

BIOLOGICAL AND MEDICAL PHYSICS,
BIOMEDICAL ENGINEERING

BIOLOGICAL AND MEDICAL PHYSICS, BIOMEDICAL ENGINEERING

The fields of biological and medical physics and biomedical engineering are broad, multidisciplinary and dynamic. They lie at the crossroads of frontier research in physics, biology, chemistry, and medicine. The Biological and Medical Physics, Biomedical Engineering Series is intended to be comprehensive, covering a broad range of topics important to the study of the physical, chemical and biological sciences. Its goal is to provide scientists and engineers with textbooks, monographs, and reference works to address the growing need for information.

Books in the series emphasize established and emergent areas of science including molecular, membrane, and mathematical biophysics; photosynthetic energy harvesting and conversion; information processing; physical principles of genetics; sensory communications; automata networks, neural networks, and cellular automata. Equally important will be coverage of applied aspects of biological and medical physics and biomedical engineering such as molecular electronic components and devices, biosensors, medicine, imaging, physical principles of renewable energy production, advanced prostheses, and environmental control and engineering.

Editor-in-Chief:

Elias Greenbaum, Oak Ridge National Laboratory, Oak Ridge, Tennessee, USA

Editorial Board:

Masuo Aizawa, Department of Bioengineering,
Tokyo Institute of Technology, Yokohama, Japan
Olaf S. Andersen, Department of Physiology,
Biophysics & Molecular Medicine,
Cornell University, New York, USA
Robert H. Austin, Department of Physics,
Princeton University, Princeton, New Jersey, USA
James Barber, Department of Biochemistry,
Imperial College of Science, Technology
and Medicine, London, England
Howard C. Berg, Department of Molecular
and Cellular Biology, Harvard University,
Cambridge, Massachusetts, USA
Victor Bloomfield, Department of Biochemistry,
University of Minnesota, St. Paul,
Minnesota, USA
Robert Callender, Department of Biochemistry,
Albert Einstein College of Medicine,
Bronx, New York, USA
Britton Chance, Department of Biochemistry/
Biophysics, University of Pennsylvania,
Philadelphia, Pennsylvania, USA
Steven Chu, Lawrence Berkeley National
Laboratory, Berkeley, California, USA
Louis J. DeFelice, Department of Pharmacology,
Vanderbilt University, Nashville, Tennessee, USA
Johann Deisenhofer, Howard Hughes Medical
Institute, The University of Texas, Dallas, Texas, USA
George Feher, Department of Physics, University of
California, San Diego, La Jolla, California, USA
Hans Frauenfelder, Los Alamos National Laboratory,
Los Alamos, New Mexico, USA
Ivar Giaever, Rensselaer Polytechnic Institute,
Troy, New York, USA
Sol M. Gruner, Cornell University, Ithaca,
New York, USA

Judith Herzfeld, Department of Chemistry,
Brandeis University, Waltham, Massachusetts, USA
Mark S. Humayun, Doheny Eye Institute,
Los Angeles, California, USA
Pierre Joliot, Institut de Biologie Physico-Chimique,
Fondation Edmond de Rothschild, Paris, France
Lajos Keszthelyi, Institute of Biophysics,
Hungarian Academy of Sciences, Szeged, Hungary
Robert S. Knox, Department of Physics
and Astronomy, University of Rochester,
Rochester, New York, USA
Aaron Lewis, Department of Applied Physics,
Hebrew University, Jerusalem, Israel
Stuart M. Lindsay, Department of Physics
and Astronomy, Arizona State University,
Tempe, Arizona, USA
David Mauzerall, Rockefeller University,
New York, New York, USA
Eugenie V. Mielczarek, Department of Physics
and Astronomy, George Mason University,
Fairfax, Virginia, USA
Markolf Niemz, Medical Faculty Mannheim,
University of Heidelberg, Mannheim, Germany
V. Adrian Parsegian, Physical Science Laboratory,
National Institutes of Health, Bethesda,
Maryland, USA
Linda S. Powers, University of Arizona,
Tucson, Arizona, USA
Earl W. Prohofsky, Department of Physics,
Purdue University, West Lafayette, Indiana, USA
Andrew Rubin, Department of Biophysics,
Moscow State University, Moscow, Russia
Michael Seibert, National Renewable Energy
Laboratory, Golden, Colorado, USA
David Thomas, Department of Biochemistry,
University of Minnesota Medical School,
Minneapolis, Minnesota, USA

For further volumes:

<http://www.springer.com/series/3740>

Claus Hélix-Nielsen
Editor

Biomimetic Membranes for Sensor and Separation Applications

 Springer

Editor

Claus Hélix-Nielsen
Department of Physics
Technical University of Denmark
Fysikvej 309
2800 Kgs. Lyngby
Denmark
claus.helix.nielsen@fysik.dtu.dk

ISSN 1618-7210

ISBN 978-94-007-2183-8 e-ISBN 978-94-007-2184-5

DOI 10.1007/978-94-007-2184-5

Springer Dordrecht Heidelberg London New York

Library of Congress Control Number: 2011943096

© Springer Science+Business Media B.V. 2012

No part of this work may be reproduced, stored in a retrieval system, or transmitted in any form or by any means, electronic, mechanical, photocopying, microfilming, recording or otherwise, without written permission from the Publisher, with the exception of any material supplied specifically for the purpose of being entered and executed on a computer system, for exclusive use by the purchaser of the work.

Printed on acid-free paper

Springer is part of Springer Science+Business Media (www.springer.com)

Pour Laura et Jonathan

Preface

Biological membrane processes and phenomena have been studied for more than 250 years since 1748 where Jean-Antoine Nollet described osmosis in pig bladders, whereas synthetic membranes constitute a rather recent scientific topic with large scale technological applications beginning just 50 years ago. Since the first report by Moritz Traube in 1864 on synthetic membranes in the form of glue droplets in water and Wilhelm Pfeffer later in the nineteenth century precipitated cupric ferrocyanide on thin porous structures, membranes studies have emerged as two more or less separate scientific topics and associated scientific communities. One topic focused on understanding biological membrane processes and one focused on developing membranes as separation devices. With the advent of biomimetics this topical distinction may be less obvious in the future.

The biological membrane research field has its roots in seventeenth and eighteenth century light microscopy – but a clear understanding of membrane molecular structure only emerged during the 1960s expressed in the seminal 1972 Singer-Nicolson fluid-mosaic model for biological membranes. However due to theoretical advances by Adolf Fick, Jacobus van't Hoff, Walther Nernst, Julius Bernstein and others, the basic membrane barrier properties and ionic differential selectivity were experimentally established in the early twentieth century. A major step forward came in the 1950s with the Hodgkin-Huxley model description of the nerve impulse highlighting the significance of regulated mechanisms for selective transport of ions across the membrane. However it would take another 40 years before molecular insight into how a biological membrane could have differential selectivity to water and ions such as sodium and potassium was provided by protein structures with atomistic resolution. The number of membrane proteins with known structure now amounts to more than 200 and by atomistic (molecular dynamics) simulations the mechanisms behind the combined high selectivity and permeability is now being elucidated. Interestingly this work has also stimulated research in the molecular mechanisms underlying selective transport properties of non-biological materials such as water permeation through carbon nanotubes.

The synthetic membrane research field progressed from Traube and Pfeffers work and in the early twentieth century nitrocellulose membranes with graded pore

sizes were developed. They became commercially available in the 1930s and the first significant application of industrial membranes was for testing of drinking water in the aftermath of the Second World War. However, it was not before the early 1960s that the membrane field was transformed from a laboratory scale to truly large scale applications as we know them today for example in the form of reverse osmosis desalination plants. The turning point was the development of the Loeb-Sourirajan process by which defect-free high-flux anisotropic membranes with a thin dense layer supported by a thicker porous structure can be produced. The dense non-porous layer (also known as the active layer or the rejection layer) enables transport of water but has barrier properties towards small (charged) solutes. Other developments in membrane technology during the last 40 years include microfiltration, ultrafiltration, and electrodialysis membranes. The vast majority of these membranes are polymer-based, but in recent years more 'unconventional' membrane materials have attracted attention. These include supported liquid membranes or films developed for carrier-facilitated transport processes. Carrier-facilitated transport is a major transport form in biological membranes and seen in this light liquid membranes represent an interesting interface between biological membrane science and membrane engineering with biomimetic potential.

The biomimetic membrane field has expanded significantly since the first scientific papers appeared with the title words 'biomimetic membranes' in the mid 1990s. However the concept of an artificial cell emerged much earlier. In fact Charles Darwin in the 1870s corresponded with Traube on cell wall formation and cell growth in physico-chemical terms. The immediate appeal of mimicking nature stems from the fact that biological membranes carry out very complex and specific sensing and transport tasks in living organisms. They accomplish these tasks efficiently with highly specialized proteins for transport exemplified by ion- and water-permeable proteins where separation is driven by electrochemical and osmotic gradients. Another class of proteins perform active transport most notably represented by the activity of ATPases/ATP synthases and rhodopsins where the energy comes from hydrolysis of ATP and from light respectively. Furthermore, biological membranes are capable of reproducing and repairing themselves continuously and biological membrane processes are seemingly not marred by issues such as fouling which represent a major problem in the operation of synthetic membranes.

However mimicking biological membrane processes also presents formidable obstacles to surmount. The membranes defining a biological cell and its compartments are very complex structures. Being a capsular material only a few nanometer thick biological membranes are flexible and strong. Flexibility arises as a consequence of its thinness – it is only two molecules thick – and strength arises from its cohesive properties defined by the composition of its constituent elements. However, any large-scale biomimetic application of lipid bilayer-type materials will require sophisticated supporting encapsulation capable of protecting the thin lipid film from the hardships of our macroscopic world without compromising its integrity.

Also, biological membranes contain several hundred different lipid species and the interaction between lipids and protein likely involves both specific and unspecific interactions. Preserving membrane protein activity in a biomimetic membrane

thus requires a thorough understanding of protein function but also of its chemical and physical interactions with the host membrane. A promising way to create and stabilize biomimetic membranes includes the use of amphiphilic substitutes for lipids. Both di- and triblock-copolymers as well as dendrimers are capable of forming membrane structures in aqueous solutions. The challenges with these systems include controlling a complex aggregation polymorphism and development of strategies for efficient protein incorporation.

While secreted proteins and enzymes today are manufactured routinely on an industrial basis, no integral membrane protein is currently commercially available in large (kilogram) quantities. In order for biomimetic membranes to develop from nanoscale laboratory devices (where typically only a few milligram of purified proteins is needed) to mass-produced industrial devices (potentially requiring many kilograms of purified protein) it is vital to consider the challenges in upscaling the production of natural and de novo designed biomimetic membrane proteins.

This volume seeks to highlight a range of aspects in the biomimetic membrane field: from biological inspirations to applied membrane technology. The aim is to present the status and challenges as seen by different scientific and engineering communities in a single volume and facilitate dialogs across subject borders to further stimulate the truly multidisciplinary field of biomimetics.

I am indebted to those friends and colleagues who have generously and enthusiastically contributed with their ideas and concepts described in this book. I thank Springer Verlag and in particular Mieke van der Fluit and Maria Bellantone for making this book possible.

Claus Hélix-Nielsen
Copenhagen

Contents

1 Sensing Meets Separation: Water Transport Across Biological Membranes	1
Stanley D. Hillyard	
2 Nature Meets Technology: Forward Osmosis Membrane Technology	21
Filicia Wicaksana, Anthony G. Fane, Chuyang Tang, and Rong Wang	
3 Polymer-Based Biomimetic Membranes for Desalination	43
Manish Kumar, Michelle M. Payne, Sean K. Poust, and Julie L. Zilles	
4 Ion-Selective Biomimetic Membranes	63
Henk Miedema	
5 Vesicle Arrays as Model-Membranes and Biochemical Reactor Systems	87
Sune M. Christensen and Dimitrios Stamou	
6 Active Biomimetic Membranes	113
Flemming Cornelius	
7 Passive Transport Across Biomimetic Membranes	137
Karin Stibius, Sania Bäckström, and Claus Hélix-Nielsen	
8 Multi-scale Modeling of Biomimetic Membranes	157
Hans Enggrob, Lars Yde, Mathias Gruber, and Himanshu Khandelia	
9 Regulation of Protein Function by Membrane Elastic Properties	187
Jens A. Lundbæk and Olaf S. Andersen	
10 Large Scale Biomimetic Membrane Arrays	205
Mark Perry, Christian Rein, and Jörg Vogel	
11 Systems for Production of Proteins for Biomimetic Membrane Devices	233
Nicola Altamura and Giuseppe Calamita	

12 Strategies for Integrating Membrane Proteins in Biomembranes	251
Jesper S. Hansen, Inés Plasencia, and Kamila Pszon-Bartosz	
13 Microfluidic Encapsulation of Biomimetic Membranes.....	273
Oliver Geschke	
Index.....	285

Contributors

Nicola Altamura Institute of Biomembranes and Bioenergetics (IBBE), National Council of Researches, University of Lecce, Via Monteroni, 73100 Lecce, Italy, n.altamura@ibbe.cnr.it

Olaf S. Andersen Department of Physiology and Biophysics, Weill Cornell Medical College, Rm C-501B 1300 York Avenue, New York, NY, 10065, USA, sparre@med.cornell.edu

Sanja Bäckström Department of Physics (DTU), Technical University of Denmark, Building 309, Fysikvej 309, DK-2800 Kgs. Lyngby, Denmark, sania.ibragimov@gmail.com

Giuseppe Calamita Department of General and Environmental Physiology, University of Bari Aldo Moro and Apulian Network of Research Laboratories, “WAFITECH” – Via Amendola 165/AI-70126, Bari, Italy, calamita@biologia@uniba.it

Flemming Cornelius Department of Physiology and Biophysics, Aarhus University, Ole Worms Allé 6, DK-8000, Aarhus C, Denmark, fc@biophys.au.dk

Sune M. Christensen Bio-Nanotechnology Laboratory, Department of Neuroscience and Pharmacology, Nano-Science Center & Lundbeck Foundation Center Biomembranes in Nanomedicine, Center for Pharmaceutical Nanotechnology and Nanotoxicology, University of Copenhagen, The HC Ørsted Institute, Universitetsparken 5, DK-2100 Copenhagen, Denmark, sunemc@nano.ku.dk

Hans Enggrob DHI, Agern Allé 5, DK-2970 Hørsholm, Denmark, hge@dhigroup.dk

Anthony G. Fane Singapore Membrane Technology Centre, Nanyang Technological University, 50 Nanyang Avenue, 639798, Singapore

School of Civil and Environmental Engineering, Nanyang Technological University, 50 Nanyang Avenue, 639798, Singapore, agfane@ntu.edu.sg

Oliver Geschke Aquaporin A/S, Ole Maaløes Vej 3, DK-2200, Copenhagen, Denmark, oge@aquaporin.dk

Mathias Gruber Nano-Science Center, The HC Ørsted Institute, University of Copenhagen and Aquaporin A/S, Universitetsparken 5, DK-2200 Copenhagen, Denmark, mathiasgruber@nano.ku.dk

Jesper S. Hansen Aquaporin A/S, Copenhagen, Denmark

DTU Physics, Technical University of Denmark, Building 309, Rm 142 Fysikvej 309, DK-2800 Kgs. Lyngby, Denmark, jsha@fysik.dtu.dk

Claus Hélix-Nielsen Department of Physics (DTU), Technical University of Denmark, Building 309, Rm 138 Fysikvej 309, DK-2800 Kgs. Lyngby, Denmark, claus.helix.nielsen@fysik.dtu.dk

Stanley D. Hillyard Department of Biomedical Sciences, University of Nevada, Las Vegas School of Dental Medicine, 1001 Shadow Lane MS 7410, Las Vegas, NV 89106-4124, USA, stanley.hillyard@unlv.edu

Himanshu Khandelia MEMPHYS, Center for Biomembrane Physics, Department of Physics and Chemistry, University of Southern Denmark, Campusvej 55, DK-5230, Odense, Denmark, hkhandel@memphys.sdu.dk

Manish Kumar Department of Chemical Engineering, Pennsylvania State University, 16802 University Park, PA, USA, mkumar.psu@gmail.com

Jens A. Lundbæk Department of Physiology and Biophysics, Weill Cornell Medical College, Rm C-501B 1300 York Avenue, New York, NY, 10065, USA

Department of Physics, Biomimetic Membranes Group, Danish Technical University, Building 309, Rm 142 Fysikvej 309, Kgs. Lyngby, DK-2800, Denmark, lundbaek@dadlnet.dk

Henk Miedema Wetsus, Centre of Excellence for Sustainable Water Technology, Agora 1, NL 8900 CC, Leeuwarden, The Netherlands, Henk.Miedema@wetsus.nl

Michelle M. Payne Department of Civil and Environmental Engineering, 3230C Newmark Civil Engineering Laboratory, University of Illinois, Urbana Champaign, 205 N. Mathews Avenue, 61801 Urbana, IL, USA, marincel@illinois.edu

Mark Perry Aquaporin A/S, Ole Maaløes Vej 3, DK-2200 Copenhagen, Denmark, mpe@aquaporin.dk

Inés Plasencia MEMPHYS-Center for Biomembrane Physics, Department of Physics and Chemistry, University of Southern Denmark, Campusvej 55, DK-5230, Odense, Denmark, miplasen@gmail.com

Sean K. Poust Joint BioEnergy Institute, 5885 Hollis Street, 94608 Emeryville, CA, USA, poust@berkeley.edu

Kamila Pszon-Bartosz Aquaporin A/S, Copenhagen, Denmark

DTU Nanotech, Technical University of Denmark, Building 423, Rm 110, Produktionstorvet, DK-2800, Kgs. Lyngby, Denmark, Kamila.Pszon@nanotech.dtu.dk

Christian Rein Aquaporin A/S, Ole Maaløes Vej 3, DK-2200 Copenhagen, Denmark, cr@aquaporin.dk

Dimitrios Stamou Bio-Nanotechnology Laboratory, Department of Neuroscience and Pharmacology, Nano-Science Center & Lundbeck Foundation Center Biomembranes in Nanomedicine, Center for Pharmaceutical Nanotechnology and Nanotoxicology, University of Copenhagen, The HC Ørsted Institute, Universitetsparken 5, 2100 Copenhagen, Denmark, stamou@nano.ku.dk

Karin Stibius Department of Physics (DTU), Technical University of Denmark, Building 309, Rm 142 Fysikvej 309, DK-2800, Kgs. Lyngby, Denmark, karin.stibius@fysik.dtu.dk

Chuyang Tang Singapore Membrane Technology Centre, Nanyang Technological University, 50 Nanyang Avenue, 639798, Singapore

School of Civil and Environmental Engineering, Nanyang Technological University, 50 Nanyang Avenue, 639798, Singapore, CYTang@ntu.edu.sg

Jörg Vogel Aquaporin A/S, Ole Maaløes Vej 3, DK-2200, Copenhagen, Denmark, jvo@aquaporin.dk

Rong Wang Singapore Membrane Technology Centre, Nanyang Technological University, 50 Nanyang Avenue, 639798, Singapore

School of Civil and Environmental Engineering, Nanyang Technological University, 50 Nanyang Avenue, 639798, Singapore, RWang@ntu.edu.sg

Filicia Wicaksana Singapore Membrane Technology Centre, Nanyang Technological University, 50 Nanyang Avenue, 639798, Singapore, Filicia@ntu.edu.sg

Lars Yde DHI, Agern Allé 5, DK-2970, Hørsholm, Denmark, lay@dhigroup.dk

Julie L. Zilles Department of Civil and Environmental Engineering, 3230C Newmark Civil Engineering Laboratory, University of Illinois, Urbana Champaign, 205 N. Mathews Ave, 61801 Urbana, IL, USA, jzilles@illinois.edu

Chapter 1

Sensing Meets Separation: Water Transport Across Biological Membranes

Stanley D. Hillyard

Abstract Water has been recognized as an essential component of living systems since antiquity. One must drink to stay alive and water is essential for growing food crops. With the development of the microscope it was possible to visualize cells and make observations that indicated the movement of water across cell membranes. Experiments conducted in the eighteenth, nineteenth and early twentieth centuries developed concepts and terminology that are used to this day. The discovery of aquaporins as water conducting channels provided a mechanism for understanding water transport across cell membranes. Selected examples are provided to describe functions of aquaporins in water balance physiology in animals and plants. Historically, many investigators have contributed to the understanding of water transport, sometime in collaboration and other times completely independent of one another. Thus, what may appear to be a linear advancement is only possible by selecting landmark studies and attempting a synthesis of how we know what we know.

1.1 History of Water Transport Across Cell Membranes

Among the first biological structures described by early microscopists were red blood cells (Malphigi 1666, translated by Forrester 1995) and compartments formed by cell walls in cork (Hooke 1664). These structures became instrumental in experiments leading to our understanding of water transport across cell membranes. The English anatomist, William Hewson (1773) described experiments in which human and animal red blood cells were observed while rolling down a tilted slide so their shape could be visualized. The cells were observed to swell in dilute media and

S.D. Hillyard (✉)

Department of Biomedical Sciences, University of Nevada, Las Vegas School of Dental Medicine, 1001 Shadow Lane MS 7410, Las Vegas, NV 89106-4124, USA
e-mail: stanley.hillyard@unlv.edu

shrink in concentrated media leading to the hypothesis of a cell membrane. This study predates the experiments by Nageli and Kramer (1855) who observed that plant cell membranes would shrink within the cell wall when exposed to concentrated solutions, a process termed plasmolysis. Kleinzeller (1996) summarized these studies in the context of similar experiments by other investigators during the nineteenth century and observed that concepts of osmotic water movement developed rather independently within the zoological/medical and botanical communities. For example, in 1799 the English naturalist, Robert Townson, determined that living frogs obtain water solely by absorption across the skin (Jørgensen 1997). Like the red blood cell, the frog skin has played an important role in the elucidation of mechanisms for osmotic water flow across biological membranes.

The concept of osmosis was further developed by Dutrochet (1827) who devised an osmometer consisting of an upper and lower chamber separated by a membrane, such as the caecum of a fowl or the pig bladder. The lower chamber contained water and the lower chamber a more concentrated solution. Endosmosis was evaluated as an increase in the fluid level in the upper chamber while diffusion back into the lower chamber resulted in a slow outward movement as the concentration gradient diminished (exosmosis). This discovery and its contribution to subsequent understanding of water permeability is summarized by Richet (2001). About 20 years later, Matteucci and Cima (1845) used a Dutrochet-like osmometer to measure osmotic water movement across the isolated frog skin which became a tissue of choice for studying water permeability in medically oriented studies.

The botanist Wilhelm Pfeffer (1877) developed an osmometer like the one of Dutrochet but used an artificial membrane of copper ferrocyanide precipitated on a porous ceramic surface and a mercury manometer to evaluate the pressure that developed as water moved osmotically into the solution chamber. The artificial membrane was assumed to allow only water and not solutes (i.e. it was semipermeable) to pass. Thus, it was possible to establish a relationship between molar concentration and osmotic pressure. Both Pfeffer and another botanist, Hugo DeVries (1871), observed plant cells to shrink within their cell walls when placed in concentrated solutions and developed the concept of isoosmotic concentrations in which cells did not shrink.

van't Hoff analyzed Pfeffer's and DeVries' data quantitatively with the assumption that solute molecules in solution behave like ideal gas molecules (van't Hoff 1877, 1901). From this analysis, he derived the famous Van't Hoff equation (and was awarded the first Nobel Prize in chemistry in 1901):

$$\pi = C_s RT \quad (1.1)$$

where π is the osmotic pressure that develops when a solution is separated from pure water by a semipermeable membrane, C_s is the molar concentration of an ideal solute, R is the appropriate gas constant and T the absolute temperature. The non-ideal behavior of a given solute is corrected by an empirically determined dimensionless osmotic coefficient ϕ_s times the molar concentration ($\phi_s \cdot C_s$) to give the effective osmotic concentration (C_{osm}). For physiological solutions ϕ_s is typically about 0.9. A more general case can be applied for separation of two solutions having a different

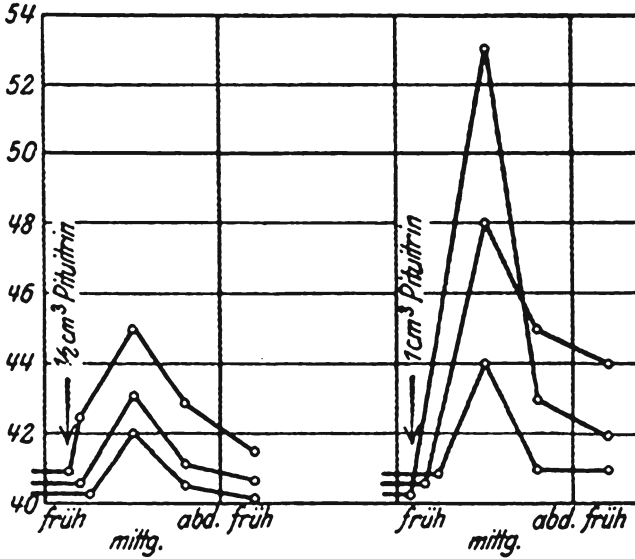


Fig. 1.1 An original figure from Brunn (1921) showing the rapid increase in body weight (ordinate) of frogs placed in water and give two doses (0.5 and 1 ml) of a neurohypophyseal extract (pituitin)

osmotic concentration by empirically correcting for non ideality of the solute and semipermeable membrane:

$$\pi = \sigma_s RT\Delta C_{\text{osm}} \tag{1.2}$$

where σ_s is the reflection coefficient for the solute. A reflection coefficient of 1 indicates the membrane is completely impermeable to the solute while a value of 0 indicates the solute is equally permeable with water and unable to establish an osmotic gradient. The osmotic permeability coefficient P_f [$\text{cm} \cdot \text{s}^{-1}$] is calculated from the equation:

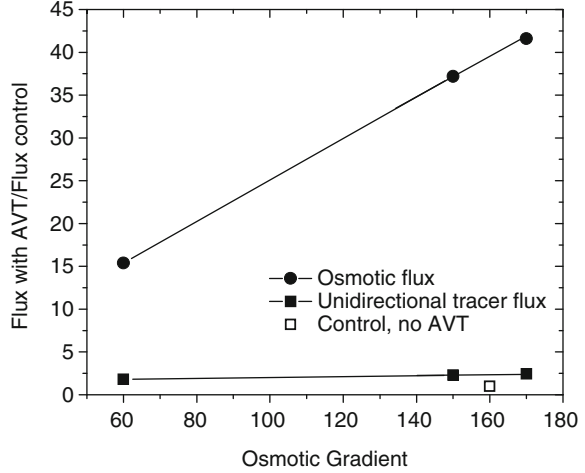
$$P_f = (RT / V_w) \cdot L_p \tag{1.3}$$

where V_w is the partial molal volume for water ($18 \text{ cm}^3 \text{ mol}^{-1}$) and L_p is the hydraulic conductivity which is the rate of water movement across a given area, per unit of osmotic gradient. The area specific osmotic water flux J_v [$\text{cm}^3 \text{ cm}^{-2} \text{ s}^{-1} = \text{cm s}^{-1}$] is calculated from the equation:

$$J_v = P_f V_w \sigma_s \Delta C_{\text{osm}} \tag{1.4}$$

The discovery by Brunn (1921) that water uptake by frogs was stimulated by posterior pituitary extracts was replicated in numerous anuran species and again made frog skin an important contributor to the study of osmotic water flow, see Fig. 1.1.

Fig. 1.2 Increase in water movement across the toad bladder following treatment with antidiuretic hormone AVT. The *upper trace* shows the larger value determined from osmotic flow versus the small value calculated from diffusion of isotopically labeled water (Plotted from tabular data taken from Hays and Leaf 1962)



The introduction of isotopic water (D_2O and later 3H_2O) allowed comparison between osmotic and diffusional water flow across the skin of living frogs (Hevesy et al. 1935). Diffusional water flow (J_{H_2O}) is calculated from the equation:

$$J_{H_2O} = P_{dw} \left([H_2O]_b - [H_2O]_f \right) \quad (1.5)$$

In Eq. 1.5 P_{dw} is the diffusional coefficient for water and, assuming isotopic water has the same properties as water itself, J_{H_2O} should equal J_v from Eq. 1.4. Although initial studies were inconclusive, Koefoed-Johnsen and Ussing (1953) made further experiments with isolated frog skin and found osmotic water flow was stimulated by over two times following treatment of the skin with neurohypophyseal extracts while diffusional flow was stimulated by only about 10%. Similar observations were made by Hays and Leaf (1962) for water flow across the isolated toad urinary bladder that also became an important tissue for studying the effects of neurohypophyseal hormones on water transport, see Fig. 1.2.

From these and other observations (reviewed in Parisi et al. 2007) it was suggested that water was moving across the tissue via water filled pores that were activated by the hormones because volume flow Q [$m^3 s^{-1}$] through a pore would be described by the Poiseuille equation:

$$Q = \pi \Delta P \cdot r^4 / 8 \eta L \quad (1.6)$$

where ΔP [Pa] is the pressure gradient, η [Pa·s] is the viscosity, and L [m] is the length of the pore. Q is proportional to the radius to the fourth power whereas diffusional flux J [$mol m^{-2} s^{-1}$] (i.e. amount of substance flowing through a finite area during a finite time interval) would be proportional to the area only as described by Fick's first law:

$$J = -A \cdot D \cdot (dC / dx) \quad (1.7)$$

where A [m^2] is the area, D [$\text{m}^2 \text{s}$] the diffusion coefficient and dC/dx [mol m^{-1}] the concentration gradient.

Related studies with toad bladder (Parisi et al. 1985) showed that disrupting microtubules by colchicine and actin filaments by cytochalasin B inhibited the increase in water permeability produced by neurohypophyseal hormones (also termed antidiuretic hormone, ADH). For mammals the ADH is arginine vasopressin, AVP, while for amphibians the ADH is arginine vasotocin, AVT. Both AVT and AVP stimulate water permeability of toad bladder and frog skin. Electrical measurements of membrane capacitance also showed that the increase in water permeability of toad bladder produced by ADH was associated with an increase in apical membrane area of the epithelium (Stetson et al. 1982). Together, these observations gave rise to the hypothesis that the stimulation of water permeability by antidiuretic hormones, termed the hydroosmotic response, resulted from exocytosis of vesicles containing putative water channels into the apical membrane of the epithelial cells.

1.2 Identification and Characterization of Water Channels

With the development of the electron microscope it was possible to visualize cellular structures at the macromolecular level. In particular, freeze fracture electron microscopy in which the lipid bilayer of cell membranes is split open revealed major intrinsic proteins (MIPs) that formed clusters in toad bladder epithelial cells following stimulation of osmotic water flow by neurohypophyseal peptides (Chevalier et al. 1974; Kachadorian et al. 1975). The evidence for pores and observations of MIPs in many tissues led to efforts to isolate and characterize the specific molecules associated with water permeability.

Among the first MIPs to be characterized was a 26 kD protein from lens (Kistler and Bullivant 1980). With improving technology for construction and analyzing cDNA libraries, Gorin et al. (1984) were able to isolate mRNA for a 26 kD MIP in bovine lens and deduce an amino acid sequence for a protein with six transmembrane domains and at least one amphiphilic transmembrane segment “*as expected if the protein were to participate in the formation of an aqueous channel*”. In red blood cells, it was known that HgCl_2 and organomercurial compounds blocked water permeability across a putative water channel (Macey and Farmer 1970). Benga et al. (1986) demonstrated the inhibition of water flow across membranes of red blood cell ghosts by (chloromercuri) benzene sulfonate (PCMBS) using ^{130}Hg as a label to identify proteins associated with water permeability. Two labeled bands were identified with gel electrophoresis that the authors concluded “*...have to be considered as playing a role in water transport*”.

The final demonstration of a MIP as an aquaporin was accomplished by the laboratory of Peter Agre who received the 2003 Nobel Prize in Chemistry.

Table 1.1 List of aquaporins based on phylogenetic analyses, based on Kruse et al. (2006), Ikeda et al. (2011), and Itoh et al. (2005)

Mammals	Plants	Yeast	E. coli
AQP0	PIPs (Plasma	AQY1	AQPZ
AQP1	membrane	AQY2	GlpF**
AQP2	Intrinsic Proteins)	GLPY1**	
AQP3**	TIPs* (Tonoplast	GLPY2**	
AQP4	Intrinsic Proteins)		
AQP5	NIPs* (Nodulin-like		
AQP6	Intrinsic Proteins)		
AQP7**	SIPs (Small basic		
AQP8	Intrinsic Proteins)		
AQP9**	XIPs (X Intrinsic		
AQP10**	Proteins)		
AQP11***			
AQP12***			

The single asterisk (*) indicates that the PIPs, TIPs and NIPs constitute groups of plant aquaporins with some members of each group having permeability to glycerol

The double asterisk (**) indicates aquaglyceroproteins that are also permeable to glycerol and other small solutes

The triple asterisk (***) indicates aquaporins with non-NPA motifs (NPC in AQP11 and NPT in AQP12)

In studying a 32 kD Rh protein in human erythrocytes they discovered a 28 kD protein, initially termed CHIP28, to be very abundant. Isolation of the cDNA for the 28 kD MIP revealed sequence homology with the MIP 26 from lens. When the cRNA corresponding to this protein was injected into oocytes of the clawed frog, *Xenopus laevis* suspended in a dilute saline solution, the oocytes rapidly swelled and burst (Preston et al. 1992). (The oocyte expression system is based on the need for amphibian oocytes to synthesize many proteins that are needed early in development. Heterologous mRNA is translated as are intrinsic mRNAs and newly translated membrane proteins become incorporated into the oocyte membrane.) In addition, purified CHIP 28 protein incorporated into artificial phospholipid vesicles resulted in a similar increase in water permeability relative to vesicles without the protein (Zeidel et al. 1994). Soon after the demonstration that CHIP28 was a water channel and that other water channels exist, a nomenclature for designating aquaporins (AQP) was established. CHIP28 became AQP1 while MIP26 from the lens, having been described earlier became AQP0.

Once the cDNA sequence for AQP1 had been identified it became possible to construct primers to investigate the expression of other aquaporin isoforms from cDNA libraries, in mammals and non-mammalian systems. Thirteen aquaporins were identified in humans (Ishibashi et al. 2009) and they were also characterized in other vertebrates, insects, plants, and in microbial systems including both bacteria and archaeobacteria (Borgnia et al. 1999; Kruse et al. 2006). It is evident that aquaporins are an ancient class of membrane proteins that date back to the earliest cellular organisms, see Table 1.1.

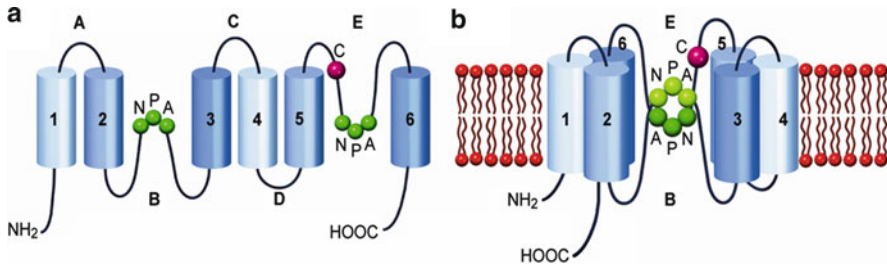


Fig. 1.3 (a) The basic structure of aquaporin subunits. Each has six transmembrane domains with the amino and carboxy terminals in the cytosol and two Asn-Pro-Ala (NPA) domains. (b) The arrangement of transmembrane domains forms an “hour glass” shape with the juxtaposed NPA domains forming the water selective pore

The basic aquaporin structure consists of four subunits, each having six transmembrane domains. Unlike ion channels, each subunit forms a water conducting channel. Figure 1.3a shows the arrangements of the transmembrane domains (1–6) and linking segments (A–E) for a typical subunit. Figure 1.3b shows the hour glass model in which the transmembrane domains form an entry site for water to diffuse through the selective pore formed by the juxtaposition of the two NPA (asparagine-proline-alanine) domains on segments B and E. A cysteine residue (C) can bind mercury ions which are known to inhibit water flow across aquaporins.

1.3 Functional Organization of Aquaporins in Animal and Plant Tissues

The intent of this volume is to examine biomimetic functions for membrane proteins such as the aquaporins. Such applications often require the utilization of osmotic and hydrostatic pressure gradients for applications such as reverse osmosis while biologically aquaporins generally mediate forward osmosis. As examples for forward osmosis in biological systems I have chosen aquaporins in the mammalian kidney and amphibian water homeostasis because they mediate large volume flows via well characterized mechanisms of epithelial transport. These are compared with plant tissues which have a larger diversity of aquaporins than animal tissues and develop large hydrostatic (turgor) pressures associated with fluid transport and growth.

1.4 Kidney Aquaporins

The paired human kidneys, each about the size of a small person’s fist, filter about 180 l of plasma per day and reabsorb all but about 1% of that volume as the filtrate moves through a series of tubules called nephrons. The final urine may be concentrated to

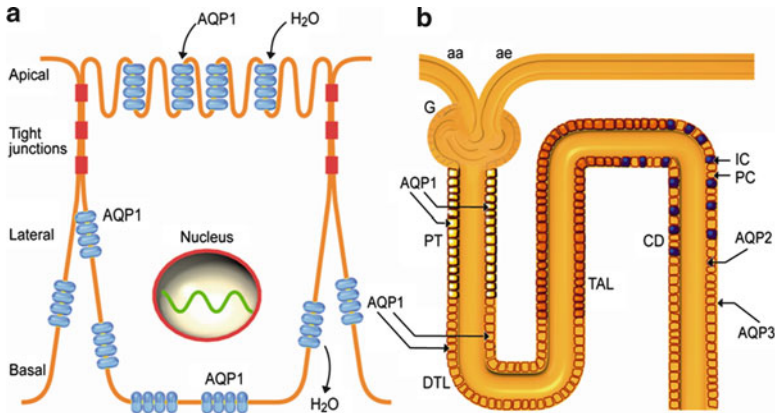


Fig. 1.4 (a) Epithelial cells in the proximal tubule (PT) and descending thin limb (DTL) of the loop of Henle express *AQP1* in both the apical (luminal) and basolateral membranes (lateral and basal membranes) (Adapted from Agre 2000). (b) NaCl transport out of the thick ascending limb (TAL) draws water out of the DTL, increasing the salt concentration reaching the TAL. Salt and urea accumulation in the peritubular fluid creates a gradient to draw water out of the collecting duct (CD) to reduce the volume of urine formed (Adapted from Sabolic and Brown 1995). Water permeability of the CD is regulated by AVP stimulation of *AQP2* insertion into the apical membrane of principal cells (PC). Water leaves the PCs via an aquaglyceroprotein (*AQP3*) in the BLM

conserve plasma volume in the face of dehydration or dilute to eliminate excess fluid and metabolic wastes. Small adjustments in tubular reabsorption can have dramatic impact on blood pressure and abnormalities are associated with a number of cardiovascular diseases (Nielsen et al. 1999; Agre 2000). Each kidney has about one million nephrons. Each nephron consists of a series of tubules formed by epithelial cells that are specialized for solute and water reabsorption. Reabsorption requires entry of solutes and water from the tubular lumen into the cells across the apical membrane and transport out of the cells across the basolateral membrane. Solute and water reabsorbed across the epithelial cells are then taken back into peritubular capillaries that surround the nephrons and returned to the venous circulation. The first tubular segment is the proximal tubule that is located in the outer or cortical zone of the kidney.

Approximately 60% of the volume of the glomerular filtrate is reabsorbed in the proximal tubule. *AQP1* is localized in both the apical and basolateral membranes of proximal tubular cells, see Fig. 1.4, and it facilitates reabsorption of a large fluid volume that is mediated by a small osmotic gradient created by active ion transport, primarily Na⁺ and Cl⁻, across the epithelium. Because glomerular filtration prevents protein loss to the tubular fluid, there is an elevated colloid osmotic pressure that facilitates uptake of the reabsorbed fluid back into the circulation. Values for tubular reabsorption and capillary colloid osmotic pressure, obtained from Boron and Boulpaep (2005), are given in Fig. 1.5.

The nephron continues as the loop of Henle that descends into the medulla and ascends back up to the cortex. The descending loop of Henle is made of thin squamous epithelial cells that, like proximal tubular cells, have *AQP1* in the apical

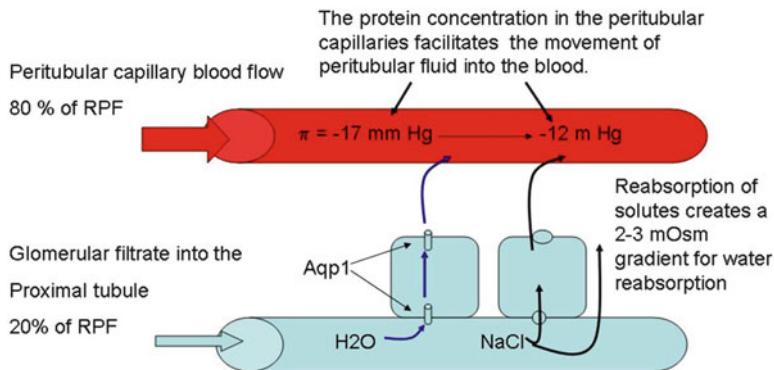


Fig. 1.5 Approximately 20% of renal plasma flow (*RPF*) to the glomeruli forms a protein free ultrafiltrate that enters the proximal tubule. Tubular solute reabsorption creates a small osmotic gradient in the peritubular fluid that is sufficient to reabsorb 2/3 of the glomerular filtrate (ca 180 L/day). This is possible because of the high permeability produced by *AQP1*. The plasma proteins become concentrated in the remaining 80% of plasma that flows to the peritubular capillaries to produce an increased colloid osmotic pressure that facilitates water uptake from the peritubular fluid (Values from Boron and Boulpaep 2005)

and basolateral membranes but do not transport salt. Epithelial cells in the thick ascending loop of Henle become more columnar and transport Na^+ and Cl^- into the peritubular fluid surrounding the thin descending loop. This draws water out of the descending loop and concentrates the solutes so that a higher Na^+ and Cl^- concentration reaches the ascending thick loop to transport even more solute. This process is termed counter current multiplication and results in the accumulation of high concentrations of Na^+ and Cl^- in the peritubular fluid in the medulla. The ascending thick loop continues as the distal tubule that regulates reabsorption of NaCl and K^+ secretion but mediates little water reabsorption. The result is a dilute tubular fluid that enters the collecting ducts.

As fluid travels down the collecting duct, the osmotic concentration of the peritubular fluid, established by the loop of Henle and also urea recycling, creates an osmotic gradient for water reabsorption that permits urine concentration to as much as 1,200 mOsm. Of interest, desert rodents may concentrate their urine to as much as 6,000 mOsm and require no water in their diet (Schmidt-Nielsen and Schmidt-Nielsen 1952). The degree to which this gradient is utilized depends on the permeability of the collecting duct epithelial cells that is highly regulated according to the requirement for fluid retention (antidiuresis) or excretion (diuresis). Antidiuretic hormone released from the posterior pituitary (neurohypophysis) in response to increased plasma osmolality or hypotension promotes fluid reabsorption to compensate for dehydration or hemorrhage.

Fluid reabsorption across the collecting duct epithelium utilizes separate aquaporins in the apical and basolateral membrane, see Figs. 1.6 and 1.7. Transepithelial transport is regulated by the insertion of vesicles that contain *AQP2* into the apical membrane by exocytosis. Exocytosis is stimulated by *ADH* that binds to a membrane

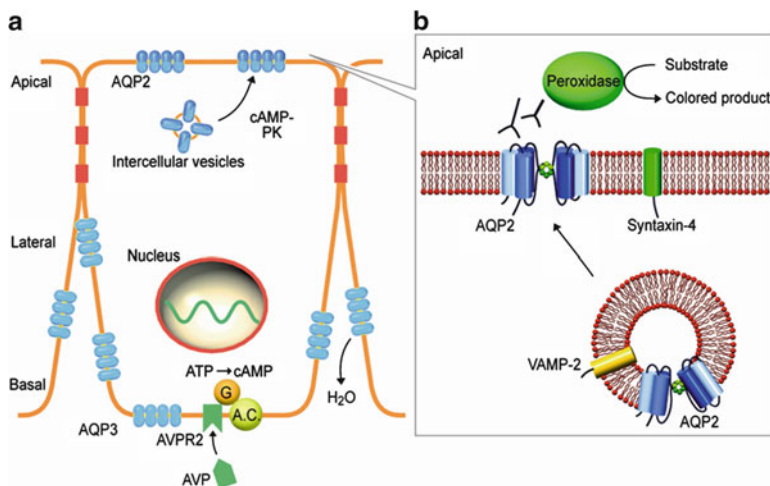


Fig. 1.6 (a) The pathway for AVP-stimulated water reabsorption across the collecting duct (CD) epithelium begins with transport into the cells via AVP stimulated AQP2 and out of the cells via AQP3 aquaglyceroproteins in the basolateral membrane. ADH activates a AVP type 2 receptor (AVPR2) in the basolateral (lateral+basal) membrane that stimulates protein insertion, see Fig. 1.7 for details. (b) Inset: AQP2 containing vesicles contain the docking protein VAMP-2 that binds to Syntaxin-4 in the apical membrane to facilitate fusion and AQP2 insertion. Anti-AQP2 C-loop antibodies can be used to monitor the AQP2 density on the plasma membrane (Figure based on Gouraud et al. 2002)

receptor (V2) and activates adenylate cyclase to form cyclic AMP (cAMP). C-AMP then activates protein kinase A (PKA) and phosphorylation events lead to vesicle transport to the apical membrane and exocytosis. Although the exact signaling mechanism is not fully understood, it is known that AQP2 has an amino acid residue (serine 256) that becomes phosphorylated within minutes following AVP treatment of kidney slices, that vesicle transport requires microtubules and microfilaments and that vesicles and the cytosolic face of the apical membrane both contain docking proteins that are similar to soluble neuronal synaptic attachment protein receptors (SNAREs; Nielsen et al. 1999). More recently, Gouraud et al. (2002) demonstrated interaction between SNARE proteins VAMP-2 in aquaporin containing vesicles and syntaxin-4 in the apical membrane associated with cyclic AMP induced insertion of AQP2-containing vesicles in cultured renal cells.

Water leaves the cell via two aquaporins, AQP3 and AQP4 that have been identified in the basolateral membrane of collecting duct cells. AQP3 was found to also be permeable to small molecules such as glycerol and represents a group of aquaglyceroproteins versus aquaporins that are more selective for water. Of comparative interest, aquaglyceroproteins are related to the bacterial glycerol transport protein GlpF found in *E. coli* and occur in the basolateral membrane of the mammalian skin. Knockout mice that have the AQP3 gene deleted display dry skin and it has been suggested that this condition in humans might result from a defect in the expression of AQP3 in the skin (Verkman 2009).

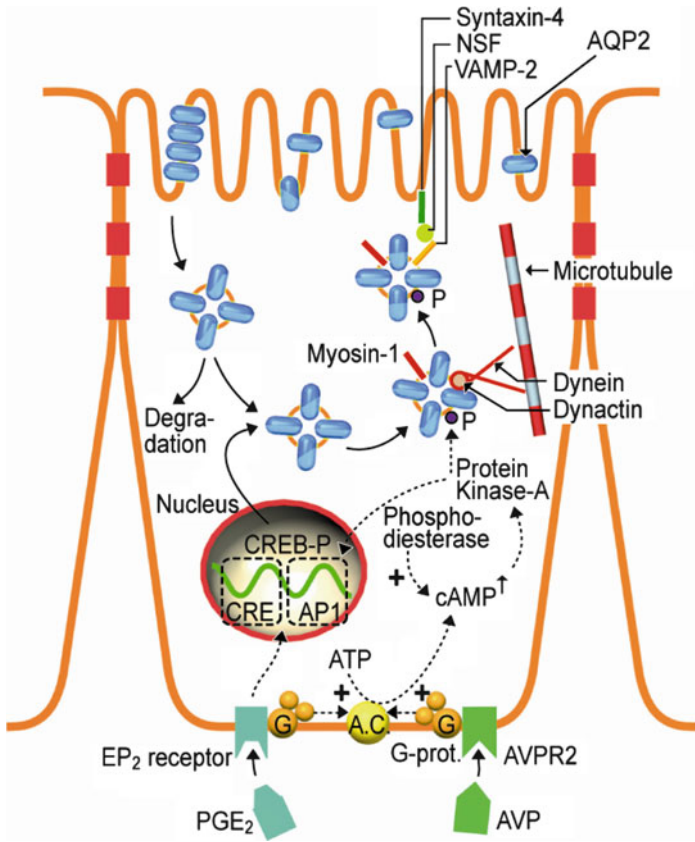


Fig. 1.7 A more detailed drawing shows pathways for the stimulation of *AQP2* insertion into apical membrane of collecting duct (CD) epithelial cells. *AVP* binding to the *AVP* type 2 receptor (*AVPR2*) stimulates adenylate cyclase (*A.C.*) activity. Elevated levels of Cyclic AMP (*cAMP*) activate protein kinase A mediated phosphorylation (*P*) of *AQP2* serine residues and also *cAMP* response element binding protein (*CREB-P*) that stimulates gene expression. *AQP2* containing vesicles are carried by dynein and dynactin along microtubules. Syntaxin-4 in the apical membrane binds to *VAMP-2* in the vesicle to promote vesicle fusion (see also Fig. 1.6b) Note also that other hormones may affect *A.C.* and *cAMP* production, for example prostaglandin *PGE₂* inhibits *A.C.* activity and thereby *cAMP* production (Figure based on Nielsen et al. 1999)

1.5 Amphibian Water Balance

Unlike mammals, amphibians cannot form concentrated urine and have skin that is not resistant to evaporative water loss. Despite this limitation, many anuran (frog and toad) species are able to inhabit arid regions of the world (Hillman et al. 2009). When available, water is absorbed across the skin and the kidneys form a large volume of dilute urine that can be stored in the urinary bladder which, unlike the mammalian bladder, is a water storage organ. In some terrestrial species this volume may

be equivalent to half of the body weight, or more, and animals may remain for many months in subterranean burrows when water is not available.

When foraging away from water urine formation basically ceases and the animals reabsorb water via aquaporins in the bladder epithelium to offset hemoconcentration due to evaporative water loss (Ruibal 1962). Like the collecting duct of the mammalian kidney the bladder epithelial cells have an ADH stimulated aquaporin in the apical membrane and an aquaglyceroprotein in the basolateral membrane. When water is again available, water is taken up across the skin to restore plasma osmolality and replenish urine storage. As with the urinary bladder, the apical membrane of the outer living cell layer of skin epithelial cells contains AVT-stimulated aquaporins that become inserted by exocytosis of vesicles.

Anuran amphibians have a distinct group of AVT-stimulated aquaporins that are analogous with mammalian AQP2 but differ sufficiently that they form a separate class, AQP-a2 (Suzuki et al. 2007). The designation of anuran aquaporins also refers to the species where a particular isoform was obtained. For example, Hasegawa et al. (2003) characterized two AVT-stimulated aquaporins in the AQP-a2 subclass from ventral skin of the Japanese treefrog, *Hyla japonica* and named them AQP-h2 and AQP-h3. AQP-h2-homologues are also found in the urinary bladder of all species examined and in the skin of species that tend to be more terrestrial. AQP-h3 homologues are found in more terrestrial and more semi-aquatic species. In the completely aquatic species, *Xenopus laevis*, messenger RNA for AQP-h3 can be isolated from the ventral skin but contains an additional nucleotide sequence that prevents translation of the functional AQP-h3 aquaporin which is not necessary for purely aquatic species (Ogushi et al. 2010a). Amphibians are the first group of vertebrates to successfully colonize terrestrial habitats and have evolved a variety of mechanisms to utilize aquaporins in osmoregulatory tissues.

As with the mammalian collecting duct, water that enters epithelial cells of the skin and urinary bladder leaves via aquaglyceroporins in the basolateral membranes that share homologies with mammalian AQP3. Akabane et al. (2007) have characterized and immunolocalized an aquaglyceroporin, from *Hyla japonica* and named it AQP-h3BL to distinguish it from the apically expressed AQP-h3. Zimmerman et al. (2007) have characterized a similar aquaglyceroprotein (HC-3) in many tissues of Cope's treefrog, *Hyla chrysosalis*, that routinely freeze during cold months of the year and suggested that HC-3 allows cryoprotectant molecules, such as glycerol, to enter the cells.

Some terrestrial species have specialized regions of ventral skin, called the seat patch, that allow dehydrated animals to rehydrate at rates as high as 30% of the body weight per hour, see Fig. 1.8a. In conjunction with the increase in cutaneous water permeability produced by AVT many anuran species show a behavior, termed the water absorption response, in which the skin is pressed to a moist surface and capillary blood flow to skin increases markedly, see Fig. 1.8b. Historically, Christensen (1975) found that AVT – stimulation of water uptake across isolated toad skin required perfusion of the cutaneous vasculature. If not perfused, the electrolyte content of the tissue became diluted and the osmotic gradient across the epidermis dissipated. Viborg and Rosenkilde (2004) showed the increase in water absorption by

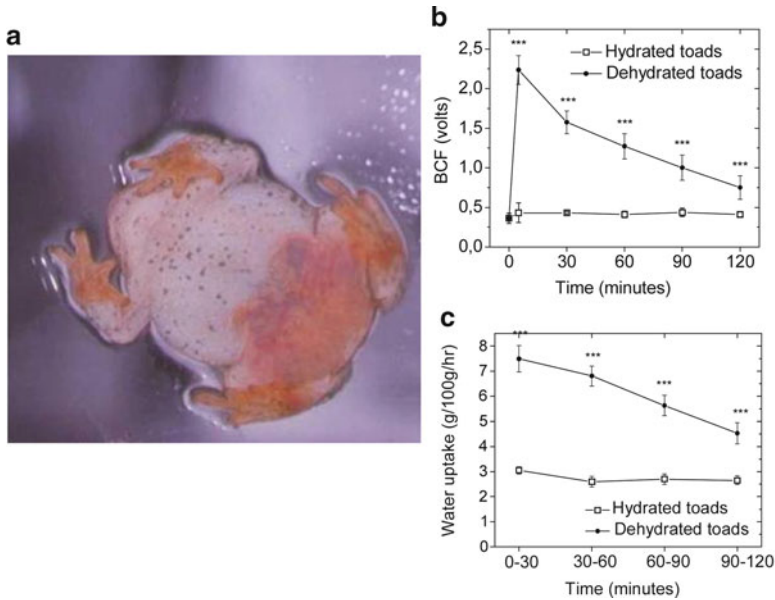


Fig. 1.8 (a) Many semiterrestrial and terrestrial anurans have a region of skin on the posterior-ventral surface that is specialized for water absorption. This region is highly vascularized and blood flow, measured with laser-Doppler flow cytometry, increases (b) to facilitate rehydration (c) (From Viborg and Rosenkilde 2004)

dehydrated toads was accompanied by an increase in capillary perfusion of the seat patch region, see Fig. 1.8c.

Of interest, AVT had no effect on blood flow but produced a transient increase in water absorption of hydrated toads while injection of the beta adrenergic agonist, isoproterenol, increased both blood flow and water absorption to levels similar to that of dehydrated toads, see Fig. 1.9. More recently, Ogushi et al. 2010b, found that beta adrenergic stimulation also promotes incorporation of aquaporins into the apical membrane of the skin.

Thus, cutaneous blood flow and insertion of aquaporins into the apical membrane of the skin are coordinated by a sympathetic response when a suitable hydration source is detected by chemoreceptors in the skin. Finally, the capillaries that serve the seat patch area are richly supplied with AQP1 – like aquaporins that facilitate water movement into the vasculature. The overall flow of water across the skin and into the circulation thus requires serial transport involving three aquaporins, see Fig. 1.10.

Of interest, a number of studies have reported toads to rehydrate more rapidly from dilute NaCl solutions (10–50 mM) than from deionized water, despite the reduced osmotic gradient (Ferriera and Jesus 1972; Hillyard and Larsen 2001). This has been ascribed to solute coupled water absorption (Guo et al. 2003) but is not inhibited by amiloride, an inhibitor of epithelial Na^+ transport. A possible explanation is provided by Bowen and Yousef (2003) who examined the effect of electrolytes

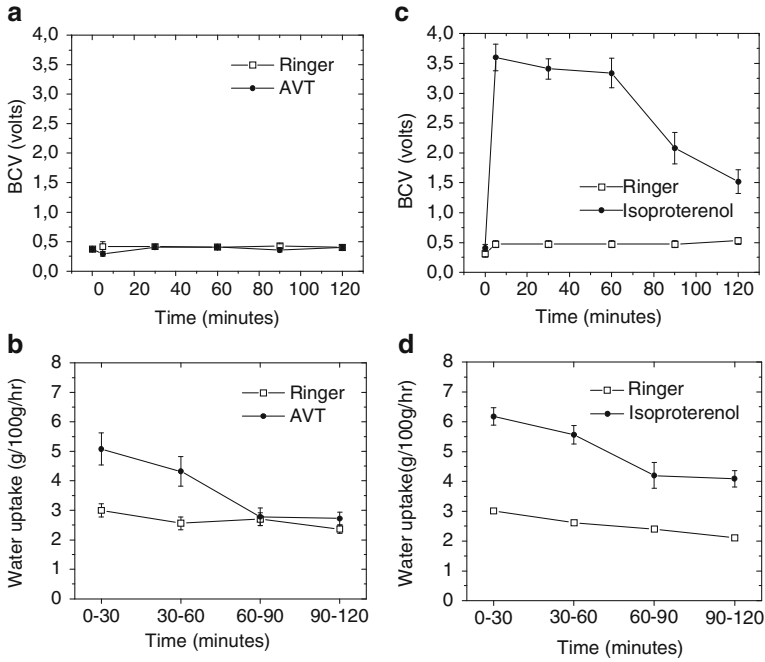


Fig. 1.9 (a, b) Injection of AVT into hydrated toads has negligible effect on seat patch blood flow and water uptake is only transiently stimulated. (c, d) In comparison, injection of the beta adrenergic agonist, isoproterenol, stimulates both blood flow and water absorption to levels comparable to those seen for dehydrated toads in Fig. 1.6b (From Viborg and Rosenkilde 2004)

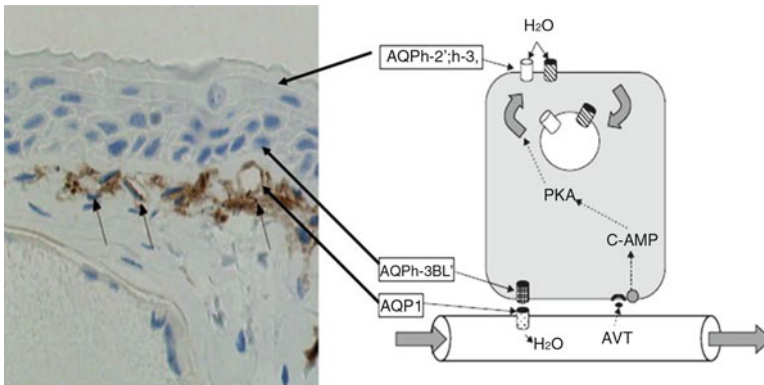


Fig. 1.10 The pathway for water absorption across anuran skin and its flow into the circulation. A. The epithelial cells form a functional syncytium so water absorbed across the apical membrane of the outer most living cell layer flows through the collective basolateral membranes of the underlying cell layers. The apical membrane contains AVT stimulated aquaporins that are homologous to those characterized in the Japanese tree frog. (*AQP-h2* and *AQP-h3*). The basolateral membrane contains an aquaglyceroprotein homologous to *AQP-h3BL* and subepidermal capillaries, stained brown in this figure, contain an aquaporin homologous to the mammalian *AQP1*

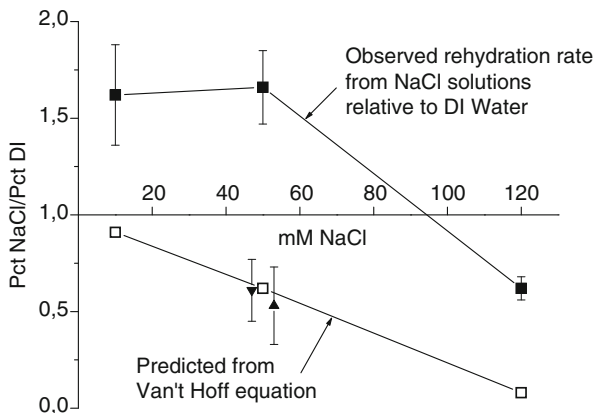


Fig. 1.11 Rehydration by *Bufo marinus* is more rapid from dilute (10–50 mM) NaCl solutions than from deionized water (*DI*). The observed rates are expressed as a ratio of the values measured with *DI* to the values obtained from the NaCl solutions. The ratio predicted from the van't Hoff equation is plotted below the line of unity. The values obtained for rehydration from 100 mM sucrose (*inverted triangle*) and 50 mM Na gluconate (*triangle*) lie on or near the value predicted from the van't Hoff equation (From Hillyard and Larsen 2001)

on the viscosity of vicinal or confined water as they might affect membrane separation processes that use very finely porous polymeric films.

Significantly, they found Cl^- was particularly effective as a “structure breaker” that reduced the viscosity of water in pores having a radius of approximately 1.69 nm. Hillyard and Larsen (2001) found that water absorption by toads, *Bufo marinus* was greater from 10–50 mM NaCl solutions but absorption from an equal concentration of Nagluconate, see Fig. 1.11 was reduced as predicted from the van't Hoff equation. Furthermore, water absorption by toads, *Bufo punctatus*, was similarly greater from dilute solutions of NaCl and CaCl_2 (Hillyard et al. 2007). Whether Cl^- exerts a similar effect on aquaporins and porous polymeric films presents an interesting case where the biological provides insight into the biomimetic.

1.6 Plant Water Balance

Maurel et al. (2008) have recently reviewed the literature on plant aquaporins that mediate water movements into and within plant tissues. The interested reader may consult this reference for access to the primary literature. Note that the forces that drive water into or out of plant cells have hydrostatic and gravitational components in addition to osmotic gradients. The plant physiological literature often uses hydraulic conductivity with these units of driving force. Water turnover in plants begins with absorption across the roots, transfer to the leaves in vascular bundles (xylem) and evaporative loss through stomata that open to allow carbon

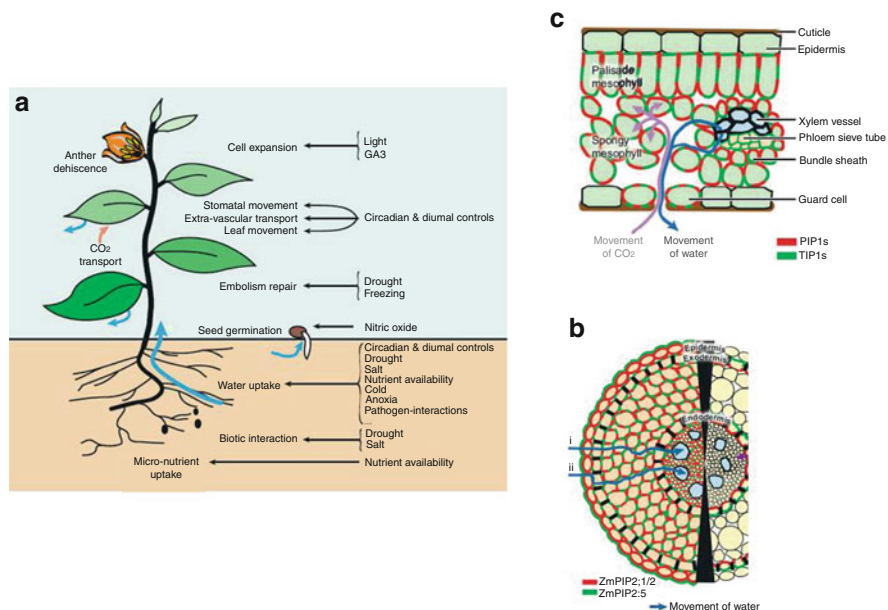


Fig. 1.12 (a) The general pathway for water absorption by roots and transport by xylem to the leaves. Water reaching the leaves creates turgor pressure to prevent wilting while the stomata open to allow carbon dioxide entry for photosynthesis. Water loss by transpiration creates suction to draw water upwards. (b) Detailed cross section of a corn (*Zea mays*) root showing cellular layers that contain plasma membrane aquaporins ZmPIP2;1/2 and ZmPIP2;5. Transcellular transport (indicated by *i*) mediates water movement to the xylem bundles that carry fluid to the upper regions of the plant. (c) Detailed cross section showing water transfer from xylem bundles to cellular components of a leaf. Transfer to cells is mediated by PIPs while uptake by tonoplasts, via TIPs, creates turgor pressure to prevent wilting and regulate opening of guard cells in the stomata. Transpiration of water from the stomata is important for creating suction to draw water upwards from the roots. Carbon dioxide entry into photosynthetic cells is also believed to be mediated by PIPs (From Maurel et al. 2008)

dioxide entry for photosynthesis, see Fig. 1.12a. Water uptake by plant cells creates turgor pressure that can be transmitted to adjacent cells by cytoplasmic connections called plasmodesmata. Water stress can occur when uptake from the roots is less than transpiration and the plant wilts. The soil water potential at which this occurs is the wilting point and varies among drought sensitive and drought resistant species. Plant cells also differ from animal cells in that the intracellular space is dominated by a central vacuole or tonoplast. The hydraulic conductivity of the tonoplast membrane is greater than the cell membrane and it has been suggested that fluid transfer from tonoplast to cytosol might minimize changes in cytosolic volume during water stress. Cell volume increases are essential for plant growth and water uptake by the cell and tonoplast are elevated during growth.

1.7 Plant Aquaporins

At the time of the Maurel et al. (2008) review there were 35 aquaporin homologs in the model organism *Arabidopsis thaliana* and similar numbers in other plant species. The nomenclature for plant aquaporins is different than for animals and reflects their localization in plant cells and diversity of function. There are four subgroups two of which are primarily associated with water uptake and distribution within plant tissues. Plasma membrane intrinsic proteins (PIPs) are located in the plasma membrane and tonoplast intrinsic proteins (TIPs) are located in the tonoplast (vacuolar) membrane.

Overall water balance begins with water uptake by the roots. Root tissue has an outer epidermal cell layer, a multilayered exodermis and an endodermis all of which have PIP isoforms that can facilitate water uptake and transfer to vascular (xylem) vessels that transport fluid upward to the plant tissues, see Fig. 1.12b. In herbaceous plants water taken up by the cells accumulates in the tonoplast that swells to generate turgor pressure within the cell wall. Elongation and cell growth is also mediated by fluid accumulation in the tonoplast. Water movement up the xylem bundles is mediated by capillary flow and transpiration across leaves draws xylem fluid upwards. PIPs and TIPs contribute to the transfer of xylem flow to cells within the leaf tissues and prevent wilting, see Fig. 1.12c. In this regard, PIP and TIP isoforms have been identified in guard cells that regulate stomatal opening and closing in response to K⁺ transport. It has also been suggested that the movement of carbon dioxide into photosynthetic cells of the leaf is mediated by diffusion through PIP channels. A considerable amount of research with plant cells has been conducted after dissolution of the cell wall to give a protoplast in which transport events can be more easily measured.

As with animal tissues, HgCl₂ blocks water flow through plant aquaporins in protoplasts and intact tissues. In this capacity, HgCl₂ reversibly inhibits water uptake by *Arabidopsis* roots and reduces hydraulic conductivity of leaves of sunflower and some deciduous trees. The opening of leaves in response to sunlight requires an increase in leaf hydraulic conductivity that is associated with changes in expression of PIP2 mRNA transcripts. These events can be detected within an hours' time indicating regulation occurs at the level of gene activity over a rapid time course. Drought and salt stress reduce the hydraulic conductivity of roots in most plant species. Most aquaporin transcripts in roots of *Arabidopsis* become downregulated within 24 h following salt stress. In leaves, the picture is more complex. Some PIP isoforms are downregulated while others are upregulated suggesting water is directed towards critical cell types. The plant hormone abscisic acid (ABA) can transiently stimulate hydraulic conductivity of roots in maize by enhancing the expression of PIP isoforms. A more drought resistant strain of rice that exhibits a greater production of ABA during water restriction also shows a greater expression of PIP isoforms in root tissue. It has been suggested that this response would allow the plant to obtain water that might remain in the soil when drying conditions began. *Arabidopsis* with transgenic inhibition of PIP1 and PIP2 expression have lower leaf water potentials and recover more slowly when rewatering. The role of plant aquaporins in drought

tolerance and recovery during rewatering are active areas of research. Given the projections for increased temperature and regional drought conditions caused by global climate change, it will be important to better understand these processes and possibly use transgene technology to sustain agricultural productivity.

1.8 Perspective

The discovery of aquaporins revealed an ancient family of MIPs and has provided a mechanistic understanding of water transport within cells, between tissues and between organisms and their environment. Analysis of amino acid sequences for the diversity of aquaporin isoforms suggests the variety of aquaporins is the result of gene duplication and natural selection for functional specialization in plant, animal and microbial systems. Zardoya (2005) compiled an extensive collection of amino acid sequences for 450 members of the MIP family from the National Center for Biotechnology Information (NCBI) data bases and established phylogenetic trees that suggest the earliest duplication resulted in the split between aquaporins (AQPs) and aquaglyceroproteins (GLPs). Microbes, including archaeobacteria, eubacteria and fungi, typically express a single copy of GLP while vertebrates express up to four copies. Microbes typically express a single copy of AQP in comparison with plants and vertebrates that express a wide diversity of AQPs, some of which have been described in the preceding chapter. Understanding how natural selection has addressed specific biological functions can provide insight into biomimetic applications.

References

- Agre, P.: Aquaporin water channels in kidney. *J. Am. Soc. Nephrol.* **11**, 764–777 (2000)
- Akabane, G., Ogushi, Y., Hasegawa, T., Suzuki, M., Tanaka, S.: Gene cloning and expression of an aquaporin (AQP-h3BL in the basolateral membrane of water-permeable epithelial cells in osmoregulatory organs of the tree frog. *Am. J. Physiol.* **292**, R2340–R2351 (2007)
- Benga, G., Popescu, O., Pop, V.I., Holmes, R.P.: p-(chloromercuri)benzenesulfonate binding by membrane proteins and the inhibition of water transport in human erythrocyte. *Biochemistry* **25**, 1535–1538 (1986)
- Borgnia, M., Nielsen, S., Engel, A., Agre, P.: Cellular and molecular biology of the aquaporin water channels. *Annu. Rev. Biochem.* **68**, 425–458 (1999)
- Boron, W.F., Boulpaep, E.L.: *Medical Physiology a Cellular and Molecular Approach*. Elsevier Saunders, Philadelphia (2005)
- Bowen, W.R., Yousef, H.N.S.: Effect of salts on water viscosity in narrow membrane pores. *J. Colloid Interface Sci.* **264**, 452–457 (2003)
- Brunn, F.: Beitrag zur Kenntnis der Wirkung von hypophysenextrakten auf den Wasserhaushalt des Frosches. *Zeit. f. Gesam. Exp. Med.* **25**, 120–125 (1921)
- Chevalier, J., Bourget, J., Hugon, J.S.: Membrane associated particles: distribution in frog urinary bladder epithelium at rest and after oxytocin treatment. *Cell Tissue Res.* **152**, 129–140 (1974)
- Christensen, C.U.: Correlation between net water flux, osmotic concentration of the interstitial fluid and osmotic water permeability of the isolated skin of *Bufo bufo*. *J. Comp. Physiol.* **96**, 95–100 (1975)

- De Vries, H.: Sur la permeabilite du protoplasme de betteraves rouges. Arch. Neer Sci. Exacte Naturelles **6**, 117–126 (1871)
- Dutrochet, R.J.R.: Nouvelles observations sur l'endosmos et l'exosmos, et sur la cause de ce double phenomene. Anal. Chim. Phys. **35**, 393–400 (1827)
- Ferriera, H.G., Jesus, C.H.: Salt adaptation in *Bufo bufo*. J. Physiol. **228**, 583–600 (1972)
- Forrester, J.M.: Malpighi's *De Polyypo Cordis*: an annotated translation. Med. Hist. **39**, 477–492 (1995)
- Gorin, W.B., Yancey, S.B., Cline, J., Revel, J.P., Horwitz, J.: The major intrinsic protein (MIP) of the bovine lens fiber membrane: characterization and structure based on cDNA cloning. Cell **39**, 49–59 (1984)
- Gouraud, S., Laera, A., Calamita, G., Carmosino, M., Procino, G., et al.: Functional involvement of VAMP/synaptobrevin-2 in cAMP-stimulated aquaporin 2 translocation in renal collecting duct cells. J. Cell Sci. **115**, 3667–3674 (2002)
- Guo, P., Hillyard, S.D., Fu, B.M.: A two-barrier compartment model for volume flow across amphibian skin. Am. J. Physiol. **285**, R1384–R1394 (2003)
- Hasegawa, T., Tani, H., Suzuki, M., Tanaka, S.: Regulation of water absorption in the frog skins by two vasotocin-dependent water channel aquaporins, AQP-h2 and AQP-h3. Endocrinology **144**, 4087–4096 (2003)
- Hays, R.M., Leaf, A.: Studies on the movement of water through the isolated toad bladder and its modification by vasopressin. J. Gen. Physiol. **45**, 905–919 (1962)
- Hevesy, G.V., Hofer, E., Krogh, A.: The permeability of the skin of frogs to water as determined by D₂O and H₂O. Skand. Arch. Physiol. **72**, 199–214 (1935)
- Hewson, R.: On the figure and composition of the red particles of the blood, commonly called the red globules. Philos. Tran. R. Soc. Lond. **63**, 306–324 (1773)
- Hillman, S.S., Withers, P.C., Drewes, R.C., Hillyard, S.D.: Ecological and Environmental Physiology of Amphibians. Oxford University Press, New York (2009). 469 pp
- Hillyard, S.D., Larsen, E.H.: Lymph osmolality and rehydration from NaCl solutions by toads, *Bufo marinus*. J. Comp. Physiol. B **171**, 283–292 (2001)
- Hillyard, S.D., Viborg, A., Nagai, T., Hoff, K.: Chemosensory function of salt and water transport by the amphibian skin. Comp. Biochem. Physiol. **148A**, 44–54 (2007)
- Hooke, R. (ed.): Micrographia Some Physiological Descriptions of Minute Bodies Made by Magnifying Glasses with Observations and Inquiries Thereupon. Martyn, and Allestry, London (1664)
- Ikeda, M., Andoo, A., Shimono, M., Takamatsu, N., Taki, A., Muta, K., Matsushita, W., Uechi, T., Matsuzaki, T., Kenmochi, N., Takata, K., Sasaki, S., Ito, K., Ishibashi, K.: The NPC motif of aquaporin-11, unlike the NPA motif of known aquaporins, is essential for full expression of molecular function. J. Biol. Chem **286**(5), 3342–3350 (2011)
- Ishibashi, K., Hara, S., Kondo, S.: Aquaporin water channels in mammals. Clin. Exp. Nephrol. **13**, 107–117 (2009)
- Itoh, T., Rai, T., Kuwahara, M., Ko, S.B.H., Uchida, S., Sasaki, S., Ishibashi, K.: Identification of a novel aquaporin, AQP12, expressed in pancreatic acinar cells. Biochem. Biophys. Res. Commun. **330**, 832–838 (2005)
- Jørgensen, C.B.: 200 years of amphibian water economy: from Robert Townson to the present. Biol. Rev. **72**, 153–237 (1997)
- Kachadorian, W.A., Wade, J.B., Di Scala, V.A.: Vasopressin induced structural change in toad bladder luminal membrane. Science **190**, 67–69 (1975)
- Kistler, J., Bullivant, S.: Lens gap junctions and orthogonal arrays are unrelated. FEBS Lett. **111**, 73–78 (1980)
- Kleinzeller, A.: William Hewson's studies of red blood corpuscles and the evolving concept of a cell membrane. Am. J. Physiol. **271**, C1–C8 (1996)
- Koefoed-Johnsen, V., Ussing, H.H.: The contributions of diffusion and flow to the passage of D2O through living membranes. Acta Physiol. Scand. **28**, 60–76 (1953)
- Kruse, E., Uehlein, N., Kaldenhoff, R.: Protein family review, the Aquaporins. Genome Biol. **7**, 206.1–206.6 (2006)

- Macey, R.I., Farmer, R.E.I.: Inhibition of water and solute permeability in human red cells. *Biochim. Biophys. Acta* **211**, 104–106 (1970)
- Matteucci, C., Cima, A.: Memoire sur l'endosmose. *Annal. Chim. et Phys.* **13**, 63–86 (1845)
- Maurel, C., Verdoucq, L., Luu, D.-T., Santoni, V.: Plant aquaporins: membrane channels with multiple integrated functions. *Annu. Rev. Plant Biol.* **59**, 595–624 (2008)
- Nageli, C., Kramer, C. (eds.): *Pflanzenphysiologische Untersuchungen*. 1. Heft. Schulthess, Zurich (1855)
- Nielsen, S., Kwon, T.-H., Christensen, B.M., Promeneur, D., Frokiaer, J., Marples, D.: Physiology and pathophysiology of renal aquaporins. *J. Am. Soc. Nephrol.* **10**, 647–663 (1999)
- Ogushi, Y., Akabane, G., Hasegawa, T., Mochida, H., Matsuda, M., et al.: Water adaptation strategy in anuran amphibians: molecular diversity of aquaporin. *Endocrinology* **151**, 165–173 (2010a)
- Ogushi, Y., Kitagawa, D., Hasegawa, T., Suzuki, M., Tanaka, S.: Correlation between aquaporin and water permeability in response to vasotocin, hydrin, and beta-adrenergic effectors in the pelvic skin of the tree frog, *Hyla japonica*. *J. Exp. Biol.* **213**, 288–294 (2010b)
- Parisi, M., Pisam, M., Merot, J., Chevalier, J., Bourget, J.: The role of microtubules and microfilaments in the hydrosmotic response to antidiuretic hormone. *Biochim. Biophys. Acta – Biomembr.* **817**, 333–342 (1985)
- Parisi, M., Dorr, R.A., Ozu, M., Toriano, R.: From membrane pores to aquaporins: 50 years measuring water fluxes. *J. Biol. Phys.* **33**, 331–343 (2007)
- Pfeffer, W. (ed.): *Osmotische Untersuchungen*. Studien zur Zellmechanik. Engelmann, Leipzig (1877)
- Preston, G.M., Carroll, T.P., Guggino, W.B., Agre, P.: Appearance of water channels in *Xenopus* oocytes expressing red cell CHIP28 protein. *Science* **256**, 385–387 (1992)
- Richet, G.: The osmotic pressure of urine—from Dutrochet to Koranyi, a trans-european interdisciplinary epic. *Nephrol. Dial. Transplant.* **16**, 420–424 (2001)
- Ruibal, R.: The adaptive value of bladder water in the toad *Bufo cognatus*. *Physiol. Zool.* **35**, 218–223 (1962)
- Sabolic, I., Brown, D.: Water channels in renal and non renal tissues. *News Physiol. Sci.* **10**, 12–17 (1995)
- Schmidt-Nielsen, K., Schmidt-Nielsen, B.: Water metabolism of desert mammals. *Physiol. Rev.* **32**, 135–166 (1952)
- Stetson, D.L., Lewis, S.A., Alles, W., Wade, J.B.: Evaluation by capacitance measurements of antidiuretic hormone induced membrane area changes in toad bladder. *Biochim. Biophys. Acta – Biomembr.* **689**, 267–274 (1982)
- Suzuki, M., Hasegawa, T., Ogushi, Y., Tanaka, S.: Amphibian aquaporins and adaptation to terrestrial environments: a review. *Comp. Biochem. Physiol.* **148A**, 72–81 (2007)
- van't Hoff, J.H.: Die Rolle des osmotischen Druckes in der Analogie zwischen Lösungen und Gasen. *Zeitschrift für Physikalische Chemie* **1**, 481–508 (1877)
- van't Hoff, J.H.: Osmotic pressure and chemical equilibrium. Nobel Lecture, 13 Dec (1901)
- Verkman, A.S.: Aquaporins: translating bench research to human disease. *J. Exp. Biol.* **212**, 1707–1715 (2009)
- Viborg, A., Rosenkilde, P.: Water potential receptors in the skin regulate blood perfusion in the ventral pelvic skin of toads. *Physiol. Biochem. Zool.* **77**, 39–49 (2004)
- Zardoya, R.: Phylogeny and evolution of the major intrinsic protein family. *Biol. Cell* **97**, 397–414 (2005)
- Zeidel, M.L., Nielsen, S., Smith, B.L., Ambudkar, S.V., Maunsbach, A.B., Agre, P.: Ultrastructure, pharmacologic inhibition, and transport selectivity of aquaporin channel-forming integral protein in proteoliposomes. *Biochemistry* **33**, 1606–1615 (1994)
- Zimmerman, S.L., Frisbie, J., Goldstein, D.L., West, J., Rivera, K., Krane, C.M.: Ecretion of glycerol, and expression of aquaporins and glyceroporins, during cold acclimation in Cope's gray tree frog *Hyla chrysoscelis*. *Am. J. Physiol.* **292**, R544–R555 (2007)

Chapter 2

Nature Meets Technology: Forward Osmosis Membrane Technology

Filicia Wicaksana, Anthony G. Fane, Chuyang Tang, and Rong Wang

Abstract Biomimetic membranes may find a potential application in forward osmosis due to its capability of mimicking the highly-selective transmission of water or solutes through natural cell membranes and the gentle operating conditions of the forward osmosis process. The integration of these novel technologies for desalination may significantly reduce the energy consumption when compared to the reverse osmosis desalination technique. To further understand the process, this chapter presents fundamental concepts of forward osmosis, FO membrane characteristics, draw solute properties, as well as potential applications of FO processes.

2.1 Introduction

Biomimetic membranes are based on mimicking natural membrane phenomena (Nielsen 2009). One of the phenomena is direct osmosis. This has been used in the membrane technology process commonly known as Forward Osmosis (FO). FO has recently drawn significant interest, due to its potentially lower energy requirement and lower capital cost. There is also growing interest in the use of biomimetic membranes in FO, particularly if the very effective salt exclusion properties of certain

F. Wicaksana (✉)

Singapore Membrane Technology Centre, Nanyang Technological University,
50 Nanyang Avenue, 639798, Singapore
e-mail: Filicia@ntu.edu.sg

A.G. Fane • C. Tang • R. Wang

Singapore Membrane Technology Centre, Nanyang Technological University,
50 Nanyang Avenue, 639798, Singapore

School of Civil and Environmental Engineering, Nanyang Technological University,
50 Nanyang Avenue, 639798, Singapore
e-mail: agfane@ntu.edu.sg; CYTang@ntu.edu.sg; RWang@ntu.edu.sg

biomimetic materials can be achieved. Another attraction of FO in the use of biomimetic membranes is the benign low pressure environment of FO. This would avoid the need for highly robust biomimetic membrane structures as would be required for high pressure reverse osmosis (RO). In relation to these matters, this chapter provides a review of the fundamental concepts of FO membrane characteristics, draw solute properties, as well as potential applications of FO processes.

2.2 Osmotic Processes: Basic Principles and Classification

FO utilizes a semi permeable dense membrane that separates two aqueous solutions (known as feed and draw solutions) with different osmotic pressures or different chemical potentials. The osmotic pressure difference acts as the driving force that causes the movement of water through the dense membrane from a region of low solute concentration (feed stream) to a region of high solute concentration (draw solution stream). FO is a physical phenomenon that occurs without applied pressure (non-pressure driven process). Conversely, RO is an energy intensive process that requires substantial hydraulic pressure in excess of the osmotic pressure of saline water to force the water through a dense semi-permeable membrane. However, if FO is intended for fresh water production there will be an energy demand to remove this water from the draw solution.

Pressure Retarded Osmosis (PRO) possesses characteristics intermediate between FO and RO, where water from a low salinity feed solution diffuses through a membrane into a pressurized high salinity draw solution. In order for water transport to occur, the osmotic pressure difference between the feed and draw solutions should exceed the hydrostatic pressure of the draw solution side. A proposed application of PRO is for power generation (Achilli 2009a; Loeb 1998, 2002) which can be achieved by de-pressurizing the diluted seawater through a hydro-turbine or generator set. The principles of FO, PRO and RO are shown in Fig. 2.1.

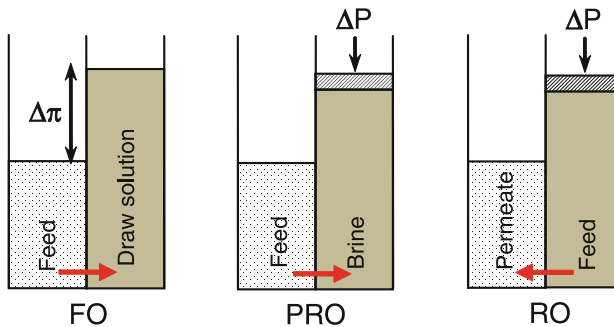


Fig. 2.1 Principles of FO, PRO and RO processes (Adapted from Cath et al. 2006). In FO the water transport (red horizontal arrow) through a semipermeable membrane separating two compartments is driven by the osmotic pressure gradient $\Delta\pi$ between the feed and the draw solution. In PRO the process is similar but retarded by an exerted pressure ΔP . In RO the exerted pressure is used to drive the water transport from the concentrated feed to a diluted permeate

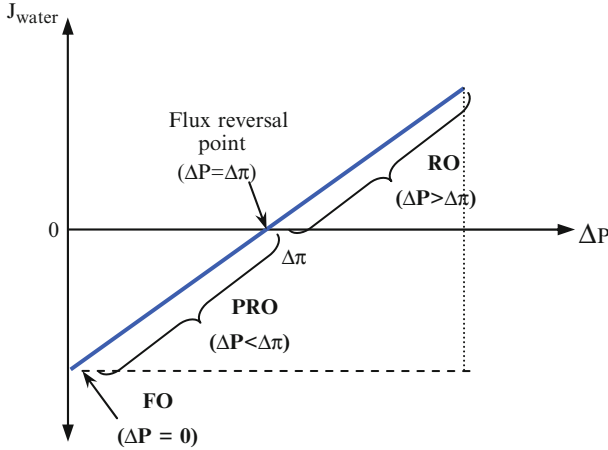


Fig. 2.2 The relationship between water flux and applied pressure in FO, RO and PRO (Adapted from Lee et al. 1981)

The transport of water in FO, PRO and RO can be described using the general equation:

$$J_w = A(\sigma\Delta\pi - \Delta P) \quad (2.1)$$

where J_w is the water flux, A is the water permeability coefficient of the membrane, σ is the reflection coefficient, $\Delta\pi$ is the osmotic pressure difference across the membrane and ΔP is the applied pressure. For non-permeating solutes, the reflection coefficient approaches unity. ΔP is zero for FO processes, while for PRO, ΔP is smaller than $\Delta\pi$. In contrast, the applied pressure is greater than $\Delta\pi$ for RO. The relationship between water flux and applied pressure in FO, PRO and RO processes is illustrated in Fig. 2.2.

2.3 Basic Properties of Draw Solutions for FO

The driving force in FO process is generated by passing a concentrated solution across the permeate side of the membrane. This concentrated solution is commonly known as the draw solution (Choi et al. 2009; McCutcheon et al. 2006b; Cornelissen et al. 2008; Garcia-Costello et al. 2009; Xu et al. 2010; Hancock 2009; McCutcheon et al. 2005), although different terms can be found in the literatures such as osmotic agent (Babu et al. 2006; Miller 2006; Nayak 2010; Lampi et al. 2005), osmotic media (Petrotos et al. 2010), working substance (Khaydarov 2007), extracting agent (Glew 1965) or driving solution (Kessler 1976; Moody 1976). The selection of appropriate draw solution plays an important role in the efficiency and performance of the process.

Since forward osmosis is an osmotically-driven process, an ideal draw solute used for FO must have a higher osmotic pressure than the feed solution, exhibit minimum

reverse transport from the draw solution side to the feed side, be easily separated and re-used upon water extraction or be readily available if regeneration is not required. Further to these characteristics, a desirable draw solute should be non-toxic, highly soluble, of neutral pH, inert and causing a minimum chemical or physical impact on the membrane, have a low molecular weight, be relatively low cost, and stable.

The osmotic pressure of a solution can be defined as the amount of pressure that has to be applied to the solution to prevent water from entering the solution through an ideal semi-permeable membrane. More concentrated solutions will produce greater osmotic pressures. The osmotic pressure of a solution depends upon the total number of ions or molecules in the solution. For an ideal solution, the osmotic pressure is proportional to the concentration of the solute:

$$\pi = iRTC_s \quad (2.2)$$

where i is the number of ions in the solution, R is the universal gas constant, T is the absolute temperature in K, and C_s is the solute concentration. Equation 2.2 is known as van't Hoff equation. The van't Hoff equation applies only to dilute solutions. For concentrated solutions, a virial equation (with second order terms) can be used or the van't Hoff equation has to be corrected by applying an osmotic coefficient (Φ):

$$\pi = \Phi iRTC_s \quad (2.3)$$

In general, highly soluble draw solutes with low molecular weight can produce higher osmotic pressure compared to draw solutes with low solubility and high molecular weight.

2.4 Types of Draw Solutions

There are several types of solution that have been tested for use as draw solutions in FO applications. The draw solutes can be categorized as follows:

- inorganic salts;
- organic microsolutives;
- organic macrosolutives;
- dissolved gases;
- magnetic particles

The reported literature for each category is presented below, along with comments on the potential and prospects for these draw solutes.

2.4.1 Inorganic Salts

Various inorganic salts have been assessed as draw solutes with sodium chloride being the most commonly used draw solute (Xu et al. 2010; Choi et al. 2009;

Martinetti et al. 2009; Mi 2008, 2010; McCutcheon 2008; Adham et al. 2007) due to its low cost, high solubility and it can be re-concentrated for reuse with RO with no scaling risk (Cath et al. 2006). However, the application of reverse osmosis process for the separation of product water could contribute to an increase in energy consumption and operating cost. Moreover, a FO membrane with high salt rejection is needed if sodium chloride is to be used as a draw solute. Otherwise, divalent or multivalent salts such as $MgCl_2$ would be more favorable than monovalent salts if minimum back-diffusion is required (Yang et al. 2009a).

2.4.2 *Organic Microsolutes*

A natural material such as cane sugar has been used as draw solute due to its high solubility in water and high osmotic pressure (Yaeli 1992). Other low molecular weight sugars such as glucose solution (Kravath 1975), concentrated fructose solution (Stache 1989) and a mixed solution containing glucose and fructose (Kessler 1976) were used to produce a nutritious drink from seawater or contaminated water. The advantage of using sugars is that additional process for clean water recovery is unnecessary as the product water can be consumed without further treatment. The product water is suitable for use as emergency potable water supply for military applications, in circumstances where storage capacity is limited (e.g., lifeboats) or in locations with severe water shortage.

2.4.3 *Organic Macrosolutes*

Different types of organic macrosolute have been reported and explored for their potential as the draw solution such as bovine serum albumin (BSA) and dendrimers.

Albumin is a protein that can control the osmotic pressure stability within the blood vessels. Based on this ability, its suitability was tested as a draw solution for dewatering RO concentrate (Adham et al. 2007). Unfortunately, the findings indicated that the highest osmotic pressure generated by albumin (approximately 66,000 g/mol molecular weight) was only 48 kPa (or 0.48 bar) for 30% (w/w) BSA solution which was obviously too low for the intended application.

In contrast to albumin, dendrimers can produce high osmotic pressure (up to 2.28 MPa (or 22.8 bar) with 20% w/w G2-pentaerythryl) (Adham et al. 2007). Dendrimers are polymeric materials, monodisperse macromolecules with highly branched spheroid or globular nanostructures connected to a central core through covalent bonds. These substances are formed through a series of replicating chemical synthesis processes that develop from the molecular level to the nanoscale region. Upon water extraction in a FO process, dendrimer compounds can be recovered by a simple ultrafiltration technique (Adham et al. 2007; Klajnert 2001).

2.4.4 Dissolved Gases

A mixture of sulphur dioxide in water was suggested as draw solution in FO (Batchelder 1965; Glew 1965; McGinnis 2002). Upon reaching a desired level of water extraction, sulphur dioxide could either be removed by a heated gas stripping operation (Batchelder 1965) or be recycled by using distillation and condensation (Glew 1965). A more recent innovative draw solution for desalination application comprised thermally removable ammonium salts that were formed by combining a certain ratio of highly soluble ammonia and carbon dioxide gasses in water (McCutcheon et al. 2005; 2006b; McGinnis 2009). The draw solution could generate an osmotic pressure difference of up to 250 atm (McCutcheon et al. 2005). The product water was obtained by thermal decomposition of ammonium bicarbonate to ammonia and carbon dioxide under moderate heating (approximately 60°C at atmospheric pressure). The gases could subsequently be separated from the solution by low-temperature distillation.

2.4.5 Magnetic Particles

Magnetic nanoparticles have been tested as draw agents (Adham et al. 2007; Ling et al. 2010). Magnetoferritin nanoparticles are naturally non-toxic; and can be recovered from the solution by means of a magnetic field (Jones 2005; Lubik 2009). Recent work has developed various sizes of surface functionalized magnetic nanoparticles that were hydrophilic and highly soluble (Ling et al. 2010). It was suggested that the surface hydrophilicity and the size of magnetic nanoparticles played crucial role in the potential use of these nanoparticles as draw solutes in FO process.

2.5 Internal Concentration Polarization

By referring to Eq. 2.1, the water flux in FO can be primarily determined by the osmotic pressure gradient across the membrane ($\Delta\pi$) and water permeability coefficient of the membrane (A). However, the permeate water fluxes are typically lower than the anticipated value. It is recognized that the effective osmotic pressure difference across the selectively permeable membrane ($\Delta\pi_{\text{eff}}$) is substantially lower than the osmotic pressure gradient between the bulk feed and draw solutions ($\Delta\pi_{\text{bulk}}$). The decrease in effective osmotic pressure difference is reportedly related to concentration polarization (CP) phenomena and this contributes to the reduction of water flux (Ng et al. 2006; Cath et al. 2006; McCutcheon et al. 2006b; Loeb et al. 1997; Mehta 1978; Lee 1981; McCutcheon 2008). It is evident that membrane structure and orientation could be accountable for the low water flux (Cath et al. 2006; Ng et al. 2006).

When water permeates through a dense RO membrane, the retained salts and other constituents accumulate adjacent to the membrane surface creating a concentration

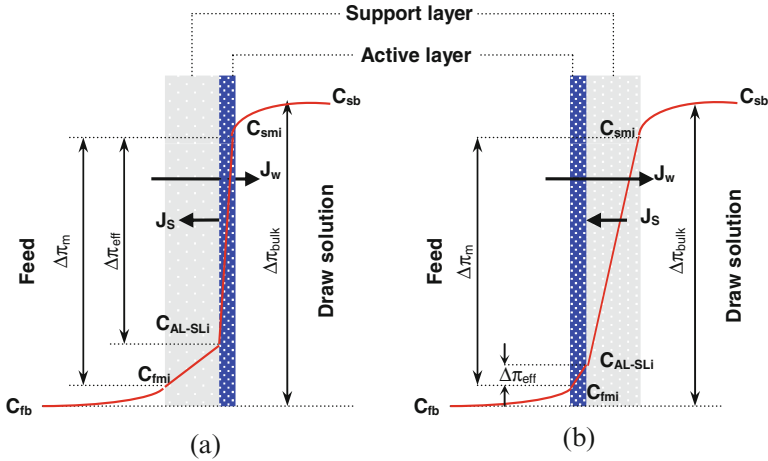


Fig. 2.3 Concentration polarization profiles across a composite FO membrane (a) concentrative ICP (b) dilutive ICP (Adapted from Cath et al. 2006) (C_{fm} is the concentration of the bulk feed solution, C_{fmi} is the concentration of the feed-membrane interface, C_{AL-SLI} is the concentration at the active layer-support layer interface, C_{smi} is the concentration of the draw solution-membrane interface, C_{sb} is the concentration of the bulk draw solution)

gradient on the feed side of the membrane. This phenomenon is known as concentration polarization (CP) that reduces the effective driving force as surface concentration increases and thereby increases $\Delta\pi$. In this case flux drops or required ΔP increases. CP can also promote scale formation and other types of membrane fouling. Similar concentration polarisation phenomena occur in osmotically driven membrane processes such as FO. However, since mass transfer occurs on both sides of FO membrane, CP will take place on both feed and draw solution sides of the membrane. In FO, water diffuses from the feed stream to the draw solution stream causing solutes to accumulate at the feed-side of the membrane, while diluting the permeate-membrane boundary layer on the draw solution side. Cath and co-workers identified these phenomena as concentrative external CP for the feed side and dilutive CP for the draw solution side (Cath et al. 2006). These polarization effects will diminish the effective osmotic pressure difference.

FO membranes are commonly composite or asymmetric membranes comprising a dense active layer and a porous support layer, hence CP phenomena would become more complex since CP can occur within the porous support layer of the membrane. We will refer to this as internal concentration polarization (ICP). While the extent of external CP can be alleviated by hydrodynamics means, it is not possible to employ a similar approach to mitigate internal CP. One option to minimize ICP is to produce a membrane with a thin support layer. This will be discussed in more detail in Sect. 2.6.

Figure 2.3 illustrates the ICP profiles across a FO composite or asymmetric membrane. The orientation with an active layer facing the draw solution (Fig. 2.3a) is denoted as the PRO mode in some publications (McCutcheon 2006a; Cath et al. 2006)

because the porous support layer of the membrane had to withstand the osmotic pressure of the permeate stream despite the fact that no hydraulic pressure is applied. In order to avoid misinterpretation with an actual pressure retarded osmosis process, this membrane orientation will be referred as AL-DS (denoting active layer in contact with draw solution) throughout this chapter. In this orientation, water and solutes can penetrate through the porous support layer causing the concentration polarization to occur within the porous layer (concentrative ICP). Similar to AL-DS orientation, ICP also occurs in the alternative membrane orientation AL-FW (referring to active layer facing the feed solution). In AL-FW, however, the permeate water will dilute the draw solution inside the porous layer (referred to as dilutive ICP) (Fig. 2.3b). It is noticeable from the figure that the osmotic pressure difference decreases from $\Delta\pi_{\text{bulk}}$ (the osmotic pressure difference between the bulk feed and bulk draw solution) to $\Delta\pi_{\text{m}}$ (the osmotic pressure difference across the membrane) due to external concentration polarization, and subsequently to $\Delta\pi_{\text{eff}}$ (the effective osmotic pressure gradient) due to internal concentration polarization.

2.5.1 Theoretical Basis

Loeb et al. (1997) derived the relationship between water flux and osmotic pressure driving force during FO operation based on a simple equation that was previously developed by Lee et al. (1981):

$$J_w = K_m \ln \left(\frac{\pi_{\text{draw}}}{\pi_{\text{feed}}} \right) \quad (2.4)$$

where K_m [$\text{L m}^{-2} \text{h}^{-1}$ or m s^{-1}] is the apparent mass transfer coefficient; π_{draw} and π_{feed} are the osmotic pressures [Pa] of the bulk draw solution and bulk feed solution, respectively, without considering the external concentration polarization effects.

In reality, however, the water flux was found to be different from the values estimated by Eq. 2.4 due to ICP effects. Hence, the equation was further modified to become (Lee et al. 1981; Loeb et al. 1997; Tang et al. 2010):

$$J_w = K_m \ln \left(\frac{A\pi_{\text{draw}} - J_w + B}{A\pi_{\text{feed}} + B} \right) \quad (2.5)$$

for concentrative ICP and for dilutive ICP:

$$J_w = K_m \ln \left(\frac{A\pi_{\text{draw}} + B}{A\pi_{\text{feed}} + J_w + B} \right) \quad (2.6)$$

where J_w [$\text{L m}^{-2} \text{h}^{-1}$ or m s^{-1}] is the water flux, and A [$\text{L m}^{-2} \text{h}^{-1} \text{Pa}^{-1}$ or $\text{m s}^{-1} \text{Pa}^{-1}$] and B [$\text{L m}^{-2} \text{h}^{-1}$ or m s^{-1}] are the water and solute permeability coefficients, respectively.

The mass transfer coefficient inside the support layer K_m can be expressed as the ration of the effective diffusion coefficient to the effective diffusion path length:

$$K_m = \frac{\varepsilon D_s}{t_h \tau} = \frac{D_s}{S} \quad (2.7)$$

where t_h [m] is the thickness of the membrane support layer, τ is the tortuosity (defined as the ratio between the length of the average pore and the material thickness) of the membrane porous support layer, ε is the porosity (defined as the total volume of the pores divided by the total volume of the material) of the porous support layer, D_s [$\text{m}^2 \text{s}^{-1}$] is the diffusion coefficient of the solute, and S [m] is the membrane structural parameter (Wang et al. 2010b; Tang et al. 2010). A larger value of K_m minimizes ICP. Hence the FO water flux can be improved by reducing the thickness of the membrane support layer (t_h) and by increasing the porosity of the support.

The solute permeability coefficient (B) can be determined based on the classical solution-diffusion theory (Lee et al. 1981):

$$B = \frac{(1 - R_s)A(\Delta P - \Delta \pi)}{R_s} \quad (2.8)$$

where R_s is the solute (salt) rejection.

Based on van't Hoff equation, the solute flux can be expressed as (Tang et al. 2010):

$$J_s = \frac{B}{A \cdot \beta RT} J_w \quad (2.9)$$

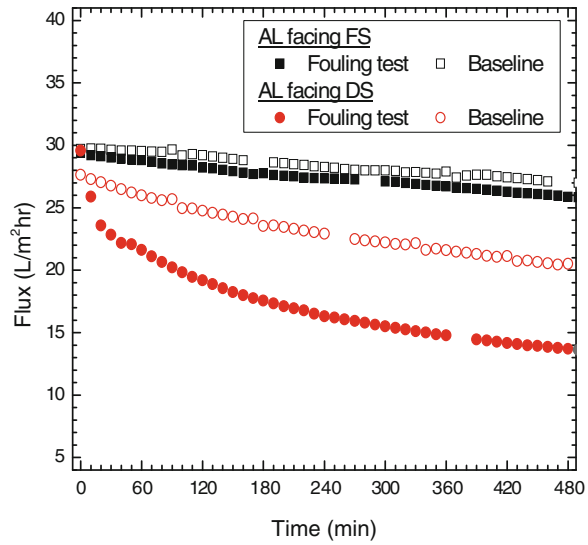
where $\beta = \Phi \cdot i$ is the van't Hoff coefficient (see Eq. 2.3), R is the universal gas constant, and T is the absolute temperature.

2.5.2 The Effect of Membrane Orientation

As described in Fig. 2.3 different membrane orientations have resulted in different water transport mechanisms and the corresponding ICP. In order to confirm this, the influence of membrane orientation on FO performance had been observed in prior studies (McCutcheon 2006a; Tang et al. 2010; Mi 2008; Wang et al. 2010c) by positioning the membrane in two different configurations: (1) with the rejection surface of the membrane facing the feed solution and the support layer facing the draw solution (AL-FW) and (2) the membrane was placed in reverse orientation as in (1) with its active surface against the draw solution (AL-DS).

Without the presence of foulants (baseline test), the membrane orientation with the active layer facing the feed solution exhibited a more stable water flux, while flux decline was more pronounced when the membrane was placed in the opposite configuration (AL-DS) (Tang et al. 2010). The flux in AL-FW orientation remained stable with the addition of foulants, see Fig. 2.4. This complements the postulation

Fig. 2.4 The influence of membrane orientation on FO membrane fouling (Tang et al. 2010)



proposed by prior studies which stated that osmotically driven membrane processes demonstrated lower fouling tendency than pressure driven membrane processes (Holloway et al. 2007; Achilli et al. 2009b). These authors believed that the lack of hydraulic pressure and smoother FO membrane would contribute to low fouling propensity. However, the absence of hydraulic pressure may not be the only factor that contributed to the low fouling propensity in FO since significant flux reduction occurred with AL-DS. ICP related effects were assumed to be accountable for causing this phenomenon (Tang et al. 2010).

2.6 FO Membrane Technology

High performance FO membranes are needed to make the FO technology technically and economically feasible. Historically, due to the lack of commercial FO membranes, the majority of studies on osmotically driven membrane processes used membranes that were initially tailored for RO processes (Cath et al. 2006; Choi et al. 2009; Cornelissen et al. 2008; Dova et al. 2007a; Garcia-Costello et al. 2009; McCutcheon et al. 2005). Typical RO membranes exhibit an asymmetric structure, comprising a thin selective layer supported by thick multiple layers of porous polymer and fabric to withstand high hydraulic pressures. The performance of these membranes in FO mode, however, has been found to be unsatisfactory, mainly due to severe internal CP in their thick support layer (Mehta 1978; Loeb et al. 1997). The thick support layer of RO membranes performs as a diffusive boundary layer that drastically reduces the osmotic pressure gradient across the active layer

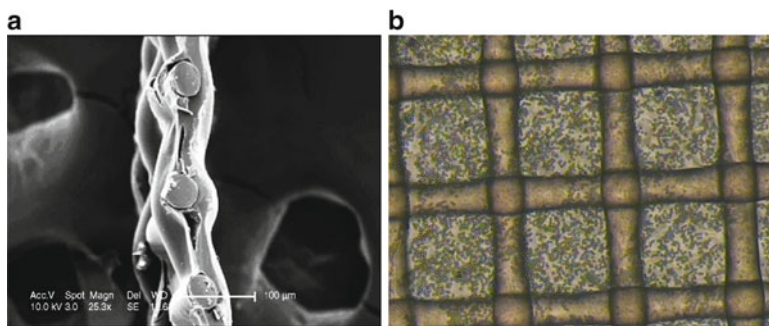


Fig. 2.5 (a) SEM image of FO membrane cross-section (Hydration Technologies Inc.) (McCutcheon et al. 2006b). (b) Particle deposition on HTI membrane (10 mM NaCl as feed solution, 3M NaCl as draw solution, AL-DS orientation, 0.09 m s^{-1} cross-flow velocity) (Wang et al. 2010c)

(Yip et al. 2010). Thus there are different criteria for membranes used in RO and FO processes. Since the FO process does not require high hydraulic pressure, a thick support layer is not necessary for FO membranes.

At present, the only commercially available FO membranes are the cellulose triacetate membranes manufactured by Hydration Technologies Inc (HTI) (Herron 2008). Being thinner and significantly smoother than typical RO membranes, the HTI proprietary membranes (see Fig. 2.5a) can achieve better FO permeate flux compared to RO membranes. However, like other membranes, the FO membrane also experiences flux decline as well as membrane fouling (Mi 2010; Cornelissen et al. 2008; Tang et al. 2010; Mi 2008; McCutcheon 2006a; Wang et al. 2010c). The decline in flux is due to the occurrence of external and internal concentration polarization during the mass transfer process, which results in the reduction of the osmotic pressure difference. Since ICP phenomena are mainly correlated to the membrane structure, an ideal FO membrane should be an ultra-thin semi-permeable membrane exclusive of a porous substrate or support to alleviate the impact of ICP. However, adequate mechanical strength is required for the FO membrane to withstand various operating conditions. Therefore, in order to facilitate the use of FO membranes in real applications, FO membranes should be supplemented with a support that can either be introduced into the thin film or fabricated underneath the thin film as a porous and very thin support layer.

Direct microscopic observation studies of FO membrane fouling indicated that particle deposition occurred even at an early stage of the FO process (20 min) with a 2M draw solution (NaCl). The membrane was almost fully covered by particles when 3M NaCl was used as draw solution (see Fig. 2.5b). Hence, other essential properties of FO membranes include being sufficiently hydrophilic to prevent irreversible fouling and having high water flux and negligible reverse flux of draw solute to the feed solution side.

Table 2.1 Various membrane materials for FO applications

Material	Membrane type	Properties	Ref.
Cellulose acetate	Double skinned flat sheet FO membranes	Highly hydrophilic, limited pH stability (4–6.5)	(Wang 2010a)
Cellulose triacetate (CTA)	Flat sheet FO membranes	More heat resistant than cellulose acetate	(Herron 2008)
Polybenzimidazole (PBI)	Hollow fibre NF membrane	Highly hydrophilic, exceptional thermal and chemical stability, very brittle	(Wang et al. 2007)
Polybenzimidazole-polyethersulfone/polyvinylpyrrolidone (PBI-PES/PVP)	Dual layer hollow fibre NF membrane	PES has good mechanical properties, high tendency to form porous and open cell structures, was blended with PVP to alter its hydrophobicity.	(Yang et al. 2009b, 2010)
Polyamide-PES substrate	Hollow fibre FO membrane	Polyamide is hydrophilic, has exceptional mechanical, chemical, and thermal resistant	(Wang et al. 2010b; Chou et al. 2010)
Polyamide-Polysulfone support	Flat sheet FO membrane	Polysulfone has high degree of chemical and thermal stability, wide pH tolerance	(Yip et al. 2010)

2.6.1 Materials for FO Membranes

Table 2.1 summarizes materials that have been used to fabricate membranes for FO applications. In general, most of these materials exhibit desirable properties for FO application such as hydrophilicity, good mechanical properties, and, in some cases, good thermal and chemical stability. Cellulose acetate was the first material used for commercial RO membranes (Carter et al. 1973; Michaels et al. 1965). This material is very hydrophilic. However, its stability is limited to a pH range of 4–6.5 and it is prone to microbial attack (Ren 2011; Baker 2004). Polybenzimidazole (PBI) is highly hydrophilic, thermally and chemically stable. However, this material is very brittle. Therefore, it should be combined with other materials that could enhance the mechanical strength of the membrane.

2.6.2 FO Membrane Structures

Considerable efforts have been made to fabricate second generation FO (flat sheet and hollow fibre) membranes with improved properties that could minimize the ICP and fouling (Chou et al. 2010; Shi et al. 2011; Wang et al. 2010a, b; Yip et al. 2010; Yang et al. 2009a, b).

- Hollow Fibres

Mono and dual layer polybenzimidazole (PBI) nanofiltration hollow fibre membranes have been studied as FO membranes (Wang et al. 2007; Yang et al. 2009a, b; Wang et al. 2009). However the draw solutions applicable for use with these newly developed membranes were restricted to multivalent salts and large biomolecules, because the nanofiltration membranes had inadequate rejection towards monovalent salts. A high degree of cross-linking was able to greatly improve the salt rejection. Unfortunately, the improved salt rejection due to reduction of pore sizes came at the price of low water flux (approximately 50% less than the original membrane after 9 h of cross-linking) (Wang et al. 2009).

A relatively low cost cellulose acetate nanofiltration hollow fibre membrane has also been fabricated and examined for FO applications (Su et al. 2010). Two stages of heat treatment were then employed to minimise the pore size of the fabricated membrane. The membrane demonstrated high salt rejection (>90% towards NaCl and MgCl₂) but low pure water permeability. Future improvement is therefore needed as the membrane also encountered severe concentrative ICP.

Most recently, a study by Wang et al. has successfully fabricated thin film composite (TFC) FO hollow fibre membranes with satisfactory intrinsic separation properties, adequate mechanical strength, high water flux and low salt passage through the membrane (Wang et al. 2010b). The membranes consisted of a porous PES hollow fibre substrate with an ultra-thin polyamide-based RO-like skin layer formed on either the outer surface (identified as #A-FO) or inner surface (#B-FO) of the hollow fibre. A practically high water flux of 32.2 L m⁻² h⁻¹ could be obtained with NaCl as the draw solution and #B-FO membrane in the AL-DS configuration at 23°C. Using only a low draw solution concentration (0.5 M), the achieved water flux level was comparable to other commercial and newly fabricated FO membranes available in the literature. The #A-FO had a thick sponge-like layer underneath the RO-like skin layer. The authors indicated that the sponge-like layer played an important role in the increase of the *S* value due to its small porosity and large tortuosity, therefore this layer should be very thin to avoid the effect of ICP. Based on these considerations, an improved version of the membrane was fabricated that comprised a polyamide-based RO-like selective skin layer, a very thin section of sponge-like layer and a finger-like layer (Chou et al. 2010). The formation of a membrane support with a thin layer of a sponge-like morphology on top of a finger-like layer is essential for fabricating a robust TFC-FO membrane (Yip et al. 2010). The sponge-like layer permits the formation of an integral active layer, while the finger-like layer contributes to greater porosity that could reduce the resistance to mass transfer thereby alleviating the ICP. It was reported that this version of the membrane could achieve a higher water flux (up to 42.6 LMH with 0.5 M NaCl as the draw solution and DI water as the feed) and a high salt rejection (~95% with 8.6 mM NaCl solution as feed).

- Flat-Sheets

Yip et al. (2010) developed a TFC FO flat sheet membrane consisting of (1) a polyamide selective layer produced by interfacial polymerization, (2) a polysulfone support layer formed by phase separation and (3) a thin polyester (PET)

non-woven fabric as a backing layer. Apart from the PET fabric layer, the membrane demonstrated similar morphological structure to the TFC hollow fibre FO membrane of Chou et al. (2010).

A double-skinned cellulose acetate flat sheet FO membrane was developed by Wang et al. through phase inversion and thermal annealing (Wang et al. 2010a). The membrane consisted of two selective layers that have different thicknesses with a porous support layer in between the selective layers. The selective layers might restrict the penetration of draw solutes into the membrane support layer depending on the size of the solutes and the pore size of the skin layers. However, it appeared that the salt rejection towards monovalent salt (NaCl) was low (~58%). Despite lower ICP, the presence of a second skin layer may provide an additional resistance to water transport across the membrane that would result in a lower water flux.

2.6.3 FO Membrane Modules

HTI commercial membranes are available in different types: cartridge membranes (Lampi et al. 2005) and pouch membranes (Hydration Technology, Inc. 2011). Compared to flat sheet membranes, the use of hollow fibre membranes for osmotically driven processes in prior studies has so far been rather limited (Mehta 1979). Having high packing density and being self-supported, hollow fibre membranes could be more suitable for FO processes than flat sheet membranes. The membranes can be simply arranged in a bundle to provide larger filtration area and liquids can move freely on both sides of the membrane. Furthermore, ICP can be alleviated as a thick support layer is no longer needed. Although hollow fibre FO membranes are not commercially available at the moment, recent development indicates an increasing trend of preparing hollow fibre membranes for FO processes (Yang et al. 2010; Wang et al. 2007, 2009, 2010b; Su et al. 2010), as discussed below.

2.6.4 FO Membrane Performance

The membrane transport parameter such as water permeability coefficient (A) can be determined by testing the membrane in a pressurised cross-flow filtration setup (RO mode). The A value can be obtained by measuring pure water flux within a certain range of applied pressure, while the solute permeability coefficient (B) can be estimated by using solute rejection data and solution-diffusion theory (Wang et al. 2010b; Tang et al. 2010).

The relationship between the membrane structural parameter (S) and transport properties in thin-film composite hollow fibre FO membrane was developed by Chou et al. (2010) and was derived from the water flux equation (Loeb et al. 1997; Lee et al. 1981; Tang et al. 2010) (Eqs. 2.5 and 2.6).

For highly concentrated feed and draw solutions, Eqs. 2.5 and 2.6 become:

$$J_w = k_m \ln \left(\frac{\pi_{\text{draw}}}{\pi_{\text{feed}}} \right) \quad (2.10)$$

It can be seen that Eq. 2.10 is identical to an initial equation developed by Loeb et al. (1997) (Eq. 2.4); which suggests that the water flux is independent of membrane orientation for highly concentrated feed and draw solutions. At higher feed concentration, the water flux for both membrane orientations (the membrane active layer facing the draw solution and the membrane active layer facing the feed water) approached identical values. Thus, under these conditions, the water flux is governed by the membrane structural parameter (S), the osmotic pressure of the feed as well as the osmotic pressure of the draw solution.

A typical resistance model can be applied by considering resistances of the RO-like skin layer and the substrate to water flux:

$$J_w = \frac{\pi_{\text{draw}} - \pi_{\text{feed}}}{\eta R_m} \quad (2.11)$$

where η is the viscosity of water, while R_m is the total resistance of the FO membrane that consists of the resistance of RO-like skin layer (R_{skin}) and the resistance of the porous substrate ($R_{\text{substrate}}$) by taking into account the contribution from ICP effect. R_{skin} is the intrinsic properties of the thin-film and can be expressed as:

$$R_{\text{skin}} = \frac{\Delta\pi_{\text{skin}}}{J_w \eta} = \frac{1}{\eta A} \quad (2.12)$$

where $\Delta\pi_{\text{skin}}$ is the osmotic pressure difference across the membrane.

$R_{\text{substrate}}$ is governed by the physical or geometrical properties of the substrate as well as the applied conditions, which includes the effect of ICP. By substituting Eq. 2.12 into Eq. 2.11, and comparing with Eq. 2.10, then for AL-DS membrane orientation, the $R_{\text{skin}}/R_{\text{substrate}}$ ratio can be written as:

$$\frac{R_{\text{skin}}}{R_{\text{substrate}}} = \frac{(\pi_{\text{draw}} - \pi_{\text{feed}} e^{\frac{J_w}{K_m}}) - \frac{B}{A} (e^{\frac{J_w}{K_m}} - 1)}{(\pi_{\text{feed}} + \frac{B}{A}) (e^{\frac{J_w}{K_m}} - 1)} \quad (2.13)$$

If the feed is DI water, $\pi_{\text{feed}}=0$, Eq. 2.13 reduces to:

$$\frac{R_{\text{skin}}}{R_{\text{substrate}}} = \frac{\pi_{\text{draw}}}{\frac{B}{A} (e^{\frac{J_w}{K_m}} - 1)} - 1 \quad (2.14)$$

It was reported that the $R_{\text{skin}}/R_{\text{substrate}}$ ratio was lower for concentrated feed and draw solutions, while the ratio increased when diluted feed and draw solutions

were used (Chou et al. 2010). A low $R_{skin}/R_{substrate}$ ratio indicated that the resistance of the RO-like skin layer was negligible compared to the resistance of the substrate due to more prominent ICP, therefore, when high feed and draw solution concentrations were used such as in food processing and desalination, the mass transfer through the substrate was the dominant step. Under this condition, a lower S value would be more crucial to the system performance compared to the A value.

A high $R_{skin}/R_{substrate}$ ratio suggests that the resistance of the substrate was significantly less compared to the resistance of the RO-like skin layer; hence, the process was governed by the water permeation through the RO-like skin layer. Furthermore, the water flux was closer to the ideal linear curve at low concentrations of feed and draw solutions, which indicated that ICP was not an important factor. In this case, a high A value of the FO membrane would become more important than the S value. For operating conditions between the above-mentioned cases such as in wastewater treatment processes, attention should be paid to both A and S values as both parameters could be equally important to the process performance (Chou et al. 2010).

2.7 Applications of FO

Although commercialisation of FO is still limited at the moment, FO processes have a number of potential applications. Several examples of FO applications are briefly discussed below:

2.7.1 Desalination

FO technology has been widely studied for desalination of brackish and seawater as a possible replacement for the reverse osmosis process (Cath 2010; Choi et al. 2009; Elimelech 2007; Khaydarov 2007; Kravath 1975; McCutcheon et al. 2006b; McGinnis 2007; Miller 2006; Tang 2008). The minimum work to separate water from saline water is defined by thermodynamics. One attraction of FO is that it may be able to achieve desalination at closer to this minimum work than by RO. Besides possible lower energy consumption, FO may have several other potential benefits. Since FO requires very low or no hydraulic pressure for its operation, it has been suggested that its fouling tendency could be lower compared to pressure-driven membrane processes (Holloway et al. 2007; Achilli et al. 2009b). However, this remains to be proven conclusively. Furthermore, the low pressure operation means that costly pressure vessels and high pressure piping can be avoided.

2.7.2 Wastewater Treatment and Reclamation

Various FO applications in wastewater treatment have been reported, such as for water reclamation in space (Cath et al. 2005), for recycling dye wastewater (Catalyx, Inc. 2009), concentration of anaerobic digestate (Holloway et al. 2007), and concentration of RO brine (Martinetti et al. 2009).

2.7.3 Food Processing

FO has been used for concentration of various fruit juices (Wrolstad et al. 1993; Petrotos et al. 1998, 1999, 2010; Babu et al. 2006), natural food additives (Nayak 2010), and liquid foods (Dova 2007a, b). The mild operating conditions of forward osmosis process such as low pressure and low temperature are advantageous for food processing since its natural taste, aroma, and nutritional values can be maintained. A more recent application of FO is for algae harvesting (Trent et al. 2010).

2.7.4 Pharmaceutical Products

Similar to food processing, the forward osmosis technique is beneficial for concentration of pharmaceutical products (Yang et al. 2009b) as the denaturation of active components can be avoided. The concept of FO can also be used as an osmotic pump to control drug delivery mechanisms (Wright et al. 2003).

2.7.5 Power Generation

Another application of the direct osmosis concept includes the use of pressure retarded osmosis (PRO) for power generation (Gerstandt et al. 2008; Achilli et al. 2009a; Lee et al. 1981; Loeb 1998, 2002) as an alternative emission-free energy source. PRO provides a means to recover energy from differences in chemical potential, by mixing fresh and salty water across a FO membrane.

2.7.6 Hybrid Processes

In addition to the above applications, forward osmosis can be combined with other processes to further enhance the system performance, such as the integration of FO and the activated sludge bioreactor process (Achilli et al. 2009b; Cornelissen et al. 2008) that is known as the forward osmosis membrane bioreactor (FOMBR) (Fig. 2.6).

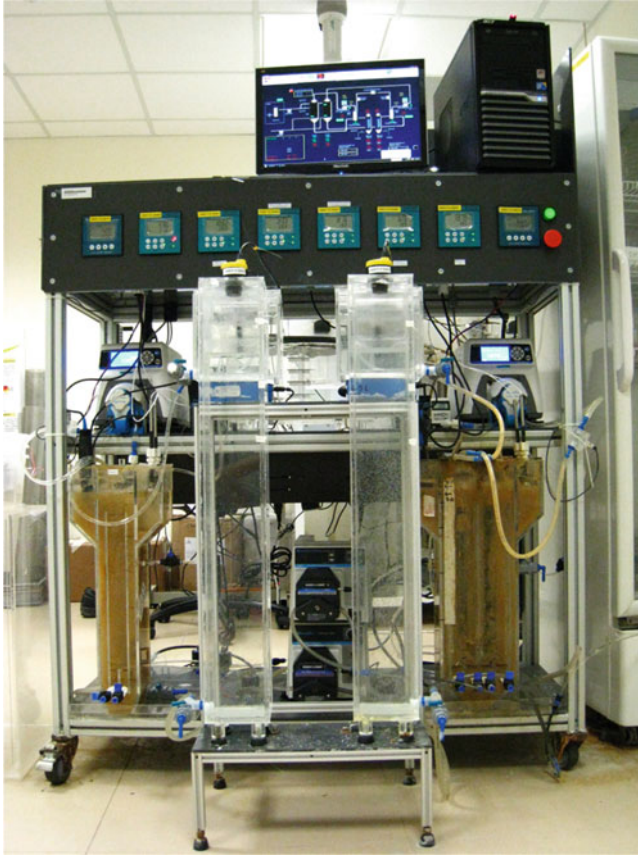


Fig. 2.6 FOMBR setup (Courtesy of Singapore Membrane Technology Centre)

The RO-like dense FO membrane provides advantages of higher quality product water, lower energy consumption and lower fouling propensity at low pressure operation.

If waste heat is available, FO can be combined with membrane distillation (MD-FO hybrid system) for separation of sodium chloride draw solution from the product water as an alternative to energy intensive reverse osmosis process (Cath 2010).

A hybrid forward osmosis-nanofiltration (FO-NF) was tested for seawater desalination (Tan 2010). Good quality product water could be obtained due to high solute rejection of FO and NF membranes.

2.8 Concluding Remarks

The increasing attention to FO processes in recent years is an indication that FO could become an alternative technology in various potential applications. Since pre-treatment of feed water is necessary to control RO membrane fouling, FO appears to

be more beneficial with less stringent pretreatment required. However, if the draw solution is to be reused or the extracted water is the intended product, extra capital and operating costs will be required for re-concentration of draw solution and water separation. As compared to RO processes, FO has not been fully established due to the lack of a suitable draw solution and an appropriate membrane. Although numerous draw solutions have been suggested, better draw solutions with clear commercial potential need to be further explored. Draw solutes with low molecular weight would be advantageous since large molecular weight solutes are not capable of diffusing rapidly through the membrane causing more severe dilutive ICP (Gray et al. 2006).

The choice of appropriate membrane material and structure could minimize the adverse ICP effects and produce high water flux with high solute rejection. In turn, ICP and water flux are also affected by the type of draw solution and operating conditions applied for FO. Further improvement and optimization of these inter-related critical factors may provide a significant reduction of FO energy consumption, thus enhance the competitiveness of FO technology. The unique separation properties of biomimetic materials may serve as inspiration for the development of improved FO membranes.

References

- Achilli, A., Cath, T.Y., Childress, A.E.: Power generation with pressure retarded osmosis: an experimental and theoretical investigation. *J. Membr. Sci.* **343**, 42–52 (2009a)
- Achilli, A., Cath, T.Y., Marchand, E.A., Childress, A.E.: The forward osmosis membrane bioreactor: a low fouling alternative to MBR processes. *Desalination* **239**, 10–21 (2009b)
- Adham, S., Oppenheimer, J., Liu, L., Kumar, M.: *Dewatering Reverse Osmosis Concentrate from Water Reuse Applications Using Forward Osmosis*. Water Reuse Foundation, Alexandria (2007)
- Babu, B.R., Rastogi, N.K., Raghavarao, K.S.M.S.: Effect of process parameters on transmembrane flux during direct osmosis. *J. Membr. Sci.* **280**, 185–194 (2006)
- Baker, R.: *Membrane Technology and Applications*, 2nd edn. Wiley, New York (2004)
- Batchelder, G.W.: Process for the demineralization of water. US Patent 3,171,799, 1965
- Carter, J.W., Psaras, G., Price, M.T.: The effect of precipitating media on the performance of porous cellulose acetate reverse osmosis membranes. *Desalination* **12**, 177–188 (1973)
- Catalyx, Inc.: Forward osmosis for recycling dye wastewater. *Filtration Sep.* **46**, 14–14 (2009)
- Cath, T.Y.: Osmotically and thermally driven membrane processes for enhancement of water recovery in desalination processes. *Desalination Water Treat.* **15**, 279–286 (2010)
- Cath, T.Y., Gormly, S., Beaudry, E.G., Flynn, M.T., Adams, V.D., Childress, A.E.: Membrane contactor processes for wastewater reclamation in space: part I. Direct osmotic concentration as pretreatment for reverse osmosis. *J. Membr. Sci.* **257**, 85–98 (2005)
- Cath, T.Y., Childress, A.E., Elimelech, M.: Forward osmosis: principles, applications, and recent developments. *J. Membr. Sci.* **281**, 70–87 (2006)
- Choi, Y.-J., Choi, J.-S., Oh, H.-J., Lee, S., Yang, D.R., Kim, J.H.: Towards a combined system of forward osmosis and reverse osmosis for seawater desalination. *Desalination* **247**, 239–246 (2009)
- Chou, S., Shi, L., Wang, R., Tang, C.Y., Qiu, C., Fane, A.G.: Characteristics and potential applications of a novel forward osmosis hollow fiber membrane. *Desalination* **261**, 365–372 (2010)
- Cornelissen, E.R., Harmsen, D., de Korte, K.F., Ruiken, C.J., Qin, J.-J., Oo, H., Wessels, L.P.: Membrane fouling and process performance of forward osmosis membranes on activated sludge. *J. Membr. Sci.* **319**, 158–168 (2008)

- Dova, M.I., Petrotos, K.B., Lazarides, H.N.: On the direct osmotic concentration of liquid foods. Part I: impact of process parameters on process performance. *J. Food Eng.* **78**, 422–430 (2007a)
- Dova, M.I., Petrotos, K.B., Lazarides, H.N.: On the direct osmotic concentration of liquid foods: part II. Development of a generalized model. *J. Food Eng.* **78**, 431–437 (2007b)
- Elimelech, M.: Yale constructs forward osmosis desalination pilot plant. *Membr. Technol.* **2007**, 7–8 (2007)
- García-Costello, E., McCutcheon, J.R., Elimelech, M.: Performance evaluation of sucrose concentration using forward osmosis. *J. Membr. Sci.* **338**, 61–66 (2009)
- Gerstandt, K., Peinemann, K.-V., Skilhagen, S.E., Thorsen, T., Holt, T.: Membrane processes in energy supply for an osmotic power plant. *Desalination* **224**, 64–70 (2008)
- Glew, D.N.: Process for liquid recovery and solution concentration. US Patent 3,216,930, 1965
- Gray, G., McCutcheon, J.R., Elimelech, M.: Internal concentration polarization in forward osmosis: role of membrane orientation. *Desalination* **197**, 1–8 (2006)
- Hancock, N., Cath, T.Y.: Solute coupled diffusion in osmotically driven membrane processes. *Environ. Sci. Technol.* **43**, 6769–6775 (2009)
- Herron, J.: Asymmetric forward osmosis membranes. US Patent 7,445,712 B2, 2008
- Holloway, R.W., Childress, A.E., Dennett, K.E., Cath, T.Y.: Forward osmosis for concentration of anaerobic digester. *Water Res.* **41**, 4005–4014 (2007)
- Hydration Technology, Inc.: HTI HydroPack forms centrepiece of water disaster-relief demonstration in Kenya. *Membrane Tech.* **5**, (2011)
- Jones, R.: Thoughts on the future of nanotechnology, <http://www.softmachines.org/wordpress/?p=68> (2005)
- Kessler, J.O., Moody, C.D.: Drinking water from sea water by forward osmosis. *Desalination* **18**, 297–306 (1976)
- Khaydarov, R.A., Khaydarov, R.R.: Solar powered direct osmosis desalination. *Desalination* **217**, 225–232 (2007)
- Klajnert, B., Bryszewska, M.: Dendrimers: properties and applications. *Acta Biochim. Pol.* **48**, 19–208 (2001)
- Kravath, R.E., Davis, J.A.: Desalination of sea water by direct osmosis. *Desalination* **16**, 151–155 (1975)
- Lampi, K., Beaudry, E., Herron, J.: Forward osmosis pressurized device and process for generating potable water. US Patent 6,849,184, 2005
- Lee, K.L., Baker, R.W., Lonsdale, H.K.: Membranes for power generation by pressure-retarded osmosis. *J. Membr. Sci.* **8**, 141–171 (1981)
- Ling, M.M., Wang, K.Y., Chung, T.-S.: Highly water-soluble magnetic nanoparticles as novel draw solutes in forward osmosis for water reuse. *Ind. Eng. Chem. Res.* **49**, 5869–5876 (2010)
- Loeb, S.: Energy production at the Dead Sea by pressure-retarded osmosis: challenge or chimera? *Desalination* **120**, 247–262 (1998)
- Loeb, S.: Large-scale power production by pressure-retarded osmosis, using river water and sea water passing through spiral modules. *Desalination* **143**, 115–122 (2002)
- Loeb, S., Titelman, L., Korngold, E., Freiman, J.: Effect of porous support fabric on osmosis through a Loeb-Sourirajan type asymmetric membrane. *J. Membr. Sci.* **129**, 243–249 (1997)
- Lubik, S.J., Garnsey, E.: Getting advanced materials to market. Paper presented at the DRUID-DIME Academy Winter 2009 Ph.D. conference on economics and management of innovation, technology and organizational change, Aalborg, 22–24 Jan 2009
- Martinetti, C.R., Childress, A.E., Cath, T.Y.: High recovery of concentrated RO brines using forward osmosis and membrane distillation. *J. Membr. Sci.* **231**, 31–39 (2009)
- McCutcheon, J.R., Elimelech, M.: Influence of concentrative and dilutive internal concentration polarization on flux behavior in forward osmosis. *J. Membr. Sci.* **284**, 237–247 (2006a)
- McCutcheon, J.R., Elimelech, M.: Influence of membrane support layer hydrophobicity on water flux in osmotically driven membrane processes. *J. Membr. Sci.* **318**, 458–466 (2008)
- McCutcheon, J.R., McGinnis, R.L., Elimelech, M.: A novel ammonia-carbon dioxide forward direct osmosis desalination process. *Desalination* **174**, 1–11 (2005)

- McCutcheon, J.R., McGinnis, R.L., Elimelech, M.: Desalination by ammonia-carbon dioxide forward osmosis: influence of draw and feed solution concentrations on process performance. *J. Membr. Sci.* **278**, 114–123 (2006b)
- McGinnis, R.L.: Osmotic desalination process. US Patent 6,391,205, 2002
- McGinnis, R.L.: Osmotic desalination process. US Patent 7,560,029, 2009
- McGinnis, R.L., Elimelech, M.: Energy requirements of ammonia-carbon dioxide forward osmosis desalination. *Desalination* **207**, 370–382 (2007)
- Mehta, G.D., Loeb, S.: Internal polarization in the porous substructure of a semi-permeable membrane under pressure-retarded osmosis. *J. Membr. Sci.* **4**, 261–265 (1978)
- Mehta, G.D., Loeb, S.: Performance of permasep B-9 and B-10 membranes in various osmotic regions and at high osmotic pressures. *J. Membr. Sci.* **4**, 335–349 (1979)
- Mi, B., Elimelech, M.: Chemical and physical aspects of organic fouling of forward osmosis membranes. *J. Membr. Sci.* **320**, 292–302 (2008)
- Mi, B., Elimelech, M.: Organic fouling of forward osmosis membranes: fouling reversibility and cleaning without chemical reagents. *J. Membr. Sci.* **348**, 337–345 (2010)
- Michaels, A.S., Bixler, H.J., Hodges, R.M.: Kinetics of water and salt transport in cellulose acetate reverse osmosis desalination membranes. *J. Colloid Sci.* **20**, 1034–1056 (1965)
- Miller, J.E., Evans, L.R.: Forward osmosis: a new approach to water purification and desalination. In: Sandia Report. vol. SAND2006-4634. Sandia National Laboratories, California (2006)
- Moody, C.D., Kessler, J.O.: Forward osmosis extractors. *Desalination* **18**, 283–295 (1976)
- Nayak, C.A., Rastogi, N.K.: Forward osmosis for the concentration of anthocyanin from *Garcinia indica* Choisy. *Sep. Purif. Technol.* **71**, 144–151 (2010)
- Ng, H.Y., Tang, W., Wong, W.S.: Performance of forward (direct) osmosis process: membrane structure and transport phenomenon. *Environ. Sci. Technol.* **40**, 2408–2413 (2006)
- Nielsen, C.H.: Biomimetic membranes for sensor and separation applications. *Anal. Bioanal. Chem.* **395**, 697–718 (2009)
- Petrotos, K.B., Quantick, P., Petropakis, H.: A study of the direct osmotic concentration of tomato juice in tubular membrane – module configuration. I. The effect of certain basic process parameters on the process performance. *J. Membr. Sci.* **150**, 99–110 (1998)
- Petrotos, K.B., Quantick, P.C., Petropakis, H.: Direct osmotic concentration of tomato juice in tubular membrane – module configuration. II. The effect of using clarified tomato juice on the process performance. *J. Membr. Sci.* **160**, 171–177 (1999)
- Petrotos, K.B., Tsiadi, A.V., Poirazis, E., Papadopoulos, D., Petropakis, H., Gkoutosidis, P.: A description of a flat geometry direct osmotic concentrator to concentrate tomato juice at ambient temperature and low pressure. *J. Food Eng.* **97**, 235–242 (2010)
- Ren, J., Wang, R.: Preparation of polymeric membranes. In: Wang, L.K., Chen, J.P., Hung, Y.-T., Shammis, N.K. (eds.) *Membrane and Desalination Technologies. Handbook of Environmental Engineering*, vol. 13. Humana Press, Inc., Totowa (2011)
- Shi, L., Chou, S.R., Wang, R., Fang, W.X., Tang, C.Y., Fane, A.G.: Effect of substrate structure on the performance of thin-film composite forward osmosis hollow fiber membranes. *J. Membr. Sci.* **382**, 116–123 (2011)
- Stache, K.: Apparatus for transforming sea water, brackish water, polluted water or the like into a nutritious drink by means of osmosis. US Patent 4,879,030, 1989
- Su, J., Yang, Q., Teo, J.F., Chung, T.-S.: Cellulose acetate nanofiltration hollow fiber membranes for forward osmosis processes. *J. Membr. Sci.* **355**, 36–44 (2010)
- Tan, C.H., Ng, H.Y.: A novel hybrid forward osmosis-nanofiltration (FO-NF) process for seawater desalination: draw solution selection and system configuration. *Desalination Water Treat.* **13**, 356–361 (2010)
- Tang, W., Ng, H.Y.: Concentration of brine by forward osmosis: Performance and influence of membrane structure. *Desalination* **224**, 143–153 (2008)
- Tang, C.Y., She, Q., Lay, C.L.W., Wang, R., Fane, A.G.: Coupled effects of internal concentration polarization and fouling on flux behavior of forward osmosis membranes during humic acid filtration. *J. Membr. Sci.* **354**, 123–133 (2010)

- Trent, J.D., Gormly, S.J., Delzeit, L.D., Flynn, M.T, Embaye, T.N.: Algae bioreactor using submerged enclosures with semi-permeable membranes. US Patent Application Publication, Pub. No.: US 2010/0216203 A1, 2010
- Wang, K.Y., Chung, T.-S., Qin, J.-J.: Polybenzimidazole (PBI) nanofiltration hollow fiber membranes applied in forward osmosis process. *J. Membr. Sci.* **300**, 6–12 (2007)
- Wang, K.Y., Yang, Q., Chung, T.S., Rajagopalan, R.: Enhanced forward osmosis from chemically modified polybenzimidazole (PBI) nanofiltration hollow fiber membranes with a thin wall. *Chem. Eng. Sci.* **64**, 1577–1584 (2009)
- Wang, K.Y., Ong, R.C., Chung, T.S.: Double-skinned forward osmosis membranes for reducing internal concentration polarization within the porous sublayer. *Ind. Eng. Chem. Res.* **49**, 4824–4831 (2010a)
- Wang, R., Shi, L., Tang, C.Y., Chou, S., Qiu, C., Fane, A.G.: Characterization of novel forward osmosis hollow fiber membranes. *J. Membr. Sci.* **355**, 158–167 (2010b)
- Wang, Y., Wicaksana, F., Tang, C., Fane, A.G.: Direct microscopic observation of forward osmosis membrane fouling. *Environ. Sci. Technol.* **44**, 7102–7109 (2010c)
- Wright, J.C., Johnson, R.M., Yum, S.I.: DUROS osmotic pharmaceutical systems for parenteral & site-directed therapy. *Drug Deliv. Technol.* **3**, 64–73 (2003)
- Wrolstad, R.E., McDaniel, M.R., Durst, R.W., Micheals, N., Lampi, K.A., Beaudry, E.G.: Composition and sensory characterization of red raspberry juice concentrated by direct osmosis or evaporation. *J. Food Sci.* **58**, 633–637 (1993)
- Xu, Y., Peng, X., Tang, C.Y., Fu, Q.S., Nie, S.: Effect of draw solution concentration and operating conditions on forward osmosis and pressure retarded osmosis performance in a spiral wound module. *J. Membr. Sci.* **348**, 298–309 (2010)
- Yaeli, J.: Method and apparatus for processing liquid solutions of suspensions particularly useful in the desalination of saline water. US Patent 5,098,575, 1992
- Yang, Q., Wang, K.Y., Chung, T.S.: Dual-layer hollow fibers with enhanced flux as novel forward osmosis membranes for water production. *Environ. Sci. Technol.* **43**, 2800–2805 (2009a)
- Yang, Q., Wang, K.Y., Chung, T.S.: A novel dual-layer forward osmosis membrane for protein enrichment and concentration. *Sep. Purif. Technol.* **69**, 269–274 (2009b)
- Yang, Q., Wang, K.Y., Chung, T.S.: Dual-layer hollow fibers with enhanced flux as forward osmosis membranes for water reuses and protein enrichment. US Patent WO 2010/045430 A2, 2010
- Yip, N.Y., Tiraferri, A., Philip, W.A., Schiffman, J.D., Elimelech, M.: High performance thin-film composite forward osmosis membrane. *Environ. Sci. Technol.* **44**, 3812–3818 (2010)

Chapter 3

Polymer-Based Biomimetic Membranes for Desalination

Manish Kumar, Michelle M. Payne, Sean K. Poust, and Julie L. Zilles

Abstract Membrane desalination technologies, such as reverse osmosis (RO) and forward osmosis (FO), have come to the forefront as excellent technologies for developing new saline source waters. The high energy requirement for current desalination membranes necessitates development of a new class of high flux membranes. Aquaporins, biological water transport proteins, demonstrate excellent water transport properties and biological membranes containing aquaporins have better permeabilities than current RO membrane technology while maintaining solute rejection. Incorporation of aquaporins in biomimetic block copolymers is a promising new approach for development of new desalination membranes. Using arrays of carbon nanotubes as synthetic analogs of aquaporin-based membranes is another potential approach for highly permeable membrane development.

3.1 Introduction

Synthetic membranes are important for environmental applications, particularly for water purification. They have become more relevant as we are faced with a scarcity of fresh water sources in many parts of the world. This water scarcity is further

M. Kumar (✉)

Department of Chemical Engineering, Pennsylvania State University,
16802 University Park, PA, USA
e-mail: mkumar.psu@gmail.com

M.M. Payne • J.L. Zilles

Department of Civil and Environmental Engineering, 3230C Newmark Civil Engineering Laboratory,
University of Illinois, Urbana Champaign, 205 N. Mathews Ave, 61801 Urbana, IL, USA
e-mail: marincel@illinois.edu; jzilles@illinois.edu

S.K. Poust

Joint BioEnergy Institute, 5885 Hollis Street, 94608 Emeryville, CA, USA
e-mail: poust@berkeley.edu

complicated by contamination of existing freshwater supplies and the emergence of new, difficult-to-remove pollutants (Koplin et al. 2002). Membrane desalination technologies, such as reverse osmosis (RO), have come to the forefront as excellent technologies for developing new water sources such as brackish surface and groundwater (Bohdziewicz et al. 1999), seawater (Matsura 2001), and even recycled wastewater (Judd 2006; del Pino and Durham 1999; Goldstein 2006). RO is also used for removal of several existing and emerging contaminants (Kimura et al. 2003; Kimura et al. 2004). Forward osmosis (FO) is another promising membrane-based technology. FO relies on the process of diffusion across a semipermeable membrane under an imposed osmotic gradient, and does not require active addition of energy (pressure), in contrast to RO which is pressure driven.

RO's environmental footprint is coming under increasing scrutiny, especially for seawater desalination (Einav et al. 2002). Current RO membrane operating pressures can range from 7 to 21 bar (~100–300 psi) for brackish water to 55–70 bar (~800–1,000 psi) for seawater. Consequently, energy consumption for RO facilities are a large fraction (up to 60%) of the operating costs (Kumar et al. 2005), and this number will increase as energy costs go up. This pressure requirement is due to the necessity of overcoming the osmotic pressure created by rejection of soluble material, in particular, salts, and to the mechanism of water transport in current RO membranes. Overcoming the osmotic pressure is required for any RO process. The advantage of proposed biomimetic membranes lies in the use of a different, faster mechanism for water transport, greatly increasing membrane permeability. Energy-intensive pumps are required to meet pressure requirements, and thus any reductions in pressure can decrease RO's inefficiencies. While FO processes do not use pressure to drive permeation, they too are limited by the mechanism of water transport, leading to large membrane area requirements or the requirements to use large concentrations of osmotic agents. Additionally, some contaminants such as endocrine disrupting compounds and pharmaceutically active compounds are not easily treated using RO processes (Kimura et al. 2004). With increasing concern regarding the impact of climate change on traditional water supplies (Kundzewicz et al. 2007), the development of alternate sources such as seawater and reclaimed water is imperative, but this should be done with attention to minimizing the energy use and environmental impacts. Despite tremendous developments in the efficacy and affordability of RO membranes in the last three decades, substantial improvements are still needed.

Cell membranes, on the other hand, provide an alternative model for solute rejecting membranes. Cell membranes are a composite filter consisting of exceptionally selective proteins that transport water, specific ions (e.g. K^+), or specific macromolecules, all embedded in a lipid bilayer. Cell membranes transport water at extremely high rates. Current high salt rejection RO membranes have a permeability of around $3\text{--}4 \cdot 10^{-12} \text{ m s}^{-1} \text{ Pa}^{-1}$ (Ladner 2009), while membranes mimicking those present in red blood cells or kidney tubules can reach $\sim 4 \cdot 10^{-11} \text{ ms}^{-1} \text{ Pa}^{-1}$ (Walz et al. 1994). This enhanced permeability is due to the presence of water channel proteins, aquaporins. Unlike purification with conventional membranes, in which water diffuses more quickly than salts through a polymer phase, aquaporins transport water rapidly through a narrow pore, while maintaining selectivity. Aquaporins

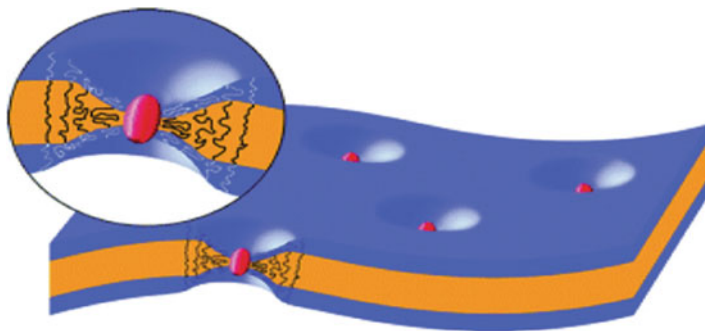


Fig. 3.1 A bioinspired approach to a highly permeable membrane. Aquaporins (*ovoid particles*) are incorporated into an amphiphilic block copolymer membrane. *Dark shading* represents the hydrophilic block of the polymer and *light shading* represents the hydrophobic block of the polymer. The “dimpled” structure of the polymer close to the incorporated aquaporin proteins are due to compression of the hydrophobic block to match the smaller hydrophobic length of the aquaporin transmembrane segments. (Mecke et al. 2006)

can transport as many as three billion water molecules per second while excluding solutes (Agre 2004).

Membranes designed to utilize this mechanism would have much higher permeabilities. A bioinspired approach to developing a highly-permeable membrane for desalination is to insert aquaporins into cell membrane-like amphiphilic block copolymer membranes, as illustrated in Fig. 3.1. These membranes are proposed as alternatives to currently used synthetic polymeric RO and FO membranes. One can think of existing RO and FO membranes as analogues of the membranes used by early single-celled organisms before the evolution of aquaporins, in which water could only be transported by slow diffusion processes. The next step for the evolution of water treatment membranes is the incorporation of specific water conducting channels, to mimic modern high-flux cellular membranes. This can be done either by incorporating aquaporins directly, as illustrated in Fig. 3.1, or by using the current understanding of aquaporins to design synthetic analogs. For example, carbon nanotubes (CNTs) are being investigated as potential membrane materials, but their diameter is currently too large for rejecting salt without functionalization as sub-nanometer CNTs would be needed for such applications (Corry 2008). By analogy to aquaporins, this problem might be overcome not only through new developments in the synthesis of smaller diameter nanotubes, but perhaps also by incorporating electrostatic repulsion into the design of CNTs (Fornasiero et al. 2008). These biomimetic membranes have the potential to reduce energy input by decreasing the feed pressures required for RO processes and the membrane area or osmotic agent concentration required for FO processes.

The following sections introduce (i) water transport in current water treatment membranes; (ii) water transport and selectivity mechanisms in aquaporins and synthetic nanochannels; (iii) block copolymers and their suitability as biomimetic membranes and as a platform for inserting functional membrane proteins; (iv) approaches for developing biomimetic membranes for desalination, and (v) some key challenges related to the development of high efficiency biomimetic desalination membranes.

3.2 Water Transport in Synthetic Membranes

Improvements in the productivity of synthetic membranes used for water and wastewater applications are required. As mentioned in Sect. 3.1, current RO membranes require high pressures to operate. Additionally, due to continuous improvement in membrane technology, the permeability of current RO membranes has allowed plants to approach the thermodynamic minimum energy required for such separations (Zhu et al. 2009). Current best practice seawater RO can achieve energy efficiencies of around 2 kiloWatt-hour per cubic meter (kWh m^{-3}), whereas the thermodynamic limit for seawater RO is about 1 kWh m^{-3} . In practice however, electrical energy consumption is about $2.5\text{--}3.5 \text{ kWh m}^{-3}$ at seawater RO plants (American Membrane Technology Association 2010; Stover 2007). A cost and productivity index (cost per unit water production) for high pressure membranes over the last few decades, calculated based on manufacturer-provided historical and projection data, is shown in Fig. 3.2. The above discussion illustrates that although there have been great improvements in productivity and decreases in cost; the cost per unit water produced has become relatively flat in recent years. Increases in productivity of current membranes are limited by the mechanism of water transport through interfacially formed and crosslinked polymers.

The mechanism of water transport in such polymer membranes is illustrated in Fig. 3.3. The rate-controlling transport step is through the top interfacial thin film layer (shown in Fig. 3.3a). In the crosslinked structure of the polymer, the pores are not connected in a static manner – and sometimes the thin-film layer is referred to as being non-porous, see Fig. 3.3b, c. Water is present in interstitial spaces of such polymers and diffuses through the polymer layer as the interstitial spaces become interconnected by thermal motion of the polymers (Kotelyanskii et al. 1998, 1999).

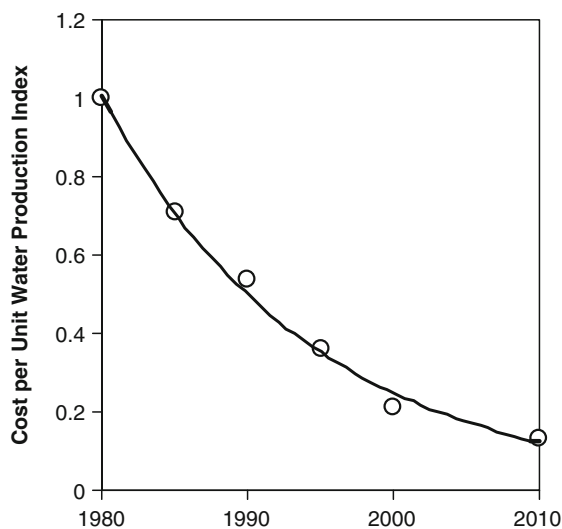


Fig. 3.2 Cost reduction and productivity improvement in synthetic membranes used in brackish water RO (Kumar 2010). The cost/productivity values were indexed to the first year data was available

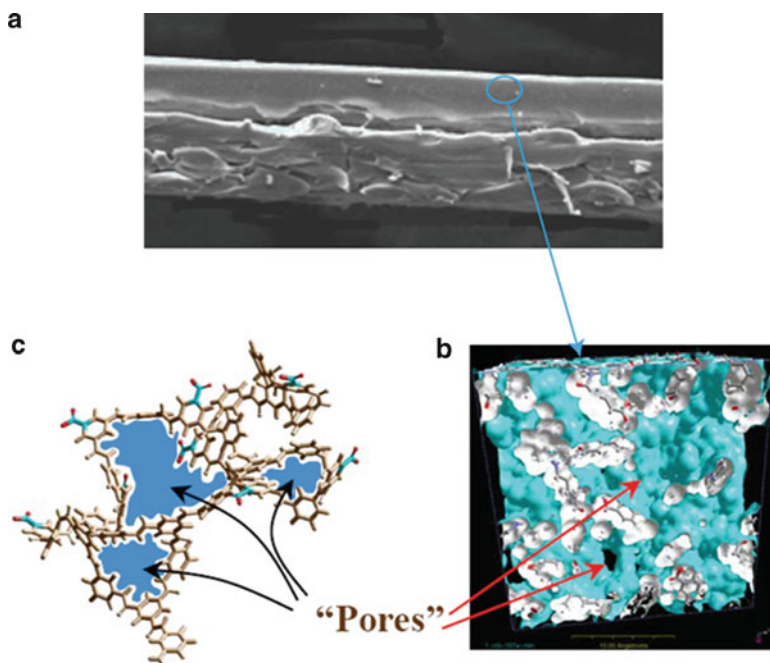


Fig. 3.3 Water transport through RO and FO membranes is limited by the slow “jump diffusion” of water. (a) Transport through the *top layer*, shown here in a Scanning Electron Micrograph of a Thin Film Composite (TFC) RO membrane, limits membrane permeability. (b) The nonporous nature of the separating layer is illustrated in this molecular model of water distribution. Transport of water through this layer requires “jump diffusion” as described in (Kotelyanskii et al. 1998). (c) A schematic of the distribution of interstitial spaces (“pores”) and water within the crosslinked polymer structure (Fig. 3.3b, c are used with permission from Kalinichev 2007)

This is called “jump diffusion” of water. Due to the statistical nature of this phenomenon, it is inherently slow. This is particularly evident when the scale of transport (~ 100 nm) is considered compared to the scale of each jump diffusion step (~ 0.3 nm) (Kotelyanskii et al. 1998). Crosslinking reduces the possible connections between adjacent pores and slows water transport. However, crosslinking is crucial in achieving high salt rejection, for example in polyamide membranes used in seawater RO.

3.3 Water Transport and Selectivity by Aquaporins and Synthetic Nanochannels

Aquaporins are a class of membrane-spanning proteins that transport water across the cell membrane (Agre 2004). Agre and coworkers first demonstrated the water channel activity of a 28 kDa erythrocyte membrane protein expressed in

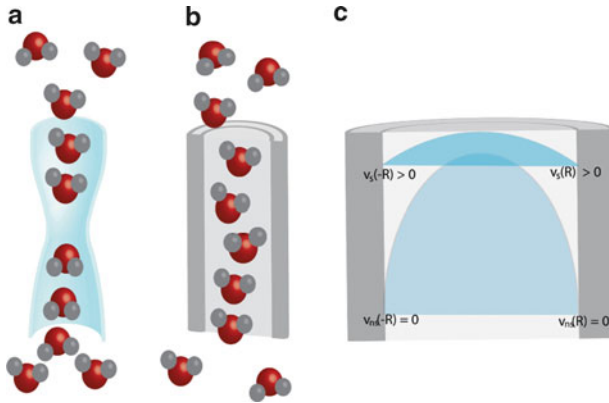


Fig. 3.4 Water transport in narrow hydrophobic channels. (a) and (b) are illustrations of water flow in an aquaporin and an idealized hydrophobic channel, respectively. (c) shows comparison of velocity profiles in non-slip Poiseuille flow (*parabolic*, shown in *light blue*, and indicated by the subscript ns) and in confined slip flow (blunted *parabolic*, *blue*, and indicated by the subscript s). Note the velocity at the walls for non-slip flow ($r=R$ or $r=-R$) is zero for non-slip flow, while it is non-zero for slip flow. Additionally, the maximum velocity as well as the total flow indicated by the profile is higher for slip flow

Xenopus laevis oocytes (Preston et al. 1992). This was the human aquaporin subsequently named AQP1. Since then 12 other human/mammalian aquaporins have been discovered (named AQP0 through AQP12) with critical physiological functions (Agre and Kozono 2003; Ishibashi et al. 2009). Additionally, aquaporins have been found in plants, yeast, and in the domains *Bacteria* and *Archaea* (Maurel 1997; Calamita et al. 1995; Kozono et al. 2003; Bonhivers et al. 1998). Most aquaporins have functions related to water transport, but solute transport (reviewed in King et al. 2004) and formation of intercellular junctions (AQP0, AQP4) have been reported (Engel et al. 2008) for specific aquaporins. For the purposes of water treatment, aquaporins are of interest due to their high fluxes and their excellent solute rejection.

Aquaporins transport water more rapidly than existing RO and FO membranes due to a fundamental difference in transport mechanism. In contrast to the “jump diffusion” mechanism of existing membranes, aquaporins transport water through small hydrophobic pores (referred to here as nanochannels). Water transport in these narrow (diameter <200 nm) hydrophobic nanochannels occurs by frictionless movement of water molecules in a single file through the short (10–20 nm) channel (Fig. 3.4a, b).

Classical fluid dynamics describes flow in channels (>200 nm) using classical Poiseuille flow (Fig. 3.4c). Due to the viscosity of the fluid, the “no slip condition” requires that the water will have zero velocity at the wall of the channel. This requirement controls the overall average velocity and thus flux through the channel. In this classical situation, understanding the behavior of individual molecules is not necessary for describing overall flow and water can be treated as a continuous fluid.

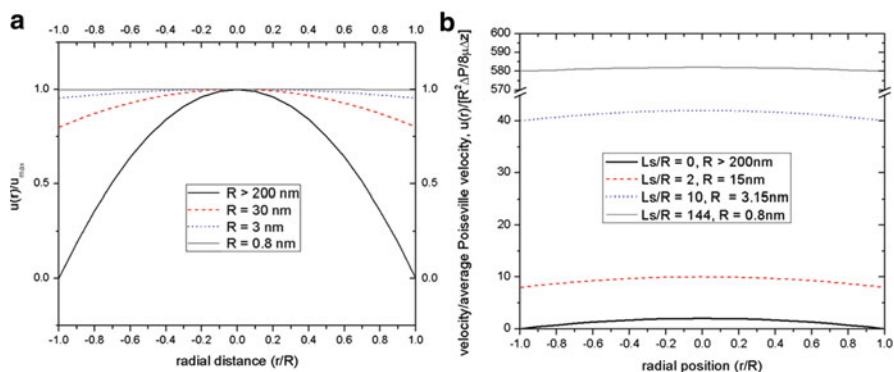


Fig. 3.5 Comparison on velocity profiles in Poiseuille flow ($R > 200$ nm) to that in confined slip flow (not considering change in water viscosity). These calculations are based on (Thomas et al. 2009). (a) Velocity profiles normalized to the maximum velocity for different channel radii showing the change in profile from parabolic to blunt profile. (b) Velocity profiles across the channel where the y axis represents the ratio of the radial velocity ($u(r)$) to the average Poiseuille velocity for different channel radii. Note the large increase in velocity (and hence flow) as the R value goes from >200 nm ($2\times$ avg. Poiseuille velocity as expected in Poiseuille flow) to 0.8 nm ($\sim 580\times$ avg. Poiseuille velocity)

However, for channels smaller than 200 nm in diameter, interesting properties arise due to noncontinuum effects both at the walls of the channel and between the confined water molecules. Aquaporin channels are ~ 0.23 nm at the narrowest part while existing CNTs can be made as narrow as 1.6 nm (Fornasiero et al. 2008), so neither of these are well described by the classical Poiseuille flow model. Thomas et al. describe a fluid dynamics description of the noncontinuum effects at the wall to illustrate one mechanism for flux enhancement seen in small hydrophobic channels between 1.6 and 200 nm (Thomas et al. 2009). The flux enhancement due to the noncontinuum effects at the walls is presented below, followed by discussion on enhancement due to noncontinuous behavior of water molecules observed in nanochannels.

In confined nanochannels (<200 nm) with frictionless hydrophobic walls there is a deviation from the classical Poiseuille flow due to “slip” at the wall. The effect of slip in these narrow hydrophobic channels is that the parabolic shape of the velocity profile seen in Poiseuille flow is “blunted” (Fig. 3.1c). This is further illustrated using numerical calculations of the flow profile in Fig. 3.5a. As the channels become narrower, the velocity increases dramatically when compared to average velocity in Poiseuille flow as predicted by classical fluid dynamics (Fig. 3.5b) due to relaxation of the “no slip condition”. Additionally, due to confinement of the water molecules, a change in viscosity of the bulk water within the nanochannels has been proposed to occur (Joseph and Aluru 2008; Thomas et al. 2009), further enhancing flow velocity.

When pore size is below the continuum limit for water (<1.6 nm), the description of transport is somewhat complicated by the structure of water in confined geometries as well as by coordinated motion of water molecules, and must be modeled using molecular dynamics simulations. Such modeling was first reported by

Hummer and colleagues (Kalra et al. 2003; Berezhkovskii and Hummer 2002; Hummer et al. 2001), who demonstrated enhanced water flow in subnanometer CNTs under the influence of an osmotic gradient. A method to conduct simulations under a hydrostatic gradient was subsequently developed (Zhu and Schulten 2003). Based on molecular dynamics simulations, there is a depletion layer next to the wall of nanochannels, where the water concentration is less than 5% of the bulk water concentration (Joseph and Aluru 2008). In this region, water molecules are oriented such that the non-hydrogen-bonded OH groups of water molecules point towards the wall, allowing the water to flow freely. This depletion layer has a direct effect on flow enhancement, and the smoothness of the nanochannels also helps in enhancement of flow rates. Simulations also suggest ion rejection capability for CNTs with diameters <0.47 nm (Corry 2008).

Enhanced water transport through aquaporins follows the main principles for transport through narrow hydrophobic channels described above and has been modeled by several groups (de Groot and Grubmüller 2001; Zhu et al. 2001; Jensen and Mouritsen 2006). Additionally, the selectivity, or solute rejection, of aquaporins is excellent. Aquaporins have a unique hourglass architecture, with pore openings of around 3 Å lined with mostly hydrophobic amino acids. Three mechanisms contributing to solute rejection are summarized here and in Fig. 3.6 (Kozono et al. 2002; de Groot and Grubmüller 2001). Large solutes are rejected through *size exclusion*, as the narrowest part of the channel is 2.3 Å. A positively charged arginine residue is located at this narrow part and helps reject positively charged solutes through *electrostatic repulsion*. Finally, during transport, water molecules undergo a molecular reorientation by hydrogen bonding with a residue near the pore (de Groot and Grubmüller 2001; Chakrabarti et al. 2004; Murata et al. 2000). This molecular reorientation (*water dipole reorientation*) breaks the extensive hydrogen bonding that normally allows rapid H⁺ transfer in bulk water, and in doing so prevents passage of H⁺ ions.

In aquaporins from different organisms, and even from different tissues in multicellular organisms, there are variations in water permeability, selectivity, and regulation of permeability. These variations allow the aquaporins to fulfill different physiological functions. For example, the aquaporin present in mammalian eye lens, AQP0, is selective for water, but does not show high permeability, while AQP2, present in kidney tissues and involved in concentrating urine, shows high selectivity and high permeability (King et al. 2004). Other members of the aquaporin family are not specific for water, transporting anions, arsenite, glycerol, and/or urea. The *Escherichia coli* aquaporin AqpZ has high water permeability and no known transport of solutes (Borgnia et al. 1999). Many aquaporins also show some control over water transport; this reversible closure is commonly called gating. For example, the PIP family of plant aquaporins closes in response to drought stress and pH changes (reviewed in Hedfalk et al. 2006). Because of the medical importance of mammalian aquaporins, the structural basis for many of these variations in activity is known. For water treatment, the choice of aquaporin must consider this variation as well as practical aspects of producing the protein. The existing variation also illustrates the potential for development of aquaporins with enhancement of specific properties.

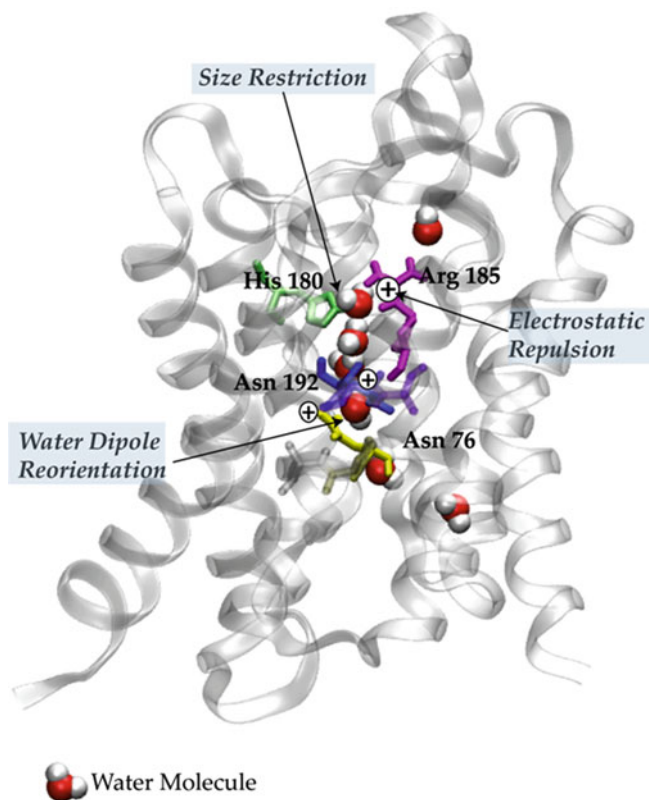


Fig. 3.6 Mechanisms for rejection of solutes illustrated using AQP1 as a model. Selected amino acid residues important for these rejection mechanisms are highlighted. Histidine 180 (His 180) and Arginine 185 (Arg 185) form the narrowest part of the channel (2.8 Å), and this size restriction is responsible for *size exclusion* of larger solutes. Arg 185 is positively charged and the presence of this residue at the narrowest part of the channel helps reject positively charged solutes by *electrostatic repulsion*. Arg 185 and two conserved asparagine-proline-alanine motifs (*not highlighted*) form a series of hydrogen bonds with the water molecules, reorienting the water and preventing passage of H⁺ ions. The above illustration is based on Kozono et al. (2002) and Jung et al. (1994) and was recreated using an example simulation (trajectory file from a molecular dynamics simulation of water passage through AQP1 by the Grubmüller group (2010)). Only a few water molecules are shown within the AQP1 molecule for clarity

3.4 Block Copolymers as Mimics of Biological Membranes

For membrane proteins such as aquaporins, the native environment is a lipid bilayer (Fig. 3.7). All membrane proteins have hydrophobic transmembrane regions, usually in the form of a band on the protein's outer surface, that interact with the hydrophobic core of the lipid bilayer. These interactions are important for the correct conformation and orientation of the aquaporin. In the absence of a hydrophobic "cushion" around the protein, hydrophobic interactions between molecules of the same protein can lead to their precipitation and inactivation. During purification of

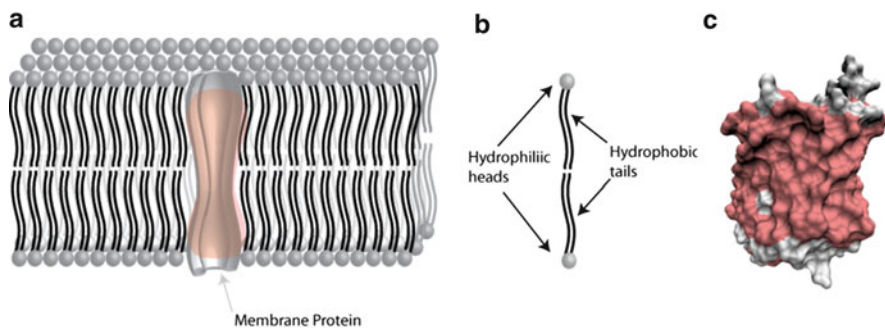


Fig. 3.7 Schematic of the lipid bilayer with inserted channel protein (transmembrane protein) (a) shows the insertion of the channel into the lipid bilayer with the *darker region* representing the hydrophobic surface of the protein that interacts with the hydrophobic core of the membrane bilayer formed from the tails of the lipid molecules illustrated in (b). (c) depicts the hydrophobic residues on the AqpZ monomer (in surface representation) in *darker shade* as an illustration of the hydrophobic band in membrane proteins

membrane proteins, the lipids are replaced by appropriate amphiphilic detergent molecules, but in order to utilize the function of these proteins they have to be placed back in a lipid bilayer-like environment. However, lipids have some limitations for water treatment applications. A promising alternative is the use of biomimetic polymers. Block copolymers that self assemble into structures similar to lipid bilayers provide a lipid-like environment for membrane protein insertion, thus emulating the biological design of bacterial cell membranes.

Triblock copolymers with a hydrophilic-hydrophobic-hydrophilic pattern self-assemble into vesicles with a structure resembling a lipid bilayer. The insertion of membrane proteins into block copolymer vesicles has been demonstrated, and in many cases the protein has also been shown to be active. In this section we summarize the advantages of block copolymers and the evidence supporting their suitability as an alternative platform for insertion of membrane proteins.

Amphiphilic block copolymers provide several advantages over artificial and synthetic lipids in engineering applications. These include:

1. *High mechanical and chemical stability when compared to lipid membranes.* Lipids have many disadvantages when used for applications (reviewed in Lee et al. 2001). Lipid membranes cannot be stretched beyond 5% of their original area without rupture under osmotic or other stresses (Needham and Zhelev 1996). Because of susceptibility to thermal phase transitions, the permeability of lipid membranes is highly variable, leading to solute leakage (Needham and Zhelev 1996). Conversely, block copolymer membranes perform much better than lipid membranes in terms of rupture strength (toughness) (Discher et al. 1999) and thermal stability (Lee et al. 2001). The cohesive energy density or toughness for polyethylene-polyethyleneoxide (EE-EO) block copolymer membranes are 5–50

times higher than lipid membranes (Discher et al. 1999). Liposomes can also be strongly affected by pH, ionic strength, and temperature (Grit and Crommelin 1993), complicating studies and applications that need to be performed under varying conditions. Poly-2-methyl-2-oxazoline-*b*-polydi-methylsiloxane-*b*-poly-2-methyl-2-oxazoline (PMOXA-PDMS-PMOXA) block copolymer vesicles are insensitive to extreme pH values (between 2 and 12) and high ionic strengths (of up to 1 M, unpublished results).

2. *Low permeability for water* (Lee et al. 2001; Kumar et al. 2007) and gases (unpublished data) while being impermeable to charged species. The structure and function of membrane transport proteins, including aquaporins, are typically studied via reconstitution in a lipid matrix. However, lipids have high permeability for water and gases, making it difficult to study transport of these molecules (Hill et al. 2004; Verkman 2002). The low permeability of block copolymers enhances the difference in transport behavior between the membranes with and without inserted proteins, allowing sensitive measurement of transport rates and the potential to control transport of these molecules.
3. *Design potential*. Amphiphilic block copolymers can be engineered to provide the desired properties such as fluidity or morphology by the choice of blocks and block lengths (Discher and Eisenberg 2002) or their length ratios (Zhang and Eisenberg 1995). Additionally, the choice of blocks can provide a range of properties to these membranes. A highly relevant example is the use of PMOXA, because in addition to its use as the hydrophilic block in many block copolymers, it has been reported to be resistant to fouling (Konradi et al. 2008), which would be useful in a variety of applications. The end groups of the polymers can also be modified (Napoli et al. 2006) by molecules such as biotin (for recognition and immobilization) (Grzelakowski et al. 2009), methacrylate (for stabilization by crosslinking) (Nardin et al. 2000a), fluorescent molecules (for imaging) (Grzelakowski et al. 2009), and even drugs (for drug delivery) (Peer et al. 2007).

Self assembled block copolymers in aqueous solutions, and in particular the PMOXA-PDMS-PMOXA system shown in Fig. 3.8a, are appropriate platforms for insertion of membrane proteins, as supported by several studies with different proteins performed over the past decade (Table 3.1). This is in spite of the mismatch between the size of the PMOXA hydrophobic block (up to 10 nm) and the hydrophobic band on most membrane protein (typically 4–5 nm). Pata and Dan (Pata and Dan 2003) have suggested that the flexibility of the PDMS hydrophobic block as well as its polydispersity could lead to regions immediately adjacent to the membrane proteins matching the hydrophobic band of the membrane protein (Fig. 3.8b, c). Regardless of the mechanism, the PMOXA-PDMS-PMOXA polymer permits functional insertion of the bacterial aquaporin AqpZ in block copolymers (Kumar et al. 2007) and may be expected to have better stability than lipid-based systems.

These polymer properties, coupled to the high permeabilities and selectivity exhibited by aquaporins, provide an excellent starting point for development of high efficiency biomimetic desalination membranes.

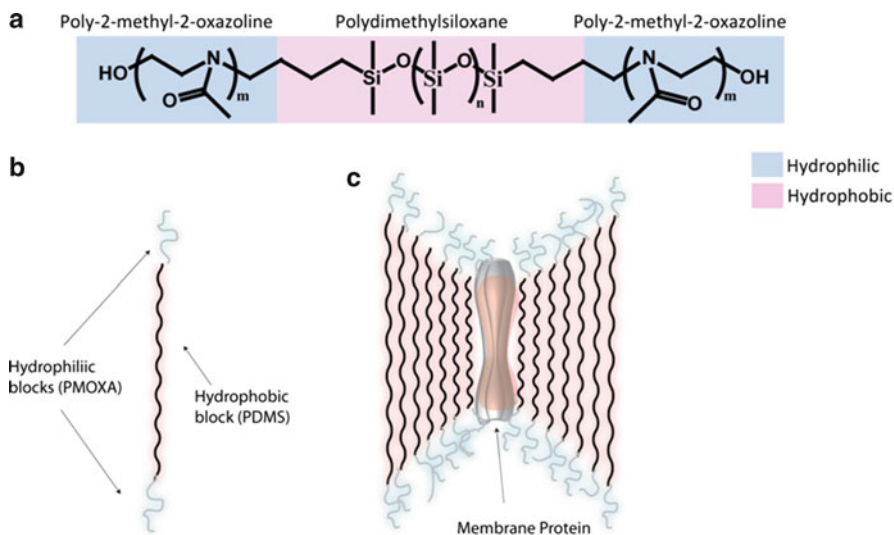


Fig. 3.8 (a) Chemical Structure of PMOXA-PDMS-PMOXA polymers and (b) schematic of a PMOXA-PDMS-PMOXA monomer (c) illustration of insertion of membrane protein in this polymer

3.5 Developing Biomimetic Membranes for Desalination

Two main directions are being taken in the development of biomimetic membranes for desalination and other water treatment applications. One involves the incorporation of aquaporins in synthetic polymer such as those described in the previous section. The other approach involves synthetic arrays of selective, hydrophobic nanochannels such as CNTs.

First we will discuss the approach of incorporating aquaporins in polymer. We have focused on the bacterial aquaporin AqpZ. In addition to its high water permeability and no known permeability for other solutes, there are practical advantages to this choice. AqpZ is relatively easily overexpressed in and purified from its native host, *E. coli*, providing a good source of the protein. In contrast, eukaryotic membrane proteins are more difficult to produce, sometimes requiring the use of tissue culture systems that have a slow growth rate and a relatively low protein yield. Additionally, AqpZ has been reported to be robust under various solution conditions and active upon reconstitution into lipid vesicles (Borgnia et al. 1999).

The potential improvements in productivity from an aquaporin-based membrane have been demonstrated by our work (Kumar et al. 2007). The PMOXA-PDMS-PMOXA polymer vesicles have low permeability, with shrinkage under osmotic shock occurring on a time scale of seconds. Incorporation of AqpZ into the vesicles shortened the time scale to 5–20 ms. The rate and thus the calculated permeability varied with the ratio of protein to polymer in the synthesis mixture (Fig. 3.9). This provides the possibility of controlling the permeability, which is useful in applications such as drug delivery. The decrease in permeability at the

Table 3.1 Summary of literature on membrane protein insertion in block copolymers

Block Copolymer system ^a	Type	Study focus	Membrane protein	Protein activity	Reference
PMOXA-PDMS-PMOXA	ABA	Antibiotic transport	OmpF	Yes	(Nardin et al. 2000b)
PMOXA-PDMS-PMOXA	ABA	Functional reconstitution	OmpF; Maltoporin; LamB	Yes	(Meier et al. 2000)
PMOXA-PDMS-PMOXA	ABA	Calcium transport	Alamethicin	Yes	(Sauer et al. 2001)
PMOXA-PDMS-PMOXA	ABA	Functional reconstitution and reversible gating	OmpF	Yes	(Nardin et al. 2001)
PMOXA-PDMS-PMOXA	ABA	Functional reconstitution	OmpF	Yes	(Nardin and Meier 2002)
PMOXA-PDMS-PMOXA	ABA	OmpF in vesicles			
PMOXA-PDMS-PMOXA	ABA	Virus assisted DNA transport	LamB	Yes	(Graff et al. 2002)
PMOXA-PDMS-PEO	ABC	Directed insertion	AQP-0	ND ^b	(Stoinescu et al. 2004)
PMOXA-PDMS-PMOXA	ABA	Proton transport	BR; COX	Yes	(Ho et al. 2004)
PEIOz-PDMS-PEIOz	ABA	ATP production	BR; Fo-F1 ATPase	Yes	(Choi and Montemagno 2005)
PMOXA-PDMS-PMOXA	ABA	Solvent-free protein reconstitution	BR; Fo-F1 ATPase	Yes	(Choi et al. 2006)
PMOXA-PDMS-PMOXA	ABA	Single molecule transport	OmpG; Alamethicin	Yes	(Wong et al. 2006)
PMOXA-PDMS-PMOXA	ABA	Single molecule transport	α -haemolysin (α HL)	No, α HL not incorporated	(Wong et al. 2006)
PMOXA-PDMS-PMOXA	ABA	Aquaporin activity	AqpZ	Yes	(Kumar et al. 2007)
PMOXA-PDMS-PMOXA	ABA	Reduction triggered channels	FhuA	Yes	(Onaca et al. 2008)
PMOXA-PDMS-PMOXA	ABA	Immobilized nanoreactors	OmpF	Yes	(Grzelakowski et al. 2009)
PMOXA-PDMS-PMOXA	ABA	Effect of hydrophobic block length on activity	NADH-ubiquinone Oxidoreductase	Yes	(Graff et al. 2009)

^aPMOXA polymethyl oxazoline, PDMS polydimethyl siloxane, PEO polyethylene oxide, PEIOz polyethyl oxazoline^bND not determined

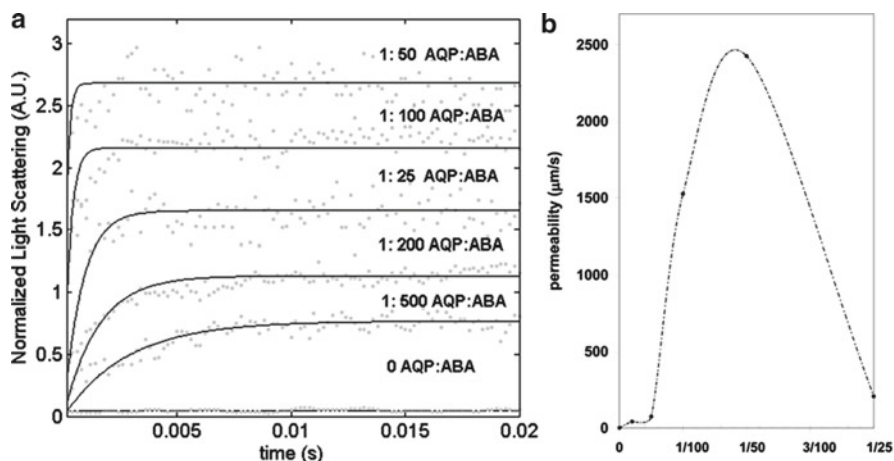


Fig. 3.9 Effect of increasing AqpZ concentrations on the permeability of ABA polymers (a) stopped flow light scattering results from osmotic shock experiments. Data were normalized to fit between 0 and 1. Curves for different ratios have been offset for clarity and fits are shown as guides. Data at 0 AQP: ABA ratio shown at a fixed offset. (b) Increase in calculated permeability with increase in protein to polymer ratio during vesicle formation (From Kumar et al. (2007), Copyright 2007, National Academy of Sciences)

highest protein concentration is surprising and may reflect reduced incorporation of the protein due to higher detergent concentrations in those samples. Good rejection of salt, glycerol, and urea was shown in the same study.

The reported productivities of AqpZ-ABA membranes exceed those for any existing salt rejecting membrane. A comparison of the measured permeability values to those measured by other researchers for block copolymer membranes and commercial RO and FO membranes is shown in Fig. 3.10. These values were measured using different procedures so the comparison is not direct, but it suggests our AqpZ-ABA membranes have provided more than an order-of-magnitude improvement over existing commercial solute-rejecting membranes in the first report on the topic.

The development of synthetic nanochannels such as CNTs for desalination and other water treatment applications has also been progressing recently. CNT membranes rely on the use of aligned, single wall CNTs in an impermeable matrix. There are two commonly used approaches to synthesizing aligned CNT that may be suitable for membrane applications (Noy et al. 2007). One is a low pressure chemical vapor deposition process that encapsulates a vertically aligned array of CNTs in silicon nitride (Holt et al. 2006). After encapsulation the ends of the CNTs are opened up using an etching process. Another approach to synthesizing aligned CNTs (Kim et al. 2007) uses a polymer matrix. In this approach the CNTs are first functionalized with amine groups and then dispersed in the solvent tetrahydrofuran. This suspension is filtered through a hydrophobic polytetrafluoroethylene filter to align the CNTs. A polymer solution of polysulfone is spin coated to make the support matrix.

Majumder et al. first provided experimental evidence for enhancement of water flow through an array of 7 nm diameter CNTs (Majumder et al. 2005). Holt et al.

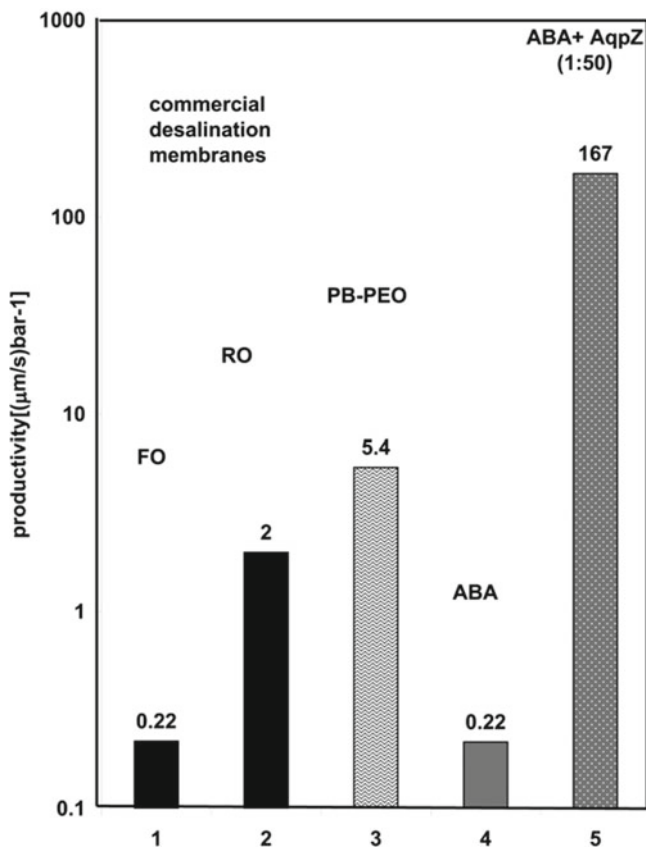


Fig. 3.10 Comparison of reported permeability values for polymeric membranes to those obtained in the study. FO data is from McCutcheon and Elimelech (2006) at 20°C. RO data is from Matsura (2001) at room temperature (assumed here to be 25°C). PB-PEO is a Polybutadiene Polyethylene diblock copolymer with data from Discher et al. (1999) at temp of 20°C. ABA represents the polymer vesicles used in study with permeability calculated at 20°C. ABA + AQP represents the polymer vesicles with incorporated AqpZ at 1:100 M ratio at 20°C. Data for ABA and AqpZ were obtained at 5.5°C and calculated at 20°C using E_a values (From Kumar et al. (2007), Copyright 2007, National Academy of Sciences)

demonstrated a similar enhancement with smaller (sub 2 nm) diameter CNTs (Holt et al. 2006) and later described ion exclusion through a CNT membrane (Fornasiero et al. 2008). Exclusion of larger ions such as $\text{Fe}(\text{CN})_6^{3-}$ molecules was demonstrated to be as high as 98% and depended on the solution pH due to ionization of the $-\text{COOH}$ groups at the ends of the CNTs. Additionally, the accompanying K^+ ion was excluded due to Donnan exclusion to maintain charge balance. Exclusion of small ions such as those present in saline water was however much lower (37% for K^+ and 45% for Cl^- for a 1 M KCl solution).

Considered together, molecular dynamics simulations and initial reports suggest great potential for desalination using narrow CNT membranes (<0.5 nm). However,

currently synthesized CNTs have diameters in the range of ~1.6 nm or more and have the major drawback of not removing small ions such as sodium and chloride. This lack of exclusion is due to the fundamental difficulty of making CNTs smaller than the hydrated diameter of these ions (Na^+ has a diameter of ~0.2 nm).

3.6 Future Research Needs and Conclusions

The aquaporin-based biomimetic membranes described above were in vesicle form. One pressing challenge is to create a larger structure suitable for use in a treatment process. Several groups are pursuing a variety of approaches, from using templates to form flat sheet PMOXA-PDMS-PMOXA membranes to immobilizing or incorporating vesicles into a matrix. However, all of this work is at an early stage. One method that shows promise for the preparation of flat sheet polymer membranes is an autopainting method. In this method small (300 μm) apertures are filled with polymer flat sheet membranes. The model protein used in the study, Gramicidin A, was shown to be functional using a voltage-clamp assay (González-Pérez et al. 2009). Kaufmann et al. have recently published a method to reliably coat a nanofiltration (NF) membrane with a lipid bilayer by depositing a tuned mixture of lipids on the surface (Kaufman et al. 2010). They have demonstrated that the lipid bilayer is continuous and could be a platform for insertion of aquaporins. However, functional insertion of aquaporins and permeability of such membranes has not been demonstrated. Other challenges for aquaporin-based biomimetic membranes will include optimizing the membrane matrix material and the incorporation of aquaporins for both permeability and stability as well as scaling up the synthesis.

In the context of water treatment, the major challenge for CNT membranes is to make narrower channels that reject salt. Attempts are underway in several research groups to make thinner CNTs and to functionalize the internal surface of these CNTs to improve ion rejection.

Longer term, as these new, higher permeability membranes are developed and commercialized, there will be new issues related to operation and system design. While many challenges, including minimizing concentration polarization and fouling, developing appropriate cleaning procedures, and optimizing overall system design, concern all membrane-based processes, the efficient incorporation of higher flux membranes will require particular attention to minimizing concentration polarization and overall system design. Concentration polarization occurs when salts are rejected and accumulate on the membrane surface, thereby reducing the driving force for permeation. Because concentration polarization increases with increasing flux, it is likely to be an important consideration for operation of the new membranes. Operating for the maximum possible flux is not likely to be the most productive mode of operation. The availability of more permeable membranes will also create new challenges and opportunities for layout and design of water treatment systems. Typically several RO membrane elements are placed in series in a pressure vessel. However, in this design, most of the water production occurs in the first few elements

because of the increased pressure drop, and more importantly, concentration polarization along the length of the pressure vessel. Biomimetic membranes, with their increased permeability and high rejection rates, will be more susceptible to this phenomenon and will be used more productively in an alternative configuration.

Water issues are gaining in importance worldwide as populations increase and climate change exacerbates potable water shortages through increasing extremes in precipitation. To alleviate these issues, membrane-based water treatment processes allow the development of new water sources, such as brackish groundwater and seawater. However, the energy use of these processes is high, and it is determined primarily by membrane permeability. Aquaporins, biological water transport proteins, demonstrate excellent water transport properties, with permeabilities exceeding current RO membrane technology. Incorporation of aquaporins in synthetic, block copolymers is a promising new approach for development of water separation membranes. CNT arrays are another promising approach for design of highly permeable membranes. The two approaches also may complement each other; increased understanding of the mechanisms used in biological water transport protein can inform our design of synthetic nanochannels, while the techniques developed for the synthesis and study of CNTs may have utility in the development of aquaporin-based membranes. However, both approaches require additional advances before scale up or commercial use.

Acknowledgments Work in our laboratories on this topic was supported by funding from primarily the US National Science Foundation (CBET 08–28512). Additional financial support was provided by fellowships from the US Environmental Protection Agency, National Water Research Institute, and the American Water Works Association to MK and fellowships from Graduate Assistance in Areas of National Need (GAANN) and Support for Under-Represented Groups in Engineering (SURGE) for MMP. We are grateful to the Wolfgang Meier Laboratory at the University of Basel, Switzerland for providing block copolymer materials and expertise to these projects.

References

- Agre, P.: Nobel lecture. Aquaporin water channels. *Biosci. Rep.* **24**, 127–163 (2004)
- Agre, P., Kozono, D.: Aquaporin water channels: molecular mechanisms for human diseases. *FEBS Lett.* **555**(1), 72–78 (2003)
- American Membrane Technology Association: Membrane desalination power usage put in perspective. http://www.amtaorg.com/amta_media/pdfs/7_MembraneDesalinationPowerUsagePutInPerspective.pdf (2009). Accessed 15 June 2010
- Berezhkovskii, A., Hummer, G.: Single-file transport of water molecules through a carbon nanotube. *Phys. rev. Lett.* **89**:064503(4 pages) (2002)
- Bohdziewicz, J., Bodzek, M., Wasik, E.: The application of reverse osmosis and nanofiltration to the removal of nitrates from groundwater. *Desalination* **121**, 139–147 (1999)
- Bonhivers, Ml, Carbrey, J.M., Gould, S.J., Agre, P.: Aquaporins in saccharomyces. *J. Biol. Chem.* **273**, 27565–27572 (1998)
- Borgnia, M.J., Kozono, D., Calamita, G., Maloney, P.C., Agre, P.: Functional reconstitution and characterization of aqpz, the e-coli water channel protein. *J. Mol. Biol.* **291**, 1169–1179 (1999)
- Calamita, G., Bishai, W.R., Preston, G.M., Guggino, W.B., Agre, P.: Molecular cloning and characterization of aqpz, a water channel from escherichia coli. *J. Biol. Chem.* **270**, 29063–29066 (1995)

- Chakrabarti, N., Tajkhorshid, E., Roux, B., Pomes, R.: Molecular basis of proton blockage in aquaporins. *Structure* **12**, 65–74 (2004)
- Choi, H.J., Montemagno, C.D.: Artificial organelle: ATP synthesis from cellular mimetic polymersomes. *Nano Lett.* **5**, 2538–2542 (2005)
- Choi, H.-J., Germain, J., Montemagno, C.D.: Effects of different reconstitution procedures on membrane protein activities in proteopolymersomes. *Nanotechnology* **17**, 1825–1830 (2006)
- Corry, B.: Designing carbon nanotube membranes for efficient water desalination. *J. Phys. Chem. B* **112**, 1427–1434 (2008)
- de Groot, B.L., Grubmuller, H.: Water permeation across biological membranes: mechanism and dynamics of aquaporin-1 and glpf. *Science* **294**, 2353–2357 (2001)
- del Pino, M., Durham, B.: Wastewater reuse through dual-membrane processes: opportunities for sustainable water resources. *Desalination* **124**, 271–277 (1999)
- Discher, D.E., Eisenberg, A.: Polymer vesicles. *Science* **297**, 967–973 (2002)
- Discher, B.M., Won, Y.Y., Ege, D.S., Lee, J.C.M., Bates, F.S., Discher, D.E., Hammer, D.A.: Polymersomes: tough vesicles made from diblock copolymers. *Science* **284**, 1143–1146 (1999)
- Einav, R., Harussi, K., Perry, D.: The footprint of desalination processes on the environment. *Desalination* **152**, 141–154 (2002)
- Engel, A., Fujiyoshi, Y., Gonen, T., Walz, T.: Junction-forming aquaporins. *Curr. Opin. Struct. Biol.* **18**, 229–235 (2008)
- Fornasiero, F., Park, H.G., Holt, J.K., Stadermann, M., Grigoropoulos, C.P., Noy, A., Bakajin, O.: Ion exclusion by sub-2-nm carbon nanotube pores. *Proc. Natl. Acad. Sci.* **105**, 17250–17255 (2008)
- Goldstein, J.: Sustainable water supplies with wastewater recycling. *Biocycle* **47**, 24–25 (2006)
- González-Pérez, A., Stibius, K.B., Vissing, T., Nielsen, C.H., Mouritsen, O.G.: Biomimetic tri-block copolymer membrane arrays: a stable template for functional membrane proteins. *Langmuir* **25**, 10447–10450 (2009)
- Graff, A., Sauer, M., Van Gelder, P., Meier, W.: Virus-assisted loading of polymer nanocontainer. *Proc. Natl. Acad. Sci. U.S.A.* **99**, 5064–5068 (2002)
- Graff, A., Fraysse-Ailhas, C., Palivan, C.G., Grzelakowski, M., Friedrich, T., Vebert, C., Gescheidt, G., Meier, W.: Amphiphilic copolymer membranes promote nadh: ubiquinone oxidoreductase activity: towards an electron-transfer nanodevice. *Macromol. Chem. Phys.* **211**, 229–238 (2009)
- Grit, M., Crommelin, D.J.A.: Chemical stability of liposomes: implications for their physical stability. *Chem. Phys. Lipids* **64**, 3–18 (1993)
- Grubmüller, H.: [Http://www.Mpibpc.Mpg.De/home/grubmueller/teaching_past_lectures/ws2007_2008/practical_05/index.html](http://www.Mpibpc.Mpg.De/home/grubmueller/teaching_past_lectures/ws2007_2008/practical_05/index.html) (2010). Accessed 2 November 2011
- Grzelakowski, M., Onaca, O., Rigler, P., Kumar, M., Meier, W.: Immobilized protein-polymer nanoreactors. *Small* **5**, 2545–2548 (2009)
- Hedfalk, K., Törnroth-Horsefield, S., Nyblom, M., Johanson, U., Kjellbom, P., Neutze, R.: Aquaporin gating. *Curr. Opin. Struct. Biol.* **16**, 447–456 (2006)
- Hill, A., Shachar-Hill, B., Shachar-Hill, Y.: What are aquaporins for? *J. Membr. Biol.* **197**, 1–32 (2004)
- Ho, D., Chu, B., Lee, H., Montemagno, C.D.: Protein-driven energy transduction across polymeric biomembranes. *Nanotechnology* **15**, 1084 (2004)
- Holt, J.K., Park, H.G., Wang, Y., Stadermann, M., Artyukhin, A.B., Grigoropoulos, C.P., Noy, A., Bakajin, O.: Fast mass transport through sub-2-nanometer carbon nanotubes. *Science* **312**, 1034–1037 (2006)
- Hummer, G., Rasaiah, J.C., Noworyta, J.P.: Water conduction through the hydrophobic channel of a carbon nanotube. *Nature* **414**, 188–190 (2001)
- Ishibashi, K., Hara, S., Kondo, S.: Aquaporin water channels in mammals. *Clin. Exp. Nephrol.* **13**, 107–117 (2009)
- Jensen, M.O., Mouritsen, O.G.: Single-channel water permeabilities of escherichia coli aquaporins aqpz and glpf. *Biophys. J.* **90**, 2270–2284 (2006)
- Joseph, S., Aluru, N.R.: Why are carbon nanotubes fast transporters of water? *Nano Lett.* **8**, 452–458 (2008)
- Judd, S.: *The MBR Book: Principles and Applications of Membrane Bioreactors for Water and Wastewater Treatment*. Elsevier, San Diego (2006)

- Jung, J.S., Preston, G.M., Smith, B.L., Guggino, W.B., Agre, P.: Molecular structure of the water channel through aquaporin chip. The hourglass model. *J. Biol. Chem.* **269**, 14648–14654 (1994)
- Kalinichev, A. from Lecture 12, Slide 22, from University of Illinois Course GEOL593 MM: Molecular modeling of aqueous solutions and substrate-solution interfaces. Spring (2007)
- Kalra, A., Garde, S., Hummer, G.: Osmotic water transport through carbon nanotube membranes. *Proc. Natl. Acad. Sci. U.S.A.* **100**, 10175–10180 (2003)
- Kaufman, Y., Berman, A., Freger, V.: Supported lipid bilayer membranes for water purification by reverse osmosis. *Langmuir* **26**, 7388–7395 (2010)
- Kim, S., Jinschek, J.R., Chen, H., Sholl, D.S., Marand, E.: Scalable fabrication of carbon nanotube/polymer nanocomposite membranes for high flux gas transport. *Nano Lett.* **7**, 2806–2811 (2007)
- Kimura, K., Amy, G., Drewes, J., Heberer, T., Kim, T., Watanabe, Y.: Rejection of organic micropollutants (disinfection by-products, endocrine disrupting compounds, and pharmaceutically active compounds) by nf/ro membranes. *J. Membr. Sci.* **227**, 113–121 (2003)
- Kimura, K., Toshima, S., Amy, G., Watanabe, Y.: Rejection of neutral endocrine disrupting compounds (edcs) and pharmaceutical active compounds (phacs) by ro membranes. *J. Membr. Sci.* **245**, 71–78 (2004)
- King, L.S., Kozono, D., Agre, P.: From structure to disease: the evolving tale of aquaporin biology. *Nat. Rev. Mol. Cell Biol.* **5**, 687–698 (2004)
- Konradi, R., Pidhatika, B., Muhlebach, A., Textor, M.: Poly-2-methyl-2-oxazoline: a peptide-like polymer for protein-repellent surfaces. *Langmuir* **24**, 613–616 (2008)
- Koplin, D., Furlong, E., Meyer, M., Thurman, E., Zaugg, S., Barber, L., Buxton, H.: Pharmaceuticals, hormones, and other organic wastewater contaminants in us streams: a national reconnaissance, (1999–2000). *Environ. Sci. Technol.* **36**, 1202–1211 (2002)
- Kotlyanskii, M.J., Wagner, N.J., Paulaitis, M.E.: Atomistic simulation of water and salt transport in the reverse osmosis membrane ft-30. *J. Membr. Sci.* **139**, 1–16 (1998)
- Kotlyanskii, M.J., Wagner, N.J., Paulaitis, M.E.: Molecular dynamics simulation study of the mechanisms of water diffusion in a hydrated, amorphous polyamide. *Comput. Theor. Polym. Sci.* **9**, 301–306 (1999)
- Kozono, D., Yasui, M., King, L.S., Agre, P.: Aquaporin water channels: atomic structure molecular dynamics meet clinical medicine. *J. Clin. Invest.* **109**, 1395–1399 (2002)
- Kozono, D., Ding, X., Iwasaki, I., Meng, X., Kamagata, Y., Agre, P., Kitagawa, Y.: Functional expression and characterization of an archaeal aquaporin. *J. Biol. Chem.* **278**, 10649–10656 (2003)
- Kumar, M.: Biomimetic membranes as new materials for applications in environmental engineering and biology. Ph.D. thesis, University of Illinois, Urbana (2010)
- Kumar, M., Adham, S.S., Pearce, W.: Model developed for brackish and reclaimed water. *Desalination Water Reuse* **15**, 38–46 (2005)
- Kumar, M., Grzelakowski, M., Zilles, J., Clark, M., Meier, W.: Highly permeable polymeric membranes based on the incorporation of the functional water channel protein aquaporin z. *Proc. Natl. Acad. Sci.* **104**, 20719–20724 (2007)
- Kundzewicz, Z.W., Mata, L.H., Arnell, N.W., Döll, P., Kabat, P., Jiménez, B., Miller, K.A., Oki, T., Sen, Z., Shiklomanov, I.A.: Freshwater resources and their management. *Climate change 2007: impacts, adaptation and vulnerability*. In: Parry, M.L., Canziani, O.F., Palutikof, J.P., van der Linden, P.J., Hanson, C.E. (eds.) *Contribution of Working Group II to the Fourth Assessment Report of the Intergovernmental Panel on Climate Change*, pp. 173–210. Cambridge University Press, Cambridge (2007)
- Ladner, D.A.: Effects of bloom-forming algae on fouling of integrated membrane systems in seawater desalination. Ph.D. thesis, University of Illinois, Urbana (2009)
- Lee, J.C.-M., Bermudez, H., Discher, B.M., Sheehan, M.A., Won, Y.-Y., Bates, F.S., Discher, D.E.: Preparation, stability, and in vitro performance of vesicles made with diblock copolymers. *Biotechnol. Bioeng.* **73**, 135–145 (2001)
- Majumder, M., Chopra, N., Andrews, R., Hinds, B.J.: Nanoscale hydrodynamics: enhanced flow in carbon nanotubes. *Nature* **438**, 44–44 (2005)
- Matsura, T.: Progress in membrane science and technology for desalination – a review. *Desalination* **134**, 47–54 (2001)

- Maurel, C.: Aquaporins and water permeability of plant membranes. *Annu. Rev. Plant Biol.* **48**, 299–429 (1997)
- McCutcheon, J., McGinnis, R., Elimelech, M.: Desalination by ammonia–carbon dioxide forward osmosis: Influence of draw and feed solution concentrations on process performance. *J. Memb. Sci.* **278**, 114–123 (2006)
- Mecke, A., Dittrich, C., Meier, W.: Biomimetic membranes designed from amphiphilic block copolymers. *Soft Matter*, **2**, 751–759 (2006)
- Meier, W., Nardin, C., Winterhalter, M.: Reconstitution of channel proteins in (polymerized) aba triblock copolymer membranes. *Angew. Chem. Int. Ed.* **39**, 4599–4602 (2000)
- Murata, K., Mitsuoka, K., Hirai, T., Walz, T., Agre, P., Heymann, J.B., Engel, A., Fujiyoshi, Y.: Structural determinants of water permeation through aquaporin-1. *Nature* **407**, 599–605 (2000)
- Napoli, A., Sebök, D., Senti, A., Meier, W.: Block copolymer vesicles. In: Lazzari, M., Liu, G., Lecommandoux, S. (eds.) *Block Copolymers in Nanoscience*, pp. 39–71. Wiley-VCH Verlag GmbH and Co. KGaA: Weinheim, Germany (2006)
- Nardin, C., Meier, W.: Hybrid materials from amphiphilic block copolymers and membrane proteins. *Rev. Mol. Biotechnol.* **90**, 17–26 (2002)
- Nardin, C., Hirt, T., Leukel, J., Meier, W.: Polymerized aba triblock copolymer vesicles. *Langmuir* **16**, 1035–1041 (2000a)
- Nardin, C., Thoeni, S., Widmer, J., Winterhalter, M., Meier, W.: Nanoreactors based on (polymerized) aba-triblock copolymer vesicles. *Chem. Commun.* **15**, 1433–1434 (2000b)
- Nardin, C., Widmer, J., Winterhalter, M., Meier, W.: Amphiphilic block copolymer nanocontainers as bioreactors. *Eur. Phys. J. E.* **4**, 403–410 (2001)
- Needham, D., Zhelev, D.: The mechanochemistry of lipid vesicles examined by micropipet manipulation techniques. *Surfactant Sci. Ser.* **62**, 373–444 (1996)
- Noy, A. et al.: Nanofluidics in carbon nanotubes. *Nano Today*, **2**, 22–29 (2007)
- Onaca, O., Sarkar, P., Roccatano, D., Friedrich, T., Hauer, B., Grzelakowski, M., Güven, A., Fioroni, M., Schwaneberg, U.: Functionalized nanocompartments (synthosomes) with a reduction-triggered release system. *Angew. Chem.* **120**, 7137–7139 (2008)
- Pata, V., Dan, N.: The effect of chain length on protein solubilization in polymer-based vesicles (polymersomes). *Biophys. J.* **85**, 2111–2118 (2003)
- Peer, D., Karp, J.M., Hong, S., Farokhzad, O.C., Margalit, R., Langer, R.: Nanocarriers as an emerging platform for cancer therapy. *Nat. Nanotechnol.* **2**, 751–760 (2007)
- Preston, G.M., Carroll, T.P., Guggino, W.B., Agre, P.: Appearance of water channels in xenopus oocytes expressing red-cell chip28 protein. *Science* **256**, 385–387 (1992)
- Sauer, M., Haefele, T., Graff, A., Nardin, C., Meier, W.: Ion-carrier controlled precipitation of calcium phosphate in giant aba triblock copolymer vesicles. *Chem. Commun.* **23**, 2452–2453 (2001)
- Stoenescu, R., Graff, A., Meier, W.: Asymmetric abc-triblock copolymer membranes induce a directed insertion of membrane proteins. *Macromol. Biosci.* **4**, 930–935 (2004)
- Stover, R.L.: Seawater reverse osmosis with isobaric energy recovery devices. *Desalination* **203**, 168–175 (2007)
- Thomas, J.A., McGaughey, A.J.H., Kuter-Arnebeck, O.: Pressure-driven water flow through carbon nanotubes: insights from molecular dynamics simulation. *Int. J. Therm. Sci.* **49**, 281–289 (2009)
- Verkman, A.S.: Does aquaporin-1 pass gas? An opposing view. *J. Physiol.* **542**, 31–31 (2002)
- Walz, T., Smith, B.L., Zeidel, M.L., Engel, A., Agre, P.: Biologically-active 2-dimensional crystals of aquaporin chip. *J. Biol. Chem.* **269**, 1583–1586 (1994)
- Wong, D., Jeon, T.-J., Schmidt, J.: Single molecule measurements of channel proteins incorporated into biomimetic polymer membranes. *Nanotechnology* **17**, 3710 (2006)
- Zhang, L., Eisenberg, A.: Multiple morphologies of “crew cut” aggregates of polystyrene-b-poly (acrylic acid) block copolymers. *Science* **268**, 1728–1731 (1995)
- Zhu, F., Schulten, K.: Water and proton conduction through carbon nanotubes as models for biological channels. *Biophys. J.* **85**, 236–244 (2003)
- Zhu, F., Tajkhorshid, E., Schulten, K.: Molecular dynamics study of aquaporin-1 water channel in a lipid bilayer. *FEBS Lett.* **504**, 212–218 (2001)
- Zhu, A., Christofides, P.D., Cohen, Y.: On RO membrane and energy costs and associated incentives for future enhancements of membrane permeability. *J. Membr. Sci.* **344**(1-2), 1–5 (2009)

Chapter 4

Ion-Selective Biomimetic Membranes

Henk Miedema

Abstract Highly selective nanopores are believed to hold an enormous potential for future nano-scaled devices and it is this promise that motivates the study of pores and channels with predictable and controllable permeation characteristics. This chapter focuses on pores and membranes exclusively selective for K^+ , Na^+ or Ca^{2+} . To date despite all the progress in membrane and separation technology, artificial membranes that can discriminate between two ion species of the same valence *and* allow high fluxes do not exist yet. After addressing how ionophores and biological ion channels achieve their high selectivity, options are discussed how Nature can provide the necessary guidance to design membranes of comparable selectivity. Three types of membranes are discussed: chemically-modified ceramic membranes, ionophore-containing polymer membranes and biological ion channel-based membranes. The pros and cons of each system are briefly addressed.

4.1 Introduction

Biological cells are enveloped by a phospholipid bilayer membrane containing ion channel proteins that mediate ion fluxes across this otherwise impermeable, low-dielectric barrier (Parsegian 1969). Ion channels are found in all types of biological membranes and implemented in all levels of cell physiology ranging from mineral uptake to signaling.

The existence of entities that can occupy an open and closed state and responsible for ion transport across the phospholipid bilayer was already anticipated by current noise analysis (Stevens 1972). It was however only after the advent of the

H. Miedema (✉)

Wetsus, Centre of Excellence for Sustainable Water Technology, Agora 1, 8900 CC
Leeuwarden, The Netherlands
e-mail: Henk.Miedema@wetus.nl

patch-clamp technique that the study and monitoring of ion currents through individual ion channel proteins became reality (Neher and Sakmann 1976, 1992; Hamill et al. 1981; Sakmann and Neher 1984). For the invention of this (single molecule!) technique, Neher and Sakmann were rewarded the Nobel Prize for Chemistry in 1991 (Barinaga 1991). Patch-clamp recordings have contributed immensely to our understanding of ion channel functioning, notably the way they open and close (gate) and discriminate (select) between different ion species. This chapter addresses two well-documented types of ion selectivity, K^+ vs Na^+ and Ca^{2+} vs Na^+ , and explores ways to design membranes of comparable high ion selectivity.

4.2 Ion Selectivity at the Nanoscale

Irrespective whether they are from biological or man-made origin, ion flow through nanometer-sized pores and channels essentially obeys the same laws of physics. The two major forces acting at the nanoscale are the van der Waals force, at distances <2 nm, and electrostatic or Coulomb forces. In relatively wide channels geometric aspects and the bulk behavior of the electrolyte solution are determinant for ion flow dynamics. When scaling down with the diameter entering the nm range, this all changes dramatically (Honig and Nicholls 1995; Hölzel and Tallarek 2007; Eijkel and van den Berg 2005; Schoch et al. 2008; Sparreboom et al. 2009). At high surface-to-volume ratios and depending on the relative magnitudes of the channel radius and the Debye screening length, the interaction between the solution and channel wall starts to dominate ion flow. In general, the wider the channel, the lower the bulk concentrations (ionic strength) needed to make this interaction become visible. For practical calculations the Debye length (in nm) is approximated by $0.304/I^{0.5}$, with the ionic strength I in mol l^{-1} (Hille 1992). The Debye length represents the distance two charges separated by a dielectric ϵ still experience the mutual electrostatic force. In a 1, 10 or 100 mM 1:1 salt solution (e.g., NaCl) the Debye length equals approximately 9.5, 3 and 0.95 nm, respectively. These numbers emphasize the long-range nature of the electrostatic force, notably at low ionic strength. Many (hypothesized) Lab-on-a-Chip devices are inspired by the behavior of ions near charged surfaces (He et al. 2009; Jiang and Stein 2010).

Selectivity of ion channels is a rather dynamic concept. Ionic strength and pH, for instance, are determining parameters (Alcaraz et al. 2004; García-Giménez et al. 2010). A key criteria for cation versus anion selectivity is a channel radius comparable to the Debye length (at that particular ionic strength of the solution), resulting in effective exclusion of co-ions. Another parameter influencing selectivity is the (negatively) charged membrane surface where counter ions can accumulate and by that affect the permeation properties of embedded ion channels (Hille 1992; Miedema 2002). Medium composition is essential also. For instance, in the absence of Ca^{2+} , Ca channels permeate Na^+ quite well. It is only in the presence of Ca^{2+} that these channels demonstrate high Ca^{2+} over Na^+ selectivity. When discussing ion-selective membranes, one should thus always bear in mind the specific application, notably the ionic conditions the membrane is exposed to.

To date despite the enormous progress in membrane technology, membranes permeable to one ion species but not to another of the same valence do not exist yet. It is believed that Nature can provide the necessary guidance to design (biomimetic) ion-selective membranes (see also Hou and Jiang 2009). To mimic Nature demands, however, understanding its working mechanisms. Therefore, we will first explore the mechanisms of ion selectivity exploited by ion-selective ionophores and ion channel proteins.

4.3 Selectivity of Ionophores and Ion Channels

4.3.1 Ionophores/Valinomycin

Ionophores bind their guest ion with high selectivity. The ionophore molecule acts as solvent for the particular ion, replacing the aqueous solvation or hydration shell surrounding the ion when dissolved in water. With the exterior of the ionophore-ion complex predominantly hydrophobic, ionophores can facilitate ion transfer across hydrophobic barriers.

The biological K^+ selective valinomycin, an antibiotic produced by several strains of *Streptomyces*, belongs to the most extensively studied ionophores (Pressman 1965; Wipf and Simon 1970; Wipf et al. 1970). Valinomycin is a macrocyclic dodecadepsipeptide comprised of enantiomers of D- and L-valine, D-hydroxyvaleric acid and L-lactic acid, all bound by alternating amide and ester bridges. The (dehydrated) K^+ ion is coordinated through ion-dipole interactions by six carbonyl oxygens present in the valinomycin molecule. The 10^5 higher stability constant of the K^+ -valinomycin complex compared to that of the Na^+ -valinomycin complex explains its high K^+ over Na^+ selectivity.

Ionophores can also be designed and synthesized in the lab. A prominent class of synthetic ionophores are the (cation-selective) crown ethers. As in valinomycin, cation coordination in crowns is by carbonyl oxygens and these compounds can indeed have a comparable K^+ over Na^+ selectivity as valinomycin. The first synthetic crown ether was discovered in 1960 by Du Pont researcher Charles Pedersen, actually resulting from the presence of an impurity. The final publication became one of the most cited papers of JACS (Pedersen 1967) and led to the Chemistry Nobel Prize in 1987 (together with Donald Cram and Jean-Marie Lehn who further expanded Pedersen's research).

The measured number of K^+ ions transported by a single valinomycin molecule typically is 10^4 s^{-1} (Stark et al. 1971). The rates of K^+ complexation and decomplexation are several orders of magnitude higher and comparable to ion channel transport rates (as cited in Pfeifer et al. 2006). The discrepancy between these two numbers may reflect a rate-limiting diffusion step of the ionophore-ion complex through the membrane. Cox et al. (1981) studied the kinetic component of ionophore selectivity. Assume the interaction between ionophore and its guest ion is characterized by a rate constant of association and dissociation of k_f and k_d , respectively.

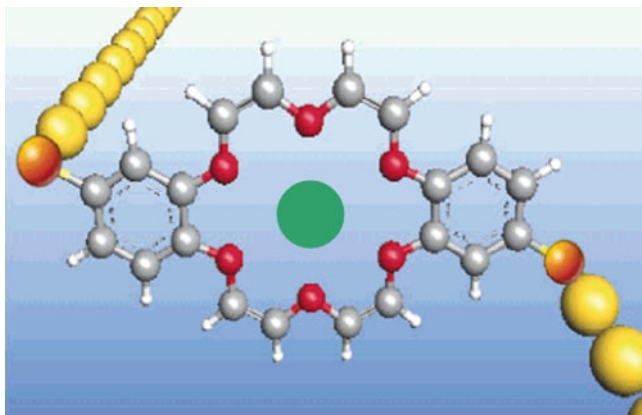


Fig. 4.1 Artistic view of a conductance measurement of crown-6, with K^+ (green) coordinated by six negatively charged oxygens (red), and attached to two gold electrodes (yellow) (Adapted from Liu et al. 2003, copied with permission from the publisher)

Plotting $\log k_d$ as a function of $\log K$ for several (combinations of) ionophores, solvents and cations, revealed large variations in k_d values but relatively small variations in those of k_f (see also Naumowicz et al. 2006). This made Cox et al. (1981) conclude that selectivity is determined more by the rate of dissociation than that of association (see also Lockhart 1986). Another relevant observation concerns the influence of water. Density functional theory (DFT) calculations show that the presence of water diminishes the selectivity of K^+ selective 18-crown-6 ether. Apparently, selectivity is not based on the mere interaction between crown-6 and the metal ion but influenced also by other interactions including those in which water molecules are involved (Rodriguez et al. 2009).

Apart from impedance spectroscopy (Steinem et al. 1998; Naumowicz et al. 2006) and flux measurements, e.g., in planar lipid bilayers (Jin 2002), ionophore-ion interactions have been monitored by conductance measurements on single crown molecules, see Fig. 4.1, or using fluorescent ionophores (Kim et al. 2002; Peng and Tang 2009).

4.3.2 Biological K Channels

Potassium channels are the most selective ion channels found in nature (Hille 1992). They are about 1,000 times more permeable to K^+ than Na^+ , a ratio that translates into a free energy difference of $\sim 10 kT$. Current insight in K channel functioning gained serious momentum after the bacterial channel KcsA could be produced in quantities large enough to crystallize the protein. Indeed, high resolution X-ray crystallography gave way for understanding the molecular basis of K^+ selectivity (Doyle et al. 1998). Elucidation (and interpretation) of the 3D structure of KcsA

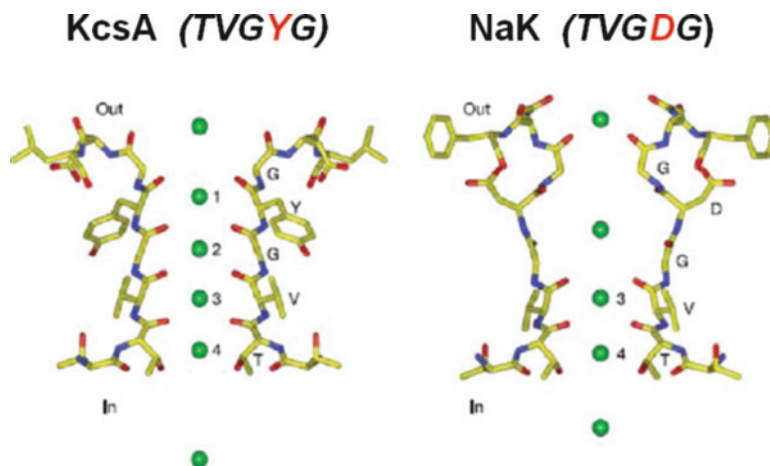


Fig. 4.2 Comparison of the permeation pathway in KcsA (*left*) and the Na/K channel (*right*). Note that only two of the four subunits are shown (From Shi et al. 2006, copied with permission from the publisher)

rendered MacKinnon the 2003 Nobel Prize for Chemistry, together with Peter Agre for his work on aquaporins (Miller 2003; MacKinnon 2004).

In the most constricted region (selectivity filter) of the tetrameric KcsA channel the pore wall is lined with backbone carbonyl oxygens belonging to the residues of the ‘signature’ sequence TVGYG. These residues, belonging to each of the four identical subunits, form a permeation pathway comprising several binding sites in series. As in valinomycin and K^+ selective crown ethers, coordination by the carbonyl oxygens compensates for the energetic cost of K^+ dehydration as it enters the narrow pore (see also Varma et al. 2008). The selectivity filter of all known K channels possesses this highly conserved sequence of amino acids. Apparently, the amino acids comprising the selectivity filter provides a physio-chemical environment that favors K^+ against Na^+ . Cyclic nucleotide-gated (CNG) channels share high sequence and structural homology with K channels. A difference is however that they possess the TVGDG or TVGDA motif instead and with that only two of the four K^+ binding sites of KcsA, see Fig. 4.2. The loss in selectivity results in a channel that is permeable to both K^+ and Na^+ (Shi et al. 2006).

A well known trade-off observed in most, if not all, artificial membranes is that an increasing flux is accompanied by a decreasing separation factor (Peters et al. 2006). The reason is that selectivity requires (somehow) interaction between the membrane pores and the permeating ions, which in turn slows down transport rates. One would expect that ion channels demonstrate (more or less) similar behavior. Despite their high selectivity, one of the most amazing aspects of K channels is their ability to combine high selectivity with conduction rates near the (bulk) diffusion limit (Miller 2000). There are two mechanisms involved in this apparent paradox. First, the presence of multiple binding sites in series and mutual repulsive forces among K^+ ions occupying neighboring sites speed up conduction. Secondly, binding

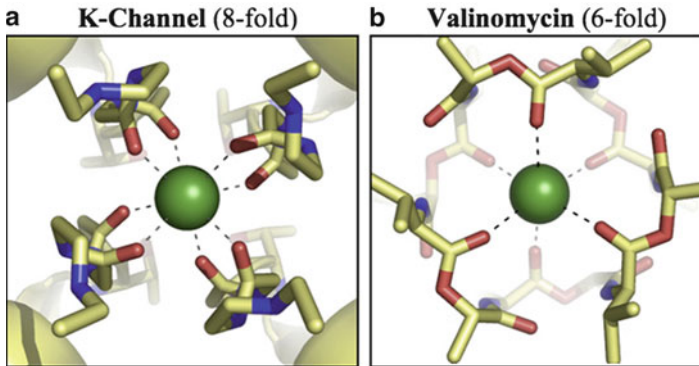


Fig. 4.3 Coordination of K^+ by KcsA (*left*) and valinomycin (*right*) (From Varma et al. 2008, copied with permission from the publisher)

of a second K^+ induces a conformational change of the protein resulting in less stronger binding of K^+ , a prerequisite for high conduction also (MacKinnon 2003).

The mechanism by which KcsA achieve its extremely high K^+ over Na^+ selectivity is still not fully elucidated yet. Several studies tried to delineate the role of different factors playing a role in KcsA selectivity (summarized and discussed by Dudev and Lim 2009), among them pore flexibility/rigidity, pore diameter, dipole moment of the coordinating oxygens (<3 Debye: K^+ selective; >4.5 Debye: Na^+ selective) and coordination architecture. Pauling ionic radii for Na^+ and K^+ are 0.95 and 1.33 Å, respectively. One theory holds that KcsA does not accommodate the smaller Na^+ because the K^+ coordinating (repulsive) carbonyl oxygens should approach each other too close, resulting in building up too much strain. Even though this view has been disputed (thermal motion would far exceed the intrinsic flexibility of the pore lumen), simulation studies show that once the strain of repulsive oxygens has been removed from the calculation, KcsA loses its K^+ over Na^+ selectivity. Valinomycin and KcsA differ for the coordination number, see Fig. 4.3, six in valinomycin versus eight in KcsA (Varma et al. 2008). Similar simulations on the influence of strain do not improve the affinity of valinomycin for Na^+ (Noskov et al. 2004). To note, Thompson et al. (2009) argue in favor of an entirely different mechanism for KcsA selectivity. High energy barriers prevent Na^+ (and Li^+) to enter the pore whereas the binding sites in the filter proper should hardly discriminate between the different alkali metal ions. A detailed discussion on KcsA and ion selectivity in general can be found in Noskov and Roux (2006).

4.3.3 *Na and Ca Channels*

The selectivity of Na and Ca channels arises from quite different chemistry (Hess and Tsien 1984). In KcsA, the side chains of the pore lining residues point away from the permeation pathway and backbone α -carbonyl oxygens coordinate the

permeating K^+ . In contrast, in Na and Ca channels the oxygens of (negatively charged) glutamates and/or aspartates form the permeation pathway (Yang et al. 1993). With four glutamates, the signature sequence of Ca channels (EEEE) comprises two negatively charged residues more than the one of Na channels (DEKA). The seminal study of Heinemann et al. (1992) showed that replacing a lysine by glutamate (DEKA \rightarrow DEEA) turns a Na^+ selective channel in one selective for Ca^{2+} . Yamaoka et al. (2003) showed the inverse by changing a Ca channel into a Na channel. To put these findings in perspective, the view that the mere presence of the EEEE-locus suffices to invoke Ca^{2+} selectivity is challenged by the bacterial NaChBac channel (Ren et al. 2001; Catterall 2001; Yue et al. 2002). Despite the presence of the EEEE-locus, NaChBac is Na^+ selective.

4.4 Charge Space Competition (CSC)

We still await the crystal structure of Na and Ca channels but even with the 64% sequence homology between the two proteins in mind (Lodish et al. 2000), it seems reasonable to assume that the positioning of the charged residues in the selectivity filter will be different. The ability to convert one channel type into the other inevitably leads to questions about the importance of the precise 3D structure of the selectivity filter. If atomic structural details of the filter were really that crucial, it is difficult to understand how a single point mutation can turn a Na channel into a functional Ca channel. Nonner, Eisenberg and co-workers developed a model that describes ion channel selectivity exclusively in terms of the fixed charge, dielectric coefficient, and volume of the selectivity filter (McCleskey 2000; Nonner et al. 2000; Eisenberg 2003; Boda et al. 2007). This so-called Charge Space Competition or CSC model uses the constraint of electroneutrality: the fixed or permanent charge of the protein is (on average) balanced by nearby mobile counter charge. The number of Na^+ ions needed to electrically balance the $-4e$ charge of the four glutamates is twice the number of Ca^{2+} ions needed to achieve the same. The crowding of the extra Na^+ ions is exactly why the channel prefers Ca^{2+} over Na^+ . According to CSC theory, all charges—fixed and mobile—float freely but are confined to the volume of the selectivity filter, emphasizing the irrelevancy of structural details to the model. The only difference between fixed and mobile charges is that the mobile charges are free to enter and leave the confined volume of the selectivity filter (or ‘electric stew’, see Fig. 4.4); fixed charges are not. The concept of crowding and its role in ion channel selectivity has also been applied to large ion selectivity (Gillespie et al. 2002), Na^+ selectivity (Boda et al. 2002) and sieving where pore diameter has been replaced with pore volume as discriminating parameter (Krauss and Gillespie 2010).

From the foregoing evaluation one may conclude that regarding selectivity K and Ca/Na channels operate essentially different. Apart from all the dissimilarities, both types seem to have a key property in common. Noskov et al. (2004) emphasize the dynamic ‘liquid-like’ nature of K^+ coordination in K channels. Selectivity arises from the intrinsic physio-chemical properties of the coordinating carbonyl oxygens

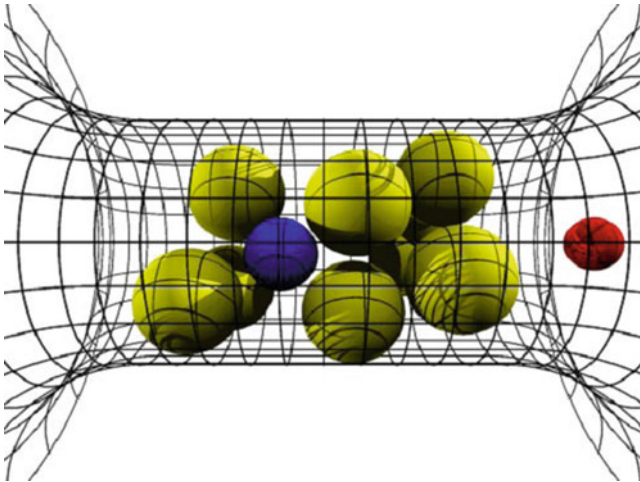


Fig. 4.4 Charge-space-competition in the ‘electric stew’ of Ca channels showing (*eight*) carboxyl oxygens (*yellow*), each charged $-1/2e$, Ca^{2+} and Na^+ . Note that a completely occupied (and electro-balanced) channel contains either 2Ca^{2+} , $1 \text{Ca}^{2+} + 2 \text{Na}^+$ or 4Na^+ ions (From Boda et al. 2002, copied with permission of the publisher)

rather than from precise architectural detail. As we have seen, the same holds for Ca channels. This view is in line with and goes back to the classical concept of ‘field strength’ as introduced by Eisenman (Eisenman and Horn 1983).

4.5 Ion-Selective Biomimetic Membranes

The application of nanopores in any putative device hinges on the ability to functionalize the system. For design purposes two approaches prevail, typified as *de novo* design and re-design, respectively (Bayley and Jayasinghe 2004). Examples that follow the first approach include, for instance, the fabrication of nanopores in synthetic films and the chemical modification of porous ceramic templates. The alternative approach takes a natural nanopore (ion channel) as a starting point, keeps its scaffold more or less intact and, if desirable, engineers (re-designs) its functionality. Here we will discuss three types of biomimetic membranes: chemically-modified ceramic membranes, ionophore-containing polymer membranes and biological ion channel-based membranes.

4.5.1 Ceramic Membranes

Pore diameter and charge density are two key parameters in membrane selectivity. Given its pores are narrow enough, the easiest way to change a non-selective membrane into one that is selective for either cations or anions, is to charge it electrically.

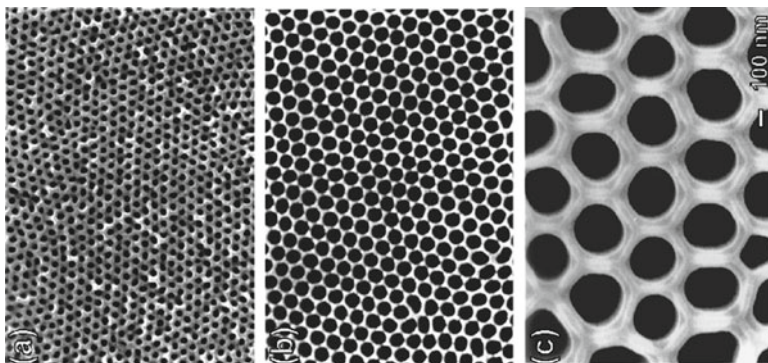


Fig. 4.5 SEM images of three different self-supporting alumina oxide membranes, anodized in sulfuric acid at 25 V (*left*), in oxalic acid at 40 V (*middle*) and in phosphoric acid at 160 V (*right*) (From Li et al. 1998, copied with permission of the publisher)

Obviously, this is only possible if the membrane is conductive. Following this approach, Martin and co-workers coated polycarbonate membranes with a thin gold layer. Applying a negative or positive potential turned the membrane selective for cations or anions, respectively (Nishizawa et al. 1995; see also Schmuhl et al. 2002).

A membrane that can distinguish two ion species of the same valence (and similar dehydrated size) requires another approach all together as charge alone lacks the necessary discriminative power. This section deals with the chemical modification of ceramic membranes, starting from self-ordered anodic alumina oxide (AAO). From a practical point of view, the use of AAO has several advantages. First, even though the surface of AAO is inherently charged and hydrophilic, thereby promoting protein adherence, coating with (neutral) polyethyleneglycol (PEG) inhibits bio-fouling (Popat et al. 2004; Lee et al. 2005). In addition, AAO membranes express high chemical and heat resistance that allows operation under harsh conditions (Song and Hong 1997; Yoshida and Cohen 2003) and sterilization and thus re-use of the membrane (Huang et al. 2007).

AAO membranes are produced by the controlled anodization (electrochemical oxidation) of plated alumina in acid solutions, resulting in nanopores aligned perpendicularly to the membrane surface (Furneaux et al. 1989; Masuda and Fukuda 1995; Thormann et al. 2007). The anodization voltage, current density, type of acid and temperature determine the pore diameter and membrane thickness, see Fig. 4.5.

Although blank nanoporous AAO is commercially available (e.g. by *Synkera* and *Whatman-Anopore*), the smallest pores still have diameters of 5–10 nm, much larger than the diameter of biological ion channels. Reduction of AAO pore diameter can be achieved in two ways; directly, i.e., making the pores smaller (adjustment of voltage and/or current density during anodization) or indirectly, i.e., by chemical modification. The standard deviation of the pore size distribution of commercially available ceramic membranes can be as high as 8%. It remains to be seen if this is small enough. Obviously, with a too large variation a lot of precious selectivity is lost due to the presence of pores with larger diameter. A strong asymmetrical pore size distribution lacking a tail at larger pore sizes helps to retain selectivity (Striemer et al. 2007; Van den Berg and Wessling 2007).

As silica oxide (Linford and Chidsey 1993), alumina oxide is very perceptible to alkoxy silane chemistry (Steinle et al. 2002; Franquet et al. 2003). Organosilane chemistry has been used frequently to develop hybrid inorganic-organic ceramic surfaces and membranes. The organosilane coupling agents self-assemble in monolayers on the nanopore surface. The chemical modification of channels with a high aspect ratio (i.e., narrow but relatively long) is challenging because the interior of the channel becomes less and less accessible to the modifying agent. Wanunu and Meller (2007) solved this problem by applying an electric field across the pores during salinization. The resulting electro-osmotic flow not only drags the organosilanes through the pore but it also prevents the silanes to oligomerize. Another advantage of this technique is that, according to the Coulter counter principle, the progress of salinization (i.e., monolayer thickness) can be monitored by measuring the ionic current through the pore simultaneously.

As we have seen in one of the previous paragraphs carbonyl or carboxyl oxygens determine to a large extent the selectivity of biological cation-selective channels. Using silane chemistry, the AAO pores can be lined with similar chemical moieties. After an initial coating with amine-terminated organosilanes, functional carboxyl and aldehyde groups can be introduced by modifying the reactive amines. Controlled radical polymerization techniques, like atom transfer radical polymerization (ATRP), possibly in combination with click chemistry (Lutz et al. 2006), provide a simple route to well-defined (co)polymers with predetermined molecular weight, narrow molecular weight distribution, and high degree of chain end functionality (Guo et al. 2010; Pasparakis et al. 2010; Zhao et al. 2010).

Now we know how to chemically modify porous AAO, the question to be answered is can we impose Ca^{2+} over Na^+ or K^+ over Na^+ selectivity to such system? In the context of CSC theory, space is one of the determining parameters for Ca^{2+} over Na^+ selectivity. Coating serves two goals, charging the pore and reducing the (effective) pore diameter. A (small) pore providing (enough) crowding can help to improve the Ca^{2+} over Na^+ selectivity. Whether a similar approach will be successful for a membrane that can discriminate between K^+ and Na^+ remains to be seen. We already addressed the several parameters (supposedly) involved in KcsA selectivity. Based on DFT calculations, Dudev and Lim (2009) conclude that KcsA selectivity results from a combination of several contributing factors that favor K^+ over Na^+ . They argue that a combination different from the one employed by KcsA may induce K^+ selectivity as well. Based on the difference in number of binding sites between channels solely permeable to K^+ and those permeable to both K^+ and Na^+ (see Fig. 4.2), membrane thickness might be one of the parameters worth to explore.

4.5.2 Ionophore-Containing (Supported) Polymer Membranes

This section deals with polymer membranes impregnated with ion-selective ionophores. Apart from their ion specificity, they can ferry their guest ion across an otherwise impermeable hydrophobic barrier (membrane). No surprise therefore that

ionophores have always been considered promising starting points for the development of ion-selective membranes.

In general, ionophores are immobilized in a (high molecular) polymer matrix like poly(vinyl chloride) (PVC) or polyimide. Inclusion of a plasticizer (e.g., NPOE or DOS) lowers the glass transition temperature of the polymer (for e.g., PVC from 80°C to -40°C) and helps to retain membrane fluidity. Even though ionophores retain their functionality after immobilization in a (plasticized) polymeric matrix, the diffusion coefficient of the ionophore-ion complex is strongly reduced and a 1,000 times lower than in aqueous solution (Armstrong and Todd 1987; Bodor et al. 2008). A generally recognized complication using this concept is leaching out of the plasticizer into the aqueous phase. This can be circumvented by taking polymers with lower glass transition temperatures that do not require the presence of a plasticizer, for instance, the methacrylic-based ones (Heng and Hall 1999, 2000). The drawback of this approach is however that a plasticizer-free polymer further reduces the diffusion coefficient of the ionophore-ligand complex (Heng et al. 2004). Apart from plasticizer, anionic sites are added. They serve to increase the cation concentration in the membrane phase and by that to lower the membrane resistance. The relative concentrations of ionophore and ionic sites and their relative affinity for the cation that is supposed to be transported determine the selectivity of the membrane (Meier et al. 1984; Eugster et al. 1991).

Ionophore-based membranes have been successfully applied already in ion-selective electrodes (Bakker 1999). An interesting account on the development and working mechanisms of such electrodes can be found in Buck and Lindner (2001). Ionophore-containing membranes for electrode applications have a thickness of 100–200 μm and an ionophore content of typically 1%. The latter value is dictated by the solubility of the ionophore in the polymer matrix and translates into a volume concentration of ~ 10 mM total valinomycin and ~ 0.4 mM valinomycin complexed with K^+ (Armstrong et al. 1986; Armstrong 1987). Ion fluxes across membranes of such potentiometric devices are virtually zero as all it has to ensure is a (near) Nernstian response. Actually, any ion (and ionophore) diffusion across and out of the membrane should be prevented as it reduces the sensitivity of the device (Heng et al. 2004; Gyurcsanyi et al. 2001). In order to prevent leaching, Sudhölter et al. (1990) suggested to covalently attach the ionophore to the polymer (e.g., to polysiloxanes as in Wienk et al. 1990).

In contrast to membranes for sensing devices, membranes for separation purposes are supposed to mediate large fluxes. The question then is how to adapt the proven recipe for synthesizing ‘potentiometric’ membranes into one suitable for a typical ‘separation’ membrane? Increasing the ionophore content and/or reducing the membrane thickness seem two obvious strategies to keep the overall membrane resistance as low as possible. Covalently attaching the ionophore to carboxylated polymer may help to increase the ionophore content beyond the limit set by its solubility in the polymer matrix (Daunert and Bachas 1990). To prevent the reaction product containing un-reacted functional COOH groups, Bereczki et al. (2005) co-polymerized ionophore and PVC monomers. More promising still is the option to apply living anionic/cationic polymerization reactions. The advantage of these

protocols is that polymer growth cannot end because of chain termination (as in regular polymerization reactions). This, in turn, implies a monomer functionalization success rate of virtually 100%. During the first step, macromolecules are functionalized by attaching, for instance, a hydroxy or amine group. The second step couples functional groups on the ionophore to those attached to the polymer. Evidently, apart from increased ionophore content, ionophore immobilization by covalently attachment to the polymer prevents leaching out of the ionophore.

There have been several attempts to model ionophore-based cation transport across membranes (see e.g., Nijenhuis et al. 1991; Christoffels et al. 1996). Cussler et al. (1989) analyzed a liquid membrane with either mobilized or covalently attached (or chained) carriers. In the case of mobile carriers, the flux (J) across the membrane is given by:

$$J = \frac{DM}{L} \left(\frac{Kc}{1 + Kc} \right) \quad (4.1)$$

where K represents the equilibrium constant of the complexation/decomplexation reactions, c the ion concentration, M the average ionophore concentration in the membrane, D the diffusion coefficient of the ionophore (including the ionophore-ligand complex) and L the membrane thickness. With the ionophores covalently linked ('chained') to the polymer, Cussler distinguished between two limit cases. Firstly, with very fast reaction kinetics at the membrane-solution interface, J is expressed by:

$$J = \frac{DM}{L} \left(\frac{Kc}{1 + Kc} \right) \left(\frac{2d/d_0}{3 - d_0/d} \right) \quad (4.2)$$

where d is the (average) distance between chained carriers that are mobile over a distance d_0 . Note that if $d = d_0/2$, Eq. 4.2 reduces to (4.1). The other case assumes very fast diffusion instead, resulting in a flux of:

$$J = \frac{(kMd^3(d_0 - d)/d_0^2)}{L} \left(\frac{KMd}{1 + Kc} \right) \quad (4.3)$$

As Cussler points out, such 'chained carrier' membrane has a clear percolation threshold. The transport chain operates only as soon as d starts to exceed d_0 because only then can the ion 'hop' from one chained carrier to the next. He also concludes that in contrast to a membrane containing mobile carriers, with the carriers covalently attached reaction kinetics rather than diffusion might be the actual rate limiting step.

Obviously, the robustness of such (ultra) thin membranes is very limited. A (low resistance) porous support (e.g., AAO, PES, PVDF or Nafion) may circumvent this complication. Such composite membranes combine the best of two worlds, i.e., the mechanical strength of the support and the selectivity of a polymer membrane. This

methodology works for tubular (Yoshida and Cohen 2003) as well as sheet membranes (Rezac and Koros 1992). Using this approach, Rezac and Koros (1992) covered AAO membranes possessing 20 nm pores with an ultra-thin (0.2–1.9 μm) defect-free layer of polyimide. An additional advantage of these hybrid membranes is to induce electric field-driven transport by applying a potential to the support, given it has been made conductive first.

4.5.3 Ion Channel-Containing Membranes

Of all the different types of biological ion channels known, bacterial porins are of special interest. Because of their thermal and chemical stability, bacterial porins are often considered ideal building blocks for biomimetic membranes and applications. Two widely used model systems for protein functionalization are α -hemolysin, a *Staphylococcus* toxin, and the mechanical sensitive large conductance channel (MscL) from *Escherichia coli*. Examples of adding novel functionalities to these two channels include incorporation of light-sensitivity (Banghart et al. 2006; Koçer et al. 2007; Fortin et al. 2008), temperature-sensitivity (Jung et al. 2006) and single-molecule detection (Wu and Bayley 2008). α -hemolysin and MscL are both relatively wide and, by implication, essentially non-selective. One way to implement ion selectivity to such wide pores is to covalently attach molecular adapters that have the required selectivity to the pore lumen (Gu et al. 2000; Wu et al. 2007). Instead of attached, Bezrukov (2004) used freely dissolved linear and circular (18-crown-6) PEG molecules that entered the pore under forward voltage bias.

Apart from aquaporins (addressed elsewhere in this volume), another well characterized model system is the outer membrane porin F (OmpF) from *Escherichia Coli* (Tieleman and Berendsen 1998; Schirmer and Phale 1999; Im and Roux 2002a, b). OmpF was the first membrane protein of which the X-ray crystal structure was resolved at high resolution (Cowan et al. 1992). OmpF is a trimer protein possessing three identical monomers, each forming a β -barrel-based structure (Schirmer 1998; Schulz 2002). Charged residues in the constriction zone of the pore lumen determine to a large extent the permeation properties of the channel (Karshikoff et al. 1994; Saint et al. 1996; Saxena et al. 1999; Phale et al. 2001). The local surface charge density in that region of (mutant) OmpF can be estimated to be as high as $\sim 300 \text{ mC m}^{-2}$, a value in the range of 1–600 mC m^{-2} calculated for synthetic nanochannels (Stein et al. 2004; Jiang and Stein 2010), see Fig. 4.6.

Ion flow through a nanopore like OmpF can be calculated by the Poisson-Nernst-Planck (PNP) formalism (Eisenberg 1996, 1999). Poisson gives the electrostatic potential (ϕ) arising from the charge density (ρ) in the pore. Its one-dimensional version reads:

$$\frac{\partial^2 \phi}{\partial x^2} = -\frac{\rho}{\epsilon_0 \epsilon} \quad (4.4)$$

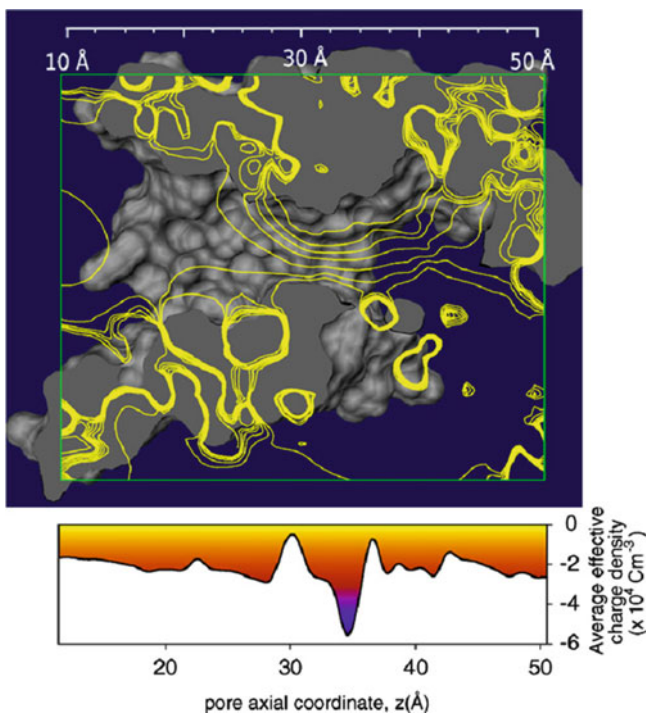


Fig. 4.6 Calculated lines of equipotential superimposed on a section of the OmpF channel. The *bottom figure* shows the profile of the effective fixed charge density (in cm^{-3}) along the channel (From Aguilera-Arzo et al. 2007, copied with permission of the publisher)

The Nernst-Planck equation for electrodiffusion relates ion flux (J) to the gradient of electrochemical potential:

$$J = -D \left(\frac{\partial c}{\partial x} \right) - \kappa \left(\frac{\partial \phi}{\partial x} \right) \quad (4.5)$$

where D is the diffusion coefficient and κ the electrical conductivity. Not only is the motion of mobile ions influenced by the electric potential, they actually contribute to it. It is therefore that the charge density ρ in Eq. 4.4 represents the collective contribution of permanent and mobile charge present in the pore lumen. The mutual interplay between potential and flux demands the two expressions to be solved self-consistently (see also Dill and Bromberg 2003). A second remark concerns the calculation of the permanent charge. A prerequisite to do so is knowledge of the ionization state (pKs) of all titratable residues, in OmpF > 100. This is far from trivial because both variations in local ϵ and charged residues nearby have an effect on pK values (Nestorovich et al. 2003; Varma and Jakobsson 2003; Miedema et al. 2006b; Vrouenraets and Miedema 2010).

From the perspective of (engineering) ion channel selectivity, OmpF is an excellent starting point because it already has the proper dimensions in that its transport characteristics are dominated by electrostatics. Because ion flow through OmpF is so sensitive to the electrostatic profile in the pore lumen, its properties can be manipulated by substituting amino acid residues by ones of different charge. Wild-type OmpF is only weakly cation-selective, a result from the combination of a low net permanent charge and a (still) relatively wide pore cross section. The cation or anion selectivity can be improved by changing the permanent charge and/or (effective) pore diameter. Volume reduction can be achieved by substituting residues by larger ones (e.g., arginines) or introducing a cysteine that can be modified by bulky cysteine-specific reagents. Following this strategy, OmpF could be turned into a channel either completely selective for cations or anions (Vrouenraets et al. 2006). These OmpF studies showed that a low permanent charge in combination with a narrow pore can render the same cation vs anion selectivity as a highly charged but wider pore.

Due to the tools of site-directed mutagenesis, protein channels allow modification at an unprecedented (sub)nanometer scale as (charged) moieties can be introduced at (almost) any preferred position(s). Among many others, one example is the creation of the liquid- or ionic-state analog of a solid state diode (Daiguji et al. 2004, 2005; Karnik et al. 2005; Hou et al. 2010). Wild-type OmpF shows (essentially) ohmic behavior, i.e. the currents through the channel recorded at negative and positive applied potential are equal in magnitude (but in opposite direction). Rectification of ion flow requires an asymmetry in the geometry of the channel and/or the charge distribution along the channel wall (Siwy 2006). An OmpF mutant possessing two separate oppositely charged selectivity filters showed strong (voltage-dependent) current rectification, analogous to the current across the np-junction of a solid state semiconductor (Miedema et al. 2007).

Attempts have been made also to trans-mutate OmpF into a channel selective for Ca^{2+} by creating an EEEE locus similar to the one in Ca channels. Compared to real Ca channels the gain in Ca^{2+} over Na^{+} selectivity was however still rather modest. With an estimated filter volume of 2 nm^3 , the filter volume of (mutant) OmpF is more than five times that of the L-type Ca^{2+} channel (0.375 nm^3). Crowding is a steep function of pore volume; apparently OmpF lacks enough crowding to exclude Na^{+} . In that sense, the observed selectivity of mutant OmpF was in accordance to CSC theory (Miedema et al. 2004, 2006a).

As powerful a tool site-directed mutagenesis might be, the limitation is that one is constrained to the natural occurring amino acid residues. As already referred to, the introduction of chemically-modified cysteines is a first step to overcome this limitation. One step further along this road is the incorporation of unnatural amino acids (Focke and Valiyaveetil, 2010). Using protein ligation techniques, this approach has been successfully applied to, for instance, KcsA (Linn et al. 2010).

Instead of semi-synthesizing an existing biological ion channel, one may choose to design the entire ion channel from scratch. This way Matile and co-workers constructed artificial rigid-rod β -barrels based on a self-assembling *p*-oligophenyl scaffold (Sakai et al. 2008). Lining the inner wall with positively

charged arginines or negatively charged aspartates evoked anion and cation selectivity, respectively (Sakai et al. 2003). Similar peptide-based nanotubes were constructed by Ghadiri and co-workers (Askenasy et al. 2006). Another example of synthetic ion channels comes from those based on β -cyclodextrin. Chemical modification with azobenzene rendered a light-gated synthetic ion channel (Jog and Gin 2008). Finally, we should mention the carbon nanotubes (Izadi-Najafabadi et al. 2010). As with peptidic nanotubes, the presence of negatively charged carboxylic groups turned the channels cation selective (Fornasiero et al. 2010). An example of an artificial chloride channel operating in and modulating a biological system can be found in Li et al. (2009).

Apart from the ion channel itself, an indispensable and crucial component of any ion channel-based device is the membrane. Proper functioning demands the ion channel to be embedded in a (defect-free) membrane that has retained its fluidity. As for device design, membrane stability and fluidity are often two conflicting requirements. Strategies to improve membrane stability or provide membrane alternatives include tethering the membrane to either a solid surface (Sackmann 2000; Atanasov et al. 2005) or porous (AAO) membrane (Römer and Steinem 2004), the encapsulation of the membrane in a hydrogel (Costello et al. 1999; Kang et al. 2007; Maurer et al. 2007; Malmstadt et al. 2008), polymerizable phospholipids (Shenoy et al. 2005) and triblock copolymer membranes (Meier et al. 2000). Another option is developing new (miniaturized) platforms for ion channel reconstitution that do not require large (unstable) membrane surface areas, for instance, membranes spanning ceramic pores (Dhoke et al. 2005; Mach et al. 2008) or membranes formed in microfluidic channels (Malmstadt et al. 2006; Domachuk et al. 2010).

4.6 Concluding Remarks

The previous paragraphs explored ways to design and synthesize biomimetic membranes. We followed a clear hierarchy in that we started with bare ceramic membranes while ending with biological ion channels. The three types of membranes discussed all have their own specific points of strength and weakness.

Even though ceramic membranes are (relatively) robust and have controllable pore diameters, achieving the desired selectivity requires the necessary chemical functionalization. Considering the subtle physio-chemical mechanisms exploited by Nature this may seem a daunting if not impossible task to perform. There are nevertheless arguments that ground optimism. First, calculation of the ion flux from the total charge accumulated in the pore (Eqs. 4.4 and 4.5) requires no less than three consecutive integration steps. As a result, despite local variations, ion flux itself is relatively insensitive to the precise charge profile (Nonner and Eisenberg 1998). Secondly, Dudev and Lim (2009) conclude that quite a different combination of chemistry and physics than the one employed by KcsA may also evoke K^+ selectivity. Third, CSC theory defines selectivity in terms of three

relatively easily adjustable and manipulative parameters. These arguments advocate the view that in order to make an ion-selective pore or membrane it is perhaps not really necessary to mimic Nature in full atomic detail, which would be a daunting task indeed! Actually, one may argue the other way around in that structural complexity is not necessarily an essential feature of protein functioning (Koder et al. 2009). Based on previous studies of Siwy et al. (2004), Gillespie et al. (2008) observed anomalous mole fraction effects in conically-shaped and carboxyl-functionalized polyethylene terephthalate (PET) pores. This study shows that it is quite well possible to impose transport characteristics typical for a biological (Ca^{2+}) ion channel to synthetic pores/membranes. Another example comes from the OmpF-diode mutant described in a previous section. Even though the crystal structure was not at hand, the protein behaved precisely as anticipated. Finally, a recent molecular dynamics study shows the ability to adjust the K^+ vs Na^+ of a single-walled carbon nanotube by patterning the inner wall with carbonyl oxygens (Gong et al. 2010).

Next we discussed the ionophore-based membranes. In contrast to AAO pores, these molecules have high selectivity already. In addition and in relation to this, for an ionophore-based membrane pore size distribution is a non-issue, i.e., virtually zero. It is for this reason that they have been applied already in numerous (zero-flux) ion-selective membranes. For a high-flux membrane, however, the Achilles heel of the system is the low transport rate due to the relatively low diffusion coefficient of the ionophore-ion complex in the polymer matrix. The most promising approach therefore seems one based on an (ultra)thin membrane combined with high ionophore content. The first requirement may be met by thin-coating a porous support; the second by covalently coupling ionophore and polymer. As Cussler et al. (1989) argue, the mechanism of ion flux in such ‘chained carrier’ system is not necessarily one based on diffusion but, instead, might be based on a (much faster) kind of a ‘hop-hop’ mechanism (Eq. 4.4). Another option not addressed yet is to combine the selectivity of ionophores with the high porosity of a ceramic membrane. Even though the ionophores were not covalently bonded, Heins et al. (2005) explored the effect of ionophores on the ionic current through synthetic nanopores.

The third type of biomimetic membranes addressed were the one based on biological ion channels. From the point of view of ion selectivity (and for that matter any other functionality), these highly specialized natural nanodevices are excellent starting points. Over the course of millions of years evolution has shaped the structure-function relationship of these molecules. As argued, here the fragility of the phospholipid bilayer poses a major challenge. Searching for a robust (synthetic) alternative for the biological phospholipid bilayer is one of the holy grails of ion channel biophysics. An inevitable consequence of a text this length is that a lot of issues remain untouched. For that reason we just briefly addressed the field of synthetic ion channels. Perhaps the ultimate biomimetic membrane is one composed of biology-inspired synthetic ion channels embedded in a synthetic membrane, e.g. oligopeptide-based ion channels in a block co-polymer membrane or (chemically-modified) carbon nanotubes in a silicon nitride matrix.

References

- Aguilella-Arzo, M., García-Celma, J.J., Cervera, J., Alcaraz, A., Aguilera, V.M.: Electrostatic properties and macroscopic electrodiffusion in OmpF porin and mutants. *Bioelectrochemistry* **70**, 320–327 (2007)
- Alcaraz, A., Nestorovich, E.M., Aguilera-Arzo, M., Aguilera, V.M., Bezrukov, S.M.: Salting out the ionic selectivity of a wide channel: the asymmetry of OmpF. *Biophys. J.* **87**, 943–957 (2004)
- Armstrong, R.D.: Mechanistic aspects of the K⁺ ion-selective electrode based on valinomycin-PVC. *Electrochim. Acta.* **32**, 1549–1552 (1987)
- Armstrong, R.D., Todd, M.: Ionic mobilities in PVC membranes. *Electrochim. Acta.* **32**, 155–157 (1987)
- Armstrong, R.D., Lockhart, J.C., Todd, M.: The mechanism of transfer of K⁺ between aqueous solutions and PVC membranes containing valinomycin. *Electrochim. Acta.* **31**, 591–594 (1986)
- Ashkenasy, N., Horne, W.S., Ghadiri, M.R.: Design of self-assembling peptide nanotubes with delocalized electronic states. *Small.* **2**, 99–102 (2006)
- Atanasov, V., Knorr, N., Duran, R.S., Ingebrandt, S., Offenhäuser, A., Knoll, W., Köper, I.: Membrane on a chip: a functional tethered lipid bilayer membrane on silicon oxide surfaces. *Biophys. J.* **89**, 1780–1788 (2005)
- Bakker, E.: Polymer membrane ion-selective electrodes – what are the limits? *Electroanalysis* **11**, 915–933 (1999)
- Banghart, M.R., Volgraf, M., Trauner, D.: Engineering light-gated ion channels. *Biochemistry* **45**, 15129–15141 (2006)
- Barinaga, M.: Ion channel research wins physiology nobel. *Science* **254**, 380 (1991)
- Bayley, H., Jayasinghe, L.: Functional engineered channels and pores. *Mol. Membr. Biol.* **21**, 209–220 (2004)
- Bereczki, R., Gyurcsányi, R.E., Agai, B., Toth, K.: Synthesis and characterization of covalently immobilized bis-crown ether based potassium ionophore. *Analyst* **130**, 63–70 (2005)
- Bezrukov, S.M.: Field-dependent effect of crown ether (18-Crown-6) on ionic conductance of a-hemolysin channels. *Biophys. J.* **87**, 3162–3171 (2004)
- Boda, D., Busath, D.D., Eisenberg, B., Henderson, D., Nonner, W.: Monte Carlo simulations of ion selectivity in a biological Na channel: charge-space competition. *Phys. Chem. Chem. Phys.* **4**, 5154–5160 (2002)
- Boda, D., Valisko, M., Eisenberg, B., Nonner, W., Henderson, D., Gillespie, D.: Combined effect of pore radius and protein dielectric coefficient on the selectivity of a calcium channel. *Phys. Rev. Lett.* **98**, 168102(1)–168102(4) (2007)
- Bodor, S., Zook, J.M., Lindner, E., Tóth, K., Gyurcsányi, R.E.: Electrochemical methods for the determination of the diffusion coefficient of ionophore-ion complexes in plasticized PVC membranes. *Analyst* **133**, 635–642 (2008)
- Buck, R.P., Lindner, E.: Tracing the history of selective ion sensors. *Anal. Chem.* **1**, 88A–97A (2001)
- Catterall, W.A.: A one-domain voltage-gated sodium channel in bacteria. *Science* **294**, 2306–2308 (2001)
- Christoffels, L.A.J., Struijk, W., de Jong, F., Reinhoudt, D.N.: Carrier mediated transport through supported liquid membranes: determination of transport parameters from single transport experiment. *J. Chem. Soc. Perkin Trans.* **2**, 1617–1622 (1996)
- Costello, R.F., Peterson, I.R., Heptinstall, J., Walton, D.J.: Improved gel-protected bilayers. *Biosens. Bioelectron.* **14**, 265–271 (1999)
- Cowan, S.W., Schirmer, T., Rummel, G., Steiert, M., Ghosh, R., Pauptit, R.A., Jansonius, J.N., Rosenbusch, J.P.: Crystal structures explain functional properties of two *E. coli* porins. *Nature* **358**, 727–733 (1992)
- Cox, B.G., Garcia-Rosas, J., Schneider, H.: Solvent dependence of the kinetics of formation and dissociation of cryptate complexes. *J. Am. Chem. Soc.* **103**, 1054–1059 (1981)
- Cussler, E.L., Aris, R., Bhowan, A.: On the limits of facilitated diffusion. *J. Membr. Sci.* **43**, 149–164 (1989)

- Daijui, H., Yang, P., Majumdar, A.: Ion transport in nanofluidic channels. *Nano Lett.* **4**, 137–142 (2004)
- Daijui, H., Oka, Y., Majumdar, A.: Nanofluidic diode and bipolar transistor. *Nano Lett.* **5**, 2274–2280 (2005)
- Dauert, S., Bachas, L.G.: Ion-selective electrodes using an ionophore covalently attached to carboxylated poly(vinyl chloride). *Anal. Chem.* **62**, 1428–1431 (1990)
- Dhoke, M.A., Ladha, P.J., Boerio, F.J., Lessard, L.B., Malinowska, D.H., Cuppoletti, J., Wiczorek, D.S.: Porous membranes for reconstitution ion channels. *Biochim. Biophys. Acta* **1716**, 117–125 (2005)
- Dill, K.A., Bromberg, S.: *Molecular Driving Forces*. Garland Science, New York (2003)
- Domachuk, P., Tsioris, K., Omenetto, F.G., Kaplan, D.L.: Bio-microfluidics: biomaterials and biomimetic designs. *Adv. Mater.* **22**, 249–260 (2010)
- Doyle, D.A., Cabral, J.M., Pfuetzner, R.A., Kuo, A., Gulbis, J.M., Cohen, S.L., Chait, B.T., MacKinnon, R.: The structure of the potassium channel: molecular basis of K^+ conduction and selectivity. *Science* **280**, 69–77 (1998)
- Dudev, T., Lim, C.: Determinants of K^+ vs Na^+ selectivity in potassium channels. *J. Am. Chem. Soc.* **131**, 8092–8101 (2009)
- Eijkel, J.C.T., van den Berg, A.: Nanofluidics: what is it and what can we expect from it? *Microfluid. Nanofluidic* **1**, 249–267 (2005)
- Eisenberg, R.S.: Computing the field in proteins and channels. *J. Membr. Biol.* **150**, 1–25 (1996)
- Eisenberg, R.S.: From structure to function in open ionic channels. *J. Membr. Biol.* **171**, 1–24 (1999)
- Eisenberg, B.: Proteins, channels and crowded ions. *Biophys. Chem.* **100**, 507–517 (2003)
- Eisenman, G., Horn, R.: Ion selectivity revisited: the role of kinetic and equilibrium processes in ion permeation through channels. *J. Membr. Biol.* **76**, 197–225 (1983)
- Eugster, R., Gehrig, P.M., Morf, W.E., Spichiger, U.E., Simon, W.: Selectivity-modifying influence of anionic sites in neutral-carrier-based membrane electrodes. *Anal. Chem.* **63**, 2285–2289 (1991)
- Focke, P.J., Valiyaveetil, F.: Studies of ion channels using expressed protein ligation. *Curr Opin Chem Biol.* **14**, 797–802 (2010)
- Fornasiero, F., In, J.B., Kim, S., Park, H.G., Wang, Y., Grigoropoulos, C.P., Noy, A., Bakajin, O.: pH-Tunable ion selectivity in carbon nanotube pores. *Langmuir* **26**, 14848–14853 (2010)
- Fortin, D.L., Banghart, M.R., Dunn, T.W., Borges, K., Wagenaar, D.A., Gaudry, Q., Karakossian, M.H., Otis, T.S., Kristan, W.B., Trauner, D., Kramer, R.H.: Photochemical control of endogenous ion channels and cellular excitability. *Nat. Methods* **5**, 331–338 (2008)
- Franquet, A., Terryn, H., Vereecken, J.: Composition and thickness of non-functional organosilane films coated on aluminum studied by means of infra-red spectroscopic ellipsometry. *Thin Solid Films* **441**, 76–84 (2003)
- Furneaux, C., Rigby, W.R., Davidson, A.P.: The formation of controlled-porosity membranes from anodically oxidized aluminium. *Nature* **337**, 147–149 (1989)
- García-Giménez, E., Alcaraz, A., Aguilera, V.M.: Overcharging below the nanoscale: multivalent cations reverse the ion selectivity of a biological channel. *Phys. Rev. E* **81**, 021912 (2010)
- Gillespie, D., Nonner, W., Henderson, D., Eisenberg, R.S.: A physical mechanism for large-ion selectivity of ion channels. *Phys. Chem. Chem. Phys.* **4**, 4763–4769 (2002)
- Gillespie, D., Boda, D., He, Y., Apel, P., Siwy, Z.S.: Synthetic nanopores as a test case for ion channel theories: the anomalous mole fraction effect without single filing. *Biophys. J.* **95**, 609–619 (2008)
- Gong, X., Li, J., Xu, K., Wang, J., Yang, H.: A controllable molecular sieve for Na^+ and K^+ ions. *J. Am. Chem. Soc.* **132**, 1873–1877 (2010)
- Gu, L.-Q., Dalla Serra, M., Vincent, J.B., Vigh, G., Cheley, S., Braha, O., Bayley, H.: Reversal of charge selectivity in transmembrane protein pores by using noncovalent molecular adaptors. *Proc. Natl. Acad. Sci.* **97**, 3959–3964 (2000)
- Guo, F., Jankova, K., Schulte, L., Vigild, M.E., Ndoni, S.: Surface modification of nanoporous 1,2-polybutadiene by atom transfer radical polymerization or click chemistry. *Langmuir* **26**, 2008–2013 (2010)

- Gyurcsanyi, R.E., Pergel, E., Nagy, R., Kapui, I., Lan, B.T.T., Toth, K., Bitter, I., Linder, E.: Direct evidence of ionic fluxes across ion-selective membranes: a scanning electrochemical microscopic and potentiometric study. *Anal. Chem.* **73**, 2104–2111 (2001)
- Hamill, O.P., Marty, A., Neher, E., Sakmann, B., Sigworth, F.J.: Improved patch-clamp techniques for high-resolution current recording from cells and cell-free membrane patches. *Pflügers Arch.* **391**, 85–100 (1981)
- He, Y., Gillespie, D., Boda, D., Vlasiouk, I., Eisenberg, R.S., Siwy, Z.S.: Tuning transport properties of nanofluidic devices with local charge inversion. *J. Am. Chem. Soc.* **131**, 5194–5202 (2009)
- Heinemann, S.H., Terlau, H., Stühmer, W., Imoto, K., Numa, S.: Calcium channel characteristics conferred on the sodium channel by single mutations. *Nature* **356**, 441–443 (1992)
- Heins, E.A., Baker, L.A., Siwy, Z.S., Mota, M.O., Martin, C.R.: Effect of crown ether on ion currents through synthetic membranes containing a single conically shaped nanopore. *J. Phys. Chem. B* **109**, 18400–18407 (2005)
- Heng, L.Y., Hall, E.A.H.: Taking the plasticizer out of methacrylic-acrylic membranes for K⁺-selective electrodes. *Electroanalysis* **12**, 187–189 (1999)
- Heng, L.Y., Hall, E.A.H.: Producing 'self-plasticizing' ion-selective membranes. *Anal. Chem.* **72**, 42–51 (2000)
- Heng, L.Y., Toth, K., Hall, E.A.: Ion-transport and diffusion coefficients of non-plasticized methacrylic-acrylic ion-selective membranes. *Talanta* **63**, 73–87 (2004)
- Hess, P., Tsien, R.W.: Mechanism of ion permeation through calcium channels. *Nature* **309**, 453–456 (1984)
- Hille, B.: *Ion Channels Excitable Membranes*, 2nd edn. Sinauer Associates Inc, Sunderland (1992)
- Höltzel, A., Tallarek, U.: Ionic conductance of nanopores in microscale analysis systems: where microfluidics meets nanofluidics. *J. Sep. Sci.* **30**, 1398–1419 (2007)
- Honig, B., Nicholls, A.: Classic electrostatics in biology and chemistry. *Science* **268**, 1144–1149 (1995)
- Hou, X., Jiang, L.: Learning from nature: building bio-inspired smart nanochannels. *ACS Nano* **3**, 3339–3342 (2009)
- Hou, X., Dong, H., Zhu, D., Jiang, L.: Fabrication of stable single nanochannels with controllable ionic rectification. *Small* **6**, 361–365 (2010)
- Huang, Z., Zhang, W., Yu, J., Gao, D.: Nanoporous alumina membranes for enhancing hemodialysis. *J. Med. Devices* **1**, 79–83 (2007)
- Im, W., Roux, B.: Ion permeation and selectivity of OmpF porin: a theoretical study based on molecular dynamics, Brownian dynamics, and continuum electrodiffusion theory. *J. Mol. Biol.* **322**, 851–869 (2002a)
- Im, W., Roux, B.: Ions and counterions in a biological channel: a molecular dynamics simulation of OmpF porin from *Escherichia coli* in an explicit membrane with 1 M KCl aqueous salt solution. *J. Mol. Biol.* **319**, 1177–1197 (2002b)
- Izadi-Najafabadi, A., Futaba, D.N., Lijima, S., Hata, K.: Ion diffusion and electrochemical capacitance in aligned and packed single-walled carbon nanotubes. *J. Am. Chem. Soc.* **132**, 18017–18019 (2010)
- Jiang, Z., Stein, D.: Electrofluidic gating of chemically reactive surface. *Langmuir* **26**, 8161–8173 (2010)
- Jin, T.: Selective transport of potassium ions across a planar lipid phospholipid bilayer by a calix[4]arene-crown-5 as a synthetic carrier. *J. Chem. Soc. Perkin Trans.* **2**, 151–154 (2002)
- Jog, P.V., Gin, M.S.: A light-gated synthetic ion channel. *Org. Lett.* **10**, 3693–3696 (2008)
- Jung, Y., Bayley, H., Movileanu, L.: Temperature-responsive protein pores. *J. Am. Chem. Soc.* **128**, 15332–15340 (2006)
- Kang, X.-F., Cheley, S., Rice-Ficht, A.C., Bayley, H.: A storable encapsulated bilayer chip containing a single protein nanopore. *J. Am. Chem. Soc.* **129**, 4701–4705 (2007)
- Karnik, R., Fan, R., Yue, M., Li, D., Yang, P., Majumdar, A.: Electrostatic control of ions and molecules in nanofluidic transistors. *Nano Lett.* **5**, 943–948 (2005)
- Karshikoff, A., Spassov, V., Cowan, S.W., Ladenstein, R., Schirmer, T.: Electrostatic properties of two porin channels from *Escherichia coli*. *J. Mol. Biol.* **240**, 372–384 (1994)

- Kim, J.S., Shon, O.J., Rim, J.A., Kim, S.K., Yoon, J.: Pyrene-armed calix[4]azacrowns as new fluorescent ionophores: 'Molecular Teakowndo' process via fluorescence change. *J. Org. Chem.* **67**, 2348–2351 (2002)
- Koçer, A., Walko, M., Feringa, B.L.: Synthesis and utilization of reversible and reversible light-activated nanovalves derived from the channel protein MscL. *Nat. Protoc.* **2**, 1426–1437 (2007)
- Koder, R.L., Anderson, J.L.R., Solomon, L.A., Reddy, K.S., Moser, C.C., Dutton, P.L.: Design and engineering of an O₂ transport protein. *Nature* **458**, 305–310 (2009)
- Krauss, D., Gillespie, D.: Sieving experiments and pore diameter: it's not a simple relationship. *Eur. Biophys. J.* **39**, 1513–1521 (2010)
- Lee, S.W., Shang, H., Haasch, R.T., Petrova, V., Lee, G.U.: Transport and functional behavior of poly(ethylene glycol)-modified nanoporous alumina membranes. *Nanotechnology* **16**, 1335–1340 (2005)
- Li, A.P., Müller, F., Birner, A., Nielsch, K., Gösele, U.: Hexagonal pore arrays with a 50–420 nm interpore distance formed by self-organization in anodic alumina. *J. Appl. Phys.* **84**, 6023–6026 (1998)
- Li, X., Shen, B., Yao, X.-Q., Yang, D.: Synthetic chloride channel regulates cell membrane potentials and voltage-gated calcium channels. *J. Am. Chem. Soc.* **131**, 13676–13680 (2009)
- Linford, M.R., Chidsey, C.E.D.: Alkyl monolayers covalently bonded to silicon surfaces. *J. Am. Chem. Soc.* **115**, 12631–12632 (1993)
- Linn, K.M., Derebe, M.G., Jiang, Y., Valiyaveetil, F.I.: Semisynthesis of NaK, a Na⁺ and K⁺ conducting ion channel. *Biochemistry*. **49**, 4450–4456 (2010)
- Liu, C., Walter, D., Neuhauser, D.: Molecular recognition in crown ethers. *J. Am. Chem. Soc.* **125**, 13936–13937 (2003)
- Lockhart, J.C.: New host-guest carriers. *J. Chem. Soc. Faraday Trans.* **82**, 1161–1167 (1986)
- Lodish, H., Berk, A., Zipursky, S.L., Matsudaira, P., Baltimore, D., Darnell, J.: *Molecular Cell Biology*, 4th edn. WH Freeman, New York (2000)
- Lutz, J.-F., Börner, H.G., Weichenhan, K.: Combining ATRP and "click" chemistry: a promising platform toward functional biocompatible polymers and polymer bioconjugates. *Macromolecules* **39**, 6376–6383 (2006)
- Mach, T., Chimere, C., Fritz, J., Fertig, N., Winterhalter, M., Fütterer, C.: Miniaturized planar lipid bilayer: increased stability, low electric noise and fast fluid perfusion. *Anal. Bioanal. Chem.* **390**, 841–846 (2008)
- MacKinnon, R.: Potassium channels. *FEBS Lett.* **555**, 62–65 (2003)
- MacKinnon, R.: Nobel lecture. Potassium channels and the atomic basis of selective ion conduction. *Biosci. Rep.* **24**, 75–100 (2004)
- Malmstadt, N., Nash, M.A., Purnell, R.F., Schmidt, J.J.: Automated formation of lipid bilayer membranes in a microfluidic device. *Nano Lett.* **6**, 1961–1965 (2006)
- Malmstadt, N., Jeon, T.-J., Schmidt, J.J.: Long-lived planar lipid bilayer membranes anchored to an in situ polymerized hydrogel. *Adv. Mater.* **20**, 84–89 (2008)
- Masuda, H., Fukuda, K.: Ordered metal nanohole arrays made by a two-step replication of honeycomb structures of anodic alumina. *Science* **268**, 1466–1468 (1995)
- Maurer, J.A., White, V.E., Dougherty, D.A., Nadeau, J.L.: Reconstitution of ion channels in agarose-supported silicon orifices. *Biosens. Bioelectron.* **22**, 2577–2584 (2007)
- McCleskey, E.W.: Ion channel selectivity using an electric stew. *Biophys. J.* **79**, 1691–1692 (2000)
- Meier, P.C., Morf, W.E., Läubli, M., Simon, W.: Evaluation of the optimum composition of neutral-carrier membrane electrodes with incorporated cation-exchanger sites. *Anal. Chim. Acta* **156**, 1–8 (1984)
- Meier, W., Nardin, C., Winterhalter, M.: Reconstitution of channel proteins in (polymerized) ABA triblock copolymer membranes. *Angew. Chem. Int. Ed.* **39**, 4599–4602 (2000)
- Miedema, H.: Surface potentials and the calculated selectivity of ion channels. *Biophys. J.* **82**, 156–159 (2002)
- Miedema, H., Meter-Arkema, A., Wierenga, J., Tang, J., Eisenberg, B., Nonner, W., Hektor, H., Gillespie, D., Meijberg, W.: Permeation properties of an engineered bacterial OmpF porin containing the EEEE-locus of Ca²⁺ channels. *Biophys. J.* **87**, 3137–3147 (2004)

- Miedema, H., Vrouenraets, M., Wierenga, J., Eisenberg, B., Gillespie, D., Meijberg, W., Nonner, W.: Ca^{2+} selectivity of a chemically modified OmpF with reduced pore volume. *Biophys. J.* **91**, 4392–4400 (2006a)
- Miedema, H., Vrouenraets, M., Wierenga, J., Eisenberg, B., Schirmer, T., Baslé, A., Meijberg, W.: Conductance and selectivity fluctuations in D127 mutants of the bacterial porin OmpF. *Eur. Biophys. J.* **36**, 13–22 (2006b)
- Miedema, H., Vrouenraets, M., Wierenga, J., Meijberg, W., Robillard, G., Eisenberg, B.: A biological porin engineered into a molecular, nanofluidic diode. *Nano Lett.* **7**, 2886–2891 (2007)
- Miller, C.: Ion channels: doing hard chemistry with hard ions. *Curr. Opin. Chem. Biol.* **4**, 148–151 (2000)
- Miller, C.: Ion channels go to Stockholm—this time as proteins. *Neuron* **40**, 1049–1051 (2003)
- Naumowicz, M., Kotynska, J., Petelska, A., Figaszewski, Z.: Impedance analysis of phosphatidylcholine membranes modified with valinomycin. *Eur. Biophys. J.* **35**, 239–246 (2006)
- Neher, E., Sakmann, B.: Single-channel currents recorded from membrane of denervated frog muscle fibres. *Nature* **260**, 799–802 (1976)
- Neher, E., Sakmann, B.: The patch clamp technique. *Sci. Am.* **266**, 44–51 (1992)
- Nestorovich, E.M., Rostovtseva, T.K., Bezrukov, S.M.: Residue ionization and ion transport through OmpF channels. *Biophys. J.* **85**, 3718–3729 (2003)
- Nijnenhuis, W.F., Buitenhuis, E.G., de Jong, F., Sudhölter, E.J.R., Reinhoudt, D.N.: Calixcrowns as selective potassium cation carriers in supported liquid membranes. *J. Am. Chem. Soc.* **113**, 7963–7968 (1991)
- Nishizawa, M., Menon, V.P., Martin, C.R.: Metal Nanotubule membranes with electrochemically switchable ion transport selectivity. *Science* **268**, 700–702 (1995)
- Nonner, W., Eisenberg, B.: Ion permeation and glutamate residues linked to Poisson-Nernst-Planck theory in L-type calcium channels. *Biophys. J.* **75**, 1287–1305 (1998)
- Nonner, W., Catacuzzeno, L., Eisenberg, B.: Binding and selectivity in L-type calcium channels: a mean spherical approximation. *Biophys. J.* **79**, 1976–1992 (2000)
- Noskov, S.Y., Roux, B.: Ion selectivity in potassium channels. *Biophys. Chem.* **124**, 279–291 (2006)
- Noskov, S.Y., Bernèche, S., Roux, B.: Control of ion selectivity in potassium channels by electrostatic and dynamic properties of carbonyl ligands. *Nature* **431**, 830–834 (2004)
- Parsegian, A.: Energy of an ion crossing a low dielectric membrane: solutions to four relevant electrostatic problems. *Nature* **221**, 844–846 (1969)
- Pasparakis, G., Krasnogor, N., Cronin, L., Davis, B.G., Alexander, C.: Controlled polymer synthesis – from biomimicry to synthetic biology. *Chem. Soc. Rev.* **39**, 286–300 (2010)
- Pedersen, C.J.: Cyclic polyethers and their complexes with metal salts. *J. Am. Chem. Soc.* **89**, 7017–7036 (1967)
- Peng, Q., Tang, H.: Synthesis of a novel calix[4]arene-based fluorescent ionophore and its metal ions recognition properties. *Chin. Chem. Lett.* **20**, 13–16 (2009)
- Peters, T.A., Poeth, C.H.S., Benes, N.E., Buijs, H.C.W.M., Vercauteren, F.F., Keurentjes, J.T.F.: Ceramic-supported thin PVA pervaporation membranes combining high flux and high selectivity; contradicting the flux-selectivity paradigm. *J. Membr. Sci.* **276**, 42–50 (2006)
- Pfeifer, J.R., Reiss, P., Koert, U.: Crown ether-gramicidin hybrid ion channels: dehydration-assisted ion selectivity. *Angew. Chem. Int. Ed.* **45**, 501–504 (2006)
- Phale, P.S., Philippsen, A., Widmer, C., Pahe, V.P., Rosenbusch, J.P., Schirmer, T.: Role of charged residues at the OmpF porin channel constriction probed by mutagenesis and simulation. *Biochemistry* **40**, 6319–6325 (2001)
- Popat, K.C., Mor, G., Grimes, C.A., Desai, T.A.: Surface modification of nanoporous alumina surfaces with poly(ethylene glycol). *Langmuir* **20**, 8035–8041 (2004)
- Pressman, B.C.: Induced active transport of ions in mitochondria. *Proc. Natl. Acad. Sci. U.S.A.* **53**, 1076–1083 (1965)
- Ren, D., Navarro, B., Xu, H., Yue, L., Shi, Q., Clapham, D.E.: A prokaryotic voltage-gated sodium channel. *Science* **294**, 2372–2375 (2001)
- Rezac, M.E., Koros, W.J.: Preparation of polymer-ceramic composite membranes with thin defect-free separating layers. *J. Appl. Polym. Sci.* **46**, 1927–1938 (1992)

- Rodriguez, J.D., Vaden, T.D., Lisy, J.M.: Infrared spectroscopy of ionophore-model systems: hydrated alkali metal ion 18-crown-6 ether complexes. *J. Am. Chem. Soc.* **131**, 17277–17285 (2009)
- Römer, W., Steinem, C.: Impedance analysis and single-channel recordings on nano-black lipid membranes based on porous alumina. *Biophys. J.* **86**, 955–965 (2004)
- Sackmann, E.: Tethered membranes. *J. Biotechnol.* **74**, 135–136 (2000)
- Saint, N., Lou, K.-L., Widmer, C., Luckey, M., Schirmer, T., Rosenbusch, J.P.: Structural and functional characterization of OmpF porin mutants selected for larger pore size. *J. Biol. Chem.* **271**, 20676–20680 (1996)
- Sakai, N., Sordé, N., Das, G., Perrotet, P., Gerard, D., Matile, S.: Synthetic multifunctional pores: deletion and inversion of anion/cation selectivity using pM and pH. *Org. Biomol. Chem.* **1**, 1226–1231 (2003)
- Sakai, N., Mareda, J., Matile, S.: Artificial β -barrels. *Acc. Chem. Res.* **41**, 1354–1365 (2008)
- Sakmann, B., Neher, E.: Patch clamp techniques for studying ionic channels in excitable membranes. *Annu. Rev. Physiol.* **46**, 455–472 (1984)
- Saxena, K., Drosou, V., Maier, E., Benz, R., Ludwig, B.: Ion selectivity reversal and induction of voltage-gating by site-directed mutations in the *Paracoccus denitrificans* porin. *Biochemistry* **38**, 2206–2212 (1999)
- Schirmer, T.: General and specific porins from bacterial outer membranes. *J. Struct. Biol.* **121**, 101–109 (1998)
- Schirmer, T., Phale, P.S.: Brownian dynamics simulation of ion flow through porin channels. *J. Mol. Biol.* **294**, 1159–1167 (1999)
- Schmuhl, R., ten Elshof, J.E., Keizer, K., van den Berg, A.: Tunable ion-selective inorganic membranes. *Desalination* **146**, 29–33 (2002)
- Schoch, R.B., Han, J., Renaud, P.: Transport phenomena in nanofluidics. *Rev. Mod. Phys.* **80**, 839–882 (2008)
- Schulz, G.E.: The structure of bacterial outer membrane proteins. *Biochem. Biophys. Acta.* **1565**, 308–317 (2002)
- Shenoy, D.K., Barger, W.R., Singh, A., Panchal, R.G., Misakian, M., Stanford, V.M., Kasianowicz, J.J.: Functional reconstitution of protein ion channels into planar polymerizable phospholipid membranes. *Nano Lett.* **5**, 1181–1185 (2005)
- Shi, N., Ye, S., Alam, A., Chen, L., Jiang, Y.: Atomic structure of a Na^+ and K^+ conducting channel. *Nature* **440**, 570–574 (2006)
- Siwy, Z.S.: Ion current rectification in nanopores and nanotubes with broken symmetry. *Adv. Funct. Mater.* **16**, 735–746 (2006)
- Siwy, Z., Heins, E., Harrell, C.C., Kohli, P., Martin, C.R.: Conical-nanotube ion-current rectifiers: the role of surface charge. *J. Am. Chem. Soc.* **126**, 10850–10851 (2004)
- Song, K.M., Hong, W.H.: Dehydration of ethanol and isopropanol using tubular type cellulose acetate membrane with ceramic support in pervaporation process. *J. Membr. Sci.* **123**, 27–33 (1997)
- Sparreboom, W., van den Berg, A., Eijkel, J.C.T.: Principles and applications of nanofluidic transport. *Nat. Nanotechnol.* **4**, 713–720 (2009)
- Stark, G., Ketterer, B., Benz, R., Lauger, P.: The rate constants of valinomycin-mediated ion transport through thin lipid membranes. *Biophys. J.* **11**, 981–994 (1971)
- Stein, D., Kruitthof, M., Dekker, C.: Surface-charge-governed ion transport in nanofluidic channels. *Phys. Rev. Lett.* **93**, 035901 (2004)
- Steinem, C., Janshoff, A., von dem Bruch, K., Reihs, K., Goossens, J., Galla, H.-J.: Valinomycin-mediated transport of alkali cations through solid supported membranes. *Bioelectrochem. Bioenerg.* **45**, 17–26 (1998)
- Steinle, E.D., Mitchell, D.T., Wirtz, M., Lee, S.B., Young, V.Y., Martin, C.R.: Ion channel mimetic micropore and nanotube membrane sensors. *Anal. Chem.* **74**, 2416–2422 (2002)
- Stevens, C.F.: Inferences about membrane properties from electrical noise measurements. *Biophys. J.* **12**, 1028–1047 (1972)
- Sriemer, C.C., Gaborski, T.R., McGrath, J.L., Fauchet, P.M.: Charge- and size-based separation of macromolecules using ultrathin silicon membranes. *Nature* **445**, 749–753 (2007)

- Sudhölter, E.J.R., van der Wal, P.D., Skowronska-Ptasinska, M., van den Berg, A., Bergveld, P., Reinhoudt, D.N.: Modification of ISFETs by covalent anchoring of poly(hydroxyethyl methacrylate) hydrogel. Introduction of a thermodynamically defined semiconductor-sensing membrane interface. *Anal. Chim. Acta* **230**, 59–65 (1990)
- Thompson, A.N., Kim, I., Panosian, T.D., Iverson, T.M., Allen, T.W., Nimigean, C.M.: Mechanism of potassium channel selectivity revealed by Na and Li binding sites within the KcsA pore. *Nat. Struct. Mol. Biol.* **16**, 1317–1324 (2009)
- Thormann, A., Teuscher, N., Pfannmöller, M., Rothe, U., Heilmann, A.: Nanoporous aluminum oxide membranes for filtration and biofunctionalization. *Small* **3**, 1032–1040 (2007)
- Tieleman, D.P., Berendsen, H.J.C.: A molecular dynamics study of the pores formed by *Escherichia coli* OmpF porin in a fully hydrated plamitoyloleoylphosphatidylcholine bilayer. *Biophys. J.* **74**, 2786–2801 (1998)
- Titov, A.V., Wang, B., Sint, K., Král, P.: Controllable synthetic molecular channels: biomimetic ammonia switch. *J. Phys. Chem. B* **114**, 1174–1179 (2010)
- Van den Berg, A., Wessling, M.: Silicon for the perfect membrane. *Nature* **445**, 726 (2007)
- Varma, S., Jakobsson, E.: Ionization states of residues in OmpF and mutants: Effects of dielectric constant and interactions between residues and ionic strength. *Biophys. J.* **86**, 690–704 (2003)
- Varma, S., Sabo, D., Rempe, S.B.: K+/Na+ selectivity in K channels and valinomycin: over-coordination versus cavity-size constraints. *J. Mol. Biol.* **376**, 13–22 (2008)
- Vrouenraets, M., Miedema, H.: The ionization state of D37 in *E. coli* porin OmpF and the nature of conductance fluctuations in D37 mutants. *Eur. Biophys. J.* **39**, 1563–1571 (2010)
- Vrouenraets, M., Wierenga, J., Meijberg, W., Miedema, H.: Chemical modification of the bacterial porin OmpF: gain of selectivity by volume reduction. *Biophys. J.* **90**, 1202–1211 (2006)
- Wanunu, M., Meller, A.: Chemically modified solid-state nanopores. *Nano Lett.* **7**, 1580–1585 (2007)
- Wienk, M.M., Stolwijk, T.B., Sudhölter, E.J.R., Reinhoudt, D.N.: Stabilization of crown ether containing supported liquid membranes. *J. Am. Chem. Soc.* **112**, 797–801 (1990)
- Wipf, H.K., Simon, W.: Models for coupling mechanisms and carrier-induced alkali ion transport in mitochondrial membranes. *Helv. Chim. Acta* **53**, 1732–1740 (1970)
- Wipf, H.K., Olivier, A., Simon, W.: Mechanism and selectivity of alkali-ion transport in model membranes in the presence of valinomycin antibiotics. *Helv. Chim. Acta* **53**, 1605–1608 (1970)
- Wu, H.-C., Bayley, H.: Single-molecule detection of nitrogen mustards by covalent reaction within a protein nanopore. *J. Am. Chem. Soc.* **130**, 6813–6819 (2008)
- Wu, H.-C., Astier, Y., Maglia, G., Mikhailova, E., Bayley, H.: Protein nanopores with covalently attached molecular adapters. *J. Am. Chem. Soc.* **129**, 16142–16148 (2007)
- Yamaoka, K., Kinoshita, E., Seyama, I.: Altering ion selectivity of the L-type Ca channel cloned from frog cardiac myocytes. *Biophys. J. Suppl.* **84**, 402a (2003)
- Yang, J., Ellinor, P.T., Sather, W.A., Zhang, J.I.F., Tsien, R.W.: Molecular determinants of Ca²⁺ selectivity and ion permeation in L-type Ca²⁺ channels. *Nature* **366**, 158–161 (1993)
- Yoshida, W., Cohen, Y.: Ceramic-supported polymer membranes for pervaporation of binary organic/organic mixtures. *J. Membr. Sci.* **213**, 145–157 (2003)
- Yue, L., Navarro, B., Ren, D., Ramos, A., Clapham, D.E.: The cation selectivity filter of the bacterial sodium channel, NaChBac. *J. Gen. Physiol.* **120**, 845–853 (2002)
- Zhao, Y.H., Wee, K.H., Bai, R.: A novel electrolyte-responsive membrane with tunable permeation selectivity for protein purification. *ACS Appl. Mater. Interfaces* **2**, 203–211 (2010)

Chapter 5

Vesicle Arrays as Model-Membranes and Biochemical Reactor Systems

Sune M. Christensen and Dimitrios Stamou

Abstract Self-assembled nanocontainers in the form of small unilamellar lipid vesicles have gathered broad interest due to their applications as intelligent drug carriers, as biophysical model-membrane systems and as biochemical reaction vessels. Immobilisation (arraying) of single vesicles on a solid support permits detailed characterisation of vesicle preparations using surface sensitive techniques, in particular fluorescence microscopy. Its biocompatible nature makes a vesicle an ideal host for water soluble and membrane integral biomolecules and in this respect a vesicle comprises an ultra-miniaturised 3D “scaffold” ($\text{\O} \geq 13 \text{ nm}$) ideally suited for reconstitution of biochemical processes. Surface-based single vesicle arrays opens new vistas for the highly parallel examination of vesicle-reconstituted biology in a high throughput format and with high spatial and temporal resolution. Here we will highlight the most prominent contributions to date on the fabrication and the applications of surface-based single vesicle systems.

5.1 Introduction

A lipid vesicle, comprising a lipid bilayer membrane enclosing an aqueous lumen, is a structure with restricted inherent function. However, vesicles can be readily functionalised with organic and inorganic moieties (see Fig. 5.1a) creating an autonomous, complex system of nanoscopic dimensions. This “scaffold” can host motifs that would allow identity encoding, specific biorecognition (sensing or screening),

S.M. Christensen (✉) • D. Stamou
Bio-Nanotechnology Laboratory, Department of Neuroscience and Pharmacology,
Nano-Science Center & Lundbeck Foundation Center Biomembranes in Nanomedicine,
Center for Pharmaceutical Nanotechnology and Nanotoxicology, University of Copenhagen,
The HC Ørsted Institute, Universitetsparken 5, 2100 Copenhagen, Denmark
e-mail: sunemc@nano.ku.dk; stamou@nano.ku.dk

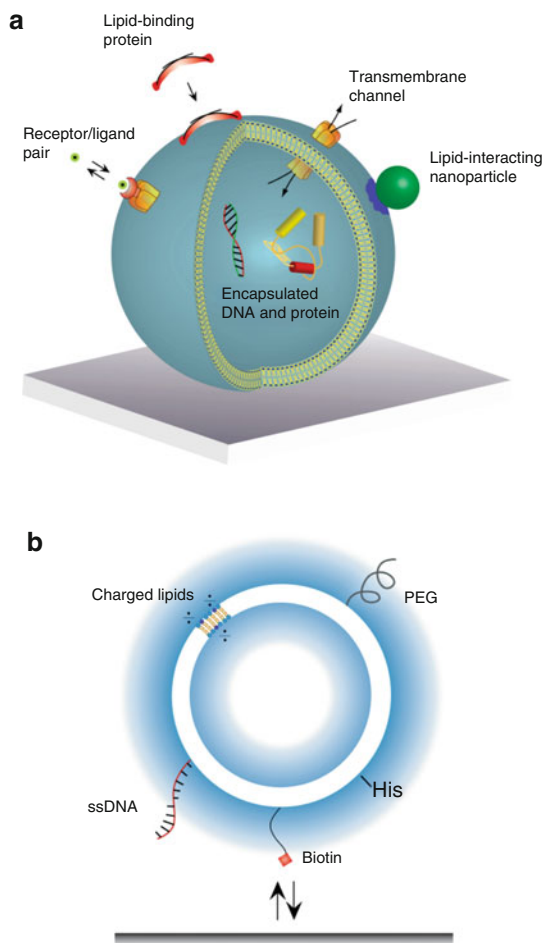


Fig. 5.1 Single surface-immobilised vesicle as an autonomous 3D biomimetic scaffold for the reconstitution of biochemical processes. **(a)** Examples on various biochemical processes reconstituted in a vesicle including ligand binding to a membrane embedded receptor (Pick et al. 2004), lipid-protein interactions (Bhatia et al. 2009), transport of solutes through a membrane integral channel (Stamou et al. 2003; Cisse et al. 2007; Okumus et al. 2009) and nanoparticle templated phase separation (Wang et al. 2008). Encapsulation of soluble entities in the vesicle lumen, e.g. DNA and proteins, allows spatial fixation of few or single molecules without the need for surface conjugation of the molecule(s) of interest (Roy et al. 2008). **(b)** Molecular determinants of vesicle-surface interactions. Specific immobilisation onto a surface can be mediated by different binding pairs, e.g. biotin/streptavidin, DNA hybridisation or histidine/NTA. To prevent non-specific interactions it is often desirable to introduce repulsive forces between the vesicle and a surface. Two strategies to obtain this are to incorporate charged lipids (electrostatic repulsion) or poly-ethylene-glycol (PEG) lipid conjugates (repulsive force of entropic origin) in the membrane

biochemical reactions or targeted delivery of reactants. Furthermore, its biomimetic nature makes it an ideal environment for the reconstitution and preservation of transmembrane or water-soluble biomolecules. The possibility to simultaneously integrate and miniaturise at the nanometre scale such a broad range of functions allows one to perform a variety of experiments in femto- to zeptolitre (10^{-15} l– 10^{-21} l) sized compartments and in an unprecedented ultra high throughput fashion using surface-based single vesicle arrays (Stamou et al. 2003; Christensen and Stamou 2007).

In this chapter we review the *fabrication* and the *applications* of surface-based vesicle systems with emphasis on single vesicles. In the first section we consider the main parameters that control vesicle immobilisation and how patterned surfaces can be used to direct the self-assembly of highly ordered arrays of static or mobile vesicles. We discuss how quantitative information on vesicle size and the concentration of encapsulated or membrane-bound molecules can be assessed from fluorescence microscopy data. Furthermore, we review essential results that underscore the potential of surface immobilised vesicles as a robust and quantitative assaying platform by showing that vesicles retain encapsulated molecules and are non-deformed upon immobilisation.

In the second part we focus on applications of single vesicle arrays for screening/sensing of (i) biochemical reactions taking place within the vesicle lumen, (ii) the activity of transmembrane protein channels and (iii) protein-lipid interactions as a function of membrane curvature.

5.2 Production and Interrogation of Surface-Based Single Vesicle Arrays

Immobilisation of vesicles on a solid support allows highly parallel single vesicle analysis using microscopy based detection schemes. In this section we outline the principle technical advancements that established single vesicle arrays as a robust biochemical assaying platform.

5.2.1 Vesicle Immobilisation on Surfaces

The fundamental step in production of single vesicle arrays on surfaces is the process of vesicle adsorption from solution. The adsorption of vesicles to inorganic substrates has been studied extensively with a number of techniques including surface plasmon resonance (SPR), acoustic devices (quartz crystal microbalance, QCM, and surface acoustic wave devices, SAW), fluorescence microscopy and atomic force microscopy (AFM). SPR provides ensemble information on vesicle adsorption (Stora et al. 2000) and has been used for quantification of adsorption kinetics. QCM also records an effective total mass but when operated in dissipation mode it yields in addition

information regarding vesicle morphology from which it can be deduced whether vesicles on average are intact or have ruptured to form a supported bilayer (Reimhult et al. 2003; Gizeli and Glad 2004; Keller and Kassemø 1998). Fluorescence microscopy allows one to follow individual vesicle adsorption events (Johnson et al. 2002). AFM resolves the topography of vesicles and bilayer patches resulting from vesicle rupture but is insufficient for recording of fast kinetics and is furthermore complicated by the non-rigid vesicle bilayer (Schönherr et al. 2004; Reviakine and Brisson 2000). Among the investigated substrates are silicon oxides (Keller and Kassemø 1998; Johnson et al. 2002), titanium dioxide (Reimhult et al. 2003), gold (Reimhult et al. 2003) and SAM modified surfaces (Jenkins et al. 2002).

Strong interactions between the bilayer of an adsorbed vesicle and the solid support leads to vesicle deformation which induces stress in the bilayer. If the stress exceeds a critical threshold the bilayer becomes unstable leading to pore opening (Lenz et al. 2006) and eventually vesicle rupture and formation of a supported membrane patch (generally considered to occur at 2–4% relative expansion of the bilayer (Boucher et al. 2007)). Vesicle rupture is promoted by surface hydrophobicity (Reimhult et al. 2003), low electrostatic repulsion (Cremer and Boxer 1999; Richter et al. 2003) and high vesicle surface density (Keller and Kassemø 1998; Johnson et al. 2002; Richter et al. 2003). Direct adsorption of a vesicle onto a surface is generally not desirable for utilising the vesicle as a model membrane system because it perturbs the bilayer and thereby influences reconstituted biochemical processes.

To achieve more gentle vesicle immobilisation a number of specific tethering methods based on chemical and biological ligation have been developed, e.g. the receptor-ligand pair of biotin/streptavidin (Bäumle et al. 2004). Soft-matter modified templates are generally more versatile compared to bare solid substrates since non-specific binding can be controlled and reduced to a minimum and the diversity of biological binding pairs (e.g. DNA) allows the assembly of systems with multiple components. Biorecognition moieties have been incorporated to lipid membranes mainly through coupling to phospholipids (Patolsky et al. 2001) or alternatively by using lipophilic anchors such as alkane chains (Yoshina-Ishii et al. 2005) or cholesterol (Pheiffer and Höök 2004). Figure 5.1b illustrates three of the most commonly applied vesicle-surface tethers: biotin, ssDNA and the histidine tag. Biotin binds to streptavidin with high affinity (González et al. 1999) ($KD \sim 10^{-15}$ M) but in an irreversible manner making it useful for the precise and stable positioning of single vesicles on a surface (Stamou et al. 2003). Histidine-NTA was originally developed for protein purification and tagging but was recently adopted for immobilising vesicles and bilayers (Stora et al. 2000; Gizeli and Glad 2004). Contrary to biotin-streptavidin it allows for reversible chelation mediated by Ni^{2+} complexation (Geissbuehler et al. 2005). The duplex formation of DNA oligonucleotides is useful as a more advanced recognition system that allows multiplexing and potentially self assembly driven sorting of mixed vesicle solutions on predefined patterns of the complementary sequences (i.e. a DNA array) (Yoshina-Ishii et al. 2005; Pheiffer and Höök 2004; Dusseiller et al. 2005; Städler et al. 2004; Yoshina-Ishii and Boxer 2003).

To fine tune vesicle-surface interactions it is often useful to integrate surface-repelling elements into the vesicle membrane (Fig. 5.1b). This can be achieved, e.g. by enhancing the percentage of charged lipids in the bilayer, thereby increasing

electrostatic repulsion. Another possibility to prevent non-specific interactions is to functionalise the vesicle membrane with lipid conjugates of poly-ethylene-glycol (PEG) of varying molecular weight (Hansen et al. 2003). At low surface densities (typically below 1 mol%) the polymer is in a mushroom conformation that acts as an entropic shield preventing vesicle adsorption on surfaces. The combination of surface repulsive elements and specific tethers is essential in achieving immobilisation of intact and non-deformed vesicles (further discussed in Sects. 5.3 and 5.4).

5.2.2 *Single Vesicle Arrays*

Single vesicles and their content can be monitored in a massively parallel manner ($>10^8$ per cm^2) by fluorescence microscopy once adsorbed onto a solid support (Fig. 5.2a). This fact motivates the idea to utilise libraries of immobilised vesicles for high throughput screening experiments. A critical issue for this concept is the identification of the individual vesicles in such a library. To date there has been no conclusive answer to this problem. However, the recent commercialisation of several imaging-based DNA sequencing platforms (Metzker 2010), with resolution down to even single DNA-oligonucleotides, has opened for the opportunity to apply DNA-based encoding schemes (Clark et al. 2009). Although the issue of encoding has to be resolved in order to harvest the full potential of single vesicle arrays for multiplexing purposes at the current stage single vesicle arrays comprise extremely useful platforms for parallelised single vesicle experiments.

Ordered arrays of single vesicles have been produced by patterning a surface into single vesicle binding sites using either colloidal particle lithography (Michel et al. 2002) or high-resolution micro-contact printing (Renault et al. 2003). Stamou et al. (2003) realised such an array by incubating an array of streptavidin functionalised spots fabricated by micro-contact printing with two types of biotinylated vesicles, each labelled with distinct fluorophores (Fig. 5.2b).

The absence of co-localisation of the red and green signals (Fig. 5.2b inset) demonstrates single vesicle positioning. In applications where the high order and (ultra) high density of immobilised vesicles is not critical it is often advantageous to work with a non-patterned (random) single vesicle array. A random single vesicle array can be obtained simply by incubating a homogenous vesicle-binding surface with a dilute solution of vesicles (Fig. 5.2c) (Hatzakis et al. 2009; Bhatia et al. 2009).

5.2.3 *Fluorescence-Based Sizing of Individual Immobilised Vesicles*

To take full advantage of single vesicle arrays for performing quantitative measurements it is critical to be able to assess the physical dimensions of individual vesicle containers. In fluorescence micrographs vesicles with sizes below the optical resolution appear as diffraction limited spots (Fig. 5.3a, b). Our lab has developed a method

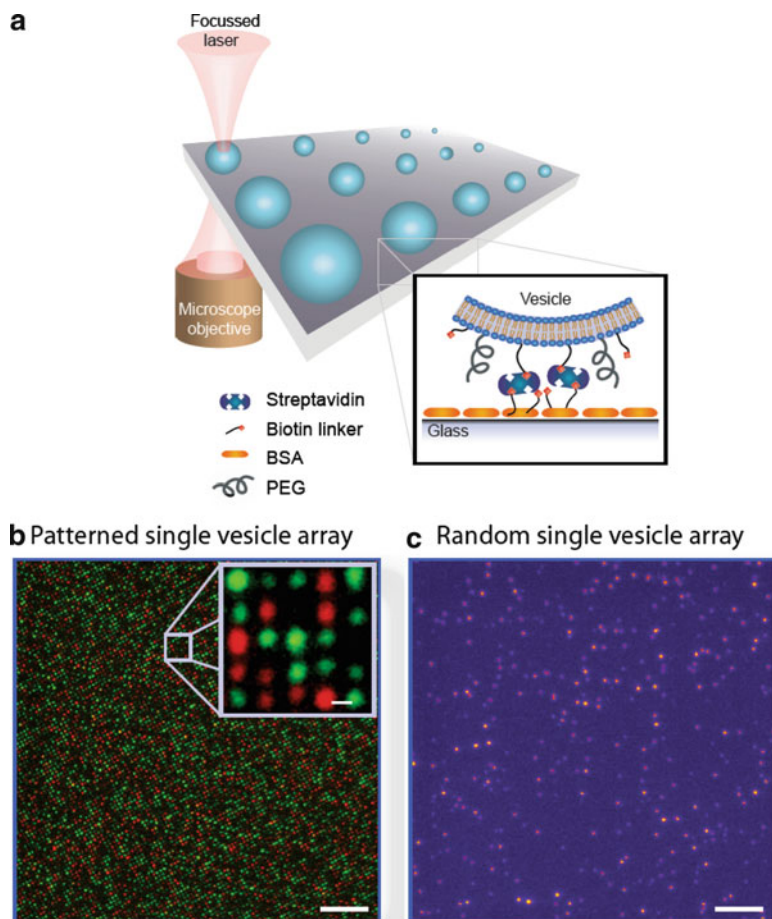


Fig. 5.2 Single vesicle arrays. **(a)** Sketch of individual vesicles arrayed on a surface. The vesicles are interrogated by fluorescence microscopy. Vesicle tethering is typically achieved using the receptor/ligand pair of streptavidin/biotin where the receptor is attached to the surface and the vesicles carry biotinylated lipids. In order to avoid non-specific interactions between vesicles and the surface the solid support is passivated using either a layer of bovine serum albumin (*BSA*) (Stamou et al. 2003), poly-L-lysine grafted poly-ethylene-glycol (*PLL-g-PEG*) (Bendix et al. 2009) or a supported lipid bilayer (Bendix et al. 2009). **(b)** Micrograph of a single vesicle array. High resolution micro-contact printing was used to define an array of vesicle binding sites (as sketched in *a*) where the dimensions of the spots were similar to the size of subsequently bound vesicles. This setup was optimised to address single vesicles at each spot. The image shows an array presenting two distinctly labelled vesicle populations (the image is an overlay of the *red* and the *green* channel) (Figure adapted from Stamou et al. (2003). Copyright Wiley-VCH Verlag GmbH & Co. KGaA. Reproduced with permission. **(c)** Micrograph of a random single vesicle array (*bright spots* correspond to individual vesicles)). Bars in **(b)** and **(c)** are 10 μm , the bar on the inset in **b** is 500 nm

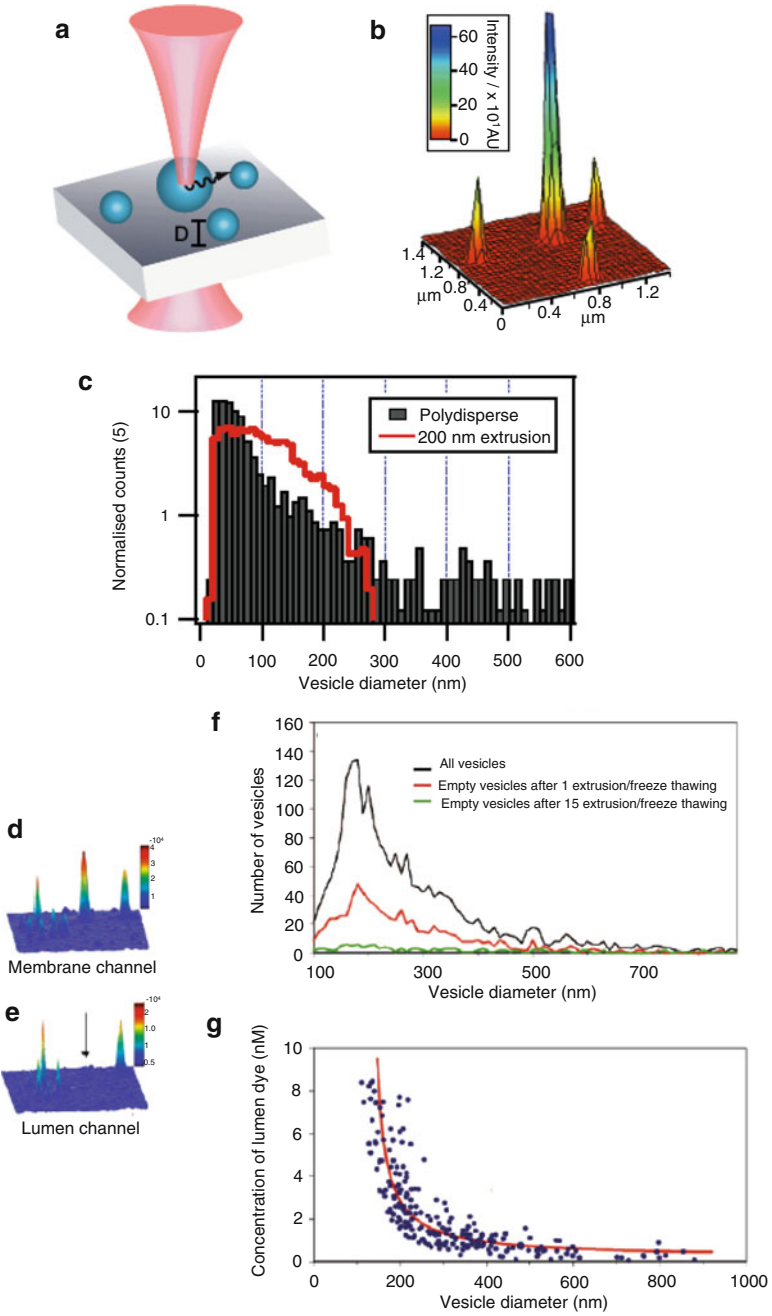
for quantifying the diameter of single imaged vesicles within 5 nm accuracy by taking advantage of the proportionality between vesicle diameter and the integrated fluorescence intensity of a dye incorporated in the vesicle membrane (vesicle diameter $\propto \sqrt{\text{membrane area}} \propto \sqrt{\text{intensity}}$) (Kunding et al. 2008; Lohr et al. 2009). To obtain the proportionality factor the intensity distribution of a calibration vesicle sample measured by fluorescence microscopy is aligned with the size distribution measured by transmission electron microscopy at cryogenic temperatures (cryoTEM) or dynamic light scattering (DLS). The calibration sample is typically vesicles extruded through polycarbonate membranes with pores of 50 or 100 nm diameter to narrow the size distribution thus allowing examination by cryoTEM and DLS that are incompatible with polydisperse samples. With the calibration factor determined the intensity of a given vesicle can be converted to its physical diameter.

This technique was used to map the size distribution of a polydisperse (non-extruded) vesicle population (Fig. 5.3c), a measurement that is inaccessible to conventional techniques. This enabled, for the first time, the comparison of a vesicle sample before and after extrusion (Fig. 5.3c) revealing that the major effect of extrusion is to introduce an upper cutoff in vesicle sizes: vesicles larger than the pore diameter of the filter are broken into smaller vesicles while vesicles below the pore size of the filter are left unaltered. The method for quantification of vesicle size from fluorescence intensity data forged the fundament for a range of quantitative studies on single vesicles. In particular, it opened up for systematic studies of size dependent phenomena (see Sects. 5.4 and 5.8) that to this end had only been qualitatively described by ensemble measurements that are compromised by averaging over the inherent polydispersity of vesicle preparations.

5.3 Encapsulation Efficiency Measured on Single Vesicles

Immobilised vesicles have been shown to be intact to large molecules (proteins and fluorophores) (Johnson et al. 2002) and capable of sustaining ionic gradients (Stamou et al. 2003). Unpublished results from our group even suggests that a small ion like Na^+ can be stably encapsulated over a matter of days. The supreme tightness is central to the potential of vesicles as biochemical reactors since it permits confining not only larger molecules like proteins and DNA but allows sustaining a stable ionic nanoenvironment.

Figure 5.3d, e show the fluorescence intensity of single immobilised vesicles carrying a lipophilic dye in the membrane and a water soluble dye in the lumen (Lohse et al. 2008). In this experiment the vesicles were immobilised on a BSA passivated glass surface decorated with streptavidin. The images demonstrate that, surprisingly, not all vesicles have encapsulated dye (arrow in Fig. 5.3e highlights an empty vesicle). Figure 5.3f shows the number of empty vesicles as a function of vesicle diameter showing that empty vesicles were present for all investigated vesicle sizes. Copious extrusion and freeze-thawing cycles, procedures known to enhance encapsulation efficiency, greatly reduced the number of empty vesicles,



demonstrating that the phenomena relates to vesicle preparation and is not induced upon immobilisation. This conclusion has been further supported by imaging of diffusing vesicles in solution that confirmed the presence of empty vesicles also before immobilisation (Lauge et al. unpublished results). By quantifying the number of encapsulated fluorophores from the fluorescence intensity of the encapsulated dye (a procedure equivalent to the size calibration scheme described above) it was possible to assess the encapsulation efficiency as a function of vesicle size revealing that the dye upconcentrated in small vesicles (Fig. 5.3g) (Lohse et al. 2008). At this stage it is, however, unclear how this tendency emerges. Single vesicle characterisation of encapsulation efficiency is important for the optimisation of vesicle-based drug delivery formulations (Lasic and Needham 1995) and is also essential to the design of single vesicle based reactor systems.

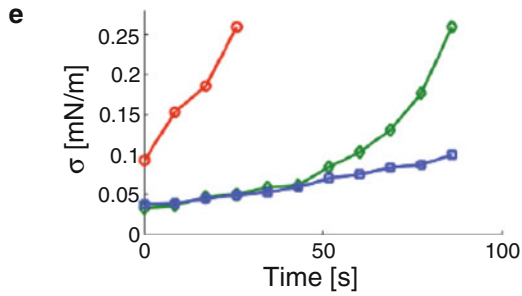
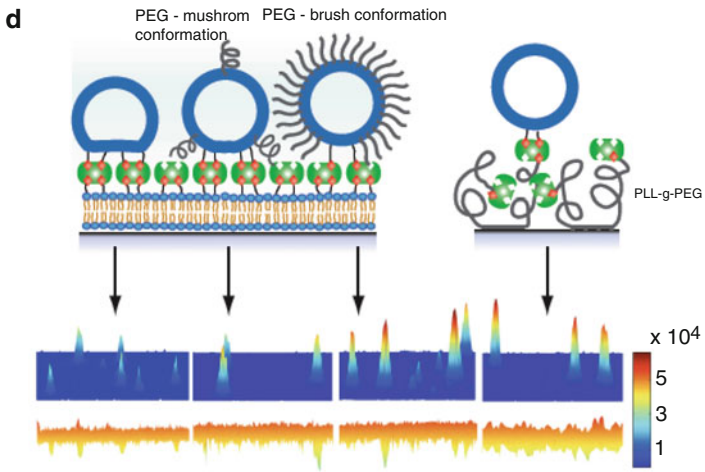
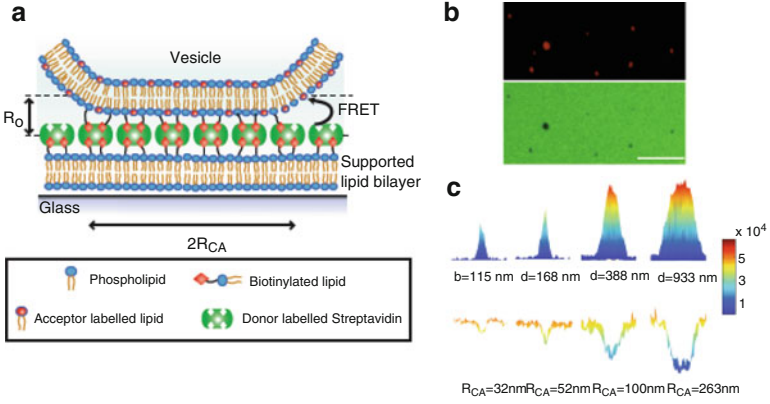
5.4 Quantification of Vesicle-Surface Contact Areas

Ideally one strives to achieve stable vesicle immobilisation without unwanted perturbations arising from strong interactions with the underlying support. Strong adhesion between the vesicle bilayer and a surface will deform the vesicle thereby inducing unwanted stress in the system. Our laboratory has developed a method for quantifying subresolution contact areas between vesicles tethered to functionalised substrates allowing the quantitative assessment of vesicle deformation (Bendix et al. 2009).

The geometry of a vesicle deformed at a streptavidin functionalised substrate due to strong adhesion is sketched in Fig. 5.4a. By embedding a fluorescence



Fig. 5.3 Fluorescence based sizing of individual immobilised vesicles and measurement of encapsulation efficiency on single vesicles. (a) Vesicles of different diameter immobilised on a solid support. The vesicles are labelled with lipophilic dyes and probed by fluorescence (confocal) microscopy. (b) Surface plot of fluorescence intensity of single vesicles appearing as diffraction limited spots. Vesicle fluorescence intensities were quantified by integrating the intensity-peaks and used for calculation of the physical size (vesicle diameter $\propto \sqrt{\text{membrane area}} \propto \sqrt{\text{intensity}}$). The proportionality factor was obtained by measuring a calibration sample (extruded vesicles) with fluorescence microscopy and either cryoTEM or dynamic light scattering (DLS) and aligning the intensity and the size distributions. With knowledge of the proportionality factor the diameter of a given vesicle in a fluorescence micrograph can be obtained. (c) The technique was applied for measuring the size distribution of a polydisperse vesicle sample which cannot be attained by conventional techniques. This permitted examination of the same sample before and after extrusion (using filters with 200 nm pore diameter) revealing that extrusion introduces an upper cut off in vesicle diameters. Note the significant overlap of the distributions before and after extrusion. (d-e) Surface plots of fluorescence intensity of a membrane label and a vesicle-encapsulated dye (CoroNa Green) revealing the presence of empty vesicles (arrow). (f) Number of loaded and empty vesicles as a function of diameter (black line) and number of empty vesicles after 1 (red line) and 15 (green line) extrusion and freeze-thawing cycles, respectively. (g) Concentration of encapsulated dye as a function of vesicle diameter showing that small vesicles encapsulate relatively more dye (Fig. a–c reprinted from (Kunding et al. 2008) with permission from Elsevier. Figure d–g adapted from (Lohse et al. 2008), Copyright 2008 American Chemical Society)



resonance energy transfer (FRET) pair in the streptavidin layer (FRET donor) and the vesicle membrane (FRET acceptor) with a Förster Radius (R_0) matching the interbilayer separation quantitative information of the contact zone geometry can be assessed by observing the reduction in donor intensity due to FRET. Figure 5.4b shows a fluorescence micrograph of immobilised vesicles (top) and the streptavidin layer (bottom), respectively. Clear FRET footprints are observed in the donor (streptavidin) channel. By theoretical calculations the footprint produced by a non-deformed vesicle of a given size was obtained. Footprints with donor reduction exceeding that of a non-deformed vesicle are indicative of vesicle deformation. By a simple calibration measurement on giant vesicles adsorbed to the streptavidin layer the expected FRET per contact zone area was obtained which allowed mapping the radius of the contact zone for vesicles with dimensions below the optical resolution (Fig. 5.4c).

Different systems were examined to determine the optimal conditions for vesicle immobilisation (Fig. 5.4d). Without PEG conjugated lipids in the vesicle membrane deformation was observed for vesicles with diameters as small as 200 nm (Fig. 5.4d). In the presence of 1% or 5% PEG lipids on the vesicles larger vesicles showed only small footprints. Alternatively, vesicles were immobilised on a PLL-*g*-PEG functionalised surface. In this setup no deformation could be observed for vesicles with diameters below 1 μm . Thus, vesicles can be securely immobilised without significant deformation either by including PEGylated lipids in the bilayer or, more conveniently, by using a PLL-*g*-PEG coated support.

Knowledge of vesicle size and the area of the contact zone is sufficient to calculate the effective contact angle between the vesicle and the surface from which the tension in the bilayer can be readily obtained (Bendix et al. 2009). This opens for



Fig. 5.4 Quantification of nanoscale contact areas between a vesicle and a functionalised surface. (a) Sketch of the contact area formed between a deformed immobilised vesicle and a streptavidin decorated substrate. Quantitative information on the radius of the contact area (R_{CA}) was obtained by measuring Förster Resonance Energy Transfer (FRET) between donor dyes on the streptavidin layer and acceptor dyes in the vesicle membrane. R_0 depicts the Förster radius. (b) Fluorescence micrographs of small vesicles with radius ≈ 100 nm (top) and the streptavidin layer (bottom). FRET footprints are observed as a reduction in donor intensity. Bar: 5 μm . (c) Surface plot of fluorescence intensity of immobilised vesicles (top) and corresponding plots of fluorescence from the donor labelled streptavidin layer (bottom). By comparing theoretical and experimental results the degree of vesicle deformation upon immobilisation can be evaluated. The obtained vesicle diameters, d , and the radii of the mapped contact areas are indicated below the single vesicle intensity plots. (d) When 1 mol% PEGylated lipids was added on the vesicles the degree of deformation was reduced (resulting in smaller FRET footprints). At 5 mol% PEG in the vesicles the polymer enters a brush conformation leading to long-range repulsion and further reduction in deformation. Coating of the glass support with PLL-*g*-PEG prevented deformation of vesicles carrying no PEGylated lipids. On this type of surface FRET footprints were never observed for vesicles with diameters below 1 μm . (e) Time resolved measurements of single vesicle contact areas used to quantitatively evaluate the tension in the bilayer as a function of time. In this example the tension increases due to strong laser illumination (Karatekin et al. 2003). The graphs shows data for three vesicles of different size (circles, vesicle diameter $d = 362$ nm, diamonds; $d = 778$ nm and squares; $d = 1,272$ nm) (Figure adapted from Bendix et al. 2009)

the application of immobilised vesicles as nanoscopic sensors of membrane tension which provides a tool for probing mechanical changes in the membrane induced, e.g. by binding of proteins on the bilayer or thermotropic phase transitions. In Fig. 5.4e time resolved measurements of single vesicle contact areas were used to probe the increase in bilayer tension upon exposing the vesicles to strong laser illumination (a procedure known to increase the tension in dye containing bilayers (Karatekin et al. 2003)). As a function of time (exposure) bilayer tensions was found to increase thus establishing a proof of concept for the method.

5.5 Mobile Surface-Tethered Vesicles

To this point we discussed single vesicle systems where the vesicles remain fixed upon immobilisation. Several laboratories (e.g. ref. (Pheiffer and Höök 2004; Yoshina-Ishii and Boxer 2003)) have developed alternative platforms where immobilised vesicles retain lateral mobility upon surface coupling. This has been accomplished by tethering of vesicles onto fluid supported bilayers via binding of a linker on the vesicle to an anchor embedded in the bilayer, Fig. 5.5a (Pheiffer and Höök 2004; Yoshina-Ishii and Boxer 2003). In this way vesicles can diffuse in the surface plane enabling imaging of single particle trajectories and, e.g. measurement of diffusion coefficients (Yoshina-Ishii and Boxer 2003; Simonsson et al. 2010). The reported diffusion coefficients vary between 0.1 and 1 $\mu\text{m}^2/\text{s}$ (Yoshina-Ishii and Boxer 2003; Benkoski and Höök 2005) which is comparable to the diffusion of lipids in supported bilayers (Tamm and McConnell 1985). The mobility of surface tethered vesicles has been found to depend on the number of anchors per vesicle, the anchor length and the interactions of the tethered vesicle with the supporting layer (Benkoski and Höök 2005).

The use of patterned bilayers allows the confinement of mobile vesicles inside well-defined fluid domains (Groves and Boxer 2002). This has been employed to selectively assemble ssDNA tagged vesicles into a chessboard array by encoding the supported bilayer with cDNA as depicted on Fig. 5.5a (Yoshina-Ishii and Boxer 2003). The type of vesicles present at each spot in the array was controlled by sequential modulation of the concentration and type of cDNA oligos (Yoshina-Ishii et al. 2005). The movement of surface-mobile vesicles inside such fluid domains can in addition be directed by applying an electric field in the surface plane, which has been proven capable of sorting two populations of vesicles due to their difference in charge (Yoshina-Ishii and Boxer 2006).

The most powerful application of the mobile vesicle platform is likely for assaying of intermembrane interactions because the interacting membranes in this setup can be tracked unambiguously through all steps of the process. Intermembrane interactions are of utmost importance to many aspects of cellular life including the secretory pathway in eukaryotes (Bonifacino and Glick 2004), synaptic transmission (Sudhof and Rothman 2009), juxtacrine signalling (Salaita et al. 2010) and virus infection. A first step in this direction was reported by Chan et al. (Chan et al. 2007) that performed single particle measurements of vesicle-vesicle docking

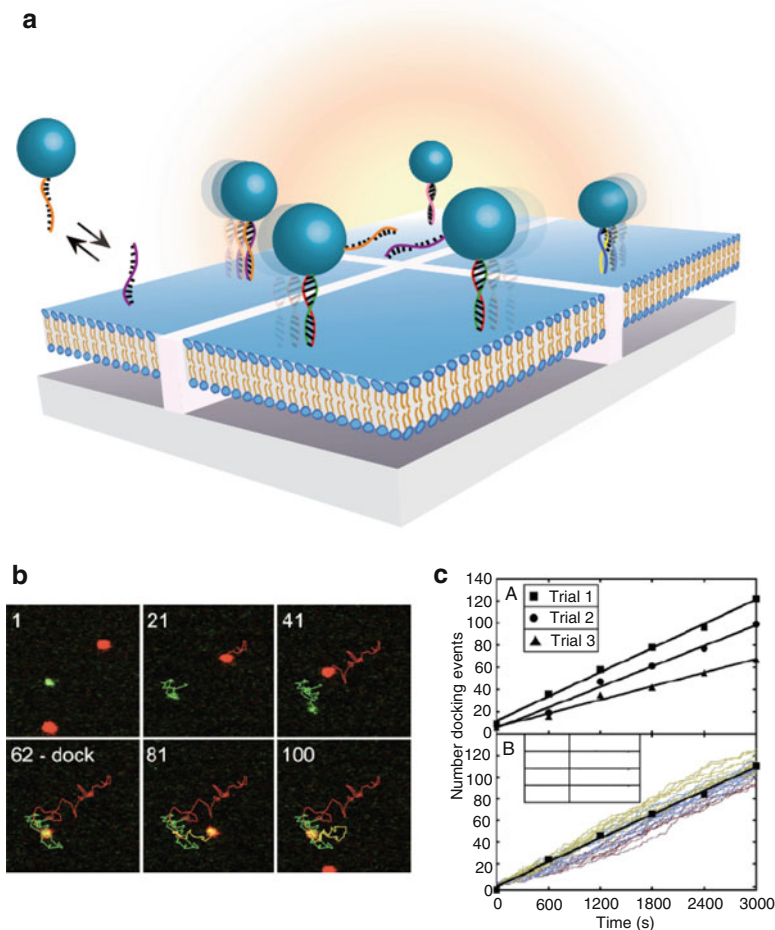


Fig. 5.5 Mobile surface-tethered vesicles. **(a)** Sketch of vesicles tethered to a supported bilayer via ssDNA conjugated to cognate bilayer embedded DNA anchors. The bound vesicles are able to diffuse parallel to the bilayer surface. Patterning of the supported bilayer can be used to constrict vesicle diffusion. **(b)** A docking reaction between two vesicles mediated by DNA hybridisation (as indicated on the two vesicles in the front in a) tracked by dual-colour fluorescence microscopy. **(c) Top:** Number of observed docking events as a function of time in three different experiments (trials). **Bottom:** the docking kinetics were modelled taking as input the initial vesicle coordinates and the diffusion coefficient of the vesicles. By iterating through possible values of the docking probability upon collision of a vesicle pair (P_{dock}) the docking probability in the given experiment was taken as the one that yielded the theoretical curve that best resembled the trend of the data (Fig. 5.5b, c adapted from Chan et al. (2007) copyright 2007 National Academy of Sciences U.S.A.)

reactions mediated by DNA hybridisation (Fig. 5.5a). Two populations of vesicles labelled with distinct fluorophores were tethered to a supported bilayer allowing the direct monitoring of docking between individual vesicle pairs (Fig. 5.5b). By counting the total number of docking events the probability that a collision leads

to docking could be extracted with the aid of a diffusion model (Fig. 5.5c). The work has not yet been extended for monitoring of vesicle-vesicle fusion reactions. Vesicle-vesicle fusion, however, has been examined quite extensively in an assay where statically immobilised vesicles are allowed to interact with vesicles diffusing freely in solution (Yoon et al. 2006; Yoon et al. 2008; Lee et al. 2010).

5.6 Applications of Surface-Based Single Vesicle Systems

An intact surface-tethered vesicle constitutes a biomimetic nanoscaffold onto which one can assemble molecular components and integrate various functions. In the previous section we considered methods to immobilise and arrange vesicles on surfaces and touched upon several applications of these systems for studying vesicle preparations. In this section we will focus on techniques and methods to access the interior of vesicles and the use of these miniaturised experimental volume-systems to perform confined reactions, sense ion channel activity and screening of lipid-protein interactions as a function of membrane curvature.

5.6.1 Methods to Mix Solutes Inside Vesicle Reactors

To carry out controlled (bio) chemical reactions in vesicles one has to devise appropriate techniques that allow the mixing of reactants. This problem has been solved by different strategies relying on electrical, mechanical, optical or thermal interaction with the lipid bilayer.

At an early stage Chiu et al. demonstrated how to mix the interior volume of selected single giant vesicle pairs (1–5 μm in diameter) in solution (Chiu et al. 1999). This was obtained by trapping two vesicles using optical tweezers, bringing the vesicles together and inducing mixing of their initially separated contents by delivering a voltage pulse causing the vesicles to fuse. Orwar and co-workers developed a novel method to create networks of surface tethered giant vesicles by establishing connections, in the form of hollow lipid nanotubes (tube diameter ≈ 100 nm), between adjacent vesicles using micromanipulators (Karlsson et al. 2001). Common to both mixing strategies is the use of micromanipulators (e.g. micropipettes or tweezers) to assemble and manipulate single vesicles with diameters larger than one micrometer (volumes in the femtolitre regime).

Bolinger et al. developed an alternative method to trigger mixing inside surface-tethered giant vesicles taking advantage of the fact that bilayers show a maximum in permeability at their phase transition temperature due to packing defects (Bolinger et al. 2004). This property of bilayers was utilised to systematically release cargo (a self-quenched dye) from small unilamellar vesicles (SUVs) with volumes in the attolitre (1 aL = 10^{-18} l) regime trapped in the lumen of the giant vesicles. This was accomplished by elevating the temperature across the membrane phase transition of the enclosed SUVs (and not the giant vesicles) giving rise to dequenching of the dye.

The nested system was produced by rehydration of the giant vesicle lipid mixture in a solution of the cargo-loaded SUVs. This platform was subsequently used to titrate an enzyme trapped in the lumen of individual giant vesicles with substrates in two consecutive steps by employing SUVs with different phase transition temperatures (Fig. 5.6a) (Bolinger et al. 2008). Figure 5.6b shows fluorescence micrographs of the process and Fig. 5.6c shows the corresponding fluorescence traces. The possibility to use nested containers, comprising SUVs with several different lipid compositions, allows one to release reactants in a programmed manner and perform a number of confined sequential reactions within single giant vesicles. This is the most advanced example to date of a fluidic soft-matter based nanoscale device.

The aforementioned strategies to mix solutes inside vesicle containers have diverse advantages. With the micromanipulation founded strategies (Karlsson et al. 2001; Karlsson et al. 2004; Lizana et al. 2009) one has to manipulate single vesicles sequentially which practically excludes high-throughput experiments but allows precise interaction with selected vesicles. The method of Bolinger et al. (2004, 2008) relies on a change in temperature as the trigger and is therefore more appropriate to address ensembles of containers in parallel.

To further tune the permeability properties of vesicles one can also use the plethora of membrane proteins and peptides naturally developed for this purpose, e.g. channels or transporters with high selectivity to the size and polarity of molecules and ions (Gouaux and MacKinnon 2005). Several examples on this topic can be found in the literature including (i) the peptide gramicidin A, used to control the pH inside immobilised vesicles (Stamou et al. 2003) (ii) pore forming bacterial proteins (OmpF or alpha-hemolysin) used to continuously fuel a reaction taking place in the vesicle lumen (Graff et al. 2001; Yoshimoto et al. 2005; Noireaux and Libchaber 2004) and (iii) reconstitution of the acceptor for λ -phage that allowed specific loading of DNA in targeted vesicles (Graff et al. 2002). Transmembrane molecules have been combined with surface-immobilised vesicles on surprisingly few occasions in comparison to ensemble studies in solution.

5.6.2 Probing of Transmembrane Protein Channels

Transmembrane protein channels are of utmost importance to cells for controlling the flow of substances over cellular membranes and they comprise important drug targets. Robust assays for functional screening of this protein family are thus important both for gaining mechanistic insight and as tools in drug discovery. The nanoscopic dimensions of vesicles could potentially provide access to functional screening of single transporters and ion channels in an unprecedented parallelised manner using the single vesicle array format. As a first step toward this vision Stamou et al. measured the activity of a pore forming peptide (Gramicidin A) on single immobilised vesicles (Stamou et al. 2003). Kuyper et al. in a subsequent contribution took advantage of single vesicles for resolving the fine structure of passive proton permeation through the bilayer (Kuyper et al. 2006).

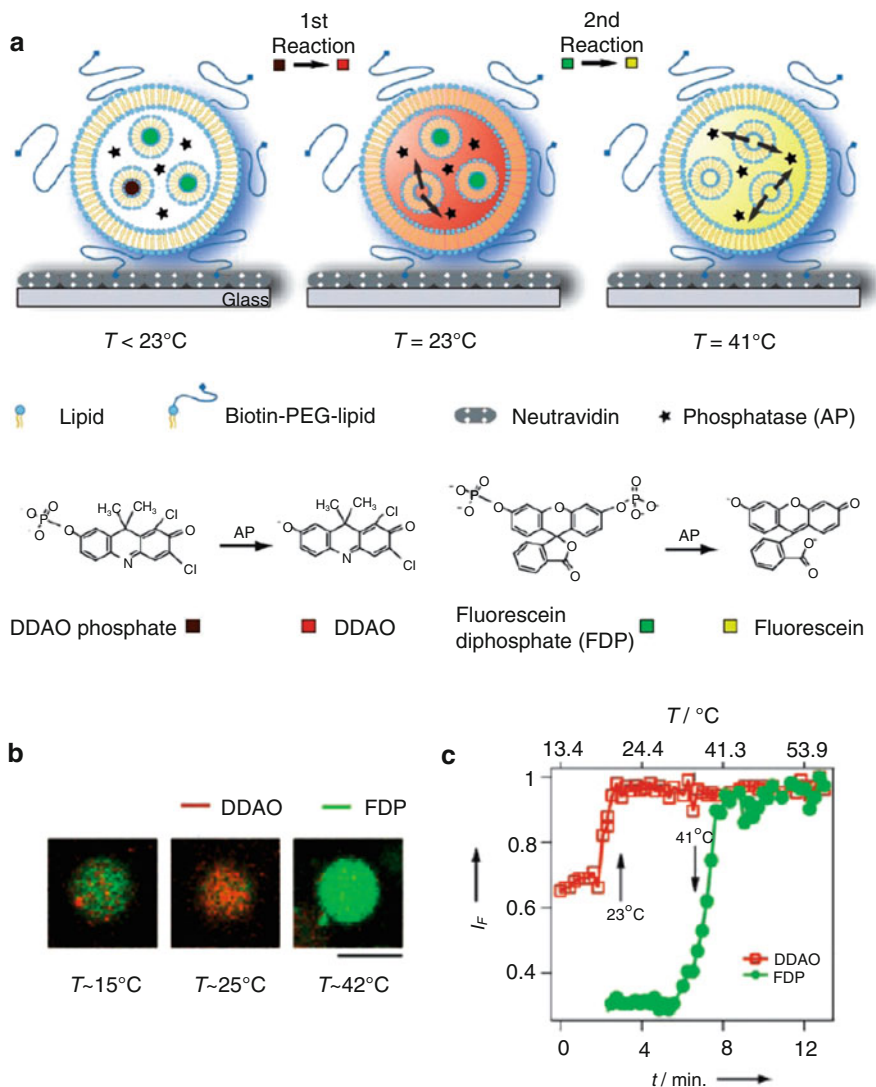


Fig. 5.6 Self-assembled fluidic device: consecutive enzymatic reactions triggered in single giant unilamellar vesicles. **(a)** The external surface of a giant vesicle is decorated with biotinylated lipids for immobilisation on a neutravidin-coated glass coverslip. Alkaline phosphatase (AP, star) is incorporated in the giant vesicle together with two different kinds of small unilamellar vesicles (SUVs), each loaded with a different non-fluorescent substrate for the enzyme. The first kind of SUV ($T_1 \approx 23^\circ\text{C}$) is loaded with dichlorodimethylacridinone (DDAO) phosphate (dark red) and the second kind of SUV ($T_2 \approx 41^\circ\text{C}$) is loaded with fluorescein diphosphate (FDP, dark green). An increase of temperature triggers the release of the substrates in two consecutive steps at the corresponding phase-transition temperatures. After release from the SUVs, the substrates are confined in the lumen of the giant vesicle where they are processed to their respective fluorescent products, DDAO (red) and FDP (green), by the enzyme. **(b)** Fluorescence micrographs of the process depicted in a. Bar: 10 μm . **(c)** Fluorescence intensity traces demonstrating sequential release of substrates and production of DDAO and FDP in a single giant vesicle during a temperature ramp (Figure adapted from Bolinger et al. (2008). Copyright Wiley-VCH Verlag GmbH & Co. KGaA. Reproduced with permission)

In a more advanced setting Pick et al. demonstrated activation of a ligand-gated ion channel (serotonin-gated 5-hydroxytryptamine type-3 receptor, 5-HT 3R) using immobilised “native” vesicles produced directly from the plasma membrane of cells overexpressing the receptor (Pick et al. 2004). The vesicles were derived by incubating surface-attached cells with cytochalasin B (a vesicle budding promoter) and applying a shear stress (vortexing). Agonist-mediated calcium influx in single vesicles evoked directly comparable responses to whole cell measurements thus supporting the idea of using vesicle arrays for screening of ion channel activity. An elegant aspect of this work is that it bypasses the need for protein purification although this is achieved on the expense of a well-defined lipid and protein composition.

It is generally challenging to resolve the kinetics of solute influx/efflux through transmembrane protein channels on individual SUVs ($\text{\AA} \leq 200$ nm) due to their small size and the speed with which solutes (especially ions) are filled/emptied from the vesicles once diffusive contact is established between the lumen and the surrounding medium. This property is, however, extremely useful for probing of channels with very low permeability. Bränden et al. recently demonstrated quantitative measurements of the permeability properties of an aquaglyceroporin by immobilising SUVs harboring the reconstituted porin on an SPR (surface-plasmon resonance) compatible surface (Bränden et al. 2010). This approach permitted label-free probing of the efflux kinetics of sugar alcohols into the immobilised vesicles. Because the vesicles in this setup were immobilised on the sensor surface permeability of the porin towards several sugar alcohols could be measured on the same set of vesicles by exchanging the sugar solution via a flow system.

With improvements in sensitivity, e.g. by employing fluorescence microscopy for detection, it should in principle be possible to push the immobilised vesicle platform to achieve quantitative measurements on single channels in individual vesicles. This would comprise an entirely new method for single channel recordings that would offer, e.g. (i) access to single channel analysis of slow transporters and, importantly, (ii) dramatically increased data throughput (hundreds to thousands of vesicles measured in one experiment compared to a single data point per run in a conventional ensemble (Bangham 1968) or patch pipette setup (Hamill et al. 1981)).

5.7 Vesicle Encapsulation for Single Molecule Studies

Encapsulation of soluble entities in a surface-tethered vesicle allows the spatial localisation of few or single macromolecules while keeping the encapsulant(s) under physiological conditions (in contrast to direct surface conjugation which remains the prevailed method for single molecule experiments) (Boukobza et al. 2001; Roy et al. 2008). In this manner the encapsulated species can be probed within single vesicles, e.g., using vibrational (Cristobal et al. 2006) or fluorescence spectroscopy (Boukobza et al. 2001). At the very limit this platform can be used to acquire measurements at the single molecule level. This was first demonstrated by Boukobza et al. who used immobilised vesicles to monitor rotational dynamics of single proteins (Boukobza

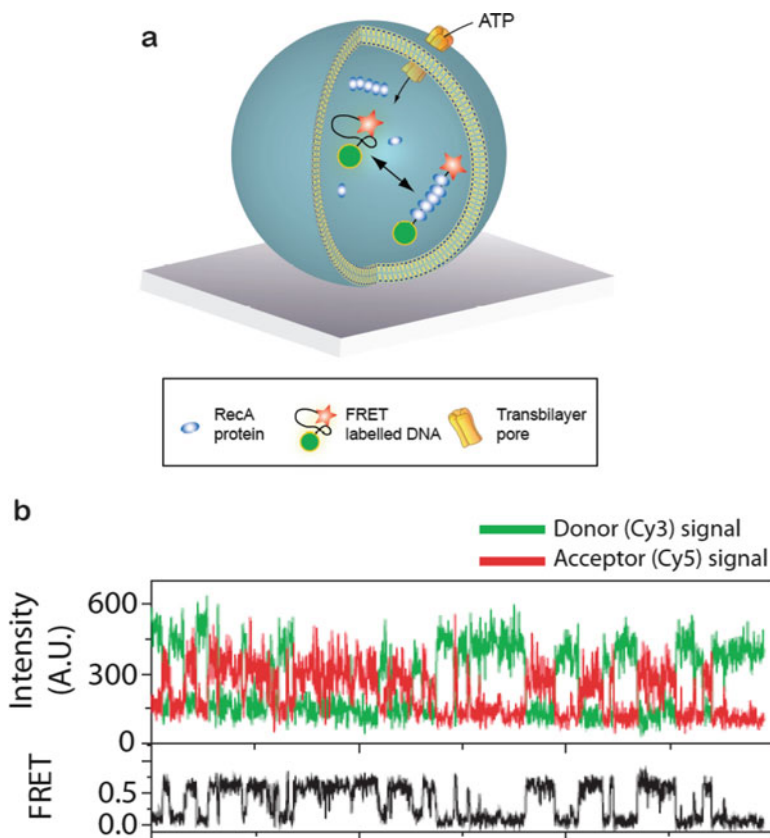


Fig. 5.7 Single molecule monitoring of protein-DNA interactions driven by ATP in a single surface-tethered vesicle. **(a)** A single strand of DNA labelled with a FRET pair encapsulated inside a surface-tethered vesicle together with the ATPase RecA (approximately seven copies per vesicle). In the cell RecA is active in DNA-repair upon ATP-regulated polymerisation on DNA. Upon RecA assembly the DNA is stretched giving rise to a reduction in FRET. The vesicle is permeable to small molecules (<1 nm diameter) via pores in the membrane introduced either by utilising a lipid mixture with a phase transition at the temperature of the experiment (Cisse et al. 2007) or using the bacterial toxin alpha-hemolysin (Okumus et al. 2009). Repeated polymerisation/dissociation reactions were triggered by exchange of ATP through the pores. **(b)** Fluctuations between stretched (low FRET) and unstretched (high FRET) states of the DNA (Fig. 5.7b adapted from Cisse et al. (2007)) copyright 2007 National Academy of Sciences U.S.A.)

et al. 2001). Comparison of surface-conjugated and vesicle-encapsulated proteins revealed that at the surface the rotational freedom of the molecule was greatly impeded while inside the vesicles the protein exhibited rotational properties identical, within detection uncertainty, to that in free solution. In a later study Rhoades et al. resolved structural fluctuations of single proteins trapped inside surface tethered vesicles using single molecule FRET (Rhoades et al. 2003) (see refs. (Choi et al. 2010; Okumus et al. 2004; Lee et al. 2005) for additional single molecule FRET experiments in vesicles).

In a more complex setup Ha and co-workers used single vesicle encapsulation to characterise intermolecular reactions between a single DNA strand and a handful of RecA proteins (Fig. 5.7a) (Cisse et al. 2007; Okumus et al. 2009). For the purpose of probing intermolecular association vesicle encapsulation is particularly useful in analysing low affinity interactions since even a single molecule in a 100 nm vesicle has a concentration of roughly 3 μM . By attaching FRET probes at the distal ends of the DNA strand folding and unfolding induced upon polymerisation of the RecA along the DNA was traced in real-time (Fig. 5.7b). An additional feature of this study is that the vesicles were made semipermeable either by employing lipids with a phase transition at the temperature of the experiment (Cisse et al. 2007) or by inserting alpha-hemolysin pores in the bilayer (Okumus et al. 2009). Both approaches allowed exchange of ATP/ADP over the vesicle membrane while retaining the proteins and DNA inside. In this way continued association/dissociation of the RecA upon ATP binding and subsequent hydrolysis could be observed enabling quantification of folding/unfolding rates.

Because vesicle composition can be easily controlled vesicle encapsulation should be an ideal experimental scene for investigating systematically how the local nanoenvironment influences the behaviour of single biomolecules. Furthermore, single vesicles offer the possibility to quantitatively examine the effect of spatial confinement on biochemical reactions.

5.8 Lipid-Protein Interactions and Membrane Curvature

In recent years it has become evident that membrane curvature has dramatic effects on a variety of membrane associated biological processes, e.g. enzymatic activity (Slater et al. 1994; Cajal et al. 2000), membrane fusion (Martens et al. 2007) and lipid-protein interactions (McMahon and Gallop 2005; Bhatia et al. 2010; Madsen et al. 2010). Traditionally, these effects have been probed by assays that measure the average activity of reconstituted proteins in the presence of vesicles extruded through polycarbonate membranes of different pore diameters. Despite extrusion, however, such preparations have in general on the order of 70% overlap (Fig. 5.3c and ref. (Kunding et al. 2008)). With the implementation of fluorescence based size calibration single vesicle arrays provide access to detailed screening of curvature dependent binding by taking advantage of the inherent polydispersity of vesicle samples; in this format each single vesicle provides a data point for a unique membrane curvature and a full spectrum of curvatures can be screened in one experiment (Bhatia et al. 2009; Hatzakis et al. 2009). Furthermore, the single particle format provides crucial information on heterogeneous behaviour among individual vesicles that is averaged out in conventional ensemble measurements (Bhatia et al. 2010; Madsen et al. 2010).

Figure 5.8a shows the setup in a single vesicle assay for screening of membrane curvature dependent protein binding. Vesicles with different diameters are immobilised on a solid support and incubated with the protein of interest. By dual colour

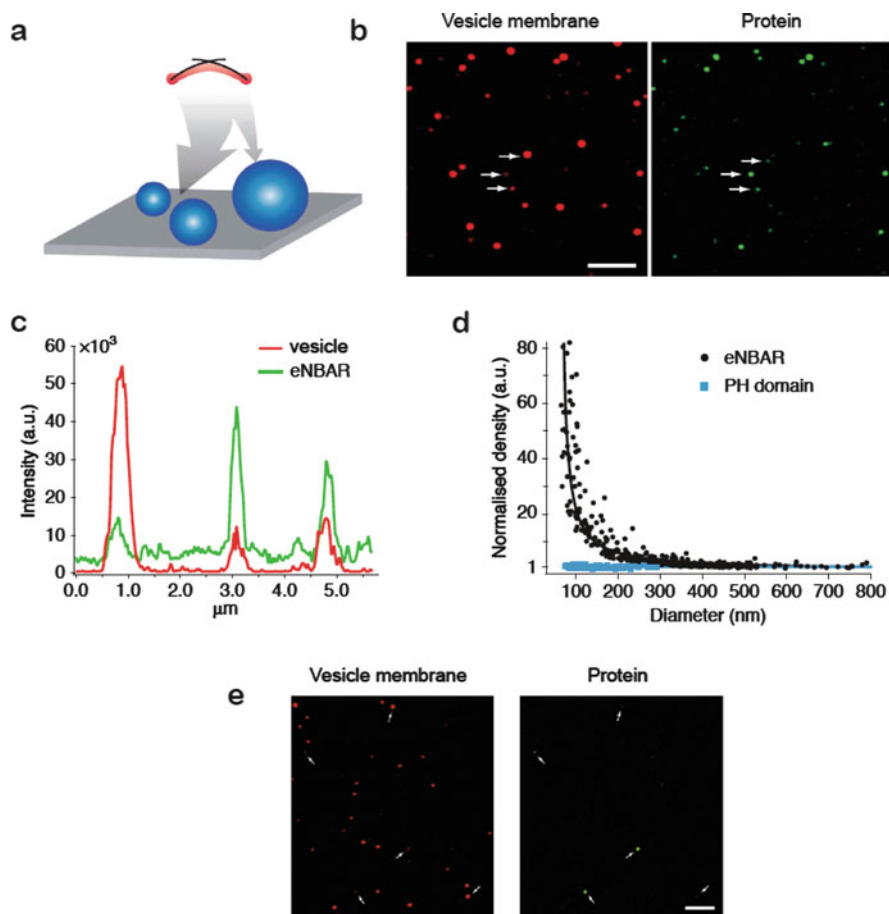


Fig. 5.8 Screening of membrane curvature dependent protein-lipid interactions. (a) Vesicles of different sizes, and therefore different membrane curvatures, are immobilised on a functionalised glass substrate and incubated with a lipid binding protein. (b) Fluorescence micrographs of vesicles and protein. Scale bar: 3 μm . (c) Line profiles of fluorescence intensity scanning over the three vesicles highlighted by the white arrows in b. (d) Density of bound protein as a function of vesicle diameter for binding of eNBAR, a protein containing a membrane curvature sensing amphiphatic helix, and a *PH* (Pleckstrin Homology) domain, which is known not to be a sensor of membrane curvature. The curves were constructed from single particle fluorescence intensities of vesicles and protein. The protein density was obtained as the ratio of protein intensity to vesicle membrane intensity (the number of bound protein molecules is directly proportional to the protein intensity and the membrane area is directly proportional to membrane intensity). The protein densities were normalised to 1 for large vesicles. (e) Fractional binding of eNBAR to vesicles at low (nM) protein concentration. Only a fraction of the vesicles is observed to have detectable amounts of protein bound. We acknowledge EMBO J. for permission to reprint the material in this figure which originally appeared in Bhatia et al. (2009)

fluorescence microscopy the location of vesicles, as well as their size, and the amount of bound protein is visualised (Fig. 5.8b, c). The ratio of the integrated intensity of the protein signal and the vesicle signal reveals the density of bound protein on each single vesicle. By performing this analysis for all vesicles at the surface a membrane curvature sensing graph can be constructed (Fig. 5.8d). Figure 5.8d shows data for protein binding mediated by an amphiphatic helix, a module that is known to be a sensor of membrane curvature, demonstrating increased protein density on highly curved vesicles. As a control, data for the PH (Pleckstrin Homology) domain is shown on Fig. 5.8d revealing a constant protein density in the investigated curvature range.

A rather surprising finding emerging from screening of protein binding on single vesicles is that for given conditions not all vesicles are observed to admit protein, Fig. 5.8e (Bhatia et al. 2009). The absolute number of vesicles that admit protein has been found to depend on vesicle size and protein concentration (Bhatia et al. 2009). This result has broad implications for ensemble assays in which such fractional binding behaviour would greatly obscure the interpretation of the average density of bound protein. If, e.g. a change in conditions leads to binding of protein on a higher number of the vesicles in an experiment while leaving the density of protein on the vesicles that have bound protein unaltered the conclusion of an ensemble assay would misleadingly be that the density of protein on the vesicles membrane increased. The hallmark of the single vesicle assay is that it can decipher such heterogeneous behaviour. For a more detailed survey of single vesicle membrane curvature screening assays see refs. (Bhatia et al. 2010; Madsen et al. 2010).

5.9 Summary and Outlook

A lipid vesicle comprises a three-dimensional nanoscopic scaffold that can group together water soluble, hydrophobic or amphiphilic molecules. The high biocompatibility and similarity to cell membranes make lipid vesicles ideal model membrane systems for the reconstitution and characterisation of various biological processes. In addition, the application of vesicles as ultra-miniaturised biochemical reactor systems has gathered attention from the single molecule community and from various biotechnological branches that could benefit from alternative technologies for reducing sample consumption and parallelise volume based experiments.

Arrays of single vesicles fabricated on solid supports provide access to high throughput examination of vesicle samples using fluorescence microscopy. Controlled immobilisation of intact and non-deformed vesicles is best achieved by tethering vesicles onto polymer (PEG) functionalised substrates that minimise non-specific interactions. Specific surface tethering can be achieved using various cognate binding pairs, e.g. biotin-streptavidin, DNA hybridisation or histidine/NTA. The single vesicle array has now proven a quantitative and robust platform with a promising potential for various niche applications where ultra-miniaturisation, biocompatibility or cost are of critical importance.

The ultimate vision of the experiments we have described in this chapter would be an ultra-high density single vesicle array ($>10^8$ per cm^2) of single nanoscopic multifunctional experimental units. The membrane of the vesicles would be used to study transmembrane events (e.g. ion channel activation) or binding of water-soluble molecules (peripheral proteins, ligands etc.). The lumen of the vesicles would be used to confine single macromolecules and observe folding, catalytic pathways of enzymes or more complex biochemical reactions. To date, the most important accomplishments toward this vision are the (i) production of surface-based arrays of single intact and non-deformed vesicles (ii) development of methods to extract quantitative information from single vesicle reactors using fluorescence microscopy and (iii) development of various methods to access the vesicle interior and trigger solute mixing. The critical outstanding issue for this vision is encoding the identity of large numbers of different single vesicles. The rise of second generation DNA sequencing platforms, however, has made commercial technology available that in principle would allow the massively parallel decoding of DNA tagged vesicle libraries. Although challenges regarding multiplexed production of such libraries still remains to be solved the presented vision now seems to have come within realisable horizons.

Acknowledgments D.S. would like to acknowledge financial support from the Lundbeck Foundation Center for Biomembranes in Nanomedicine, the Danish Councils for Independent and Strategic Research and the University of Copenhagen programs of excellence “Single Molecule Nanoscience” and “BioScaRT”.

References

- Bangham, A.D.: Membrane models with phospholipids. *Prog. Biophys. Mol. Biol.* **18**, 29–95 (1968)
- Bäumle, M., Stamou, D., Segura, J.-M., Hovius, R., Vogel, H.: Highly fluorescent streptavidin-coated CdSe nanoparticles: preparation in water, characterization, and micropatterning. *Langmuir* **20**, 3828–3831 (2004)
- Bendix, P.M., Pedersen, M.S., Stamou, D.: Quantification of nano-scale intermembrane contact areas by using fluorescence resonance energy transfer. *Proc. Natl. Acad. Sci. U.S.A.* **106**, 12341–12346 (2009)
- Benkoski, J.J., Höök, F.: Lateral mobility of tethered vesicle-DNA assemblies. *J. Phys. Chem. B* **109**, 9773–9779 (2005)
- Bhatia, V.K., Madsen, K.L., Bolinger, P.Y., Kunding, A., Hedegard, P., Gether, U., Stamou, D.: Amphipathic motifs in BAR domains are essential for membrane curvature sensing. *EMBO J.* **28**, 3303–3314 (2009)
- Bhatia, V.K., Hatzakis, N.S., Stamou, D.: A unifying mechanism accounts for sensing of membrane curvature by BAR domains, amphipathic helices and membrane-anchored proteins. *Semin. Cell Dev. Biol.* **21**, 381–390 (2010)
- Bolinger, P., Stamou, D., Vogel, H.: Integrated nanoreactor systems: triggering the release and mixing of compounds inside single vesicles. *J. Am. Chem. Soc.* **126**, 8594–8595 (2004)
- Bolinger, P.Y., Stamou, D., Vogel, H.: An integrated self-assembled nanofluidic system for controlled biological chemistries. *Angew. Chem. Int. Ed.* **47**, 5544–5549 (2008)
- Bonifacino, J.S., Glick, B.S.: The mechanisms of vesicle budding and fusion. *Cell* **116**, 153–166 (2004)
- Boucher, P.A., Joos, B., Zuckermann, M.J., Fournier, L.: Pore formation in a lipid bilayer under a tension ramp: modeling the distribution of rupture tensions. *Biophys. J.* **92**, 4344–4355 (2007)

- Boukobza, E., Sonnenfeld, A., Haran, G.: Immobilization in surface-tethered lipid vesicles as a new tool for single biomolecule spectroscopy. *J. Phys. Chem. B* **105**, 12165–12170 (2001)
- Bränden, M., Tabaei, S.R., Fischer, G., Neutze, R., Höök, F.: Refractive-index-based screening of membrane-protein-mediated transfer across biological membranes. *Biophys. J.* **99**, 124–133 (2010)
- Cajal, Y., Svendsen, A., Girona, V., Patkar, S.A., Alsina, M.A.: Interfacial control of lid opening in *Thermomyces lanuginosa* lipase. *Biochemistry* **39**, 413–423 (2000)
- Chan, Y.H.M., Lenz, P., Boxer, S.G.: Kinetics of DNA-mediated docking reactions between vesicles tethered to supported lipid bilayers. *Proc. Natl. Acad. Sci. U.S.A.* **104**, 18913–18918 (2007)
- Chiu, D.T., Wilson, C.F., Ryttsén, F., Strömberg, A., Farre, C., Karlsson, A., Nordholm, S., Gaggari, A., Modi, B.P., Moscho, A., Roberto, A., Garza-López, R.A., Orwar, O., Zare, R.N.: Chemical transformations in individual ultrasmall biomimetic containers. *Science* **283**, 1892–1895 (1999)
- Choi, U.B., Strop, P., Vrljic, M., Chu, S., Brunger, A.T., Weninger, K.R.: Single-molecule FRET-derived model of the synaptotagmin 1-SNARE fusion complex. *Nat. Struct. Mol. Biol.* **17**, 318–324 (2010)
- Christensen, S.M., Stamou, D.: Surface-based lipid vesicle reactor systems: fabrication and applications. *Soft Matter* **3**, 828–836 (2007)
- Cisse, I., Okumus, B., Joo, C., Ha, T.J.: Fueling protein-DNA interactions inside porous nanocontainers. *Proc. Natl. Acad. Sci. U.S.A.* **104**, 12646–12650 (2007)
- Clark, M.A., Acharya, R.A., Arico-Muendel, C.C., Belyanskaya, S.L., Benjamin, D.R., Carlson, N.R., Centrella, P.A., Chiu, C.H., Creaser, S.P., Cuzzo, J.W., Davie, C.P., Ding, Y., Franklin, G.J., Franzen, K.D., Gefter, M.L., Hale, S.P., Hansen, N.J.V., Israel, D.I., Jiang, J.W., Kavarana, M.J., Kelley, M.S., Kollmann, C.S., Li, F., Lind, K., Mataruse, S., Medeiros, P.F., Messer, J.A., Myers, P., O’Keefe, H., Oliff, M.C., Rise, C.E., Satz, A.L., Skinner, S.R., Svendsen, J.L., Tang, L.J., van Vloten, K., Wagner, R.W., Yao, G., Zhao, B.G., Morgan, B.A.: Design, synthesis and selection of DNA-encoded small-molecule libraries. *Nat. Chem. Biol.* **5**, 647–654 (2009)
- Cremer, P.S., Boxer, S.G.: Formation and spreading of lipid bilayers on planar glass supports. *J. Phys. Chem. B* **103**, 2554–2559 (1999)
- Cristobal, G., Arbouet, L., Sarrazin, F., Talaga, D., Bruneel, J.L., Joanicot, M., Servant, L.: On-line laser Raman spectroscopic probing of droplets engineered in microfluidic devices. *Lab Chip* **6**, 1140–1146 (2006)
- Dusseiller, M.R., Niederberger, B., Städler, B., Falconnet, D., Textor, M., Vörös, J.: A novel crossed microfluidic device for the precise positioning of proteins and vesicles. *Lab Chip* **5**, 1387–1392 (2005)
- Geissbuehler, I., Hovius, R., Martinez, K.L., Adrian, M., Ravindranathan, T., Vogel, H.: Lipid-coated nanocrystals as multifunctionalized luminescent scaffolds for supramolecular biological assemblies. *Angew. Chem. Int. Ed.* **44**, 1388–1392 (2005)
- Gizeli, E., Glad, J.: Single-step formation of a biorecognition layer for assaying histidine-tagged proteins. *Anal. Chem.* **76**, 3995–4001 (2004)
- González, M., Argarana, C.E., Fidelio, G.D.: Extremely high thermal stability of streptavidin and avidin upon biotin binding. *Biomol. Eng.* **16**, 67–72 (1999)
- Gouaux, E., MacKinnon, R.: Principles of selective ion transport in channels and pumps. *Science* **310**, 1461–1465 (2005)
- Graff, A., Winterhalter, M., Meier, W.: Nanoreactors from polymer-stabilized liposomes. *Langmuir* **17**, 919–923 (2001)
- Graff, A., Sauer, M., Gelder, P.V., Meier, W.: Virus-assisted loading of polymer nanocontainer. *Proc. Natl. Acad. Sci. U.S.A.* **99**, 5064 (2002)
- Groves, J.T., Boxer, S.: Micropattern formation in supported lipid membranes. *Acc. Chem. Res.* **35**, 149–157 (2002)
- Hamill, O.P., Marty, A., Neher, E., Sakmann, B., Sigworth, F.J.: Improved patch-clamp techniques for high-resolution current recording from cells and cell-free membrane patches. *Pflug. Arch. Eur. J. Phys.* **391**, 85–100 (1981)
- Hansen, P.L., Cohen, J.A., Podgornik, R., Parsegian, V.A.: Osmotic properties of poly(ethylene glycols): quantitative features of brush and bulk scaling laws. *Biophys. J.* **84**, 350–355 (2003)

- Hatzakis, N.S., Bhatia, V.K., Larsen, J., Madsen, K.L., Bolinger, P.Y., Kunding, A.H., Castillo, J., Gether, U., Hedegard, P., Stamou, D.: How curved membranes recruit amphipathic helices and protein anchoring motifs. *Nat. Chem. Biol.* **5**, 835–841 (2009)
- Jenkins, A.T.A., Bushby, R.J., Evans, S.D., Knoll, W., Offenhäuser, A., Ogier, S.D.: Lipid vesicle fusion on muCP patterned self-assembled monolayers. *Langmuir* **18**, 3176–3180 (2002)
- Johnson, J.M., Ha, T., Chu, S., Ajo-Franklin, M.C., Boxer, S.G.: Early steps of supported bilayer formation probed by single vesicle Fluorescence assays. *Biophys. J.* **83**, 3371–3379 (2002)
- Karatekin, E., Sandre, O., Guitouni, H., Borghi, N., Puech, P.H., Brochard-Wyart, F.: Cascades of transient pores in giant vesicles: line tension and transport. *Biophys. J.* **84**, 1734–1749 (2003)
- Karlsson, A., Karlsson, R., Karlsson, M., Cans, A.-S., Strömberg, A., Ryttsén, F., Orwar, O.: Networks of nanotubes and containers. *Nature* **409**, 150 (2001)
- Karlsson, M., Davidson, M., Karlsson, R., Karlsson, A., Bergenholtz, J., Konkoli, Z., Jesorka, A., Lobovkina, T., Hurtig, J., Voinova, M., Orwar, O.: Biomimetic nanoscale reactors and networks. *Annu. Rev. Physchem.* **55**, 613 (2004)
- Keller, C.A., Kassemo, B.: Surface specific kinetics of lipid vesicle adsorption measured with a quartz crystal microbalance. *Biophys. J.* **75**, 1397–1402 (1998)
- Kunding, A.H., Mortensen, M.W., Christensen, S.M., Stamou, D.: A fluorescence-based technique to construct size distributions from single-object measurements: application to the extrusion of lipid vesicles. *Biophys. J.* **95**, 1176–1188 (2008)
- Kuyper, C.L., Kuo, J.S., Mutch, S.A., Chiu, D.T.: Proton permeation into single vesicles occurs via a sequential two-step mechanism and is heterogeneous. *J. Am. Chem. Soc.* **128**, 3233–3240 (2006)
- Lasic, D.D., Needham, D.: The “stealth” liposome: a prototypical biomaterial. *Chem. Rev.* **95**, 2601–2628 (1995)
- Lee, J.Y., Okumus, B., Kim, D.S., Ha, T.J.: Extreme conformational diversity in human telomeric DNA. *Proc. Natl. Acad. Sci. U.S.A.* **102**, 18938–18943 (2005)
- Lee, H.-K., Yang, Y., Su, Z., Hyeon, C., Lee, T.-S., Lee, H.-W., Kweon, D.-H., Shin, Y.-K., Yoon, T.-Y.: Dynamic Ca²⁺ – dependent stimulation of vesicle fusion by membrane-anchored synaptotagmin 1. *Science* **328**, 760–763 (2010)
- Lenz, P., Johnson, J.M., Chan, Y.H.M., Boxer, S.G.: Tension-induced pore formation and leakage in adhering vesicles. *Europhys. Lett.* **75**, 659–665 (2006)
- Lizana, L., Konkoli, Z., Bauer, B., Jesorka, A., Orwar, O.: Controlling chemistry by geometry in nanoscale systems. *Annu. Rev. Phys. Chem.* **60**, 449–468 (2009)
- Lohr, C., Kunding, A.H., Bhatia, V.K., Stamou, D.: Constructing size distributions of liposomes from single-object fluorescence measurements. *Methods Enzymol.* **465**, 143–160 (2009)
- Lohse, B., Bolinger, P.Y., Stamou, D.: Encapsulation efficiency measured on single small unilamellar vesicles. *J. Am. Chem. Soc.* **130**, 14372–14373 (2008)
- Madsen, K.L., Bhatia, V.K., Gether, U., Stamou, D.: BAR domains, amphipathic helices and membrane-anchored proteins use the same mechanism to sense membrane curvature. *FEBS Lett.* **584**, 1848–1855 (2010)
- Martens, S., Kozlov, M.M., McMahon, H.T.: How synaptotagmin promotes membrane fusion. *Science* **316**, 1205–1208 (2007)
- McMahon, H.T., Gallop, J.L.: Membrane curvature and mechanisms of dynamic cell membrane remodelling. *Nature* **438**, 590–596 (2005)
- Metzker, M.L.: Applications of next-generation sequencing technologies – the next generation. *Nat. Rev. Genet.* **11**, 31–46 (2010)
- Michel, R., Reviakine, I., Sutherland, D., Fokas, C., Csucs, G., Danuser, G., Textor, M.: A novel approach to produce biologically relevant chemical patterns at the nanometer scale: selective molecular assembly patterning combined with colloidal lithography. *Langmuir* **18**, 8580–8586 (2002)
- Noireaux, V., Libchaber, A.: A vesicle bioreactor as a step toward an artificial cell assembly. *Proc. Natl. Acad. Sci. U.S.A.* **101**, 17669–17674 (2004)
- Okumus, B., Wilson, T.J., Lilley, D.M.J., Ha, T.: Vesicle encapsulation studies reveal that single molecule ribozyme heterogeneities are intrinsic. *Biophys. J.* **87**, 2798–2806 (2004)

- Okumus, B., Arslan, S., Fengler, S.M., Myong, S., Ha, T.: Single molecule nanocontainers made porous using a bacterial toxin. *J. Am. Chem. Soc.* **131**, 14844–14849 (2009)
- Patolsky, F., Lichtenstein, A., Willner, I.: Electronic transduction of DNA sensing processes on surfaces: amplification of DNA detection and analysis of single-base mismatches by tagged liposomes. *J. Am. Chem. Soc.* **123**, 5194–5205 (2001)
- Pheiffer, I., Höök, F.: Bivalent cholesterol-based coupling of oligonucleotides to lipid membrane bivalent cholesterol-based coupling of oligonucleotides to lipid membrane assemblies. *J. Am. Chem. Soc.* **126**, 10224–10225 (2004)
- Pick, H., Schmid, E.L., Tairi, A., Ilegems, E., Hovius, R., Vogel, H.: Investigating cellular signaling reactions in single attoliter vesicles. *J. Am. Chem. Soc.* **127**, 2908–2912 (2004)
- Reimhult, E., Höök, F., Kasemo, B.: Intact vesicle adsorption and supported biomembrane formation from vesicles in solution: influence of surface chemistry, vesicle size, temperature, and osmotic pressure formation from vesicles in solution: influence of surface chemistry, vesicle size, temperature, and osmotic pressure. *Langmuir* **19**, 1681–1691 (2003)
- Renault, J.P., Bernard, A., Bietsch, A., Michel, B., Bosshar, H.R., Delamarche, E., Kreiter, M., Hecht, B., Wild, U.P.: Fabricating arrays of single protein molecules on glass using microcontact printing. *J. Phys. Chem. B* **107**, 703–711 (2003)
- Reviakine, I., Brisson, A.: Formation of supported phospholipid bilayers from unilamellar vesicles investigated by atomic force microscopy. *Langmuir* **16**, 1806–1815 (2000)
- Rhoades, E., Gussakovsky, E., Haran, G.: Watching proteins fold one molecule at a time. *Proc. Natl. Acad. Sci. U.S.A.* **100**, 3197–3202 (2003)
- Richter, R., Mukhopadhyay, A., Brisson, A.: Pathways of lipid vesicle deposition on solid surfaces: a combined QCM-D and AFM study. *Biophys. J.* **85**, 3035–3047 (2003)
- Roy, R., Hohng, S., Ha, T.: A practical guide to single-molecule FRET. *Nat. Methods* **5**, 507–516 (2008)
- Salaita, K., Nair, P.M., Petit, R.S., Neve, R.M., Das, D., Gray, J.W., Groves, J.T.: Restriction of receptor movement alters cellular response: physical force sensing by EphA2. *Science* **327**, 1380–1385 (2010)
- Schönherr, H., Johnson, J.M., Lenz, P., Frank, C.W., Boxer, S.G.: Vesicle adsorption and lipid bilayer formation on glass studied by atomic force microscopy. *Langmuir* **20**, 11600–11606 (2004)
- Simonsson, L., Jonsson, P., Stengel, G., Hook, F.: Site-specific DNA-controlled fusion of single lipid vesicles to supported lipid bilayers. *Chemphyschem* **11**, 1011–1017 (2010)
- Slater, S.J., Kelly, M.B., Taddeo, F.J., Ho, C.J., Rubin, E., Stubbs, C.D.: The modulation of protein-kinase-C activity by membrane lipid bilayer structure. *J. Biol. Chem.* **269**, 4866–4871 (1994)
- Städler, B., Falconnet, D., Pfeiffer, I., Höök, F., Vörös, J.: Micropatterning of DNA-tagged vesicles. *Langmuir* **20**, 11348–11354 (2004)
- Stamou, D., Duschl, C., Delamarche, E., Vogel, H.: Self-assembled microarrays of attoliter molecular vessels. *Angew. Chem. Int. Ed.* **42**, 5580–5583 (2003)
- Stora, T., Dienes, Z., Vogel, H., Duschl, C.: Histidine-tagged amphiphiles for the reversible formation of lipid bilayer aggregates on chelator-functionalized gold surfaces. *Langmuir* **16**, 5471–5478 (2000)
- Sudhof, T.C., Rothman, J.E.: Membrane fusion: grappling with SNARE and SM proteins. *Science* **323**, 474–477 (2009)
- Tamm, L.K., McConnell, H.M.: Supported phospholipid-bilayers. *Biophys. J.* **47**, 105–113 (1985)
- Wang, B., Zhang, L.F., Bae, S.C., Granick, S.: Nanoparticle-induced surface reconstruction of phospholipid membranes. *Proc. Natl. Acad. Sci. U.S.A.* **105**, 18171–18175 (2008)
- Yoon, T.Y., Okumus, B., Zhang, F., Shin, Y.K., Ha, T.: Multiple intermediates in SNARE-induced membrane fusion. *Proc. Natl. Acad. Sci. U.S.A.* **103**, 19731–19736 (2006)
- Yoon, T.Y., Lu, X., Diao, J., Lee, S.M., Ha, T., Shin, Y.K.: Complexin and Ca²⁺ stimulate SNARE-mediated membrane fusion. *Nat. Struct. Mol. Biol.* **15**, 707–713 (2008)
- Yoshimoto, M., Wang, S., Fukunaga, K., Fournier, D., Walde, P., Kuboi, R., Nakao, K.: Novel immobilized liposomal glucose oxidase system using the channel protein OmpF and catalase. *Biotechnol. Bioeng.* **90**, 231–238 (2005)

- Yoshina-Ishii, C., Boxer, S.G.: Arrays of mobile tethered vesicles on supported lipid bilayers. *J. Am. Chem. Soc.* **125**, 3696–3697 (2003)
- Yoshina-Ishii, C., Boxer, S.G.: Controlling two-dimensional tethered vesicle motion using an electric field: interplay of electrophoresis and electro-osmosis. *Langmuir* **22**, 2384–2391 (2006)
- Yoshina-Ishii, C., Miller, G.P., Kraft, M.L., Kool, E.T., Boxer, S.G.: General method for modification of liposomes for encoded assembly on supported bilayers. *J. Am. Chem. Soc.* **127**, 1356–1357 (2005)

Chapter 6

Active Biomimetic Membranes

Flemming Cornelius

Abstract The concept of biomimetic membranes containing energy driven transport proteins has attracted considerable interest, but there still remains substantial progress to be made before we have large-scale systems based on active transport. Here I use the Na,K-ATPase as an example of a prototypical transport protein and describe functional reconstitution of Na,K-ATPase from the salt gland of shark with prior solubilization in detergent including determination of the orientation of reconstituted Na,K-ATPase and recovery of catalytic and transport activity. Reconstituted Na,K-ATPase is ideal to investigate the protein-lipid interaction by reconstitution into liposomes of defined lipid composition. The dependence of Na,K-ATPase activity on hydrophobic thickness of the bilayer and how this is affected by cholesterol is demonstrated and related to the hydrophobic matching principle. The effect of cholesterol on functional properties of Na,K-ATPase is related to the recent crystal structure in which a cholesterol is resolved at a functionally important location. Finally, the effect of polyunsaturated phospholipids is discussed in relation to the lateral pressure profile and the dependence of Na,K-ATPase regulation on acidic phospholipids is demonstrated.

List of Abbreviations

$C_{12}E_8$	octaethyleneglycol dodecyl monoether
CHL or chol	cholesterol
C_m	specific membrane capacitance
Cmc	critical micelle concentration

F. Cornelius (✉)
Department of Physiology and Biomedicine, Aarhus University,
Ole Worms Allé 6, DK-8000 Aarhus C, Denmark
e-mail: fc@biophys.au.dk

DHA	docosahexaenoyl acid
DOC	deoxycholate
DOPC	dioleoyl PC
G_m	membrane conductance
k_{cat}	turnover number
n_c	average hydrocarbon length
PC	phosphatidyl choline
PE	phosphatidyl ethanolamine
PG	phosphatidyl glycerol
PI	Phosphatidyl inositol
PKA	protein kinase A
PKC	protein kinase C
PLB	phospholamban
PUFA	polyunsaturated fatty acids
PS	phosphatidyl serine
SERCA	sarco(endo)plasmic Ca-ATPase.

6.1 Biomimetic Membranes with Active Transport

Development of membranes mimicking native biomembranes containing active transport has attracted recent interest, e.g. in desalination (Shannon et al. 2008). Incorporation of active transport proteins like Na,K-ATPase into lipid bilayer is not a trivial task, however. The transport protein must be isolated, purified, and reconstituted without denaturation and loss of activity. Moreover, protein orientation must be determined and, if possible, controlled.

Here is described how Na,K-ATPase purified from shark rectal glands can be functionally reconstituted into liposomes and how protein with a specific orientation can be selectively activated exploiting the sidedness of the system. The protein-lipid interaction is investigated using such reconstitution of Na,K-ATPase into liposomes of defined lipid composition. Recently, the method described below to reconstitute Na,K-ATPase was used to achieve an ion-pump controlled carbon nanotube protein transistor (Shih-Chieh et al. 2010).

6.2 Reconstitution of Na,K-ATPase by Solubilization

The Na,K-ATPase can be studied in purified membrane preparations using a tissue rich in this protein like kidney or brain. We have successfully employed Na,K-ATPase prepared from the rectal gland of the spiny dogfish, *Squalus acanthias*, which is highly homologous to the human one. The reason for using shark Na,K-ATPase is that it can be produced in high yield and with a high activity. Thus the shark Na,K-ATPase preparation is typically prepared with a specific activity of about 1,800 μmol

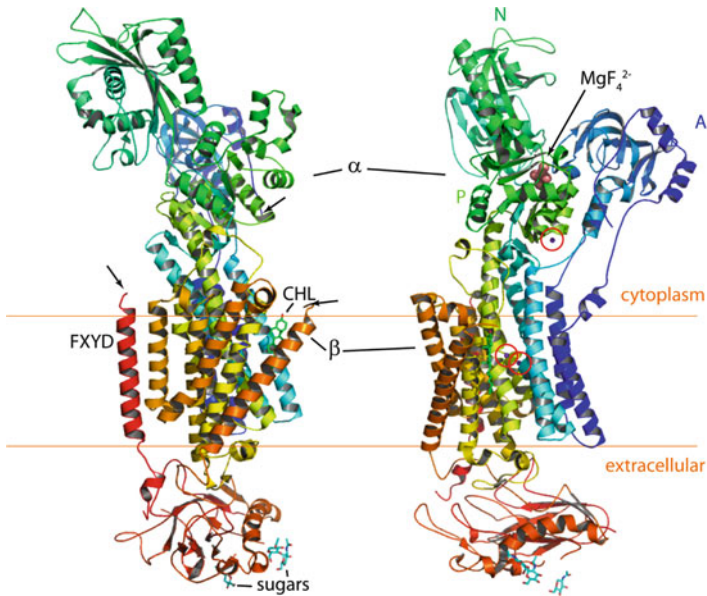


Fig. 6.1 Ribbon diagram of the structure of shark Na,K-ATPase in the E_2PK_2 -like state with MgF_4^{2-} as a MgP_i -analog (pdb 2ZXE). The structure is seen from two different views turned 90° . In the transmembrane region two K^+ -ions are bound, and one is bound in the cytoplasmic P-domain (circled in red). The β_1 -subunit is glycosylated in two of four putative glycosylation sites. The horizontal orange lines indicate the approximate boundaries of the hydrophobic core of the lipid bilayer. The 3 *arrows* point at cytoplasmic positions where residues could not be modelled (31 amino-terminal residues of α , 27 residues of β , and 33 residues of FXYD). Cholesterol (CHL) and sugars are shown in ball and stick style. Drawn using PyMol

P_i $mg^{-1} h^{-1}$ at $37^\circ C$ and a phosphorylation site density of about $2.5 \text{ nmol } mg^{-1}$ protein giving a turnover number of 200 s^{-1} . Most importantly in this context, however, is that it remains fully active after solubilization in certain detergents – a prerequisite for reconstitution as well as for crystallization. Using this preparation Na,K-ATPase can be successfully reconstituted without loss of activity (Cornelius and Skou 1984), and the first complete crystal structure including both α -, β -, and FXYD-subunits of the Na,K-ATPase was recently determined at 2.4 \AA using the shark Na,K-ATPase, as depicted in Fig. 6.1 (Shinoda et al. 2009).

The purpose of reconstituting Na,K-ATPase is to obtain a very pure preparation and to re-establish sidedness. The first purpose is in order to study function without interference from other membrane proteins. This may seem advantageous, on the other hand it is hardly physiological since *in vivo* the protein is susceptible to numerous interactions with other membrane constituents. Reestablishment of sidedness enables the study of transport processes and properties depending on it, like generation of membrane potentials (see Sects. 6.3.2 and 6.3.3). For oligomeric proteins like the Na,K-ATPase a minimum requirement for functional reconstitution is that all molecular components must be reconstituted, i.e. co-reconstitution of the $\alpha\beta$ -subunits together with the regulatory FXYD subunit must be ensured.

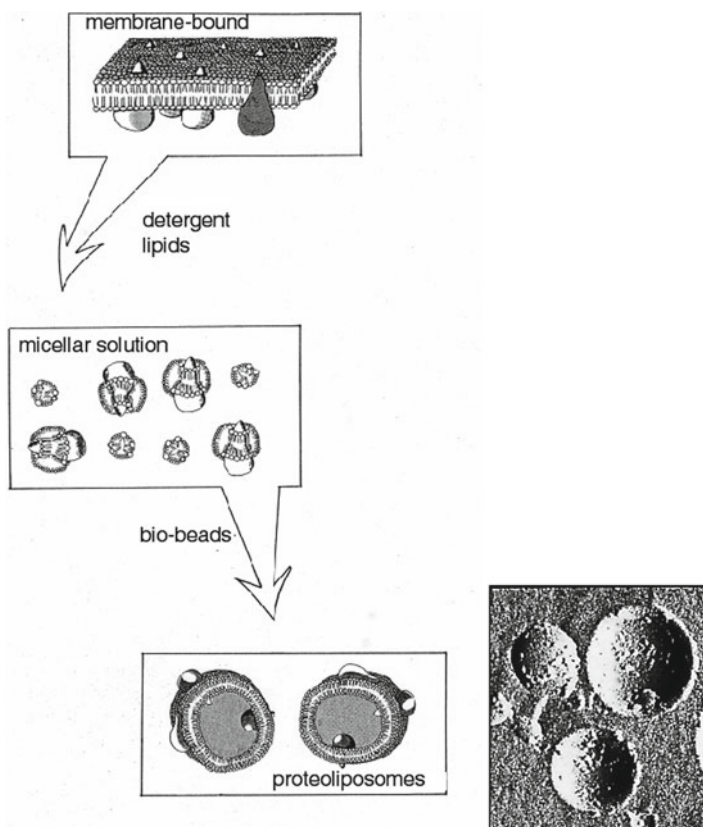


Fig. 6.2 Reconstitution of Na,K-ATPase by detergent solubilization. The Na,K-ATPase membrane preparation is initially solubilized by addition of the detergent $C_{12}E_8$ and mixed with excess lipids (protein: lipid = 1:20 w:w) also solubilized in $C_{12}E_8$. After equilibration detergent is removed by adsorption to hydrophobic polystyrene beads (bio-beads) and proteoliposomes are spontaneously formed. The micrograph shows a freeze-etch preparation of proteoliposomes with diameters of approximately 200 nm. Reconstituted Na,K-ATPases are clearly observed as small inter-membrane particles in the smooth lipid phase (Courtesy by A. B. Maunsbach)

The strategy for reconstitution by solubilization is, in principle, straightforward as depicted in Fig. 6.2. Initially protein and lipids are solubilized individually in detergent, then mixed to allow equilibration of lipid and protein in mixed micelles, and when the detergent is subsequently removed by adsorption to hydrophobic polystyrene beads liposomes with incorporated protein (proteoliposomes) are spontaneously formed. The resulting proteoliposomes are unilamellar with a bimodal size-distribution with average diameters of approximately 60 and 200 nm, respectively (Cornelius and Møller 1996). In practice things are more complicated, of course, and several important technical points must be considered before a reliable method for functional reconstitution can be devised. Often such considerations may resemble “higher French cookery” rather than physico-chemical reasoning. It is important that the protein during the entire reconstitution process is prevented from

denaturing. Indeed, factors such as the nature of the detergent and lipids are essential to consider, but many other factors may influence the outcome including temperature, mixing procedures, protein handling, etc.

6.2.1 Detergent

The first thing to consider is which kind of detergent to use in order to obtain solubilization of Na,K-ATPase with full recovery of function. For most membrane proteins this is not a trivial task. Regarding Na,K-ATPase the non-ionic detergent octaethyleneglycol dodecyl monoether ($C_{12}E_8$) is a good choice. Furthermore, Na,K-ATPase preparations from different sources may have variable resistance to the detergent. Na,K-ATPase from shark rectal gland is very resistant to $C_{12}E_8$. The starting material is a partially purified membrane preparation of shark Na,K-ATPase, which is prepared by tissue homogenization, differential centrifugation and mild treatment with deoxycholate (DOC) to selectively remove loosely associated extrinsic proteins and to open microsome vesicles (Skou and Esmann 1979).

Solubilization is a gradual process but can be considered to take place in three main stages where the detergent first partitions into the lipid phase of the membrane and, as its concentration is increased beyond saturation, partially replaces the native lipids that surround the intrinsic protein, which gradually disintegrates the membrane. Finally, when disintegration is complete, a mixture of solubilized lipids and solubilized protein is formed. The detergent shields the hydrophobic part of the protein, which would normally form the transmembrane domain of the native membrane protein. In the beginning of this stage the hydrophobic surface of the protein is still covered by a layer of disordered lipids, the so-called annulus lipids (Lee 2003).

Polyoxyethylene glycol detergents have been very successful in solubilizing Na,K-ATPase without denaturation. The critical micelle concentration (cmc) of $C_{12}E_8$ is 87 μM which precludes its removal by dialysis. However, introduction of polystyrene beads for adsorption of nonionic detergents like $C_{12}E_8$ has solved that problem (Cornelius and Skou 1984). Solubilization of shark Na,K-ATPase is achieved by gently mixing the membrane enzyme preparation with 10 mM $C_{12}E_8$ at 0°C in 150 mM NaCl, 25% glycerol, and 20 mM histidine (pH 7.0) at a detergent:protein weight ratio of 4. After centrifugation at 100.000 g 60–70% of the protein is recovered in the supernatant.

6.2.2 Lipids

Lipid composition of the plasma membrane is important for Na,K-ATPase function. The Na,K-ATPase is anchored in the lipid bilayer, and the complex soft matter properties of the lipid membrane (e.g. elasticity), fluidity and bilayer thickness, can modulate the function of membrane proteins (see Lee 2003; Jensen and Mouritsen 2004). Apart from such non-specific protein-lipid interactions some specific lipids may be needed (see Sect. 6.4).

The annulus is a statistical entity, since the annulus lipids exchange with the bulk lipids on a μs time scale. The annulus lipids are distorted by specific arrangements in grooves of the hydrophobic protein surface formed by the side-chains. The lipid chains are aligned with these grooves implying specific interactions between the lipid chains and the protein groups by van der Waals forces. These lipids have restricted mobility compared to the bulk membrane lipids. As the detergent concentration increases further the annulus or boundary lipids may be removed, which can result in irreversible protein inactivation. Also hydrophobic interactions between protein subunits may be subject to modifications by added detergent. Thus, sub-cmc concentrations of C_{12}E_8 caused a large increase in Na,K-ATPase activity (Huang et al. 1985), which later was demonstrated to be caused by dissociation of the regulatory FXYD-subunit that normally inhibits the Na,K-ATPase (Mahmoud et al. 2000).

Apart from the annulus lipids more specific lipid sites on proteins have been suggested. Such non-annular sites have been demonstrated for cholesterol on the acetylcholine receptor (Jones and McNamee 1988) and on G-coupled receptor (Cherezov et al. 2007), for squalene on bacteriorhodopsin (Luecke et al. 1999), and for cardiolipin and PE on the photosynthetic reaction centre (McAuley et al. 1999), among others. Direct crystallographic support for such sites are emerging as more membrane protein structures become available (see, Sect. 6.4.1).

A lipid composition of PC:PE:PI:CHL 48:12:2:38 that closely resembles the annulus lipid composition of shark membrane preparations is demonstrated to support optimal activity of reconstituted Na,K-ATPase (Cornelius and Skou 1984). The lipid composition of solubilized shark Na,K-ATPase is found to be PC:PE:PI:CHL=40:10:1:46 (mol%) the remainder being sphingomyelin, sulfatides, and gangliosides (Esmann et al. 1980). The presence of cholesterol (Sect. 6.4.1) and a small amounts of acidic phospholipids (Sect. 6.4.1) seem to be essential.

The protein:lipid weight ratio is an important factor that must be controlled since it can influence both the recovery of activity as well as the orientation of reconstituted Na,K-ATPase (Cornelius 1988). A protein:lipid ratio between 1:10 and 1:20 is normally used. Decreasing the lipid content may produce leaky liposomes. Increasing the lipid content, on the other hand, decreases the recovered specific activity of Na,K-ATPase, which can be taken to indicate that some kind of interaction between the protein units are important. Whether or not dimeric interaction of Na,K-ATPase is important in the native plasma membrane is still a controversial issue in the field, although many kinetic data seem to indicate it (Clarke and Kane 2007).

6.3 Characterization of Proteoliposomes

Before the proteoliposomes can be used for quantitative measurements of Na,K-ATPase functions they must be thoroughly characterized. This includes determination of the proteoliposome size distribution, the number and orientations of pumps in the proteoliposomes, i.e. the sidedness, and their morphology and leakiness.

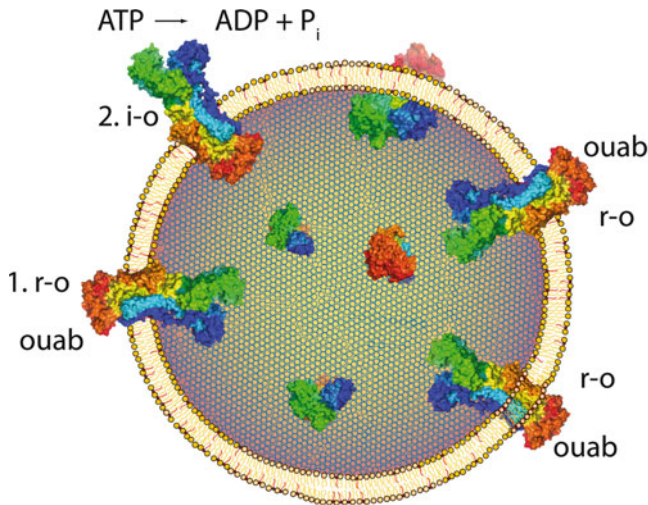


Fig. 6.3 Sketch of proteoliposome showing the kinds of protein orientations: 1. Right-side out as in the native membrane (r-o), which are inhibited by added ouabain 2. In the opposite orientation, inside out (i-o), which are activated by external ATP and insensitive to added ouabain. Leaky proteoliposomes that allow ATP to penetrate will give rise to a Na,K-ATPase fractions that can be inhibited by external ouabain and activated by added ATP (non-oriented, n-o). Phospholipids are shown in orange, cholesterol is red. The sketch is drawn approx. to scale for a vesicle with a diameter of 220 nm

6.3.1 Protein Orientation

It is often assumed that Na,K-ATPase is reconstituted with a random orientation. However, whether this is correct depends on the specific technique used for reconstitution. The protein orientation can be determined from functional tests exploiting the sidedness of the system, as described previously in details (Cornelius and Skou 1984; Cornelius 1988). In principle the activity is taken as proportional to the number of active Na,K-ATPase molecules, and the asymmetric binding of ATP, which binds from the cytoplasmic side, and inhibition by ouabain, which acts from the extracellular side, is used to detect orientations. Three possible orientations may exist (see Fig. 6.3): right-side out (r-o), where the Na,K-ATPase is oriented as in the cell. The opposite orientation, inside out (i-o), and non-oriented (n-o) representing unsided Na,K-ATPase, which is described in more details below. Thus, first the hydrolytic activity is measured of proteoliposomes reopened by detergent, which will be proportional to the total number of pumps. Then the activity of proteoliposomes in the presence of ouabain is measured, which will be proportional to inside out pumps, since only Na,K-ATPase with exposed ATP-binding sites are active and non-oriented enzyme is inhibited by ouabain. Finally, the activity is measured in the absence of ouabain, which will represent inside out plus non-oriented enzyme. The reconstitution described here produces asymmetrical reconstitution with about 65% right-side out, 10–15% inside out, and the rest incorporated with both extracellular and

cytoplasmic side exposed (non-oriented, n-o). The latter activity can in principle arise from free, un-reconstituted enzyme, from adsorbed but not fully integral enzyme, or representing a fraction of leaky proteoliposomes, which are permeable to ATP. The last possibility is considered the most likely. On the one hand all protein co-eluate with the lipid phase using gel-chromatography, excluding the presence of un-reconstituted enzyme (Cornelius and Skou 1984). Secondly, the n-o fraction is found at higher density on an isosmotic metrizamid gradient than the i-o fraction indicating that i-o activity is associated with closed proteoliposomes that float at low density due to entrapment of less dense medium (Cornelius 1988). Finally, there seems to be no indications of larger intermembrane particles in the freeze-fractured proteoliposomes arising from adsorbed Na,K-ATPase. Accordingly, increasing the lipid:protein ratio decreases significantly the fraction of n-o Na,K-ATPase, which seems to indicate that it is the increased curvature stress of reconstituted Na,K-ATPase on the lipid bilayer which is responsible for the leakiness.

The symmetry of protein reconstitution is found to depend on several parameters including the lipid composition, rate of detergent elimination, the protein:lipid ratio, and the sort of detergent used for solubilization (see Cornelius 1991).

6.3.2 *Specific Hydrolytic Activity of Reconstituted Na,K-ATPase*

Normally, after reconstitution of Na,K-ATPase only one of the three possible orientations are preferred to be active, e.g. i-o. Therefore, ATP is added to the outside, excluding ATP binding to right-side out enzyme, and n-o enzyme is inhibited by addition of ouabain in the presence of MgP_i . This leads to phosphorylation and binding of ouabain to enzyme with exposed extracellular sides (i.e. n-o and r-o), whereas the ouabain binding site of i-o enzyme is shielded inside the proteoliposome (see Fig. 6.3). The measured hydrolytic activity can now be specifically related to the fraction of Na,K-ATPase with a specific orientation, here i-o. The specific activity calculated in $\mu\text{mol}/\text{mg}$ i-o protein per hour can then be calculated by measurement of the total amount of protein in the proteoliposomes after correction by the i-o fraction. Here a method must be chosen that avoids interference from phospholipids and cholesterol (Petersen 1977), and the albumin standards should contain a lipid composition as in the proteoliposomes.

The kinetics of the Na,K-ATPase is generally described in terms of the Albers-Post scheme (Albers 1967; Post et al. 1972), which is shown in Fig. 6.4. In this model two main conformations of the Na,K-ATPase are considered, which can be either unphosphorylated, E_1 and E_2 , or phosphorylated, $E_1 \sim P$ and $E_2 \sim P$ (\sim indicates that the form can react with ADP to form ATP, a so-called energy-rich bond, and $-$ indicates that the form can only react with H_2O to be hydrolyzed). The model illustrates, furthermore, the counter-transport of Na^+ and K^+ across the plasma membrane where a consecutive binding and release of Na^+ and K^+ with a stoichiometry of $3Na^+/2 K^+$ take place. Na^+ ions bind from the cytoplasm and K^+ ions from the extracellular side.

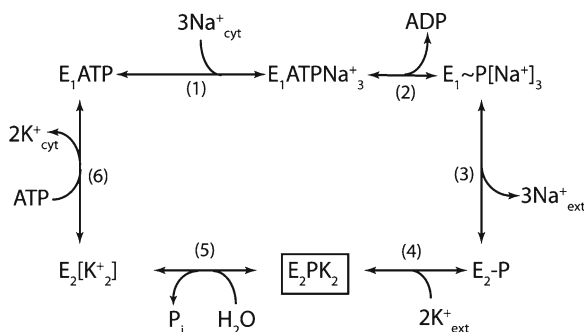


Fig. 6.4 The Albers-Post reaction cycle. The E_1 conformations have high Na^+ -affinities and low K^+ -affinities, whereas it is opposite for E_2 conformations that have low Na^+ -affinity and high K^+ -affinity. E_1ATP binds 3 Na^+ from the cytoplasmic side (1) and becomes phosphorylated (2) leading to Na^+ -occlusion (signified by sharp brackets). A spontaneous conformational change (3) leads to the release of Na^+ to the extracellular side and two extracellular K^+ ions are bound to form E_2PK_2 (4), which is the enzyme conformation that is crystallized (framed). A dephosphorylation (5) leads to occlusion of K^+ . Low-affinity binding of ATP facilitates K^+ -deocclusion to the cytoplasmic side (6), which closes the cycle

Measurements of maximum ATP hydrolysis associated with inside-out oriented Na,K-ATPase turnover should be performed at optimal conditions of substrate and ligands, i.e. mM ATP concentrations, 130 mM Na^+ , and 4 mM Mg^{2+} at the cytoplasmic side (i.e. outside the proteoliposomes) and about 20 mM K^+ at the extracellular side (i.e. inside the proteoliposomes), in a buffer at pH ~ 7.4 . Due to the small volume of the proteoliposome internal K^+ will quickly become limiting, however. To avoid this, K^+ is added to the outside together with the electroneutral K^+ -ionophore nigericin, which ensures rapid equilibration of K^+ . Indeed, rather sensitive methods are needed to measure specific ATP-hydrolysis even at optimal conditions due to the small quantities of protein present after reconstitution. Sensitive colorimetric methods like that of Baginski et al. (1967) can be used, but at suboptimal conditions the more sensitive method using ^{32}P -[ATP] must be employed (Lindberg and Ernster 1956). To obtain isosmotic conditions the extracellular osmolarity must be balanced (e.g. by sucrose) inside the proteoliposomes during their production. In Table 6.1 the activity of the membrane preparation is compared to preparations after solubilization in $C_{12}E_8$ and after reconstitution. As indicated by the site numbers a gradually purification takes place as the Na,K-ATPase is first solubilized and finally reconstituted. The lower site number in solubilized enzyme compared to reconstituted Na,K-ATPase is probably caused by interference from the detergent since re-addition of detergent to the proteoliposomes lowers the site number to the one found in solubilized Na,K-ATPase (Cornelius 1995a). Since the specific activity remains constant after reconstitution it means that the turnover number (molecular activity) of reconstituted Na,K-ATPase decreases. The measured site number of reconstituted Na,K-ATPase is identical to the theoretical site number for binding of one ATP per α/β /FXD-unit (~ 6.5 nmol mg^{-1}).

Table 6.1 Na,K-ATPase activities at 23°C of various preparations

	Membranes	Solubilized	Reconstituted
Specific activity [$\mu\text{mol}\cdot\text{mg}^{-1}\text{ h}^{-1}$]	629 \pm 26 (5)	630 \pm 23 (4)	564 \pm 21 (4)
Molecular activity [min^{-1}]	4,143 \pm 254 (5)	2,436 \pm 90 (4)	1,356 \pm 42 (4)
Site number ^a [$\text{nmol}\cdot\text{mg}^{-1}$]	2.5 \pm 0.3 (5)	4.2 \pm 0.3 (4)	6.9 \pm 0.6 (4) from ATP 6.1 \pm 0.5 (2) from MgP_i

^aMeasured as the number of phosphorylation sites per mg of protein from either ATP or from MgP_i . With a molecular mass of 154 kDa for the Na,K-ATPase ($\alpha/\beta/\text{FXD}$) the theoretical value is 6.5 nmol/mg. If the site number reflects the enzyme purity the membrane preparation is about 37% pure. Data from Cornelius (1995a)

Table 6.2 Stoichiometry for some partial reactions of Na,K-ATPase

Reaction	Catalytic turnover, s^{-1}	Charge turnover, s^{-1}	Stoichiometry charges/ATP
$\text{Na}^+:\text{Na}^+$ exchange	13.7	15.1	1.1
Uncoupled Na^+ -efflux	3.86	10.8	2.8

Data from Cornelius (1995c)

6.3.3 Ion Transport and Electrogenicity

The Na,K-ATPase is both an enzyme, which hydrolyses ATP, and a transport protein that performs vectorial energy-consuming ion-transport using the energy released from this ATP-hydrolysis. Thus, the Na,K-ATPase actively transports 3 Na^+ out and 2 K^+ into the cell for each ATP hydrolyzed. It is therefore an electrogenic ion-pump that generates an outward-directed current, which establishes a membrane potential across the proteoliposome bilayer. The membrane potential generated by activation of inside-out pumps will be inside positive and can be measured using potential sensitive fluorescent probes like oxonol VI after calibration using K^+ ionophores and known K^+ -gradients to calculate the Nernst equilibrium potentials (Cornelius 1989). The magnitude of this pump-generated membrane potential will depend on the liposome leakiness, i.e. on the membrane conductance (G_m). The higher the leak the lower a steady-state transmembrane potential can be maintained by the pump. G_m can be measured by arresting the pump after generating the steady-state membrane potential, V_{max} and follow the dissipation of membrane potential: $V_t = V_{\text{max}} e^{-t/\tau}$ where the time constant, $\tau = C_m/G_m$, and C_m is the specific membrane capacitance, which is $\sim 1 \mu\text{F cm}^{-2}$ for a lipid bilayer. The membrane conductance for the present proteoliposomes can be measured to $\sim 2.4 \text{ nS cm}^{-2}$. Due to this low conductance a very large membrane potential is generated by reconstituted Na,K-ATPase, up to several hundred mV. From the initial rate of membrane potential development one can calculate the turnover of charge and by comparing with the catalytic turnover the transport stoichiometry can be estimated (Cornelius 1995c, see Table 6.2).

The K^+ and Na^+ ion binding sites of the Na,K-ATPase are not very specific, thus the K^+ binding sites can accommodate most other alkali metal ions like Rb^+ , Li^+ , Tl^+ , NH_4^+ , H^+ , Cs^+ , and Na^+ . The Na^+ binding sites are more specific and can accommodate Li^+ and H^+ . Replacing extracellular K^+ with Na^+ the Na,K-ATPase, therefore, can exchange

three Na^+ from the cytoplasm with two Na^+ from the extracellular side accompanied by the hydrolysis of one ATP molecule. This $\text{Na}^+:\text{Na}^+$ exchange accompanied by ATP hydrolysis has been characterized in details in proteoliposomes and has been demonstrated to be electrogenic with a stoichiometry close to 3:2:1 (Forgacs and Chin 1981; Cornelius and Skou 1984; Cornelius 1995c). The intensity of hydrolytic activity accompanying this electrogenic $\text{Na}^+:\text{Na}^+$ exchange is between 5% and 10% of the $\text{Na}^+:\text{K}^+$ exchange.

Similarly, in the absence of extracellular Na^+ and K^+ the pump can expel Na^+ from the cytoplasm without any counter-ion transport, the so-called uncoupled Na^+ -efflux, and this transport mode is also accompanied by ATP hydrolysis and the stoichiometry is $3\text{Na}^+:\text{ATP}$ (Cornelius 1989, 1995b). The stoichiometry seems to vary, however, depending on pH in a way so at pH lower than 7.0 the stoichiometry decreases, probably by inducing $\text{Na}^+:\text{H}^+$ exchange (Cornelius 1990). The intensity of hydrolytic activity accompanying this uncoupled Na^+ -efflux is about 70% of the $\text{Na}^+:\text{Na}^+$ exchange.

6.4 Protein-Lipid Interactions

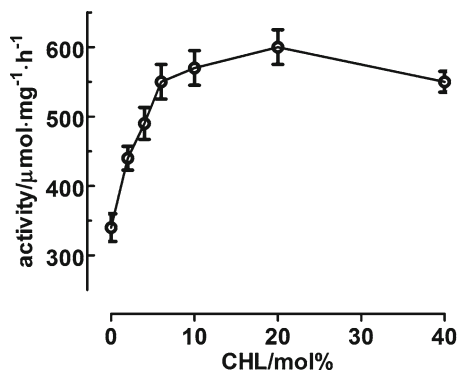
Are specific lipids necessary for reconstitution of fully functional Na,K-ATPase? The answer is *yes!* Reconstitution of Na,K-ATPase into liposomes of defined lipid composition is ideal to study the effects of lipids on Na,K-ATPase function. It is important, however, that the sidedness is determined for each lipid composition, since the orientation of Na,K-ATPase is influenced by the lipid composition of the liposomes (Cornelius 1988, 2001). The native animal plasma membrane is composed of phosphoglycerides (phospholipids), sphingolipids, and cholesterol. Previously, lipids in cell membranes were considered merely as a passive solvent into which the proteins partition. However, the very complex lipid composition of the plasma membrane with hundreds of different lipid species speaks in favour of a much more specific role. Recent research has documented this view beyond any doubt. The fatty acid composition of shark membrane preparation has an average hydrocarbon length (n_c) of 18.6, a polyunsaturation index of 210, i.e. a high content of polyunsaturated fatty acids (PUFA), and a cholesterol:phospholipid ratio of 0.6 (Cornelius et al. 2003). Below is a description of the effects of cholesterol, polyunsaturated lipids, and acidic phospholipids on various aspects of Na,K-ATPase functions and regulation as studied in reconstituted shark Na,K-ATPase.

6.4.1 Cholesterol

In most mammals and in the shark, too, the plasma membrane contains between 25 and 60 mol% cholesterol. It is well known that cholesterol has a range of important effects on membrane properties, e.g.:

1. Eliminates the sharp main transition temperature of phospholipids.
2. Promotes the liquid-ordered phase supporting lateral and rotational diffusion of lipid or protein

Fig. 6.5 Specific Na,K-ATPase activity at 23°C of Na,K-ATPase reconstituted into DOPC-liposomes with varying cholesterol (CHL) content (mol%) (Data from Cornelius 1995b)



3. Increases the conformational order of phospholipids and bilayer thickness (bending modulus)
4. Can induce lateral segregation of proteins and lipid domains formation
5. Can regulate transmembrane insertion of peptides important in targeting and membrane trafficking
6. Increases electric potential within bilayer interior
7. Decreases ion permeability.

But is there any specific interactions between the Na,K-ATPase and cholesterol? To investigate this we examined the effect of varying the cholesterol mol% in proteoliposomes on the specific Na,K-ATPase activity. The result is shown in Fig. 6.5. As seen V_{\max} (the maximum hydrolytic activity) almost doubles when the cholesterol content increases from 0 to 20 mol% where after it remains constant up to 40 mol%. Actually a whole range of functional properties are influenced by an increase in the cholesterol content in the proteoliposomes besides V_{\max} : the phosphorylation level increases, the apparent Na^+ -affinity decreases, the rate of phosphorylation and spontaneous dephosphorylation increases, the E_2 to E_1 rate constant increases, and the poise of the $E_1\text{P}$ to $E_2\text{P}$ equilibrium is shifted towards the $E_1\text{P}$ -conformation (Cornelius 1995b, 2001; Cornelius et al. 2003). The increase in the E_2 to E_1 rate constant explains the increased V_{\max} , since this step is the rate-determining reaction in the Albers-Post scheme (reaction 6 in Fig. 6.4) (Lüpfert et al. 2001; Humphry et al. 2002).

So cholesterol changes the global properties of Na,K-ATPase. How is this achieved? At least two possibilities exist: it could be due to effects of cholesterol on the bulk mechanical properties of the membrane, or it could be that cholesterol is specifically bound to Na,K-ATPase affecting its kinetic properties.

Integral membrane proteins span the lipid membrane via a hydrophobic transmembrane domain, which must be accommodated or matched by the hydrophobic thickness of the lipid membrane. If a mismatch exist the soft lipids are stretched or deformed at a certain distance from the protein (Mouritsen and Bloom 1984; Jensen and Mouritsen 2004; Lundbæk et al. 2004). The resulting free energy of deformation, ΔG_{def} , is a function of the membrane continuum physical properties, ΔG_{cont} , and the packing energy, ΔG_{pack} , due to lipid adaptation to the rough protein surface. For a protein like the Na,K-ATPase where the hydrophobic thickness may change during turnover due to a change in conformation, this free energy will contribute to the free

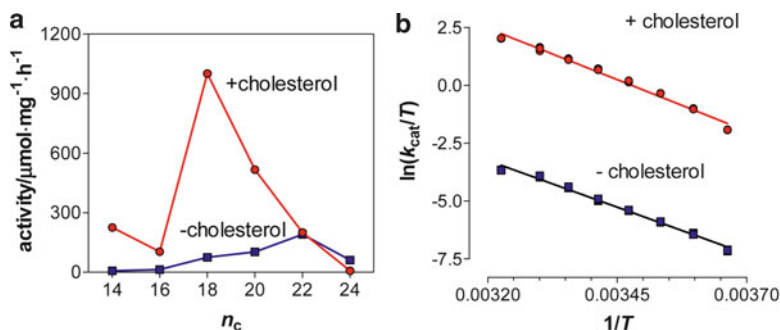


Fig. 6.6 Panel a shows Na,K-ATPase activity as a function of fatty acid acyl chain length (n_c) in proteoliposomes with and without 40 mol% cholesterol. Panel b shows Eyring plots for Na,K-ATPase reconstituted in DOPC with and without 40 mol% cholesterol from which the entropy of activation and enthalpy can be derived, which allows calculation of the free energy of activation (Data from Cornelius 2001)

energy of activation, and thus the kinetic properties of the protein. Furthermore, since the plasma membrane contains multiple lipid species there may be a tendency for lipids that match the hydrophobic thickness of the protein to become recruited at the protein-lipid interface, which may change the composition of the annulus lipids. Again this could change the properties of the protein if a specific lipid composition of the annulus is required.

In Fig. 6.6a the maximum hydrolytic activity is measured for Na,K-ATPase reconstituted into liposomes composed of monounsaturated phospholipids with increasing acyl chain length (n_c) from 14 to 24 and in the presence or absence of 40 mol% cholesterol. As seen there is an optimum activity for a certain lipid acyl chain length. In the absence of cholesterol the optimum acyl chain length is 22 whereas in the presence of cholesterol a smaller chain length of 18 is preferred.

For a monounsaturated phospholipid the relation between hydrophobic bilayer thickness in \AA and acyl chain length is $\langle d_{\text{unsat}} \rangle \cong 1.75(n_c - 2.6)$. Thus the optimum hydrophobic thickness is about 27 and 34 \AA in the presence or absence of cholesterol, respectively. This can be rationalized via the hydrophobic matching principle since one of the properties of cholesterol is that it increases the bilayer thickness due to the constraint the rigid cholesterol structure imposes on the wobbling acyl chains of the phospholipids. Actually, if similar experiments are performed with the closely related sarco(endo)plasmic Ca-ATPase (SERCA) the optimal acyl chain length in the absence of cholesterol is between 16 and 18 (Lee 2003), which is in accordance with the location of this ATPase to the cholesterol poor membranes of endoplasmic reticulum.

In Fig. 6.6b a logarithmic plot of the turnover number (k_{cat}) of Na,K-ATPase divided by the temperature, (T in Kelvin), as a function of the reciprocal temperature, the so-called Eyring plot, is shown in the presence or absence of 40 mol% cholesterol. From the slope and intercept of such plots the enthalpy and entropy of activation can be evaluated as $-\Delta H^\ddagger/R$ (R is the gas constant) and $\Delta S^\ddagger + 23.76$, respectively. From these values the free energy of activation can be calculated as $\Delta G^\ddagger = \Delta H^\ddagger - T\Delta S^\ddagger$. As seen the Eyring plots are linear, indicating that a single rate constant in the reaction cycle is rate-determining. As described in Sect. 6.3 this is in accordance with the

finding that it is the $E_2 \rightarrow E_1$ reaction that is the main rate-determining step. From the plot the slope and hence ΔH^\ddagger is very similar in the absence (about 67 kJ mol^{-1}) and presence of cholesterol (about 74 kJ mol^{-1}). However, the entropy is very different in the two cases, $-10 \text{ J}\cdot\text{K}^{-1}\cdot\text{mol}^{-1}$ and $59 \text{ J}\cdot\text{K}^{-1}\cdot\text{mol}^{-1}$, respectively. The free energy of activation at 25°C , ΔG^\ddagger , is thus 70 and 56 kJ mol^{-1} in the absence and presence of cholesterol, respectively. That the entropy of activation is particularly dependent on the presence of cholesterol could indicate that the physical property of the membrane, which is a soft material dominated by entropy, is the important factor here. Indeed, cholesterol increases the conformational order of the phospholipids, as described above.

As seen from Fig. 6.6a adjusting the hydrophobic membrane thickness to be optimal without cholesterol does not restore full activity. Thus, cholesterol must have additional and maybe more direct effects on the Na,K-ATPase others than providing an optimal hydrophobic match between the lipid bilayer and the protein. There is increasing evidence for more specific interactions of protein and lipids where certain lipids are necessary to obtain biological function.

Unfortunately only a few examples of membrane protein structures show associated lipids that are known to be important for function. Crystallization procedures typically delipidate the protein, and only tightly bound lipids show sufficient electron density to be resolved at the atomic level.

In the recent crystal structure of shark Na,K-ATPase a cholesterol molecule is resolved near the cytoplasmic face of the membrane in close proximity to M7 and the β -subunit, see Fig. 6.7 (Shinoda et al. 2009). Two conserved tyrosine residues on β , Y40 and Y44, make contact with the cholesterol and with α M7 (see Fig. 6.7b). As seen from Fig. 6.7c cholesterol is positioned in a groove on the protein surface. In contrast to Ca-ATPase the cytoplasmic helical part of M7 (M7') in Na,K-ATPase has a distinct kink of 18° , which appears to have pivotal role in K^+ binding. The unwound parts of M7 and M5 interact strongly. The unwinding is stabilized by hydrogen bonding of Y44 of β to G855 carbonyl of α . The cholesterol shields the unwound part of M7 from the bulk lipid. So β and cholesterol are necessary for stabilizing M7' unwinding and therefore for K^+ binding. A change in M5 orientation, e.g. in transition to $E_1\text{Na}_3$, will be transmitted to M7', M10, the C-terminal, and to the β -subunit. Thus M7-M10 which seem to be a static membrane anchor in SERCA may have a dynamic role in Na,K-ATPase.

Therefore, cholesterol is found at a very essential location in the Na,K-ATPase structure indicating that it may interact more directly in affecting the Na,K-ATPase activity than by influencing the bulk membrane physical properties, as discussed above.

6.4.2 Polyunsaturated Phospholipids

As mentioned above the polyunsaturation index of shark plasma membranes is high, actually as high as for mammalian brain, which is especially rich in PUFA among mammals. Thus in the shark membrane preparation more than $15 \text{ mol}\%$ of fatty

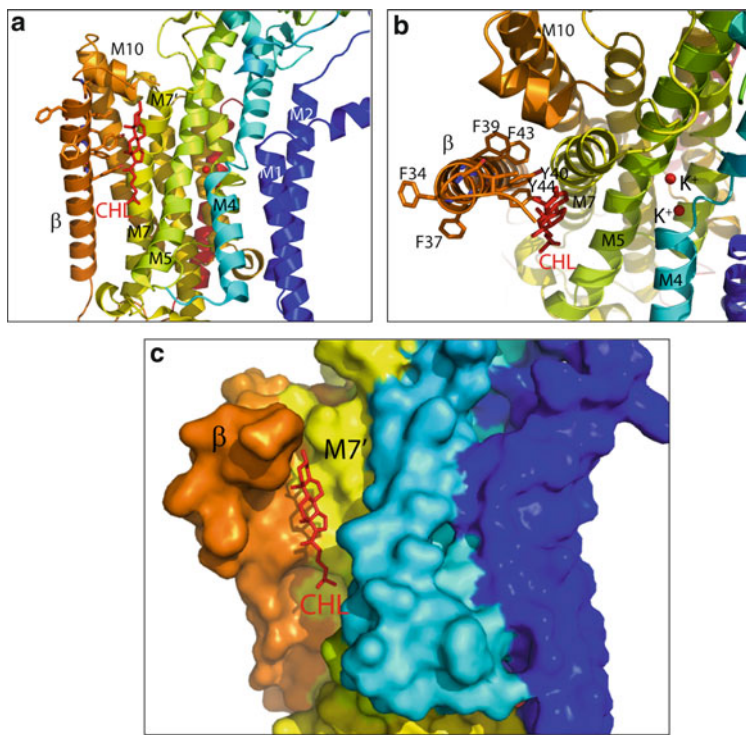


Fig. 6.7 Crystal structure of shark Na,K-ATPase showing the disposition of cholesterol (CHL, in red). Panel (a) is viewed parallel to the membrane plane with the cytoplasmic side facing upward. In panel (b) the view is from the cytoplasmic side down on the membrane. Hydrophobic residues and CHL is shielding the unwound part of M7 from the bulk lipids. In panel (c) cholesterol is shown in a groove on the hydrophobic protein surface. The figures were drawn using PyMol (pdb 2ZXE)

acids is docosahexaenoyl acid (DHA) with 22 carbon atoms and 6 double bonds. DHA has been reported to be beneficial for health in general and a large number of proteins have been demonstrated to be affected by DHA (Litman and Mitchell 1996; Stillwell et al. 2005). Therefore we measured the effect on Na,K-ATPase kinetics of adding 10 mol% polyunsaturated phospholipids like 16:0–22:6 PC and di-22:6 PC to 18:1 PC liposomes with and without 40 mol% CHL (Cornelius 2008). The results are shown in Fig. 6.8a. As seen polyunsaturates inhibit Na,K-ATPase quite drastically, especially in the absence of cholesterol. Also DHA can be demonstrated to increase apparent cytoplasmic Na^+ -affinity, Fig. 6.8b.

As mentioned above DHA affects the function of many different proteins. Thus, rather than a specific effect on proteins, DHA might work by affecting the bulk physical properties of the membrane. A marked incompatibility between DHA and cholesterol has previously been demonstrated and bilayers rich in DHA have a distinctly lower solubility to cholesterol (Huster et al. 1998; Brzustowicz et al. 2002). Cholesterol and DHA have a tendency to lateral phase separate into liquid ordered (l_o) DHA-poor/cholesterol-rich domains and liquid disordered (l_d) DHA-rich/cholesterol-poor

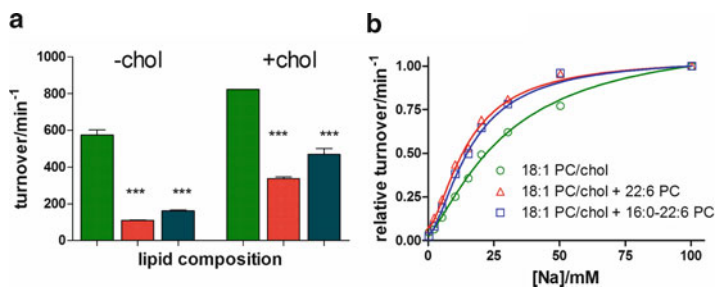


Fig. 6.8 The left panel (a) shows the effects of polyunsaturated phospholipids on the Na,K-ATPase turnover in the absence and presence of 40 mol% cholesterol in the proteoliposomes (left column PC/chol; middle column PC/chol+22:6 PC, and right column PC/chol+16:0–22:6 PC). The inhibition by polyunsaturates is noticeably, but not completely, counteracted by cholesterol. Panel B shows the activation by cytoplasmic Na⁺ of Na,K-ATPase reconstituted into DOPC/Cholesterol liposomes, or into liposomes where either 10 mol% di-22:6 PC or 16:0–22:6 PC are included. $K_{0.5}$ values are 29.7 mM (PC/chol), 15.3 mM (PC/chol+22:6 PC), and 16.4 mM (PC/chol+16:0–22:6 PC) (Data from Cornelius 2008)

domains (Zidovetzki 1997; Mitchel and Litman 1998). Such phase separation could partially exclude cholesterol from the Na,K-ATPase and thus lead to inhibition if the Na,K-ATPase is localized preferentially at inter-domain boundaries. Such a propensity for inter-domain localization of proteins results when the interaction of the l_o -domain (cholesterol) and l_d -domain (22:6 PC) forming lipids with the protein is more favourable than with each other (Yethiraj and Weisshaar 2007). This situation is illustrated in Fig. 6.9a, b where the localization of Na,K-ATPase is shifted to the l_o/l_d -domain interface by addition of polyunsaturated phospholipids.

Such an explanation does not necessary imply direct interaction of cholesterol or polyunsaturated phospholipids by actual binding to the Na,K-ATPase. The effect could also be indirect, exerted e.g. via changes in the lateral pressure profile ($\pi(z)$) in the lipid domains (Cantor 1999), see Fig. 6.9c. The lateral pressure, which varies by several hundreds of atmosphere through the bilayer, can couple to protein function via the stress it exerts on the protein transmembrane domain. As pointed out by Cantor (1999) the pressure profile can have strong effects on protein conformational equilibrium, if the different conformations have different cross-sectional area profiles. Unfortunately we only know the crystal structure of Na,K-ATPase in one conformation, the E₂PK₂-like conformation. However, comparing with the homologous Ca-ATPase it is clear that there the E₁ to E₂ conformational change is associated with a large change in cross-sectional area.

Indeed, DHA with its six double bonds supports curved bilayer structures and addition of polyunsaturated phospholipids to 18:1 PC bilayer changes the curvature stress by redistributing and increasing pressure from a broad region near the centre of the bilayer to regions closer to the aqueous interfaces near the head groups. The effect of cholesterol is opposite. Here pressure decreases (by tenths of atmospheres) near the interfaces with compensating pressure increase in the bilayer centre (Cantor 1999; Gullingsrud and Shulten 2004) (cf. Fig. 6.9c).

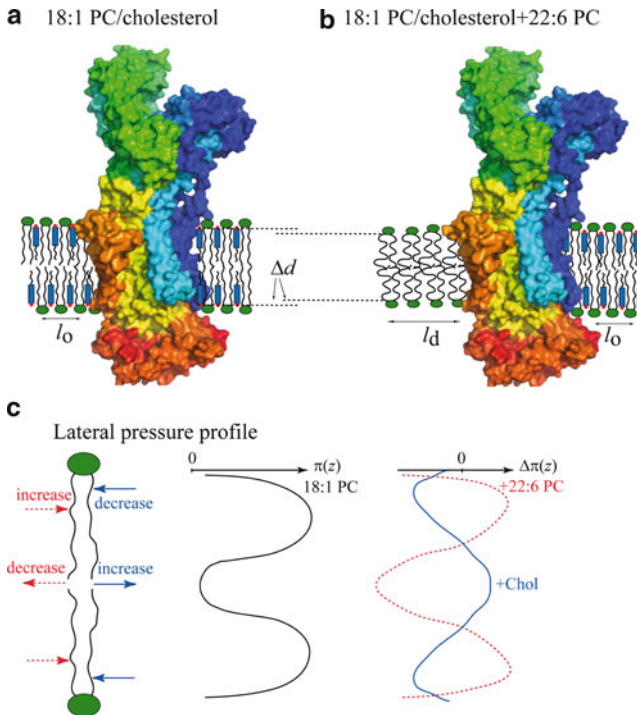


Fig. 6.9 A cartoon illustrating the phase separation and resulting increase in hydrophobic thickness of the bilayer. In panel A the Na,K-ATPase is reconstituted in the presence of 18:1 PC and cholesterol. In B di-22:6 PC is included and a phase separation results where Na,K-ATPase prefers to be situated in the interface between the two domains. Cholesterol changes the liquid disordered phase (l_d) into a liquid ordered phase (l_o) and increases the hydrophobic thickness, Δd , which match the transmembrane part of the Na,K-ATPase better. In (c) the opposing effects of cholesterol (blue) and polyunsaturates (red) on the lateral pressure profile $\Delta\pi(z)$ is illustrated. 22:6 PC increases the lateral pressure near the aqueous interfaces near the head groups and decreases it in the middle of the bilayer, whereas cholesterol has the opposite effect

6.5 Na,K-ATPase Regulation by FXYD Proteins

The FXYD family of ion transport regulators were defined by Sweadner and Rael (2000) based on the invariant FXYD motif. The functions of this family of proteins were unknown except for one, the γ -subunit of kidney Na,K-ATPase, now known as FXYD2. In 2000 another FXYD protein (FXYD10) was found to be specifically associated with and functionally regulating Na,K-ATPase from shark and that spurred the idea that this family of proteins were all specifically associated with and regulating Na,K-ATPase in different tissues (Mahmmoud et al. 2000, 2003). This has later been confirmed (for reviews see Cornelius and Mahmmoud 2003; Garty and Karlsh 2006; Geering 2006). At least one of the FXYD members, FXYD1, is found to be somewhat promiscuous and has been demonstrated also to regulate the

Na⁺/Ca²⁺ exchanger (Zhang et al. 2003) and a voltage activated L-type Ca²⁺-channel in myocytes (Wang et al. 2010).

FXVD10 is shown to inhibit Na,K-ATPase and cross-linking experiments indicate that this is probably via interacting with the Na,K-ATPase A-domain (Mahmoud et al. 2005). Unfortunately this interaction cannot yet be confirmed by the recent crystal structure of shark Na,K-ATPase since a large part of the cytoplasmic domain of FXVD10 (beyond K42) is not resolved in the crystal structure (Shinoda et al. 2009). Like FXVD1, FXVD10 contains a multi-site phosphorylation domain susceptible to PKA- and PKC-phosphorylation, which relieves the Na,K-ATPase inhibition (Mahmoud et al. 2000). This resembles the regulatory mechanism demonstrated for phospholamban (PLB)-regulation of cardiac SERCA2a (MacLennan and Kranias 2003).

Experimental evidence has demonstrated that the cytoplasmic domain of free PLB acts as a conformational switch alternating between contacts to the lipid head groups of the membrane surface and to SERCA (Zamoon et al. 2005), but it is unclear how this relates to the physiological regulation including phosphorylation.

To investigate if a similar conformational switch mechanism is operating in the FXVD-regulation of Na,K-ATPase the effects of phospholipids on the functional regulation of shark Na,K-ATPase by FXVD10 has been addressed by reconstituting Na,K-ATPase into liposomes containing the zwitterionic DOPC and cholesterol in the presence or absence of anionic phospholipids (Cornelius and Mahmoud 2007).

The structural interactions of FXVD10 with Na,K-ATPase in these different lipid environments were investigated using intermolecular cross-linking using the homobifunctional sulfhydryl cross-linker 1,4-Bismaleimidyl-2,3-dihydro-butane (BMDDB), which links C74 in the cytoplasmic domain of FXVD10 to C254 in the A-domain of Na,K-ATPase (Mahmoud et al. 2005). Taken together the results demonstrate that the presence of the anionic phospholipids is important for the detailed kinetics of FXVD regulation of Na,K-ATPase activity. Thus some of the functional effects of anionic phospholipids on Na,K-ATPase activity are mediated by changes in the FXVD/Na,K-ATPase interaction.

However, the results do definitely not indicate that FXVD is alternating between interacting with the Na,K-ATPase and with the lipid surface containing anionic phospholipids. Thus, as probed by intermolecular cross-linking anionic phospholipids do not decrease the interaction of the C-terminal domain of FXVD with the α -subunit. On the contrary, as seen from Fig. 6.10 the cross-linking intensity is *increased* in the presence of anionic phospholipids like PI, PS, or PG indicating that the interaction between FXVD10 and the Na,K-ATPase α -subunit is stabilized. This does not, however, exclude that any free FXVD10 not associated with Na,K-ATPase could attain a bent conformation with the cytoplasmic domain associated with the lipid surface, as with PLB, since the molecular structure of FXVD1 in micelles and lipid membranes seems to have a bent conformation, see Fig. 6.11 (Franzin et al. 2007).

How do anionic phospholipids change the interaction of FXVD10 with the Na,K-ATPase? It is possible, e.g., that electrostatic interactions with the phospholipid head groups of anionic phospholipids and a conserved cluster of basic residues (K42, R44, K46, see Fig. 6.11) in FXVD10 positioned close to the cytoplasmic membrane face

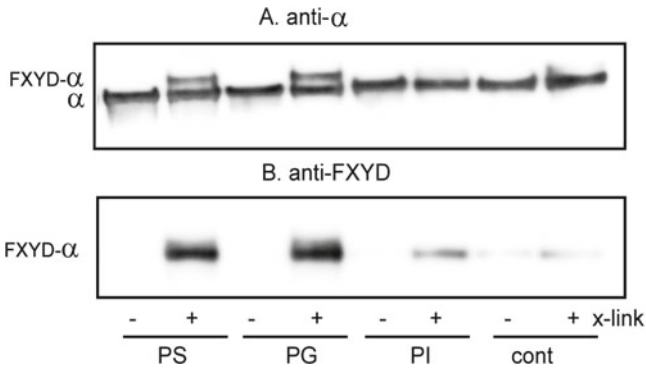


Fig. 6.10 Effects of anionic phospholipids on BMDB cross-linking of FXYD10 to Na,K-ATPase α -subunit. Immunoblot of Na,K-ATPase reconstituted into DOPC:CHL liposomes without (cont) or with 20 mol% PS, PG or PI, before and after BMDB cross-linking probed with anti- α antibody (Panel a) or anti-FXYD antiserum (Panel b). The intensity of cross-linking is clearly increased in the presence of anionic phospholipids, especially by PS and PG (Data from Cornelius and Mahmmoud 2007)

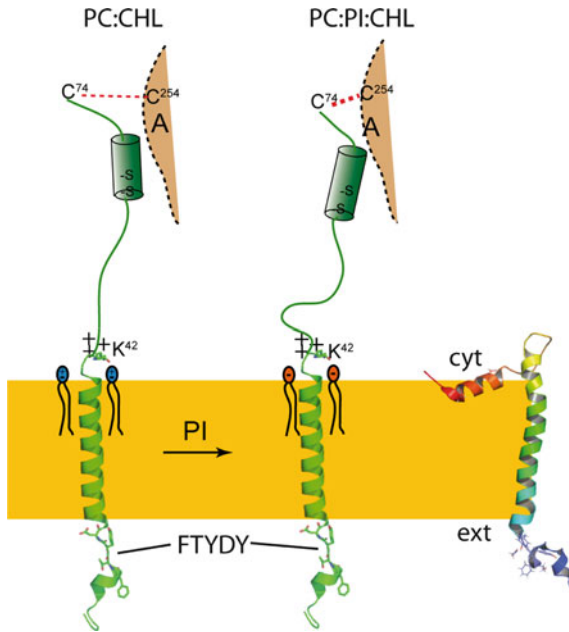


Fig. 6.11 Model illustrating the lipid-dependent interaction between FXYD10 and the Na,K-ATPase. The extracellular and TM part of FXYD is from the crystal structure of Na,K-ATPase (Shinoda et al. 2009), which terminates at K42. The cytoplasmic part of FXYD10 including the multisite phosphorylation domain is modelled. The figure illustrates the interaction between anionic phospholipids (PI, orange) and basic FXYD residues (K42, R44, K46) positioned near the lipid bilayer surface stabilizing a conformation where the modulation of the Na,K-ATPase function is changed and C74 of FXYD is in a more favourably position for cross-linking to C254 in the Na,K-ATPase A-domain. To the right the NMR-structure of FXYD1 is compared in the bend conformation in micelles (pdb 2JO1)

stabilize the cytoplasmic FXYD-Na,K-ATPase interaction, and favour cross-linking, as depicted in Fig. 6.10. This is in accord with the fact that the effect of anionic phospholipids could be screened by addition of Ca^{2+} . Such intermolecular interaction at the transmembrane level of FXYD10 could be transmitted to the cytoplasmic domain of FXYD10 via long range coupling induced by changes in the helical packing in the transmembrane domain. In SERCA the inhibitory regulation by PLB has been shown to involve the stabilization of α -helices within the Ca-ATPase transmembrane domain (Tatulian et al. 2002). Such a mechanism would be in accord with the Na,K-ATPase activation observed after addition of sub-cmc concentrations of the detergent C_{12}E_8 to Na,K-ATPase membrane preparations (Huang et al. 1985; Mahmmoud et al. 2000). Thus, the detergent will partition into the lipid bilayer and affect the interhelical packing of FXYD10 and Na,K-ATPase at the transmembrane level (Therien and Deber 2002). Indeed, there must be long range coupling throughout the entire FXYD protein from the transmembrane, hydrophobic region to the cytoplasmic C-terminal domain.

6.6 Perspective

To summarize, the following factors are found essential for functional reconstitution of Na,K-ATPase and should be considered in future design of active biomimetic membranes:

- Hydrophobic matching between protein and lipids must be achieved, i.e. lipids with a hydrophobic thickness that match the transmembrane domain of Na,K-ATPase must be employed.
- Cholesterol in high amount (20–40 mol%) is required to support optimal activity of Na,K-ATPase. This is to stabilize the structure of Na,K-ATPase around the unwound part of M7', which is pivotal for extracellular K^+ -binding. Cholesterol may also be important in promoting a liquid ordered state of the lipid bilayer that support conformational mobility of the protein.
- A small proportion of anionic phospholipids (a few mol%) is important for the fine-tuning of Na,K-ATPase regulation by FXYD-proteins.
- A proper protein:lipid weight ratio is important both for protein orientation and for supporting optimal specific activity. Excess dilution of protein decreases activity indicating some kind of protein-protein interaction. On the other hand increasing protein concentration may produce very leaky proteoliposomes.
- The detergent must ensure protein solubilization without denaturation, and should be used in concentrations that conserve the annulus lipids.
- The rate of detergent elimination in the mixed protein-lipid micelles is important for protein orientation: fast removal induced by bio-bead addition produces asymmetric protein orientations, whereas slow removal, like dialysis, produces more random protein orientation.

Acknowledgments The Danish Medical Research Foundation and The Danish Agency for Science, Technology and Innovation are kindly acknowledged for financial support.

References

- Albers, R.W.: Biochemical aspects of active transport. *Annu. Rev. Biochem.* **36**, 727–756 (1967)
- Baginsky, E.S., Foa, P.P., Zak, B.: Microdetermination of inorganic phosphate, phospholipids, and total phosphate in biological materials. *Clin. Chim. Acta* **13**, 326–332 (1967)
- Brzustowicz, M.R., Cherezov, V., Caffrey, M., Stillwell, W., Wassall, S.R.: Molecular organization of cholesterol in polyunsaturated membranes: microdomain formation. *Biophys. J.* **82**, 285–298 (2002)
- Cantor, R.S.: Lipid composition and the lateral pressure profile in bilayers. *Biophys. J.* **76**, 2625–2639 (1999)
- Cherezov, V., Rosenbaum, D.M., Hanson, M.A., Rasmussen, S.G.F., Thian, F.S., Kobilka, T.S., Choi, H.J., Kuhn, P., Weis, W.I., Kobilka, B.K., Stevens, R.: High-resolution crystal structure of an engineered human β_2 -adrenergic G protein-coupled receptor. *Science* **318**, 1258–1265 (2007)
- Clarke, R.J., Kane, D.J.: Two gears of pumping by the sodium pump. *Biophys. J.* **93**, 4187–4196 (2007)
- Cornelius, F.: Incorporation of C12E8-solubilized Na^+ , K^+ -ATPase into liposomes: determination of sidedness and orientation. *Methods Enzymol.* **156**, 156–167 (1988)
- Cornelius, F.: Uncoupled Na^+ -efflux on reconstituted shark Na, K-ATPase is electrogenic. *Biochem. Biophys. Res. Commun.* **160**, 801–807 (1989)
- Cornelius, F.: Variable stoichiometry in reconstituted shark Na, K-ATPase engaged in uncoupled efflux. *Biochim. Biophys. Acta* **1026**, 147–152 (1990)
- Cornelius, F.: Functional reconstitution of the sodium pump. Kinetics of exchange reactions performed by reconstituted Na/K-ATPase. *Biochim. Biophys. Acta* **1071**, 19–66 (1991)
- Cornelius, F.: Phosphorylation/dephosphorylation of reconstituted shark Na^+ , K^+ -ATPase: one phosphorylation site per $\alpha\beta$ protomer. *Biochim. Biophys. Acta* **1235**, 197–204 (1995a)
- Cornelius, F.: Cholesterol modulation of molecular activity of reconstituted shark Na^+ , K^+ -ATPase. *Biochim. Biophys. Acta* **1235**, 205–212 (1995b)
- Cornelius, F.: Liposomes in reconstitution of ion-pumps. Electrogenic properties of the Na^+ , K^+ -ATPase and the sarcoplasmic Ca^{2+} -ATPase. *J. Lipos. Res.* **5**, 399–412 (1995c)
- Cornelius, F.: Modulation of Na, K-ATPase and Na-ATPase activity by phospholipids and cholesterol. I. Steady-state kinetics. *Biochemistry* **40**, 8842–8851 (2001)
- Cornelius, F.: Cholesterol-dependent interaction of polyunsaturated phospholipids with Na, K-ATPase. *Biochemistry* **47**, 1652–1658 (2008)
- Cornelius, F., Mahmood, Y.A.: Functional modulation of the sodium pump: the regulatory proteins “Fixit”. *News Physiol. Sci.* **18**, 119–124 (2003)
- Cornelius, F., Mahmood, Y.A.: Modulation of FXYD interaction with Na, K-ATPase by anionic phospholipids and protein kinase phosphorylation. *Biochemistry* **46**, 2371–2379 (2007)
- Cornelius, F., Møller, J.V.: Liposomes in reconstitution of ion-pumps. In: Barenholz, Y., Lasic, D.D. (eds.) *Handbook of Nonmedical Applications of Liposomes*, vol. II, pp. 219–243. CRC Press, New York (1996)
- Cornelius, F., Skou, J.C.: Reconstitution of $(\text{Na}^+ + \text{K}^+)\text{-ATPase}$ into phospholipid vesicles with full recovery of its specific activity. *Biochim. Biophys. Acta* **772**, 357–373 (1984)
- Cornelius, F., Turner, N., Christensen, H.R.: Modulation of Na K-ATPase by phospholipids and cholesterol. II. Steady-state and presteady-state kinetics. *Biochemistry* **42**, 8541–8549 (2003)
- Esmann, M., Christiansen, C., Karlsson, K.-A., Hansson, G.C., Skou, J.C.: Hydrodynamic properties of solubilized $(\text{Na}^+ + \text{K}^+)\text{-ATPase}$ from rectal glands of *Squalus acanthias*. *Biochim. Biophys. Acta* **603**, 1–12 (1980)
- Forgac, M., Chin, G.: K^+ -independent active transport of Na^+ by the $(\text{Na}^+ + \text{K}^+)\text{-stimulated}$ adenosine triphosphatase. *J. Biol. Chem.* **256**, 3645–3646 (1981)
- Franzin, C.M., Gong, X.M., Teriete, P., Marassi, F.M.: Structures of the FXYD regulatory proteins in lipid micelles and membranes. *J. Bioenerg. Biomembr.* **39**, 379–383 (2007)
- Garty, H., Karlish, S.J.D.: Role of FXYD proteins in ion transport. *Annu. Rev. Physiol.* **68**, 431–459 (2006)

- Geering, K.: FXYP proteins: new regulators of Na-K-ATPase. *Am. J. Physiol. Renal Physiol.* **290**, F241–F250 (2006)
- Gullingsrud, J., Schulten, K.: Lipid bilayer pressure profiles and mechanosensitive channel gating. *Biophys. J.* **86**, 3496–3509 (2004)
- Huang, W.-H., Kakar, S.S., Askari, A.: Mechanisms of detergent effects on membrane-bound (Na⁺ + K⁺)-ATPase. *J. Biol. Chem.* **260**, 7356–7361 (1985)
- Humphrey, P.A., Lüpfer, C., Apell, H.-J., Cornelius, F., Clarke, R.J.: Mechanism of the rate-determining step of the Na⁺, K⁺-ATPase pump cycle. *Biochemistry* **41**, 9496–9507 (2002)
- Huster, D., Arnold, K., Gawrisch, K.: Influence of docosahexaenoic acid and cholesterol on lateral lipid organization in phospholipid mixtures. *Biochemistry* **37**, 17299–17308 (1998)
- Jensen, M.Ø., Mouritsen, O.G.: Lipids do influence protein function—the hydrophobic matching hypothesis revisited. *Biochim. Biophys. Acta* **1666**, 205–226 (2004)
- Jones, O.T., McNamee, M.G.: Annular and nonannular binding sites for cholesterol associated with the nicotinic acetylcholine receptor. *Biochemistry* **27**, 2364–2374 (1988)
- Lee, A.G.: Lipid-protein interactions in biological membranes: a structural perspective. *Biochim. Biophys. Acta* **1612**, 1–40 (2003)
- Lindberg, O., Ernster, L.: Determination of organic phosphorus compounds by phosphate analysis. *Methods Biochem. Anal.* **3**, 1–22 (1956)
- Litman, B.R., Mitchell, D.C.: A role for phospholipid polyunsaturation in modulating membrane protein function. *Lipids* **31**, S193–S197 (1996)
- Luecke, H., Schobert, B., Richter, H.-T., Cartailler, J.-P., Lanyi, J.K.: Structure of bacteriorhodopsin at 1.55 Å resolution. *J. Membr. Biol.* **291**, 899–911 (1999)
- Lundbæk, J.A., Birn, P., Hansen, A.J., Søgård, R., Nielsen, C., Grishman, J., Bruno, M.J., Tape, S.E., Egebjerg, J., Greathouse, D.V., Mattice, G.L., Koeppe II, R.E., Andersen, O.S.: Regulation of sodium channel function by bilayer elasticity – the importance of hydrophobic coupling. *J. Gen. Physiol.* **121**, 599–621 (2004)
- Lüpfer, C., Grell, E., Pintschvius, V., Apell, H.-J., Cornelius, F., Clarke, R.J.: Rate limitation of the Na⁺, K⁺-ATPase pump cycle. *Biophys. J.* **81**, 2069–2081 (2001)
- MacLennan, D.H., Kranias, E.G.: Phospholamban: a crucial regulator of cardiac contractility. *Nat. Rev. Mol. Cell Biol.* **4**, 566–577 (2003)
- Mahmoud, Y.A., Vorum, H., Cornelius, F.: Identification of a phospholemman-like protein from shark rectal glands. Evidence for indirect regulation of Na, K-ATPase by protein kinase C via a novel member of the FXYP family. *J. Biol. Chem.* **275**, 35969–35977 (2000)
- Mahmoud, Y.A., Cramb, G., Maunsbach, A.B., Cutler, C.P., Meischke, L., Cornelius, F.: Regulation of Na, K-ATPase by PLMS, the phospholemman-like protein from shark. Molecular cloning, sequence, expression, cellular distribution, and functional effects of PLMS. *J. Biol. Chem.* **278**, 37427–37438 (2003)
- Mahmoud, Y.A., Vorum, H., Cornelius, F.: Interaction of FXYP10 (PLMS) with Na, K-ATPase from shark rectal glands. Close proximity of Cys74 of FXYP10 to Cys254 in the A domain of the α -subunit revealed by intermolecular cross-linking. *J. Biol. Chem.* **280**, 27776–27782 (2005)
- McAuley, K.E., Fyfe, P.K., Ridge, J.P., Isaacs, N.W., Cogdell, J.R., Jones, M.R.: Structural details of an interaction between cardiolipin and an integral membrane protein. *Proc. Natl. Acad. Sci. U.S.A.* **96**, 14706–14711 (1999)
- Mitchel, D.C., Litman, B.J.: Effect of cholesterol on molecular order and dynamics in highly polyunsaturated phospholipid bilayers. *Biophys. J.* **75**, 896–908 (1998)
- Mouritsen, O.G., Bloom, M.: Mattress model of lipid-protein interactions in membranes. *Biophys. J.* **46**, 141–153 (1984)
- Peterson, G.L.: A simplification of the protein assay method of Lowry et al. which is more generally applicable. *Anal. Biochem.* **83**, 346–356 (1977)
- Post, R.L., Hegyvary, C., Kume, S.: Activation by adenosine triphosphate in the phosphorylation kinetics of sodium and potassium ion transport adenosine triphosphatase. *J. Biol. Chem.* **247**, 6530–6540 (1972)

- Shannon, M.A., Bohn, P.W., Elimelech, M., Georgiadis, J.G., Marinas, B.J., Mayes, A.M.: Science and technology for water purification in the coming decades. *Nature* **452**, 301–310 (2008)
- Shih-Chieh, J.H., Artyukhin, A.B., Misra, N., Martinez, J.A., Stroeve, P.A., Grigoropoulos, C.P., Ju, J.-W.W., Noy, A.: Carbon nanotube transistor controlled by a biological ion pump gate. *Nano Lett.* **10**, 1812–1826 (2010)
- Shinoda, T., Ogawa, H., Cornelius, F., Toyoshima, C.: Crystal structure of the sodium-potassium pump at 2.4 Å resolution. *Nature* **459**, 446–450 (2009)
- Skou, J.C., Esmann, M.: Preparation of membrane-bound and solubilized (Na⁺+K⁺)-ATPase from rectal glands of *Squalus acanthias*. The effect of preparative procedures on purity, specific and molar activity. *Biochim. Biophys.* **567**, 436–444 (1979)
- Stillwell, W., Shaikh, S.R., Zerouga, M., Siddiqui, R., Wassall, S.R.: Docosahexaenoic acid affects cell signalling by altering lipid rafts. *Reprod. Nutr. Dev.* **45**, 559–579 (2005)
- Sweadner, K.J., Rael, E.: The FXFD gene family of small ion transport regulators or channels: cDNA sequence, protein signature sequence, and expression. *Genomics* **68**, 41–56 (2000)
- Tatulian, S.A., Chen, B., Li, J., Negash, S., Middaugh, C.R., Bigelow, D.J., Squiere, T.C.: The inhibitory action of phospholamban involves stabilization of α -helices within the Ca-ATPase. *Biochemistry* **41**, 741–751 (2002)
- Therien, A.G., Deber, C.M.: Interhelical packing in detergent micelles. Folding of a cystic fibrosis transmembrane conductance regulator construct. *J. Biol. Chem.* **277**, 6067–6072 (2002)
- Wang, X., Goa, G., Guo, K., Yarotsky, V., Huang, C., Elmslie, K.S., Peterson, B.Z.: Phospholemman modulates the gating of cardiac L-type calcium channels. *Biophys. J.* **98**, 1149–1159 (2010)
- Yethiraj, A., Weisshaar, J.C.: Why are lipid rafts not observed in vivo? *Biophys. J.* **93**, 3113–3139 (2007)
- Zamoon, J., Nitu, F., Karim, C., Thomas, D.D., Veglia, G.: Mapping the interaction surface of a membrane protein: unveiling the conformational switch of phospholamban in calcium pump regulation. *Proc. Natl. Acad. Sci. U.S.A.* **102**, 4747–4752 (2005)
- Zhang, X.Q., Ureshi, A., Song, J., Carl, L.L., Tian, Q., Stahl, R.C., Carey, D.J., Rothblum, L.I., Cheung, J.Y.: Phospholemman modulates Na⁺/Ca²⁺ exchange in adult rat cardiac myocytes. *Am. J. Physiol. Heart Circ. Physiol.* **284**, H225–H233 (2003)
- Zidovetzki, R.: Membrane properties and the activation of protein kinase C and phospholipase A₂. *Curr. Top. Membr.* **44**, 255–283 (1997)

Chapter 7

Passive Transport Across Biomimetic Membranes

Karin Stibius, Sania Bäckström, and Claus Hélix-Nielsen

Abstract An ideal biomimetic sensor/separation device requires the supporting membrane matrix to be virtually impermeable to anything but the solute in question. In practice, however, a biomimetic support matrix will generally have finite permeabilities to water, electrolytes, and non-electrolytes. The feasibility of a biomimetic device thus depends on the relative transport contribution from both protein and biomimetic support matrix. Here we will discuss models for passive membrane permeability of solutes and water in the framework of lipid and polymer based biomimetic membranes.

7.1 Energetic Barriers

A fundamental question to be addressed in the development of biomimetic membrane separation devices is how much transport is mediated by the proteinaceous pathways inserted into the supporting matrix and how much transport it mediated by the matrix itself? A general answer to this question depends on the solute, the transporting protein and the structure of the support. Although the phenomenon seems quite simple: solutes and water move in response to transmembrane gradients (electrochemical, hydrostatic, and osmotic gradients), the intricate mechanistic details of protein and membrane selectivity have remained a major obstacle for understanding biological membrane transport for more than a century.

K. Stibius • S. Bäckström • C. Hélix-Nielsen (✉)
Department of Physics (DTU), Technical University of Denmark,
Building 309, Rm 138 Fysikvej 309, DK-2800 Kgs. Lyngby, Denmark
e-mail: karin.stibius@fysik.dtu.dk; sania.ibragimov@gmail.com;
claus.helix.nielsen@fysik.dtu.dk

The mechanism by which water and solutes permeate membranes has been much debated. The classical description (Graham 1866) has been the solubility-diffusion model in which the permeant solute molecule leaves the external phase by dissolving in the membrane. It then undergoes molecular diffusion in the membrane, driven towards the other side of the membrane by for example a concentration or pressure gradient, after which it enters (evaporates/resolvates) into the external phase. Thus the permeability coefficient P is defined by the ratio between the flux J of the permeant species and its concentration gradient Δc over the membrane of thickness d . Using Fick's first law P may be expressed as

$$P = KD/d \quad (7.1)$$

where D is the diffusion coefficient of the permeant species, K is the partition coefficient for the solute between water and the membrane low dielectric interior (Finkelstein 1987; Gennis 1989). P conveniently is expressed in units of cm s^{-1} and K may be expressed based on molarities as

$$K = \frac{V_w}{V_{HC}} \exp(-\Delta G/RT) \quad (7.2)$$

where V_w is the molar volume of water ($18.1 \text{ cm}^3 \text{ mol}^{-1}$ or 30 \AA^3 per molecule) and V_{HC} is the molar volume of the low dielectric part of the membrane, and ΔG is the associated change in Gibbs free energy. The change in Gibbs free energy associated with permeants crossing a barrier can be regarded as arising from several component energies. The component energies depend on the permeant species (Paula et al. 1996; Volkov and Hampton 2008; Volkov et al. 1997). These components will be presented in the following.

7.1.1 Charged Permeants

An important class of permeants is formed from ions such as Na^+ , K^+ , Ca^{2+} , Mg^{2+} , and Cl^- . For ions, part of the total Gibbs free energy can be described as arising from the dielectric polarization of the medium surrounding the ion. To a first approximation the potential energy of the ion at a point located in the membrane interior far from the boundary is the sum of the energies associated with (1): discharging of a sphere with charge q and radius r in an aqueous medium with a dielectric constant ϵ_w ; (2) transfer of the uncharged sphere across the boundary; (3) recharging (to q) of the sphere in a medium corresponding to the hydrocarbon interior of a biological membrane with a corresponding dielectric constant ϵ_{HC} . According to the Born model (1920), the energy associated with steps (1) and (3) above can be expressed as:

$$\Delta G_{\text{Born}} = \frac{N_a q^2}{8\pi\epsilon_0 r} \left(\frac{1}{\epsilon_{HC}} - \frac{1}{\epsilon_w} \right) \quad (7.3)$$

where N_a is Avogadro's number and ϵ_0 the absolute vacuum permittivity.

The second step mentioned above corresponds to the transfer of the uncharged sphere from the aqueous phase to the membrane interior and involves removal of a spherical cavity in the aqueous phase and its recreation in the membrane interior. The associated energy can be approximated as

$$\Delta G_H = -N_a 4\pi r^2 \gamma_{W/HC} \quad (7.4)$$

where $\gamma_{W/HC}$ is the difference in interfacial tensions per unit area between the two media. This energy component is always negative and will therefore lower the total free energy. Thus the formation of a cavity *per se* is more favorable in the hydrophobic phase versus in the aqueous phase.

However, Eq. 7.3 overestimates the energy of transfer as an ion moving from the aqueous phase across the boundary into the hydrocarbon phase of a membrane is subjected to image forces as the membrane is only a few nm thick. Thus the ion is repelled from the boundary while in the aqueous phase but attracted toward the boundary while in the hydrocarbon phase. The associated image energy can be expressed as

$$\Delta G_I = \frac{N_a q^2}{16\pi\epsilon_0\epsilon_{HC}} \left(\frac{1}{x} + \frac{1}{d} \sum_{n=1}^{\infty} \left[\frac{\vartheta^{2n}}{n+x/d} + \frac{\vartheta^{2n-2}}{n-x/d} - \frac{\vartheta^{2n}}{n+r/d} - \frac{\vartheta^{2n-2}}{n-r/d} \right] \right) \quad (7.5)$$

where x denotes the position of the ion sphere in the membrane ($0 < x < d$) and

$$\vartheta = \frac{\epsilon_W - \epsilon_{HC}}{\epsilon_W + \epsilon_{HC}} \quad (7.6)$$

see (Neumcke and Luger 1969) for a derivation. Since the dielectric constant of the bilayer interior is always lower than the dielectric constant of water, the sign of ΔG_I is negative and this energy component will therefore also lower the total free energy.

Judged from Eqs. 7.1 and 7.3 cation and anion associated energies and membrane permeabilities are equal. However, permeability studies of hydrophobic ions surprisingly revealed that the permeability of the lipid bilayer membrane for hydrophobic anions was approximately 10^5 greater than that of hydrophobic cations (Lieberman and Topaly 1969). To explain this difference in behavior it was hypothesized that the interior of the membrane must initially be positively charged.

Haydon and coworkers (Hladky and Haydon 1973; Haydon and Myers 1973) later recognized that the positive charge within the membrane must arise from oriented molecular dipoles in the membrane surface and coined the term ‘‘dipole potential.’’

Although the total lipid membrane interfacial dipolar moment may have contributions from various lipid molecule moieties, the carbonyls just below the glycerol backbone seem to play a major role. As a consequence interfacial dipole potentials $\Delta\phi$ are induced and the measured values are in the order of hundreds of mV.

Also oriented water molecules that are tightly bound in the lipid headgroup region might contribute to interfacial dipole potential. The contribution of the dipole potential to the total Gibbs free energy can be expressed as

$$\Delta G_D = -qN_a\Delta\phi \quad (7.7)$$

The negative sign in Eq. 7.7 implies that the barrier for anions is smaller than for cations. The interplay between hydrated ions and the hydrated hydrophilic moieties of the membrane molecules (lipids or block co-polymers) is complex. Thus the dipolar interfacial potential will effectively be reduced by the ion hydration shell(s) due to the screening of ion charge by the hydration shells. Reciprocally, ion hydration shell water molecules can interact with dipolar moments and fixed charges in the hydrophilic region of the membrane. Paula et al. (1998) discuss this issue in detail and describe how the effects can be captured either by reducing the interfacial dipole potential or keeping the dipolar energy term (Eq. 7.7) unaltered (with 250 mV as a representative value for $\Delta\phi$) and including an extra energy term ΔG_{SP} to describe specific ionic interactions. The extra term can be quantified by fitting experimental ionic permeabilities as functions of membrane thickness to the predicted permeabilities calculated using Eqs. 7.1–7.7

Dipole potentials of lipid have been determined from the difference in conductance between hydrophobic cation/anion pairs (e.g. tetraphenylarsonium (+)/tetraphenylborate (-)) where it is assumed that the magnitude of the hydration energies of the anions and cations is equal. The validity of this assumption has been tested by quantum mechanical calculations of the hydration energies (Schamberger and Clarke 2002) resulting in additive corrections up to more than 100 mV for some lipids. Thus the corrected $\Delta\phi$ or di-oleoylphosphatidylcholine amounts to 334 mV (as compared to a previously determined value of 224 mV (Gawrisch et al. 1992)). This brings the $\Delta\phi$ values estimated from hydrophobic cation/anion experiments close to lipid monolayer based determinations of $\Delta\phi$ which generally are 100–200 mV higher than uncorrected $\Delta\phi$ values (Hladky and Haydon 1973; Beitinger et al. 1989; Smaby and Brockman 1990). Thus the value of the corrective energy term ΔG_{SP} mentioned above depends on the estimate of $\Delta\phi$. Figure 7.1 shows the calculated values for ΔG_{Born} , ΔG_H , ΔG_I , ΔG_D and their sum ΔG_{Total} .

For small values of r the Born term is positive and dominates ΔG_{Total} , all other terms are <0 . For $r > 4 \text{ \AA}$ the sum of the ΔG_H , ΔG_I , and ΔG_D terms is larger than ΔG_{Born} leading to effectively negative values for ΔG_{Total} . While ΔG_D is independent of r , and ΔG_I is only weakly dependent on r , $\Delta G_H \sim r^2$. This quadratic relation is the basis for the relative high permeability of large anions. Thus for biomimetic membranes based on lipids envisioned for applications where the separation of small negatively charged molecules is crucial for function, this may be problematic. An approach to circumvent this issue could be to use block co-polymer membranes instead where the effective interfacial dipole potential may be tuned so the ΔG_D can to some extent counterbalance ΔG_H at least for smaller values of r . It should be noted that the energetic analysis presented here is essentially a macroscopic description neglecting energetic contributions arising from the molecular packing of membrane

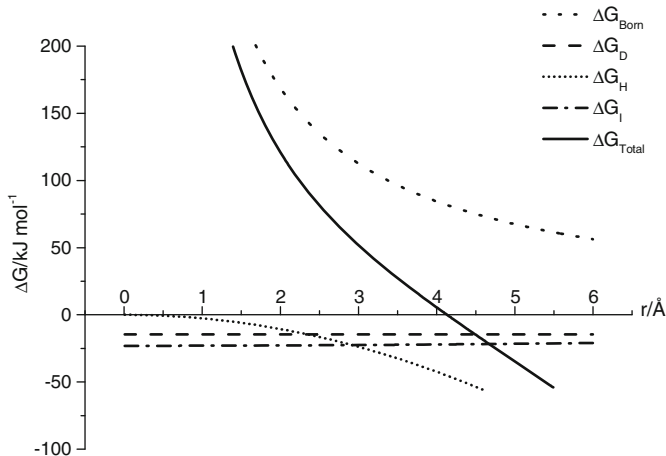


Fig. 7.1 The total free energy ΔG_{Total} for transferring a cation with charge $+1e$ and radius r from an aqueous phase ($\epsilon_w=78$) into the center of a low dielectric interior ($x=d/2$) of a membrane ($\epsilon_{HC}=2$) arising from component energies: the Born term (Eq. 7.3), the hydration term (Eq. 7.4) with $\gamma_{WHC}=0.035 \text{ mNm}^{-1}$, the image force term (Eq. 7.5) with $d=6 \text{ nm}$ and the dipole term (Eq. 7.7) with $\Delta\phi=150 \text{ mV}$. Equations are all implemented in Origin and the script-code is given below (the summation in Eq. 7.5 converges well within 50 terms)

```
col(B)=1*((78-2)/(78+2)); (* Eq. 7.6 *)
col(C)=(col(A)/100)*1e-10; (* range of radius values *)
dummyT=60e-10; (* membrane thickness *)
dummyS=0; (* dummy for storing evaluation of Eq. 7.5 *)
for(ii=1; ii<=50; ii++) (* summation loop for bracket term in Eq. 7.5 *)
{
dummyA=((1*col(B))^(2*ii))/(ii+0.5); (* 1. term in bracket *)
dummyB=((1*col(B))^(2*ii-2))/(ii-0.5); (* 2. term in bracket *)
dummyC=((1*col(B))^(2*ii))/(ii+(col(c)/(dummyT))); (* 3. term in bracket *)
dummyD=((1*col(B))^(2*ii-2))/(ii-(col(c)/(dummyT))); (* 4. term in bracket *)
dummyS=(dummyA+dummyB-dummyC-dummyD)+dummyS; (* accumulated value *)
}
Col(H)=dummyS; (* result from summation in Eq. 7.5 for each radius value *)
avogadro=6.022e23; (* avogadros number *)
charge=1.6e-19; (* elementary charge *)
epsilonz=8.85e-12; (* epsilon zero *)
Col(I)=-((avogadro*charge*charge*col(B))/(16*3.1416*epsilonz*2))*
((2/dummyT)+(1/dummyT)*col(H));
(* Col(I) stores the image force term *)
col(K)=(avogadro*charge*charge)/(8*3.1416*epsilonz*col(C))*((1/2)-(1/78));
(* born term *)
col(P)=-charge*avogadro*0.15*(col(A)/col(A)); (* dipole term *)
col(Q)=-avogadro*4*pi*col(C)*Col(C)*0.035; (* hydration term *)
col(T)=col(O)+col(P)+col(Q); (* total free energy *)
```

components. Thus when solute size is comparable with membrane component size, the cohesive energies of the membrane assembly will also contribute to the overall energetic barrier for translocation.

7.1.2 Dipolar Permeants

Water and non-electrolyte permeabilities in protein-free lipid bilayers have been investigated intensely over the last 40 years. For water the permeability has been determined both by tracer diffusion measurements yielding the diffusional membrane permeability P_d and osmotic flow measurements giving the P_f , for a comprehensive review see (Finkelstein 1987).

Although the osmotic membrane permeability P_f is clearly a function of bilayer composition, the mechanism by which water permeates lipid bilayers has been much debated. The classical description has been the solubility diffusion model in which the water permeability is proportional to the partition coefficient for water into the bilayer hydrocarbon core (Overton's rule) and the diffusion within that region and inversely proportional to the hydrophobic bilayer thickness. However this correlation predicts a thickness (derived from permeability measurements) for egg lecithin bilayers which is three times higher than measured from structural measurements (Finkelstein 1987; Nagle and Tristram-Nagle 2000). Recently a theory for passive water permeation has been proposed that is consistent with refined measurements (Nagle et al. 2008; Mathai et al. 2008). In short, the simple solubility-diffusion model is extended to include a term proportional to the interfacial area per lipid at each interface effectively creating a three layer model. This provides a framework for understanding how passive water permeability of biomimetic membranes may be controlled by tuning both interfacial and bulk membrane properties.

In a general continuum description of partitioning of dipolar molecules such as water into low-dielectric media such as the interior of lipid bilayers or block co-polymer mono- and bilayers one may proceed in a manner similar to the description of charged solutes: define the Gibbs energy of transfer and correct for image forces following the approach of (Volkov and Hampton 2008). According to (Bell 1931) the energy of transferring an ideal dipole in a spherical cavity with radius r from water (ϵ_w) to a 'hydrocarbon' medium (ϵ_{HC}) is:

$$\Delta G_{Bell} = \frac{N_a \mu^2}{4\pi\epsilon_0 r^3} \left(\frac{\epsilon_w - \epsilon_{HC}}{(2\epsilon_w + 1)(2\epsilon_{HC} + 1)} \right) \quad (7.8)$$

The image forces for a dipole in a medium (membrane) with thickness d surrounded by aqueous media on each side give rise to a Gibbs energy (Arakelyan and Arakelyan 1983; Arakelyan et al. 1985):

$$\Delta G_{I,Dip} = -\frac{N_a \mu^2}{6\pi\epsilon_0 \epsilon_{HC} d^3} \sum_{n=1}^{\infty} \left(\frac{\vartheta^{2n-1}}{(2n-1-\alpha)^3} + \frac{\vartheta^{2n-1}}{(2n-1+\alpha)^3} \right) \quad (7.9)$$

with ϑ as defined in Eq. 7.6 and $\alpha=2x/d$ where x is the 'depth' position in the membrane. Thus the total energy for water transfer in this description is the sum of Eqs. 7.8 and 7.9 where a numerical evaluation of Eq. 7.9 can be performed similar to that of Eq. 7.5 (see legend to Fig. 7.1).

7.2 Osmotic Barrier Properties

In the following osmotic water transport across a barrier will be briefly described followed by an introduction to methods for evaluation of membrane osmotic water permeability of a membrane with focus on the stopped-flow light scattering method.

7.2.1 Water Permeability

Water volume flux J_v [cm s^{-1}] per unit area through a permeable membrane is a function of the hydrostatic pressure difference ($\Delta P = P_2 - P_1$ [$\text{Pa} = \text{Nm}^{-2}$]) and the osmotic pressure difference ($\Delta \Pi = \Pi_2 - \Pi_1$ [$\text{Pa} = \text{Nm}^{-2}$]), see Fig. 7.2. For an ideal semipermeable membrane only water can pass the membrane, no solutes $J_s = 0$. The water flux is proportional to the pressure, thus the water volume flux, J_v , can be described as:

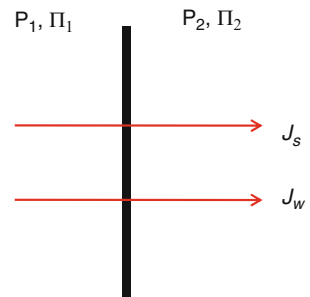
$$J_v = L_p (\Delta \Pi - \Delta P) \quad (7.10)$$

where L_p [$\text{cm N}^{-1} \cdot \text{s}^{-1}$] is the hydraulic permeability per unit area of the membrane and can be written as a function of the membrane permeability, P_f [cm s^{-1}], the partial molar volume of water, V_w and the product of the molar gas constant $R = 8.314 \text{ JK}^{-1} \cdot \text{mol}^{-1}$ and the temperature T [K]:

$$L_p = \frac{P_f V_w}{RT} \quad (7.11)$$

Equation 7.10 may be corrected to take into account the reflection factor σ_i which describes the membrane's ability to reflect the i^{th} solute where for $\sigma_i = 1$ the membrane is completely impermeable to the i^{th} solute and for $\sigma_i = 0$ the membrane is completely permeable to the i^{th} solute. The volume flux can be described as:

Fig. 7.2 Water and solute transport across a membrane separating compartments 1 and 2 with osmotic and hydrostatic pressures Π and P . Positive water volume flux, J_v , and positive solute flux, J_s , are indicated



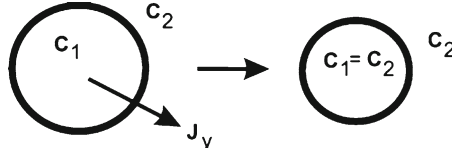


Fig. 7.3 Water transport across a membrane separating compartments 1 and 2 leading to shrinking of the closed compartment 1 from an initial equilibrium volume V_0 to a new equilibrium volume V_∞ . Positive water volume flux, J_v , is indicated. The system reaches equilibrium when $C_1 = C_2$

$$J_v = L_p \left(\sum_{i=0}^n \sigma_i \Delta \Pi_i - \Delta P \right) \quad (7.12)$$

where n is the number of different solutes. The osmotic pressure, Π , can be defined as, $\Pi = \Phi i R T C$, where C [mol/cm³] is the solute concentration, Φ is the molar osmotic coefficient which accounts for the deviation of the solution from ideal behavior, and i the number of ionic species (see also Chap. 2). Thus from Eqs. 7.11 and 7.12 the volume flux, J_v , can be written as:

$$\begin{aligned} J_v &= L_p \left(R T \sum_{j=0}^n i \sigma_j \Phi_j (C_{2j} - C_{1j}) - \Delta P \right) \\ &= P_f V_w \left(\sum_{j=0}^n i \sigma_j \Phi_j (C_{2j} - C_{1j}) - \frac{\Delta P}{R T} \right) \end{aligned} \quad (7.13)$$

where C_{1j} is the concentration of the j^{th} solute on one side of the membrane and C_{2j} is the concentration of the j^{th} solute on the other side of the membrane.

For osmotic swelling/shrinking experiments $\Delta P = 0$. A schematic drawing can be seen in Fig. 7.3. With the assumption that no solutes escape the inside of the vesicles or cells and $n = C \cdot V$ then $C_1(t) \cdot V_1(t) = C_1(0) \cdot V_1(0)$, since the number of solutes, n , is constant. Thus the reaction of the osmotic shrinking/swelling will end when $C_1 = C_2$, and the volume water flux J_v is found by:

$$J_v = P_f V_w \left(\sum_{j=0}^n i \sigma_j \Phi_j (C_{2j} - C_{1j}) \right) = P_f V_w (C_2 - C_1) \quad (7.14)$$

Also the initial change in volume can be found as the change in number of water molecules, n_w , times the molar volume of water, which is equal to the volume water flux multiplied with the area of the membrane, A [cm²]:

$$\frac{dV}{dt} = - \frac{dn_w}{dt} \cdot V_w = -J_v A = -P_f V_w A (C_2 - C_1) \quad (7.15)$$

Table 7.1 Different experimental methods for measurement of P_f

Method	Typical membrane	Output
Cell swelling	Oocytes, Protoplasts, vacuoles, sufficient in size for visualization	Cell diameter versus time
NMR	Cells, vesicles, plants, tissue	NMR signal relaxation times
Stopped-flow fluorescence quenching	Oocytes, vesicles, dependent on sufficient concentration of loadable fluorophores	Fluorescence intensity versus time
Stopped-flow light scattering	Small cells and vesicles in suspensions	Scattered light intensity versus time

Thus the membrane permeability, P_f , can be found from Eq. 7.15 to be:

$$P_f = -\frac{dV}{dt} \frac{1}{V_w A (C_2 - C_1)} \quad (7.16)$$

7.2.2 Experimental Methods

Different experimental methods can be used to estimate the osmotic water permeability of cells, vesicles and proteoliposomes. As seen from Eq. 7.16 the experiments need to provide knowledge about dV/dt , A , C_1 and C_2 . C_1 and C_2 are typically measured using an osmometer. Alternatively the concentration of the solutes can be calculated however this does not take into account any deviation from ideal behaviour, $\Phi \neq 1$. The surface area, A , at time $t=0$ is typically calculated from a measurement of the cell/vesicle diameter from microscopy imaging, transmission electron microscopy or dynamic light scattering. The remaining challenge is to measure the initial volume change upon a rapid change in environment, dV/dt . Table 7.1 gives an overview of some different methods for measuring the volume change. For reviews see (Verkman et al. 1989; Verkman 2000).

7.2.2.1 Cell Swelling Assay

Volume change is followed in real time under a microscope. This method allows for direct calculation of P_f using the volume change over time recorded from the microscope images, the surface area of the oocytes and the osmotic difference in Eq. 7.16 (Ramahaleo et al. 1999; Fetter et al. 2004). The experiment is commonly done using defolliculated oocytes containing an expression vector of the aquaporin (AQP) cDNA of interest. The main drawback of the method is the need for an animal-based laboratory and the fact that expression of the AQPs of interest does not guarantee insertion into the oocyte plasma membrane (Bienert and Jahn 2010).

A similar method is permeability measurements on immobilized cells. By tracking the position of a fluorescent bead attached to the external cell surface of a cell immobilized on a coverglass the response to changes in the osmolarity can be followed (Verkman 1993).

7.2.2.2 Nuclear Magnetic Resonance, NMR

Proton NMR uses the magnetic properties of hydrogen (^1H). It detects changes in water protons as they change physical state or chemical configuration and can thus be used to detect water movement from one compartment to another (Verkman 1993; Bienert and Jahn 2010; Ionenko et al. 2010). A widely used approach is to add a paramagnetic compound such as Mn to the external environment which will decrease proton relaxation and make it possible to distinguish between internal and external water molecules (Snaar and Van As 1992). This technique is not dependent on a volume change and can be used to measure not only the osmotic water permeability but also the diffusional water permeability.

7.2.2.3 Osmotic Water Permeability by Fluorescence Quenching

Several fluorescent probes are self-quenching at high concentration. Thus a reduction in vesicle size following an inward directed osmotic gradient in a stopped-flow apparatus can be detected by the reduction in fluorescence intensity of a self-quenching fluorescent dye such as 6-carboxyfluorescein (Verkman 1993; Liu et al. 2002; Solenov et al. 2004; Gao et al. 2006). Stopped-flow uses rapid mixing of a vesicle suspension of one osmolarity with a solution of a different osmolarity. The mixing generates an osmotic gradient which results in efflux of water from the vesicles (vesicles mixed with hypertonic solution), see Fig. 7.3. The efflux of water results in a change in vesicle size and thus a change in the concentration of a membrane impermeable dye. By choosing the starting concentration of the self-quenching dye to be sufficiently high the change in fluorescence intensity can be detected and the resulting time constant can be used to estimate P_f .

7.2.3 Stopped-Flow Light Scattering Measurements

Light scattering of suspended particles has been shown to be dependent on the size of the particles and the viscosity of the surrounding media. Similar to the fluorescence quenching assay a stopped-flow apparatus can be used to measure the change in intensity of scattered light at a 90° angle as a function of time after mixing, see Fig. 7.4. The light scattering changes resulting from osmotically induced changes in vesicle size have been used extensively to estimate P_f .

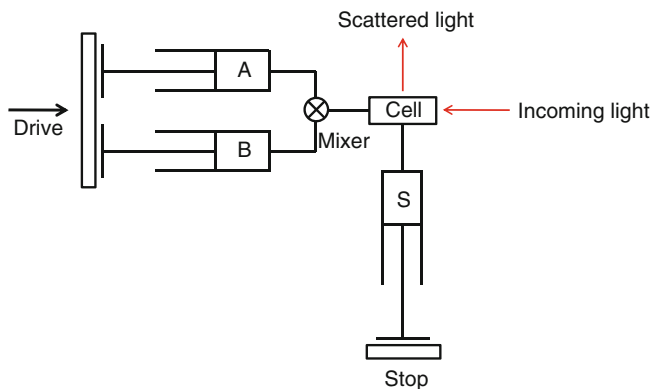


Fig. 7.4 Stopped-flow principle for measuring osmotic water permeability in lipid/polymer vesicles by monitoring vesicle volume decrease (shrinking). Two syringes are loaded with small volumes of two solutions, one with high osmolarity (*A*) and one with low osmolarity containing vesicles (*B*). The *A* and *B* solutions are rapidly driven from their syringes into a high efficiency mixer to create a fast-mixed solution. The resultant reaction volume then displaces the contents of an observation cell prefilled with a mixture of the *A* and *B* solutions (without vesicles) filling it with freshly mixed *A+B*+vesicle solution. The volume injected is limited by the stop syringe which provides the “stopped-flow”. The solution entering the flow cell is mixed only a few milliseconds before entering. This time is also known as the dead time of the stopped-flow system. As the solution fills the stopping syringe, the plunger is blocked, causing the flow to be stopped instantaneously at which point scatter monitoring begins

However, several different expressions for calculating P_f from similar obtained data are used, making evaluation and comparison between different studies more difficult. In the following we describe some of the expressions used for analysing experimental data and calculating P_f .

7.2.4 Analysis of Light Scattering Data

For the calculation of P_f from stopped-flow light scattering data it is necessary to find the relationship between the volume, V , of the particles and the scattering light intensity, I . This has been done in different ways starting with the expression by Lord Rayleigh (Rayleigh 1881) which gives the relationship between the particle volume and the scattered light intensity in the regime where the particle size is much smaller than the wavelength of the incident light. For these very small particles the intensity is proportional to the volume of the particles, however as shown by Mie (Mie 1908) when the particles become larger the intensity of the light scattered decreases with increasing particle size.

The relationship between the volume and the scattered light intensity can be approached both theoretically (Rayleigh 1918; Mie 1908; Koch 1961, 1968; van Heeswijk and van Os 1986) and experimentally (Verkman et al. 1989; Mlekoday

et al. 1983; Levitt and Mlekoday 1983; White et al. 1996). If the relationship between intensity and volume is known then P_f from Eq. 7.16 can be found by differentiation of the scattered light intensity, I , according to the equation:

$$\frac{dV}{dt} = \frac{dV}{dI} \frac{dI}{dt} \quad (7.17)$$

where dI/dt is found from the experimental measurements of I as a function of time, t . One of the simplest relationships between V and I is assuming that V/V_0 is proportional to I (Verkman 1993):

$$\frac{V}{V_0} = A \cdot I + B \quad (7.18)$$

where V_0 is the initial volume, and A , B are constants. By assuming a conserved number, N , of solutes inside the vesicle: $N = C_1 V_0 = CV$, and using Eq. 7.16, the derivative of the intensity, dI/dt can be found as:

$$\frac{dI}{dt} = \frac{P_f V_w S}{A V_0} \left(C_2 - C_1 \frac{1}{A I + B} \right) \quad (7.19)$$

Here V_w is known, S , V_0 , C_1 , C_2 are determined by the experimental conditions and $I(t)$ is measured. In principle experimental scatter intensity curves can be iteratively fitted using Eq. 7.19 and A , B and P_f estimated. However iterative fitting using Eq. 7.19 is not straightforward and in fact Eq. 7.16 does not account for the osmotically inactive volume. Denoting this volume b we have

$$C(V - b) = C_1(V_0 - b) = C_2(V_\infty - b) \quad (7.20)$$

Following (van Heeswijk and van Os 1986) one may formulate Eq. 7.15 to

$$J_v = \frac{dV}{Adt} = -L_p RT \Delta C = -V_w P_f \Delta C \quad (7.21)$$

and integrate to

$$\ln \left(\frac{V_\infty - V}{V_\infty - V_0} \right) - \frac{V - V_0}{V_\infty - V_0} \cdot \frac{\Delta C_1}{C_1} = -k \cdot t \quad (7.22)$$

where k is the rate constant associated with the volume change, $\Delta C_1 = C_2 - C_1$ and

$$k = V_w P_f \frac{A}{V_0} \left(1 - \frac{b}{V_0} \right)^{-1} \cdot \frac{C_2}{C_1} \quad (7.23)$$

As the logarithmic term in Equation 7.22 is small in the initial stage of the osmotically induced volume change (van Heeswijk and van Os 1986), Eqs. 7.22–7.23 can be simplified to

$$\ln\left(\frac{V_\infty - V}{V_\infty - V_0}\right) = -k \cdot t \quad (7.24)$$

where

$$k = V_w P_f \frac{A}{V_0} \left(1 - \frac{b}{V_0}\right)^{-1} \cdot C_2 \quad (7.25)$$

or

$$P_f = \frac{k(1 - b/V_0)}{V_w S C_2} \quad (7.26)$$

where S is the initial surface area to volume ratio A/V_0 . In the limit where the osmotically inactive volume is small Eq. 7.26 simplifies to

$$P_f = \frac{kV_0}{V_w A C_2} = \frac{k}{V_w S C_2} \quad (7.27)$$

Equation 7.24 represents a single exponential function with k proportional to C_2 . Thus by fitting the scattered intensity $I(t)$ to

$$I = \alpha e^{-kt} + \beta \quad (7.28)$$

one obtains a value for k which can be inserted in Eq. 7.27 to give a value for P_f . This approach seems to have become *de rigueur* in characterization of biomimetic membrane/reconstituted aquaporin osmotic permeability e.g. (Kumar et al. 2007; Yakata et al. 2011; Borgnia et al. 1999).

7.3 Biomimetic Barrier Materials

As lipids constitute the main component of most biological membranes it is not surprising that the early biomimetic membranes were realized by forming films and vesicular structures using various lipid extracts, for reviews see (Tien 1974; Tien and Ottova-Leitmannova 2003; Hauser 1993). With recent advances in polymer and lipid synthesis alternatives in the form of bolalipids and di- and triblock copolymers are now emerging as building blocks for biomimetic membranes.

7.3.1 Lipid-Based Barriers

Today we have a wide range of lipid and sterol species including headgroup modified and polymerizable variants allowing construction of complex membranes in the

form of supported membranes and vesicular structures see also Chap. 5. The lipid bilayer membrane is flexible and strong where flexibility is achieved by the membrane being only two lipid molecules thick corresponding to about 3 nm, and strength is achieved by mixing in sterols with cholesterol as the main component. The result is a matrix with remarkable properties which have implications for both protein reconstitution see Chap. 6 and protein function, see Chap. 9.

Lipid bilayer permeability to water and solutes depends strongly on the state of lateral cohesion and presence of any molecular packing defects. Generally lipid permeability to small charged solutes is low (see Fig. 7.1), for Na^+ it is in the range of 10^{-14} – 10^{-13} cm s^{-1} (Hauser et al. 1973; Papahadjopoulos 1971; Papahadjopoulos et al. 1972). Micropipette experiments where water permeability is measured by osmotic deflation of vesicles in hypertonic salt solutions above the gel-liquid-crystalline phase transition temperature reveal a progressive decrease in water osmotic permeability as the compressibility of the bilayers decreases. Thus the least compressible cholesterol-containing membranes show the lowest water permeability. For lipid bilayers made from diC14:0PC (dimyristoylphosphatidylcholine (DMPC)) P_f is around $70 \cdot 10^{-4}$ cm s^{-1} whereas for C18:0-C18:1PC (1-stearoyl-2-oleoyl-*sn*-glycero-3-phosphocholine (SOPC) and cholesterol in equimolar concentration P_f is around $2 \cdot 10^{-4}$ cm s^{-1} (Bloom et al. 1991).

An interesting class of lipids is found in organisms from *Archaea*. They are dominant in extreme environments (van de Vossenberg et al. 1998) and may provide versatile biomimetic membrane inspiration. Some of these organisms have membranes with very low proton permeability combined with a high stability. Of particular interest are the bipolar lipids (bolalipids) (De Rosa and Gambacorta 1988). The membrane spanning structure of the bolalipid confers increased structural stability (Dannenmuller et al. 2000) and membranes formed from (tetra)ether lipids are more resistant to oxidation and high temperature due to their ether linkage compared to the more labile ester links found in lipids from *Bacteria* and *Eukaryota* (Chang 1994). For liposomes made from macrocyclic archaeol and caldarcheol lipids the water, ammonia, urea and glycerol permeabilities are reduced 6–120 fold (Mathai et al. 2001) compared to phospholipids. Interestingly neither the presence of phytanoyl chains nor the ether bond (instead of the usual ester bond in phospholipids) significantly affects the water and solute permeability. It rather seems that the presence of macrocyclic structures decreases the mobility of the midplane hydrocarbon and this is the reason behind the reduced permeability.

7.3.2 Polymer-Based Barriers

Triblock copolymers have attracted substantial interest not only as building blocks for vesicular structures with embedded integral membrane proteins but also as vesicular drug carriers where the drug is released via (controlled) passive diffusion through the membrane. In both applications it is important to determine and control permeabilities to water and solutes.

However, the hydrophobic thickness d of polymersomes made from block copolymers ranges from 3 nm e.g. for polymersomes made from the triblock ABA block copolymer poly(ethylene glycol)-poly(propylene glycol)-poly(ethylene glycol) PEO5-PPO68-PEO5 (Schillen et al. 1999) up to ~25 nm for PS-PAA, PS-PEO, and PBD-PAA diblock copolymer vesicles (Yu and Eisenberg 1998; Zhang and Eisenberg 1996) depending on composition, molecular weight and the degree of stretching of the hydrophobic block. This is in contrast to the very narrow range in hydrophobic thickness around 3 nm in biological membranes despite the natural lipid diversity. d of a membrane made from block copolymers is not directly related to the contour length of the hydrophobic block. For example, polymersomes made of PEO5-PPO68-PEO5 (Schillen et al. 1999) have relatively small d values of 3–5 nm, compared to the 25 nm contour length of the PPO68. These membranes are probably this thin because of the tendency for interfacial localization of the mid-block oxygen. Generally, however, d increases with block copolymer molecular weight M_{block} as evidenced by cryo-TEM and for some AB block copolymers $d \sim M_{block}(1-f)^{0.5}$ where f is the hydrophilic volume fraction (Bermudez et al. 2002).

The osmotic water permeability P_f of polymersomes made from diblock polyethyleneoxide-polyethyleneethylene (EO40-EE37) with a mean contour length of 23 nm and $d=8$ nm, is $2.5 \cdot 10^{-4}$ cm s⁻¹ (Discher et al. 1999) and for polymersomes made of poly-(2-methyloxazoline)-poly-(dimethylsiloxane)-poly-(2-methyloxazoline) PMOXA15-PDMS110-PMOXA15 triblock copolymer an even lower P_f of $0.8 \cdot 10^{-4}$ cm s⁻¹ has been reported (Kumar et al. 2007). These P_f values are at least an order of magnitude lower than those obtained for vesicular membranes composed purely of phospholipids with acyl chains ≤ 18 carbon atoms which typically have permeabilities in the fluid state around $25\text{--}150 \times 10^{-4}$ cm s⁻¹ (Bloom et al. 1991). Thus polymersomes are apparently less permeable to water as compared to phospholipid vesicles. However, on a per area basis, polymersome membranes and phospholipid membranes (with comparable mechanical moduli) exhibit similar fluctuations in area. This suggests that the ratio of permeabilities largely reflects the relative probability for water diffusion across the membrane and decreases with relative core thickness as $\exp(-d_{EO40-EE37}/d_{lipid}) \approx e^{8/3} = 0.07$, which is a value close to the measured ratio of permeabilities for polymersomes versus lipid vesicles.

Recently dendrimers have attracted attention as biomimetic membrane components (Percec et al. 2010). The properties of giant dendrimersomes indicate that they can form biomimetic membrane structures with a membrane thickness of 5–8 nm in a wide range of buffers. The thickness and stability indicate good barrier properties although no quantitative permeability measurements have been reported yet. The dendrimersome thickness is comparable to that of block copolymer membranes and thus in principle suitable for incorporating membrane spanning proteins (Kumar et al. 2007). Although successful incorporation has been demonstrated for the pore-forming melittin (Percec et al. 2010) the greater membrane thicknesses (generally >8 nm) will be a challenge for protein reconstitution into dendrimer based membranes (see also Chap. 6).

7.4 Perspective

In conclusion, the passive membrane barrier properties for water and polar and charged solutes arise from the amphiphilic structure where a central hydrophobic volume is interfaced by hydrophilic moieties. Macroscopic theories for describing solute and water transport build on describing the energy needed to cross the barrier. The change in Gibbs free energy associated with permeants crossing a barrier can be regarded as arising from several component energies capturing the physics of translocating charged and polar solutes from a highly polarisable medium into a thin film containing a medium with a low dielectric constant.

The stopped-flow technique is a powerful technique to accurately measure osmotic permeability of biomimetic vesicular membranes. However the relation between light scatter (or fluorescence) and volume change following osmotic stress is complex and several models for the relation between experimentally obtained scatter curves and P_f have been proposed. Lipids being the main component of biological membranes form the basis of many biomimetic membrane designs. Recently the emergence of effective syntheses for amphiphilic di- and triblock copolymers and dendrimers opens for new designs where the barrier for water and electrolytes is based on the hydrophobic core as for lipids, but where the hydrophilic blocks are readily amendable for modifications leading to increased stability and compatibility with supporting materials. However, the challenge for these biomimetic membrane components is that the hydrophobic thickness is substantially larger than the hydrophobic thickness of biological membranes and this has implications for both protein incorporation and function. Perhaps the future lies in a happy marriage between lipid and polymer components in a mixed system where annular lipids cushion proteins in a polymeric matrix.

Acknowledgements The Danish National Advanced Technology Foundation and MEMBAQ, a Specific Targeted Research Project (STREP) supported by the European Commission under the Sixth Framework Programme, are kindly acknowledged for financial support.

References

- Arakelyan, V.B., Arakelyan, S.B.: Energetic profile of a dipole molecule in the thin membrane. *Biolog. Zh. Armenii* **36**, 775–779 (1983)
- Arakelyan, V.B., Arakelyan, S.B., Avakyan, Ts.M., Aslanyan, V.M.: Electrostatic effects on transport of water across bilayer lipid membranes. *Biofizika* **30**, 170–171 (1985)
- Beitinger, H., Vogel, V., Mobius, D., Rahmann, H.: Surface potentials and electric dipole moments of ganglioside and phospholipid bilayers: contribution of the polar headgroup at the water/lipid interface. *Biochim. Biophys. Acta* **984**, 293–300 (1989)
- Bell, R.P.: The electrical energy of dipole molecules in solution and solubilities of ammonia, hydrogen chloride and hydrogen sulfite in various solvent. *J. Chem. Soc.* **32**, 1371–1382 (1931)
- Bermudez, H., Brannan, A.K., Hammer, D.A., Bates, F.S., Discher, D.E.: Molecular weight dependence of polymersome membrane structure, elasticity, and stability. *Macromolecules* **35**, 8203–8208 (2002)

- Bienert, G.P., Jahn, T.P.: Major intrinsic proteins and arsenic transport in plants: new players and their potential role. *Adv. Exp. Med. Biol.* **679**, 111–125 (2010)
- Bloom, M., Evans, E., Mouritsen, O.G.: Physical properties of the fluid lipid-bilayer component of cell membranes: a perspective. *Q. Rev. Biophys.* **24**, 293–397 (1991)
- Borgnia, M.J., Kozono, D., Calamita, G., Maloney, P.C., Agre, P.: Functional reconstitution and characterization of AqpZ, the E. coli water channel protein. *J. Mol. Biol.* **291**, 1169–1179 (1999)
- Chang, E.L.: Unusual thermal stability of liposomes made from bipolar tetraether lipids. *Biochem. Biophys. Res. Commun.* **202**, 673–679 (1994)
- Dannenmuller, O., Arakawa, K., Eguchi, T., Kakinuma, K., Blanc, S., Albrecht, A.M., Schmutz, M., Nakatani, Y., Ourisson, G.: Membrane properties of archaeal macrocyclic diether phospholipids. *Chemistry* **6**, 645–654 (2000)
- De Rosa, M., Gambacorta, A.: The lipids of archaeobacteria. *Prog. Lipid Res.* **27**, 153–175 (1988)
- Discher, B.M., Won, Y.Y., Ege, D.S., Lee, J.C., Bates, F.S., Discher, D.E., Hammer, D.A.: Polymersomes: tough vesicles made from diblock copolymers. *Science* **284**, 1143–1146 (1999)
- Fetter, K., Van Wilder, V., Moshelion, M., Chaumont, F.: Interactions between plasma membrane aquaporins modulate their water channel activity. *Plant Cell* **16**, 215–228 (2004)
- Finkelstein, A. (ed.): *Water Movement Through Lipid Bilayers, Pores, and Plasma Membranes. Theory and Reality.* Wiley-Interscience, New York (1987)
- Gao, J., Wang, X., Chang, Y., Zhang, J., Song, Q., Yu, H., Li, X.: Acetazolamide inhibits osmotic water permeability by interaction with aquaporin-1. *Anal. Biochem.* **350**, 165–170 (2006)
- Gawrisch, K., Ruston, D., Zimmerberg, J., Parsegian, V.A., Rand, R.P., Fuller, N.: Membrane dipole potentials, hydration forces, and the ordering of water at membrane surfaces. *Biophys. J.* **61**, 1213–1223 (1992)
- Gennis, R.B.: *Biomembranes. Molecular Structure and Function.* Advanced Texts in Chemistry. Springer, New York (1989)
- Graham, T.: On the absorption and dialytic separation of gases by colloid septa. *Philos. Mag. J. Sci.* **32**, 401–420 (1866)
- Hauser, H.: Phospholipid vesicles. In: Cevc, G. (ed.) *Phospholipids Handbook*, pp. 603–637. Marcel Dekker, New York (1993)
- Hauser, H., Oldani, D., Phillips, M.C.: Mechanism of ion escape from phosphatidylcholine and phosphatidylserine single bilayer vesicles. *Biochemistry* **12**, 4507–4517 (1973)
- Haydon, D.A., Myers, V.B.: Surface charge, surface dipoles and membrane conductance. *Biochim. Biophys. Acta* **307**, 429–443 (1973)
- Hladky, S.B., Haydon, D.A.: Membrane conductance and dipole potential. *Biochim. Biophys. Acta* **318**, 464–468 (1973)
- Ionenko, I.F., Anisimov, A.V., Dautova, N.R.: Effect of temperature on water transport through aquaporins. *Biol. Plantarum* **54**, 488–494 (2010)
- Koch, A.L.: Some calculations on the turbidity of mitochondria and bacteria. *Biochim. Biophys. Acta* **51**, 429–441 (1961)
- Koch, A.L.: Theory of the angular dependence of light scattered by bacteria and similar-sized biological objects. *J. Theor. Biol.* **18**, 133–156 (1968)
- Kumar, M., Grzelakowski, M., Zilles, J., Clark, M., Meier, W.: Highly permeable polymeric membranes based on the incorporation of the functional water channel protein Aquaporin Z. *Proc. Natl. Acad. Sci. U.S.A.* **104**, 20719–20724 (2007)
- Levitt, D.G., Mlekoday, H.J.: Reflection coefficient and permeability of urea and ethylene glycol in the human red cell membrane. *J. Gen. Physiol.* **81**, 239–253 (1983)
- Lieberman, E.A., Topaly, V.P.: Permeability of bimolecular phospholipid membranes for fat-soluble ions. *Biofizika* **14**, 452–461 (1969)
- Liu, J., Christian, J.A., Critser, J.K.: Canine RBC osmotic tolerance and membrane permeability. *Cryobiology* **44**, 258–268 (2002)
- Mathai, J.C., Sprott, G.D., Zeidel, M.L.: Molecular mechanisms of water and solute transport across archaeobacterial lipid membranes. *J. Biol. Chem.* **276**, 27266–27271 (2001)
- Mathai, J.C., Tristram-Nagle, S., Nagle, J.F., Zeidel, M.L.: Structural determinants of water permeability through the lipid membrane. *J. Gen. Physiol.* **131**, 69–76 (2008)

- Mie, G.: Beiträge zur Optik trüber Medien, speziell kolloidaler Metallösungen. *Ann. Phys. Vierte Folge* **25**, 377–445 (1908)
- Mlekoday, H.J., Moore, R., Levitt, D.G.: Osmotic water permeability of the human red cell. Dependence on direction of water flow and cell volume. *J. Gen. Physiol.* **81**, 213–220 (1983)
- Nagle, J.F., Tristram-Nagle, S.: Structure of lipid bilayers. *Biochim. Biophys. Acta* **1469**, 159–195 (2000)
- Nagle, J.F., Mathai, J.C., Zeidel, M.L., Tristram-Nagle, S.: Theory of passive permeability through lipid bilayers. *J. Gen. Physiol.* **131**, 77–85 (2008)
- Neumcke, B., Läger, P.: Nonlinear electrical effects in lipid bilayer membranes II. Integration of the generalized Nernst-Planck equations. *Biophys. J.* **9**, 1160–1170 (1969)
- Papahadjopoulos, D.: Na⁺–K⁺ discrimination by “pure” phospholipid membranes. *Biochim. Biophys. Acta* **241**, 254–259 (1971)
- Papahadjopoulos, D., Nir, S., Oki, S.: Permeability properties of phospholipid membranes: effect of cholesterol and temperature. *Biochim. Biophys. Acta* **266**, 561–583 (1972)
- Paula, S., Volkov, A.G., Deamer, D.W.: Permeation of halide anions through phospholipid bilayers occurs by the solubility-diffusion mechanism. *Biophys. J.* **74**, 319–327 (1998)
- Paula, S., Volkov, A.G., Van Hoek, A.N., Haines, T.H., Deamer, D.W.: Permeation of protons, potassium ions, and small polar molecules through phospholipid bilayers as a function of membrane thickness. *Biophys. J.* **70**, 339–348 (1996)
- Percec, V., Wilson, D.A., Leowanawat, P., Wilson, C.J., Hughes, A.D., Kaucher, M.S., Hammer, D.A., Levine, D.H., Kim, A.J., Bates, F.S., Davis, K.P., Lodge, T.P., Klein, M.L., DeVane, R.H., Aqad, E., Rosen, B.M., Argintaru, A.O., Sienkowska, M.J., Rissanen, K., Nummelin, S., Ropponen, J.: Self-assembly of Janus dendrimers into uniform dendrimersomes and other complex architectures. *Science* **328**, 1009–1014 (2010)
- Ramahaleo, T., Morillon, R., Alexandre, J., Lassalles, J.P.: Osmotic water permeability of isolated protoplasts. Modifications during development. *Plant Physiol.* **119**, 885–896 (1999)
- Rayleigh, L.: On the electromagnetic theory of light. *Philos. Mag.* **12**, 81–101 (1881)
- Rayleigh, L.: On the scattering of light by spherical shells, and by complete spheres of periodic structure, when the refractivity is small. *Proc. R. Soc. A* **94**, 296–300 (1918)
- Schamberger, J., Clarke, R.J.: Hydrophobic ion hydration and the magnitude of the dipole potential. *Biophys. J.* **82**, 3081–3088 (2002)
- Schillen, K., Bryshke, K., Melnikova, Y.: Vesicles formed from a poly(ethylene oxide)-poly(propylene oxide)-poly(ethylene oxide) triblock copolymer in dilute aqueous solution. *Macromolecules* **32**, 6885–6888 (1999)
- Smaby, J.M., Brockman, H.L.: Surface dipole moments of lipids at the argon-water interface. Similarities among glycerol-ester-based lipids. *Biophys. J.* **58**, 195–204 (1990)
- Snaar, J.E., Van As, H.: Probing water compartments and membrane permeability in plant cells by H NMR relaxation measurements. *Biophys. J.* **63**, 1654–1658 (1992)
- Solenov, E., Watanabe, H., Manley, G.T., Verkman, A.S.: Sevenfold-reduced osmotic water permeability in primary astrocyte cultures from AQP-4-deficient mice, measured by a fluorescence quenching method. *Am. J. Physiol. Cell Physiol.* **286**, C426–C432 (2004)
- Tien, H.T.: *Bilayer Lipid Membranes (BML) Theory and Practice*, 1st edn. Marcel Dekker, New York (1974)
- Tien, H.T., Ottova-Leitmannova, A. (eds.): *Planar Lipid Bilayers (BLMs) and Their Applications*. Elsevier, Amsterdam (2003)
- van de Vossenberg, J.L., Driessen, A.J., Konings, W.N.: The essence of being extremophilic: the role of the unique archaeal membrane lipids. *Extremophiles* **2**, 163–170 (1998)
- van Heeswijk, M.P., van Os, C.H.: Osmotic water permeabilities of brush border and basolateral membrane vesicles from rat renal cortex and small intestine. *J. Membr. Biol.* **92**, 183–193 (1986)
- Verkman, A.S.: *Water Channels*. Molecular Biology Intelligence Unit. R.G. Landes, Austin (1993)
- Verkman, A.S.: Water permeability measurement in living cells and complex tissues. *J. Membr. Biol.* **173**, 73–87 (2000)

- Verkman, A.S., Weyer, P., Brown, D., Ausiello, D.A.: Functional water channels are present in clathrin-coated vesicles from bovine kidney but not from brain. *J. Biol. Chem.* **264**, 20608–20613 (1989)
- Volkov, A.G., Hampton, T.: Energetics of membrane permeability. In: Leitmannova Liu, A. (ed.) *Advances in Planar Lipid Bilayers and Liposomes*, vol. 8, pp. 155–199. Elsevier Academic Press, Amsterdam (2008)
- Volkov, A.G., Paula, S., Deamer, D.W.: Two mechanisms of permeation of small neutral molecules and hydrated ions across phospholipid bilayers. *Bioelectrochem. Bioenerg.* **42**, 153–160 (1997)
- White, G., Pencer, J., Nickel, B.G., Wood, J.M., Hallett, F.R.: Optical changes in unilamellar vesicles experiencing osmotic stress. *Biophys. J.* **71**, 2701–2715 (1996)
- Yakata, K., Tani, K., Fujiyoshi, Y.: Water permeability and characterization of aquaporin-11. *J. Struct. Biol.* **174**, 315–320 (2011)
- Yu, K., Eisenberg, A.: Bilayer morphologies of self-assembled crew-cut aggregates of amphiphilic PS-*b*-PEO diblock copolymers in solution. *Macromolecules* **31**, 3509–3518 (1998)
- Zhang, L., Eisenberg, A.: Morphogenic effect of added ions on crew-cut aggregates of polystyrene-*b*-poly(acrylic acid) block copolymers in solutions. *Macromolecules* **29**, 8805–8815 (1996)

Chapter 8

Multi-scale Modeling of Biomimetic Membranes

Hans Enggrob, Lars Yde, Mathias Gruber, and Himanshu Khandelia

Abstract For designing and optimizing the performance of biomimetic membranes, numerical models are useful and powerful tools. The scientific background, application and experience within different scales of models are described: Computational Fluid Dynamics (CFD) modeling is being done typically by hydraulic engineers of larger flow systems at macro-scale. Molecular Dynamics (MD) modeling of molecule systems at micro-scale is carried out by physics-biochemistry scientists. Similarities as well as basic differences between the two approaches are highlighted: Whereas the physical-chemical formulations of the problem are fundamentally different, the numerical and mathematical expressions are quite similar. Attempts to combine the model approaches at meso-scales include coarse grain MD and micro-CFD modeling, and there appears to be substantially more potential for further exploration of numerical modeling at different length and time scales such as biofouling or control of the hydrodynamic, chemical and biological conditions inside the membrane material. A systematic approach to assessment of the reliability of model results at any scale is provided at the end of the chapter.

H. Enggrob (✉) • L. Yde
DHI, Agern Allé 5, DK-2970 Hørsholm, Denmark
e-mail: hge@dhiigroup.dk; lay@dhiigroup.dk

M. Gruber
Nano-Science Center, The HC Ørsted Institute, University of Copenhagen, &
Aquaporin A/S, Universitetsparken 5, DK-2200 Copenhagen, Denmark
e-mail: mathiasgruber@nano.ku.dk

H. Khandelia
MEMPHYS, Center for BioMembrane Physics, Department of Physics and chemistry,
University of Southern Denmark, Campusvej 55, DK-5230 Odense, Denmark
e-mail: hkhandel@memphys.sdu.dk

8.1 Introduction

Numerical models are used to simulate flow and transport processes and other key phenomena with the objective to optimize design or operation of flow systems. With adequate conceptual description, mathematical formulation, numerical schemes, calibration and validation at appropriate time and lengths scales, such models are ideal to supplement measurements and not least to explain and explore new coherences and phenomena, which can be utilized in the design and operation of membranes.

This chapter describes the use of numerical models of biomimetic membranes at various spatial and time scales. Emphasis is on describing the various phenomena which can be modeled at the different scales and to demonstrate the connectivity between the model types (Fig. 8.1).

Section 8.2 describes the use of atomistic and semi-atomistic models starting with classical mechanical MD (molecular dynamics) exemplified by simulations of water permeation through single aquaporin proteins at a detailed atomic level in the nanometer scale. We then discuss how membrane properties (channel conductivity) at a larger length and timescale can be simulated using CGMD (coarse grained molecular dynamics) simulations and DPD (dissipative particle dynamics). Section 8.3 provides an overview of conventional computational fluid dynamic CFD models of membrane system at millimeter scale and how this can be extended to micrometer scale (Micro CFD). Section 8.4 gives guidelines to the choice of models depending on the scope of investigations, and the inherent computational efforts, costs of calibrations and validation as well as systematic approach to uncertainty assessment.

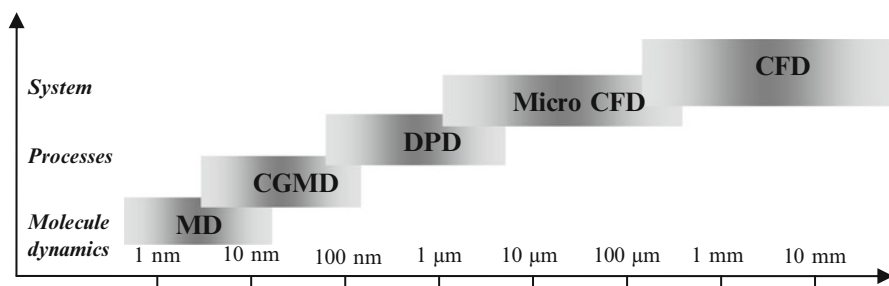


Fig. 8.1 Computational methods covering the spatial range from 1 to 10 mm. *MD* molecular dynamics, *CGMD* coarse grained molecular dynamics, *DPD* dissipative particle dynamics, *Micro CFD* micro computational fluid dynamics, *CFD* computational fluid dynamics. The *y*-axis description levels also comprise a time resolution range in simulated time, from ps in MD simulations to minutes in CFD simulations

8.2 Atomistic and Semi-atomistic Modeling

After Alder and Wainwright introduced the MD simulation technique in 1957 (Alder and Wainwright 1957), it emerged as a useful tool in biology two decades later, when the first simulations of proteins were reported (Levitt and Warshel 1975). MD continues to be a powerful tool in solid and liquid state physics, where Monte Carlo methods have also thrived. The soft nature and chemical complexity of biological molecules makes them particularly amenable to analysis by MD in which it is possible to trace the motion of individual atoms over time in response to forces of magnitude comparable to thermal fluctuations in liquids. The technique is now applied to a wide range of problems in biology including calculation of the free energy of ligand-protein binding, folding of small peptides, design of protein inhibitors, calculation of physical properties of biomembranes, and deciphering the mechanism of action or selectivity of molecular machines such as active or passive transmembrane protein transporters. Aquaporin (AQP) molecules fall into the last category. With the standardization and development of methodology and software, and the ever-increasing availability of essential inexpensive computational power, the breadth of problems and the time and length scales tractable by MD simulations continues to expand. In the following sections, the theory and implementation of MD is introduced, followed by a description of the application of the method to setup simulations of AQPs embedded in a biomimetic membrane. We then cite a few examples to expound upon the possible useful information that can be extracted from such simulations of AQPs, the limitations of and uncertainties in the calculations, and conclude with a short description of newly popular coarse-grained MD method, and a perspective for the future.

8.2.1 Molecular Dynamics (MD) Simulations

The idea behind MD is to solve the equations of motion of a set of interacting particles, and use the resulting trajectories to calculate microscopic and macroscopic thermodynamic quantities. In principle, one would do this most accurately by solving Schrödinger's equation. However, such a solution of quantum mechanical (QM) equations of motion is analytically possible for only very simple systems, and numerically possible for a very small number of atoms. Thus, one resorts to classical mechanics instead. In MD, each atom of the interacting chemical species in the simulated system is modeled by a single point-charge point-mass particle. The time evolution of a set of interacting atoms is followed by integrating the classical equations of motion, based on Newton's second law of motion:

$$-\nabla_i E(\mathbf{r}_i) = \mathbf{F}_i = m_i \frac{d^2 \mathbf{r}_i}{dt^2} \quad (8.1)$$

Table 8.1 Commonly used force fields for atomistic of united-atom lipid simulations

Force field	Advantages	Shortcomings
CHARMM C36	Can be easily combined with other types of biological molecules such as proteins or DNA, for which accurate compatible parameters are available. Reproduces experimental properties of model bilayers accurately in the NPT ensemble	Only available in the all-atom form, thus being computationally more expensive. Has not been tested extensively for longer time scales
GAFF	Can be easily combined with other types of biological molecules such as proteins or DNA, for which accurate compatible parameters are available. Reproduces experimental properties of model bilayers accurately	Same as above, but has been tested for longer time scales, but not in the tensionless NPT ensemble
BERGER	Most extensively tested lipid force field. Reproduced experimental properties of model lipid bilayer accurately. A united-atom approach results in cheaper simulations	Not straightforward to combine with other biomolecules with accurate compatible parameters sets. Membranes get too condensed in the presence of sodium ions

where the interaction energy function $E(\mathbf{r}_i)$ is a function of the positions \mathbf{r}_i of the nuclei, representing the potential energy of the system in that particular configuration, m_i , \mathbf{r}_i and \mathbf{F}_i are the mass, the position of and the force on the i^{th} particle. MD simulations thus generate information at the microscopic level, including atomic positions and velocities. The conversion of this microscopic information to macroscopic observables such as pressure, diffusion constants, and heat capacities requires the application of the principles of statistical mechanics, a branch of physics that essentially applies probability theory to the laws of mechanics. Notice that in MD, no electronic rearrangements are possible on the orbital scale, i.e. bonds cannot be broken and formed, and in most cases, electronic polarizability is not included in the equations of motion (Table 8.1).

The energy function $E(\mathbf{r}_i)$, also called a “force field”, is semi-empirical, and in the simplest case, is typically approximated by a sum of pair wise interactions between the atoms of the system. Three-body and higher interactions are excluded from standard semi-empirical force fields for MD simulations. A typical form of $E(\mathbf{r}_i)$ is shown in Eq. 8.2. For a detailed mathematical description of the force field, the reader can refer to any standard text on molecular simulations.

$$E(\mathbf{r}_i) = E_{\text{bond stretch}} + E_{\text{angle bend}} + E_{\text{dihedral torsion}} + E_{\text{improper dihedral}} + E_{\text{vdW}} + E_{\text{electrostatic}} \quad (8.2)$$

The energy of the system is calculated as a sum of the energies arising from bonded and non-bonded forces. The bonded forces correspond to the energies associated with stretching of bonds between atoms A and B ($E_{bond\ stretch}$), the bending of the angles are described by three atoms A–B–C ($E_{angle\ bend}$), the rotation of the bond between atoms B and C in the A–B–C–D dihedral ($E_{dihedral}$). The bond and angle vibrations are modeled by Hookean springs, while a periodic function is used for the dihedral rotations. The energy arising from the non-bonded forces are divided in E_{vdW} and $E_{electrostatic}$. The first of these terms is the energy arising from dispersion or van der Waals (vdW) forces and can be described by various potentials such as the Lennard-Jones potential. The second term models the electrostatic interactions between the various charged particles of the system and is described by Coulomb's law. Thus, the potential energy function $E(\mathbf{r}_i)$ contains a large number of tunable parameters, such as spring constants, and barriers for dihedral rotations. For each force field, these parameters are typically optimized to accurately predict experimental properties such as heat of vaporization, or to replicate energies calculated from quantum mechanics (QM) calculation of small molecules.

The complexity of the force field makes an analytical solution to the Equation of motion impossible. This necessitates a numerical solution to Eq. 8.1. Most integration algorithms are based on a Taylor series approximation of the particle position and its derivatives:

$$\begin{aligned}\mathbf{r}(t + \delta t) &= \mathbf{r}(t) + \delta t \mathbf{v}(t) + \frac{1}{2} \delta t^2 \mathbf{a}(t) + \frac{1}{6} \delta t^3 \mathbf{b}(t) + \frac{1}{24} \delta t^4 \mathbf{c}(t) + \dots \\ \mathbf{v}(t + \delta t) &= \mathbf{v}(t) + \delta t \mathbf{a}(t) + \frac{1}{2} \delta t^2 \mathbf{b}(t) + \frac{1}{6} \delta t^3 \mathbf{c}(t) + \dots\end{aligned}\quad (8.3)$$

One of the more popular integration algorithms is the Leap-frog Verlet, where the velocity at a later time is calculated before the positions (hence the term ‘‘Leap-frog’’):

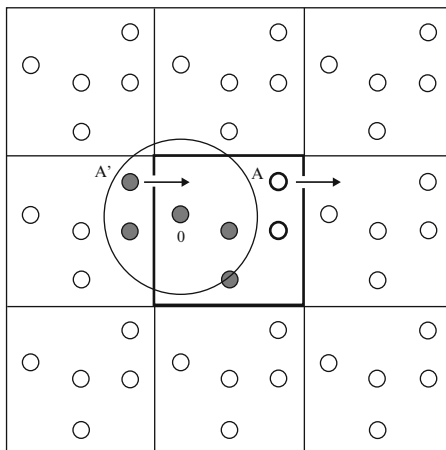
$$\begin{aligned}\mathbf{v}(t + \frac{1}{2} \delta t) &= \mathbf{v}(t - \frac{1}{2} \delta t) + \delta t \mathbf{a}(t) \\ \mathbf{r}(t + \delta t) &= \mathbf{r}(t) + \delta t \mathbf{v}(t + \frac{1}{2} \delta t)\end{aligned}\quad (8.4)$$

The time step δt is typically limited to 2 fs (femtoseconds, 10^{-15} s) to conserve energy and to prevent unrealistic conformations. The small time step and the complexity of the energy function make MD simulations computationally very intensive.

8.2.1.1 Initial and Periodic Boundary Conditions, and Potential Cutoffs

The position and velocity vectors for all atoms and the box dimensions describe the initial state of the system. The initial atomic coordinates can be obtained from experimentally measured structures, or from pre-equilibrated structures from

Fig. 8.2 Periodic boundary conditions and minimum image convention. If particle *A* leaves the simulation from one side, particle *A'* enters it from the other side. Particle *O* interacts with particles or their nearest images, whichever are closer



previous simulations. For aquaporins, the initial coordinates of the protein are typically obtained from published crystal structures. The initial velocities of atoms are usually determined from a random or Maxwellian distribution with the magnitudes conforming to the required temperature, and corrected so that the overall momentum is zero.

The non-bonded potential in Eq. 8.2 has an infinite spatial range in theory. However, the contribution of interacting particles to the non-bonded energy is very low for particles very far apart. It is thus common practice to cut off or smoothly switch off non-bonded interactions beyond a certain radius, typically of the order of $\sim 12 \text{ \AA}$. Cutoffs result in substantial savings in computational cost with very little loss of accuracy.

Periodic boundary conditions allow for a simulation to be performed using a relatively small number of particles in such a way that the particles experience forces as if they were in a bulk solution. The central simulation cell is replicated infinitely along all three axes, and the calculations are made for the central simulation cell. Thus, a particle *A* that leaves a 2-D central simulation cell from the $+x$ box edge (Fig. 8.2) reenters it from the $-x$ box edge instantaneously as particle *A'*. Each particle sees only one image of the particles it interacts with. Such a scheme eliminates wall effects, and the model is effectively simulated infinitely in all three dimensions. However, the size of the simulation cell should still be large enough to eliminate finite-size artifacts, which arise when molecules interact with their own periodic images of an adjoining cell.

8.2.1.2 Simulation Ensemble

To completely determine the thermodynamic state of the simulation box, two intensive thermodynamic variables need to be fixed along with the number of atoms of the system, unless one is interested in “open box” simulations where particles are allowed

to leave and reenter the simulation cell. Typically, the *NPT* ensemble, where the number of particles (N), pressure (P) and temperature (T) are kept constant is used to replicate experimental conditions and to easily calculate the Gibbs free energy (G). However, from the point of view of statistical mechanics, the thermodynamic state of the system is independent of the ensemble used, if the sampling is sufficient. In practice, the type of ensemble chosen depends on the quantity of interest. For example, if one wants to calculate the area-per-lipid of a lipid bilayer, it is best to use the *NPT* ensemble, so that the box dimensions can fluctuate and equilibrate. The pressure and temperature of the central simulation cell can be kept constant using a variety of techniques, most of which involve either introducing an extra degree of freedom for the box dimensions, or coupling to an external heat bath. The details of pressure and temperature control are beyond the scope of this chapter.

8.2.1.3 MD Simulations of Aquaporins in Biomimetic Membranes

Aquaporins are nature's most efficient water filtration devices, and have a sub-nanometer sized pore in which salt and other impurities are screened out. Detailed descriptions of the molecular-scale interactions and phenomena that drive the water-filtration mechanism and accurate quantification of water transport rates through the pore can contribute significantly to the design, development and optimization of an aquaporin-containing biomimetic membrane. Such a description is difficult to attain with analytical techniques alone, and the void is filled by MD simulation. The objectives of modeling transport through aquaporins by MD simulations are threefold:

- **Calculation of water transport rates through individual aquaporin molecules:** Accurate knowledge of the rate at which water gets transported through individual aquaporin pores is essential in determining the density and concentration of aquaporins to be used in the final aquaporin-containing biomimetic membrane to meet specified filtration throughput targets. Such information is not easily accessible from experimental measurements alone.
- **Enhancement of water transport rate through the aquaporin:** MD simulations have provided atomic-scale insight not only into the mechanism of action of aquaporin molecules, but also into how water transport through aquaporins is regulated by structural features far from the central pore. Optimization of the pore structure and of other regulating structural features can be easily performed using MD simulations by designing mutants of wild-type aquaporins. A small increase in the permeability of a mutant can translate into a large increase in water filtration efficiency in an industrial scale filtration device.
- **Optimization of the Structural Matrix of the Biomimetic Membrane:** The mechanical properties of the membrane matrix are determined by the chemical and physical properties, and by the composition of lipids or other amphiphiles that constitute the matrix. MD simulations at the all-atom and coarse-grained scales (see later) can aid in the design of the membrane matrix. We will not describe this section in detail, since all-atom MD can only have limited applications in this regime.

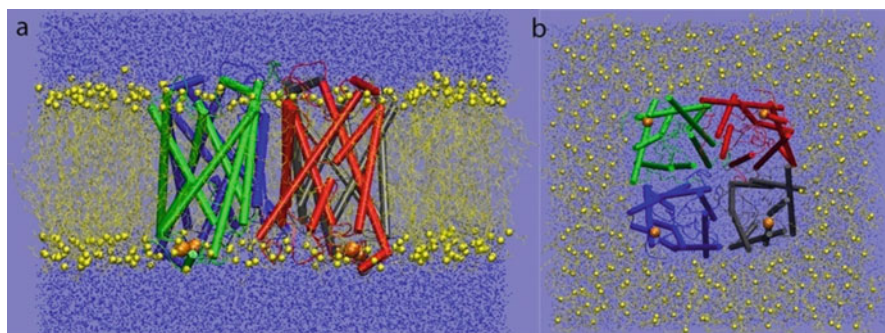


Fig. 8.3 Simulation setup of an aquaporin tetramer embedded in a POPC lipid matrix, and hydrated with water, viewed from (a) the xy -plane and (b) from the bilayer normal. Lipids are shown as *yellow lines*, lipid headgroups are shown as *yellow spheres*. Water is shown as *blue dots*. Each monomer has a pore in the *middle*, through which water diffuses across the membrane

8.2.1.4 Model Description

The underlying matrix of a biological membrane is a lipid bilayer. The simplest biomimetic membrane is thus a well-hydrated lipid bilayer, composed of a single lipid type. The standard lipid of choice is palmitoyl-oleoyl-phosphatidylcholine (POPC) that is commonly used in model lipid bilayers in both experiments and simulations. Coordinates of the lipid bilayer are obtained from existing simulations of a POPC lipid bilayer. An aquaporin tetramer containing four pores is then embedded into the lipid matrix. The initial coordinates of the protein are obtained from X-ray structures available in the *pdb* data bank (www.pdb.org). Thus, a typical simulation setup consists of one aquaporin molecule, ~ 270 lipids, 17000 water molecules and ions to keep the system electrostatically neutral. The system contains more than 100,000 atoms, and the simulation box measures $12 \text{ nm} \times 12 \text{ nm} \times 10 \text{ nm}$, with the bilayer normal typically oriented along the z -axis, see Fig. 8.3. The simulation is then carried out long enough till sufficient number of water molecules have permeated across the pore. Typically, reliable simulations are 30–100 ns long, as about one molecule of water passes through the aquaporin pore every nanosecond.

The two key quantities characterizing transport properties of the water channel are the single-channel osmotic permeability constant p_f and the single-channel diffusive permeability constant p_d (Zhu et al. 2004). Both quantities are measured in $\text{cm}^3 \text{ s}^{-1}$, and can be directly compared to experimental measurements, if available. The osmotic permeability of a channel is defined through:

$$j_w = p_f \Delta C_s \quad (8.5)$$

where j_w is the net molar flux of water through the channel, and ΔC_s is the concentration gradient across the two compartments, in this case, the two reservoirs of water on each side of the membrane. The osmotic permeability constant p_f is calculated by measuring the collective diffusion constant (D_n) of a collective

coordinate $n(t)$. The collective coordinate $n(t)$ is related to the aggregate displacement of all water molecules within the constriction region $CR(t)$ in the time interval between t and $(t - \delta t)$, normalized by the lumen length $L(t)$ at that time. The constriction region refers to the segment of the water pore that constricts larger molecules out of the pore. Please see Zhu et al. (2004) for details.

$$n(t) = \int_0^t \frac{dt'}{L(t')} \sum_{i \in CR(t)} [z_i(t') - z_i(t' - \delta t)] \quad (8.6)$$

$$D_n = \langle n^2(t) \rangle / 2t \quad (8.7)$$

$$p_f = v_w D_n \quad (8.8)$$

The diffusive permeability constant p_d can be calculated by counting the total number of water molecules that traverse the channel per unit time (k_o):

$$p_d = v_w k_o \quad (8.9)$$

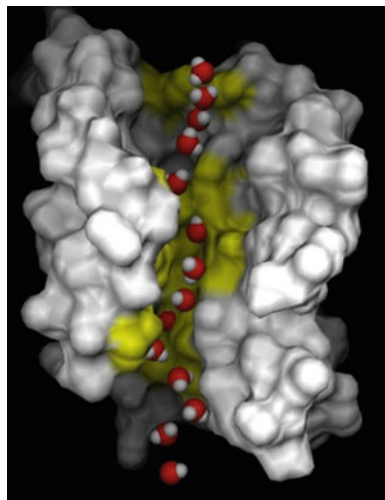
where v_w is the molar volume of water. Although both p_f and p_d are quantities that can be measured from experiments, such measurements are riddled with several assumptions and difficulties (Jensen and Mouritsen 2006). In simulations, the above equations make it possible to measure the quantities without having to resort to establishing osmotic or chemical potential differences across the membrane.

8.2.1.5 Simulation Outcomes

The first simulations of the human aquaporin AQP1 in a lipid bilayer established the exact pathway of a single file of water transport through the pore, and showed that water dipole reorientation at the center of the pore was essential for water selectivity (de Groot and Grubmuller 2001), see Fig. 8.4. The mechanism of action of proton and ion exclusion, while maintaining a high flux of water was also established, and then refined in the following years. Simulations insights were thus indispensable in deciphering the molecular mechanism (MM) of action of aquaporins.

The first accurate simulation measurements of p_f without application of a pressure across the membrane appeared in 2006 (Jensen and Mouritsen 2006), after the above equation set was established. It was possible to measure the single channel water permeability of bacterial aquaporins using MD simulations, and the agreement with experiments was quite accurate for water-selective aquaporins (Jensen and Mouritsen 2006). The quantitative agreement to experimental values was somewhat surprising, and perhaps even fortunate, because it is well known that the model of water used for the simulations severely overestimates even the bulk diffusion constant of water (Jorgensen et al. 1983). Moreover, simulations predict a higher water permeability of the aquaporin AqpZ compared to the aquaglyceroporin GlpF (de Groot and Grubmuller 2001; Jensen and Mouritsen 2006), in stark disagreement

Fig. 8.4 The trajectory of a single water molecule through an AQP1 monomer. The water dipole is oriented in different directions in the upper and lower halves of the pore, thus preventing proton hopping on the water wire (Reproduced from de Groot and Grubmüller (2001) with permission)



with experimental measurements. The discrepancy is yet unresolved, and can arise from large-scale conformational changes not accessible in simulations, or uncertainties in the measurement of the number of correctly folded and oriented membrane protein in experiments.

More recently, MD simulation has helped unfold (Tornroth-Horsefield et al. 2006; Nyblom et al. 2009; Khandelia et al. 2009) the gating mechanism of the plant aquaporin SoPIP2;1. SoPIP2;1 is an excellent candidate for use in biomimetic filtration membranes owing to its high water permeation rate and easier ethical acceptance associated with a plant (instead of a bacterial) product in a water-filtration device. However, SoPIP2;1 is a gated water channel and can possibly remain in the “closed” state when isolated from cultured cells. Since the closed conformation of the protein has lower water permeability, it becomes important to be able to design mutants of the protein that would remain constitutively open, thus making it suitable for use in a water-filtration device. Based on the knowledge of the crystal structure of the protein and its gating mechanism (Tornroth-Horsefield et al. 2006), it was possible to design SoPIP2;1 mutants which retained the wild-type’s water selectivity, and had a single channel permeability comparable to the open conformation of the protein (Khandelia et al. 2009).

It is apparent from the three examples above that MD simulations can harness atomistic X-ray crystallography data to unravel the mechanism of action of aquaporins, compare the permeability of different aquaporin molecules, and design mutants that might be more suitable in a biomimetic membrane device. All the examples illustrate the ability of MD to provide qualitative information on the sub-nanometer scale. However, quantitative reconciliation with experiments is still out of reach, although this should soon become achievable with the improvements in force field parameters, longer simulations and emergence of advanced experimental techniques to probe difficult questions like the dynamics of a single file of water 15 Å long.

It is important to note that MD trajectories are not entirely deterministic and suffer from damping or artifacts induced by the introduction of barostats or thermostats in the system. Moreover, numerical errors can accumulate in simulations, and although such errors do not affect accurate sampling of the phase space, it is important to keep in mind the somewhat stochastic nature of the results.

8.2.2 *Coarse Grained MD Simulations*

The potential of all-atom MD simulations is constrained by the limited time and length scales that can be accessed with finite computer resources. Sometimes however, atomistic detail is not necessary to address interesting questions in the design and analysis of a biomimetic membrane. In such a case, the model can be coarse-grained, such that each particle in the simulation represents multiple atoms instead of a single atom. In the simplest case, the methylene groups on hydrophobic lipid tails can be represented as single united-atom particles, because the low polarity of the C–H bond is unlikely to affect a macroscopic property such as the surface tension of the lipid-water interface. The coarse graining procedure has two desirable consequences. First, the number of particles in the system is drastically reduced; one thus has to integrate Eq. 8.1 far fewer times. Secondly, because the overall system description becomes much simpler, the potential energy surface is smoother, the system encounters lower free energy barriers across the phase space, and sampling is accelerated. Thus, it becomes possible to explore systems containing millions of atoms (micron-sized patches of membranes) for up to millisecond time scales with state-of-the-art computing infrastructure. However, the coarse-grained force field must be carefully accurately parameterized. The most popular CG force field for lipids and proteins is the MARTINI force field (Marrink et al. 2007). In MARTINI, each particle typically represents four united atoms. The model represents four water molecules as a single particle, and thus does not have the resolution to simulate water transport through aquaporins. However, the MARTINI model has been used successfully to address a large variety of physical problems in bio-membrane research such as the spontaneous formation of domains in model lipid mixtures (Risselada and Marrink 2008) For a review, see (Marrink et al. 2009).

The potential applications of CGMD are immense, because it bridges the gap between all-atom MD simulations to more continuum-based approaches such as dissipative particle dynamics (DPD) and ultimately computational fluid dynamics (CFD). The obvious limitations are the loss of atomistic detail in the trajectories, and need to reparameterize the force field for novel molecules.

8.2.3 *Dissipative Particle Dynamics (DPD) Simulations*

Bridging particle based simulations such as CGMD to continuum fluid simulations is the relatively modern technique of Dissipative particle dynamics (DPD) simulations. In DPD, particles represent fluid elements that evolve in continuum space and

discrete time steps and where the correct hydrodynamic behavior of the particles is realized. Particles interact by pairwise additive forces which consist of a conservative term, a dissipative frictional force, and a random force. However, unlike Brownian dynamics, momentum is locally conserved in DPD. With recent advances in the parallelization of DPD codes (Julian Shillcock, personal communication 2010), it is expected that DPD will be able to address systems as large as microns or even millimeters, thus providing an excellent link between short length scale particle based simulations and computational fluid dynamics which operates in the continuum regime.

8.3 Computational Fluid Dynamics (CFD) Simulations

Computational Fluid Dynamics (CFD) has been used for several years within engineering disciplines dealing with motion of liquids and gasses such as the aviation and car industries. Within recent years, the use of CFD has expanded and today, it is a widely used tool in the engineering design and analysis of many aspects of fluid dynamics.

CFD modelling is today regarded as the most exact mathematical tool which can be applied in the analysis of many macro-scale flow problems. With the increasing performance of computers today, CFD modelling is even often regarded as an alternative to physical laboratory tests. CFD results are not limited to a few measuring points, but give a complete and detailed insight into e.g. the hydrodynamic performance. Thus, design alternatives or methods for optimizing fluid dynamic systems are readily analysed.

CFD modelling requires a solid underlying appreciation of both fluid dynamics as well as numerical analysis. In order to avoid misinterpretations and significant errors it is important that the person using the technology has a good understanding of the basic theory of CFD. The objective of following sections is to provide a general but short introduction to Computational Fluid Dynamics (CFD). The reader is encouraged to refer to specialised literature to get deeper insight understanding of the topic.

8.3.1 CFD Theory

The fundamental equations of all fluid dynamic problems are conservation of mass and momentum, which can be expressed as:

$$\begin{aligned} \frac{dm}{dt} &= 0 \\ \frac{d(m\mathbf{v})}{dt} &= \sum \mathbf{f} \end{aligned} \quad (8.10)$$

where t is time, m is the mass, \mathbf{v} is the velocity vector and \mathbf{f} is the forces acting on the control mass. Description of the hydrodynamic performance of a fluid can in principle be done with two different approaches, the Euler or the Lagrangian description. In the Euler description properties of the fluid are described relative to a fixed location in space, characterised by the location \mathbf{x} , while in the Lagrangian description properties are described relative to the individual flow particles at a given time. The presentation in this chapter is based on an Euler description.

In an Euler description, the conservation of the mass, Eq. 8.10 can be expressed as:

$$\frac{\partial \rho}{\partial t} + \nabla \cdot (\rho \mathbf{v}) = 0 \quad (8.11)$$

where ρ is the density of the fluid and ∇ the gradient operator. In the following it is assumed that the compressibility of the fluid is negligible, which is a fully acceptable assumption in most practical cases of analysis of fluid dynamic problems related to membranes. In this case, the equation for conservation of mass is simplified to

$$\nabla \cdot (\mathbf{v}) = 0 \quad (8.12)$$

The forces acting on a fluid are normally classified in two groups: Body and surface forces. The body forces are forces that work on the entire body. An example of the body forces is gravitational forces, which can be expressed as:

$$\mathbf{f}_b = \rho \mathbf{g} \quad (8.13)$$

Depending on the fluid dynamic applications investigated it may be relevant to include other types of body forces, for example forces due to rotation of the body or electrical forces.

Expressions for the surface forces are derived on the basis of an expression of the stress tensor, the deformation tensor and the constitutive relation which relates the stress tensor to the deformation tensor. For a Newtonian flow (where it is assumed that there is a linear relation between the stress tensor and the deformation tensor) the stress tensor \mathbf{T} can be expressed as:

$$\mathbf{T} = -\left(p + \frac{2}{3}\mu \nabla \cdot \mathbf{v}\right) \mathbf{I} + 2\mu \left(\frac{1}{2}(\nabla \mathbf{v} + (\nabla \mathbf{v})^T)\right) \quad (8.14)$$

where \mathbf{I} is the unity tensor and μ the dynamic viscosity. Applying Eqs. 2.5 and 2.6 it can be derived that the conservation of momentum, in an Euler description, can be expressed as:

$$\rho \frac{\partial \mathbf{v}}{\partial t} + \rho (\mathbf{v} \cdot \nabla) \mathbf{v} = -\nabla p + \mu \nabla^2 (\mathbf{v}) + \rho \mathbf{g} \quad (8.15)$$

The pair of Eqs. 8.14 and 8.15 is called the Navier–Stokes equation for incompressible flow and is the basic set of equations which is solved in a CFD model.

In Eq. 8.15 the first term on the left hand is called the local acceleration term, the second term on the left hand is called the convective term, the first term on the right hand side the pressure gradient term, the second term on the right hand the viscosity term and the third term on the right hand is the gravity force term.

8.3.2 *Turbulence*

In principle, the Navier–Stokes equation could be applied directly to model any flow problems, but turbulence encountered at high flow will often require special turbulence model in order to solve hydrodynamic problem. Turbulence is a highly complex hydrodynamic phenomena and it is characterized by a series of properties:

- Turbulence is generated and dissipated where friction forces are converted to heat and evolves through a wide range of time and space scales, and is therefore not easily represented in one numerical model.
- A turbulent flow consists of random fluctuations. Turbulent flow is often modelled as a mean flow superseded by irregular fluctuation around the mean value.
- A turbulent flow consists of many vortices in different size and frequency. The flow fluctuates on a large variation in time and length scale.
- Turbulence is always a three dimensional phenomenon, which should be taken into consideration when the hydrodynamic problem is analysed in a two dimensional model.
- Turbulence increases the mixing of the flow, and the effect must be included in modelling of the transport of any conservative or reactive substance.

The turbulence introduces mixing of flow with different levels of momentum. This effect is often modelled as an “additional” viscosity of the flow, where the additional viscosity is called the eddy viscosity. The so-called Reynolds number in a given flow is the ratio between inertia and friction forces, and is therefore often used as a number for the level of turbulence in that flow.

Turbulent flow conditions are often encountered in membranes. Flow conditions, and in particular mixing and turbulence, in the vicinity of membrane surfaces are of high importance for the overall performance of membrane systems. Thus, typical issues are: what is the ideal cross-flow velocity? How can the cross-flow be reduced (energy to pump water around) while at the same time maintain sufficient shear stress to minimize fouling? How can the concentration profile of suspended or dissolved material in the water in the vicinity of the surface membranes be changed? And finally how can a hydraulic system be designed in a way so that uniform filtering overall across the membrane surface is obtained? Such analyses require assessment of turbulence effects.

Throughout history different approaches have been developed and applied to model the effect of turbulence, see for example (Wilcox 2006) and (Ferziger and Peric 1999). In principle it is possible to simulate the turbulence directly on the

basis of Eqs. 8.14 and 8.15. This approach is termed Direct Numerical Simulation (DNS). It is by far the simplest way to model the turbulence, no additional modelling is required, but the major problem in DNS is that capture of all turbulence effects requires a very refined computational grid and a corresponding very small time step. In a DNS simulation the length of the grids should be less than the Komologov length scale η , which is an estimate of the smallest size of the turbulence scale and given by:

$$\eta = \left(\frac{\nu^3}{\varepsilon} \right)^{1/4} \quad (8.16)$$

where ε is the dissipation per unit mass of the energy and ν is the kinematic viscosity. It can be demonstrated (see for example Wilcox 2006) that in many engineering applications with high Reynolds number, this requirement results in a mesh size in the order of 10^8 – 10^9 , which means that from a practical point of view DNS is only possible for low Reynolds number and simple geometry. Another central issue with DNS is the definition of boundary conditions, which can be difficult. DNS is, however, a very valuable method, that can be used to understand the turbulence structure and processes at a fundamental level. Large Eddy Simulation (LES), could be an alternative to DNS. In LES the large scale eddies are computed directly, while the small scale turbulence is modelled. As the small scale turbulence is modelled in LES, it is possible to relax the requirements to maximum grid size, and LES simulation can typically be carried out in mesh with a factor of 10–100 fewer cells than DNS model. The LES method is based on a modified version of Navier–Stokes equation where the resolvable-scale is separated from the sub-grid scale by filtering the velocity field and introducing a model of the effect from sub-grid turbulence, the sub-grid scale Reynolds Stress. With the increased capacity, in terms of speed and memory, of computers, the LES method is applied in an increasing number of projects today.

An alternative to the DNS and LES is the Reynolds-average approach to turbulence modelling (RANS – Reynolds averaged Navier–Stokes equations). Although the increased computational speed of computers today allows for application of more advanced turbulence modelling techniques in many projects, the RANS approach is still effectively the industrial standard today.

8.3.3 *Suspended and Dissolved Matter in the Fluid*

In many fluid dynamic problems there is a strong coupling between the fluid dynamic and transport of suspended, dissolved organic and non-organic matter, as well as chemical and biological processes. Traditionally, CFD has been used to optimize especially the hydrodynamics (flow mechanics) and focus has often been on the hydrodynamic performance and has not included an assessment of the interaction

between hydrodynamic and chemical-biological processes. Process-modeling with CFD offers the opportunity to develop and test new innovative ideas on another level of accuracy. By use of an advanced hydrodynamic model coupled with transport and chemical-biological process models it is possible to predict the effect of a given design modification without having to go through the cumbersome, lengthy and costly pilot testing process.

On the basis of an Euler description, the transport of a conservative constituent is often modelled by the transport equation:

$$\frac{\partial c}{\partial t} + \mathbf{v} \cdot \nabla c = \nabla \cdot (\boldsymbol{\varepsilon} \nabla c) \quad (8.17)$$

where c is the concentration of the constituent modelled, the dispersion coefficient $\boldsymbol{\varepsilon}$ is given by

$$\boldsymbol{\varepsilon} = \nu + \nu_t \quad (8.18)$$

The dispersion coefficient includes both the molecular dispersion coefficient ν and the (mechanical) hydrodynamic dispersion coefficient ν_t due to turbulence. Non-conservative constituent problems are often modelled by adding source or sink terms to Eq. 8.17. A description based on (8.17) is called an Euler-Euler model where constituents or particles are not described individually, but as a scalar in the flow. This scalar may have properties that feed back to the fluid and affect the liquid physical properties and modify the turbulence. The advantage of these types of models is that it is possible to calculate flows with high Reynolds numbers and complex geometries. The disadvantage is that the models must handle particles in a continuum. Properties of a particle with a dimension of e.g. 1 μm are distributed over a grid scale, e.g. 10 cm. Another widely used method is the so-called multiphase models, where particles and fluids are modelled as separate phases, taking up a fraction of the total volume. This type of models includes a description of the exchange of energy, inertia and mass between phases. The different phases may for example be water, air or solids (sludge).

The main challenge in modelling solids is that the particles do not follow the flow in which they are suspended. As a result of surface chemistry, geometry and mass particles will often break out of the turbulent eddies of the fluid. This has the consequence that models of subgrid scale turbulence in fluids and gases cannot be applied directly to the description of particle motion. A solution to this problem has been to model all sub turbulence processes of the fluid in great detail. The governing equations for fluid and gas flows are solved in their filtered or direct form (LES: Large Eddie Simulation, DNS: Direct Numerical Simulation) basically trying to solve the turbulence down to the viscous scale.

Alternatively, the particle motion can be described in an Euler-Lagrange model, where particles are described individually or as representative particles that represent thousands of sub particles. The disadvantage of this type of model is that it is very computational resource demanding for even the simplest fluid problem.

8.3.4 Numerical Model Setup

In a CFD model, the exact solution to the fundamental differential equations is approximated by a system of algebraic equations with a set of variables at a set of discrete locations in space and time. There are many different approaches to this, but the most common approach is the Finite Volume (FV) Method. The FV method is based on an integral form of the differential equation. The solution domain is subdivided into a numbers of control volumes (computational cells, or grid cells) where the integral equations are applied to each control volume. Often the computational point, for all solution variables, is located at the centre of each grid cell and interpolation is used to describe the variation of the variables in between. By aim of e.g. the Gaussian quadrature integration methods, the momentum and mass equations are converted into algebraic equations in each node and with links to the equations in the neighbouring nodes. The solution variables (e.g. velocity vector and pressure) in each computation point are found by numerical solution of matrix equations.

The quality of the results from a CFD model is strongly depending on the quality of the computational grid. Often, it is possible to take advantage of symmetrical conditions and hereby reduce the computational domain. The grid has to be designed in such a manner that the resolution (size of each grid cell) is sufficiently dense to capture the important physical phenomena, see Fig. 8.5. On the other hand, the computational power demand increases with the number of grid cells. Thus, to keep down the computation costs, the design of the mesh if often a tradeoff between these two considerations.

The boundary conditions represent the influence of the surroundings that have been cut off when defining the computational domain. The solution inside the computational domain may strongly depend on the boundary conditions. Proper choice of these is therefore very important. Alternatively the boundaries of the computational domain should be far away from the region of interest in order not to “contaminate” the solution with the inaccurate boundary conditions.

Boundary conditions are typically separated into different categories such as inflow, outflow, wall and symmetry boundary conditions. At the inflow boundary the velocity is often prescribed and it is assumed that the pressure gradient is zero. At the outlet boundary, zero gradient in the velocity together with a hydrostatic pressure distribution is often prescribed (a so-called open boundary condition). At solid walls a no-slip boundary condition is used for the velocities. At walls, two different approaches are typically applied in a RANS simulation. One approach is to resolve the boundary layer including the viscous sublayer close to wall and to compute the wall shear stress from the local velocity gradient normal to the wall. This requires however, a very fine mesh resolution in wall-normal direction (as a rule of thumb the model must include at least five computational points in the viscous sub layer in order to simulate the boundary layer correctly). Another approach is to assume that the velocity profile close to the wall is logarithmic. This enables a substantial reduction in the number of grid cells in the wall-normal direction.

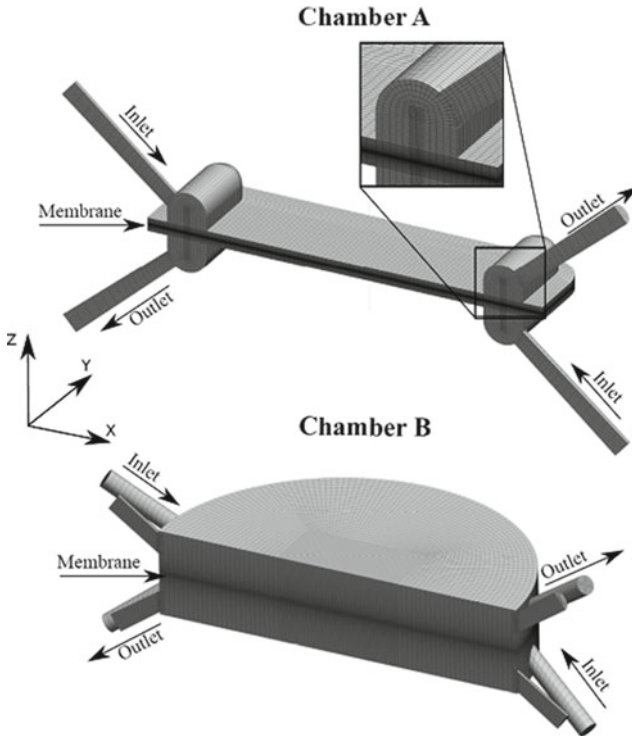


Fig. 8.5 The computational meshes for two three-dimensional flow chambers. The membranes are modeled as planes in the middle of the chambers, lying in the symmetry-planes normal to the z -axis. Both chambers have a symmetry-plane in the x - z plane, which is why only half the chambers are presented. The chambers are presented in counter-current cross-flow configuration with the feed and draw solutions being pumped through the chamber compartments in opposite directions. The zoom-in on *chamber A* demonstrates how the computational domains are finely graded towards the membrane so as to accurately describe concentration polarization effects

In many flows there are one or more symmetry planes. When the flow is steady there is a solution which is symmetric with respect to this plane. The symmetric solution can be obtained by solving the problem in a part of the domain and applying the symmetric conditions at the boundary. Also periodic boundary conditions can be used to reduce the computation domain and number of grid points.

Selection of appropriate numerical schemes is an important part of the model setup. Selection of these schemes is often a trade off between stability and accuracy. An upwind scheme is for instance typically more stable (simulates with longer time steps) than a central difference scheme, but on the other hand an upwind scheme tends to introduce numerical diffusion in the solution.

In unsteady simulations, the time step is an important parameter. The Courant number (Cr) is defined by:

$$Cr = \frac{v_{\max} dt}{dx} \quad (8.19)$$

where v_{\max} is the maximum velocity and dt the time step and dx grid size. A criterion based on the Cr number is often used to define an appropriate time step. Explicit time schemes are unconditionally unstable for $Cr > 1$, while implicit schemes are in principle stable for large Cr numbers. It is, however, normal practice to limit the Cr number to 0.5 for all type of schemes.

If a characteristic frequency range for the flow problem can be estimated, then the highest frequency should be resolved with at least 10–20 time steps per period.

8.3.5 *Micro CFD*

Classical CFD models (of e.g. flow in pumps, flow and turbulence around suspended pipelines etc.) usually operate with computational domains which have an extent of in meter, decimeter or even centimeter scale. The total number of grid cells (computational points) describing the geometry can typically be say 100,000 or even 1 million points in three dimensions. Thus, the grid cell size (dx) can typically be in cm or mm scale.

When focus is on the interaction between hydrodynamic, suspended or dissolved particles and chemical-biological processes in the boundary layers along membrane surfaces, catalytic surfaces or similar in water treatment systems, it become relevant to reduce the spatial and temporal scale of the CFD models substantially. In particular as nanotechnology makes it possible to actually engineer surfaces, it is important to be able to simulate the resulting fluid dynamics, turbulence and associated chemical-biological processes on that scale. New questions to be answered are: Which is the impact of a certain type of surface roughness on the near-wall flow conditions few microns or even nm from the wall? Can boundary layer thickness, diffusion through the boundary layer and turbulence mixing outside the layer be controlled in time and space in an intelligent way?

Fouling is by far the biggest barrier for a more wide-spread use of membrane systems. Thus, for both non-organic and organic fouling there is substantial potential in coupling e.g. various types of growth models to traditional CFD models including the evolution of fouling in time. The advanced state-of-art phenomenological descriptions of fouling processes may be expressed in deterministic CFD models to explore the complex fouling processes further. As described below, this development has started.

Expanding CFD models to the μm and nm scale is not without difficulties for various reasons: Data measurements at that scale to calibrate and validate the model results are difficult if not impossible with existing measurement instruments. Explicit thresholds in some of the commercial available CFD codes may prevent simulations in μm and nm scale. Some of the turbulence models, which have been successfully applied in traditional CFD applications, may only have a certain range of validity, and some of the turbulence constants in the equations may not be valid any longer. Finally, as also described above, CFD inherently assumes that flow and suspended or dissolved matter in the water behave like a continuum. When particles

are much larger than the size of the grid cells, the underlying mathematical formulation may no longer be valid.

Nevertheless, when the uncertainties and shortcomings are identified and appropriately handled, CFD modeling (which is called “micro CFD” herein) of much smaller systems is a very powerful tool in design and optimization of membrane systems.

8.3.6 Example of Application of CFD Models in Membrane Systems

Since the late 1990s CFD has been applied to investigate the flow phenomena in membrane filtration systems. In the literature results from several simulations on membrane spacer effects are given (Schwinge et al. 2004; Koutsou et al. 2007, 2009; Cao et al. 2001; Li et al. 2009; Shakaib et al. 2007). Especially membrane spacers have been the objective of many of the studies reported in these references. The spacer acts as mechanical stabilizer of the membrane geometry, but at the same time spacers are also turbulence promoters that may reduce concentration polarisation near membrane surfaces. Although the spacers may reduce polarisation they will inevitably increase the hydraulic resistance in the feeder channels and thus increase the required pressure to operate the membrane system. Therefore, there is often a tradeoff between increased mass transfer and increased cross flow power consumption. The topic for almost all of the above-mentioned references has been to analyse and optimise this problem.

In (Shakaib et al. 2007) it is demonstrated how CFD can be used to analyse flow field with diamond and parallel spacers. In the diamond spacers a set of filaments overlay upon another set of filaments in a different orientation on two different planes. The two sets of filaments added together define the channels height. In the parallel spacer there is a set of thin cross filaments which are transversely connected to thick axial filaments where the axial direction of the thick filaments creates channels for the main flow. A three dimensional approach is applied, with a zero velocity boundary condition at the membrane wall. This boundary condition corresponds to zero permeation, which is justified by the fact that the permeation velocity is typically very low compared to the cross flow velocity. The applied model covers only one cell of the diamond spacer or two thin cross filaments of the parallel spacer as periodic boundary conditions in flow plane are applied. In (Shakaib et al. 2007) it is demonstrated that a CFD simulation can be used to simulate the effect of filament height (channel height), spacing between filament, orientation of the filaments (or in other words the flow attack angle). Results are presented in terms of shear stress at the membrane faces and pressure distribution.

Although a detailed description of the flow pattern is of high value in the process of optimizing a membrane system, an accurate modeling of effects such as

concentration polarization, fouling etc. are essential in order to achieve a complete picture of the functioning of the membrane system. Several attempts to model such advanced features have been proposed (Wiley and Fletcher 2003; Fletcher and Wiley 2004; Wardeh and Morvan 2008; Schausberger et al. 2009; Vrouwenvelder et al. 2010). The model applied in (Wardeh and Morvan 2008) is typical for this type of simulation and can be summarized as follows. The model is based on the Navier–Stokes equation which is solved together with a transport equation of the solute concentration. The model approach does not include any turbulence modeling, and thus the approach is limited to laminar flow conditions. Standard boundary conditions are applied at inlets and outlets, with the specification of velocities variation at inlets (a parabolic variation) together with zero gradient in the pressure and zero gradient in the velocity and specification of the pressure at the outlet. At the walls no slip conditions are imposed on the velocity and zero gradient in the pressure. A uniform value of the concentration is specified at the inlet together with a zero gradient condition at walls and the outlet. At the membrane, conditions are more complex as the flow permeates through the membrane. In (Wardeh and Morvan 2008) it is assumed that the flux v_w is normal to the membrane and in the feeder channel given by:

$$v_w = A(\Delta p - \Delta\pi) \quad (8.20)$$

where Δp is the pressure difference between the feed and permeate channels, $\Delta\pi$ is the osmotic pressure difference, and A the water permeability coefficient (and assuming $\sigma=1$), see also Chap. 2. In (Wardeh and Morvan 2008) it is assumed that the hydrostatic pressure difference is constant, which is obviously a simplification. For the concentration (which is solved in terms of mass fraction m) the boundary conditions are:

$$\rho_w D \frac{\partial c}{\partial n} + \rho_w c v_w R = 0 \quad (8.21)$$

where D is the diffusion coefficient ρ_w is the density of the fluid in the feeder channel and R is a rejection coefficient taking into account the rejection of the salt at the membrane. This boundary condition expresses that the diffusive and the convective flux must be in balance at the membrane. In the permeate channel the boundary conditions are given by:

$$v_p = v_w \rho_w / \rho_p \quad (8.22)$$

$$\rho_p D \frac{\partial c}{\partial n} + \rho_p c v_p = \rho_w c v_w (1 - R) \quad (8.23)$$

where the index p refers to the permeate side of the membrane. The velocity boundary conditions in the permeate channel are corrected by the ratio of the density of the fluid on the two sides of the membrane in order to ensure that mass flux is conserved. In the paper presented by (Wardeh 2008) it is demonstrated that the model

can simulate variation in the concentration profile with different spacer configuration and the flow disturbance created by spacer has a positive effect on the concentration polarisation.

In (Vrouwenvelder 2010) a CFD model that couples a solute transport model with a biofouling description is presented. In practice biofouling is the primary fouling process in many reversed osmosis and nanofiltration membranes which is fed with extensively pre-treated water. It is important to obtain insight into the factors that have an impact on the development of the biofouling. Biofouling is caused by growth of biomass (biofilms) in the membrane.

In the model presented in (Vrouwenvelder 2010) it is assumed that the biofilm growth is a function of the concentration of a single soluble substrate. Assuming that growth depends on a single substrate is of course a simplification, but the concept could be extended to cover several substrates. The development of the biofilm is simulated on the basis of a biomass balance model, taking into account growth, transport and attachment of the biomass. The computational domain is divided into two regions, the fluid region and the biofilm region, the latter being the sub domain where the concentration of the biomass is larger than zero. The biofilm growth is given by:

$$\frac{\partial c_x}{\partial t} = \frac{\mu_m c_s c_x}{(k_s + c_s)} \quad (8.24)$$

where c_s is the concentration of the substrate and c_x is the biomass concentration, and k_s is the half-saturation coefficient. The biomass transportation is triggered when the concentration of the biomass exceeds a threshold value. The biomass redistribution is described by a cellular automaton biofilm model (Picoreanu 1998).

Biomass attachment is included with a constant rate (mass per area per day). The attachment is limited to areas where the fluid shear stress is below a threshold value, where the attachment occurs randomly in the available area. The concentration of the limiting substrate is modeled by an equation of the form of Eq. 8.17 including a sink term, in accordance with Eq. 8.24 taking into account consumption of the substrate by the formation of the biofilm. The model presented in (Vrouwenvelder et al. 2010) is one of the first attempts to describe the complex process of biofouling. In the paper it is demonstrated that such a model is able to predict the fouling process reasonably well.

Interfacial concentration polarization is another challenge for osmotic membrane operation. In Chap. 2 internal concentration polarization (ICP) was discussed and here we illustrate how CFD can be used to describe external concentration polarization (ECP). Figure 8.6 shows how the distribution of water flux and can be visualized from results obtained using CFD (Gruber et al. 2011) to simulate forward osmosis in systems with asymmetric membranes. It is observed that significant differences in water flux exist throughout the membrane domain, highlighting the power of CFD for system geometry optimization.

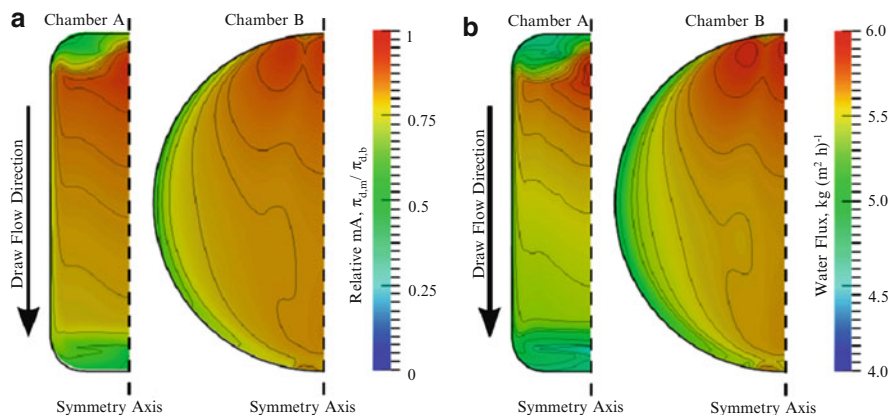


Fig. 8.6 External concentration polarization (ECP) and flux maps on the draw side of the membrane obtained from forward osmosis simulations in the chambers seen in Fig. 8.4. (a) ECP maps where the concentrations at the membrane are scaled relative to the bulk draw concentration, i.e. the concentration at the draw inlet. (b) Spatial distribution of membrane water flux in the two chambers. The flow directions in both (a) and (b) indicate that the draw inlets of both chambers are at the *top* of the figure, and correspondingly the outlets are at the *bottom*. Both simulations were performed with 1 M draw solutions, pure water feed solutions and a 50 mL/min cross-flow velocity. Contour lines are shown for arbitrary scalars merely to guide the eye

8.4 The Potential of Multi-scale Modeling

Whereas MD simulates discrete particles in a Lagrangian description and CFD simulations assume a continuum with a Eulerian description, the model applications have overlaps in the same critical mesoscopic length and timescale. MD originates from protein and biology engineering and is very suitable to simulate the transport through the aquaporin channels including the influence of external forces like osmotic pressure, electrical field, temperature gradient, pH value. Micro CFD can simulate the fluid conditions in the vicinity of the inlet and outlet channels and not least the transport of suspended or dissolved matter which controls the above mentioned forces (temperature, ions, salts, etc.).

Thus, there is scope for closer coupling between the two model types, which are evolved from two research communities usually working in quite different fields. A coherent description of processes from macro-scale (the membrane system), through meso-scale (the membrane surface) to nano-scale (the membrane pores) is possible with a set of models at different scales, which feed each others with information. From large to small scale: As described above, a model of flow and transport along the membrane surface provides the boundary conditions in terms of force fields to a detailed model of the aquaporin channels. From small to large scale: Turbulence is a determining factor in mixing processes on macroscale, and is

usually described through empirical turbulence models based on experiments and measurements. However, using small-scale models, the turbulence structure may actually be deterministically simulated and applied to estimate the parameters for the empirical turbulence model in the large-scale model.

Biofouling is an overwhelming challenge within membrane technologies where substantial research is already going on. There is a big potential in combining the biological model tradition on molecule scale in MD with fluid dynamic model tradition on macroscale in CFD in a new deterministic discipline by which fouling can be understood and controlled to a much higher degree than today.

8.4.1 Differences and Similarities

The main difference between MD and CFD is that the former assumes a set of discrete interacting particles whereas the latter assumes a continuum with given properties. Also the force field is inherently different when different scales are considered.

The similarity is that the same set of equation of motion is basically solved (Newton's second law). The solution is divided into a finite number of computation points (or particles), where a set of linear algebraic equations are derived from partial differential equations, and subsequently solved in a matrix equation.

Also considerations regarding initial conditions and boundary conditions are similar, including the need to reduce the computation domain using periodic boundary conditions, symmetry conditions or reduction of full three-dimensional spatial descriptions to two-dimensional (or even one-dimensional) models. The same type of numerical schemes, such as the leap frog explicit schemes, is found in both MD and CFD, and considerations of how to optimize model stability and accuracy at the same time.

8.4.2 Systematic Assessment of Model Reliability

For complex physical/chemical/biological phenomena which are modeled using advanced modeling systems which in turn require a number of different types of data for calibration and validation, there is a range of possible sources of uncertainties which must be taken into account when results are interpreted. The description of reliability and uncertainty analyses in hydraulic design by (Tung et al. 1993) is a good basis for understanding and assessing sources of uncertainties which influence model reliability. These include (Fig. 8.7):

- Inherent stochastic uncertainty (natural randomness)
- Data uncertainty
- Model uncertainty
- Model parameter uncertainty
- Operational uncertainty

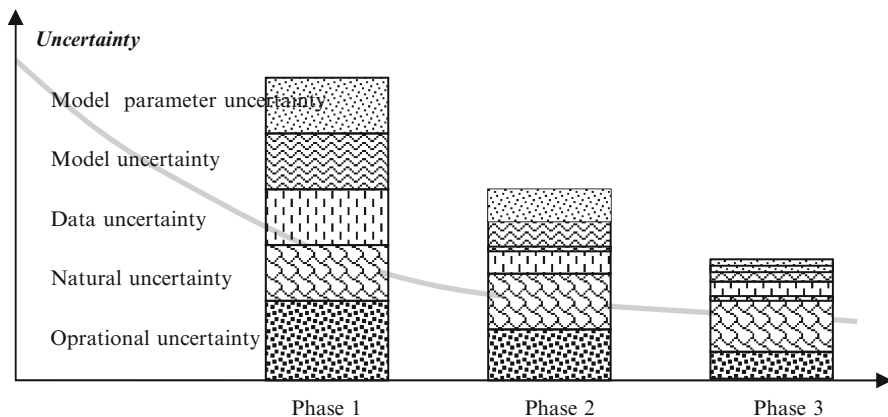


Fig. 8.7 Following the assessment and description of the uncertainty sources, a systematic approach can be applied through various phases of the model study to effectively document, reduce or eliminate uncertainties to enhance model reliability. Various probabilistic methods may be applied within each category to quantify uncertainties. However, in this description, focus is on identification and addressing the key elements of model reliability

Inherent stochastic uncertainty

The value of a numerical model basically depends on its ability to predict the natural processes under consideration. Such physical, chemical or biological processes may be associated with inherent randomness. Basically the question to be answered is: under given conditions, what will be the phenomenological behavior in the future?

MD trajectories are inherently chaotic. However, the averages drawn from several different chaotic trajectories (evolved under similar thermodynamic conditions) will converge if the sampling of the phase space is sufficient.

The relevant time scales and length scales, respectively, must be determined. In practice, the model operates with a number of time steps over a given period of time, and similarly with space steps. On a short-term small scale, processes may seem random in nature and impossible to predict although easy to simulate. However, if results from such a model are being averaged over longer time or wider areas, distinct patterns may occur which could only be simulated using such high-resolution model. One such example is turbulence modeling, where the precise velocity and pressure field at one specific point in time and at one particular place may be unpredictable, but the time-averaged results are useful.

As a rule of thumb, a good modeler will be able to describe in qualitative terms the evolution of processes prior to establishing the model and use the model itself for quantification only (with given levels of confidence). Exception from this is when a model can be applied to discover and explore non-linear processes such as cyclic phenomena, physical-based singularities or new complex correlations. The latter requires a thorough insight and understanding for proper interpretation.

Data uncertainty

A typical challenge for modelers is to have access to high-quality data, both for model setup (e.g. geometric description, inflow conditions at the boundaries, initial conditions of concentrations etc.), as well as for model calibration and validation (time series of flow velocity, pressure, concentrations etc.).

Data uncertainties include (1) measurement errors, (2) inconsistency and non-homogeneity of data, (3) data handling and transcription errors, and (4) inadequate representativeness of data sample due to time and space limitations. Measurement from the interior of membrane modules may be particularly challenging because of compact designs of e.g. spiral-wound membranes unless sensors are integrated in the design. Another difficulty is to measure data such as pressure, velocity or concentrations at micrometer scale i.e. in diffusive boundary layers because of the influence of such measurement instruments.

Efficient data sampling programs in turn significantly enhance the understanding of the functionality of membrane modules under various short-term and long-term operation conditions. For planning of such sampling programs, a pilot model which is only partly calibrated can be a valuable tool to identify critical or important places in the membrane module where data should be measured.

MD often struggles for high quality data, particularly because it is often unclear if the sampled trajectory is accurate enough to represent equilibrium conditions. This arises from time limitations.

Model uncertainty

A model's inability to accurately represent the system's true physical behavior is represented by the model uncertainty. A process description (e.g. fluid dynamic, biological or chemical) must be expressed as differential equations (mathematical formulae), which again must be translated to difference equations through the selected numerical schemes.

In practice, the computational grid (the discretization of time and lengths into distinct intervals), depends on the time and length scales which are considered. Thus, to simulate 1 month development of fouling, it makes no sense to simulate flow patterns down to micro-second details. The chosen differential equations depend on the numerical schemes, and the numerical schemes depend on the differential equations to be solved. For instance, if the resolution (time and space step in the computational grid) of the numerical scheme is coarse it may not be relevant to formulate the fully dynamic Navier-Stokes equations of flow patterns which are not resolved any way in the computational grid. The turbulence closure problem is a typical example of the considerations of a modeler in which an adequate turbulence model must be selected.

Model parameter uncertainty

The accuracy by which the input parameters can be quantified depends on the model parameter uncertainty. Parameters are boundary conditions and initial conditions (i.e. driving forces) as well as calibration parameters (e.g. flow resistance).

Key calibration parameters in fluid dynamics are resistance, viscosity and dispersion coefficients. Whereas typical values are often found in literature and/or can be reused from previous model studies of similar systems, it is essential to understand the range of validity of such calibration parameters, and to document the validity. For MD simulations, calibration parameters are in a state of constant evolution as problems with existing parameters become apparent as simulations run longer and longer with increasing computing power.

The valid range of given calibration parameters strongly depends on the model formulation itself. If for instance the model is developed and calibrated to describe average conditions, and the model is applied afterwards to simulate an extreme event, the calibration may no longer be valid. Therefore, the data collection and the subsequent calibration should ideally cover the whole range of possible applications afterwards.

To document the validity, there are different methods depending on the availability of data. Ideally, a large set of independent calibration data are used to repeat the calibration with each set to get a large set of samples of the same calibration parameter. The probability distribution of this calibration parameter can then be established and the mean and the variance of the parameter can be derived. Another method with less available data sets is to reserve one set for calibration and use the other sets for validation: The calibration parameter found initially is applied to carry out the validation simulations. The difference between the simulated and the actual validation data represent the model parameter uncertainty. Finally, if only one (or no) set of data is available, the modeler must carry out sensitivity analyses by which a number of simulations are carried out with small changes of the established calibration parameters to see the effect on the simulation results. The variance of the simulation results documents the uncertainty of the model parameters.

For advanced reliability analyses of model results, a variety of reliability analyses tools exist such as Monte Carlo simulations, Importance sampling, Latin Hypercube simulations, FORM first order reliability method. Some are useful for extreme value analyses and some are suitable for average conditions.

Operational uncertainty

A final element in the uncertainty analysis is the operational uncertainty, which reflects the human factors in terms of skills, knowledge and knowhow as well as errors during the modeling process. Definition of model requirements and interpretation and proper application of model results are essential. A specific challenge is that experts in various types of numerical models, whether it is MD or CFD, and experts in membrane systems, biological and physio-chemical processes are rarely the same.

As an example, MD simulation codes are often freely available and have become easy to use for biologists untrained in physics. The ideal modeler has expertise in (1) physical processes, (2) mathematical formulations, and (3) numerical schemes, and has the ability to interpret and distinguish whether model output are results of the real physical behavior, of erroneous mathematical expressions, or of amplified numerical effects.

8.5 Summary

Multi-scale modeling is an approach to carry out analyses of membrane flow and transport processes from different angles. MD models are used in protein engineering and have been successfully applied to simulate flow through aquaporin channels, and can now be applied to optimize the protein structures. CFD model in turns are used to optimize design and operation of membrane systems, and can also be applied on a micro-scale to analyse flow and transport in the vicinity of the membrane pore structures. There is significant potential in further exploiting different model techniques to solve the problem with biofouling in membrane systems, and to control the hydrodynamic as well as the chemical and biological conditions inside the membrane material. Numerical modeling at various scales supplements the experimental approach and is an efficient tool for design and for optimization.

References

- Alder, B., Wainwright, T.: Phase transition for a hard sphere system. *J. Chem. Phys.* **27**, 1208–1209 (1957)
- Cao, Z., Wiley, D., Fane, A.: CFD simulation of net-type turbulence promoters in a narrow channel. *J. Membr. Sci.* **185**, 157–176 (2001)
- de Groot, B.L., Grubmuller, H.: Water permeation across biological membranes: mechanism and dynamics of aquaporin-1 and GlpF. *Science* **294**, 2353–2357 (2001)
- Ferziger, J., Peric, M.: *Computational Methods for Fluid Dynamics*. Springer, Berlin/Heidelberg/New York (1999)
- Fletcher, D., Wiley, D.: A computational fluids dynamics study of buoyancy effects in reverse osmosis. *J. Membr. Sci.* **245**, 175–181 (2004)
- Gruber, M.F., Johnson, C., Tang, C.Y., Jensen, M.H., Yde, L., Hélix-Nielsen, C.: Computational fluid dynamics simulations of flow and concentration polarization in forward osmosis membrane systems. *J. Membr. Sci.* **379**(1–2), 488–495 (2011)
- Jensen, M.O., Mouritsen, O.G.: Single-channel water permeabilities of *Escherichia coli* aquaporins AqpZ and GlpF. *Biophys. J.* **90**, 2270–2284 (2006)
- Jorgensen, W.L., Chandrasekhar, J., Medura, J.D., Impey, R.W., Klein, M.L.: Comparison of simple potential function for simulating liquid water. *J. Chem. Phys.* **79**, 926–935 (1983)
- Khandelia, H., Jensen, M.O., Mouritsen, O.G.: To gate or not to gate: using molecular dynamics simulations to morph gated plant aquaporins into constitutively open conformations. *J. Phys. Chem. B* **113**, 5239–5244 (2009)
- Koutsou, C., Yiantsios, S., Karabelas, A.J.: Direct numerical simulation of flow in spacer-filled channels: effect on spacer geometric characteristics. *J. Membr. Sci.* **291**, 53–69 (2007)
- Koutsou, C., Yiantsios, S., Karabelas, A.: A numerical and experimental study of mass transfer in spacer-filled channels: effects of spacer geometrical characteristics and Schmidt number. *J. Membr. Sci.* **326**, 234–251 (2009)
- Levitt, M., Warshel, A.: Computer-simulation of protein folding. *Nature* **253**, 694–698 (1975)
- Li, Y., Tung, K., Lu, M., Huang, S.: Mitigating the curvature effect on spacer-filled channel in spiral-wound membrane module. *J. Membr. Sci.* **329**, 106–118 (2009)
- Marrink, S.J., Risselada, H.J., Yefimov, S., Tieleman, D.P., de Vries, A.H.: The MARTINI force field: coarse grained model for biomolecular simulations. *J. Phys. Chem. B* **111**, 7812–7824 (2007)
- Marrink, S.J., de Vries, A.H., Tieleman, D.P.: Lipids on the move: simulations of membrane pores, domains, stalks and curves. *Biochim. Biophys. Acta* **1788**, 149–168 (2009)

- Nyblom, M., Frick, A., Wang, Y., Ekvall, M., Hallgren, K., Hedfalk, K., Neutze, R., Tajkhorshid, E., Tornroth-Horsefield, S.: Structural and functional analysis of SoPIP2;1 mutants adds insight into plant aquaporin gating. *J. Mol. Biol.* **387**, 653–668 (2009)
- Picoreanu, C., van Loosdrecht, M.C.M., Heijnen, J.J.: Mathematical modeling of biofilm structure with a hybrid differential-discrete cellular automaton approach. *Biotechnol. Bioeng.* **58**, 101–116 (1998)
- Risselada, H.J., Marrink, S.J.: The molecular face of lipid rafts in model membranes. *Proc. Natl. Acad. Sci. U.S.A.* **105**, 17367–17372 (2008)
- Schausberger, P., Norazman, N., Li, H., Chen, V., Friedl, A.: Simulation of protein ultrafiltration using CFD: comparison of concentration polarisation and fouling effects with infiltration and protein adsorption experiments. *J. Membr. Sci.* **337**, 1–8 (2009)
- Schwinge, J., Neal, P., Wiley, D., Fletcher, D., Fane, A.: Spiral wound modules and spacers review and analysis. *J. Membr. Sci.* **242**, 129–153 (2004)
- Shakaib, M., Hasani, S., Mahmood, M.: Study on the effect of spacer geometry in membrane feed channels using three-dimensional computational flow modelling. *J. Membr. Sci.* **297**, 74–89 (2007)
- Tornroth-Horsefield, S., Wang, Y., Hedfalk, K., Johanson, U., Karlsson, M., Tajkhorshid, E., Neutze, R., Kjellbom, P.: Structural mechanism of plant aquaporin gating. *Nature* **439**, 688–694 (2006)
- Tung, Y.-K., Yen, B.-C., Melching, C.S. *Hydrosystems engineering reliability assessment and risk analysis*. 512 p. McGraw-Hill Chemical Engineering Series 2005 (1993)
- Vrouwenvelder, J., Picoreanu, C., Kruithof, J., van Loosdrecht, M.: Biofouling in spiral wound membrane systems: three-dimensional CFD model based evaluation of experimental data. *J. Membr. Sci.* **346**, 71–85 (2010)
- Vrouwenvelder, J.S., Radu, A.I., van Loosdrecht, M.C.M., Picoreanu, C.: Modeling the effect of biofilm formation on reverse osmosis performance: Flux, feed channel pressure drop and solute passage. *J. Membr. Sci.* **365** (1–2), 1–15 (2010)
- Wardeh, S., Morvan, H.P.: CFD simulations of flow and concentration polarization in spacer-filled channels for application to water desalination. *Chem. Eng. Res. Des.* **86** (10A), 1107–1116 (2008)
- Wilcox, D.C.: *Turbulence Modelling for CFD*, 3rd edn. DCW Industries, La Canada, USA (2006)
- Wiley, D., Fletcher, D.: Techniques for computational fluid dynamics modelling of flow in membrane channels. *J. Membr. Sci.* **211**, 127–137 (2003)
- Zhu, F., Tajkhorshid, E., Schulten, K.: Collective diffusion model for water permeation through microscopic channels. *Phys. Rev. Lett.* **93**, 224501 (2004)

Chapter 9

Regulation of Protein Function by Membrane Elastic Properties

Jens A. Lundbæk and Olaf S. Andersen

Abstract Integral membrane proteins are regulated by changes in the host bilayer lipid composition. We show how it is possible to get mechanistic insights in this type of regulation using proteins and other bilayer inclusions embedded in biomimetic membranes. Taking advantage of the simplicity that is conferred by studying ion channels embedded in planar lipid bilayers, one can show how membrane proteins are functionally regulated by the elastic properties of the host membranes' lipid bilayer. The chapter provides an introduction to the regulation of membrane protein function by the bilayer elastic properties, as given by the bilayer thickness, elastic moduli and monolayer intrinsic curvature. The use of gramicidin channels as molecular force as probes to study this type of regulation is described.

9.1 Introduction

The cell membrane's lipid bilayer serves as a barrier to non-selective solute movement, thus enabling cells to maintain different chemical compositions in the intracellular and extracellular fluid compartments. This barrier function is central to cellular electrolyte and volume homeostasis and it has at times led to the notion

J.A. Lundbæk (✉)

Department of Physiology and Biophysics, Weill Cornell Medical College,
Rm C-501B 1300 York Avenue, New York, NY, 10065, USA

Department of Physics, Biomimetic Membranes Group, Danish Technical University,
Building 309, Rm 142 Fysikvej 309, Kgs. Lyngby, DK-2800, Denmark
e-mail: lundbaek@dadlnet.dk

O.S. Andersen

Department of Physiology and Biophysics, Weill Cornell Medical College,
Rm C-501B 1300 York Avenue, New York, NY, 10065, USA
e-mail: sparre@med.cornell.edu

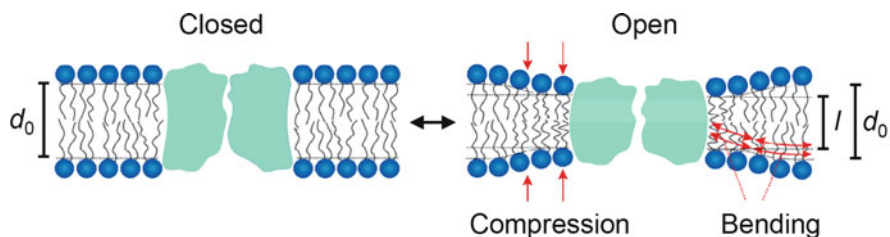


Fig. 9.1 Hydrophobic coupling between a lipid bilayer and an embedded protein. A change in protein hydrophobic length is associated with a bilayer deformation involving bilayer compression and monolayer bending (Modified from Lundbæk et al. 2010a)

that the membranes' lipid bilayer component is just a passive slab of liquid hydrocarbon—an anisotropic fluid element that merely provides the structural arrangement necessary for membrane protein organization and function.

This view is incomplete because membrane-embedded proteins are regulated by the molecular composition of the lipid bilayer—be it due to specific chemical interactions with individual bilayer-forming lipids (e.g., Evans and Hutchinson 2010; Fyrst and Saba 2010; Gimpl 2010; Kutateladze 2010)—or due to physical interactions with the bilayer behaving as a mesoscopic structure with collective material properties (e.g., Andersen and Koeppe II 2007; Lee 2004; Lundbæk 2006; Lundbæk et al. 2010a; Marsh 2008).

The present chapter provides an introduction to the regulation of membrane-embedded proteins by the bilayer elastic properties, which in the present context are given by: bilayer thickness, elastic moduli and monolayer intrinsic curvature (for more extensive reviews, see Andersen and Koeppe II 2007; Lundbæk 2006; Lundbæk et al. 2010a). This type of regulation is based on the “hydrophobic coupling” between a bilayer-embedded protein and its host bilayer, which arises as a consequence of the energetic penalty for exposing a hydrophobic surface to water. Because of this penalty, bilayer-spanning proteins and their host bilayer will adapt to each other in order to minimize exposure of hydrophobic residues to the aqueous surroundings (Fig. 9.1).

The adaptation involves local changes in lipid packing (Mouritsen and Bloom 1984), as well as changes in protein structure, e.g., (Soubias et al. 2008). The latter are likely to be more subtle than the former because the membrane lipids are organized as a liquid-crystalline soft material (e.g., Fig. 9.1). Nevertheless, despite the bilayer being relatively soft, the protein-induced changes in lipid packing incur an energetic cost—the bilayer deformation energy, ΔG_{def} .

Because of the need to maintain hydrophobic matching, protein conformational changes that involve the hydrophobic exterior of the proteins' bilayer-spanning domain will be associated with altered packing of the surrounding lipid molecules (Fig. 9.1). This is important because the difference between the bilayer deformation energies associated with two protein conformations A and B ($\Delta G_{\text{bilayer}}^{A \rightarrow B} = \Delta G_{\text{def}}^B - \Delta G_{\text{def}}^A$) contributes to the total energetic cost of the protein

conformational change (ΔG_{total}). ΔG_{def} , and thus $\Delta G_{\text{bilayer}}$, will vary as a function of the lipid bilayer elastic properties. The protein-bilayer hydrophobic interactions thus provide for an energetic coupling between protein conformations and the bilayer elastic properties—and for a Hydrophobic Coupling Mechanism (HCM), whereby protein function is regulated by changes in these properties (Lundbæk et al. 2004).

The first two sections of this chapter describe the HCM and the relation between the bilayer elastic properties and ΔG_{def} . The third section describes the use of gA channels as molecular force probes to study the bilayer regulation of protein function. The following sections describe the regulation of membrane protein function by maneuvers that alter bilayer elastic properties (thickness, monolayer intrinsic curvature and the associated elastic moduli) and studies using gA channels that have investigated the underlying mechanisms.

9.2 The Hydrophobic Coupling Mechanism

Membrane protein function generally seems to involve protein conformational changes at the protein/bilayer boundary (see (Lundbæk et al. 2010a), Table 1, for a list of examples). Figure 9.2 shows a recently described case: the KcsA channel in a partly open and an open-inactivated state (Cuello et al. 2010). The protein conformational changes involve structural rearrangements at the protein/bilayer boundary, as well as changes in protein hydrophobic length (length of the hydrophobic bilayer-spanning segment).

The relation between the energetic cost of a protein conformational change and the equilibrium distribution between the conformational states is given by:

$$\frac{n_B}{n_A} = \exp \left\{ -\frac{\Delta G_{\text{total}}^{A \rightarrow B}}{k_B T} \right\}, \quad (9.1)$$

where n_A and n_B denote the number of proteins (per unit area) in each of the states A and B, and k_B and T are Boltzmann's constant and the temperature in Kelvin. Equation 9.1 applies generally, and in case of bilayer-embedded, proteins $\Delta G_{\text{total}}^{A \rightarrow B}$ will include an energetic contribution due to any bilayer deformation caused by conformational changes at the protein/bilayer boundary. $\Delta G_{\text{total}}^{A \rightarrow B}$ therefore may be decomposed as:

$$\Delta G_{\text{total}}^{A \rightarrow B} = \Delta G_{\text{protein}}^{A \rightarrow B} + \Delta G_{\text{bilayer}}^{A \rightarrow B}, \quad (9.2)$$

where $\Delta G_{\text{protein}}^{A \rightarrow B}$ is the “intrinsic” cost of the protein conformational change (see Lundbæk et al. 2010a). Changes in bilayer elastic properties will alter the $\Delta G_{\text{bilayer}}^{A \rightarrow B}$ contribution to $\Delta G_{\text{total}}^{A \rightarrow B}$ (cf. Eqs. 9.1 and 9.2)—and thus the protein conformational distribution and protein function. That is, the bilayer becomes a regulator of membrane protein function. So what determines the magnitude of ΔG_{def} ?

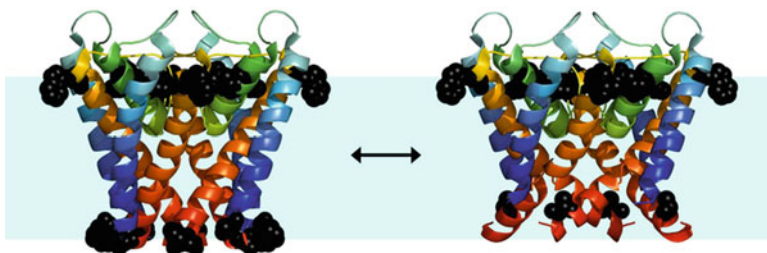


Fig. 9.2 Bilayer spanning segment of the KcsA channel in a partially open (*left*) and an open-inactivated (*right*) state (PDB: 3FB5 and 3F5W (Cuello et al. 2010)). Tryptophan (Trp) residues, usually considered to reside at the bilayer/solution interface, are shown as *black spheres* (Both structures lack coordinates for some of the atoms in TRP 113; 3F5W lack all, and 3FB5 lacks some, atom coordinates for TRP26)

9.3 Relation Between Bilayer Elastic Properties and ΔG_{def}

The energetic cost of adjusting the hydrophobic thickness of a lipid bilayer to match the hydrophobic length of a cylindrical embedded protein has been analyzed using continuum theories of elastic bilayer deformations (Helfrich and Jakobsson 1990; Huang 1986; Nielsen et al. 1998; Nielsen and Andersen 2000; Partenskii and Jordan 2002). Using this approach the bilayer deformation energy is described as the sum of two major energetic contributions that arise from the bilayer compression and monolayer bending in the vicinity of the protein (cf. Fig. 9.1).

Bilayer compression/expansion is associated with a compression energy density (CED):

$$\text{CED} = \frac{1}{2} K_a \cdot \left(\frac{d - d_0}{d_0} \right)^2, \quad (9.3)$$

where K_a is the bilayer compression modulus, d_0 the equilibrium thickness of the unperturbed bilayer, and d the thickness of the perturbed bilayer (Fig. 9.3).

Monolayer bending, correspondingly, is associated with a bending energy density (BED), which can be approximated as:

$$\text{BED} = \frac{1}{2} K_{c,m} \cdot \left(\frac{c_1 + c_2}{2} - c_0 \right)^2, \quad (9.4)$$

where $K_{c,m}$ is the monolayer bending modulus, c_1 and c_2 are the principal curvatures and c_0 is the intrinsic monolayer curvature (Fig. 9.3).

The energetic cost (ΔG_{def}) of adjusting the hydrophobic thickness of a lipid bilayer to match a bilayer-spanning protein with a radius, r_0 , thus becomes the integral of the contributions from bilayer compression and monolayer bending (cf. Eqs. 9.3 and 9.4):

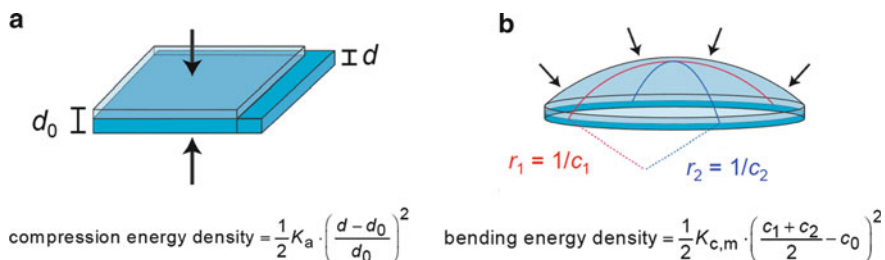


Fig. 9.3 Bilayer and monolayer deformations. **(a)** Bilayer compression and associated energy density. **(b)** Monolayer bending and associated energy density; c_0 is the curvature of the relaxed monolayer, c_1 and c_2 are the principal curvatures of the deformed monolayer (given by the corresponding radii of curvature as $1/r_1$ and $1/r_2$, respectively) (Modified from Lundbæk et al. 2010a)

$$\Delta G_{\text{def}} = \int_{r_0}^{\infty} \left\{ \frac{K_a}{2} \left(\frac{d-d_0}{d_0} \right)^2 + \frac{K_c}{2} \left(\frac{c_1+c_2}{2} - c_0 \right)^2 \right\} 2\pi r dr - \int_{r_0}^{\infty} \frac{K_c}{2} c_0^2 2\pi r dr \quad (9.5)$$

where d denotes the bilayer thickness at a radial distance $r-r_0$ from the protein/bilayer boundary, and K_c is the bilayer bending modulus ($=2K_{c,m}$). The second integral denotes the curvature frustration energy of the unperturbed (flat) bilayer (see Lundbæk et al. 2010a; Nielsen et al. 1998; Nielsen and Andersen 2000).

Equation 9.5 appears forbidding—but can be solved analytically (Goulian et al. 1998; Nielsen et al. 1998; Nielsen and Andersen 2000) to yield the following expression (see also Lundbæk et al. 2004):

$$\Delta G_{\text{def}} = H_B \cdot (l-d_0)^2 + H_X \cdot (l-d_0) \cdot c_0 - H_C \cdot c_0^2, \quad (9.6)$$

where the elastic coefficients H_B , H_X and H_C can be determined from d_0 , c_0 , K_a and K_c using the scaling relations derived in (Nielsen and Andersen 2000); the sign convention is chosen such that all three coefficients are positive, see (Lundbæk et al. 2010a).

d_0 , c_0 , K_a and K_c can be measured in protein-free lipid systems. So, based on results of such measurements (and Eqs. 9.5 or 9.6) one should, in principle, be able to determine the energetic cost of adjusting the bilayer thickness to match an embedded protein. In practice this is not possible for several reasons.

First, in continuum theories of elastic bilayer deformations, the CED and BED are treated as separable energetic contributions to ΔG_{def} . Nevertheless, they are coupled, in the sense that it is the sum of the two contributions to ΔG_{def} that is minimized (for a given deformation and set of bilayer physical properties). The underlying elastic parameters should, *in principle*, be transferable from measurements in protein-free lipid systems—assuming that the protein does not alter the local values of the underlying parameters, cf. (Partenskii and Jordan 2002). But, a change in bilayer composition will always alter more than one of the elastic parameters

(Lundbæk et al. 2005), and the changes in each of the parameters, *per se*, may have opposite effects on ΔG_{def} (Lundbæk et al. 2005; Bruno et al. 2007). This raises the question, which change will be energetically dominant?

Second, the continuum elastic parameters measured in protein-free systems are determined using global mono- or bilayer deformations that extend over length scales ranging from nm to μm (Evans and Needham 1987; Evans and Hochmuth 1978; Gruner 1985; Rand and Parsegian 1997; Helfrich 1973). The bilayer perturbation surrounding an embedded protein, in contrast, occurs on a molecular length scale and is likely to extend, at most, a few nm (Nielsen et al. 1998). It is, *a priori*, not obvious that the bilayer continuum elastic properties are relevant for the energetics of such deformations—a problem that may be further aggravated if the bilayer composition adjacent to a protein differs from that of the bulk bilayer (Andersen et al. 1992; Bruno et al. 2007).

Third, membrane proteins are not the smooth cylinders or cone-sections that usually are considered when implementing Eqs. 9.5 and 9.6 (see also (Dan and Safran 1998)). It is not obvious how to introduce the molecular details, but it is encouraging that the bilayer deformation profiles deduced from atomistic bilayer molecular dynamics simulations (Khelashvili et al. 2010) are very similar to those deduced from the continuum description.

Fourth, the “shape” of the protein-induced bilayer deformations may not be the same as in protein-free lipid systems. For example, the bending modulus usually is measured in bilayer bending experiments in which the monolayer curvatures have opposite sign, whereas the monolayer curvatures imposed by a hydrophobic mismatch between a symmetric protein and a bilayer having the same lipid composition in both leaflets are likely to be of the same sign (cf. Fig. 9.1). (It is in this context encouraging that the bending moduli measured using x-ray scattering of inverse hexagonal phases are similar to those determined from measurements on lipid bilayers (Marsh 2006).

It thus may be difficult to predict even the sign of the change in G_{def} induced by altered bilayer composition—in particular if the change in each of the elastic parameters (e.g., c_0 and elastic moduli (Bruno et al. 2007; Lundbæk et al. 2005), *per se*, would be expected to have opposite effects on ΔG_{def} (Lundbæk et al. 2010a, b). It therefore becomes important to have technologies that allow for experimental determination of changes in $\Delta G_{\text{bilayer}}$. One such method, which we will focus on in this chapter, is to use the bilayer-spanning gramicidin (gA) channel as molecular force probes to measure the effects of changes in bilayer composition on $\Delta G_{\text{bilayer}}$ for a change in hydrophobic length of an embedded protein.

9.4 Gramicidin Channels as Molecular Force Probes

gA is a pentadecapeptide that forms cation-selective ion channels by the bimolecular association of two monomeric subunits (Bämberg and Lauger 1973; Veatch et al. 1975), one residing in each bilayer leaflet (O’Connell et al. 1990) (Fig. 9.4a). The channels are mini-proteins with a very well-defined function; the channel structure,

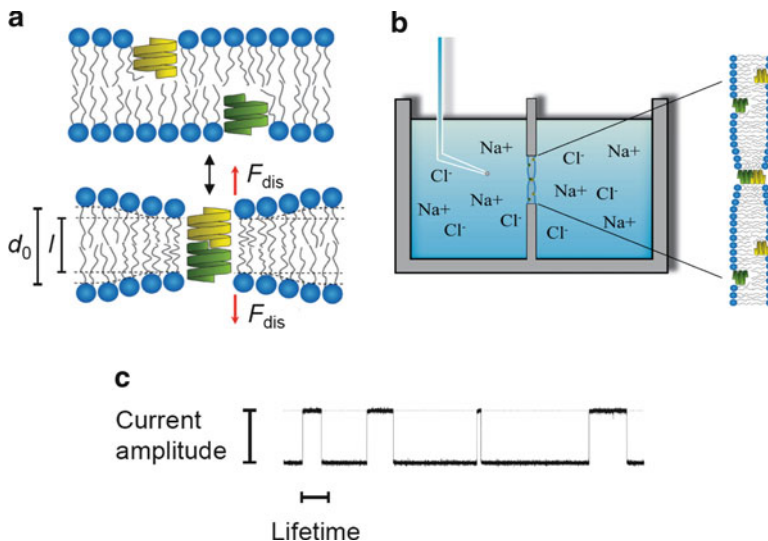


Fig. 9.4 Gramicidin channel function and experimental setup. (a) Gramicidin channels form by the trans-bilayer dimerization of a monomer from each bilayer leaflet. Channel formation is associated with a local bilayer deformation. (b) Experimental setup. (c) Experimental current trace showing the current transitions due to channel formation and disappearance; channels are “visible” as abrupt changes in the current across the bilayer (Modified from Lundbæk et al. 2010a)

the β^6 -helical dimer, is known at atomic resolution (Ketchum et al. 1993; Townsley et al. 2001), and channel function can be studied at single-molecule level using electrophysiological methods (voltage clamp). The experimental setup is shown in Fig. 9.4b. For further details see (cf. Lundbæk et al. 2010a).

gA channels do not open and close, they form and disappear (Bämborg and Lauger 1973; Veatch et al. 1975). The kinetics of gA channel formation and disappearance may be described as:



where M and D denote the monomers and channel-forming dimer, respectively, and k_1 and k_{-1} the association and dissociation rate constants. The energetics of channel formation is given by:

$$K_D = \frac{k_1}{k_{-1}} = \frac{[D]}{[M]^2} = \exp \left\{ \frac{-\Delta G_{\text{tot}}^{M \rightarrow D}}{k_B T} \right\}, \tag{9.8}$$

where K_D is the channel dimerization constant, and $[M]$ and $[D]$ are the concentrations of monomers and dimers in the bilayer (per unit area). In the experiments, changes in k_1 , k_{-1} and K_D are reported as changes in channel appearance frequency ($f = k_1 \cdot [M]^2$), channel lifetime ($\tau = 1/k_{-1}$) and activity ($n = f \cdot \tau$, the time-averaged number of conducting channels per unit area).

The hydrophobic length of the standard [Val¹]gA channel (~ 2.2 nm (Elliott et al. 1983; Harroun et al. 1999; Huang 1986)) is less than the thickness of the typical host lipid bilayer ($\sim 3\text{--}5$ nm). Channel formation therefore involves a bilayer deformation, in which the bilayer hydrophobic thickness (d_0) locally adjusts to match the channel hydrophobic length (l). The bilayer deformation energy ($\Delta G_{\text{bilayer}}^{\text{M} \rightarrow \text{D}}$) contributes to the energetic cost of channel formation (Huang 1986) ($\Delta G_{\text{tot}}^{\text{M} \rightarrow \text{D}}$):

$$\Delta G_{\text{tot}}^{\text{M} \rightarrow \text{D}} = \Delta G_{\text{prot}}^{\text{M} \rightarrow \text{D}} + \Delta G_{\text{bilayer}}^{\text{M} \rightarrow \text{D}}, \quad (9.9)$$

where $\Delta G_{\text{prot}}^{\text{M} \rightarrow \text{D}}$ is the ‘‘intrinsic’’ cost of channel formation. The relation between $\Delta G_{\text{bilayer}}^{\text{M} \rightarrow \text{D}}$ and the bilayer elastic properties is given by (cf. Eq. 9.6):

$$\Delta G_{\text{bilayer}}^{\text{M} \rightarrow \text{D}} = \Delta G_{\text{def}}^{\text{D}} - \Delta G_{\text{def}}^{\text{M}} = H_{\text{B}} \cdot (l - d_0)^2 + H_{\text{X}} \cdot (l - d_0) \cdot c_0, \quad (9.10)$$

where we approximate $\Delta G_{\text{def}}^{\text{M}}$ to be $-H_{\text{c}} c_0^2$ (cf. Eq. 9.6 with $d_0 = l$). In response to the deformation, the bilayer exerts a disjoining force (F_{dis}) on the channel, where F_{dis} is given by:

$$F_{\text{dis}} = 2H_{\text{B}} \cdot (d_0 - l) - H_{\text{X}} \cdot c_0 \quad (9.11)$$

A change in the bilayer elastic properties that increases $\Delta G_{\text{bilayer}}^{\text{M} \rightarrow \text{D}}$ is reported as a decrease in n (decrease in the product $f \cdot \tau$, where usually both f and τ will be decreased). The decrease in τ can be understood in terms of a change in the disjoining force, F_{dis} , because an increase in F_{dis} lowers the transition energy barrier for channel dissociation (see Lundbæk et al. 2010a). We will in the following focus on information gathered by studying the effects of changes in bilayer elastic properties on F_{dis} , as reported by changes in τ .

Channel dissociation involves the separation of the monomers by a distance δ (~ 0.16 nm (Durkin et al. 1993; Lundbæk and Andersen 1999; Lundbæk et al. 2010b; Miloshevsky and Jordan 2004)), where the transition state is reached and the channel conduction is lost. The corresponding activation energy ($\Delta G_{\text{tot}}^{\ddagger, \text{D} \rightarrow \text{M}}$) is given by:

$$\Delta G_{\text{tot}}^{\ddagger, \text{D} \rightarrow \text{M}} = \Delta G_{\text{prot}}^{\ddagger, \text{D} \rightarrow \text{M}} + \Delta G_{\text{bilayer}}^{\ddagger, \text{D} \rightarrow \text{M}}, \quad (9.12)$$

where $\Delta G_{\text{prot}}^{\ddagger, \text{D} \rightarrow \text{M}}$ denotes the ‘‘intrinsic’’ energy cost due to loss of contributions such as hydrogen bonds that stabilize the channel dimer and $\Delta G_{\text{bilayer}}^{\ddagger, \text{D} \rightarrow \text{M}}$ is the change in bilayer elastic energy associated with adjusting the local bilayer thickness from l to $l + \delta$, which may be approximated as:

$$\Delta G_{\text{bilayer}}^{\ddagger, \text{D} \rightarrow \text{M}} \approx -\delta \cdot F_{\text{dis}} = -\delta \cdot (2 \cdot H_{\text{B}} \cdot (d_0 - l) - H_{\text{X}} \cdot c_0) \quad (9.13)$$

In the experiments, the effects of changes in bilayer elastic properties on $\Delta G_{\text{bilayer}}^{\ddagger, \text{D} \rightarrow \text{M}}$ are reported as:

$$\Delta \Delta G_{\text{bilayer}}^{\ddagger, \text{D} \rightarrow \text{M}} = -k_{\text{B}} T \cdot \ln \left\{ \frac{k_{-1}}{k_{-1, \text{ref}}} \right\} = k_{\text{B}} T \cdot \ln \left\{ \frac{\tau}{\tau_{\text{ref}}} \right\}, \quad (9.14)$$

where the subscript “ref” denotes the reference situation. Using Eqs. 9.13 and 9.14, gA channels thus provide for direct measurements of the effects of changes in bilayer elastic properties on the energetic cost of the bilayer deformation associated with a change in hydrophobic length of an embedded “protein”.

Based on Eqs. 9.11, 9.13, and 9.14, one would expect F_{dis} to be increased, and τ to be decreased, by:

- Increasing channel-bilayer mismatch ($d_0 - l$)
- More negative monolayer intrinsic curvature (c_0)
- Larger bilayer elastic moduli (as reflected in H_B and H_x)

9.5 Changes in Bilayer Thickness

A number of structurally very different membrane proteins (e.g., Na^+ , K^+ -ATPase (Johannsson et al. 1981); rhodopsin (Brown 1994); nicotinic acetylcholine receptor (Criado et al. 1984); Ca^{2+} -activated potassium channels (Yuan et al. 2004); and the mechanosensitive MscL channel (Perozo et al. 2002)) are functionally regulated by the thickness of host lipid bilayer (see (Andersen and Koeppel II 2007) for a recent review and a list of membrane proteins regulated by changes in bilayer thickness). Though the results provide strong evidence for regulation of membrane protein function by the host bilayer physical properties, the mechanism(s) underlying the regulation are not well understood. In most cases the protein conformational changes underlying protein function are not known—and even in cases where high resolution structural information about such changes is available (e.g., Ca^{2+} -ATPase (Toyoshima et al. 2000; Toyoshima and Nomura 2002); KcsA channel (Cuello et al. 2010); mechano-sensitive MscS channel (Bass et al. 2002; Wang et al. 2008); maltose transporter (MalFGK2) (Khare et al. 2009), see also Lundbæk et al. 2010a), the structural changes at the protein/bilayer boundary are complex and the bilayer deformations/perturbations associated with the different structures are unknown.

Using continuum theories of elastic bilayer deformations, one would expect that a larger bilayer thickness would be associated with a larger cost of adjusting the bilayer to match a shorter protein. The thickness-dependent changes in protein function therefore suggest that protein function involves changes in protein hydrophobic length, as can be seen in the structures of KcsA (cf. Fig. 9.2). Studies using gA channels provide energetic insight into such regulation.

Figure 9.5a shows the effects of altering lipid bilayer thickness, by changing lipid (monoacylglyceride) acyl chain length, on $\ln\{\tau\}$ for bilayer-embedded gA channels (after Lundbæk and Andersen 1999). The bilayers were formed using either squalene or *n*-decane as solvent (results on τ from (Elliott et al. 1983) and (Kolb and Bamberg 1977); d_0 from bilayer capacitance measurements (Benz et al. 1975; Elliott et al. 1983)). $\ln\{\tau\}$ is a linear decreasing function of bilayer thickness, which provides for a simple measure of the channel-bilayer interactions. The linear

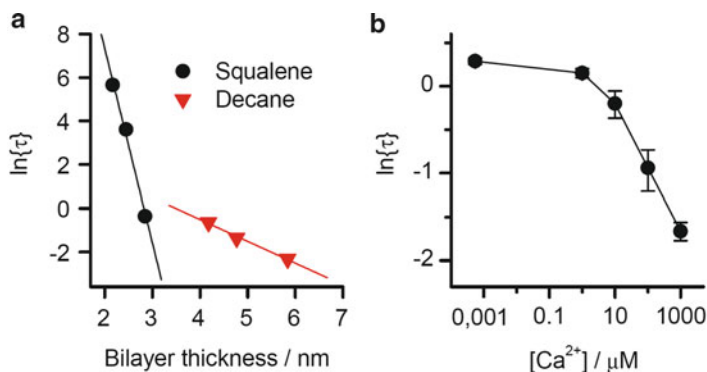


Fig. 9.5 gA channel lifetime as function of bilayer thickness and monolayer intrinsic curvature. (a) Relation between $\ln\{\tau\}$ and hydrophobic thickness (d_0) of monoacylglyceride using squalene or decane in the bilayer-forming solution. After (Lundbæk and Andersen 1999) using results from (Benz et al. 1975; Elliott et al. 1983; Kolb and Bamberg 1977). (b) Concentration-dependent effects of Ca^{2+} on τ . The monolayer intrinsic curvature is changed in the negative direction by increasing $[Ca^{2+}]$ (Experimental results from Lundbæk et al. 1997)

relation, moreover, provides support for approximating the bilayer deformation energy using the theory of elastic bilayer deformations (using Eqs. 9.13 and 9.14, $\Delta G_{\text{bilayer}}^{\text{D} \rightarrow \text{M}}$ and thus $\ln\{\tau\}$ should vary as a linear function of d_0). Further, the slope of the τ - d_0 relation provides for a measure of the bilayer elastic coefficient, H_B (Lundbæk and Andersen 1999; Lundbæk et al. 2010a) cf. Eqs. 9.6, 9.11, 9.13 and 9.14. The smaller slope of the relation obtained using *n*-decane *vs.* squalene reflects that bilayers formed using decane contain a significant fraction of hydrocarbon and therefore are softer than bilayers formed using squalene, which are virtually hydrocarbon-free (Seaman 1972; Simon et al. 1977). The value of H_B derived from the slope of the relation using squalene ($69 \text{ kJ}/(\text{mol} \cdot \text{nm}^2)$) agrees well with that expected from independent measurements of the bilayer elastic moduli in protein free lipid systems (Lundbæk and Andersen 1999). Bilayer-embedded gA channels thus represent a system where the effects of changes in bilayer thickness on protein function are well understood.

Importantly, changes in bilayer thickness and channel length have comparable effects on the channel lifetime (Lundbæk et al. 2010a). That is the changes in channel lifetimes result from changes in the hydrophobic mismatch, not bilayer thickness per se.

9.6 Changes in Monolayer Curvature

As is the case for changes in bilayer thickness, a number of structurally very different membrane proteins (e.g., Ca^{2+} -ATPase (Navarro et al. 1984); rhodopsin (Brown 1994), Ca^{2+} -activated potassium channels (Chang and Reistetter 1995; Park et al. 2003) and

mechanosensitive MscL channel (Moe and Blount 2005) are functionally regulated by maneuvers that change c_0 of the bilayer-forming lipids (see (Andersen and Koeppe II 2007) for a recent review and a list of such proteins, and (Lundbæk et al. 2010a) for a discussion of the difficulties associated with interpreting the experimental results). As for the effects of changes in bilayer thickness, the effects of changes in curvature are not well understood. It is, indeed, not clear whether the changes in protein function are caused by the changes in curvature, per se, as changes in lipid curvature alter also lipid bilayer thickness, cf. (Lundbæk et al. 2010a). For gA channels in lipid bilayers, continuum analysis predicts that a more negative curvature would increase the bilayer-disjoining force on the channel, and thus decrease f , τ and n . This is indeed the case. Figure 9.5b shows results from experiments studying gA channels in dioleoylphosphatidylserine (DOPS)/*n*-decane bilayers (Lundbæk et al. 1997). Because the experiments were done with bilayers that were formed using *n*-decane, the changes in lipid bilayer thickness are minimal. This simplifies the mechanistic interpretation because it becomes possible to focus on the changes in curvature. Because the lipid head group of DOPS is negatively charged, the electrostatic repulsion among the head groups in the bilayer—and thus c_0 —can be varied by altering the concentration of Ca^{2+} in the surrounding electrolyte solution. That is, higher $[\text{Ca}^{2+}]$ induces a more negative c_0 . As expected from Eqs. 9.13 and 9.14, a more negative c_0 leads to a decreased τ . Similar effects were observed for the changes in f , and thus n .

Our understanding of the effects of changes in c_0 , induced by altered lipid head group interactions, does not extend to changes in the bilayer-forming lipids that involve the bilayer hydrophobic core. An increase in lipid acyl chain unsaturation—which produces a more negative c_0 (Tate et al. 1991)—leads to a decrease in τ (Girshman et al. 1997)—contrary to the predictions of Eqs. 9.13 and 9.14. A possible explanation of this finding may be that an increased acyl chain unsaturation also will tend to thin lipid bilayers (Lewis and Engelman 1983) and reduce the bilayer bending moduli (Rawicz et al. 2000)—changes that in their own right will tend to reduce F_{dis} —and oppose any effect of a more negative c_0 . These findings, however, emphasize the importance of having a system, such as the bilayer embedded gA channels, where the effects of changes in the bilayers elastic properties can be tested on a well-defined protein structural change.

9.7 Amphiphile-Induced Changes in Bilayer Elastic Moduli

Amphiphilic compounds may regulate the function of bilayer-embedded proteins by direct chemical interactions with a specific protein target, as well as by adsorbing to the host lipid bilayer and thereby altering the bilayer elastic properties (Lundbæk et al. 2010a). Historically, the bilayer-mediated regulation of proteins has been ascribed to the “membrane active” or “membrane stabilizing” properties of amphiphiles (Sackmann 1984; Seeman 1972), terms that, though commonly used, are remarkably vague. Amphiphiles have complex effects on lipid bilayer physical properties that may involve changes in thickness (Ebihara et al. 1979),

intrinsic curvature (Lundbæk et al. 2005), as well as in the associated elastic moduli (Evans et al. 1995; Ly and Longo 2004; Zhelev 1998), some of which may have opposing effects on the bilayer deformation energy (Lundbæk et al. 2010a). The regulation of membrane protein function by amphiphiles therefore has been difficult to pin down.

Studies using gA channels have shown that small amphiphiles—at the concentrations where membrane protein function is modulated—have very similar effects on $\Delta G_{\text{bilayer}}$ for a change in hydrophobic length of an embedded protein. That is, a large number of structurally different amphiphiles (e.g., lipid metabolites (Bruno et al. 2007; Lundbæk and Andersen 1994); detergents (Lundbæk et al. 1996, 2004); capsaicin and capsaizepine (Lundbæk et al. 2005); and curcumin (Ingolfsson et al. 2007)) all decrease F_{dis} , irrespective of the sign of the curvature changes. The fact that amphiphiles decrease F_{dis} , most likely, reflects that such compounds tend to decrease the bilayer elastic moduli due to their reversible adsorption to lipid bilayers (Evans et al. 1995; Ly and Longo 2004)—and that the associated changes in $\Delta G_{\text{bilayer}}$ are more important than those associated with the changes in c_0 .

We compared the effects of structurally diverse amphiphiles—at the concentrations where they regulate a number of different membrane proteins—on the function of gA channels of different lengths and chirality (Lundbæk et al. 2010b). The analysis shows that the amphiphile-induced changes in gA channel function can be understood in terms of changes in H_B —with seemingly little effect of changes in c_0 . Figure 9.6a shows the concentration-dependent effects of amphiphiles on τ for channels formed by subunits having 13 amino acid residues ($[\text{des-Val}^1\text{-Gly}^2]\text{gA}^-$) or 15 amino acid residues ($[\text{Ala}^1]\text{gA}$). The compounds all increase τ (and thus $\Delta G_{\text{tot}}^{\ddagger, \text{D} \rightarrow \text{M}}$, cf. Eq. 9.14), with the larger effects on the shorter channel type, indicating that they alter bilayer elasticity (decrease the H_B).

A plot of the changes in channel lifetime of $[\text{des-Val}^1\text{-Gly}^2]\text{gA}$ as function of the changes in lifetime of $[\text{Ala}^1]\text{gA}$ (given as $\ln\{\tau_{13}/\tau_{13,\text{ref}}\}$ vs. $\ln\{\tau_{15}/\tau_{15,\text{ref}}\}$, where “ref” denotes the control situation) can be described by a shared linear relation for all the compounds (Fig. 9.6b). Similar results were obtained using dioleoylphosphatidylcholine as bilayer-forming lipid (Lundbæk et al. 2010b). The results cannot be ascribed to the presence of the hydrocarbon “solvent” that is used to form the bilayers, because experiments in solvent-free lipid vesicles show a similar insensitivity to changes in c_0 (Ingolfsson and Andersen 2010).

That the effects of structurally very different amphiphiles can be described by a shared relation implies that specific chemical interactions with the channel do not contribute to the changes in channel lifetime. The linear relation is due to a corresponding linear relation between $\Delta G_{\text{bilayer}}^{\ddagger, \text{D} \rightarrow \text{M}}$ for the bilayer deformations imposed by the two channels types, cf. Eqs. 9.12–9.14. The changes in $\Delta G_{\text{bilayer}}^{\ddagger, \text{D} \rightarrow \text{M}}$, moreover, can be shown to be described by changes in a single parameter, H_B , that summarizes the changes in the bilayer elastic properties (Lundbæk et al. 2010b).

Amphiphile-induced changes in H_B provide for quantitative predictions of their effects on voltage dependent sodium channels in living cells (Lundbæk et al. 2010b). That is, when the effects of a number of structurally different amphiphiles on sodium channel inactivation are plotted as a function of the changes in H_B , the results are

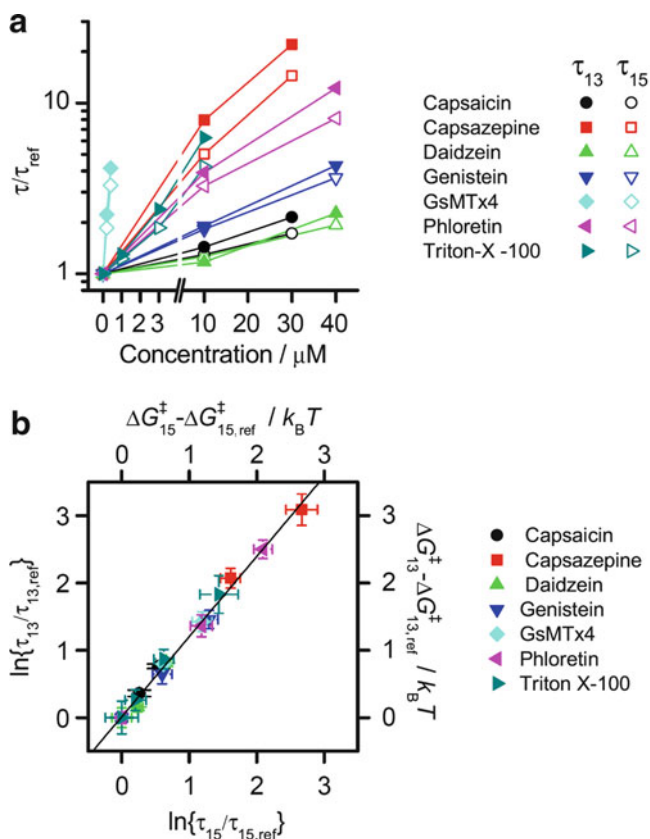


Fig. 9.6 Effects of amphiphiles on lifetimes of channels formed by monomers of 13-residues or 15 residues. **(a)** Concentration-dependent effects of Triton X-100 (Lundbæk et al. 2010b), capsaicin, capsazepine (Lundbæk et al. 2005), daidzein, genistein, phloretin (Hwang et al. 2003) or GsMTx4 (Suchyna et al. 2004) on $\ln\{\tau/\tau_{ref}\}$ for channels formed by monomeric subunits having 13 or 15 amino acid residues in their sequence, which therefore differ in length by ~ 0.32 nm (Hwang et al. 2003). **(b)** Effects on $\ln\{\tau_{13}/\tau_{13,ref}\}$ versus corresponding effects on $\ln\{\tau_{15}/\tau_{15,ref}\}$ (Modified after Lundbæk et al. 2010b)

superimposable. This raises the possibility that it will be possible to use gA channels for quantitative studies of the “membrane effects” of amphiphiles on protein function—effects that for so long have been elusive.

More generally, we note that the energetic coupling between membrane proteins and their host bilayer provide for a regulatory mechanism that is not shared with globular proteins (Andersen et al. 2008). Because many bioactive molecules and drugs are quite hydrophobic/amphiphilic (Tyrchan et al. 2009) it becomes important to consider the full spectrum of the mechanisms by which these molecules can alter membrane protein function (Lundbæk 2008; Andersen 2008).

9.8 Conclusion

In summary, the function of lipid bilayer-embedded proteins can be regulated by the elastic properties of the host lipid bilayer. This regulation can be understood in terms of the Hydrophobic Coupling Mechanism, whereby changes in the bilayer elastic properties alter the bilayer deformation energy associated with protein conformational changes at the protein-bilayer boundary. The use of gA channels as molecular force probes provides a method for studying such regulation in a system where the underlying “conformational changes” are well understood, which allows for detailed mechanistic studies.

Acknowledgments This work was supported in part by National Institutes of Health grant GM021342. We thank Helgi I. Ingólfsson, Roger E. Koeppe II, Ruchi Kapoor and Radda Rusinova for helpful discussions.

References

- Andersen, O.S.: Perspectives on how to drug an ion channel. *J. Gen. Physiol.* **131**, 395–397 (2008)
- Andersen, O.S., Koeppe II, R.E.: Bilayer thickness and membrane protein function: an energetic perspective. *Annu. Rev. Biophys. Biomol. Struct.* **36**, 107–130 (2007)
- Andersen, O.S., Sawyer, D.B., Koeppe II, R.E.: Modulation of channel function by the host bilayer. In: Easwaran, K.R.K., Gaber, B. (eds.) *Biomembrane Structure and Function*. Adenine Press, Schenectady (1992)
- Andersen, O.S., Ingólfsson, H.I., Lundbæk, J.A.: Ion channels. In: *Wiley Encyclopedia of Chemical Biology*, pp. 1–14. Wiley, Hoboken, N.J. (2008)
- Bämberg, E., Lauger, P.: Channel formation kinetics of gramicidin A in lipid bilayer membranes. *J. Membr. Biol.* **11**, 177–194 (1973)
- Bass, R.B., Strop, P., Barclay, M., Rees, D.C.: Crystal structure of *Escherichia coli* MscS, a voltage-modulated and mechanosensitive channel. *Science* **298**, 1582–1587 (2002)
- Benz, R., Fröhlich, O., Läger, P., Montal, M.: Electrical capacity of black lipid films and of lipid bilayers made from monolayers. *Biochim. Biophys. Acta* **394**, 323–334 (1975)
- Brown, M.F.: Modulation of rhodopsin function by properties of the membrane bilayer. *Chem. Phys. Lipids* **73**, 159–180 (1994)
- Bruno, M.J., Koeppe II, R.E., Andersen, O.S.: Docosahexaenoic acid alters bilayer elastic properties. *Proc. Natl. Acad. Sci. U.S.A.* **104**, 9638–9643 (2007)
- Chang, H.M., Reistetter, R.G.: Lipid-ion channel interactions: increasing phospholipid headgroup size but not ordering acyl chains alters reconstituted channel behavior. *J. Membr. Biol.* **145**, 13–19 (1995)
- Criado, M., Eibl, H., Barrantes, F.J.: Functional properties of the acetylcholine receptor incorporated in model lipid membranes. Differential effects of chain length and head group of phospholipids on receptor affinity states and receptor-mediated ion translocation. *J. Biol. Chem.* **259**, 9188–9198 (1984)
- Cuello, L.G., Jogini, V., Cortes, D.M., Perozo, E.: Structural mechanism of C-type inactivation in K(+) channels. *Nature* **466**, 203–208 (2010)
- Dan, N., Safran, S.A.: Effect of lipid characteristics on the structure of transmembrane proteins. *Biophys. J.* **75**, 1410–1414 (1998)

- Durkin, J.T., Providence, L.L., Koeppe 2nd, R.E., Andersen, O.S.: Energetics of heterodimer formation among gramicidin analogues with an NH₂-terminal addition or deletion. Consequences of missing a residue at the join in the channel. *J. Mol. Biol.* **231**, 1102–1121 (1993)
- Ebihara, L., Hall, J.E., MacDonald, R.C., McIntosh, T.J., Simon, S.A.: Effect of benzyl alcohol on lipid bilayers. A comparison of bilayer systems. *Biophys. J.* **28**, 185–196 (1979)
- Elliott, J.R., Needham, D., Dilger, J.P., Haydon, D.A.: The effects of bilayer thickness and tension on gramicidin single-channel lifetime. *Biochim. Biophys. Acta* **735**, 95–103 (1983)
- Evans, E.A., Hochmuth, R.M.: Mechanochemical properties of membranes. *Curr. Top. Membr. Transp.* **10**, 1–64 (1978)
- Evans, J.F., Hutchinson, J.H.: Seeing the future of bioactive lipid drug targets. *Nat. Chem. Biol.* **6**, 476–479 (2010)
- Evans, E., Needham, D.: Physical properties of surfactant bilayer membranes: thermal transitions, elasticity, rigidity, cohesion, and colloidal interactions. *J. Phys. Chem.* **91**, 4219–4228 (1987)
- Evans, E., Rawicz, W., Hofmann, A.F.: Lipid bilayer expansion and mechanical disruption in solutions of water-soluble bile acid. In: Hofmann, A., Paumgartner, G., Stiehl, A. (eds.) *Bile Acids in Gastroenterology: Basic and Clinical Advances*, pp. 59–68. Kluwer Academic, Dordrecht (1995)
- Fyrst, H., Saba, J.D.: An update on sphingosine-1-phosphate and other sphingolipid mediators. *Nat. Chem. Biol.* **6**, 489–497 (2010)
- Gimpl, G.: Cholesterol-protein interaction: methods and cholesterol reporter molecules. *Subcell. Biochem.* **51**, 1–45 (2010)
- Girshman, J., Greathouse, D.V., Koeppe 2nd, R.E., Andersen, O.S.: Gramicidin channels in phospholipid bilayers with unsaturated acyl chains. *Biophys. J.* **73**, 1310–1319 (1997)
- Goulian, M., Mesquita, O.N., Fygenson, D.K., Nielsen, C., Andersen, O.S., Libchaber, A.: Gramicidin channel kinetics under tension. *Biophys. J.* **74**, 328–337 (1998)
- Gruner, S.M.: Intrinsic curvature hypothesis for biomembrane lipid composition: a role for nonbilayer lipids. *Proc. Natl. Acad. Sci. U.S.A.* **82**, 3665–3669 (1985)
- Harroun, T.A., Heller, W.T., Weiss, T.M., Yang, L., Huang, H.W.: Experimental evidence for hydrophobic matching and membrane-mediated interactions in lipid bilayers containing gramicidin. *Biophys. J.* **76**, 937–945 (1999)
- Helfrich, W.: Elastic properties of lipid bilayers: theory and possible experiments. *Z. Naturforsch* **28C**, 693–703 (1973)
- Helfrich, P., Jakobsson, E.: Calculation of deformation energies and conformations in lipid membranes containing gramicidin channels. *Biophys. J.* **57**, 1075–1084 (1990)
- Huang, H.W.: Deformation free energy of bilayer membrane and its effect on gramicidin channel lifetime. *Biophys. J.* **50**, 1061–1070 (1986)
- Hwang, T.C., Koeppe II, R.E., Andersen, O.S.: Genistein can modulate channel function by a phosphorylation-independent mechanism: importance of hydrophobic mismatch and bilayer mechanics. *Biochemistry* **42**, 13646–13658 (2003)
- Ingolfsson, H.I., Andersen, O.S.: Screening for small molecules' bilayer-modifying potential using a gramicidin-based fluorescence assay. *Assay Drug Dev. Technol.* **8**, 427–436 (2010)
- Ingolfsson, H.I., Koeppe II, R.E., Andersen, O.S.: Curcumin is a modulator of bilayer material properties. *Biochemistry* **46**, 10384–10391 (2007)
- Johannsson, A., Smith, G.A., Metcalfe, J.C.: The effect of bilayer thickness on the activity of (Na⁺ + K⁺)-ATPase. *Biochim. Biophys. Acta* **641**, 416–421 (1981)
- Ketchum, R.R., Hu, W., Cross, T.A.: High-resolution conformation of gramicidin A in a lipid bilayer by solid-state NMR. *Science* **261**, 1457–1460 (1993)
- Khare, D., Oldham, M.L., Orelle, C., Davidson, A.L., Chen, J.: Alternating access in maltose transporter mediated by rigid-body rotations. *Mol. Cell* **33**, 528–536 (2009)
- Khelashvili, G., Mondal, S., Andersen, O.S., Weinstein, H.: Cholesterol modulates the membrane effects and spatial organization of membrane-penetrating ligands for G-protein coupled receptors. *J. Phys. Chem. B* **114**, 12046–12057 (2010)
- Kolb, H.A., Bamberg, E.: Influence of membrane thickness and ion concentration on the properties of the gramicidin a channel. Autocorrelation, spectral power density, relaxation and single-channel studies. *Biochim. Biophys. Acta* **464**(1), 127–141 (1977)

- Kutateladze, T.G.: Translation of the phosphoinositide code by PI effectors. *Nat. Chem. Biol.* **6**, 507–513 (2010)
- Lee, A.G.: How lipids affect the activities of integral membrane proteins. *Biochim. Biophys. Acta* **1666**, 62–87 (2004)
- Lewis, B.A., Engelman, D.M.: Lipid bilayer thickness varies linearly with acyl chain length in fluid phosphatidylcholine vesicles. *J. Mol. Biol.* **166**, 211–217 (1983)
- Lundbæk, J.A.: Regulation of membrane protein function by lipid bilayer elasticity—a single molecule technology to measure the bilayer properties experienced by an embedded protein. *J. Phys. Condens. Matter* **18**, S1305 (2006)
- Lundbæk, J.A.: Lipid bilayer-mediated regulation of ion channel function by amphiphilic drugs. *J. Gen. Physiol.* **131**, 421–429 (2008)
- Lundbæk, J.A., Andersen, O.S.: Lysophospholipids modulate channel function by altering the mechanical properties of lipid bilayers. *J. Gen. Physiol.* **104**, 645–673 (1994)
- Lundbæk, J.A., Andersen, O.S.: Spring constants for channel-induced lipid bilayer deformations. Estimates using gramicidin channels. *Biophys. J.* **76**, 889–895 (1999)
- Lundbæk, J.A., Birn, P., Girshman, J., Hansen, A.J., Andersen, O.S.: Membrane stiffness and channel function. *Biochemistry* **35**, 3825–3830 (1996)
- Lundbæk, J.A., Maer, A.M., Andersen, O.S.: Lipid bilayer electrostatic energy, curvature stress, and assembly of gramicidin channels. *Biochemistry* **36**, 5695–5701 (1997)
- Lundbæk, J.A., Birn, P., Hansen, A.J., Søgaaard, R., Nielsen, C., Girshman, J., Bruno, M.J., Tape, S.E., Egebjerg, J., Greathouse, D.V., Mattice, G.L., Koeppe 2nd, R.E., Andersen, O.S.: Regulation of sodium channel function by bilayer elasticity: the importance of hydrophobic coupling. Effects of micelle-forming amphiphiles and cholesterol. *J. Gen. Physiol.* **123**, 599–621 (2004)
- Lundbæk, J.A., Birn, P., Tape, S.E., Toombes, G.E., Søgaaard, R., Koeppe II, R.E., Gruner, S.M., Hansen, A.J., Andersen, O.S.: Capsaicin regulates voltage-dependent sodium channels by altering lipid bilayer elasticity. *Mol. Pharmacol.* **68**, 680–689 (2005)
- Lundbæk, J.A., Collingwood, S.A., Ingolfsson, H.I., Kapoor, R., Andersen, O.S.: Lipid bilayer regulation of membrane protein function: gramicidin channels as molecular force probes. *J. R. Soc. Interface* **7**, 373–395 (2010a)
- Lundbæk, J.A., Koeppe II, R.E., Andersen, O.S.: Amphiphile regulation of ion channel function by changes in the bilayer spring constant. *Proc. Natl. Acad. Sci. U.S.A.* **107**, 15427–15430 (2010b)
- Ly, H.V., Longo, M.L.: The influence of short-chain alcohols on interfacial tension, mechanical properties, area/molecule, and permeability of fluid lipid bilayers. *Biophys. J.* **87**, 1013–1033 (2004)
- Marsh, D.: Elastic curvature constants of lipid monolayers and bilayers. *Chem. Phys. Lipids* **144**, 146–159 (2006)
- Marsh, D.: Protein modulation of lipids, and vice-versa, in membranes. *Biochim. Biophys. Acta* **1778**, 1545–1575 (2008)
- Miloshevsky, G.V., Jordan, P.C.: Gating gramicidin channels in lipid bilayers: reaction coordinates and the mechanism of dissociation. *Biophys. J.* **86**, 92–104 (2004)
- Moe, P., Blount, P.: Assessment of potential stimuli for mechano-dependent gating of MscL: effects of pressure, tension, and lipid headgroups. *Biochemistry* **44**, 12239–12244 (2005)
- Mouritsen, O.G., Bloom, M.: Mattress model of lipid-protein interactions in membranes. *Biophys. J.* **46**, 141–153 (1984)
- Navarro, J., Toivio-Kinnucan, M., Racker, E.: Effect of lipid composition on the calcium/adenosine 5'-triphosphate coupling ratio of the Ca²⁺ – ATPase of sarcoplasmic reticulum. *Biochemistry* **23**, 130–135 (1984)
- Nielsen, C., Andersen, O.S.: Inclusion-induced bilayer deformations: effects of monolayer equilibrium curvature. *Biophys. J.* **79**, 2583–2604 (2000)
- Nielsen, C., Goulian, M., Andersen, O.S.: Energetics of inclusion-induced bilayer deformations. *Biophys. J.* **74**, 1966–1983 (1998)
- O'Connell, A.M., Koeppe II, R.E., Andersen, O.S.: Kinetics of gramicidin channel formation in lipid bilayers: transmembrane monomer association. *Science* **250**, 1256–1259 (1990)

- Park, J.B., Kim, H.J., Ryu, P.D., Moczydlowski, E.: Effect of phosphatidylserine on unitary conductance and Ba²⁺ block of the BK Ca²⁺ – activated K⁺ channel: re-examination of the surface charge hypothesis. *J. Gen. Physiol.* **121**, 375–398 (2003)
- Partenskii, M.B., Jordan, P.C.: Membrane deformation and the elastic energy of insertion: perturbation of membrane elastic constants due to peptide insertion. *J. Chem. Phys.* **117**, 10768–10776 (2002)
- Perozo, E., Kloda, A., Cortes, D.M., Martinac, B.: Physical principles underlying the transduction of bilayer deformation forces during mechanosensitive channel gating. *Nat. Struct. Biol.* **9**, 696–703 (2002)
- Rand, R.P., Parsegian, V.A.: Hydration, curvature, and bending elasticity of phospholipid monolayers. *Curr. Top. Membr. Transp.* **44**, 167–189 (1997)
- Rawicz, W., Olbrich, K.C., McIntosh, T., Needham, D., Evans, E.: Effect of chain length and unsaturation on elasticity of lipid bilayers. *Biophys. J.* **79**, 328–339 (2000)
- Sackmann, E.: Physical basis of trigger processes and membrane structures. In: Chapman, D. (ed.) *Biological Membranes*, vol. 5, pp. 105–143. Academic, London (1984)
- Seeman, P.: The membrane actions of anesthetics and tranquilizers. *Pharmacol. Rev.* **24**, 583–655 (1972)
- Simon, S.A., Lis, L.J., MacDonald, R.C., Kauffman, J.W.: The noneffect of a large linear hydrocarbon, squalene, on the phosphatidylcholine packing structure. *Biophys. J.* **19**, 83–90 (1977)
- Soubias, O., Niu, S.L., Mitchell, D.C., Gawrisch, K.: Lipid-rhodopsin hydrophobic mismatch alters rhodopsin helical content. *J. Am. Chem. Soc.* **130**, 12465–12471 (2008)
- Suchyna, T.M., Tape, S.E., Koeppe 2nd, R.E., Andersen, O.S., Sachs, F., Gottlieb, P.A.: Bilayer-dependent inhibition of mechanosensitive channels by neuroactive peptide enantiomers. *Nature* **430**, 235–240 (2004)
- Tate, M.W., Eikenberry, E.F., Turner, D.C., Shyamsunder, E., Gruner, S.M.: Nonbilayer phases of membrane lipids. *Chem. Phys. Lipids* **57**, 147–164 (1991)
- Townsley, L.E., Tucker, W.A., Sham, S., Hinton, J.F.: Structures of gramicidins A, B, and C incorporated into sodium dodecyl sulfate micelles. *Biochemistry* **40**, 11676–11686 (2001)
- Toyoshima, C., Nomura, H.: Structural changes in the calcium pump accompanying the dissociation of calcium. *Nature* **418**, 605–611 (2002)
- Toyoshima, C., Nakasako, M., Nomura, H., Ogawa, H.: Crystal structure of the calcium pump of sarcoplasmic reticulum at 2.6 Å resolution. *Nature* **405**, 647–655 (2000)
- Tyrchan, C., Blomberg, N., Engkvist, O., Kogej, T., Muresan, S.: Physicochemical property profiles of marketed drugs, clinical candidates and bioactive compounds. *Bioorg. Med. Chem. Lett.* **19**, 6943–6947 (2009)
- Veatch, W.R., Mathies, R., Eisenberg, M., Stryer, L.: Simultaneous fluorescence and conductance studies of planar bilayer membranes containing a highly active and fluorescent analog of gramicidin A. *J. Mol. Biol.* **99**, 75–92 (1975)
- Wang, W., Black, S.S., Edwards, M.D., Miller, S., Morrison, E.L., Bartlett, W., Dong, C., Naismith, J.H., Booth, I.R.: The structure of an open form of an E. coli mechanosensitive channel at 3.45 Å resolution. *Science* **321**, 1179–1183 (2008)
- Yuan, C., O'Connell, R.J., Feinberg-Zadek, P.L., Johnston, L.J., Treistman, S.N.: Bilayer thickness modulates the conductance of the BK channel in model membranes. *Biophys. J.* **86**, 3620–3633 (2004)
- Zhelev, D.V.: Material property characteristics for lipid bilayers containing lysolipid. *Biophys. J.* **75**, 321–330 (1998)

Chapter 10

Large Scale Biomimetic Membrane Arrays

Mark Perry, Christian Rein, and Jörg Vogel

Abstract The construction of large scale biomimetic membrane arrays is a multi-step process. Here we give an overview of the key steps involved in this process. Depending on the particular application of the array, a wide range of different membrane components is available. Typically, the biomimetic membrane precursor consists of chosen membrane components dissolved in an organic solvent. To create a membrane, the precursor solution is deposited onto a suitable scaffold separating two aqueous compartments. Depending on the preparation method, bilayer membrane regions self assemble from the precursor solution. Here, membrane stability and ease of preparation depends on the choice of material and design of the array scaffold. Another influence on preparation, stability and membrane dynamics stems from the design of the scaffold housing. Once created, membrane integrity can be monitored over time through changes in its electrical properties. Finally, membrane longevity can be increased by including a support structure close to the bilayer regions and physically coupling biomimetic membrane components in the bilayer to the support.

10.1 Applications of Large Scale Biomimetic Membrane Arrays

Biomimetic membrane systems have traditionally been used extensively in the field of transmembrane protein research (Janshoff and Steinem 2006). By reconstituting transmembrane proteins into an artificial membrane system where the cis and trans

M. Perry (✉) • C. Rein • J. Vogel
Aquaporin A/S, Ole Maaløes Vej 3, DK-2200 Copenhagen, Denmark
e-mail: mpe@aquaporin.dk; cr@aquaporin.dk; jvo@aquaporin.dk

sides are addressable for electrodes and water soluble ligands, researchers are able to probe the protein's electrical gating properties, ion transport potential and interaction with ligands. In this kind of experimental set-up, only small biomimetic membrane areas are needed since the goal is to measure single protein activity. In fact, using small membrane areas is often preferred due to their high signal to noise ratio during electrophysiological measurements and the simple fact that it is easier to isolate single proteins in a small membrane area.

In other – and more recent – applications such as biosensing devices, drug screening platforms and biomembranes containing selective peptides or proteins (such as aquaporins) for filtration and separation systems, the ability to cost-effectively upscale the biomimetic membrane area is a key factor when considering the feasibility of commercializing said systems. Another – and equally – important factor when it comes to constructing biomimetic membrane systems for “real life” applications is the ability to increase membrane stability both over time and towards external destabilizers such as mechanical agitation, lipases, detergents etc.

In the following sections we describe the current state-of-the-art knowledge we have accumulated with regards to up-scaling and increasing the stability of biomimetic membrane arrays.

10.2 Biomimetic Membrane Components

Most applications of large scale biomimetic arrays require high membrane stability as well as membrane compatibility to peptides and transmembrane proteins. Both membrane stability and protein compatibility put demands on the choice of membrane components. In this chapter we give examples of membrane components that have traditionally been used to establish biomimetic membrane systems in addition to more recent cutting edge components. We also present examples of components selected for specific applications in our lab. Finally we bring up the cost issue of membrane components since this is an important aspect when considering commercialization of biomimetic arrays.

In nature, cellular membranes are a complex mix of amphiphilic molecules (such as lipids), transmembrane proteins and other membrane bound components (Alberts et al. 2002) which organize themselves in a bilayer structure in which a double layer of amphiphilic molecules arrange themselves with their polar moieties facing outwards and their hydrophobic moieties buried inside the double layer (Alberts et al. 2002). The highly unfavorable packing of water molecules around non-polar substances is the major driving force for the packing of amphiphilic molecules into a bilayer. Besides this so called hydrophobic force, the van der Waals forces, forces due to hydrogen bonding and Coulomb interactions in the case of charged molecules, also stabilize the overall structure (Gennis 1989).

Since membranes in nature exhibit mechanical and chemical stability to a wide range of different external stresses, they have been a primary source of inspiration for artificial biomimetic membrane systems. Therefore lipids – both natural and

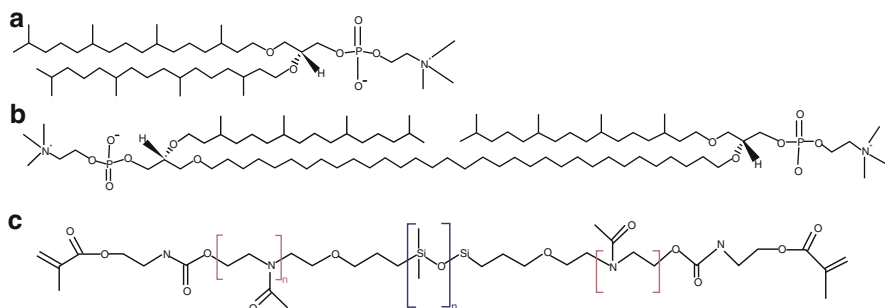


Fig. 10.1 A selection of biomimetic membrane components used for making membrane arrays. (a) Ether phospholipid 1,2-diphytanoyl-sn-glycero-3-phosphocholine (DPhPC). (b) Bolalipid 2,2'-di-O-(3,7,11,15-tetramethylhexadecyl)-3,3'- di-O-(1'',32''-ditriacontanyl)-bis-(rac-glycerol)-1,1'-diphosphocholine (C22PhytBAS). (c) Triblock copolymer poly(2-methyloxazoline)-block-poly(dimethylsiloxane)-block-poly(2-methyloxazoline) (PMOXAPDMS-PMOXA) (Figure obtained from Nielsen 2009)

synthetic – are extensively used as membrane components and will be the main focus of this chapter. However, polymer building blocks such as tri-block co-polymers have also been used as membrane building blocks and deserve mentioning.

Not all lipid molecules have a propensity towards forming bilayer structures when hydrated. Depending on the molecular shape and concentration of the molecule, lipids form bilayers, micelles, hexagonal and inverted hexagonal structures. Bilayer forming lipids have a cylindrical shape whereas lipids forming micelles or hexagonal phases have inverted cone and cone shapes respectively (Gennis 1989).

1,2-diphytanoyl-sn-glycero-3-phosphocholine (Fig. 10.1) (DPhPC in short) originates from plants (Han et al. 2007) and has been widely used for single aperture biomimetic membrane systems (Pohl et al. 1997; Han et al. 2007) and in the establishment of large scale biomimetic membrane arrays supported on hydrophobic materials, such as ethylene tetrafluoroethylene (ETFE) (Vogel et al. 2009). DPhPC is a standard lipid of choice when it comes to establishing biomimetic membranes, partly because planar lipid structures of DPhPC have been studied for some time (Benz and Janko 1976) and its behavior in several organic solvents is well described (McIntosh et al. 1980). In addition, the complete saturation of the chains and the ether bond significantly improves chemical stability of the resulting membrane. Finally, several studies have shown that transmembrane proteins fold correctly when reconstituted into biomimetic membranes consisting of DPhPC (Hansen et al. 2009a).

Block-copolymers have recently been used as membrane building blocks (Mecke et al. 2006). By using triblock copolymers such as polymethyloxazoline-polydimethylsiloxane-poly(2-methyloxazoline) (PMOXA-PDMS-PMOXA) it is possible to incorporate ion channels in large-scale planar membranes (Ho et al. 2004; Meier et al. 2000) and water channels in polymersomes (Kumar et al. 2007). The main advantages of using block-copolymers are their chemical stability and the possibility of designing them with a thicker hydrophobic core, which can enhance membrane stability (McIntosh et al. 1980).

Bolalipids (Cornell et al. 1997; Thompson et al. 1992) are found in the membranes of extremophiles such as Archaeobacteria living in hot spring (De Rosa et al. 1986). The membrane components of these organisms are characterized by a high degree of chemical and enzymatic stability (Benvegna et al. 2004) necessary for living in a harsh environment. The membrane stability inferred by bolalipids is due to their bipolar structure that can make them span across both leaflets in a lipid bilayer, the complete saturation of the chains and the ether bonds (Benvegna et al. 2004). These properties make them an obvious choice for constructing stable membrane systems (Gliozzi et al. 1982) while still allowing the insertion and function of proteins in the membrane (Febo-Ayala et al. 2006).

Custom designed polymerisable lipids (Daly et al. 2006; Shenoy et al. 2005) in which, e.g., acrylate, diene or diyne reactive moieties in the acyl chain (or head-group) region can be used for cross-linking lipids thus creating stable biomimetic structures (Nielsen 2009). The cross-linking is facilitated either using UV-light or chemical components, depending on the placement and reactivity of the cross-linkable moieties. In our lab we have worked mainly with 1,2 diphytanoyl-*sn*-glycero-3-phosphoethanolamine-*N*-acrylate (in short DPhPE-acrylate). This custom made lipid molecule has an acrylate group coupled to the head group region, which enables us to crosslink molecules by use of UV light or chemical initiators (for example ammonium persulfate / N, N, N', N'-tetramethylethylenediamine). We chose to work with a head group polymerizable lipid over an acyl chain polymerizable lipid since the polymerizable group is more accessible to chemical initiators in the former. This gave us improved control of the degree of polymerization. In addition, upon polymerization, head group polymerizable lipids retain their mobility in the hydrophobic tail regions where the bulk of transmembrane proteins are situated.

Vesicle fusion of proteoliposomes is a method that has been used in several studies to load biomimetic membrane systems with transmembrane proteins (Nielsen 2009; Woodbury and Hall 1988). Studies have described how the proteoliposome membrane composition can be tweaked to enhance the fusiogenic properties (Haque et al. 2001). In our lab we have enhanced vesicle fusion through electrostatic interactions (Lei and MacDonald 2003) by adding a positively charged lipid species (1,2-dioleoyl-3-trimethylammonium-propane, in short DOTAP) to the biomimetic membrane composition and a negatively charged lipid species (1-palmitoyl-2-oleoyl-*sn*-glycero-3-phospho-L-serine, in short POPS) to the proteoliposomes.

When it comes to up-scaling biomimetic membrane arrays, the price of lipid components needs to be taken into consideration. The price of lipid components can vary greatly from around one US dollar/g for bulk lipid extracts from soybean up to 5,000\$ per gram for custom made lipids such DPhPE-acrylate. When the price varies this much it becomes necessary to judge if the improvement to the membrane properties is worth the cost of each of the components used. For example, 1,2-dioleoyl-*sn*-glycero-3-phosphocholine (DOPC), an ester lipid commonly used to establish membranes, has the disadvantage of being prone to hydrolysis and oxidation, but at 1/8 the price of DPhPC it is more interesting to use for up-scaling purposes. When it comes to selecting the right components for making large scale membrane arrays it is often a matter of optimizing a problem with more parameters than is traditionally described in literature.

10.3 Biomimetic Membrane Scaffolds, Chambers and Formation Techniques

Having all the membrane components in place is only the first step to form large scale biomimetic membrane arrays. To successfully form a biomimetic membrane it is equally important to employ a suitable membrane scaffold, membrane formation chamber and membrane formation technique. Here we present an overview of the most recent developments in scaffold and chamber design as well as commonly used membrane formation techniques.

10.3.1 Scaffold Designs

Many biomimetic membrane applications, such as filtration devices, require a stabilizing support structure. Its main purpose is to stabilize the lipid bilayer or block-copolymer-based biomimetic matrix against hydraulic pressure driven forces. The geometry of such a micro-porous structure plays a key role in establishing a long-lasting and stable biomimetic membrane. Preferably, the surface of the entire support structure should be smooth and hydrophobic. The apertures themselves need to have a smooth, round edge to facilitate the formation of a biomimetic membrane and to stabilize the contact between the membrane components and the aperture rim (White 1972). Furthermore, for the application in water purification devices based on aquaporin proteins embedded in a lipid bilayer, it is important to densely pack the apertures in arrays to ensure a high water flux across the membrane.

The production of such support membranes can be carried out using the full spectrum of known micro technologies in combination with polymers and/or silicon. The simplest of techniques is to use a hot needle in a plastic cup (Wonderlin et al. 1990) or by micro-drilling a small hole into a polymeric material using. However, the quality of these apertures is low. They suffer from burrs, rough edges and an uneven overall shape (Fig. 10.2).

Other techniques include photolithography and etching to produce submicron apertures in silicon (Simon et al. 2007) or silicon nitride (Rijn et al. 1999), spark erosion where an electrical spark is used to burn a hole in a polymer membrane as well as the multitude of techniques within the field of polymer micro-technology. For example, Mayer et al. (2003) report of the fabrication of arrays by the casting of thin Teflon films onto a PDMS mould. With this technique precisely placed apertures with a wide controlled range of diameters (2–800 μm) could be fabricated. However, spark erosion as well as the approach by Mayer et al. suffer from a limited overall perforation area and long production time (4–24 h). In our lab we used laser ablation in order to achieve drastically decreased production times and easily reproduced results.

In laser ablation, a laser beam is directed at the surface of the substrate where the energy of the beam is absorbed and transformed. Depending on the type of laser used, different processes take place in the material. An Excimer (Excited Dimer)

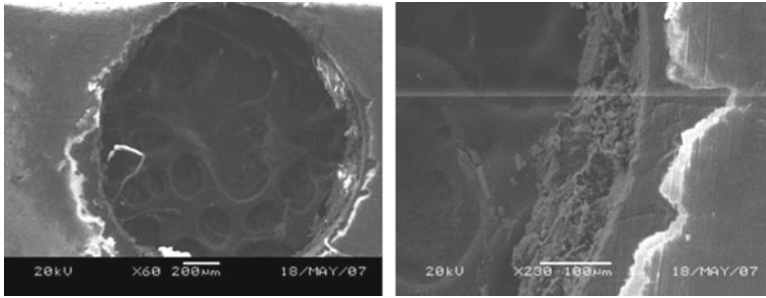


Fig. 10.2 Micro drilled hole with a diameter of 1 mm; the close up of the edge (*right*) shows that the drilling results in rough edges with sharp and uneven. The porous structure that can be seen underneath is carbon tape that secures the foil on the stage and ensures electrical contact. Pictures were taken using a Jeol JSM 5500 LV SEM from GNNettest

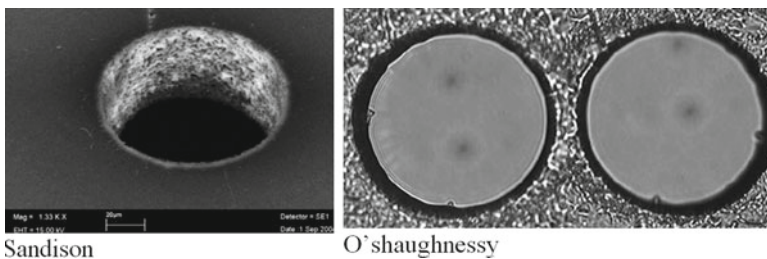


Fig. 10.3 Excimer laser ablated 100 μm apertures in PMMA by Sandison et al. (2005) (*left*) and in PC by O'Shaughnessy et al. (2007). Pictures were acquired using a SEM (*right*)

laser with its wave length of 196 nm (ArF) or 248 nm (KrF) decomposes the material through a complex mix of chemical and thermal processes. Basically, the chemical bonds between the molecules are broken by photon absorption as well as by heat from vibrating molecules. In contrast, a CO_2 laser works with light in the infrared range and vaporizes and melts the material within its focal spot. The aperture characteristics, range of applicable material and production time depend on the choice of laser. Sandison (2005) fabricated apertures in PTFE, PMMA, FET and PET foils where the best results could be achieved for PMMA (Fig. 10.3 left). Also O'Shaughnessy et al. (2007) report of Excimer laser ablated apertures in PC. Here, the production of one aperture with a diameter of about 100 μm took about 1930s. The relatively long production time is caused by the layer-by-layer ablation typical for the Excimer laser. In contrast, a CO_2 laser can generate an aperture with a single shot. Vogel et al. (2009) report of a CO_2 laser fabricated array of apertures in ethylene tetrafluoroethylene (ETFE). It consists of 64 apertures with a diameter of 300 μm and a centre-to-centre distance of 400 μm . This array could be fabricated in only 0.8 s. The typical characteristics of apertures ablated via CO_2 laser are smooth and round edges, bulges that are formed around the aperture rims and diamond-shaped pockets formed between adjacent apertures (Figs. 10.4 and 10.5). These characteristics

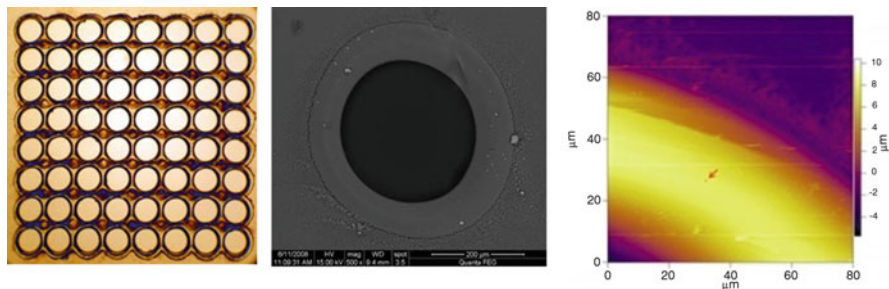


Fig. 10.4 ETFE partition with an 8 × 8 array of apertures with a diameter of 300 μm (A), a SEM picture of a single aperture in ETFE and a close up AFM picture of the smooth bulge surrounding the aperture – here the red arrow indicates a sample area where a surface roughness of 3.5 nm was measured

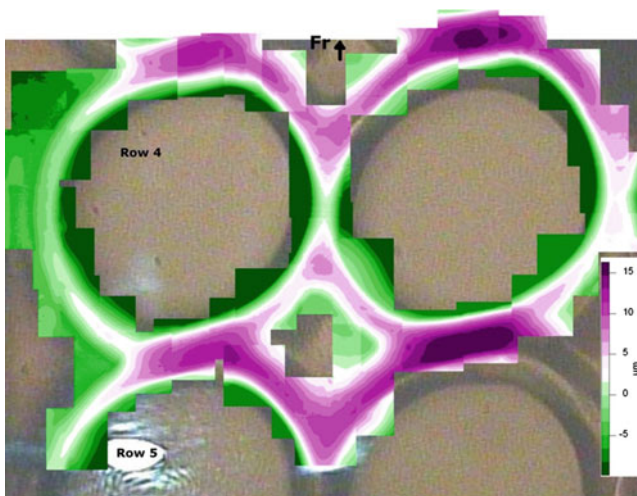


Fig. 10.5 Optical image of the front side (side facing the CO₂ laser) of a CO₂ laser ablated ETFE rectangular array overlaid with 37 AFM topological maps. The mosaic image clearly shows the presence of a diamond-shaped pocket between the apertures

are generated by melted material that is ejected from the focal spot of the laser and redeposited around the edge of the generated hole. The diameter of the apertures is mainly defined by the lens that is used to focus the beam but can also be varied by adjusting the different parameters of the laser like Spot Lase Time, power and the Off Vector Delay. Due to the Gaussian shape of the beam in a CO₂ laser these parameters can be used to make structures that are smaller than the initial focal spot diameter of the laser lens. The Spot Lase Time defines the time the beam is focused on one spot. Together with the chosen laser power this setting defines the amount off heat that is introduced in one given spot. The Off Vector Delay describes the time when the laser is switched off between two production steps. This gives the mirrors time to settle

over the starting point of a new structure before starting a new ablation process. When this delay is too short it can cause the formation of tails (ablation starts before the mirrors are adjusted) and if too long the whole production process is slowed down unnecessarily.

10.3.2 Chamber Designs

Typically, biomimetic membranes in hydrophobic scaffolds are formed in chambers where the scaffold separates two aqueous compartments (Tien and Ottova-Leitmannova 2003). Essentially, BLMs can be established via two basic techniques; the Mueller-Rudin painting technique (Mueller and Rudin 1969) and the Montal-Mueller folding technique (Montal and Mueller 1972). The technique to be applied depends on the chamber design. A typical test-setup consists of two reservoirs/chambers (*cis* and *trans*) that contain buffer solution, a support membrane with one or multiple apertures and two electrodes that are used for electrical characterization.

Standard chamber

The simplest chamber design consists of two Teflon parts which can be clamped together via screws. When assembled with the support scaffold placed in the interface between the two Teflon parts, an open two chamber system is created where electrodes can be inserted into the aqueous solutions from above. Due to its simplicity, this setup is cheap to fabricate. However, we have observed that silicone grease used for sealing tends to dissolve due to the organic solvents (i.e. decane) used in the biomimetic membrane matrix. This results in both loss of sealing over time (usually within a couple of hours) as well as partial coverage of scaffold apertures with grease which greatly reduces both the quality (i.e. electrical tightness) and the lifetime of the biomimetic membranes.

APM-chamber (Auto-Painted-Membrane)

Recently, Hansen et al. (2009a) developed an improved chamber design for biomimetic membrane formation (Fig. 10.6) in laser ablated ETFE partitions (see Sect. 10.3.1). The main advantages of this design are the reduced amount of silicone grease used for sealing and the possibility of semi-automating membrane formation resulting in a higher degree of reproducibility between experiments. When properly assembled it is possible to maintain a low leak current for several days and even weeks between the two chamber compartments.

The complete chamber setup consists of a main Teflon chamber with two axi-symmetrically drilled holes of different diameter, a cylindrical Teflon tube, two circular Teflon inter spacers where one has a slit, six Viton (DuPont Fluopolymers, US) O-ring seals, two cover slip glasses where one is cut and a brass screw to tighten the bilayer chamber (Fig. 10.6a). Both chamber compartments have identical volumes. Porous regenerated cellulose is used to further stabilize the biomimetic

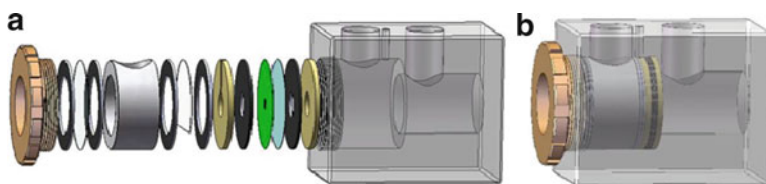


Fig. 10.6 Biomimetic membrane chamber design and assembly. **(a)** The assembly of the main Teflon chamber. The component order of the assembly into the main Teflon chamber (grey – Vink A/S, DK) is from right to left: a Teflon spacer (tawny – Vink A/S, DK), a Viton O-ring (black – DuPont, US), a circular cellulose sheet (light blue – Alfa Laval, DK), an ETFE LZ200 partition (green – DuPont, US), a Viton O-ring (black), a Teflon spacer with a slit (tawny), a Viton O-ring (black), a cut glass cover slip (transparent – VWR-Bie & Berntsen, DK) and another Viton O-ring (black). **(b)** The biomimetic membrane chamber fully assembled

membrane from mechanical agitation. The complete assembled biomimetic membrane chamber can be seen in Fig. 10.6b. Electrodes for membrane recording are inserted through the top large diameter inlets. The small diameter inlet is used to inject biomimetic matrix solution. The actual membrane formation procedure will be explained further in 10.3.3.

Horizontal chamber

The two previously shown chambers both form a biomimetic membrane over a vertically placed aperture. In experiments where visual inspection of membrane arrays is necessary (i.e. fluorescence based experiments) it is necessary to place the arrays horizontally. This also allows for physical access to the actual lipid membrane formation area, which is difficult to obtain with the simple membrane formation chamber and close to impossible with the APM chamber. Therefore, Hansen et al. (2009b) developed another chamber design where the partition is placed horizontally.

The entire chamber design with all its components can be seen in Fig. 10.7. It is made from commercially available culture dishes, where the bigger dish constitutes the lower and the smaller dish the upper compartment. An ETFE partition is glued to the upper dish. This gluing functions as a seal from upper to lower chamber. The custom made Viton ring is then used as a spacer so that two separate chambers are created. The slit in the Viton ring functions as the connection between the area underneath the array and the lower reservoir. A reusable, homemade metal sample holder is used to clamp the upper dish to the lower and ensure sealing and proper alignment. The chamber made to fit onto a microscope stage which makes it possible to combine electrical measurements with fluorescence microscopy.

Horizontal chamber with removable membrane unit

All the previously mentioned chambers had one drawback in common – the partition where the biomimetic membrane is formed is fixed within the chamber. If however, the biomimetic membrane is to be taken out and used for other experiments, then another chamber design has to be considered. The further use can for example

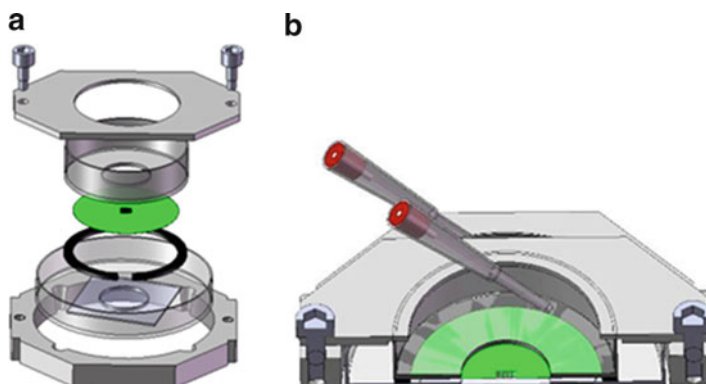


Fig. 10.7 The horizontal lipid membrane formation chamber (a) The chamber is assembled by first inserting the big dish into the *bottom* holder, placing the Viton ring in its *centre*, placing the to the smaller dish with the glued partition on top and finally clamping the system with the upper metal plate and screws; (b) shows a cross section of the assembled chamber with inserted electrodes

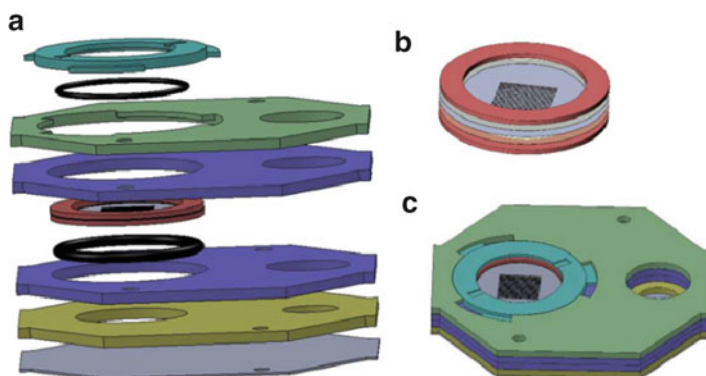


Fig. 10.8 Biomimetic membrane formation chamber in an exploded view (a), and as a complete assembly (c) with clamp (blue) and PaR (b)

include the incorporation of aquaporin proteins and the application of that setup as a water filtration device. Typically, flow through membranes are tested in commercially available flow cells. Here, the sample is placed onto a sample holder and clamped into the cell. Afterwards, the reservoir is filled with water, pressure is applied and thus the flow through the sample is tested.

To create a biomimetic membrane directly in such flow cells is considered to be problematic. This means that the bilayer has to be created in a special partition that can be taken out of the membrane formation chamber, and placed into the flow cell. To make the device cheap and disposable, PMMA rings were fitted via double sided adhesive tape onto a perforated partition (Fig. 10.8b). This assembly of partition and ring (PaR) can then be clamped into a custom made chamber and the bilayer created.

Afterwards, the PaR with bilayer can be removed from the chamber and used for further testing.

This bilayer formation chamber needs to have a *trans* and a *cis* chamber which both should be accessible by electrodes. Furthermore, it needs to make a tight seal between PaR and chamber.

The developed chamber consists of CO₂ laser structured PMMA parts that are bonded via double sided adhesive and O-rings for sealing (Fig. 10.8a, c). The clamp mechanism consists of a rotatable lid with three noses that fit underneath three counterparts that are situated at the top of the chamber and thus clamp the PaR. The lower chamber is accessible via a channel in the bottom chamber.

10.3.3 Establishing Large Scale Biomimetic Membrane

There are essentially two methods available for establishing large scale biomimetic arrays. The first method is based on “painting” the matrix across apertures submerged in aqueous solution (Mueller et al. 1962) while the second method is based on folding two monolayers of amphiphiles at an air-water interphase across the apertures of a scaffold lowered into the aqueous phase (Montal and Mueller 1972). This technique is similar to the deposition method used for making Langmuir-Blodgett (LB) films (Cruz and Perez-Gil 2007).

When using either method it is important to ensure good coupling/adhesion at the interface between the biomimetic membrane and its surrounding scaffold. One way to improve this is by pre-painting the scaffold surface. The pre-painting procedure typically involves drying down a layer of biomimetic matrix solution around the surface of the apertures in the scaffold (Hansen et al. 2009a; White et al. 1976). The presence of a pre-painting layer both aids in the formation of biomimetic membranes across apertures in a hydrophobic scaffold as well as increases the lifetime of said membranes.

Establishing biomimetic membranes in scaffolds with multiple arrays

The traditional painting and folding methods are primarily used for creating biomimetic membranes in single aperture scaffolds (Mayer et al. 2003; O’Shaughnessy et al. 2007). For up-scaling purposes, several developments of the painting method have recently been developed in our group (Hansen et al. 2009a, b). The automated painted membrane (APM) method (Fig. 10.9) was invented in parallel with the chamber design shown in Fig. 10.6. The APM method is based on the principle of raising a layer of matrix, floating on top of an aqueous electrolyte solution, across a vertical scaffold with an aperture array. A cut piece of glass will keep the amount of matrix to a minimum and separate from the rest of the solution while the membrane formation process takes place. We have routinely used the APM method to create membranes in arrays ranging from 64 to 648 0.3 mm diameter apertures.

As mentioned in Sect. 10.3.2 visual membrane inspection requires a horizontal configuration of the scaffold (Fig. 10.8). In this case membranes are created by

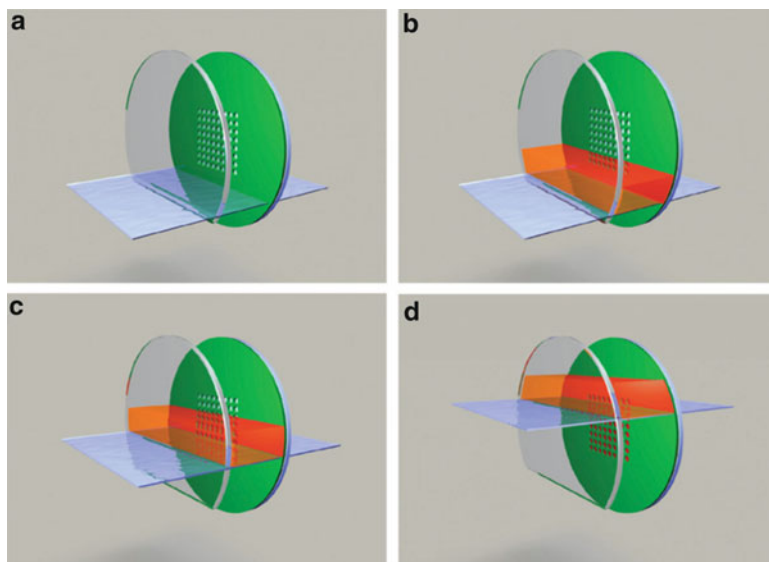


Fig. 10.9 Principle of the automation technique for the establishment of multiple bilayers in the array. The aqueous electrolyte solution is filled up to the cut glass cover slip (a) and a small amount of the matrix is added to the space between the glass and the scaffold with apertures (b). The aqueous electrolyte solution is then slowly applied to the cis chamber thereby raising the bilayer-forming solution across the multiple aperture partition to form an array of lipid bilayers (c–d) (Hansen et al. 2009a)

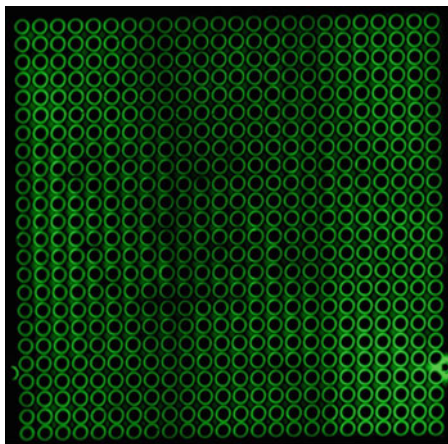
distributing 2–4 μl (depending on experimental parameters) of matrix solution evenly on the submerged array with a pipette tip or inoculation needle. Membrane creation in individual apertures is monitored both optically and electrically. In case of membrane breakage in individual apertures, repairs can be made by simply moving excess matrix present around the array across the aperture in question. Alternatively, additional matrix solution can be added until a stable membrane array is formed (Fig. 10.10).

General observations when establishing biomimetic membrane arrays

We have found that increasing the size of the membrane array enhances the stability of the entire array. An effect thought to be contributed by the reduced ratio of membranes that are at the edge of the array, where breakages often appear. The observed increase in stability could be caused by a synergetic effect when matrix solution around stable membranes inside the array can diffuse outwards to help stressed membranes at the edge of the array.

Adding to the possibility of matrix diffusion is the presence of diamond shaped pockets between apertures in rectangular distributed membrane arrays prepared in ETFE by CO_2 laser ablation (Fig. 10.5). The pockets function as reservoirs of surplus matrix both helping towards stabilizing (by allowing matrix material to

Fig. 10.10 24×27 hexagonal bilayer arrays formed across apertures (\varnothing : 0.3 mm) in ETFE-scaffold (Hansen et al. 2009b)



diffuse into arrays) and thinning (by allowing excess matrix material to diffuse out of arrays). Figure 10.5 also illustrates the low barrier between each aperture in a row, which promotes a more free diffusion of matrix among the apertures in each row.

The use of a horizontal setup for membrane creation has enabled us to visualize the process of biomimetic membrane formation inside individual apertures by use of fluorescently labeled matrix components. Immediately after matrix deposition, apertures are filled by a thick matrix film indicated by a high intensity fluorescence signal throughout the aperture. In some cases, matrix diffuses automatically out of apertures leading to the formation of a bilayer area in the center of the aperture which gradually expands towards the edge. The surplus matrix builds up a reservoir either between the apertures or in a toroidal shape along the edge of the aperture (White 1972). An example of the latter is shown in Fig. 10.10 and can be seen as green rings in the array. Here, the matrix, containing a small concentration of fluorescent dye, is most abundant.

While this thinning process often takes place automatically, in other cases it is necessary to aid the process by brushing over the array in order to reduce the amount of matrix in apertures to a point where thinning takes place.

10.4 Monitoring Electrical Characteristics of Membrane Arrays

Biomimetic membrane systems are designed to resemble naturally occurring biomembranes such as the cell wall. Biomembranes are typically 4–5 nm thick bilayer sheets of lipid molecules orientated with their hydrophobic tails towards the centre of the membrane and their hydrophilic head groups towards the aqueous

environments on either side of membrane. Therefore, biomimetic membranes consist of amphiphilic molecules having a propensity towards forming similar bilayer structures when hydrated.

When working with large scale biomimetic membrane systems it is necessary to be able to quantify the active (i.e. bilayer) area and the overall membrane quality. First of all, a high ionic seal of the membrane is needed to measure ion channel activity. Secondly, the bilayer area is a dynamic quantity. Upon sealing of the membrane array with matrix solution, the total bilayer areas is usually small compared to the total aperture area due to the fact that the matrix components do not immediately self assemble into bilayer regions. In later stages, the bilayer area increases either spontaneously or due to manual thinning, but it usually ends up at a fraction of the actual aperture area (Perry et al. 2009).

Since the bilayer structure consists of two sheets capable of accumulating charge (the head-group regions) separated by a high resistance layer (the hydrophobic tail regions) it behaves in a similar fashion to a parallel plate capacitor. The equivalent electrical circuit for a biomimetic membrane patch can thus be approximated by an electrolyte resistance in series with a parallel combination of the membrane capacitance and the membrane resistance (Perry et al. 2009). Hence the measured capacitance of the system is proportional to the membrane area and the membrane quality (high quality=low ionic leak=high resistance) can be quantified by the ionic resistance.

Electrical measurements are therefore an obvious choice of characterization method for biomimetic membrane systems. Impedance spectroscopy can be used if a detailed analysis of the capacitive contributions in a membrane system is needed (Perry et al. 2009). However, for simple biomimetic systems, such as membrane arrays, classical voltage clamp techniques, where the overall membrane capacitance and resistance is measured, are sufficient. The overall capacitance of the membrane system is a good measure of the area of active bilayer region (Perry et al. 2009). The reason being, that the capacitance of a parallel plate capacitor is inversely proportional to the distance between the capacitor plates and as such the bulk capacitance contribution comes from the thinnest (i.e. bilayer) parts of the membrane system.

From a practical point of view, capacitance values for a specific biomimetic system are converted to areas by using specific capacitance values of similar biomimetic systems determined in previous studies. Specific capacitance values for a wide variety of systems have been determined to lie in the range 0.4–1 $\mu\text{F}/\text{cm}^2$ (White 1970, 1978) depending primarily on the amount and type of solvent present in the hydrophobic core of the membranes. If specific capacitance data has not been determined for the biomimetic system in question, the bilayer area can be determined microscopically by observing the black region formed in reflected light in the areas where the matrix solution thins to a bilayers (Tien and Dawidowicz 1966; White 1970). By performing simultaneous measurements of membrane capacitance, the specific capacitance of the system in question can be determined for future reference.

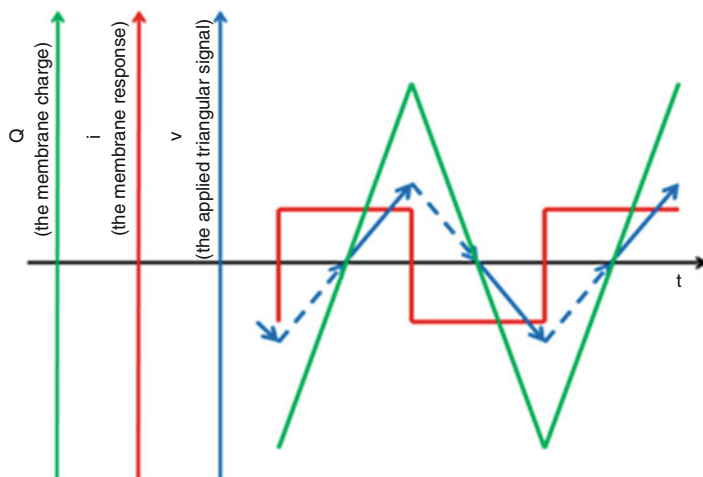


Fig. 10.11 Theoretical relationships between applied triangular input signal, the resulting membrane current response and the membrane charge. The membranes can be regarded as parallel plate capacitors that continuously cycle between charging (*full blue arrows*) and discharging (*dotted blue arrows*). The charge $Q = C \cdot V$, where C is the membrane capacitance and V is the applied voltage across the capacitor. From this relationship we can calculate the circuit current $I = dq/dt = c \cdot dV/dt$. So whenever dV/dt changes sign the capacitive current changes direction. In the case of a triangular shaped input signal, dV/dt is constant, and as a result the charging and discharging currents are constant in between the direction changes. This gives rise to the *square shaped* membrane response signal shown above

10.4.1 Determining Overall Membrane Capacitance and Resistance

In order to have a reliable and fast way of determining membrane capacitance values, triangular shaped voltage signals can be applied to the membrane systems in order to determine their capacitance. The membrane response to this signal is rectangular for low conductance (tightly sealed) membranes, and the rectangular wave current response is proportional to the value of bilayer capacitance (Fig. 10.11). In our work we routinely applied 50 Hz triangular (10 mVpp) voltage clamp waveforms for capacitance measurements. The membrane capacitance C is calculated from the peak-to-peak amplitude I of the square-shaped current response signal through: $I = C \cdot dV/dt$, where dV/dt is the constant slope of the applied triangular shaped voltage signal.

The overall membrane resistance can be determined by applying rectangular shaped voltage signals. In our work we routinely applied 50 Hz rectangular (10 mVpp) voltage clamp waveforms for resistance measurements (Perry et al. 2009). The membrane response will consist of short-lived transients occurring when the input signal changes sign, followed by periods of steady state (Fig. 10.12).

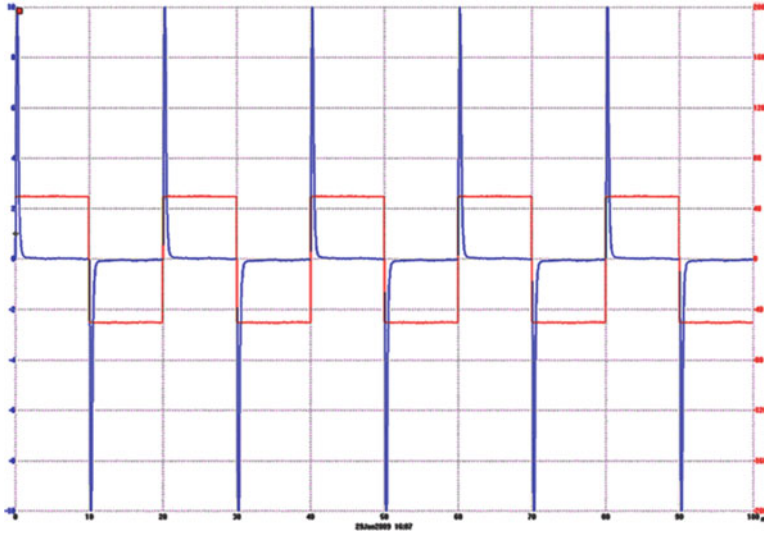


Fig. 10.12 Screenshot of a typical membrane resistance measurement. A PicoScope combined analog–digital converter and oscilloscope (Pico Technology Ltd., United Kingdom) was used for data recording

The current I across the membrane in response to the applied signal is calculated from the difference in amplitude of the steady-state values of two successive transients (a positive transient followed by a negative transient or vice versa). An ohmic relationship is assumed between the input voltage signal (U) and the membrane current (I); the membrane resistance $R = U/I$.

Care needs to be taken when interpreting overall membrane system resistance measurements of large scale biomimetic membrane systems. If background leaks exist between the two electrolyte compartments in the chamber housing, these will typically be arranged in parallel with the actual membrane resistance of the system. The typical specific resistance of defect-free biomimetic membrane patches has been previously determined to around $10 \text{ M}\Omega\text{-cm}^2$ (Bielawski et al. 1966), which depending on the size of the membrane patch typically results in the actual membrane resistance being several orders of magnitude larger than the background leak resistance. Consequently the overall membrane system resistance will often be very close to the background leak resistance and thus not reflect the actual membrane resistance of the biomimetic membrane patch. In our chamber housings, the background leak resistance could not be increased to more than $20 \text{ M}\Omega$ and usually took on values between 4 and $10 \text{ M}\Omega$. As a result, resistance measurements of the overall membrane system could not be used as a quantitative tool for probing membrane area. Instead we used these measurements as a quality check of the biomimetic membrane patch, since a leaky patch would decrease the overall resistance of the system to below $4 \text{ M}\Omega$. It is important to point out here that a 4 – $20 \text{ M}\Omega$ seal is still sufficiently large to measure single ion channel activity (Hansen et al. 2009b).

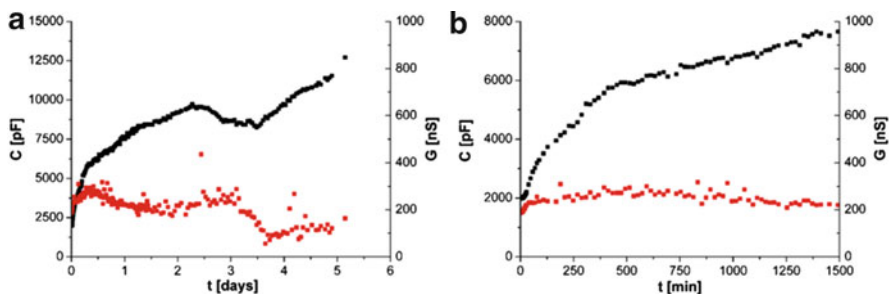


Fig. 10.13 Experimental capacitance and conductance values derived from a long-lived biomimetic membrane. **(a)** Long term recording of capacitance (*black squares* primary *y*-axis) and conductance values (*red squares* secondary *y*-axis) for a biomimetic membrane. **(b)** Zoom on the first 24 h of recording. Membrane capacitance and conductance values were recorded every 2 min for the first 30 min after membrane creation, every 10 min for the next 60 min and every 20 min for the remainder of the experiment

10.4.2 Monitoring Time-Development of Biomimetic Membranes

When dealing with large scale biomimetic membrane arrays it is essential to be able to monitor membrane performance over extended periods of time – from hours to days and even in some cases weeks. In these scenarios, manual recording and analysis of membrane performance simply is not feasible. Recently, we developed a custom designed software solution, capable of automated data acquisition, analysis and storage in a database (Perry et al. 2009). Figure 10.13 shows a routine example of an experiment where membrane characteristics are recorded over time.

10.5 Increasing Stability of Biomimetic Membrane Arrays

Increasing the stability of large scale biomimetic membrane arrays is one of the major challenges in filtration and separation applications, where long term use of the systems under potentially harsh operating conditions is a key factor in reducing the operational cost. Similar considerations apply for biosensing and drug screening applications. Traditionally, biomimetic membrane arrays to be used for the aforementioned applications have been freestanding for free access to either side of the membranes (Mueller et al. 1962). This complicates the task of stabilization compared to supported biomimetic membrane systems, where the matrix components can be physically coupled to the underlying support (Janshoff and Steinem 2006). In our lab we work with unit cells where the 5 nm thick fluid membrane system spans a 300 μm aperture. If these dimensions are scaled up, the challenge of stabilizing a freestanding biomimetic membrane system is intimidating. Imagine being given the job of making sure a 1 m thick and almost 3,000 km^2 free-standing sheet spanning a 60 km wide canyon does not collapse over an extended period of time

under operating conditions such as an applied hydrostatic pressure or mechanical agitation. In our group we have focused mainly on the following three strategies for increasing stability:

- Coating of the membrane scaffolds through plasma treatment to improve the affinity between the scaffold surface and the matrix components.
- Integrating a porous hydrophilic support into the apertures of the membrane scaffolds to stabilize the membranes by dampening membrane vibrations caused by flow of electrolyte solution close to the freestanding membrane.
- Building a cushion layer of poly-electrolytes on top of the porous hydrophilic support and physically coupling selected matrix components to the cushion. Ultimately this construction should resemble the cytoskeleton seen in nature to stabilize membrane systems (Gratzer 1981).

In the following sections we describe our current state of art within these strategies.

10.5.1 Plasma Treatment of Membrane Scaffolds

In Sect. 10.3.3 the importance of prepainting aperture arrays for the formation of large scale biomimetic arrays was briefly touched. A prepainted surface presents the matrix with a familiar surface chemistry where the components can easily attach to. Unfortunately, the application of a prepaint layer on the scaffold is difficult to control and to reproduce, though some advances have been made improve this (Hansen et al. 2009a). For the purpose of upscaling a biomimetic membrane array formation process, it might therefore be more convenient to use other pre-treatment methods to change the scaffold surface to mimic the traditional prepainted surface. As described in Sect. 10.3.1 a hydrophobic scaffold like Teflon is often desired and adjusting the surface chemistry of the scaffold material – mimicking the traditional prepainting by adding more hydrophobic groups such as alkanes – can improve the stability of biomimetic membrane arrays. A widely know technique for surface functionalization and modification is plasma polymerization. This technique facilitates a change in chemical properties of the top 10–100 nm of a substrate surface by covalently attaching chemical groups while maintaining the bulk physio-chemical substrate properties (Yasuda 1977). In recent work we tested plasma polymerization of three different hydrophobic compounds (Fig. 10.14) on EFTE scaffold containing 64 apertures. We found that adding n-hexene monomers to both sides of the scaffold significantly improved both the quality and the lifetime of the produced biomimetic membrane arrays.

Interestingly, adding any of the three monomers resulted in a decrease of water contact angle which indicates a lowering of the surface hydrophobicity. The use of n-hexene actually gave the lowest contact angle (90°) compared to the others (98° for 1-decene, 102° for HDMSO and 106° for pure ETFE). Because the contact

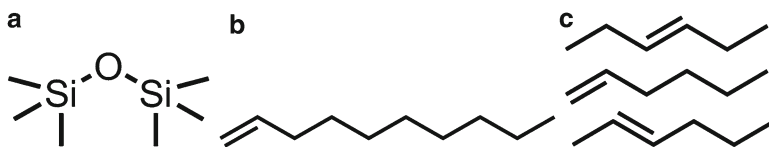


Fig. 10.14 Monomer structures. (a) Hexamethyldisiloxane (HDMSO) monomer. (b) 1-decene monomer. (c) n-hexene monomers

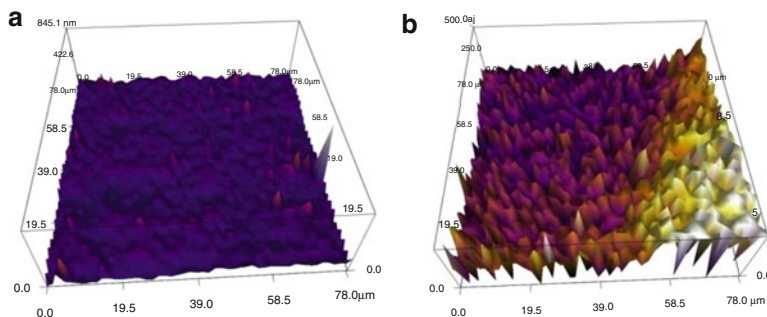


Fig. 10.15 AFM imaging of an n-hexene modified partition surface where a triangular area in the lower right corner has been shielded during plasma treatment leaving an unmodified ETFE surface. Measurements were done in Milli-Q grade water with a hydrophobic (hexadecane coated) AFM tip. (a) Topographic map. (b) 50×50 pixel force volume (FV) map generated from force-distance curves for each pixel for the area shown in a. For the untreated surface area the average adhesion energy $W_{ad} = 665 \pm 152$ aJ (average of 251 FV measurements), while for the n-hexene modified surface $W_{ad} = 345 \pm 90$ aJ (average of 902 FV measurements). For the silicon wafer (natural oxide layer) mounting surface $W_{ad} = 122 \pm 21$ aJ (average of 100 FV measurements)

angle of water is a macroscopic parameter it might not only be influenced by the surface chemistry but also the surface topology on nanoscale – an effect best illustrated by the lotus leaves.

By using atomic force microscopy (AFM) on ETFE, plasma-treated on half its surface, the topology was found to be unchanged in the process (Fig. 10.15a), while the adhesion to the hydrophobic AFM probe was decreased (Fig. 10.15b). This confirms that the surface hydrophobicity had been slightly reduced by the plasma-treatment with the hydrophobic monomers, and that this parameter alone is responsible for enhancing the properties of the biomimetic membrane array. While this seems counterintuitive it does however suggest that the energetics of the interaction between modified surfaces and a lipid/hydrocarbon phase not only relates to hydrophobic wetting but also involves contributions due to the amphiphilic nature of the lipids. A similar phenomenon has been observed for lactobacilli where hydrophobic strains do not always adhere best to hydrophobic surfaces (Millsap et al. 1997; Vadillo-Rodriguez et al. 2004).

10.5.2 Integrating Membrane Scaffolds with a Porous Support

Prior to constructing the support we specified the following demands on the material:

- The support should be integrated on the trans side of the membrane scaffold and adhere sufficiently to the scaffold surface so no delamination takes place under operating conditions, such as application of hydrostatic pressure from the cis side.
- The support should fill the apertures halfway or more in order to bring the hydrophilic surface in close proximity to the biomimetic membrane areas. This becomes especially important in later steps when a cushion layer is added on top of the hydrophilic support and coupled to matrix components.
- The support should have a highly porous structure that does not create a bottleneck for water flux in filtration and separation applications.
- The surface of the support should be smooth and flat on a micrometer scale in order to provide a well defined platform for further modifications. From a basic reasoning point of view, we also believe a flat smooth surface to be the preferred geometry since the bilayer itself has an inherent propensity towards adopting a fleet sheet structure and any deviation from this will cause internal stresses that could potentially destabilize the membrane.

Choice of support material and surface modification of partitions

To ensure that the support material does not create a bottleneck for water flux we use a highly permeable hydrogel formed by in situ radical polymerization of an aqueous solution of 2-hydroxyethyl methacrylate (HEMA), 1,4-butane-dioldiacrylate (BDDA) and poly(ethylene glycol) dimethacrylate (PEG-DMA) and in the presence of silica particles. HEMA constitutes the bulk polymeric material of the material while BDDA and PEG-DMA work as crosslinkers increasing the material strength and flexibility. We have shown that the presence of silica particles in the polymer hydrogel greatly enhances both the mechanical stability of the gel and the flux of water through the hydrogel. Radical polymerization is initiated through the ammonium persulfate (APS)/*N,N,N',N'*-Tetra-methyl-ethylenediamine (TEMED) redox pair initiator system.

Adhesion between the hydrogel support material (hereafter referred to as PHEMA) and the structured ETFE array functioning as the membrane scaffold (see Sect. 10.3.1) is achieved by plasma treating one side of the ETFE array with the HEMA monomer in a similar manner to the plasma treatment described in Sect. 10.5.1.

The actual process of integration

Depending on the material there are, in our experience, three different ways of integrating a porous, hydrophilic support with a structured membrane scaffold.

- **Clamping.** If the desired support material already exists in a solid state it can be clamped onto the back of the partition. Here, the support material will function mainly as a mechanical carrier. In some cases, if it is soft enough, it might penetrate slightly into the apertures and thus also works in the desired way of giving

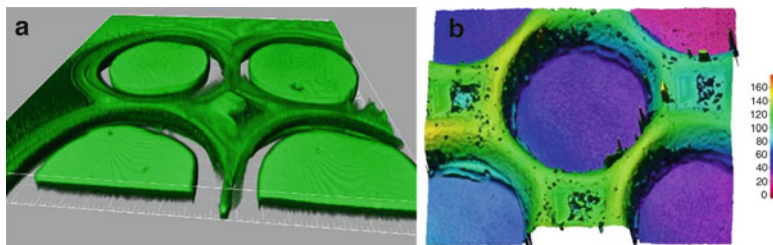


Fig. 10.16 Negative plug approach – (a) shows a Laser Scanning Confocal Microscopy image of the surface of the PDMS that was used to generate a negative plug inside apertures with a diameter of $300\ \mu\text{m}$, (b) shows an optical surface scan image (achieved via Infinite Focus, Alicona) of the surface of the porous support after pouring it onto the plug and removal of the PDMS (the spikes are artefacts from the measurement)

the biomimetic membrane more stability. However, clamping always induces mechanical stress and tension and this might actually pose a hindrance to membrane formation.

- **Direct Integration.** Here, the porous support is applied directly to the structured membrane in its liquid state and then cured. In order to achieve halfway filling of the apertures either a mold or a thinly spread (e.g. spin coated) layer of porous support solution is needed.
- **Negative Plug.** This procedure aims at creating a well defined plug inside the apertures. The plug is used as a template for the PHEMA support which is applied in its liquid state to the partition/negative plug construct. Once cured, the sacrificial plug material (e.g. PDMS (polydimethylsiloxane), PVA (polyvinyl acetate)) is removed leaving a smooth and flat support surface inside the apertures.

The following example illustrates the negative plug technique, which has yielded the best overall results in our lab with regards to the four success criteria listed in the beginning of this chapter.

The first step involves spin-coating PDMS onto a silicon wafer to create an approximately $80\text{--}100\ \mu\text{m}$ thick layer. Immediately after spin-coating, the ETFE membrane scaffolds are placed on the PDMS layer. The degree of filling is visualized by laser-scanning-confocal-microscopy (LSCM) (Fig. 10.16a). To produce the final composite material, the PHEMA precursor solution is mixed rapidly with a solution of the APS/TEMED redox pair, poured onto the PDMS-plugged scaffold and cured. Upon curing, the PDMS plug is removed from the scaffold yielding the final product (Fig. 10.16b)

Membrane characteristics in supported scaffolds

The presence of a PHEMA support in close proximity to biomimetic membranes significantly alters their electrical characteristics (Fig. 10.17). Usually the deposition of membrane matrix on scaffolds results in thick matrix films (Fig. 10.17a) which require manual thinning in order for bilayer areas to appear (Fig. 10.17b, c).

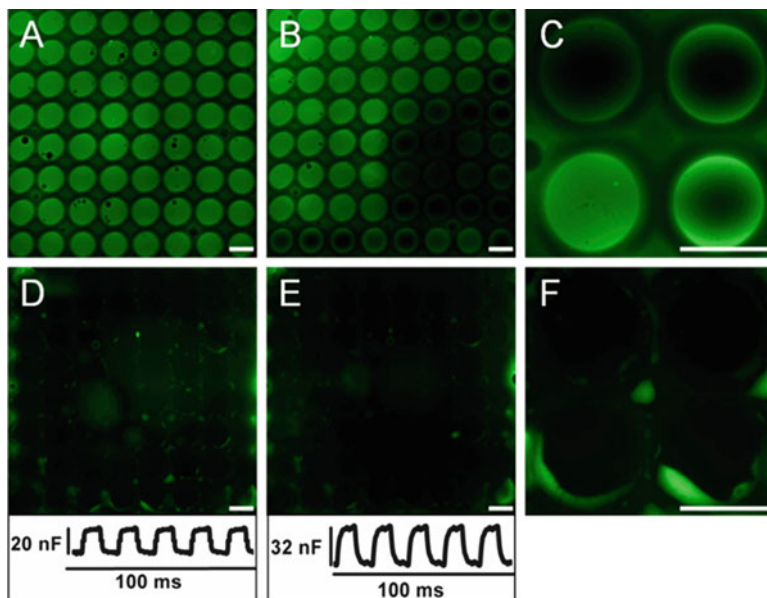


Fig. 10.17 Fluorescent images of established free-standing (panels a–c) and PHEMA-supported (panels d–f) bilayer arrays. Membrane composition: 25 mg/ml DPhPC:DOTAP:DSPE-PEG2000-Biotin:NBD-PC 71:18:10:1 (molar ratio) in decane. (a) Thick free-standing membranes taken with a 2.5 \times air-corrected objective (b) Appearance of several thinned free-standing membranes obtained after manual thinning, taken with a 2.5 \times air-corrected objective (c) Thinned and thick free-standing membranes obtained after manual thinning, taken with a 10 \times water-corrected objective. (d) PHEMA-supported membranes taken with a taken with a 2.5 \times air-corrected objective directly after membrane formation. The inset shows the corresponding membrane capacitance. (e) PHEMA-supported membranes taken with a 2.5 \times air-corrected objective 20 min after formation. The inset shows the corresponding membrane capacitance. (f) PHEMA-supported membranes taken with a taken with a 10 \times water-corrected objective directly after membrane formation. The scale bar is 300 μ m (Figure courtesy of Sania Ibragimova)

Some effort is needed to achieve a heterogeneous population of apertures containing fully thinned bilayer regions.

Supported membranes however, directly form thin membranes (Fig. 10.17d–f including capacitance values), without the need for manual thinning, indicating that in this case membrane formation occurs by a self-assembly process. In addition, the absence of both toroidal matrix films around the aperture edges (the so-called Plateau-Gibbs borders (Tien 1968)), and excess matrix in the diamond shaped pockets between apertures, indicate that the matrix solvent is squeezed out from both regions. This hypothesis is supported by the fact that the specific membrane capacitance in Fig. 10.17e is 0.7 μ F/cm² (assuming a bilayer area corresponding to 64 0.3 mm diameter apertures) which is close to the value observed for solvent free biomimetic membranes (0.8 μ F/cm²) (White 1978). In similar experiments we have reached capacitance values in 64 aperture arrays in excess of 45 nF, and thus achieving in effect solvent free biomimetic membranes.

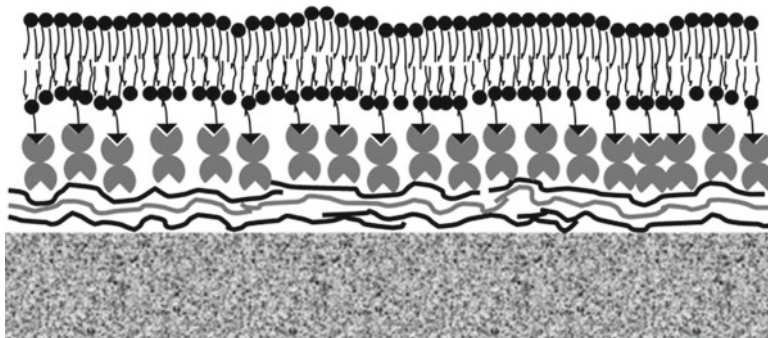


Fig. 10.18 Schematic of biomimetic membrane anchoring to the PHEMA surface inside scaffold apertures. From *bottom to top*: PHEMA (grey rectangle), PSS (black lines), PEI (grey lines), PSS (black lines), avidin (attached semi-circles), biotin (triangles), biotinylated lipid molecules (triangles+line (e.g. poly-ethylene glycol polymer)+filled circle (lipid head group)) with attached lines (acyl chains) and regular lipid molecules (black circles with attached lines)

Anchoring of biomimetic membranes to an underlying support

We have shown that the physical properties of biomimetic membranes are significantly altered when a PHEMA support is integrated into the membrane scaffold. However, the average lifetimes of membranes formed in the composite scaffold remains unchanged as compared to freestanding membranes. We are currently working towards increasing the overall stability and lifetimes of membranes by anchoring them to the underlying support material through poly-electrolyte cushion layers and avidin/biotin bonds (Fig. 10.18). The function of the poly-electrolyte cushion layer is to soften the surface/membrane interphase to better accommodate the physical undulations of a fluid biomimetic membrane system.

The poly-electrolyte cushion layer is constructed by layer-by-layer deposition of alternating negatively (PSS) and positively (PEI) charged poly-electrolytes (Lvov et al. 1995) from aqueous solutions. Since poly-electrolytes also bind to the scaffold surface during this process thus covering scaffold surface modifications (see Sect. 10.5.1) it is necessary to selectively remove the poly-electrolyte layers from the scaffold surface without removing them from the PHEMA support surfaces within the apertures. We have successfully implemented a sonication cleaning procedure for this purpose (Fig. 10.19). With this method it is possible to selectively remove PSS from the scaffold surface but not PEI which binds more strongly as quantified by contact angle measurements.

Once a poly-electrolyte cushion layer has been constructed, avidin –which binds strongly to PSS (Fig. 10.19) – is added from aqueous solution. Finally, matrix solution containing a certain mole percentage (usually from 1% to 10%) of biotinylated lipids is added as described in Sect. 10.3.3. Our current focus is to quantify and improve the anchoring of biotinylated lipid molecules to the underlying avidin layer.

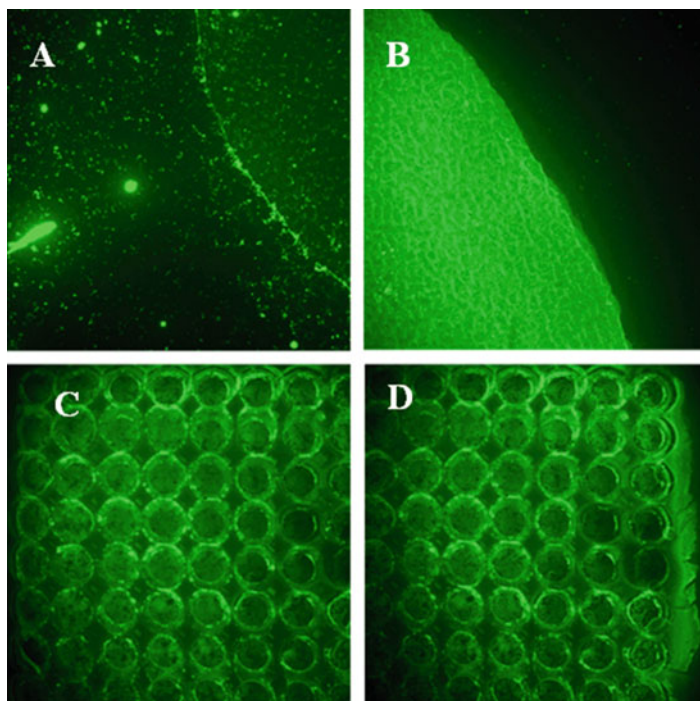


Fig. 10.19 Visualization of avidin binding to PHEMA incubated with polyelectrolytes. Images were acquired using an upright fluorescence microscope set-up. (a) PHEMA surface incubated with a droplet of aqueous PEI solution followed by incubation with fluorescently labelled Avidin in aqueous solution. The image of the PEI droplet border was acquired at 10 \times and with 1,000 ms exposure time. (b) PHEMA surface incubated with a droplet of aqueous PSS solution followed by incubation with fluorescently labelled Avidin in aqueous solution. The image of the PSS droplet border was acquired with a 10 \times objective 150 ms exposure time. (c) 8 \times 8 ETFE scaffold array with PHEMA support incubated with PSS and fluorescently labelled avidin prior to cleaning by use of sonication. Image acquired with a 2.5 \times objective and 500 ms exposure time. (d) The same ETFE scaffold array after sonication illustrating the preservation of Avidin and PSS inside the apertures. Image acquired with a 2.5 \times objective and 500 ms exposure time

10.6 Perspectives

In this chapter we have presented an overview of our research into large scale biomimetic arrays. Creating a stable, functional, addressable and ultimately commercialized large scale biomimetic array is a multi-faceted discipline which requires integration of several key components:

- The biomimetic membrane matrix (Sect. 10.2)
- The biomimetic membrane scaffold and its surface (Sects. 10.3.1 and 10.5.1)
- The method of formation (Sect. 10.3.2)
- The formation chamber (Sect. 10.3.3)
- The porous support structure (Sect. 10.5.2)

Our current research is focused on simplifying the production procedure of the integrated scaffold and support as well as quantifying and improve the anchoring of biomimetic membranes to the underlying support.

References

- Alberts, B., Johnson, A., Lewis, J., Raff, M., Roberts, K., Walter, P.: *Molecular Biology of the Cell*, 4th edn. Garland Science, New York (2002)
- Benvegna, T., Brard, M., Plusquellec, D.: Archaeobacteria bipolar lipid analogues: structure, synthesis and lyotropic properties. *Curr. Opin. Colloid Interface Sci.* **8**, 469–479 (2004)
- Benz, R., Janko, K.: Voltage-induced capacitance relaxation of lipid bilayer membranes. Effects of membrane composition. *Biochim. Biophys. Acta* **455**, 721–738 (1976)
- Bielawski, J., Thompson, T.E., Lehninger, A.L.: The effect of 2,4-dinitrophenol on the electrical resistance of phospholipid bilayer membranes. *Biochem. Biophys. Res. Commun.* **24**, 948–954 (1966)
- Cornell, B.A., Braach-Maksyvtis, V.L., King, L.G., Osman, P.D., Raguse, B., Wieczorek, L., Pace, R.J.: A biosensor that uses ion-channel switches. *Nature* **387**, 580–583 (1997)
- Cruz, A., Perez-Gil, J.: Langmuir films to determine lateral surface pressure on lipid segregation. *Methods Mol. Biol.* **400**, 439–457 (2007)
- Daly, S.M., Heffernan, L.A., Barger, W.R., Shenoy, D.K.: Photopolymerization of mixed monolayers and black lipid membranes containing gramicidin A and diacetylenic phospholipids. *Langmuir* **22**, 1215–1222 (2006)
- De Rosa, M., Gambacorta, A., Gliozzi, A.: Structure, biosynthesis, and physicochemical properties of archaeobacterial lipids. *Microbiol. Rev.* **50**, 70–80 (1986)
- Febo-Ayala, W., Morera-Felix, S.L., Hrycyna, C.A., Thompson, D.H.: Functional reconstitution of the integral membrane enzyme, isoprenylcysteine carboxyl methyltransferase, in synthetic bolalipid membrane vesicles. *Biochemistry* **45**, 14683–14694 (2006)
- Gennis, R.B.: *Biomembranes Molecular Structure and Function*. Springer, New York (1989)
- Gliozzi, A., Rolandi, R., De Rosa, M., Gambacorta, A.: Artificial black membranes from bipolar lipids of thermophilic Archaeobacteria. *Biophys. J.* **37**, 563–566 (1982)
- Gratzer, W.B.: The red cell membrane and its cytoskeleton. *Biochem. J.* **198**, 1–8 (1981)
- Han, X., Struder, A., Sehr, H., Geissbühler, I., DiBerardino, M., Winkler, F., Tiefenauer, L.: Nanopore arrays for stable and functional free-standing lipid bilayers. *Adv. Mater.* **19**, 4466–4470 (2007)
- Hansen, J., Perry, M., Vogel, J., Vissing, T., Hansen, C., Geschke, O., Emnéus, J., Nielsen, C.: Development of an automation technique for the establishment of functional lipid bilayer arrays. *J. Micromech. Microeng.* **19**, 025014 (2009a)
- Hansen, J.S., Perry, M., Vogel, J., Groth, J.S., Vissing, T., Larsen, M.S., Geschke, O., Emnéus, J., Bohr, H., Nielsen, C.H.: Large scale biomimetic membrane arrays. *Anal. Bioanal. Chem.* **395**, 719–727 (2009b)
- Haque, M.E., McIntosh, T.J., Lentz, B.R.: Influence of lipid composition on physical properties and peg-mediated fusion of curved and uncurved model membrane vesicles: “nature’s own” fusogenic lipid bilayer. *Biochemistry* **40**, 4340–4348 (2001)
- Ho, D., Chu, B., Lee, H., Montemagno, C.: Protein-driven energy transduction across polymeric biomembranes. *Nanotechnology* **15**, 1084–1094 (2004)
- Janshoff, A., Steinem, C.: Transport across artificial membranes—an analytical perspective. *Anal. Bioanal. Chem.* **385**, 433–451 (2006)
- Kumar, M., Grzelakowski, M., Zilles, J., Clark, M., Meier, W.: Highly permeable polymeric membranes based on the incorporation of the functional water channel protein Aquaporin Z. *Proc. Natl. Acad. Sci. U.S.A.* **104**, 20719–20724 (2007)
- Lei, G., MacDonald, R.C.: Lipid bilayer vesicle fusion: intermediates captured by high-speed microfluorescence spectroscopy. *Biophys. J.* **85**, 1585–1599 (2003)
- Lvov, Y., Ariga, K., Ichinose, I., Kunitake, T.: Assembly of multicomponent protein films by means of electrostatic layer-by-layer adsorption. *J. Am. Chem. Soc.* **117**, 6117–6123 (1995)

- Mayer, M., Kriebel, J.K., Tosteson, M.T., Whitesides, G.M.: Microfabricated teflon membranes for low-noise recordings of ion channels in planar lipid bilayers. *Biophys. J.* **85**, 2684–2695 (2003)
- McIntosh, T.J., Simon, S.A., MacDonald, R.C.: The organization of n-alkanes in lipid bilayers. *Biochim. Biophys. Acta* **597**, 445–463 (1980)
- Mecke, A., Dittrich, C., Meier, W.: Biomimetic membranes designed from amphiphilic block copolymers. *Soft Matter* **2**, 751–759 (2006)
- Meier, W., Nardin, C., Winterhalter, M.: Reconstitution of channel proteins in (polymerized) ABA triblock copolymer membranes. *Angew. Chem. Int. Ed Engl.* **39**, 4599–4602 (2000)
- Millsap, K.W., Reid, G., van der Mei, H.C., Busscher, H.J.: Adhesion of *Lactobacillus* species in urine and phosphate buffer to silicone rubber and glass under flow. *Biomaterials* **18**, 87–91 (1997)
- Montal, M., Mueller, P.: Formation of bimolecular membranes from lipid monolayers and a study of their electrical properties. *Proc. Natl. Acad. Sci. U.S.A.* **69**, 3561–3566 (1972)
- Mueller, P., Rudin, D.: Translocators in bimolecular lipid membranes: their role in dissipative and conservative bioenergetic transduction. *Curr. Top. Bioenerg.* **3**, 157–249 (1969)
- Mueller, P., Rudin, D.O., Tien, H.T., Wescott, W.C.: Reconstitution of cell membrane structure in vitro and its transformation into an excitable system. *Nature* **194**, 979–980 (1962)
- Nielsen, C.H.: Biomimetic membranes for sensor and separation applications. *Anal. Bioanal. Chem.* **395**, 697–718 (2009)
- O'Shaughnessy, T.J.H.J.E., Kulp III, J.L., Daly, S.M., Ligler, F.S.: Laser ablation of micropores for formation of artificial planar lipid bilayers. *Biomed. Microdevices* **9**, 863–868 (2007)
- Perry, M., Vissing, T., Boesen, T.P., Hansen, J.S., Emneus, J., Nielsen, C.H.: Automated sampling and data processing derived from biomimetic membranes. *Bioinspir. Biomim.* **4**, 044001 (2009)
- Pohl, P., Saparov, S.M., Antonenko, Y.N.: The effect of a transmembrane osmotic flux on the ion concentration distribution in the immediate membrane vicinity measured by microelectrodes. *Biophys. J.* **72**, 1711–1718 (1997)
- Rijn, C.J.M.v., Nijdam, W., Kuiper, S., Veldhuis, G.J., Wolferen, H.V., Elwenspoek, M.: Microsieves made with laser interference lithography for micro-filtration applications. *J. Micromech. Microeng.* **9**, 170–172 (1999)
- Sandison, M.: Artificial bilayer lipid membranes (BLMs) on-chip for single molecule sensing. In: *Microtechnologies for the New Millennium 2005 SPIE*, pp. 252–257. SPIE, Seville (2005)
- Shenoy, D.K., Barger, W.R., Singh, A., Panchal, R.G., Misakian, M., Stanford, V.M., Kasianowicz, J.J.: Functional reconstitution of protein ion channels into planar polymerizable phospholipid membranes. *Nano Lett.* **5**, 1181–1185 (2005)
- Simon, A., Girard-Egrot, A., Sauter, F., Pudda, C., Picollet D'Hahan, N., Blum, L., Chatelain, F., Fuchs, A.: Formation and stability of a suspended biomimetic lipid bilayer on silicon submicrometer-sized pores. *J. Colloid Interface Sci.* **308**, 337–343 (2007)
- Thompson, D., Wong, K., Humphry-Baker, R., Wheeler, J., Kim, J., Rananavare, S.: Tetraether bolaform amphiphiles as models of archaeobacterial membrane lipids: Raman spectroscopy, phosphorus-31 NMR, x-ray scattering, and electron microscopy. *J. Am. Chem. Soc.* **114**, 9035–9042 (1992)
- Tien, H.T.: Black lipid membranes at bifaces. Formation characteristics, optical and some thermodynamic properties. *J. Gen. Physiol.* **52**, 125S–143S (1968)
- Tien, H.T., Dawidowicz, E.A.: Black lipid films in aqueous media: a new type of interfacial phenomenon. *J. Colloid Interface Sci.* **22**, 438–453 (1966)
- Tien, H., Ottova-Leitmannova, A.: *Planar Lipid Bilayers (BLMs) and Their Applications*. Membrane Science and Technology. Elsevier, Amsterdam (2003)
- Vadillo-Rodriguez, V., Busscher, H.J., Norde, W., de Vries, J., van der Mei, H.C.: Dynamic cell surface hydrophobicity of *Lactobacillus* strains with and without surface layer proteins. *J. Bacteriol.* **186**, 6647–6650 (2004)
- Vogel, J., Perry, M., Hansen, J., Bolinger, P.-Y., Nielsen, C., Geschke, O.: Support structure for biomimetic applications. *J. Micromech. Microeng.* **19**, 025026 (2009)
- White, S.H.: A study of lipid bilayer membrane stability using precise measurements of specific capacitance. *Biophys. J.* **10**, 1127–1148 (1970)

- White, S.H.: Analysis of the torus surrounding planar lipid bilayer membranes. *Biophys. J.* **12**, 432–445 (1972)
- White, S.H.: Formation of “solvent-free” black lipid bilayer membranes from glyceryl monooleate dispersed in squalene. *Biophys. J.* **23**, 337–347 (1978)
- White, S.H., Petersen, D.C., Simon, S., Yafuso, M.: Formation of planar bilayer membranes from lipid monolayers. A critique. *Biophys. J.* **16**, 481–489 (1976)
- Wonderlin, W.F., Finkel, A., French, R.J.: Optimizing planar lipid bilayer single-channel recordings for high resolution with rapid voltage steps. *Biophys. J.* **58**, 289–297 (1990)
- Woodbury, D.J., Hall, J.E.: Vesicle-membrane fusion. Observation of simultaneous membrane incorporation and content release. *Biophys. J.* **54**, 345–349 (1988)
- Yasuda, H.: Modification of polymers by plasma treatment and by plasma polymerization. *Radiat. Phys. Chem.* **9**, 805–817 (1977)

Chapter 11

Systems for Production of Proteins for Biomimetic Membrane Devices

Nicola Altamura and Giuseppe Calamita

Abstract Production of large amounts of highly efficient membrane proteins (MPs) is one of the most challenging tasks in biomimetic (BM) membrane technology. Bottlenecks in protein expression approaches are raised by the hydrophobic nature of MPs and their complex mechanism of targeting, translocation and stable integration into native membranes. Over the last decade, new and more efficient protocols have been developed to overcome these problems and enhance the overexpression of MPs. Methods to produce MPs as a precipitate or synthesize them directly into detergents or into given liposomes have been also devised. This chapter focuses on the newly modified *Escherichia coli*, *Saccharomyces cerevisiae*, *Pichia pastoris* and cell-free systems as the most flexible and cost effective technologies for preparative scale production of MPs. Recent works reporting production of high quality samples of aquaporins (AQPs), a class of MPs with unique water conductance properties, are reviewed. Finally, we discuss the feasibility of exploiting the AQP channels for developing biomimetic water filtration and sensor devices of superior performance.

Abbreviations

AQP Aquaporins
BM Biomimetic membrane
CECF Two-compartment continuous exchange cell-free

N. Altamura
Institute of Biomembranes and Bioenergetics (IBBE), National Council of Researches,
University of Lecce, Via Monteroni, 73100 Lecce, Italy
e-mail: n.altamura@ibbe.cnr.it

G. Calamita (✉)
Department of General and Environmental Physiology,
University of Bari Aldo Moro and Apulian Network of Research Laboratories,
“WAFITECH” – via Amendola 165/AI-70126 Bari, Italy
e-mail: calamita@biologia.uniba.it

CF	Cell-free
MP	Membrane protein

11.1 Introduction

Production of high amounts of functional membrane proteins (MPs) to be embedded in artificial support matrix is one of the most challenging tasks in biomimetic membrane (BM) technology (Nielsen 2009). Major bottlenecks come from the low levels of expression of MPs in natural biological membranes as well as from their hydrophobic nature and specific requirements frequently preventing efficient synthesis and correct protein folding (Wagner et al. 2006; Grisshammer 2006). In addition, overproduction of recombinant MPs could cause disintegration and destabilization of host cell membranes and exert toxic effects upon membrane insertion due to system overloads or to transport and pore forming activities (Tate 2001). Last but not least, MP solubilization and purification may be difficult resulting in losses of yield and/or functional activity of the expressed proteins (Grisshammer 2006).

Over the last decade, generation of DNA templates with the optimal configuration have strongly improved expression conditions. Moreover, driven by the increasingly importance of having at one's disposal large amounts of functional MPs, new insights into the response of host cells to MP expression and mechanism of membrane insertion have been provided. This has led to considerable advance in production of even complex integral MPs. Several genes that are either upregulated or downregulated when yields of a membrane-inserted protein are poor have been identified (Luirink et al. 2005; White and von Heijne 2005). Progress has also been made in understanding how the translocon, which is the site of protein translocation and membrane insertion, establishes whether a protein segment is integrated into the membrane or not (Hessa et al. 2005). Remarkable advance has characterized the cell-free (CF) production systems, a tool known already for decades for its analytical relevance. Setups of current protocols allow preparation of milligram amounts of correctly folded and functional MPs of both prokaryotic and eukaryotic origin in less than 24 h (Schwarz et al. 2007). Expression of MPs as a fusion with an N- or C-terminal tag is often exploited to facilitate detection and/or purification of recombinant protein. Besides extending considerably in functional proteomics and structural biology applications (Dyson and Durocher 2007) the improved performance and dynamicity of both cell-based and CF expression systems is proving feasible tool for production of highly efficient MPs to be incorporated in biomimetic artificial supports. A flow-chart of the essential steps in producing preparative amounts of MPs to be incorporated in artificial support matrix is shown in Fig. 11.1.

Besides providing a brief overview of the available protein expression systems this chapter focuses on the *Escherichia coli*, *Saccharomyces cerevisiae*, *Pichia pastoris* and CF expression systems as the most flexible and cost effective technologies for preparative scale production of MPs. Despite being valuable tools for functional, regulatory and structural studies expression systems such as those using lentiviral

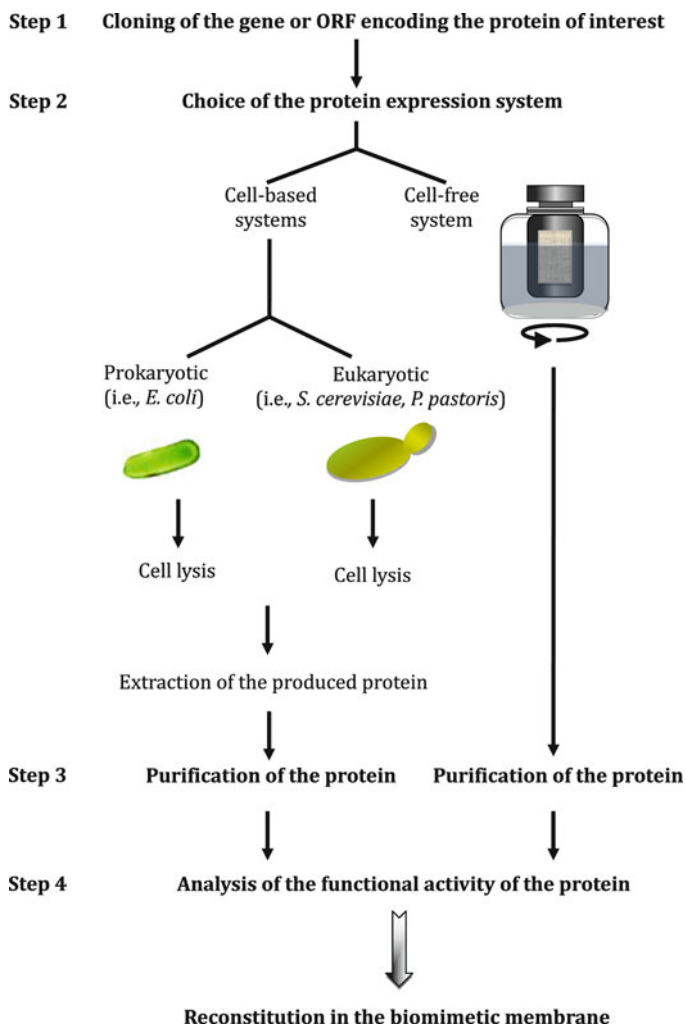


Fig. 11.1 Scheme of the production of large-scale amounts of membrane proteins for biomimetic membrane devices. (After cloning its gene or ORF (open reading frame), the protein of interest is produced by cell-based or cell-free technologies. Engineering a recombinant protein fused with a poly-His tag at its C- or N- terminus facilitates its purification by nickel affinity. After verifying its correct folding, functionality and stability, the protein is delivered to the lipid or polymer matrix. Functional embedding of MPs in the biomimetic artificial matrix is one of the most challenging tasks in the design of biomimetic membranes)

vectors, Gram-positive bacteria (*Lactococcus lactis*) and those of mammalian or insect origin will not be covered here due to cost, handling or scalability constraints. A paragraph addressing the most promising expression strategies and the possible biotechnological relevance of aquaporins, a widespread family of membrane water channel proteins, in biomimetic water filtration is also included.

11.2 *Escherichia coli* Expression Systems

The easy handling and fast growth makes *Escherichia coli* a widely used host for the production of heterologous proteins, especially in the areas of structural proteomics and genomics (Kim 2007; Yokoyama 2003). Robust engineered strains suitable for the cost effective production of complex eukaryotic proteins are also becoming available.

The *E. coli* system is being used since decades as an efficient approach for the production of a variety of soluble globular proteins (Kapust and Waugh 1999; Zhan et al. 2001; LaVallie et al. 2000). However, only a limited number of MPs have been efficiently produced by such technology due to the highly hydrophobic nature of MPs often promoting misfolding and aggregation followed by insoluble inclusion-body formation or even proteolysis. Over the last decade, new and more efficient protocols have been developed to overcome these problems and enhance the overexpression of MPs in *E. coli* (Kim 2007). In particular, the use of fusion protein expression vectors leading to the genetic fusion of the MP of interest to the N- or C- termini of soluble proteins has become increasingly common in order to increase yield and solubility and simplify detection and affinity purification of overproduced MPs (Daley et al. 2005; Laage and Langosch 2001). Examples of soluble partner proteins that are commonly used for constructing fusion MPs are thioredoxin (LaVallie et al. 1993; Begum et al. 2000), glutathione-S-transferase (Nygren et al. 1994; Zhan et al. 2001), maltose-binding protein (Pryor and Leiting 1997; Kapust and Waugh 1999), NuSA (Davis et al. 1999), protein A (Samuelsson et al. 1994), and ubiquitin (Power et al. 1990). A combinatorial system comprising two fusion cassettes consisting of short hydrophilic bacterial proteins, YaiN and YbeL, fused to the ends of MPs has been recently developed to produce stable, monodispersed MPs with functional activities comparable with the related native proteins (Leviatan et al. 2010).

Substantial developments have been also made in isolation, refolding and purification of biologically active MPs from inclusion bodies (Mukhopadhyay 1997). The effect of several refolding additive and buffers has been studied, sometimes in parallel on the same proteins. It is now accepted that more than 50% of the proteins in inclusion bodies could be refolded as also shown by the flourishing literature describing successful renaturation of proteins from inclusion bodies (Singh and Panda 2005; Vincentelli 2007; Michalke et al. 2009, 2010). A book chapter describing the main techniques and strategies for achieving successful refolding of expressed MPs has recently been published (Burgess 2009).

Certain post-translational modifications (e.g., glycosylation) remain beyond the reach of *E. coli*. However, the easy handling, low cost and fast growth together with the newly devised strategies to solubilize and refold proteins into their native and fully functional structure make the *E. coli* expression system one of the most promising technologies for mass production of MPs to be used in biomimetic membrane technology. A suitable DNA construct to produce large amounts of MPs by the *E. coli* system is described in Fig. 11.2c.

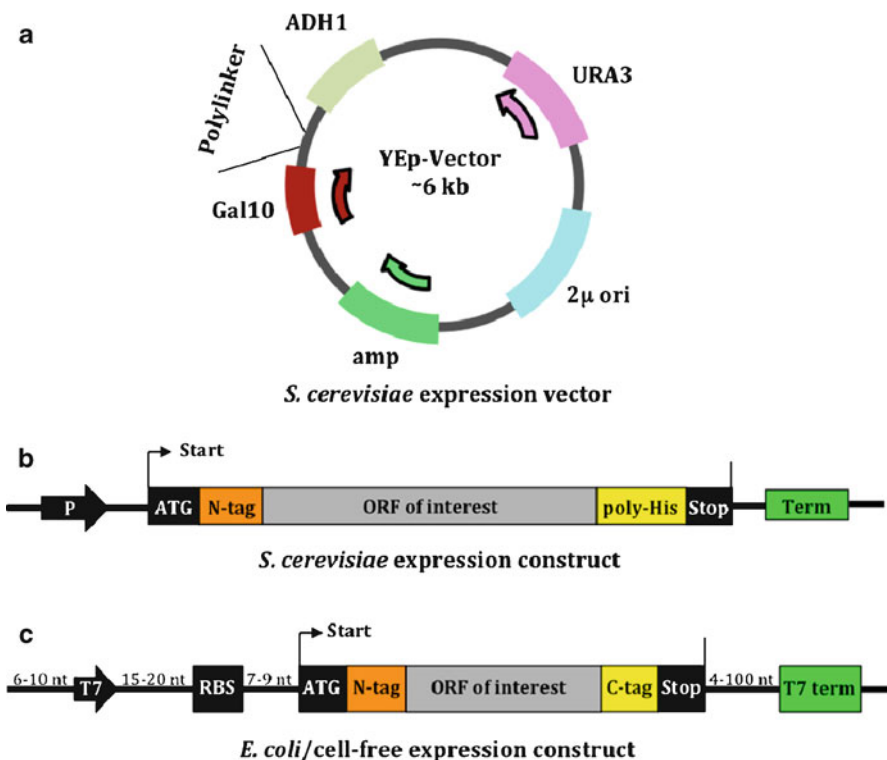


Fig. 11.2 DNA constructs used for cell-based and cell-free expressions of proteins. **(a, b)** Scheme of a typical yeast expression plasmid (high-copy vector). **(a)** Several high-copy 2 μ based episomal expression vectors (YEpl) are available with different genetic elements to initiate (P, promoter; shown is Gal10 promoter) and terminate transcription (i.e., ADH1 terminator). Generally, these plasmids combine genetic elements from the bacterium *E. coli* and the yeast *S. cerevisiae* that allow replication and propagation of the plasmids in both the organisms (shuttle vectors). In addition, the shuttle vectors contain genetic materials ensuring selection of the cell harbouring the plasmid. These shuttle vectors consist of a sequence conferring *E. coli* resistance to an antibiotic, mainly ampicillin (the β -lactamase gene, Amp) and a yeast gene sequence that, conventionally, encodes an enzyme for the synthesis of a particular amino acid, for example the *LEU2*, *HIS3* *LYS2* or *TRP1* gene, or the synthesis of a nucleotide like the *URA3* or *ADE2* gene. These genes are used as selectable markers of auxotrophy as they are able to complement the growth defect of a yeast mutant of the corresponding gene marker. **(b)** The ORF to be expressed by the host is cloned in the polylinker and may contain, fused in frame, an epitope tag (FLAG, c-myc, etc.) and/or a poly-histidine tract (poly-His) to facilitate the monitoring of the protein expression and its purification. Term, terminator. **(c)** Suitable DNA construct for the *E. coli*/cell-free expression of proteins. The DNA template contains a T7 promoter (T7) and a Shine-Dalgarno ribosome binding site (RBS) upstream of the ORF of interest that must contain an initiation codon (ATG) and a stop codon (STOP). Sequence upstream of T7 promoter contains at least 6–10 nucleotides (nt) to ensure efficient promoter binding. A potential stem-and-loop structure (Studier et al. 1990) is formed by a 15–20 nt sequence located between T7 and RBS. Optimal translation efficiency is favoured by a 7–9 nt sequence located between the RBS and the ATG initiation codon. T7 term, terminator. The ORF of interest may contain an epitope N-tag (i.e., FLAG, c-myc) and/or a C-tag (i.e., a poly-His tract) fused in frame to facilitate the monitoring of the protein expression and its purification. Such expression construct are cloned in high-copy vectors and propagated by *E. coli*

11.3 Yeast Expression Systems

Heterologous expression of an eukaryotic protein in unicellular eukaryotes like fungi, particularly yeasts, is an alternate advantageous choice because they perform the post translational steps typical of eukaryotic organisms, ensuring correct folding, assembly and post-translational modifications such as phosphorylation, proteolytic processing, disulfide bond formation and N- or O-glycosylation. The most documented yeast hosts include the non-methylotrophic *Saccharomyces cerevisiae*, *Kluyveromyces lactis* and *Yarrowia lipolytica* and the methylotrophic *Pichia pastoris* and *Hansenula polymorpha*. The methylotrophic differ from the non-methylotrophic yeasts in that they are able to metabolize a single compound (e.g., methanol) as carbon and energy source. Methylotrophic yeasts combine the important advantages to grow to high cell densities without difficulty and possess strong regulated promoters to ensure high levels of the expression of the oxidizing enzymes required for methanol metabolism (e.g., alcohol oxidase, AOX). However, fundamental knowledge of genetics and molecular biology of these yeasts is rather poor thus the possibility of engineering improved expression strains is limited (Porro et al. 2005). Undoubtedly, among the “conventional” yeasts, *S. cerevisiae* is the best representative one being the first organism whose genome has been entirely sequenced and, therefore, offering the most complete annotation of eukaryotic gene functions repertoire (Goffeau et al. 1996).

The complete sequencing of the *S. cerevisiae* genome has allowed the development of many novel tools for the analysis of the gene functions and interactions of their products. Among these, the high-throughput collection of deletion mutants has allowed many novel exhaustive screens for phenotypes that occur under a variety of physiological conditions (Scherens and Goffeau 2004). Overall, these powerful tools have re-launched *S. cerevisiae* as one of the most successful genetic systems for recombinant protein expression, particularly to set up innovative strategies to maximize protein production.

Several factors make the high yield production of heterologous proteins a challenging task. The low production yields in terms of soluble proteins may be related to the low expression level, or a toxic effect of overexpressed proteins, especially membrane proteins, or an intense proteolytic activity by endogenous proteases thus preventing accumulation of the expressed protein. These shortcomings have been alleviated in both *S. cerevisiae* and *P. pastoris* by combining the use of multicopy expression vectors (see Fig. 11.2a,b), strong constitutive or inducible promoters, protease-deficient yeast strains and tagged versions of the expressed protein for rapid and efficient purification (Andre et al. 2006; David et al. 1997; Hays et al. 2010). In the last years, efforts have been made to optimize the level of the produced proteins by altering expression parameters such as growth temperature and culture condition refinements in either *P. pastoris* or *E. coli* (Andre et al. 2006; Islam et al. 2007). Also, it has been recently reported that the overproduction level of eukaryotic membrane proteins in *P. pastoris* could be improved by mutations influencing the maturation, folding and stability of the nascent peptide chain (Oberg et al. 2009).

Although these studies further our understanding into factors directing high production of eukaryotic membrane proteins, they do not help in understanding the mechanisms activated by the host cell in response to the stress produced by the overexpression of the foreign protein (Bonander and Bill 2009). This crucial aspect of the recombinant protein expression can be investigated by using post-genomic array methods in the yeast *S. cerevisiae* (Bonander et al. 2005). The rationale is to look at the transcriptome of the host and identify those genes whose expression is significantly altered following the overproduction of the membrane protein. Such a comparative transcriptome analysis of high-yielding production conditions versus low-yielding conditions allowed the identification of 39 distinct genes (Bonander et al. 2005). Subsequently, it was shown that three of these genes, when deleted from the *S. cerevisiae* chromosomes, could each increase protein yields (Bonander et al. 2009). Moreover, it was shown that altering the transcript levels of a fourth gene, *BMS1*, involved in ribosome biogenesis, maximizes yield of membrane and soluble recombinant protein.

Altogether, there is no doubt that these advances in understanding the host organism response to the stress imposed by the recombinant membrane protein overproduction offer a rational way to relieve the bottleneck of MP production (Bonander and Bill 2009). Such a systemic approach could be soon extended to the methylotrophic yeast *P. pastoris* since its complete genome sequence is now available (De Schutter et al. 2009). The *S. cerevisiae* and *P. pastoris* systems represent powerful and promising technologies for preparative scale production of highly efficient MPs for biotechnological purposes.

11.4 Cell-Free Systems

Cell-free expression systems are emerging as fast, efficient and versatile technologies for the production of functional integral MPs (Klammt et al. 2004, 2007b; Liguori et al. 2007). A considerable variety of CF produced MPs has been already object of investigation in the areas of genomics, proteomics and biophysics regardless whether from a structural or functional standpoint. CF expression systems could either be established according to published protocols or, alternatively, having recourse to commercial kits from well recognized companies. A DNA construct suitable to produce preparative amounts of MPs by the cell-free system is described in Fig. 11.2c. Individual amino acids or selected combinations of MPs can be easily and efficiently replaced in CF reactions by labeled derivatives (Ozawa et al. 2006). The potentials of this approach are by far not completely explored yet and the high yield expression mode (Kigawa et al. 1999; Spirin et al. 1988; Chen et al. 2007) makes the CF expression a very promising tool for the preparative scale production of MPs for biomimetics.

The elimination of natural cytoplasmic cell environments during protein overexpression combined with the open accessibility of the reaction offers multiple important advantages. (i) Many of the key problems of MP over-production that affect the

physiology of the living host (i.e., incorrect membrane targeting and translocation, altered post-translational modifications, proteolysis, overload of transport mechanism, toxic or inhibitory effects) are overcome. Even large MPs containing multiple transmembrane segments can be synthesized directly into artificial hydrophobic environments like detergent micelles making CF expression strategies independent from complex and inefficient transport and translocation systems necessary for the localization of MPs into lipid membranes (Wagner et al. 2006). (ii) CF expression reduces the remarkable complexity that characterizes the *in vivo* translation of MP production. Any compound can thus be directly added to the expression reaction without considering transport or metabolic conversion problems. Protease inhibitors, ligands, cofactors, or substrates can be considered as possible additives that might be helpful in stabilizing the freshly translated MPs. (iii) MP expression by CF systems is fast, robust and straightforward. CF expression can be performed in small handling volumes of only few milliliters with short reaction times that usually shorter than 1 day. The setups of expression reactions can be made in analytical and preparative scale and several milligrams of protein per milliliter of reaction can be obtained (Kim and Swartz 1999; Klammt et al. 2005; Goffeau et al. 1996; Schwarz et al. 2007). CF systems feature high tolerance for a wide variety of substances like detergents or lipids and high efficiency in label incorporation combined with almost no background protein expression (Klammt et al. 2007a).

Several CF expression modes, extract sources and reaction setups for the CF production of MPs have been established, and the optimization and modification of these protocols is still a highly dynamic field. Membrane proteins can be CF expressed as precipitate (P-CF) and solubilised in different detergents after expression (Klammt et al. 2004; Keller et al. 2008) as well as produced directly in soluble modes by providing hydrophobic environments with detergents (D-CF), lipids (L-CF) or mixtures thereof (Klammt et al. 2005; Ishihara et al. 2005; Nozawa et al. 2007). The most frequently used extract sources are currently *E. coli* cells (Schwarz et al. 2007), wheat germs (Sawasaki and Endo 2007; Takai et al. 2010) and rabbit reticulocytes (Craig et al. 1992). However, post-translational modifications other than disulphide bridge formation have not been reported from either *E. coli* or wheat germ systems (Knapp et al. 2007). Some evidence of glycosylations in the less-productive rabbit reticulocyte extracts exists (Arduengo et al. 2007).

Reaction setups can be one-compartment batch or two-compartment continuous exchange cell-free (CECF) formats. CECF formats are more complicated but more efficient and overcome limitations resulting from the short life of translational activity which leads to low yield in protein production (Kigawa and Yokoyama 1991; Spirin et al. 1988; Shirokov et al. 2007). The more efficient CECF configuration contains a reservoir of low molecular weight precursors in a feeding mixture that is separated from the reaction mixture by a semi-permeable membrane. This ensures the exchange of substrates and by-products between the two compartments over a certain time period resulting in higher production efficiency that can yield several milligrams of MP per 1 mL of reaction mixture. CECF reactions can be scaled up to reaction mixture volumes of several milliliters

without significant loss of efficiency. A valuable chapter illustrating the setups of basic protocols for the general CF production of MPs in the CECF configuration using *E. coli* source extracts has been recently published by Frank Bernhard and coworkers (Schneider et al. 2010).

11.5 Production of Aquaporins for Biomimetic Separation/Sensor Devices

Aquaporins (AQPs) are a family of membrane-channel proteins widespread in nature making biological membranes 10- to 100-fold more permeable to water than related phospholipid bilayers (Calamita 2005; Gena et al. 2011; Verkman 2009). The water conductance featured by aquaporins is extraordinarily high: each single aquaporin pore can conduct billions of water molecules per second. AQPs are subdivided in *orthodox aquaporins*, which are selectively permeable only to water, and *aquaglyceroporins*, which in addition to water conduct small neutral solutes such as glycerol and urea and, other permeants such as ammonia, hydrogen peroxide and the metalloids antimonite, arsenite, silicic and boric acid depending on the effective restriction mechanism (Wu and Beitz 2007). The biological importance of the AQP family of water channels was recently acknowledged by the 2003 Nobel Prize for Chemistry awarded to the discovering scientist Peter Agre (Agre 2004).

The unique biophysical feature of allowing selective transport of water molecules and rejecting solutes makes orthodox AQPs of attractive interest in biomimetic separation technology (Nielsen 2009, 2010; Taubert 2007). Embedding orthodox aquaporins in artificial biocompatible supports (i.e., amphiphilic triblock copolymers) may lead to useful materials for several water-related applications, like ultrapure water production, wastewater purification, seawater desalination and salinity power production (Gerstandt et al. 2008; Pattle 1955). While extremely attractive and innovative, the fulfillment of a hybrid polymer/AQP channel membrane (Kaufman et al. 2010) constitutes a serious yet non-trivial scientific and technological challenge the low level of expression of AQPs in natural sources and their hydrophobic nature being among the hardest tasks. Feasibility of incorporating functional AQPs in artificial supports is suggested by a recent work constructing nanofiltration biomimetic membrane vesicles featuring a permeability up to several orders of magnitudes than the related pure matrix (Kumar et al. 2007). Likewise, the conductance properties (i.e., the permeability to some metalloids) of aquaglyceroporins (Bienert et al. 2008) seem to be a good requisite for production of sensor devices with potential applications in the early detection of toxic feed water contaminants such as arsenic (Nielsen 2009).

Up to date, most recombinant AQPs have been expressed for screening, functional, regulatory or structural studies (Kaldenhoff et al. 2007; Shi et al. 1995). Recently, feasibility of large scale production of functional AQPs for technological applications

is proved by a work reporting the fast and efficient production of up to 2 mg of AQP4, an eukaryotic orthodox aquaporin, per mL of reaction mixture (Kai et al. 2010). High quality AQP samples have been produced by both cell-based and CF expression systems (Table 11.1).

High expression (200 mg/L) of the orthodox aquaporin AqpZ was recently achieved by the *E. coli* system using maltose binding protein (MBP) as fusion partner protein and subsequent condition optimization (Lian et al. 2009). The same technology has been also employed by Kumar and coworkers for high yield production of functional AqpZ that was incorporated into the walls of self-assembled polymeric vesicles made of an amphiphilic triblock copolymer (PMOXA-PDMS-PMOXA) by leading to BMs that had up to several order of magnitude higher water permeability than the pure polymer vesicles (Kumar et al. 2007). *E. coli* expression methods providing milligram quantities of protein have also been successfully employed to solve the X-ray structure of the eubacterial water and glycerol channels, AqpZ (Savage et al. 2003) and GlpF (Fu et al. 2000), respectively, as well as of the archaeal aquaporin AqpM (Lee et al. 2005).

While already largely used for the expression of both orthodox aquaporins and aquaglyceroporins (Bienert et al. 2007; Fischer et al. 2009; Hedfalk et al. 2008; Kaldenhoff et al. 2007; Laize et al. 1997; Pettersson et al. 2006) the *S. cerevisiae* system may prove efficient and versatile to produce high amounts of functional AQPs to be used in biomimetic technology.

The methylotrophic yeast *Pichia pastoris* has been successfully employed to produce a large number of distinct AQPs. Exceptional high yields of functionally active human AQP1 have also been obtained arguing for the more widespread use of *P. pastoris* as a potential host in combination with rational optimization of culturing conditions (Nyblom et al. 2007). Comparative overproduction of all 13 human AQPs has provided valuable insights into the understanding of factors that direct a high production of correctly folded and stable eukaryotic MPs (Oberge et al. 2009). Moreover, efficient *P. pastoris*-based methods have been devised to produce high quantities of a number of active plant orthodox AQPs (Azad et al. 2008, 2009; Daniels et al. 2006; Karlsson et al. 2003; Kukulski et al. 2005; Tornroth-Horsefield et al. 2006; Verdoucq et al. 2008). PfAQP, an aquaglyceroporin of *Plasmodium falciparum* representing a potential drug target for treatment of malaria, has been expressed (64 mg/L culture) in *P. pastoris* to be then purified at homogeneity (18 mg/L) and crystallized for structural purposes (Hedfalk et al. 2008).

Large-scale expression of many functional recombinant AQPs have been produced by the baculovirus/insect cell system (Yang et al. 1997; Swamy-Mruthinti and Schey 1997; Werten et al. 2001; Drake et al. 2002a, Drake et al. 2002b; Hiroaki et al. 2006; Yakata et al. 2007; Hayakawa et al. 2008).

Multiple AQPs have been expressed at analytical level by reticulocyte lysate-based CF methods (La Vallie et al. 2000; Lu et al. 2000; Paul and Goodenough 1983; Shi et al. 1995). Fast and efficient production of preparative amounts of AQPs has been obtained after the recent development of new CF reaction designs and protocols. High expression of correctly folded AqpZ and a plant AQP have

Table 11.1 Aquaporins overproduced by cell-based and cell-free expression systems

Aquaporin	Origin	System	Yield (mg/L)	Quality control	References
AqpM	<i>M. marburgensis</i>	Ec	3–5	Structure	Lee et al. (2005), and Hovijitra et al. (2009)
AqpZ	<i>E. coli</i>	Ec	10–50	Structure/function, selectivity	Lian et al. (2009), Kumar et al. (2007), and Savage et al. (2003)
		CF-Ec	200	Large scale production	Xu et al. (2010), Schwarz et al. (2007), and Hovijitra et al. (2009)
GlpF	<i>E. coli</i>	Ec	10	Structure/function	Fu et al. (2000)
PfAQP	<i>P. falciparum</i>	Pp	3–5	Structure	Hedfalk et al. (2008)
SoPIP2;1 ^a (PM28A)	<i>S. oleracea</i>	Pp	25	Proteomics, functional	Karlisson et al. (2003)
	<i>S. oleracea</i>	Pp	ND	Structure, gating	Törnroth-Horsefield et al. (2006) and Kukulski et al. (2005)
AtPIP2;1	<i>A. thaliana</i>	Pp	<0.1	Structure/function, gating	Verdoucq et al. (2008)
TgPIP2;1	<i>T. gesneriana</i>	Pp	ND	Activity, gating, production	Azad et al. (2009)
TgPIP2;2					
AQP0	Rat	BI	ND	Structure/function	Drake et al. (2002a, b)
AQP1	Human	Pp	90	Overproduction	Nyblom et al. (2007)
	Human	Sc	ND	Function, regulation	Laizé et al. (1997)
AQP1, 3, 5 & 9	Mammalian	Sc	ND	Function, regulation	Pettersson et al. (2006)
AQP2	Human	BI	ND	Structure/function	Wertzen et al. (2001)
AQP4	Rat	BI	2–3	Preparative production	Yang et al. (1997), Hiroaki et al. (2006), and Hayakawa et al. (2008)
	Mouse	CF-Ec	2,000	Large scale production	Kai et al. (2010)
AQP10	Human	Pp	55	Overproduction	Oberg et al. (2009)
AQP11	Mouse	BI	1–2	Functional activity	Yakata et al. (2007)
AQP1–3, 5, 7, 12	Human	Pp	ND	Overproduction	Oberg et al. (2009)

Abbreviations: *Ec* Escherichia coli, *Sc* Saccharomyces cerevisiae, *Pp* Pichia pastoris *BI* Baculovirus/Insect, *CF-Ec* Cell-Free using *E. coli* extract sources, *ND* not determined

^aSoPIP2;1 was formerly called PM28A

been obtained with *E. coli* CF protocols using different fusion vectors (Xu et al. 2010; Schwarz et al. 2007). Milligram quantities of highly efficient AqpZ have been produced in synthetic liposomes by a CF approach with the supplementation of FtsY, the signal recognition particle receptor (Hovijitra et al. 2009). Different CF expression modes have been recently established for the fast and convenient production at a preparative scale of functional mouse AQP4 (Kai et al. 2010). CF expression methods using extract sources from *E. coli* and wheat germ embryos appear to be among the most promising perspective for the preparative scale production of functional AQPs.

11.6 Future Perspectives

The advances in understanding the processes that occur in host cells in response to the recombinant expression of MPs and the considerable success rate and efficiency in preparative production of MPs open a very promising perspective in producing functional MPs for biomimetic sensor and separation technologies. However, expression protocols and incorporation of stable MPs in BMs must be viewed in an integrated manner, the delivery of proteins in the artificial polymer matrix being one of the major challenges in the design of BMs. The potentials of the newly developed strategies to synthesize MPs directly into detergents or into given liposomes have by far not explored in terms of biomimetic technology, yet. Aquaporin water channels attract strong interest in biomimetic sensor and separation. The feasibility of orthodox AQP/polymer hybrid membranes for water purification is being demonstrated. Nevertheless, the potential application of aquaglyceroporins in biomimetic sensor device must be addressed. BMs incorporating AQPs may also reveal of exceedingly important relevance in power-producing biomimetic devices built on reverse osmosis principles. Undoubtedly, there are many good reasons to accelerate and streamline the current systems for massive and efficient production of membrane proteins to be exploited in sustainable and profitable biomimetic technologies.

Acknowledgments We thank Drs. Marialuisa Pellegrini-Calace and Patrizia Gena for help and critical reading of the manuscript and Dr. Eric Beitz for the valuable discussions. Financial support from Regione Puglia (Apulian Network of Research Laboratories “WAFITECH”), Fondazione Cassa di Risparmio di Puglia (FCRP – Ricerca Scientifica e Tecnologica) and Ministero dell’Istruzione, dell’Università e della Ricerca (MIUR – PRIN20089SRS2X_003) to G.C. and Fondazione per la Fibrosi Cistica (FFC) to N.A. are gratefully acknowledged.

References

- Agre, P.: Aquaporin water channels (nobel lecture). *Angew. Chem. Int. Ed. Engl.* **43**(33), 4278–4290 (2004)
- Andre, N., Cherouati, N., Prual, C., Steffan, T., Zeder-Lutz, G., Magnin, T., Pattus, F., Michel, H., Wagner, R., Reinhart, C.: Enhancing functional production of g protein-coupled receptors in *pichia pastoris* to levels required for structural studies via a single expression screen. *Protein Sci.* **15**(5), 1115–1126 (2006)
- Arduengo, M., Schenborn, E., Hurst, R.: The role of cell-free rabbit reticulocyte expression system in functional proteomics. In: Kudlicki, W., Katzen, F., Bennett, R. (eds.) *Cell-Free Expression*. Landes Bioscience, Austin (2007)
- Azad, A.K., Katsuhara, M., Sawa, Y., Ishikawa, T., Shibata, H.: Characterization of four plasma membrane aquaporins in tulip petals: A putative homolog is regulated by phosphorylation. *Plant Cell Physiol.* **49**(8), 1196–1208 (2008)
- Azad, A.K., Sawa, Y., Ishikawa, T., Shibata, H.: Heterologous expression of tulip petal plasma membrane aquaporins in *pichia pastoris* for water channel analysis. *Appl. Environ. Microbiol.* **75**(9), 2792–2797 (2009)
- Begum, R.R., Newbold, R.J., Whitford, D.: Purification of the membrane binding domain of cytochrome b5 by immobilised nickel chelate chromatography. *J. Chromatogr. B Biomed. Sci. Appl.* **737**(1–2), 119–130 (2000)
- Bienert, G.P., Moller, A.L., Kristiansen, K.A., Schulz, A., Moller, I.M., Schjoerring, J.K., Jahn, T.P.: Specific aquaporins facilitate the diffusion of hydrogen peroxide across membranes. *J. Biol. Chem.* **282**(2), 1183–1192 (2007)
- Bienert, G.P., Schussler, M.D., Jahn, T.P.: Metalloids: Essential, beneficial or toxic? Major intrinsic proteins sort it out. *Trends Biochem. Sci.* **33**(1), 20–26 (2008)
- Bonander, N., Bill, R.M.: Relieving the first bottleneck in the drug discovery pipeline: Using array technologies to rationalize membrane protein production. *Expert Rev. Proteomics* **6**(5), 501–505 (2009)
- Bonander, N., Hedfalk, K., Larsson, C., Mostad, P., Chang, C., Gustafsson, L., Bill, R.M.: Design of improved membrane protein production experiments: Quantitation of the host response. *Protein Sci.* **14**(7), 1729–1740 (2005)
- Bonander, N., Darby, R.A., Grgic, L., Bora, N., Wen, J., Brogna, S., Poyner, D.R., O'Neill, M.A., Bill, R.M.: Altering the ribosomal subunit ratio in yeast maximizes recombinant protein yield. *Microb. Cell Fact.* **8**, 10 (2009)
- Burgess, R.R.: Refolding solubilized inclusion body proteins. *Methods Enzymol.* **463**, 259–282 (2009)
- Calamita, G.: Aquaporins: Highways for cells to recycle water with the outside world. *Biol. Cell* **97**(6), 351–353 (2005)
- Chen, Y.J., Pornillos, O., Lieu, S., Ma, C., Chen, A.P., Chang, G.: X-ray structure of emre supports dual topology model. *Proc. Natl. Acad. Sci. U.S.A.* **104**(48), 18999–19004 (2007)
- Craig, D., Howell, M.T., Gibbs, C.L., Hunt, T., Jackson, R.J.: Plasmid cDNA-directed protein synthesis in a coupled eukaryotic in vitro transcription-translation system. *Nucleic Acids Res.* **20**(19), 4987–4995 (1992)
- Daley, D.O., Rapp, M., Granseth, E., Melen, K., Drew, D., von Heijne, G.: Global topology analysis of the *escherichia coli* inner membrane proteome. *Science* **308**(5726), 1321–1323 (2005)
- Daniels, M.J., Wood, M.R., Yeager, M.: In vivo functional assay of a recombinant aquaporin in *pichia pastoris*. *Appl. Environ. Microbiol.* **72**(2), 1507–1514 (2006)
- David, N.E., Gee, M., Andersen, B., Naider, F., Thorner, J., Stevens, R.C.: Expression and purification of the *saccharomyces cerevisiae* alpha-factor receptor (ste2p), a 7-transmembrane-segment g protein-coupled receptor. *J. Biol. Chem.* **272**(24), 15553–15561 (1997)
- Davis, G.D., Elisee, C., Newham, D.M., Harrison, R.G.: New fusion protein systems designed to give soluble expression in *escherichia coli*. *Biotechnol. Bioeng.* **65**(4), 382–388 (1999)

- De Schutter, K., Lin, Y.C., Tiels, P., Van Hecke, A., Glinka, S., Weber-Lehmann, J., Rouze, P., Van de Peer, Y., Callewaert, N.: Genome sequence of the recombinant protein production host *pichia pastoris*. *Nat. Biotechnol.* **27**(6), 561–566 (2009)
- Drake, K.D., Schuette, D., Chepelinsky, A.B., Crabbe, M.J.: Heterologous expression and topography of the main intrinsic protein (mip) from rat lens. *FEBS Lett.* **512**(1–3), 191–198 (2002a)
- Drake, K.D., Schuette, D., Chepelinsky, A.B., Jacob, T.J., Crabbe, M.J.: Ph-dependent channel activity of heterologously-expressed main intrinsic protein (mip) from rat lens. *FEBS Lett.* **512**(1–3), 199–204 (2002b)
- Dyson, M.R., Durocher, Y.: Expression System. *Methods Express.* Scion Publishing Ltd, Oxfordshire (2007)
- Fischer, G., Kosinska-Eriksson, U., Aponte-Santamaria, C., Palmgren, M., Geijer, C., Hedfalk, K., Hohmann, S., de Groot, B.L., Neutze, R., Lindkvist-Petersson, K.: Crystal structure of a yeast aquaporin at 1.15 angstrom reveals a novel gating mechanism. *PLoS Biol.* **7**(6), e1000130 (2009)
- Fu, D., Libson, A., Miercke, L.J., Weitzman, C., Nollert, P., Krucinski, J., Stroud, R.M.: Structure of a glycerol-conducting channel and the basis for its selectivity. *Science* **290**(5491), 481–486 (2000)
- Gena, P., Pellegrini-Calace, M., Biasco, A., Svelto, M., Calamita, G.: Aquaporin membrane channels: Biophysics, classification, functions and possible biotechnological applications. *Food Biophys. (Special issue)*, 1–9 (2011). doi: 10.1007/s11483-010-9193-9
- Gerstandt, K., Peinemann, K.-V., Skilhagen, S., Thorsen, T., Holt, T.: Membrane processes in energy supply for an osmotic power plant. *Desalination* **224**(1–3), 64–70 (2008)
- Goffeau, A., Barrell, B.G., Bussey, H., Davis, R.W., Dujon, B., Feldmann, H., Galibert, F., Hoheisel, J.D., Jacq, C., Johnston, M., Louis, E.J., Mewes, H.W., Murakami, Y., Philippsen, P., Tettelin, H., Oliver, S.G.: Life with 6000 genes. *Science* **274**(5287), 546–563 (1996). 547
- Grisshammer, R.: Understanding recombinant expression of membrane proteins. *Curr. Opin. Biotechnol.* **17**(4), 337–340 (2006)
- Hayakawa, S., Mori, M., Okuta, A., Kamegawa, A., Fujiyoshi, Y., Yoshiyama, Y., Mitsuoka, K., Ishibashi, K., Sasaki, S., Hattori, T., Kuwabara, S.: Neuromyelitis optica and anti-aquaporin-4 antibodies measured by an enzyme-linked immunosorbent assay. *J. Neuroimmunol.* **196**(1–2), 181–187 (2008)
- Hays, F.A., Roe-Zurz, Z., Stroud, R.M.: Overexpression and purification of integral membrane proteins in yeast. *Methods Enzymol.* **470**(1), 695–706 (2010)
- Hedfalk, K., Pettersson, N., Oberg, F., Hohmann, S., Gordon, E.: Production, characterization and crystallization of the plasmodium falciparum aquaporin. *Protein Expr. Purif.* **59**(1), 69–78 (2008)
- Hessa, T., Kim, H., Bihlmaier, K., Lundin, C., Boekel, J., Andersson, H., Nilsson, I., White, S.H., von Heijne, G.: Recognition of transmembrane helices by the endoplasmic reticulum translocator. *Nature* **433**(7024), 377–381 (2005)
- Hiroaki, Y., Tani, K., Kamegawa, A., Gyobu, N., Nishikawa, K., Suzuki, H., Walz, T., Sasaki, S., Mitsuoka, K., Kimura, K., Mizoguchi, A., Fujiyoshi, Y.: Implications of the aquaporin-4 structure on array formation and cell adhesion. *J. Mol. Biol.* **355**(4), 628–639 (2006)
- Hovijitra, N.T., Wu, J.J., Peaker, B., Swartz, J.R.: Cell-free synthesis of functional aquaporin z in synthetic liposomes. *Biotechnol. Bioeng.* **104**(1), 40–49 (2009)
- Ishihara, G., Goto, M., Saeki, M., Ito, K., Hori, T., Kigawa, T., Shirouzu, M., Yokoyama, S.: Expression of g protein coupled receptors in a cell-free translational system using detergents and thioredoxin-fusion vectors. *Protein Expr. Purif.* **41**(1), 27–37 (2005)
- Islam, R.S., Tisi, D., Levy, M.S., Lye, G.J.: Framework for the rapid optimization of soluble protein expression in *escherichia coli* combining microscale experiments and statistical experimental design. *Biotechnol. Prog.* **23**(4), 785–793 (2007). doi:10.1021/bp070059a
- Kai, L., Kaldenhoff, R., Lian, J., Zhu, X., Dotsch, V., Bernhard, F., Cen, P., Xu, Z.: Preparative scale production of functional mouse aquaporin 4 using different cell-free expression modes. *PLoS One* **5**(9), e12972 (2010). doi:10.1371/journal.pone.0012972
- Kaldenhoff, R., Bertl, A., Otto, B., Moshelion, M., Uehlein, N.: Characterization of plant aquaporins. *Methods Enzymol.* **428**, 505–531 (2007)

- Kapust, R.B., Waugh, D.S.: Escherichia coli maltose-binding protein is uncommonly effective at promoting the solubility of polypeptides to which it is fused. *Protein Sci.* **8**(8), 1668–1674 (1999)
- Karlsson, M., Fotiadis, D., Sjøvall, S., Johansson, I., Hedfalk, K., Engel, A., Kjellbom, P.: Reconstitution of water channel function of an aquaporin overexpressed and purified from *pichia pastoris*. *FEBS Lett.* **537**(1–3), 68–72 (2003)
- Kaufman, Y., Berman, A., Freger, V.: Supported lipid bilayer membranes for water purification by reverse osmosis. *Langmuir* **26**(10), 7388–7395 (2010)
- Keller, T., Schwarz, D., Bernhard, F., Dotsch, V., Hunte, C., Gorboulev, V., Koepsell, H.: Cell free expression and functional reconstitution of eukaryotic drug transporters. *Biochemistry* **47**(15), 4552–4564 (2008)
- Kigawa, T., Yokoyama, S.: A continuous cell-free protein synthesis system for coupled transcription-translation. *J. Biochem.* **110**(2), 166–168 (1991)
- Kigawa, T., Yabuki, T., Yoshida, Y., Tsutsui, M., Ito, Y., Shibata, T., Yokoyama, S.: Cell-free production and stable-isotope labeling of milligram quantities of proteins. *FEBS Lett.* **442**(1), 15–19 (1999)
- Kim, R.: Protein Expression in Escherichia coli. In *Methods Express: Expression Systems*. Dyson, M. R. and Durocher, Y. (eds.) Scion Publishing Ltd, Bloxham, pp. 13–28 (2007)
- Kim, D.M., Swartz, J.R.: Prolonging cell-free protein synthesis with a novel atp regeneration system. *Biotechnol. Bioeng.* **66**(3), 180–188 (1999)
- Klammt, C., Lohr, F., Schafer, B., Haase, W., Dotsch, V., Ruterjans, H., Glaubitz, C., Bernhard, F.: High level cell-free expression and specific labeling of integral membrane proteins. *Eur. J. Biochem.* **271**(3), 568–580 (2004)
- Klammt, C., Schwarz, D., Fendler, K., Haase, W., Dotsch, V., Bernhard, F.: Evaluation of detergents for the soluble expression of alpha-helical and beta-barrel-type integral membrane proteins by a preparative scale individual cell-free expression system. *FEBS J.* **272**(23), 6024–6038 (2005)
- Klammt, C., Schwarz, D., Dotsch, V., Bernhard, F.: Cell-free production of integral membrane proteins on a preparative scale. *Methods Mol. Biol.* **375**, 57–78 (2007a). doi:1-59745-388-9:57 [pii]
- Klammt, C., Schwarz, D., Eifler, N., Engel, A., Piehler, J., Haase, W., Hahn, S., Dotsch, V., Bernhard, F.: Cell-free production of g protein-coupled receptors for functional and structural studies. *J. Struct. Biol.* **158**(3), 482–493 (2007b)
- Knapp, K.G., Goerke, A.R., Swartz, J.R.: Cell-free synthesis of proteins that require disulfide bonds using glucose as an energy source. *Biotechnol. Bioeng.* **97**(4), 901–908 (2007)
- Kukulski, W., Schenk, A.D., Johanson, U., Braun, T., de Groot, B.L., Fotiadis, D., Kjellbom, P., Engel, A.: The 5a structure of heterologously expressed plant aquaporin *sopip2*;1. *J. Mol. Biol.* **350**(4), 611–616 (2005)
- Kumar, M., Grzelakowski, M., Zilles, J., Clark, M., Meier, W.: Highly permeable polymeric membranes based on the incorporation of the functional water channel protein aquaporin z. *Proc. Natl. Acad. Sci. U.S.A.* **104**(52), 20719–20724 (2007)
- Laage, R., Langosch, D.: Strategies for prokaryotic expression of eukaryotic membrane proteins. *Traffic* **2**(2), 99–104 (2001)
- Laize, V., Ripoché, P., Tacnet, F.: Purification and functional reconstitution of the human *chip28* water channel expressed in *saccharomyces cerevisiae*. *Protein Expr. Purif.* **11**(3), 284–288 (1997)
- LaVallie, E.R., DiBlasio, E.A., Kovacic, S., Grant, K.L., Schendel, P.F., McCoy, J.M.: A thioredoxin gene fusion expression system that circumvents inclusion body formation in the *e. Coli* cytoplasm. *Biotechnology (N Y)* **11**(2), 187–193 (1993)
- LaVallie, E.R., Lu, Z., Diblasio-Smith, E.A., Collins-Racie, L.A., McCoy, J.M.: Thioredoxin as a fusion partner for production of soluble recombinant proteins in *escherichia coli*. *Methods Enzymol.* **326**, 322–340 (2000)
- Lee, J.K., Kozono, D., Remis, J., Kitagawa, Y., Agre, P., Stroud, R.M.: Structural basis for conductance by the archaical aquaporin *aqpM* at 1.68 Å. *Proc. Natl. Acad. Sci. U.S.A.* **102**(52), 18932–18937 (2005)
- Leviatan, S., Sawada, K., Moriyama, Y., Nelson, N.: Combinatorial method for overexpression of membrane proteins in *escherichia coli*. *J. Biol. Chem.* **285**(31), 23548–23556 (2010)

- Lian, J., Ding, S., Cai, J., Zhang, D., Xu, Z., Wang, X.: Improving aquaporin z expression in *escherichia coli* by fusion partners and subsequent condition optimization. *Appl. Microbiol. Biotechnol.* **82**(3), 463–470 (2009)
- Liguori, L., Marques, B., Villegas-Mendez, A., Rothe, R., Lenormand, J.L.: Production of membrane proteins using cell-free expression systems. *Expert Rev. Proteomics* **4**(1), 79–90 (2007)
- Lu, Y., Turnbull, I.R., Bragin, A., Carveth, K., Verkman, A.S., Skach, W.R.: Reorientation of aquaporin-1 topology during maturation in the endoplasmic reticulum. *Mol. Biol. Cell* **11**(9), 2973–2985 (2000)
- Luirink, J., von Heijne, G., Houben, E., de Gier, J.W.: Biogenesis of inner membrane proteins in *escherichia coli*. *Annu. Rev. Microbiol.* **59**, 329–355 (2005)
- Michalke, K., Graviere, M.E., Huyghe, C., Vincentelli, R., Wagner, R., Pattus, F., Schroeder, K., Oschmann, J., Rudolph, R., Cambillau, C., Desmyter, A.: Mammalian g-protein-coupled receptor expression in *escherichia coli*: I. High-throughput large-scale production as inclusion bodies. *Anal. Biochem.* **386**(2), 147–155 (2009)
- Michalke, K., Huyghe, C., Lichiere, J., Graviere, M.E., Siponen, M., Sciara, G., Lepaul, I., Wagner, R., Magg, C., Rudolph, R., Cambillau, C., Desmyter, A.: Mammalian g protein-coupled receptor expression in *escherichia coli*: II. Refolding and biophysical characterization of mouse cannabinoid receptor 1 and human parathyroid hormone receptor 1. *Anal. Biochem.* **401**(1), 74–80 (2010)
- Mukhopadhyay, A.: Inclusion bodies and purification of proteins in biologically active forms. *Adv. Biochem. Eng. Biotechnol.* **56**, 61–109 (1997)
- Nielsen, C.H.: Biomimetic membranes for sensor and separation applications. *Anal. Bioanal. Chem.* **395**(3), 697–718 (2009)
- Nielsen, C.H.: Major intrinsic proteins in biomimetic membranes. *Adv. Exp. Med. Biol.* **679**, 127–142 (2010)
- Nozawa, A., Nanamiya, H., Miyata, T., Linka, N., Endo, Y., Weber, A.P., Tozawa, Y.: A cell-free translation and proteoliposome reconstitution system for functional analysis of plant solute transporters. *Plant Cell Physiol.* **48**(12), 1815–1820 (2007)
- Nyblom, M., Oberg, F., Lindkvist-Petersson, K., Hallgren, K., Findlay, H., Wikstrom, J., Karlsson, A., Hansson, O., Booth, P.J., Bill, R.M., Neutze, R., Hedfalk, K.: Exceptional overproduction of a functional human membrane protein. *Protein Expr. Purif.* **56**(1), 110–120 (2007)
- Nygren, P.A., Stahl, S., Uhlen, M.: Engineering proteins to facilitate bioprocessing. *Trends Biotechnol.* **12**(5), 184–188 (1994)
- Oberg, F., Ekvall, M., Nyblom, M., Backmark, A., Neutze, R., Hedfalk, K.: Insight into factors directing high production of eukaryotic membrane proteins; production of 13 human aqps in *pichia pastoris*. *Mol. Membr. Biol.* **26**(4), 215–227 (2009)
- Ozawa, K., Wu, P.S., Dixon, N.E., Otting, G.: N-labelled proteins by cell-free protein synthesis. Strategies for high-throughput nmr studies of proteins and protein-ligand complexes. *FEBS J.* **273**(18), 4154–4159 (2006). doi:EJB5433 [pii] 10.1111/j.1742-4658.2006.05433.x
- Pattle, R.E.: Properties, function and origin of the alveolar lining layer. *Nature* **175**(4469), 1125–1126 (1955)
- Paul, D.L., Goodenough, D.A.: In vitro synthesis and membrane insertion of bovine mp26, an integral protein from lens fiber plasma membrane. *J. Cell Biol.* **96**(3), 633–638 (1983)
- Petersson, N., Hagstrom, J., Bill, R.M., Hohmann, S.: Expression of heterologous aquaporins for functional analysis in *saccharomyces cerevisiae*. *Curr. Genet.* **50**(4), 247–255 (2006)
- Porro, D., Sauer, M., Branduardi, P., Mattanovich, D.: Recombinant protein production in yeasts. *Mol. Biotechnol.* **31**(3), 245–259 (2005)
- Power, R.F., Conneely, O.M., McDonnell, D.P., Clark, J.H., Butt, T.R., Schrader, W.T., O'Malley, B.W.: High level expression of a truncated chicken progesterone receptor in *escherichia coli*. *J. Biol. Chem.* **265**(3), 1419–1424 (1990)
- Pryor, K.D., Leiting, B.: High-level expression of soluble protein in *escherichia coli* using a his6-tag and maltose-binding-protein double-affinity fusion system. *Protein Expr. Purif.* **10**(3), 309–319 (1997)
- Samuelsson, E., Moks, T., Nilsson, B., Uhlen, M.: Enhanced in vitro refolding of insulin-like growth factor i using a solubilizing fusion partner. *Biochemistry* **33**(14), 4207–4211 (1994)

- Savage, D.F., Egea, P.F., Robles-Colmenares, Y., O'Connell 3rd, J.D., Stroud, R.M.: Architecture and selectivity in aquaporins: 2.5 a x-ray structure of aquaporin z. *PLoS Biol.* **1**(3), E72 (2003)
- Sawasaki, T., Endo, Y.: Protein expression in the wheat germ cell-free system. In *Methods Express: Expression Systems*. Dyson, M. R. and Durocher, Y. (eds.) Scion Publishing Ltd, Bloxham pp. 87–108 (2007)
- Scherens, B., Goffeau, A.: The uses of genome-wide yeast mutant collections. *Genome Biol.* **5**(7), 229 (2004)
- Schneider, B., Junge, F., Shirokov, V.A., Durst, F., Schwarz, D., Dotsch, V., Bernhard, F.: Membrane protein expression in cell-free systems. *Methods Mol. Biol.* **601**, 165–186 (2010)
- Schwarz, D., Junge, F., Durst, F., Frolich, N., Schneider, B., Reckel, S., Sobhanifar, S., Dotsch, V., Bernhard, F.: Preparative scale expression of membrane proteins in escherichia coli-based continuous exchange cell-free systems. *Nat. Protoc.* **2**(11), 2945–2957 (2007)
- Shi, L.B., Skach, W.R., Ma, T., Verkman, A.S.: Distinct biogenesis mechanisms for the water channels miwc and chip28 at the endoplasmic reticulum. *Biochemistry* **34**(26), 8250–8256 (1995)
- Shirokov, V.A., Kommer, A., Kolb, V.A., Spirin, A.S.: Continuous-exchange protein-synthesizing systems. In: Grandi, G. (ed.) *Methods of Molecular Biology*. Humana Press, Totowa (2007)
- Singh, S.M., Panda, A.K.: Solubilization and refolding of bacterial inclusion body proteins. *J. Biosci. Bioeng.* **99**(4), 303–310 (2005)
- Spirin, A.S., Baranov, V.I., Ryabova, L.A., Ovodov, S.Y., Alakhov, Y.B.: A continuous cell-free translation system capable of producing polypeptides in high yield. *Science* **242**(4882), 1162–1164 (1988)
- Studier, F.W., Rosenberg, A.H., Dunn, J.J., Dubendorff, J.W.: Use of t7 rna polymerase to direct expression of cloned genes. *Methods Enzymol.* **185**, 60–89 (1990)
- Swamy-Mruthinti, S., Schey, K.L.: Mass spectroscopic identification of in vitro glycosylated sites of mip. *Curr. Eye Res.* **16**(9), 936–941 (1997)
- Takai, K., Sasaki, T., Endo, Y.: The wheat-germ cell-free expression system. *Curr. Pharm. Biotechnol.* **11**(3), 272–278 (2010)
- Tate, C.G.: Overexpression of mammalian integral membrane proteins for structural studies. *FEBS Lett.* **504**(3), 94–98 (2001)
- Taubert, A.: Controlling water transport through artificial polymer/protein hybrid membranes. *Proc. Natl. Acad. Sci. U.S.A.* **104**(52), 20643–20644 (2007)
- Tomroth-Horsefield, S., Wang, Y., Hedfalk, K., Johanson, U., Karlsson, M., Tajkhorshid, E., Neutze, R., Kjellbom, P.: Structural mechanism of plant aquaporin gating. *Nature* **439**(7077), 688–694 (2006)
- Verdoucq, L., Grondin, A., Maurel, C.: Structure-function analysis of plant aquaporin atip2:1 gating by divalent cations and protons. *Biochem. J.* **415**(3), 409–416 (2008)
- Verkman, A.S.: Aquaporins: Translating bench research to human disease. *J. Exp. Biol.* **212**(Pt 11), 1707–1715 (2009)
- Vincentelli, R.: Refolding Proteins from Inclusion Bodies. In *Methods Express: Expression Systems*. Dyson, M. R. and Durocher, Y. (eds.) Scion Publishing Ltd, Bloxham, pp. 53–64 (2007)
- Wagner, S., Bader, M.L., Drew, D., de Gier, J.W.: Rationalizing membrane protein overexpression. *Trends Biotechnol.* **24**(8), 364–371 (2006)
- Werten, P.J., Hasler, L., Koenderink, J.B., Klaassen, C.H., de Grip, W.J., Engel, A., Deen, P.M.: Large-scale purification of functional recombinant human aquaporin-2. *FEBS Lett.* **504**(3), 200–205 (2001)
- White, S.H., von Heijne, G.: Transmembrane helices before, during, and after insertion. *Curr. Opin. Struct. Biol.* **15**(4), 378–386 (2005)
- Wu, B., Beitz, E.: Aquaporins with selectivity for unconventional permeants. *Cell. Mol. Life Sci.* **64**(18), 2413–2421 (2007)
- Xu, Z., Lian, J., Cai, J.: Efficient expression of aquaporin z in escherichia coli cell-free system using different fusion vectors. *Protein Pept. Lett.* **17**(2), 181–185 (2010)

- Yakata, K., Hiroaki, Y., Ishibashi, K., Sohara, E., Sasaki, S., Mitsuoka, K., Fujiyoshi, Y.: Aquaporin-11 containing a divergent npa motif has normal water channel activity. *Biochim. Biophys. Acta* **1768**(3), 688–693 (2007)
- Yang, B., van Hoek, A.N., Verkman, A.S.: Very high single channel water permeability of aquaporin-4 in baculovirus-infected insect cells and liposomes reconstituted with purified aquaporin-4. *Biochemistry* **36**(24), 7625–7632 (1997)
- Yokoyama, S.: Protein expression systems for structural genomics and proteomics. *Curr. Opin. Chem. Biol.* **7**(1), 39–43 (2003)
- Zhan, Y., Song, X., Zhou, G.W.: Structural analysis of regulatory protein domains using *gst*-fusion proteins. *Gene* **281**(1–2), 1–9 (2001)

Chapter 12

Strategies for Integrating Membrane Proteins in Biomembranes

Jesper S. Hansen, Inés Plasencia, and Kamila Pszon-Bartosz

Abstract Correct integration of membrane proteins with biomimetic membranes is crucial for designing novel sensor and separation technologies based on the functionality of membrane proteins. Membrane proteins are generally delicate molecules and care need to be taken in order to retain protein structure and function during handling and reconstitution into model membranes. This chapter will give a detailed overview of available and novel membrane protein reconstitution strategies in both vesicular and planar model membrane designs.

12.1 Protein Reconstitution

Membrane proteins function among others as receptors, ion channels, transporters and pore formers. They carry out important cellular functions in many physiologic processes in normal physiology, and may cause or contribute to several disease

J.S. Hansen (✉)
Aquaporin A/S, Copenhagen, Denmark

DTU Physics, Technical University of Denmark, Building 309, Rm 142 Fysikvej 309,
DK-2800 Kgs. Lyngby, Denmark
e-mail: jsha@fysik.dtu.dk

I. Plasencia
MEMPHYS-Center for Biomembrane Physics, Department of Physics and Chemistry,
University of Southern Denmark, Campusvej 55, DK-5230, Odense, Denmark
e-mail: miplasen@gmail.com

K. Pszon-Bartosz
Aquaporin A/S, Copenhagen, Denmark

DTU Nanotech, Technical University of Denmark, Building 423, Rm 110,
Produktionstorvet, DK-2800 Kgs. Lyngby, Denmark
e-mail: Kamila.Pszon@nanotech.dtu.dk

states. For the same reason membrane proteins are key targets for therapeutic intervention (Fang et al. 2003). Membrane proteins can moreover be chemically modified or genetically engineered, giving unprecedented control over membrane binding and transport properties (Castellana and Cremer 2006). Therefore, membrane proteins, either in native forms or modified versions, may give rise to the creation of novel protein-based biosensors, biomedical screening platforms and novel separation technologies.

Reconstitution of membrane proteins into artificially made lipid bilayers represent a powerful technique to study and functionally work with membrane proteins under controlled experimental conditions (Woodbury 1999). However, membrane protein reconstitution is not a trivial process. Here we will give a practical approach to the strategies and considerations for functionally reconstituting membrane proteins into vesicular and planar model membranes. The requirements for protein reconstitution yield in sensor or separation applications may not be the same. Thus, reconstitution approaches and considerations to meet the requirements of reconstitution yield in sensor or separation technologies are also discussed here.

12.2 Reconstitution in Vesicles

Vesicles are spherical shells of lipid bilayers and represent one of the most widely used methods for reconstituting membrane proteins into biomimetic model membranes. When lipids are the principal component of the vesicles, they may also be called liposomes. Polymersomes on the other hand refers to vesicles formed by synthetic polymers (Lorenceanu et al. 2005; Rastogi et al. 2009; Rosenkranz et al. 2009).

There are presently several methods available for reconstituting membrane proteins into vesicles. The protein purification conditions will be an initial parameter defining the reconstitution methodology to choose. Although few membranes proteins can be extracted by organic solvents, e.g. pulmonary surfactant proteins SP-B and SP-C (Johansson et al. 1988; Curstedt et al. 1988), most membrane protein purification protocols rely on solubilizing the cell membrane to obtain an aqueous detergent-solubilized protein state. Subsequently the membrane proteins may be reconstituted into model membranes.

12.2.1 Preparation of Liposomes and Proteoliposomes

Various techniques exist for preparing liposomes, and the method of choice may result in different types of liposomes. The types of liposomes may be classified on the basis of size and number of bilayers forming the vesicles (Deamer and Uster 1983; Szoka and Papahadjopoulos 1980). The classifications used for the different types of liposomes are often divided into:

1. *Multilamellar vesicles (MLV)*. This type of vesicles contains multiple lipid bilayer vesicles inside each other. They vary in size, internal volume (Singer et al. 1990) and osmotic activity (Yoshikawa et al. 1983). This can make liposome analysis and result interpretation difficult.
2. *Small unilamellar vesicles (SUV)*. SUVs consist of a single lipid bilayer and the vesicle sizes are between 4 and 20 nm. These vesicles are very small, resembling the sizes of biological vesicles carrying neurotransmitters in the nerve synapses.
3. *Large unilamellar vesicles (LUV)*. These vesicles also consist of a single lipid bilayer and are defined by having sizes between 50 nm and up to 10 μm . These vesicles are often the preferred type for protein reconstitution.
4. *Giant Unilamellar vesicles (GUV)*. They are also known as cell-size unilamellar vesicles, because their size approximately mimics biological living cell sizes. GUVs are defined by having a size of $\geq 10 \mu\text{m}$.

Vesicle size will not be the only parameter influenced by the preparation method, the polydispersity, surface potential, degree of ionization, thermotropic phase behavior, permeability and physical stability will also be affected (Feitosa et al. 2000; Szoka and Papahadjopoulos 1980; Joannic et al. 1997; Angelova et al. 1992). Many applications of vesicles rely on a narrow size distribution and a concomitant high stability during a long time period (Fendler 1987). When natural or synthetic long-tailed phospholipids are dispersed in aqueous solution, they form large multilamellar structures (Gabriel and Roberts 1984).

There are several methods to form unilamellar vesicles from multilamellar. This is relevant for creating vesicles suitable for reliable and reproducible protein reconstitution and may also be of importance in many analytical techniques. A straightforward method to create unilamellar vesicles from multilamellar vesicles is sonication. However, it does not produce a uniform size distribution and moreover the method may potentially cause metal contamination, lipid degradation and generation of heat and aerosols (Maguire et al. 2003). Another method is mechanical extrusion of multilamellar vesicles through a filter membrane with a defined pore size, resulting in unilamellar vesicles with a narrow size distribution. Vesicle extrusion may be carried out by small inexpensive hand-held extruders or with nitrogen pressurized barrel extruders. The latter can range in capacities from 1 to 10 ml and up to industrial scale (many liters). Generally, we have good experience with both hand-held and pressurized barrel extruders. However, hand-held extruders tend to produce a slightly more polydisperse vesicle solution and vesicles produced in this manner also tend to be slightly more instable compared to the barrel extruded vesicles (higher tendency of vesicle-vesicle fusions).

An important consideration in protein reconstitution is which strategy to choose for delivering membrane proteins into model membranes. As mentioned the majority of membrane protein reconstitution procedures involve the use of a detergent. The detergent plays a dual role for membrane proteins in solution: (i) the solubilization of the native membrane to release the contained membrane spanning protein into solution and (ii) maintain the protein folded and soluble in an aqueous state (le Maire et al. 2000). Moreover, the physio-chemical properties of the detergent

Table 12.1 Non-denaturing detergents commonly used for membrane protein reconstitution

Type	Detergent	Mw micelle (Da)	CMC (mM) ^b	Dialyzable
Anionic	Sodium cholate	900–1,300	9–15	Yes
	Sodium deoxycholate	1,200–5,000	2–6	Yes
Cationic	CTAB	62,000	1	Yes
Zwitterionic	CHAPS	6,150	6–10	Yes
	CHAPSO	7,000	8	Yes
	LDAO	ND ^a	1	Yes
Nonionic	OG	25,000	20–25	Yes
	OTG	ND	9	Yes
	Triton X-100	90,000	0.24	No
	C12E8	65,000	0.09	No
	DDM	50,000	0.15	No
	Digitonin	70,000	0.5	No
	MEGA-9	ND	6–7	Yes
	MEGA-10	ND	19–25	Yes

Abbreviations: *CTAB* hexadecyltrimethylammonium bromide, *LDAO* lauryldimethylamine N-oxide, *OG* octyl- β -glycopyranoside, *OTG* octyl β -D-thioglucopyranoside, *C12E8* dodecyl octaethylene glycol ether, *DDM* *n*-Dodecyl β -D-maltoside

^aND indicates that the detergent molecular weight micelles have not or cannot be determined

^bNotice: CMC changes with temperature and salt concentration. Given values are 20°C–25°C

may be important for the integrity and activity of the protein upon reconstitution into model membranes (Paternostre et al. 1988; Rigaud et al. 1988).

To produce protein reconstituted liposomes (proteoliposomes), removal of the detergent is necessary in order to transfer the proteins from an aqueous detergent stabilized state and into the model membrane lipid bilayer. Conventional techniques for removing the detergent include among others dialysis, gel exclusion chromatography and adsorption onto polymeric materials. A detailed description and comparison of the various techniques for detergent removal is reviewed in (Ollivon et al. 2000; Silvius 1992). Generally the choice of detergent removal technique is often a choice between using dialysis or adsorption onto polymeric materials such as hydrophobic Bio-Beads or a combination of both these techniques. Both methods are straightforward and do not require costly technical equipment. The decision of which method to use for detergent removal is typically based on the nature of the detergent. Detergents with a high critical micelle concentration (CMC) and with low to moderate molecular weight micelles can be dialyzed away, whereas dialysis is not an appropriate technique for detergent removal if the opposite is the case. Table 12.1 gives a brief overview of some of the more commonly used non-denaturing detergents for membrane protein reconstitution and also indicates whether the detergent is dialyzable.

Another parameter to consider before carrying out the protein reconstitution process is the lipid-to-protein ratio (LPR). The LPR is the mol of lipids per mol protein to be reconstituted into the vesicles. There is an upper limit of how much protein that physically can be incorporated into a defined amount of lipid (or polymer). This limit depends on the surface area of the protein and the area of the lipid. The area

per lipid of phosphatidylcholines has for example been characterized by NMR spectroscopy and may provide useful information in LPR calculations (Petrache et al. 2000). Since the lipid membrane exists as a bimolecular structure, lipid molecules are needed in both bilayers to cover a single transmembrane protein. Similarly the crystal structure has been determined for various membrane proteins from which the protein monomer surface has been published. The spinach aquaporin SoPIP2;1 is just one example (Tomroth-Horsefield et al. 2006). Thus, based on the area values of the lipid and protein a minimum mol/mol ratio of lipid molecules to protein may be estimated. It is often necessary to test different LPRs (e.g. LPR 200, 100, 50, etc.) to find the optimal protein reconstitution conditions.

In our laboratory we work with aquaporins which are tetrameric α -helical water channel forming membrane proteins. We have good experience with octyl- β -D-glycopyranoside (OG) and generally use this detergent for protein solubilization and reconstitution. Since OG is dialyzable the preferred detergent removal technique is dialysis (Table 12.1). To ensure complete detergent removal a second (optional) Bio-Beads step may be included. Our scheme for protein reconstitution into liposomes to produce proteoliposomes is:

1. *Preparation of detergent containing MLVs.* The MLVs are prepared either by drying down the lipid from a chloroform phase followed by rehydration or directly dissolving lyophilized lipids in lipid hydration buffer. The lipid hydration buffer is usually matched to the buffer of the protein (note: it also contains detergent).
2. *Formation of detergent containing LUVs.* LUVs are prepared from MLVs typically by extrusion using a pressurized barrel extruder with 100, 200 or 400 nm filters depending on the desired proteoliposomes size.
3. *Mixing of detergent LUVs with detergent solubilized protein.* Detergent solubilized protein is mixed with the formed detergent containing LUVs to the desired LPR (e.g. 200, 100, 50, etc.).
4. *Detergent removal.* To remove the detergent dialysis is applied. An efficient way is to use dynamic dialysis where a continuous flow of the detergent-free dialysate buffer passes the dialysis tubing containing the lipid-protein-detergent sample (with flow rates of 2–10 ml dialysate/min).
5. *Optionally, second detergent removal step.* To ensure that all detergent has been removed from the formed proteoliposomes absorption Bio-Beads may be added to the proteoliposomes sample. This may be relevant for carrying out stopped-flow permeability measurements of aquaporin function, where the presence of residual detergent can hamper the result interpretation. Following the additional detergent removal step, the supernatant is collected and used (the proteoliposomes).

The simplified scheme represented above for reconstitution aquaporins into model membrane vesicles is in many aspects a general methodology and may be followed as a flow chart for preparing proteoliposomes using a dialyzable detergent. Parameters such as the detergent type, detergent concentration, dialysis times, the optimal LPR and buffer composition may vary from protein to protein. Moreover, various protein isoforms may often require different buffer conditions.

12.2.2 *How Lipid Composition May Affect Protein Folding*

A stable integration of a membrane protein into a lipid bilayer will be affected among other factors by the hydrophobic interactions of the hydrophobic protein segment(s) with the acyl chains of the lipids. The difference between the hydrophobic length of a membrane integral protein and the hydrophobic thickness of the membrane is known as hydrophobic mismatch. In order to avoid unfavorable exposition of the protein to the hydrophilic environment the length of the hydrophobic thickness of the membrane and the hydrophobic segment of the protein are expected to be matched so they are approximately equal.

Elastic properties of the lipid bilayer are vital to the folding and function of membrane proteins (Booth 2005). Membrane proteins have a percentage of apolar residues that is much higher than for their water soluble counterparts (Samatey et al. 1995; Hong et al. 2009). However, membrane proteins cannot bury all the hydrophobic residues in a hydrophobic core. Therefore, the membrane proteins associate with lipid bilayers both *in vivo* (Van den Berg et al. 2004; Osborne et al. 2005) and *in vitro* (Seddon et al. 2004) and tend to aggregate in aqueous solutions in order to escape the hydrophilic environments. The bilayer thickness is determined by several factors, where some of them for example are the lipid chain length and the degree of saturation of the lipid acyl chains (Rawicz et al. 2000), cholesterol content (Mouritsen and Zuckermann 2004) and the membrane proteins themselves (Mitra et al. 2004). When the lipids forming the model membrane constitute a hydrophobic environment shorter than the hydrophobic protein segment the protein tend to aggregate or oligomerize to minimize the exposed hydrophobic areas. Alternatively, they can change the conformation or induce a tilt of the protein in the membrane. In the opposite situation, where the protein chain length is longer than the hydrophobic protein segment the mismatch can also result in protein aggregation.

Membrane proteins may also have specific requirements for phospholipids and sterols, which may be essential for folding, oligomerization and/or activity. Moreover, the lipid composition of biological membranes varies, so it may be a good idea to consider what the origin of the protein in question is and in which host organism the proteins have been expressed and purified from. A detailed review of specific lipid requirements of selected membrane proteins as well as the lipid composition of various biological membranes are given by Opekarová and Tanner (Opekarova and Tanner 2003). A good starting point, however, for membrane protein reconstitution is to use total lipid extracts such as soybean asolectin or *E. coli* total lipid extract. These lipid mixtures are total lipid membrane extracts and therefore contain all the natural constituents of a biological membrane. They also generally tend to result in good protein reconstitution yield.

12.3 **Reconstitution in Planar Membranes**

Planar biomimetic membranes constitute an important platform for studying membrane protein function and protein-lipid interactions. The planar membrane design creates a possibility to study the transport processes of a membrane protein across

the lipid bilayer (Janshoff and Steinem 2006). Techniques available to study processes across planar artificially made membranes include among others electrophysiological measurements (Montal and Mueller 1972; Mueller and Rudin 1969) and optical techniques such as fluorescence microscopy or a combination (Hansen et al. 2009a; Hemmler et al. 2005; Wilburn et al. 2006). The structural and dynamic processes of proteins in the membrane may also be studied by surface sensitive techniques (Buzhynskyy et al. 2007a, b; Goennenwein et al. 2003).

The potential biotechnological applications of planar membrane designs are large and include both sensor and separation technologies. The creation of membrane protein microarrays for high-throughput screening of protein-drug interactions has attracted much attention (Fang et al. 2002; Majd and Mayer 2008). Designs that fit into modern plate readers are attractive in the development of high-throughput membrane protein assays for the pharmaceutical industry (Fang et al. 2006; Le Pioufle et al. 2008; Suzuki et al. 2009). Provided that the effective functional membrane area can be scaled up sufficiently, planar biomimetic membranes may also be suitable for novel separation technologies using membrane protein channels (Nielsen 2009).

Small fusogenic depsipeptides or peptides such as valinomycin, gramicidin or alamethicin, respectively, spontaneously self-insert into pre-established membranes (Zagnoni et al. 2007). These membrane spanning molecules are therefore well-characterized and due to the ease of reconstitution they are often applied to demonstrate the functionality of artificially made lipid membranes (Hansen et al. 2009a, b). In contrast, medium to large membrane proteins (35–500 kDa) do generally not reliably self-insert into pre-established membranes (Zagnoni et al. 2007). An exception is the heptameric α -hemolysin channel pore from *S. aureus* (Suzuki et al. 2007). In addition, several *E. coli* outer membrane porins such as OmpA, OmpF and FomA may be reconstituted into planar membranes directly from a detergent solubilized state (Schmitt et al. 2006; Pocanschi et al. 2006; Arora et al. 2000). It should be noted, however, that although the detergent solubilized proteins can be added in a few microliter aliquots to the lipid bilayer chamber, the detergent present tends to make the established membrane(s) unstable.

In order to study most membrane proteins, reliable and controllable reconstitution methods are required for the delivery of functionally active membrane proteins into planar membranes.

12.3.1 Vesicle Fusion with Planar Lipid Bilayers

The conventional technique to deliver membrane proteins to pre-established planar lipid bilayers is by vesicle fusion. The methodology can be viewed as a biomimicry of the ubiquitous biological phenomena of exocytosis. In exocytosis intracellular vesicles fuse with the plasma membrane and subsequently release the extracellular content (Zimmerberg et al. 1980a). Exocytosis is involved in important biological processes such as neurotransmitter release from nerve synapses and the release of hormones and messenger substances from endocrine and

exocrine glands (Zimmerberg et al. 1980a). Vesicles fusion with artificially made membranes is inspired by these elegant biological processes in nature, albeit *in vitro* model systems of vesicle fusion with model membranes are greatly simplified compared to the naturally occurring processes.

The approach of vesicle fusion with model membrane systems can be simplified to four discrete steps:

1. *Preparation of proteoliposomes.* Reconstitute the membrane protein of interest into vesicles, usually LUVs, resulting in formation of proteoliposomes (see Sect. 12.2).
2. *Establishment of a planar model membrane.* Planar lipid bilayers are typically created across a Teflon aperture and commonly by using the Müller-Rudin (Mueller and Rudin 1969) or the Montal-Müller technique (Montal and Mueller 1972).
3. *Addition of the proteoliposomes to the planar model membrane.* Aliquots of the prepared proteoliposomes are added (usually) to the *cis* side of the chamber design, which per definition consist of a *cis* and a *trans* side separated by the established membrane (Montal and Mueller 1972; Mueller and Rudin 1969).
4. *Induction of fusion of the proteoliposomes with the membrane.* There are various means to stimulate vesicles fusion with the established lipid bilayers, including creating an osmotic gradient, magnetic stirring, addition Ca^{2+} , vesicle buoyancy and LPR. This will be discussed in details below.

The reality is often more nuanced than simplified schemes and vesicle fusion with planar membranes is no exception. The fusion efficiency is often influenced by several factors that may be difficult to pinpoint. These may both be related to the applied biomimetic membrane chamber design, the stability of the established biomimetic membrane and the specific nature of the membrane protein in question.

In general, adding proteoliposomes to a pre-established lipid model membrane results in a low basal rate of fusion. Efficient reconstitution of membrane proteins into the planar membrane thus requires stimulation of the fusion rate. An efficient way to induce fusion events of vesicles to planar membranes is by creating an osmotic gradient across the membrane (Cohen et al. 1980). Creation of an osmotic gradient across the membrane may be established by addition of an osmolyte (i.e. salt or sugar) to the same side of the membrane as the vesicles (*cis* side). An effective way to do this is to add a 3 M KCl solution to the *cis* chamber side to a final concentration in the chamber of around 800–900 mM KCl (Woodbury 1999). The established osmotic gradient across the membrane is believed to result in vesicle instability which eventually causes them to burst and subsequently fuse to the planar bilayer membrane (Cohen et al. 1982; Zimmerberg et al. 1980b).

In exocytosis calcium ions play a crucial role for biological membrane fusion (Furber et al. 2009). For *in vitro* vesicle fusion to planar membranes divalent cations (i.e. Ca^{2+} , Mg^{2+} , Ba^{2+}) in millimolar concentrations have been described to enhance vesicle fusion to planar lipid bilayers in the presence of an osmotic gradient (Cohen et al. 1980). In contrast, with vesicles derived from brain syn-

Table 12.2 Dynamic light scattering measurements of initially 200 nm extruded lipid vesicles under various buffer conditions

Solution outside vesicles	Vesicle size (nm)	PDI
Phosphate buffered saline (PBS)	137 ± 2	0.11
300 mM KCl, PBS	134 ± 0	0.09
10 mM CaCl ₂ , PBS	8,253 ± 469	0.63
10 mM CaCl ₂ , 300 mM KCl, PBS	4,952 ± 2,097	1.00
17.5 wt% PEG(6,000), PBS	1,015 ± 79	0.28

Vesicles consisted of POPE:POPC:POPS:Ergosterol (2:1:1:1). Results are n=3 measurements ± standard deviation.

PDI is the polydispersity index, where in this case a value of 0 represents a monodisperse, while a value of 1 indicates a completely polydisperse solution (Ibragimova and Rein unpublished results).

apses or proteoliposomes reconstituted with Ca²⁺ binding proteins, only Ca²⁺ specifically stimulates fusion events (not Mg²⁺ or Ba²⁺) and it does so in micromolar concentrations (Zimmerberg et al. 1980b). This indicates that the effect of calcium ions on vesicle fusion events arise from protein interactions rather than lipid interactions. This also fits well with the mechanism of biological exocytosis, where the soluble *N*-ethylmaleimide sensitive factor attachment receptor (SNARE) protein complexes dock the vesicles to the plasma membrane, and a subsequent influx of Ca²⁺ triggers vesicle fusion (Carr and Munson 2007; Ungermann and Langosch 2005; Jeremic et al. 2004). However, although Ca²⁺ has an important role in biological membrane fusion, it may not necessarily be beneficial to include Ca²⁺, or other divalent cations, for that matter in model membrane systems. In this relation, Woodbury (1999) described that the vesicles may clump or fuse together prior to reaching the planar membrane, leading to suboptimal fusion conditions (Woodbury 1999). Indeed, we also noticed in our laboratory that Ca²⁺ does not necessarily stimulate vesicle fusion to planar membranes. In support of Woodbury (1999), we also find that Ca²⁺ appears to result in vesicle-vesicle fusions and formation of vesicle aggregation before reaching the planar membrane. That this is the case may be evidenced by dynamic light scattering measurements (Table 12.2). It is likely that these larger fused vesicle or vesicle aggregates loses the ability to fuse with the established planar membrane. Therefore, it is recommended to carefully test and evaluate whether including Ca²⁺ in model membrane systems are beneficial.

Poly(ethylene glycol) (PEG) has been described to stimulate vesicle-vesicle fusion (Lee and Lentz 1997; Lentz 1994). Stimulation of vesicle-bilayer fusion events have not been described in the literature. Like CaCl₂ we observed that the presence of PEG in the buffer stimulated vesicle-vesicle fusion events (Table 12.2). Again, it is likely that these larger fused vesicle or vesicle aggregates loses the ability to fuse with the established planar membrane. In relation to this it has been described that PEG-mediated vesicle fusion is favored by lipid bilayer curvature (Lentz 1994). Moreover, in vesicle-lipid bilayer fusions the buffer viscosity due to the high PEG concentration (17.5 wt%) may pose a problem.

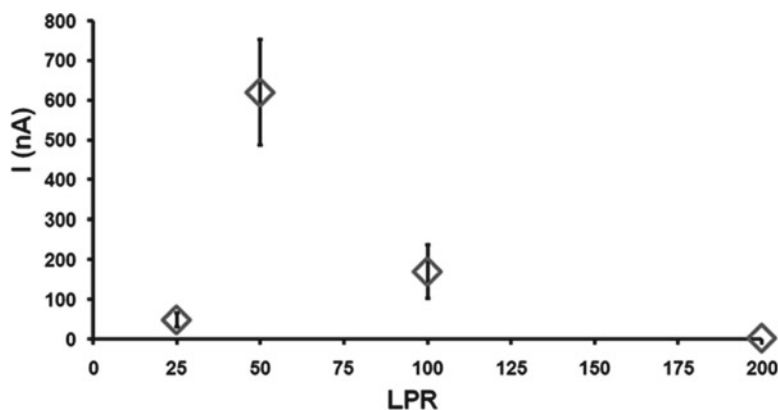


Fig. 12.1 Dependence of LPR on FomA proteoliposomes fusion with planar lipid membrane arrays. Planar lipid bilayers arrays were established as described by Hansen et al. (2009a)

Magnetic stirring of the model membrane system may be important to keep a continuous motion of the vesicles in the chamber (Woodbury 1999). This may increase the likelihood that vesicles come so close to the planar membrane that they can interact and fuse with the planar membrane.

The buoyancy of vesicles may possess a problem for obtaining optimal fusion efficiency with the planar membrane. In biological exocytosis docking of the vesicles to the plasma membrane is a crucial step for fusion, which is mediated by SNARE proteins (Carr and Munson 2007). In model membrane systems, we usually do not have SNAREs, but what we can do is altering the vesicle density. The vesicle density may be increased to ensure that the vesicles sink down to the planar membrane, thereby ensuring close proximity of the vesicles with the membrane. In principle this should be able to increase the likelihood for membrane fusion. In practice, increasing the density of vesicles may be created by encapsulating 200–300 mM of a sugar, preferably a membrane impermeant sugar such as sorbitol or mannitol, inside the vesicles. This may be done by (i) creating the vesicles in a sugar containing buffer and (ii) removing the sugar outside the vesicles. Removal of sugar outside the vesicles may essentially be done by the techniques briefly mentioned in Sect. 12.2.1 for removal of detergent during protein reconstitution into vesicles.

A factor that may also be considered for optimizing the fusion efficiency of proteoliposomes with planar membranes is the LPR of the proteoliposomes. We have found that the LPR may affect the fusion efficiency of FomA with planar membranes in a LPR dependent manner. Our results demonstrate that fusion events with planar membranes are significantly increased with decreasing LPR (200 to 50) with maximal fusion efficiency at LPR 50 (Fig. 12.1). However, with LPR 25 fusion events cease and become comparable to LPR 200. The theoretical proteoliposome coverage with FomA porins is 18, 31%, 47% and 68% for LPR values 200, 100, 50 and 25, respectively. Clearly something happens with fusion efficiency between

LPR 50 and 25, but exactly what causes the fusion efficiency to decrease is difficult to address. It may be that 68% protein coverage in the proteoliposomes is too high and this may cause or stimulate protein aggregation rather than functional protein reconstitution.

The fusion efficiency of vesicles with planar membranes is influenced by numerous factors as discussed in this section. Clearly creating an osmotic gradient across the established lipid bilayers and having magnetic stirring in the model membrane chamber design are likely the most important parameters for getting started with model membrane vesicle fusion experiments. Subsequently, factors such as including divalent cations in the model membrane buffers, increase vesicle density or adjusting the LPR may be considered to achieve optimal vesicle fusion efficiency.

12.3.2 Addressing Vesicle Fusion Events with Planar Membranes

How do we address the vesicle fusion efficiency in our model membrane system? Vesicle fusion with planar membranes is characterized by (i) the transfer of vesicular contents across the planar membrane to the *trans* chamber side and (ii) the incorporation of vesicular membrane with the planar membrane (Zimmerberg et al. 1980b). These two criteria may be utilized to create sensor systems for assessing the degree of vesicle fusion events with planar membranes.

To utilize (i) vesicles may be loaded with a fluorescent dye, which upon fusion with the planar membrane is released to the *trans* chamber and following may be quantified (e.g. by fluorescence spectroscopy or microscopy). The water soluble impermeant dye calcein is often used for these purposes. A good feature of calcein is that its fluorescence emission can be quenched, either by self-quenching at high concentrations (≥ 6 mM) or by cobalt ions. Self-quenching may be utilized by encapsulating millimolar calcein concentrations in vesicles, resulting in a low fluorescence emission yield. Upon fusion with the planar membrane calcein is released and diluted, resulting in a high fluorescence emission yield (Perin and MacDonald 1989). To utilize calcein quenching by cobalt ions, the vesicles may be encapsulated with a micromolar calcein concentration, while having cobalt ions in the *trans* chamber buffer. Upon fusion of the calcein-cobalt loaded vesicles the vesicular content is released. Cobalt effectively chelates the released calcein and quenches the fluorescence signal (Niles and Cohen 1987; Woodbury and Hall 1988a, b). Alternatively, ethylenediaminetetraacetic acid (EDTA) which is a divalent cation chelating agent may be applied to chelate cobalt. The assay could then be designed to encapsulate saturating amounts of cobalt with calcein to create fluorescently quenched calcein-cobalt complexes in vesicles (Kendall and MacDonald 1982). Having included EDTA in the *trans* chamber buffer, results in chelation of cobalt upon release of the calcein-cobalt complexes by vesicle fusion, yielding fluorescent calcein (Kendall and MacDonald 1982).

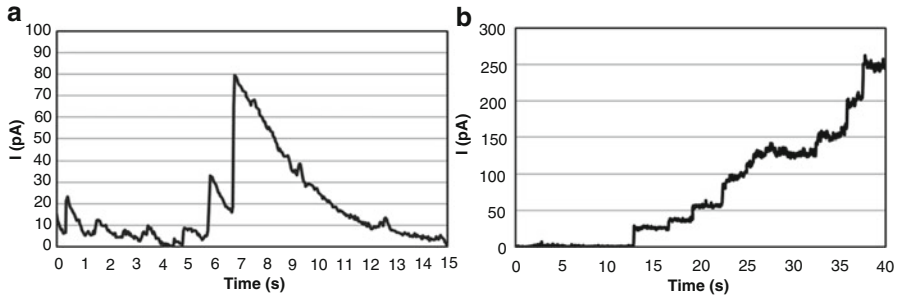


Fig. 12.2 Vesicle fusion with N/E vesicles and FomA proteoliposomes. (a) Current trace of N/E vesicle fusion activity. (b) Current trace of FomA proteoliposomes vesicle fusion. Measurements were carried out using voltage clamp technique

There are several ways to utilize (ii) the incorporation of vesicular membrane with the planar membrane upon membrane fusion:

- *Fluorescent tracer fusion assay.* Fluorescence may be used to label the receiving planar lipid membrane, say green fluorescence, while having a different fluorescence label, say red fluorescence, of the lipid vesicles or a labeled protein reconstituted into the fusiogenic vesicles. In this case vesicle fusion will result in incorporation of the red fluorescent dye of the vesicles or of the labeled proteins reconstituted in the vesicles, respectively, into the planar fluorescently green membrane (Ganesan and Boxer 2009).
- *Nystatin/ergosterol fusion activity assay.* The Nystatin/ergosterol (N/E) fusion activity assay is a very neat way to assess vesicle fusion activity (Woodbury and Miller 1990). Nystatin is a pore-forming antibiotic, which binds to ergosterol and when the ergosterol concentration is high enough, ten nystatin monomers associate to form a membrane pore (Woodbury 1999). If vesicles are prepared to include both nystatin and ergosterol, the nystatin molecules form functional pores in the lipid vesicles. When the N/E vesicles fuse with the planar membrane functional nystatin pores is being transferred to the planar membrane. The nystatin pore conductance can be measured shortly, because the ergosterol will diffuse into the planar membrane, which in turn causes the nystatin to dissociate into monomers and the nystatin becomes nonfunctional (Woodbury and Miller 1990). In conductance measurements the fusion event of N/E vesicles will be seen as a “current spike” in voltage clamp measurements (Fig. 12.2a). The number of “spikes” per time can be seen as a measure of fusion efficiency. The advantage of this assay is that it can co-include a membrane protein of interest (Woodbury 1999; Zagnoni et al. 2007). Since the nystatin becomes nonfunctional upon fusion to the planar membrane most measurements of reconstituted membrane protein using N/E vesicles will not be affected by the presence of nystatin. A disadvantage may be that care has to be taken for interpretation of the N/E fusion events, since it can be hampered by air bubbles that may arise during formation

of the planar membrane. If an entrapped air bubble burst in the membrane this may be misinterpreted as a fusion event (our unpublished data). Another disadvantage may also be that the amount of molecules loaded into the planar membrane cannot be directly determined – it only shows if fusion has taken place. To get started with the vesicle N/E fusion activity assay we recommend reading the review by Dixon J. Woodbury (1999) on this topic (Woodbury 1999)

- *Outer membrane porin fusion efficiency assay.* A reporter membrane protein may be used to address the amount of protein that can be reconstituted into a model membrane system with vesicle fusion. As stated in the beginning of Sect. 12.3 several *E. coli* outer membrane porins may be reconstituted into planar membranes directly from a detergent solubilized state. However, they may also be reconstituted into vesicles. Many of these β -barrel proteins have a specific conductance that is well-characterized. Thus, outer membrane porin proteoliposomes may conveniently be used to address fusion efficiency with a model membrane system. The voltage dependent anion channel (VDAC) has in the literature been used as a reporter for vesicle fusion activity with planar membranes (Cohen et al. 1980). In our laboratory we use the trimeric FomA as reporter for vesicle fusion efficiency with planar membranes (Fig. 12.2b). In the following we use FomA as example. In voltage clamp measurements FomA porin has a single channel current value of approximately 15 pA in 1.0 M KCl saline solution with an applied potential of ± 60 mV (Kleivdal et al. 1995; Pocanschi et al. 2006). Thus, reconstitution of a single functional FomA porin gives rise to a current increase of approximately 15 pA (Fig. 12.3b). Incorporation of multiple FomA porins is seen as a “ladder-like” increase in the current trace (Fig. 12.2b). Since the current value for a single functional FomA porin is known (15 pA) we can calculate how many porins that reconstituted with the planar model membrane during vesicle fusion. For further details about voltage clamp measurements we refer to Perry et al. (2009).

In summary, transfer of vesicular content following vesicle fusion may be used as a measure of whether vesicle fusion takes place. The fluorescence calcein assay is an example of a way to address vesicle fusion by measuring the amount of fluorescent molecules released to the trans chamber side. Fluorescence may also be utilized to address transfer of vesicular membrane to the planar membrane, which occurs during membrane fusion. Fluorescent labels may be positioned in the membranes and/or on the membrane protein of interest. Voltage clamp measurements of fusion of N/E vesicles with planar membranes may be utilized to address vesicle fusion activity, whereas reconstitution of outer membrane porin(s) may be used to address vesicle fusion efficiency.

12.3.3 Direct Incorporation into Planar Membranes

A novel strategy for reconstituting membrane proteins into planar membranes is by direct incorporation, which refers to reconstitution of membrane proteins

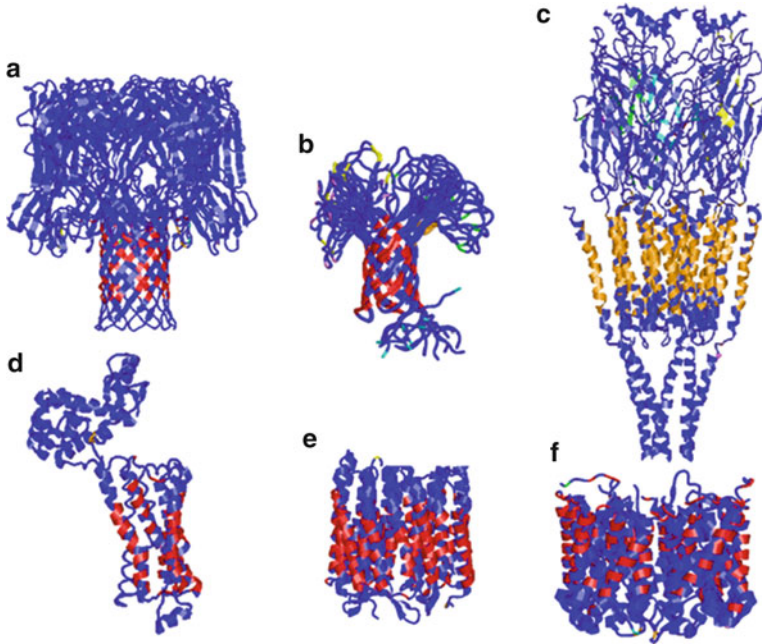


Fig. 12.3 Hydrophobic and hydrophilic regions of membrane protein surfaces. The extracellular domains of membrane proteins vary. Examples shown are (a) α -hemolysin, (b) outer membrane porin A (*OmpA*), (c) Nicotinic acetylcholine receptor, (d) human B_2 -adrenergic G-protein coupled receptor, (e) Bacteriorhodopsin and (f) Spinach aquaporin SoPIP2;1. Analysis of lipid interaction patches (hydrophobicity) was carried out using HotPatch statistical analysis. It is an algorithm-based program for the analysis of protein surface patches (Pettit et al. 2007). Identified (individual) hydrophobic protein surface patches are shown as red, orange, yellow and green, respectively, while blue correspond to hydrophilic surface regions

simultaneously with establishing the planar model membrane. Although, a general methodology for direct reconstitution would potentially revolutionize the field of biomimetic membrane research, only a few reports have dealt with the topic of direct reconstitution. Here we will describe the practical approach of direct incorporation described for bacteriorhodopsin (BR) and the nicotinic acetylcholine receptor, respectively, and use these examples to discuss some of the considerations and concerns of this strategy of reconstituting membrane proteins.

A clear advantage of the direct incorporation approach is that the LPR, and thereby also the amount of the protein reconstituted into the model membrane, may be precisely controlled. The ability to incorporate large quantities of protein into model membranes may especially be important for using planar protein-based biomimetic membranes for separation techniques, such as water purification through aquaporin water channel-based biomimetic membranes (Nielsen 2009).

Bamberg et al. (1981) reported successful direct reconstitution of the proton-pump BR from a proteo–lipid solvent–containing solution (Bamberg et al. 1981).

The approach was to solubilize BR purple membranes in an aqueous solution and then transfer the protein into an asolectin/*n*-alkane (e.g. *n*-decane) lipid bilayer forming solution. The methodology was to add 100 μL of the BR solution (10 mg/ml) to a 1 ml asolectin/*n*-decane solution (50 mg/ml). The sample was then sonicated and the suspension was subsequently added successive aliquots of CaCl_2 (100 μL , 0.1 M) until a clear purple BR apolar phase developed. The clear purple apolar phase was then used to successfully create a BR-based lipid bilayer membrane while maintaining the functionality of the protein (Bamberg et al. 1981). It should be noted however, that BR as lyophilized purple membranes can be solubilized in aqueous solutions without the use of detergent. This makes BR a somewhat special case that is not general for most other membrane proteins.

Beddow et al. (2004) reported a similar approach to functionally reconstitute nicotinic acetylcholine receptors into lipid bilayer model membranes (Beddow et al. 2004). The main differences were that the bilayer forming solution consisted of glycerol monooleate and *n*-hexane, the receptor extracts were prepared as vesicles and the bilayer forming solution was emulsified with receptor extract without using CaCl_2 (Beddow et al. 2004).

Membrane proteins are generally delicate structures, especially α -helical proteins whereas β -barrel proteins often are somewhat more stable. A concern for the transfer of membrane protein to a solvent containing lipid phase is that the protein structure and function will be affected by the solvent. Several reports have described that membrane proteins can be extracted in a functional state by harsh solvents such as diethyl ether, toluene or chloroform/methanol/water mixtures (Ayala et al. 1985, 1986; Dmitriev et al. 2004; Reiken et al. 1996). However, it is difficult to predict the long term effects of solvent exposure on protein structure and function. In this context protein functionality has been shown to be affected considerably by solvent exposure and to decrease in a time-dependent manner (Ayala et al. 1985; Beddow et al. 2004).

To circumvent the potential deleterious effects of solvent on membrane protein structure and function it may be considered to use a less harmful solvent in the bilayer forming solution. Solventless bilayer forming solutions using squalene, a naturally derived oil, as substitute for *n*-alkanes have been described for formation of planar lipid bilayers (White 1978).

A major issue to be solved for creating a successful general formulation for direct protein incorporation is to make an amphiphilic bilayer forming solution that is sufficiently polar to shield and protect the hydrophilic residues of membrane proteins, while at the same time being hydrophobic enough to make a homogeneous solution that can shield the hydrophobic membrane protein regions (Fig. 12.3). In Sect. 12.2.2 we discussed considerations of hydrophobic matching lipid species to the protein hydrophobic regions for protein reconstitution in vesicles. The same considerations also apply for matching the hydrophobic regions of the protein in a direct protein incorporation formulation.

A likely more demanding challenge is to create an amphiphilic bilayer forming solution that sufficiently shield the hydrophilic protein regions, since the extent of the hydrophilic regions varies considerably among membrane proteins (Fig. 12.3).

For direct protein incorporation it would be advantageous to be able to transfer the protein directly from a detergent-solubilized state to the bilayer forming solution. This may be carried out by the use of hydrophobic absorption polymer beads (such as Bio-Beads SM absorbents or similar). In this approach an appropriate amount of the absorption beads (e.g. matching the amount of detergent to be removed) is included to the protein/lipid/solvent dispersion. By placing the protein-lipid dispersion with Bio-Beads end-over-end rotation at 4°C over night the protein is transferred to the apolar phase while removing the detergent. Using this approach we have been able to create lipid bilayers reconstituted with spinach aquaporin SoPIP2;1 (our unpublished results). If the detergent was not sufficiently removed during the described procedure it would not be possible to create sealed lipid bilayers.

Direct protein incorporation would be a powerful tool to reconstitute large quantities of membrane protein into model membranes. In this light it is surprising that there are still very limited reports on this subject. Major contributions to biomimetic membrane research may be envisaged provided that attention is directed towards the topic of direct protein incorporation.

12.4 Requirements for Protein Reconstitution Yield

The planar membrane design for protein reconstitution may be suitable for sensor and separation technologies. The protein reconstitution yield into model membrane is almost never addressed, but it makes good sense to include protein reconstitution yield as a biomimetic membrane design criteria. The requirements of the amount of protein to be reconstituted for the different applications may not be the same. Considerations of the protein reconstitution methodology to apply may therefore be of importance in the design criteria for the biomimetic membrane application in question. For sensor applications the reconstitution yield may not be that important per se, instead it may be more important to have an optimized reliable and reproducible protein reconstitution protocol. Sensitive sensor designs may be created with a reasonable low amount of functionally reconstituted protein. Here vesicle fusion with planar membranes may be considered as a first choice reconstitution method.

The maximum protein reconstitution yield that can be reached with vesicle fusion is rather low. Using the outer membrane porin fusion efficiency assay, Cohen et al. (1980) showed that the fusion efficiency that could be reached was approximately 513 porin insertions in 10 min into a single bilayer suspended across a 1-mm² aperture (Cohen et al. 1980). We have addressed the maximum vesicle fusion efficiency of a membrane array consisting of 8×8 apertures with an average aperture diameter of 300 μm. Here the maximal fusion efficiency was approx. 147,600 porin insertions during the vesicle fusion experiment. Although this sounds as a high

number of protein insertions it corresponds to less than 1% of the total effective membrane area. While this protein reconstitution yield may be sufficient for designing sensor based assays, it is clearly insufficient to create novel separation technologies based on membrane proteins. Alternative methods for reconstitution membrane proteins in high yield need to be sought. Direct protein reconstitution may be the novel strategy to consider for obtaining a high protein reconstitution yield into biomimetic membranes. Since the protein and lipid are simultaneously included in a combined bilayer forming solution prior to establishing the biomimetic membranes it may be possible to control the LPR. Thereby it should also be possible to control the amount of protein reconstituted into biomimetic membranes per se.

12.5 Perspectives

To summarize, the following key elements in protein reconstitution should be considered to create novel sensor and separation technologies based on membrane proteins:

- Protein reconstitution into vesicles is the conventional strategy in membrane protein biomimetic designs.
- Proteoliposomes may be applied directly in protein analytical methods or may be further used to reconstitute membrane proteins into planar membrane designs.
- Fluorescence assays, N/E vesicle fusion activity assay or outer membrane porin fusion efficiency assay may be applied to evaluate and optimize protein reconstitution into planar model membranes.
- Direct membrane protein reconstitution may represent a novel strategy to reconstitute large amounts of protein into planar model membranes.
- In both conventional and novel protein reconstitution strategies the LPR and hydrophobic matching of the protein hydrophobic regions to the model membrane hydrophobic regions are crucial considerations for optimal and functional protein reconstitution.
- Reconstitution yield should be included as a biomimetic membrane design criteria.
- Proteoliposomes fusion with planar membrane may be applied for the creation of novel protein biosensor and drug–screening applications.
- Proteoliposomes fusion efficiency is likely insufficient to support fabrication of large scale separation technologies based on membrane protein function. Here alternative protein reconstitution strategies need to be explored. Direct protein reconstitution may be a promising approach; albeit technical advances in this protein reconstitution strategy is required.

Acknowledgments We thank the Danish National Advanced Technology Foundation for financial support.

References

- Angelova, M.I., Soleau, S., Melerd, P., Faucon, J.F., Bothorel, P.: Preparation of giant vesicles by external AC electric fields. Kinetics and applications. *Prog. Colloid Polym. Sci.* **89**, 127–131 (1992)
- Arora, A., Rinehart, D., Szabo, G., Tamm, L.K.: Refolded outer membrane protein A of *Escherichia coli* forms ion channels with two conductance states in planar lipid bilayers. *J. Biol. Chem.* **275**, 1594–1600 (2000)
- Ayala, G., Nascimento, A., Gomez-Puyou, A., Darszon, A.: Extraction of mitochondrial membrane proteins into organic solvents in a functional state. *Biochim. Biophys. Acta* **810**, 115–122 (1985)
- Ayala, G., de Gomez-Puyou, M.T., Gomez-Puyou, A., Darszon, A.: Thermostability of membrane systems in organic solvents. *FEBS Lett.* **203**, 41–43 (1986)
- Bamberg, E., Dencher, N.A., Fahr, A., Heyn, M.P.: Transmembranous incorporation of photoelectrically active bacteriorhodopsin in planar lipid bilayers. *Proc. Natl. Acad. Sci. U.S.A.* **78**, 7502–7506 (1981)
- Beddow, J.A., Peterson, I.R., Heptinstall, J., Walton, D.J.: Reconstitution of nicotinic acetylcholine receptors into gel-protected lipid membranes. *Anal. Chem.* **76**, 2261–2265 (2004)
- Booth, P.J.: Sane in the membrane: designing systems to modulate membrane proteins. *Curr. Opin. Struct. Biol.* **15**, 435–440 (2005)
- Buzhynskyy, N., Girmens, J.F., Faigle, W., Scheuring, S.: Human cataract lens membrane at subnanometer resolution. *J. Mol. Biol.* **374**, 162–169 (2007a)
- Buzhynskyy, N., Hite, R.K., Walz, T., Scheuring, S.: The supramolecular architecture of junctional microdomains in native lens membranes. *EMBO Rep.* **8**, 51–55 (2007b)
- Carr, C.M., Munson, M.: Tag team action at the synapse. *EMBO Rep.* **8**, 834–838 (2007)
- Castellana, E.T., Cremer, P.S.: Solid supported lipid bilayers: from biophysical studies to sensor design. *Surf. Sci. Rep.* **61**, 429–444 (2006)
- Cohen, F.S., Zimmerberg, J., Finkelstein, A.: Fusion of phospholipid vesicles with planar phospholipid bilayer membranes. II. Incorporation of a vesicular membrane marker into the planar membrane. *J. Gen. Physiol.* **75**, 251–270 (1980)
- Cohen, F.S., Akabas, M.H., Finkelstein, A.: Osmotic swelling of phospholipid vesicles causes them to fuse with a planar phospholipid bilayer membrane. *Science* **217**, 458–460 (1982)
- Curstedt, T., Johansson, J., Barros-Soderling, J., Robertson, B., Nilsson, G., Westberg, M., Jornvall, H.: Low-molecular-mass surfactant protein type 1. The primary structure of a hydrophobic 8-kDa polypeptide with eight half-cystine residues. *Eur. J. Biochem.* **172**, 521–525 (1988)
- Deamer, D.W., Uster, P.S.: Liposome preparation: methods and mechanism. In: Ostro, M.J. (ed.) *Liposomes*, pp. 27–51. Marcel Dekker, New York (1983)
- Dmitriev, O.Y., Altendorf, K., Fillingame, R.H.: Subunit A of the *E. coli* ATP synthase: reconstitution and high resolution NMR with protein purified in a mixed polarity solvent. *FEBS Lett.* **556**, 35–38 (2004)
- Fang, Y., Frutos, A.G., Lahiri, J.: Membrane protein microarrays. *J. Am. Chem. Soc.* **124**, 2394–2395 (2002)
- Fang, Y., Lahiri, J., Picard, L.: G protein-coupled receptor microarrays for drug discovery. *Drug Discov. Today* **8**, 755–761 (2003)
- Fang, Y., Hong, Y., Webb, B., Lahiri, J.: Applications of biomembranes in drug discovery. *MRS Bull.* **31**, 5 (2006)
- Feitosa, E., Barreleiro, P.C., Olofsson, G.: Phase transition in dioctadecyldimethylammonium bromide and chloride vesicles prepared by different methods. *Chem. Phys. Lipids* **105**, 201–213 (2000)
- Fendler, H.: Atomic and molecular clusters in membrane mimetic chemistry. *Chem. Rev.* **87**, 877–899 (1987)
- Furber, K.L., Churchward, M.A., Rogasevskaia, T.P., Coorsen, J.R.: Identifying critical components of native Ca²⁺-triggered membrane fusion. Integrating studies of proteins and lipids. *Ann. N. Y. Acad. Sci.* **1152**, 121–134 (2009)

- Gabriel, N.E., Roberts, M.F.: Spontaneous formation of stable unilamellar vesicles. *Biochemistry* **23**, 4011–4015 (1984)
- Ganesan, P.V., Boxer, S.G.: A membrane interferometer. *Proc. Natl. Acad. Sci. U.S.A.* **106**, 5627–5632 (2009)
- Goennenwein, S., Tanaka, M., Hu, B., Moroder, L., Sackmann, E.: Functional incorporation of integrins into solid supported membranes on ultrathin films of cellulose: impact on adhesion. *Biophys. J.* **85**, 646–655 (2003)
- Hansen, J.S., Perry, M., Vogel, J., Groth, J.S., Vissing, T., Larsen, M.S., Geschke, O., Emneus, J., Bohr, H., Nielsen, C.H.: Large scale biomimetic membrane arrays. *Anal. Bioanal. Chem.* **395**, 719–727 (2009a)
- Hansen, J.S., Perry, M., Vogel, J., Vissing, T., Hansen, C.R., Geschke, O., Emneus, J., Nielsen, C.H.: Development of an automation technique for the establishment of functional lipid bilayer arrays. *J. Micromech. Microeng.* **19**, 025014 (2009b)
- Hemmler, R., Bose, G., Wagner, R., Peters, R.: Nanopore unitary permeability measured by electrochemical and optical single transporter recording. *Biophys. J.* **88**, 4000–4007 (2005)
- Hong, H., Joh, N.H., Bowie, J.U., Tamm, L.K.: Methods for measuring the thermodynamic stability of membrane proteins. *Methods Enzymol.* **455**, 213–236 (2009)
- Janshoff, A., Steinem, C.: Transport across artificial membranes-an analytical perspective. *Anal. Bioanal. Chem.* **385**, 433–451 (2006)
- Jeremic, A., Kelly, M., Cho, J.A., Cho, S.J., Horber, J.K., Jena, B.P.: Calcium drives fusion of SNARE-apposed bilayers. *Cell Biol. Int.* **28**, 19–31 (2004)
- Joannic, R., Auvray, L., Lasic, D.D.: Monodisperse vesicles stabilized by grafted polymers. *Phys. Rev. Lett.* **78**, 3402–3405 (1997)
- Johansson, J., Curstedt, T., Robertson, B., Jornvall, H.: Size and structure of the hydrophobic low molecular weight surfactant-associated polypeptide. *Biochemistry* **27**, 3544–3547 (1988)
- Kendall, D.A., MacDonald, R.C.: A fluorescence assay to monitor vesicle fusion and lysis. *J. Biol. Chem.* **257**, 13892–13895 (1982)
- Kleivdal, H., Benz, R., Jensen, H.B.: The *Fusobacterium nucleatum* major outer-membrane protein (FomA) forms trimeric, water-filled channels in lipid bilayer membranes. *Eur. J. Biochem.* **233**, 310–316 (1995)
- le Maire, M., Champeil, P., Møller, J.V.: Interaction of membrane proteins and lipids with solubilizing detergents. *Biochim. Biophys. Acta Rev. Biomembr.* **1508**, 86–111 (2000)
- Le Piouffe, B., Suzuki, H., Tabata, K.V., Noji, H., Takeuchi, S.: Lipid bilayer microarray for parallel recording of transmembrane ion currents. *Anal. Chem.* **80**, 328–332 (2008)
- Lee, J., Lentz, B.R.: Evolution of lipidic structures during model membrane fusion and the relation of this process to cell membrane fusion. *Biochemistry* **36**, 6251–6259 (1997)
- Lentz, B.R.: Polymer-induced membrane fusion: potential mechanism and relation to cell fusion events. *Chem. Phys. Lipids* **73**, 91–106 (1994)
- Lorenceau, E., Utada, A.S., Link, D.R., Cristobal, G., Joanicot, M., Weitz, D.A.: Generation of polyerosomes from double-emulsions. *Langmuir* **21**, 9183–9186 (2005)
- Maguire, L.A., Zhang, H., Shamlou, P.A.: Preparation of small unilamellar vesicles (SUV) and biophysical characterization of their complexes with poly-L-lysine-condensed plasmid DNA. *Biotechnol. Appl. Biochem.* **37**, 73–81 (2003)
- Majd, S., Mayer, M.: Generating arrays with high content and minimal consumption of functional membrane proteins. *J. Am. Chem. Soc.* **130**, 16060–16064 (2008)
- Mitra, K., Ubarretxena-Belandia, I., Taguchi, T., Warren, G., Engelman, D.M.: Modulation of the bilayer thickness of exocytic pathway membranes by membrane proteins rather than cholesterol. *Proc. Natl. Acad. Sci. U.S.A.* **101**, 4083–4088 (2004)
- Montal, M., Mueller, P.: Formation of bimolecular membranes from lipid monolayers and a study of their electrical properties. *Proc. Natl. Acad. Sci. U.S.A.* **69**, 3561–3566 (1972)
- Mouritsen, O.G., Zuckermann, M.J.: What's so special about cholesterol? *Lipids* **39**, 1101–1113 (2004)
- Mueller, P., Rudin, D.O.: Translocators in bimolecular lipid membranes: their role in dissipative and conservative bioenergetic transduction. *Curr. Top. Bioenerg.* **3**, 157–249 (1969)

- Nielsen, C.H.: Biomimetic membranes for sensor and separation applications. *Anal. Bioanal. Chem.* **395**, 697–718 (2009)
- Niles, W.D., Cohen, F.S.: Video fluorescence microscopy studies of phospholipid vesicle fusion with a planar phospholipid membrane. Nature of membrane-membrane interactions and detection of release of contents. *J. Gen. Physiol.* **90**, 703–735 (1987)
- Ollivon, M., Lesieur, S., Grabielle-Madelmont, C., Paternostre, M.: Vesicle reconstitution from lipid-detergent mixed micelles. *Biochim. Biophys. Acta* **1508**, 34–50 (2000)
- Opekarova, M., Tanner, W.: Specific lipid requirements of membrane proteins—a putative bottleneck in heterologous expression. *Biochim. Biophys. Acta* **1610**, 11–22 (2003)
- Osborne, A.R., Rapoport, T.A., van den Berg, B.: Protein translocation by the Sec61/SecY channel. *Annu. Rev. Cell Dev. Biol.* **21**, 529–550 (2005)
- Paternostre, M.T., Roux, M., Rigaud, J.L.: Mechanisms of membrane protein insertion into liposomes during reconstitution procedures involving the use of detergents. 1. Solubilization of large unilamellar liposomes (prepared by reverse-phase evaporation) by triton X-100, octyl glucoside, and sodium cholate. *Biochemistry* **27**, 2668–2677 (1988)
- Perin, M.S., MacDonald, R.C.: Fusion of synaptic vesicle membranes with planar bilayer membranes. *Biophys. J.* **55**, 973–986 (1989)
- Perry, M., Vissing, T., Boesen, T.P., Hansen, J.S., Emneus, J., Nielsen, C.H.: Automated sampling and data processing derived from biomimetic membranes. *Bioinspir. Biomim.* **4**, 044001 (2009)
- Petrache, H.I., Dodd, S.W., Brown, M.F.: Area per lipid and acyl length distributions in fluid phosphatidylcholines determined by (2)H NMR spectroscopy. *Biophys. J.* **79**, 3172–3192 (2000)
- Pettit, F.K., Bare, E., Tsai, A., Bowie, J.U.: HotPatch: a statistical approach to finding biologically relevant features on protein surfaces. *J. Mol. Biol.* **369**, 863–879 (2007)
- Pocanschi, C.L., Apell, H.J., Puntervoll, P., Hogh, B., Jensen, H.B., Welte, W., Kleinschmidt, J.H.: The major outer membrane protein of *Fusobacterium nucleatum* (FomA) folds and inserts into lipid bilayers via parallel folding pathways. *J. Mol. Biol.* **355**, 548–561 (2006)
- Rastogi, R., Anand, S., Koul, V.: Flexible polymerosomes—an alternative vehicle for topical delivery. *Colloids Surf. B Biointerfaces* **72**, 161–166 (2009)
- Rawicz, W., Olbrich, K.C., McIntosh, T., Needham, D., Evans, E.: Effect of chain length and unsaturation on elasticity of lipid bilayers. *Biophys. J.* **79**, 328–339 (2000)
- Reiken, S.R., Van Wie, B.J., Sutisna, H.: Bispecific antibody modification of nicotinic acetylcholine receptors for biosensing. *Biosens. Bioelectron.* **11**, 91–102 (1996)
- Rigaud, J.L., Paternostre, M.T., Bluzat, A.: Mechanisms of membrane protein insertion into liposomes during reconstitution procedures involving the use of detergents. 2. Incorporation of the light-driven proton pump bacteriorhodopsin. *Biochemistry* **27**, 2677–2688 (1988)
- Rosenkranz, T., Katranidis, A., Atta, D., Gregor, I., Enderlein, J., Grzelakowski, M., Rigler, P., Meier, W., Fitter, J.: Observing proteins as single molecules encapsulated in surface-tethered polymeric nanocontainers. *ChemBiochem* **10**, 702–709 (2009)
- Samatey, F.A., Xu, C., Popot, J.L.: On the distribution of amino acid residues in transmembrane alpha-helix bundles. *Proc. Natl. Acad. Sci. U.S.A.* **92**, 4577–4581 (1995)
- Schmitt, E.K., Vroenenraets, M., Steinem, C.: Channel activity of OmpF monitored in nano-BLMs. *Biophys. J.* **91**, 2163–2171 (2006)
- Seddon, A.M., Curnow, P., Booth, P.J.: Membrane proteins, lipids and detergents: not just a soap opera. *Biochim. Biophys. Acta* **1666**, 105–117 (2004)
- Silvius, J.R.: Solubilization and functional reconstitution of biomembrane components. *Annu. Rev. Biophys. Biomol. Struct.* **21**, 323–348 (1992)
- Singer, M.A., Finegold, L., Rochon, P., Racey, T.J.: The formation of multilamellar vesicles from saturated phosphatidylcholines and phosphatidylethanolamines: morphology and quasi-elastic light scattering measurements. *Chem. Phys. Lipids* **54**, 131–146 (1990)
- Suzuki, H., Tabata, K.V., Noji, H., Takeuchi, S.: Electrophysiological recordings of single ion channels in planar lipid bilayers using a polymethyl methacrylate microfluidic chip. *Biosens. Bioelectron.* **22**, 1111–1115 (2007)

- Suzuki, H., Le Pioufle, B., Takeuchi, S.: Ninety-six-well planar lipid bilayer chip for ion channel recording fabricated by hybrid stereolithography. *Biomed. Microdevices* **11**, 17–22 (2009)
- Szoka Jr., F., Papahadjopoulos, D.: Comparative properties and methods of preparation of lipid vesicles (liposomes). *Annu. Rev. Biophys. Bioeng.* **9**, 467–508 (1980)
- Tornroth-Horsefield, S., Wang, Y., Hedfalk, K., Johanson, U., Karlsson, M., Tajkhorshid, E., Neutze, R., Kjellbom, P.: Structural mechanism of plant aquaporin gating. *Nature* **439**, 688–694 (2006)
- Ungermann, C., Langosch, D.: Functions of SNAREs in intracellular membrane fusion and lipid bilayer mixing. *J. Cell Sci.* **118**, 3819–3828 (2005)
- Van den Berg, B., Clemons Jr., W.M., Collinson, I., Modis, Y., Hartmann, E., Harrison, S.C., Rapoport, T.A.: X-ray structure of a protein-conducting channel. *Nature* **427**, 36–44 (2004)
- White, S.H.: Formation of “solvent-free” black lipid bilayer membranes from glyceryl monooleate dispersed in squalene. *Biophys. J.* **23**, 337–347 (1978)
- Wilburn, J.P., Wright, D.W., Cliffel, D.E.: Imaging of voltage-gated alamethicin pores in a reconstituted bilayer lipid membrane via scanning electrochemical microscopy. *Analyst* **131**, 311–316 (2006)
- Woodbury, D.J.: Nystatin/ergosterol method for reconstituting ion channels into planar lipid bilayers. *Methods Enzymol.* **294**, 319–339 (1999)
- Woodbury, D.J., Hall, J.E.: Role of channels in the fusion of vesicles with a planar bilayer. *Biophys. J.* **54**, 1053–1063 (1988a)
- Woodbury, D.J., Hall, J.E.: Vesicle-membrane fusion. Observation of simultaneous membrane incorporation and content release. *Biophys. J.* **54**, 345–349 (1988b)
- Woodbury, D.J., Miller, C.: Nystatin-induced liposome fusion. A versatile approach to ion channel reconstitution into planar bilayers. *Biophys. J.* **58**, 833–839 (1990)
- Yoshikawa, W., Akutsu, H., Kyogoku, Y.: Light-scattering properties of osmotically active liposomes. *Biochim. Biophys. Acta* **735**, 397–406 (1983)
- Zagnoni, M., Sandison, M.E., Marius, P., Lee, A.G., Morgan, H.: Controlled delivery of proteins into bilayer lipid membranes on chip. *Lab Chip* **7**, 1176–1183 (2007)
- Zimmerberg, J., Cohen, F.S., Finkelstein, A.: Fusion of phospholipid vesicles with planar phospholipid bilayer membranes. I. Discharge of vesicular contents across the planar membrane. *J. Gen. Physiol.* **75**, 241–250 (1980a)
- Zimmerberg, J., Cohen, F.S., Finkelstein, A.: Micromolar Ca^{2+} stimulates fusion of lipid vesicles with planar bilayers containing a calcium-binding protein. *Science* **210**, 906–908 (1980b)

Chapter 13

Microfluidic Encapsulation of Biomimetic Membranes

Oliver Geschke

Abstract This chapter introduces the basic theory necessary needed for designing microfluidic problems. As an example, the flow resistance will be calculated in dependence of geometrical factors and the Reynolds Number will be introduced. Following a short excursion into current polymer microfabrication techniques, the challenges in constructing a biomimetic membrane device will be discussed based on an chamber for automatic microfluidic membrane formation.

13.1 Introduction

In the previous chapters the intricacies of membrane technology, transmembrane proteins reconstitution and biomimetic membrane construction have been discussed in detail. In order to make use of biomimetic systems as technological devices we need to interface the nanoscale world of proteins in membranes with our everyday world. For example a biomimetic membrane for sensing or separation will need some sort of plumbing in the sense, that fluids must be brought to and (in the case of separation) also across the membrane. Here, microfluidics presents several options and in this Chapter I will introduce to the fascinating world of microfluidic systems, how they can be set up, and how they can be a useful tool in biomimetic membrane design.

Is there any difference between normal plumbing and microfluidics apart from the size of the items? The short answer is: yes! Shrinking systems down to micrometer scale makes actually a very big difference – not only in terms of costs but also in the flow behavior. Whereas in a macroscopic system two fluids are mixed immediately, a microsystem exposes a totally different behavior.

O. Geschke (✉)

Aquaporin A/S, Ole Maaløes Vej 3, DK-2200, Copenhagen, Denmark
e-mail: oge@aquaporin.dk

Every day life experience from macrosystems tells us, that for instance a conventional shower head, that is connected to a hot and a cold water pipe gives us a convenient shower temperature somewhere between the extreme temperatures, depending on the mixing ratio of cold and hot water. If we now try to manufacture a miniaturized shower head – let us say we produce a toy showerhead for ants and connect it with small capillary tubes to hot and cold water, we probably experience a slightly different situation: The water at the shower head will be as hot as it comes from the hot pipe on one side of the shower head and on the other side, cold water from the cold pipe will run out. Changing the mixing ratio will just change the amount of hot and cold water jets exiting this miniaturized shower head. How can this happen? I will try to give an answer in the following sections without using too much of mathematical formulas.

13.2 Theoretical Background of Microfluidics

How can our miniaturized shower head act so differently from our macroscopic daily experience? This has to do with the basic law of (micro)fluidics – the Navier-Stokes equation, named after Claude-Louis Navier and George Gabriel Stokes, see also Chap. 8. The basic idea behind this equation is based on Newton’s second law: the conservation of momentum, often alongside with mass and energy conservation can be written for an arbitrary portion of a fluid as:

$$\rho \left(\frac{\partial \mathbf{v}}{\partial t} + \mathbf{v} \cdot \nabla \mathbf{v} \right) = -\nabla p + \nabla \cdot \mathbf{T} + \mathbf{f} \tag{13.1}$$

where \mathbf{v} is the flow velocity, ρ is the fluid density, p is the pressure, \mathbf{T} is the (deviatoric) stress tensor, and \mathbf{f} represents body forces (per unit volume) acting on the fluid. If we consider an incompressible, Newtonian fluid such as water, the Navier-Stokes equation can be simplified to

$$\rho \left(\frac{\partial \mathbf{v}}{\partial t} + \mathbf{v} \cdot \nabla \mathbf{v} \right) = -\nabla p + \mu \nabla^2 \mathbf{v} + \mathbf{f} \tag{13.2}$$

The shear stress term $\nabla \cdot \mathbf{T}$ becomes the useful quantity $\mu \nabla^2 \mathbf{v}$ when we introduce the dynamic viscosity μ .

In other words, the different terms in Eq. 13.2 can be regarded as a connection between inertial forces and viscous forces:

$$\rho \left[\underbrace{\frac{\partial \mathbf{v}}{\partial t}}_{\text{Unsteady acceleration}} + \underbrace{\mathbf{v} \cdot \nabla \mathbf{v}}_{\text{Convective acceleration}} \right] = \underbrace{-\nabla p}_{\text{Pressure gradient}} + \underbrace{\mu \nabla^2 \mathbf{v}}_{\text{Viscosity}} + \underbrace{\mathbf{f}}_{\text{Other body forces}} \tag{13.3}$$

Equation 13.1 however is difficult to solve exactly and it is not within the scope of this chapter to provide a lot of mathematical derivations. As Albert Einstein wrote

in a private letter to Barbara Lee Wilson in January 1943, “*Do not worry about your difficulties in Mathematics. I can assure you mine are still greater*”. (Bucky and Weakland 1993) The reader is referred to an excellent theoretical and mathematical approach in (Bruus 2007). A recent article on transit times in turbulent flows can be found in (Pecseli and Trulsen 2010).

There are, however, a couple of other well known equations derived from the Navier-Stokes equation by using reasonable assumptions and simplifications. This includes for instance a very practical equation: The Hagen-Poiseuille equation. This gives us a relation between a fluidic resistance and the viscosity of a substance. Our experience tells us already, that the flow resistance in a tube is dependent on the length and the diameter of that tube. But what exactly is the relation?

Again, let us use an example of the everyday life: it is harder, to drink through a thin straw than through a thick one and the longer the straw is, the harder it is to suck a drink through as well. Also, we know intuitively it is much harder to drink viscous honey with a straw than water – so somehow the viscosity η has to play a role in the calculation of a flow resistance.

Assuming the straw has a circular cross section, the flow resistance R can be described by the following equation:

$$R = \frac{8\eta L}{\pi r^4} \quad (13.4)$$

where L is the length and r the diameter of the tube. The term η is the so called kinematic viscosity (literally, the resistance of a fluid to flow, so the larger this term is, the more viscous the fluid is).

Seen from Eq. 13.4 (the Hagen Poiseuille Equation) we can see that the cross-sectional area of our system (in this case the radius of the straw) has the largest effect. If we decrease the radius of our straw with a factor 10, the flow resistance will increase with a factor $10^4 = 10,000!$ Different cross-sectional shapes lead to different flow resistances. The following table demonstrates this dependency of the flow resistance from the shape however the used numbers were gained from numerical solutions of the Navier-Stokes equation. Therefore, this table should only be used to estimate a flow resistance for a given system.




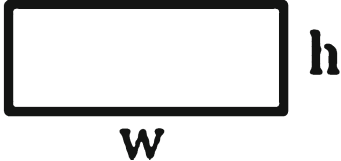
Let us assume we have a channel with a squared cross-section as often used in microfluidics. According to Table 13.1 the flow resistance in such geometry is

$$R = \frac{28.454\eta L}{a^4} \quad (13.5)$$

where a is the side length of the square. If we plug in numbers we will find out, that we will get an about 15% higher flow resistance in a quadratic system than in a circular system while maintaining the cross-sectional area.

This means that in the real world, a microfluidic system will act much less ideal as Eq. 13.2 suggests. Surface roughness for instance can play an important role in terms of flow resistance. Another issue will be the polarity of the fluid compared with the hydrophobicity of the system material. If for example the system is very

Table 13.1 Flow resistance at various cross sectional shapes

Cross section	Example	Flow resistance
Circular		$R = \frac{8\eta L}{\pi r^4}$
Regular triangle		$R = \frac{184.751\eta L}{a^4}$
Square		$R = \frac{28.454\eta L}{a^4}$
Rectangular ($W \gg h$)		$R = \frac{12\eta L}{wh^3}$

hydrophobic, it will be extremely difficult if not impossible to prime the system with an aqueous solution.

This shows one of the obvious challenges of shrinking down fluidic systems: if we want to move fluids around in a miniaturized system, we will have to apply a much higher pressure to do so than in larger systems, simply to overcome the flow resistance.

Let us go back to our picture of the straw in your drink. What do you do if you are thirsty? Usually, you will increase the flow rate by sucking stronger (increasing the pressure difference between the drink and your mouth). This is obviously one way in treating this “problem”, but the clever engineering way would be using two straws (since you normally lack one with a larger diameter). Luckily, the flow resistance of such a system can be calculated analogue to an electrical resistor according to the Kirchhoff-rules:

Two flow resistors (“straws”) in sequential order can be just added to one larger resistance:

$$R_{\text{tot}} = R_1 + R_2 + \dots + R_n \quad (13.6)$$

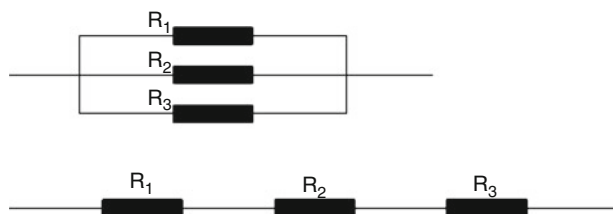


Fig. 13.1 Parallel and sequential connections of flow resistors. The equivalent flow resistance is given by Eqs. 13.7 and 13.6 respectively

In a sequential (or serial) order the flow resistance is simply the sum of all individual flow resistors – in our case two straws mounted to one long straw just gives twice as much fluidic resistance. In parallel order the flow resistance will add according to:

$$\frac{1}{R_{\text{tot}}} = \frac{1}{R_1} + \frac{1}{R_2} + \dots + \frac{1}{R_n} \quad (13.7)$$

Two straws mounted in parallel have a much smaller resistance than switched in series – just a result from the r^4 dependence in Eq. 13.4 (Fig. 13.1).

13.3 The Reynolds Number and Non-Newtonian Fluids

Yet another important practical equation derived from the Navier-Stokes equation is the so-called Reynolds Number Re . It also gives a relation between the viscous forces and the inertial forces and in practice it is a very good indication for the expected flow behavior of an object, for instance a ship model (Duvigneau et al. 2003), in a given fluid (water). Obviously, a small ship model will behave differently than a large 1:1 scale model if immersed into the same liquid because the inertia forces such as speed, size and density will be quite different. However, this effect can be compensated if the viscous forces would be changed accordingly. It has been exactly this challenge that brought ship construction engineers to “invent” the Reynolds number – to compare ship model behavior with reality. The Reynolds number is defined to be:

$$Re = \frac{\rho v l}{\mu} \quad (13.8)$$

where μ is the dynamic viscosity, ρ the density, v the velocity and l describes a characteristic length scale such as the width of a microchannel or in our example, the width of the ship model.

This means, that in our example of a miniature ship model, we have to make the viscous forces on our ship model equally larger. If we can manage to increase the viscosity of the liquid, the ship model is immersed into, we should get a much more realistic behavior.

Let us go back to the core of this chapter: in the case of microfluidic behavior this number has another, but nonetheless less important meaning. At Reynolds numbers above 2,300 we will always experience turbulent flow meaning we will get a lot of unstable vortices and two fluids would mix instantly. This is exactly the reason, why our normal shower head delivers a uniform jet of water as you experience in everyday life!

Reynolds numbers below 2,000 will indicate the tendency of the system to be more and more laminar. In common dimensions of microsystems Reynolds numbers seldom exceed values of 10 – meaning our toy shower head for the ants will have a number of very hot and very cold jets according to the set conditions.

Another important feature when going microfluidics is the following aspect: The surface to volume ratio increases dramatically. In itself, this is not a big challenge however as a consequence, evaporation becomes a severe issue. Nilsson et al. actually used this feature to up-concentrate small samples in order to perform chemical analysis (Santesson et al. 2000). What they did was the following: they levitated a droplet in a knot created from ultrasound waves (100 kHz), so it got immobilized as a free suspended, spherical droplet. To counteract for the evaporation, they shot microdroplets of water into the captured droplet using a microfluidic nozzle, similar to those from a conventional ink jet printer. Vice versa, this method could be used to up-concentrate biological samples.

Did you ever wonder, why ketchup is so hard to get out of the bottle, and once, it has decided to leave this bottle it comes with one big splash? Well, the reason is as simple or as complicated as Nature. Ketchup is a so called non-Newtonian fluid, meaning that its viscosity changes with applied shear stress (Yilmaz et al. 2011). If the shear stress is high, the ketchup gets less viscous and it can leave the orifice of the bottle. Once, it has reached its destination, ideally the French fries and not your shirt, it will stick there because the ketchup's viscosity gets back to normal as no shear forces are applied to it. In fact, ketchup is partially designed to act like this.

Mother Nature has used this trick since many centuries: our blood is also a non-Newtonian fluid. This is obviously very good because otherwise our blood could never reach the very small blood vessels we do have almost everywhere. The shear stress in the small blood vessels simply results in low viscous blood inside, so it actually can run through our body. On the contrary, the properties of blood helps the mosquitoes to survive – it would be much harder for them to “steal” our blood if it would be Newtonian – certainly our wise Mother Nature would have equipped them with a “straw” that has a much larger cross sectional area, leading unfortunately to more painful stitches.

13.4 Fabrication of Microfluidic Devices

A lot of books e.g. (Madou 1997; Geschke et al. 2004) are written about this subject and it cannot be the scope of this chapter to present the tremendous amount of available technology to fabricate a lot of different microfluidic devices. Here, we just need to learn how we can combine our macroscopic world of “ordinary plumbing”

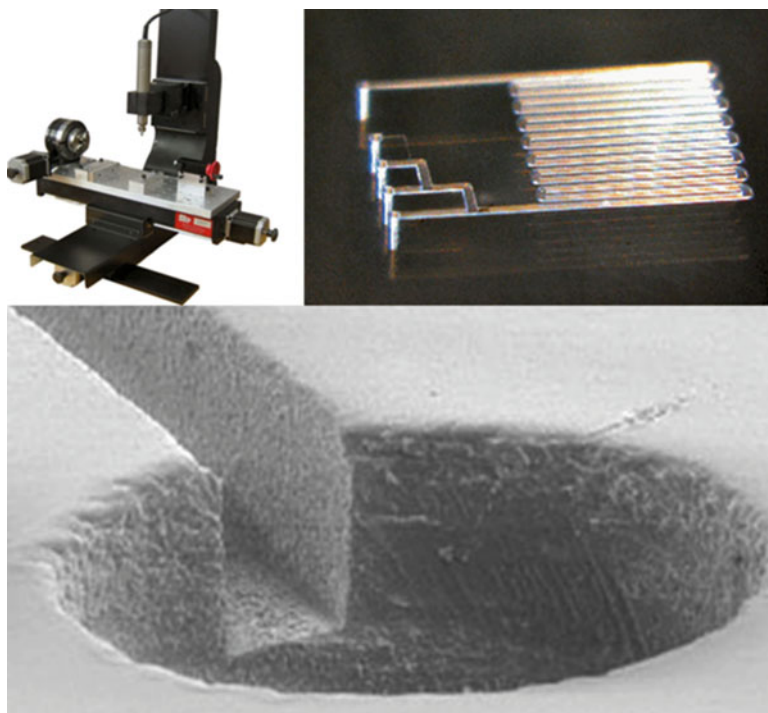


Fig. 13.2 Micromilling setup (*upper left*) and example of microfluidic polymer structures (*upper right*). The lower picture shows a scanning electron micrograph of a close up of this structure (channel size $50\ \mu\text{m} \times 50\ \mu\text{m}$) (Adapted from F. Bundgaard 2008)

to microfluidic systems. What technologies are favorable and at what costs? Often microfluidics is strongly connected to microtechnology, unfortunately often attributed to high cost technology such as silicon clean room technology.

This has however changed dramatically in the last decade where polymer microtechnology became mature enough to enable inexpensive mass production. The driving force of this has actually not been the microfluidic market but rather the information technology. The need of inexpensive data storage has driven the polymer technology to inventions such as compact discs, DVDs and Blu-ray discs. Microfluidics took advantage of these fabrication techniques and refined them – some of the commercial microfluidic systems even use the same format as a compact disc and use the centrifugal forces of a spinning disc to move liquids through the system. Those and other systems can now be fabricated routinely for a few cents by injection moulding and/or hot embossing. There is also technology available to generate low cost prototypes for microfluidic devices. Micromilling, for instance, can generate channel dimensions of $50\ \mu\text{m}$ and less as a cross section, see Fig. 13.2.

13.5 Microfluidic Formation of Biomimetic Membranes

How can we now take advantage of microfluidic techniques to build up biomimetic membranes? The fabrication techniques used to generate microfluidic structures can be used for making membrane scaffolds – for instance fabricating an array of regular apertures in a hydrophobic membrane, see Chap. 10. To generate a lipid bilayer spanning over all individual apertures, painting methods and blotting methods have been successfully proven. They, however have their drawbacks as most often, the membrane scaffold material is very thin and flexible, leading to immediate damage of the lipid bilayer.

Instead of moving the scaffold in a bilayer forming solution, microfluidics can help to direct the fluid along the membrane scaffold. This way has recently been shown (Pszon-Bartosz et al. 2011). They defined microchannels in a soft material on either side of a hydrophobic, microstructured membrane scaffold. The entire device was fabricated with a CO₂ laser leading to production times of only a few minutes and thereby reducing the fabrication costs to a minimum (Vogel et al. 2009). The system is comprised of a total of five layers that are clamped together, see Fig. 13.3.

The device was built as a completely closed chamber in order to improve the membrane stability. It consists of two compartments separated by the hydrophobic membrane scaffold in the centre of the device. This membrane scaffold has been fabricated from a thin (50 μm) ETFE membrane by laser machining an array of 8 × 8 = 64 holes (300 μm diameter, 400 μm pitch) into it.

The compartments are connected to a microfluidic system including conventional syringe pumps, thereby enabling fast and reliable injection and removal of liquids independently above and below the membrane scaffold.

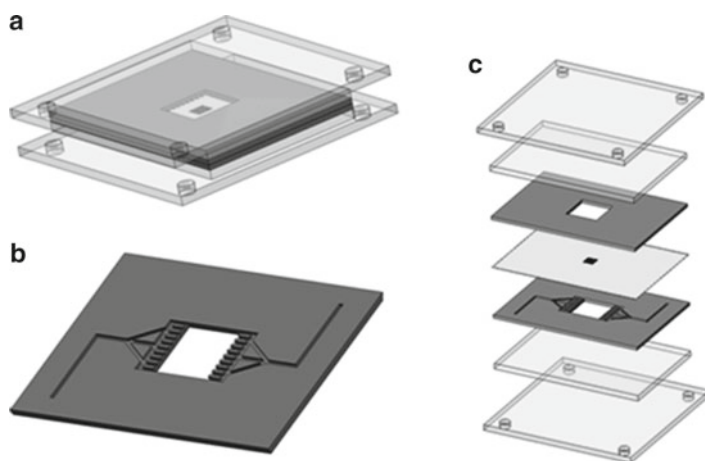
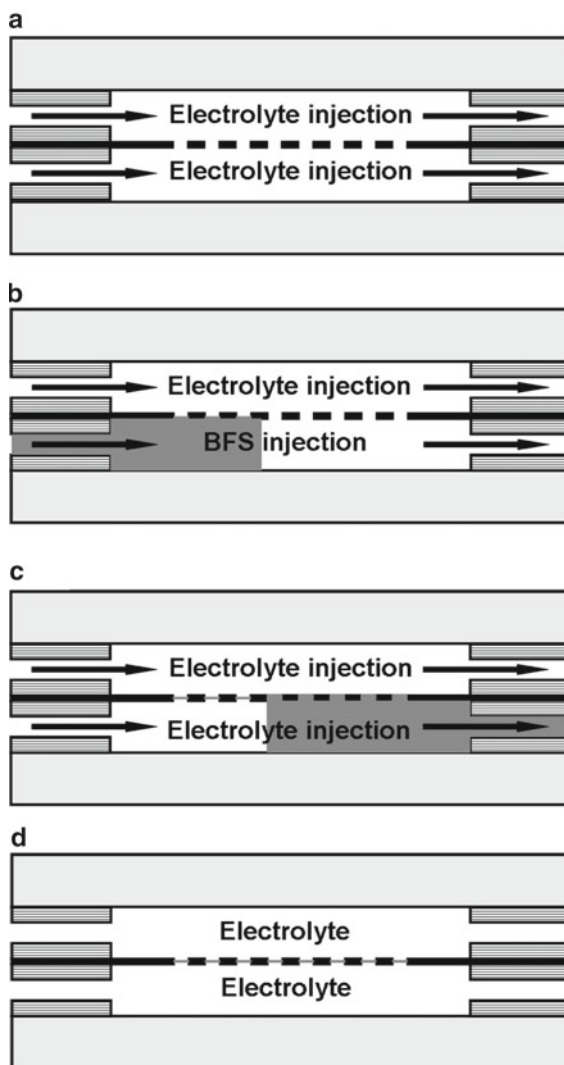


Fig. 13.3 Microfluidic system to generate an array of lipid bilayers. Schematic drawing of entire system (a), channel design (b) and arrangement of individual layers (c). Note, that the central layer is the actual membrane scaffold. The comb-like structure (b) acts as a flow equalizer

Fig. 13.4 Schematic drawing of establishing a lipid bilayer array (*center*). The system is primed with electrolyte (**a**), a plug of bilayer forming solution (*BFS*) is injected into the system (**b** and **c**), and after the plug has passed, a stable lipid bilayer has been generated in the membrane scaffold (**d**)



The system is initially primed with an aqueous solution of an electrolyte on both sides of the membrane. This step has to be performed very carefully as air bubbles can spoil the entire experiment of generating stable lipid bilayers on the membrane scaffold in the following step. Introducing the lipid bilayers is done by flushing one channel (here the lower one) with a plug of bilayer forming solution.

After the lipid bilayer has been established, both channels are rinsed with electrolyte solution and electrochemical measurements can be performed.

The procedure for bilayer membrane formation in the microfluidic device has been the following: Fig. 13.4a: The device compartments are filled with an electrolyte at a flow rate of 50 $\mu\text{L}/\text{min}$. In the next step (Fig. 13.4b) 40 μL of bilayer

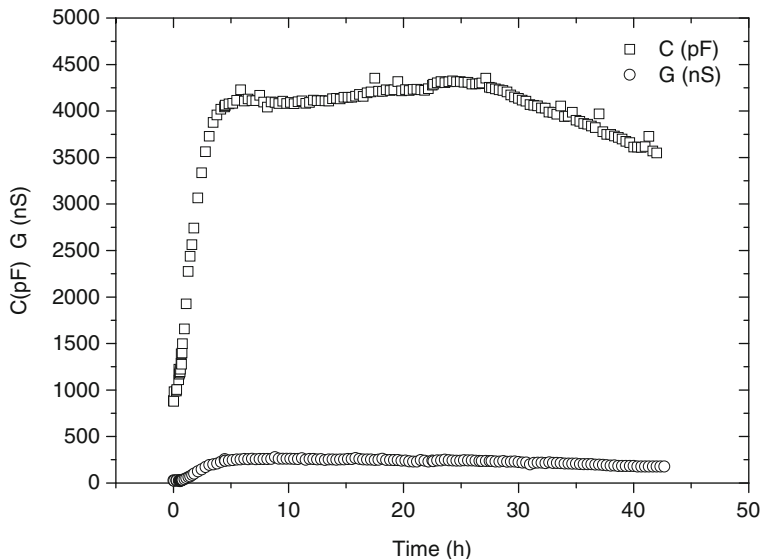


Fig. 13.5 Development of conductance G and capacitance C during the membrane thinning process. The lifetime of this experiment with an $8 \times 8 = 64$ aperture array (each $300 \mu\text{m}$ diameter) approached 2 days at continuous monitoring

forming solution (5 mg/ml DPhPC in decane) are injected into the bottom compartment at a flow rate of $50 \mu\text{l}/\text{min}$. Afterwards (Fig. 13.4c), the electrolyte is injected into both of the compartments on either side of the membrane with the same flow rate ($50 \mu\text{l}/\text{min}$) to remove an excess amount of lipids and induce a membrane thinning process (Fig. 13.4d).

This looks pretty straight forward on the sketch, but we need a proof, that we actually have a lipid bilayer. Here, electrochemistry comes in handy, see Chap. 10. If we include two electrodes into the system on either side of the membrane, we can prove the existence of this lipid bilayer by tracking the capacitance which is supposed to be high and stable and the conductance being low through the entire measurement. We can “quasi online” see the membrane thinning process resulting in a continuous rise of the capacitance during the process, see also Chap. 10. A typical measurement curve is shown in Fig. 13.5.

We can apparently conclude now, that we can fabricate an array of lipid bilayers by applying simple microfluidic techniques. The only remaining but obviously very important thing to do is now to get a transmembrane protein into the system and show that this is actually functioning.

Again, microfluidics serves as an easy accessible tool without getting poor because of using too much of expensive protein. For instance, we can use reconstitution of a transmembrane protein by simple flushing a bolus of a protein-containing stock solution in an electrolyte solution through the bottom chamber of our microfluidic system. In our case we have used a $10 \mu\text{g}/\text{ml}$ stock solution of α -Hemolysin

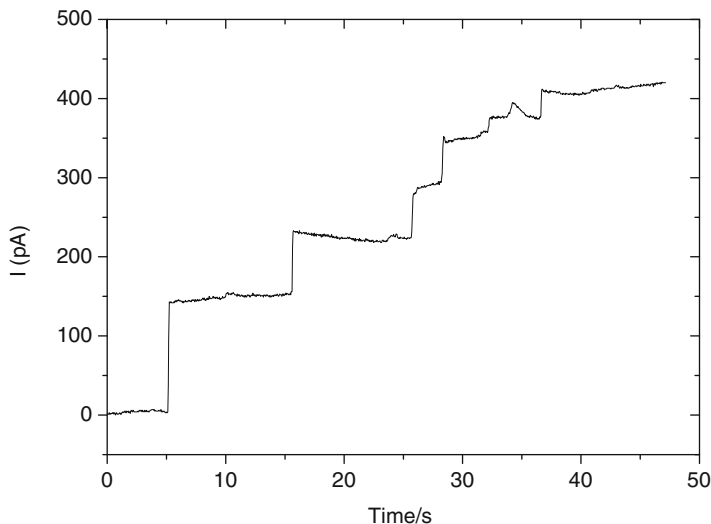


Fig. 13.6 Current trace showing reconstitution of α -Hemolysin. The current amplitude jumps correspond to insertion of α -Hemolysin pore-forming complexes

in 1.0 M KCl-solution but this is just one example. Other transmembrane proteins could be used however this is all a matter of an experimental optimization. In Fig. 13.6 we have used the same electrodes as previously described for monitoring the current across the membrane. Each step in the curve represents the insertion of one or more α -Hemolysin proteins somewhere in the 8×8 aperture array. The current value is comparable to previously reported signals (Hemmler et al. 2005).

13.6 Conclusion and Outlook

Using microfluidic devices to study proteins and to stabilize them in biomimetic devices seems to be a very good combination due to a number of reasons. First of all, it is a good research tool as the device costs are negligible compared to the high expenses attributed to the fabrication and purification of a protein. Even very tiny amounts of precious protein can be handled and analyzed. As the previous example showed, microfluidics can be used to create complex systems such as a lipid bilayer including a transmembrane protein – something Nature has done for millions of years. The most important advantage of microfluidics is simply, that the size of the systems matches the size of the proteins natural environment. I have personally no doubt that microfluidics will continuously impact the rapidly growing community working with biomimetic membranes – not only for the sake of research and understanding nature but also to generate highly innovative biomimetic solutions to man-made problems.

References

- Bruus, H.: *Theoretical Microfluidics*. Oxford Master Series in Physics. Oxford University Press, Oxford (2007)
- Bucky, P., Weakland, A.: *The Private Albert Einstein*. Andrews McMeel Publishing, Kansas City (1993)
- Bundgaard, F.: Thesis, Technical University of Denmark (2008)
- Duvigneau, R., Visonneau, M., Deng, G.: On the role played by turbulence closures in hull shape optimization at model and full scale. *J. Mar. Sci. Technol.* **8**, 11–25 (2003)
- Geschke, O., Klank, H., Telleman, P. (eds.): *Microsystem Engineering of Lab-on-a-Chip Devices*. Wiley-VCH, Weinheim (2004)
- Hemmler, R., Bose, G., Wagner, R., Peters, R.: Nanopore unitary permeability measured by electrochemical and optical single transporter recording. *Biophys. J.* **88**, 4000–4007 (2005)
- Madou, M.: *Fundamentals of Microfabrication*. CRC Press, Boca Raton (1997)
- Pecseli, H., Trulsen, J.: Transit times in turbulent flows. *Phys. Rev. E* **81**, 046310–046316 (2010)
- Pszon-Bartosz, K., Perry, M., Hansen, J., Vogel, J., Helix-Nielsen, C., Emneus, J., Geschke, O.: Automation formation and regeneration of biomimetic membranes in microfluidic devices. *J. Micromech. Microeng.* (2011) (in press)
- Santesson, S., Andersson, M., Degerman, E., Johansson, T., Nilsson, J., Nilsson, S.: Airborne cell analysis. *Anal. Chem.* **72**, 3412–3418 (2000)
- Vogel, J., Perry, M.E., Hansen, J.S., Bollinger, P.-Y., Nielsen, C.H., Geschke, O.: Support structure for biomimetic applications. *J. Micromech. Microeng.* **19**, 025026 (2009)
- Yilmaz, M., Karamanb, S., Cankurta, H., Kayacierb, A., Sagdic, O.: Steady and dynamic oscillatory shear rheological properties of ketchup-processed cheese mixtures: effect of temperature and concentration. *J. Food. Eng.* **103**, 197–210 (2011)

Index

A

Abscisic acid (ABA), 17
Acyl chain unsaturation, 197
Agre, P., 5, 47, 67
Akabane, G., 12
Albers, R.W., 120, 121, 124
Albers-Post scheme, 120
Albert Einstein, 274
Albumin, 120
Alder, B., 159
Alpha-hemolysin, 104, 105
Altamura, N., 233
Alumina oxide, 71, 72
Ammonium persulfate, 208
Andersen, O.S., 187
Anionic phospholipids, 129, 131, 132
Annulus lipids, 117, 118, 125, 132
Anodic alumina oxide (AAO), 71
Anodization, 71
Antidiuretic hormone
 ADH, 5, 10, 12
 arginine vasopressin (AVP), 5
 arginine vasotocin (AVT), 5
Antifouling surface, 53
Apparent mass transfer coefficient, 28
Aquaglyceroporins
 AQP3, 10
 AQP8, 6
 AQP9, 6
 AQP10, 6
 GlpF, 10
Aquaporins, 44, 45, 47, 48, 50, 51, 53, 54, 58,
 59, 161, 163, 165–167
 AQP0, 51
 AQP1, 6, 8, 9, 13, 14, 50, 165
 AQP2, 6, 10–12, 50

AQP3, 6
AQP4, 6, 10
AQP5, 6
AQP6, 6
AQP7, 6
AqpM, 242–244
AqpZ, 52, 242, 243
CHIP 28, 6
major intrinsic proteins (MIPs), 5, 18
PIP family, 50
plasma membrane intrinsic proteins (PIPs),
 6, 17
SoPIP2;1, 166, 255
tonoplast intrinsic proteins (TIPs), 6, 17
Arabidopsis, 17
Arabidopsis thaliana, 17
Archaeol lipids, 150
Atomic force microscopy (AFM), 89, 211,
 212, 223
Automated painted membrane (APM) method,
 215
Azad, A.K., 243

B

Bäckström, S., 137
Bacteriorhodopsin (BR), 118, 264
Baginsky, 121
Bamberg, E., 264
Barbara Lee Wilson, 275
Basolateral membrane, 8–10, 12, 14
Beddow, J.A., 265
Bending energy density (BED), 190
Benga, G., 5
Bereczki, R., 73
Bernhard, F., 241

Bezrukov, S.M., 75
 Bhatia, V.K., 106
 Bilayer bending modulus, 191
 Bilayer capacitance measurements, 195
 Bilayer compression modulus, 190
 Bilayer deformation energy, ΔG_{def} , 188
 Bilayer elastic properties, 187–190, 194, 195, 197, 198, 200
 Bilayer thickness, 187, 188, 191, 194–196
 Biofilm, 178
 Biofouling, 178
 Biomimetic membrane arrays, 206
 Biomimetic membranes, 45, 54, 58, 59
 Biotin, 53, 90
 Biotinylated lipids, 88, 227
 Block copolymer, 45, 52, 53, 55, 56, 59
 Block copolymers, 54
 Body forces, 169
 Bolalipids, 149, 150, 208
 Bolinger, P.Y., 100–102
 Born model, 138
 Boron, W.F., 8
 Boukobza, E., 103
 Boulpaep, E.L., 8
 Bovine serum albumin, 25
 Bowen, W.R., 13
 Bränden, M., 103
 Brownian dynamics, 167, 168
 Brunn, F., 3
 Buck, R.P., 73
Bufo marinus, 15
Bufo punctatus, 15
 1,4-Butane-dioldiacrylate (BDDA), 224

C

Ca²⁺-ATPase, 195, 196
 Calamita, G., 233
 Calcein, 146, 261, 263
 Caldarcheol lipids, 150
 Cantor, R.S., 128
 Carbon nanotubes (CNT), 45, 50, 55, 57, 58
 Carbonyl oxygens, 65
 6-Carboxyfluorescein, 146
 Cardiolipin, 118
 Cath, T.Y., 27
 Cell-free expression systems, 239
 Cell-free (CF) production systems, 234
 Cell membrane, 44, 47, 52
 Cell swelling assay, 145–146
 Cellulose triacetate membranes, 31
 Chan, Y.H.M., 98, 99
 Charge space competition (CSC) model, 69
 Chiu, D.T., 100

Chloromercuri benzene sulfonate (PCMBs), 5
 Cholesterol, 113, 118–120, 123–129, 150
 Chou, S., 34
 Christensen, C.U., 12
 Christensen, S.M., 87
 Cima, A., 2
 Coarse grained molecular dynamics (GCMD), 158, 167
 Coarse graining, 167
 Cohen, F.S., 266
 CO₂ laser, 210, 211, 215, 216, 280
 Colloidal particle lithography, 91
 Computational fluid dynamics (CFD), 158
 Concentration polarization (CP), 26, 58, 59, 176, 178
 Concentrative ICP, 28
 Constitutive promoters, 238
 Continuous exchange cell-free (CECF) format, 240
 Cornelius, F., 113, 122
 Cost and productivity index, 46
 Coulomb forces, 64
 Coulomb's law, 161
 Courant number (*Cr*), 174
 Cox, B.G., 65, 66
 Critical micelle concentration (CMC), 254
 Crowding, 69
 Curvature frustration energy, 191
 Cussler, E.L., 74, 79
 Cytochalasin B, 103

D

Dan, N., 53
 Debye screening length, 64
 Dendrimers, 151
 Density functional theory (DFT), 66
 Deoxycholate (DOC), 117
 Dephosphorylation, 124
 Desalination, 43, 45, 53–57
 Detergent, 117
 Detergent dialysis, 255
 Detergent removal, 255
 De Vries, H., 2
 Dialysis, 254, 255
 Diblock copolymer vesicles, 151
 Diblock polyethyleneoxide-polyethylene (EO40-EE37), 151
 Dichlorodimethylacridinone (DDAO) phosphate, 102
 Diffusional coefficient, 4, 177
 Diffusional water flow, 4
 Diffusive permeability constant, 165
 Dilutive ICP, 28
 Dimyristoylphosphatidylcholine (DMPC), 150

Dioleoylphosphatidylcholine (DOPC), 125
 Dioleoylphosphatidylserine (DOPS), 197
 1,2-Dioleoyl-*sn*-glycero-3-phosphocholine (DOPC), 208
 1,2-Dioleoyl-3-trimethylammonium-propane (DOTAP), 208
 Diphtanoylphosphatidylcholine (DPhPC), 207
 Dipole potential, 139
 Direct numerical simulation (DNS), 170
 Discher, D.E., 57
 Dispersion coefficient, 172
 DNA, 88, 90, 91, 93, 97, 99, 101, 104, 107
 Docosahexaenoyl acid (DHA), 127
 Dodecyl octaethylene glycol ether (C12E8), 254
 Donnan exclusion, 57
 Drake, K.D., 243
 Draw solution, 23
 dendrimers, 25
 magnetic nanoparticles, 26
 thermally removable ammonium salts, 26
 Driving solution. *See* Draw solution
 Dudev, T., 72, 78
 Dutrochet, R.J.R., 2
 Dynamic viscosity, 169

E

E. coli, 54
E. coli total lipid extract, 256
 Eddy viscosity, 170
 Eisenberg, B., 69
 Eisenman, G., 70
 Elastic moduli, 188
 Electrogenic exchange, 123
 Electronic polarizability, 159
 Electrostatic repulsion, 45, 50
 Elimelich, M., 57
 Endodermis, 17
 Endoplasmic reticulum, 125
 Energy consumption, 44
 Enggrob, H., 157
 Entropy of activation, 126
 Erythrocytes, 6
 Ethylenediaminetetraacetic acid (EDTA), 261
 Ethylene tetrafluoroethylene (ETFE), 207,
 210–213, 216, 217, 222–225, 228
 Euler description, 169
 Euler-Euler model, 172
 Excimer laser, 209–210
 Exocytosis, 257, 260
 Exodermis, 17
 External concentration polarization (ECP), 178
 Extracting agent. *See* Draw solution
 Eyring plot, 125

F

Fane, A.G., 21
 Fick's first law, 4
 Finite Volume (FV) Method, 173
 Flat sheet, 58
 Flow resistance, 273, 275–277
 Fluorescein diphosphate (FDP), 102
 Fluorescence microscopy,
 213, 257
 Fluorescence resonance energy transfer (FRET), 97, 104
 Fluorophores, 91, 95
 Force field, 160
 Förster radius, 97
 Forward osmosis (FO), 7, 44, 45, 48, 55,
 178, 179
 Forward osmosis membrane bioreactor (FOMBR), 37
 Foullants, 29
 Fouling, 170, 175, 177, 178, 180, 182
 Friction forces, 170
 Fu, D., 243
 Fusiogenic vesicles, 262
 Fusion protein expression vectors, 236
 FXYP proteins, 129

G

Gangliosides, 118
 Geschke, O., 273
 Ghadiri, M.R., 78
 Giant unilamellar vesicles (GUV), 253
 Gillespie, D., 79
 Glass transition temperatures, 73
 Glutathione-S-transferase, 236
 Glycosylation, 115
 Gorin, W.B., 5
 Gouraud, S., 10
 Gruber, M., 157
 Grubmüller, H., 51

H

Ha, T.J., 105
 Hansen, J.S., 213, 251
Hansenula polymorpha, 238
 Hasegawa, T., 12
 Hayakawa, S., 243
 Haydon, D.A., 139
 Hays, R.M., 4
 Hedfalk, K., 243
 Heinemann, S.H., 69
 Heins, E.A., 79
 Hélix-Nielsen, C., 137

Hexadecyltrimethylammonium
 hexadecyltrimethylammonium bromide
 (CTAB), 254
 Hillyard, S.D., 1, 15
 Hiroaki, Y., 243
 Histidine tag, 90
 Hollow fibres, 33
 Holt, J.K., 56
 Hovijitra, N.T., 243
 Hummer, G., 50
 Hydrolytic activity, 124
 Hydrophobic anions, 139
 Hydrophobic coupling mechanism (HCM),
 188, 189
 Hydrophobic interactions, 118
 Hydrophobic match, 126
 Hydrophobic mismatch, 192
 Hydrophobic thickness, 124, 151, 256
 2-Hydroxyethyl methacrylate (HEMA), 224
Hyla japonica, 12

I

Ikeda, M., 6
 Image energy, 139
 Image forces, 139, 142
 Immobilised vesicles, 89
 Inclusion bodies, 236
 Inducible promoters, 238
 Interfacial dipole potential, 140
 Internal concentration polarization (ICP), 27
 Ion channels, 63
 acetylcholine receptor, 118
 alpha-hemolysin, 75, 101
 aspect ratio, 72
 bacterial channel KcsA, 66
 bacterial NaChBac, 69
 Ca²⁺-activated potassium channels, 195
 carbonyl oxygens, 65, 67–69, 79
 DEKA locus, 69
 EEEE locus, 69
 hemolysin, 75
 KcsA, 65, 68, 69, 72, 78, 195
 mechanical sensitive large conductance
 channel (MscL), 75, 195, 197
 nicotinic acetylcholine receptor, 195
 outer membrane porin A (FomA), 260
 outer membrane porin F (OmpF), 75–77,
 79, 80, 82, 101
 potassium channels, 66
 selectivity filter, 69
 sodium channels, 68
 voltage dependent anion channel
 (VDAC), 263

Ion hydration shell, 140
 Ionophores, 65
 alamethicin, 257
 alpha-hemolysin, 257, 283
 crown ethers, 65
 cyclic nucleotide-gated (CNG)
 channels, 67
 gramicidin, 58, 101, 187, 189,
 192–200, 257
 melittin, 151
 nigericin, 121
 nystatin, 262
 selectivity filter, 67
 valinomycin, 65, 67, 68, 73, 257
 Ion-selective electrodes, 73
 Ion selectivity, 64
 Itoh, T., 6

J

Jung, J.S., 51

K

Kai, L., 243
 Karlsson, M., 243
 Kaufmann, Y., 58
 K⁺ complexation, 65
 Khandelia, H., 157
 Kidney
 collecting duct, 9
 fluid reabsorption, 9
 glomerular filtrate, 8
 loop of Henle, 8
 nephrons, 8
 proximal tubule, 8
 tubules, 8
 Kleinzeller, A., 2
Kluyveromyces lactis, 238
 Koefoed-Johnsen, V., 4
 Koros, W.J., 75
 Kozono, D., 51, 243
 Kramer, C., 2
 Kruse, E., 6
 Kukulski, W., 243
 Kumar, M., 43, 242, 243
 Kuyper, C.L., 101

L

Lagrangian description, 169
 Laizé, V., 243
 Large eddy simulation (LES), 171
 Large unilamellar vesicles (LUV), 253

Larsen, E.H., 15
 Laser ablation, 209
 Lateral pressure profile, 128
 Lauryldimethylamine N-oxide (LDAO), 254
 Leaf, A., 4
 Leap-frog Verlet, 161
 Lee, J.K., 243
 Lee, K.L., 28
 Lennard-Jones potential, 161
 Li, A.P., 78
 Lian, J., 243
 Lim, C., 72, 78
 Lindner, E., 73
 Lipid annulus, 118
 Lipid bilayer, 5, 44, 50, 52, 58
 Lipid membrane, 52
 Lipid packing, 188
 Lipid-to-protein ratio (LPR), 254, 255, 258, 260, 261, 264, 267
 Liposomes, 52, 116, 244, 252–255
 Liquid disordered (*ld*) domain, 128
 Liquid ordered (*lo*) domain, 128
 Loeb, S., 28, 35
 Lundbæk, J.A., 187

M

MacKinnon, R., 67
 Majumder, M., 56
 Maltose-binding protein, 236, 242
 Mammalian supraquaporins
 AQP11, 6
 AQP12, 6
 Mannitol, 260
 Martin, C.R., 71
 MARTINI force field, 167
 Matile, S., 77
 Matsura, T., 57
 Matteucci, C., 2
 Maurel, C., 15, 17
 Mayer, M., 209
 McCutcheon, J., 57
 Mecke, A., 45
 Meller, A., 72
 Membrane capacitance, 218, 282
 Membrane curvature, 105
 Membrane protein reconstitution, 252–254, 256, 267
 Membrane proteins, 45, 47, 51–55, 251–267
 Membrane resistance, 218
 Membrane scaffold, 209, 280
 Membrane thickness, 72
 Mesh design, 173
 Micro-drilling, 209

Microfluidics, 273
 Mie, G., 147
 Miedema, H., 63
 Molecular dynamics (MD), 157
 Molecular force probes, 200
 Monolayer intrinsic curvature, 187–189, 195, 196
 Montal-Mueller folding technique, 212
 Mueller, P., 258
 Mueller-Rudin painting technique, 212
 Multicopy expression vectors, 238
 Multilamellar vesicles (MLV), 253

N

Nageli, C., 2
 Na,K-ATPase, 113–132
 Nanochannels, 45, 48, 50, 54–56, 59
 Nanocontainers, 87
 Nanofiltration, 241
 Navier-Stokes equation, 169, 274
n-Dodecyl β -D-maltoside (DDM), 254
 Neher, E., 64
 Nernst-Planck equation, 76
 Neurohypophysis, 9
 Newtonian fluid, 274
n-hexene, 222
 Non-annular sites, 118
 Non-denaturing detergents, 254
 Nonner, W., 69
 Non-Newtonian fluid, 278
 Noskov, S.Y., 68–70
 NPT ensemble, 163
 Nyblom, M., 243
 Nystatin/ergosterol (N/E) fusion activity assay, 262

O

Oberg, F., 243
 Octaethyleneglycol dodecyl monoether (C₁₂E₈), 117
 Octyl β -D-thioglucopyranoside (OTG), 254
 Octyl- β -glycopyranoside (OG), 254
 Off vector delay, 211
 Ogushi, Y., 13
 Oligomerization, 256
 Omiloride, 13
 Opekarová, M., 256
 Organomercurial compounds, 5
 Organosilanes, 72
 Orwar, O., 100
 O'Shaughnessy, T.J.H.J.E., 210

Osmosis, 2
 endosmosis, 2
 exosmosis, 2
 Osmotic agent, 23
 Osmotic coefficient, 24
 Osmotic gradient, 3, 8, 9, 12, 13, 44, 49, 146,
 258, 261
 Osmotic membrane permeability, 142
 Osmotic permeability coefficient, 3
 Osmotic pressure, 2, 8, 9, 23
 Ouabain, 119
 Oxonol VI, 122

P

Palmitoyl-oleoyl-phosphatidylcholine
 (POPC), 164
 1-Palmitoyl-2-oleoyl-*sn*-glycero-3-phospho-
 L-serine (POPS), 208
 Pata, V., 53
 Patch-clamp, 64
 Paula, S., 140
 Pauling ionic radii, 68
 Payne, M.M., 43
 Pedersen, C.J., 65
 Periodic boundary conditions, 162
 Permeability, 44, 46, 47, 50, 52–55,
 58, 59
 Permeability coefficient, 138
 Perry, M., 205, 263
 PEtOz, polyethyl oxazoline, 55
 Pettersson, N., 243
 Pfeffer, W., 2
 Phosphorylation, 124
Pichia pastoris, 233, 234, 238,
 239, 242
 Pick, H., 103
 Planar lipid bilayers, 66, 257–266
 Plasencia, I., 251
 Plasma polymerization, 222
 Plasmolysis, 2
 Plasticizer, 73
 Plateau-Gibbs border, 226
 PMOXA, polymethyl oxazoline, 55
 Poiseuille equation, 4, 275
 Poiseuille flow, 48, 49
 Poisson-Nernst-Planck (PNP) formalism, 75
 Polydimethyl siloxane (PDMS), 55, 207,
 209, 225
 Polydispersion, 93, 253
 Poly-electrolyte cushion, 226, 227
 Poly-electrolytes, 222
 Poly(ethylene glycol) dimethacrylate
 (PEG-DMA), 224

Poly(ethylene glycol)-poly(propylene
 glycol)-poly(ethylene glycol) PEO5-
 PPO68-PEO5, 151
 Polyethylene-polyethyleneoxide (EE-EO)
 block copolymer, 52
 Poly(2-hydroxyethyl methacrylate) (PHEMA),
 224–228
 Polymer, 44–47, 52–55, 58, 59
 Polymerizable lipids, 208
 Polymersomes, 151, 207, 252
 Poly-(2-methyloxazoline)-poly-
 (dimethylsiloxane)-poly-
 (2-methyloxa-zoline)
 PMOXA15-PDMS110-
 PMOXA15, 151
 Polymethyloxazoline-polydimethylsiloxane-
 polymethyloxazoline (PMOXA-PDMS-
 PMOXA), 207
 Polyunsaturated lipids, 123
 Polyunsaturated phospholipids, 113, 127, 128
 Polyunsaturation index, 123
 Poly(vinyl chloride) (PVC), 73
 Porosity, 29
 Post, R.L., 120, 121, 124
 Post-translational modifications, 236,
 238, 240
 Poust, S.K., 43
 Pressure retarded osmosis (PRO), 37
 Protease-deficient yeast strains, 238
 Protein A, 236
 Protein aggregation, 256, 261
 Protein conformational equilibrium, 128
 Protein purification, 252
 Proteoliposomes, 116, 118–125, 128, 132,
 252–255, 258–260, 262, 263
 Proton permeability, 150
 Pszon-Bartosz, K., 251
 Purification, 234

Q

Quartz crystal microbalance (QCM), 89

R

Rael, E., 129
 Rayleigh, L., 147
 RecA proteins, 105
 Reflection coefficient, 3, 23
 Rein, C., 205
 Reticulocyte lysate-based CF method, 242
 Reverse osmosis (RO), 44
 Reynolds averaged Navier-Stokes equations
 (RANS), 171

- Reynolds number, 170, 171, 277
 Rezac, M.E., 75
 Rhoades, E., 104
 Richet, G., 2
 Robert Townson, 2
 Rosenkilde, P., 12
 Roux, B., 68
 Rudin, D.O., 258
- S**
Saccharomyces cerevisiae, 233, 234, 238, 239, 242
 Sakmann, B., 64
 Sandison, M., 210
 Sarco(endo)plasmic Ca-ATPase (SERCA), 125
 Savage, D.F., 243
 Schwarz, D., 243
 Selectivity filter, 67
 Self-quenching dye, 146
 Semipermeable membrane, 2, 3, 44, 143
 Shear forces, 278
 Silicon nitride, 209
 Single-channel osmotic permeability constant *pf*, 164
 Siwy, Z.S., 79
 Size exclusion, 50
 Slip enhancement, 49
 Small unilamellar vesicles (SUVs), 100, 253
 Solubility diffusion model, 138, 142
 Solubilization, 115, 234
 Soluble partner proteins, 236
 Sorbitol, 260
 Soybean asolectin, 256
 Spark erosion, 209
 Sphingomyelin, 118
 Spiny dogfish, *Squalus acanthias*, 114
 Spot lase time, 211
 Stamou, D., 87, 91, 101
 1-Stearoyl-2-oleoyl-*sn*-glycero-3-phosphocholine (SOPC), 150
 Sterols, 150
 Stibius, K., 137
 Stopped flow principle, 147
 Streptavidin, 88, 90, 91, 93, 95, 97, 107
 Streptavidin/biotin, 88
 Stress tensor, 169
 sub-grid scale Reynolds Stress, 171
 Sudhölter, E.J.R., 73
 Sulfatides, 118
 Surface forces, 169
 Surface functionalization, 222
 Sweadner, K.J., 129
- Synaptic attachment protein receptors
 SNAREs, 10, 260
 Synthetic ion channels, 79
- T**
 Tang, C., 21
 Tanner, W., 256
 Tethering, 88
 Tetra-methyl-ethylenediamine (TEMED), 208, 224
 Tetraphenylarsonium, 140
 Thin film composite (TFC), 33
 Thioredoxin, 236
 Thomas, J.A., 49
 Thompson, A.N., 68
 Tonoplast, 16, 17
 Tonoplast (vacuolar) membrane, 17
 Törnroth-Horsefield, S., 243
 Tortuosity, 29
 Transmission electron microscopy at cryogenic temperatures (cryoTEM), 93
 Turbulence, 170
 Turgor pressure, 7, 15, 16
 Turnover number (*kcat*), 125
- U**
 Unilamellar vesicles, 253
 Ussing, H.H., 4
- V**
 van't Hoff, J.H., 2
 van't Hoff equation, 2, 24
 Verdoucq, L., 243
 Vesicle fusion, 257–259, 261–263, 266, 267
 Vesicles, 52–56, 58
 Viborg, A., 12
 Vogel, J., 205
 Voltage-clamp, 58, 193, 263
- W**
 Wainwright, T., 159
 Wang, R., 21
 Wanunu, M., 72
 Water dipole reorientation, 165
 Water permeability coefficient, 23
 Water transport, 1, 44–48, 50, 59
 Werten, P.J., 243
 Wicaksana, F., 21
 William Hewson, 1

Wilson, B.L., 275
Woodbury, D.J., 259, 263

X

Xenopus laevis, 6, 12
Xu, Z., 243

Y

Yakata, K., 243
Yamaoka, K., 69

Yang, L., 243
Yarrowia lipolytica, 238
Yde, L., 157
Yip, N.Y., 33
Yousef, H.N.S., 13

Z

Zardoya, R., 18
Zhu, F., 165
Zilles, J.L., 43
Zimmerman, S.L., 12